

Univerza
v Ljubljani

Fakulteta
*za gradbeništvo
in geodezijo*



PRIMOŽ MOŽE, univ. dipl. inž. grad.

**DUCTILITY AND RESISTANCE OF BOLTED CONNECTIONS IN
STRUCTURES MADE OF HIGH STRENGTH STEELS**

DOCTORAL THESIS

**DUKTILNOST IN NOSILNOST VIJAČENIH SPOJEV V
KONSTRUKCIJAH, NAREJENIH IZ JEKEL VISOKE TRDNOSTI**

DOKTORSKA DISERTACIJA

PODIPLOMSKI ŠTUDIJ GRADBENIŠTVA

LJUBLJANA, 2008

Univerza
v Ljubljani

Fakulteta
*za gradbeništvo
in geodezijo*



*PODIPLOMSKI ŠTUDIJ
GRADBENIŠTVA
KONSTRUKCIJSKA SMER
DOKTORSKI ŠTUDIJ*

Kandidat:

PRIMOŽ MOŽE, univ. dipl. inž. grad.

**DUCTILITY AND RESISTANCE OF BOLTED
CONNECTIONS IN STRUCTURES MADE OF HIGH
STRENGTH STEELS**

Doctoral thesis No.: 180

**DUKTIILNOST IN NOSILNOST VIJAČENIH SPOJEV V
KONSTRUKCIJAH, NAREJENIH IZ JEKEL VISOKE
TRDNOSTI**

Doktorska disertacija štev.: 180

Temo doktorske disertacije je odobril
Senat Univerze v Ljubljani na 7. seji dne 27. junija 2006
in imenoval mentorja prof. dr. Darka Bega.

Pisanje doktorske disertacije v angleškem jeziku je odobril
Senat Univerze v Ljubljani na 7. seji dne 27. junija 2006.

Ljubljana, 6. maj 2008



Univerza
v Ljubljani

Fakulteta
*za gradbeništvo
in geodezijo*



Komisijo za oceno ustreznosti teme doktorske disertacije v sestavi
prof. dr. Darko Beg
izr. prof. dr. Jože Korelc
prof. dr. Dan Dubina, Politehnica University of Timisoara, Romunija

je imenoval Senat Fakultete za gradbeništvo in geodezijo na 9. redni seji dne
19. aprila 2006.

Komisijo za oceno doktorske disertacije v sestavi
prof. dr. Darko Beg
izr. prof. dr. Jože Korelc
prof. dr. Dan Dubina, Politehnica University of Timisoara, Romunija

je imenoval Senat Fakultete za gradbeništvo in geodezijo na 16. redni seji dne
26. marca 2008.

Komisijo za zagovor doktorske disertacije v sestavi
prof. dr. Bojan Majes, dekan, predsednik
prof. dr. Darko Beg
izr. prof. dr. Jože Korelc
prof.dr. Dan Dubina, Politehnica University of Timisoara, Romunija

je imenoval Senat Fakultete za gradbeništvo in geodezijo na 17. redni seji dne
23. aprila 2008.

Univerza
v Ljubljani

Fakulteta
*za gradbeništvo
in geodezijo*



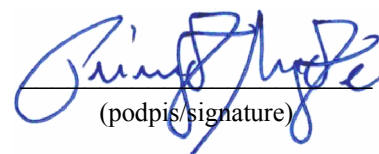
IZJAVA O AVTORSTVU

Podpisani **PRIMOŽ MOŽE**, univ. dipl. inž. grad., izjavljam, da sem avtor doktorske disertacije z naslovom: **“DUKTILNOST IN NOSILNOST VIJAČENIH SPOJEV V KONSTRUKCIJAH, NAREJENIH IZ JEKEL VISOKE TRDNOSTI”**.

STATEMENT OF AUTHORSHIP

I, undersigned **Primož Može**, Univ. B.C.E., hereby declare that I am the author of the doctoral thesis titled: **“DUCTILITY AND RESISTANCE OF BOLTED CONNECTIONS IN STRUCTURES MADE OF HIGH STRENGTH STEELS”**.

Ljubljana, 6.5.2008


(podpis/signature)

ERRATA

Page	Line	Error	Correction
------	------	-------	------------

BIBLIOGRAPHIC-DOCUMENTALISTIC INFORMATION

UDC: 624.014.2:624.078(043.3)
Author: Primož Može
Supervisor: Prof Darko Beg
Title: Ductility and resistance of bolted connections in structures made of high strength steels
Notes: 156 p., 29 tab., 130 fig., 118 eq., 6 app.
Keywords: high strength steel, ductility, bolted connections, net cross-section, tension splices

Abstract

Structural steel grades with yield strength higher than 420 MPa are considered as high strength steels. They undoubtedly have lower ductility than mild steels in terms of engineering measures of ductility, such as ultimate-to-yield strength ratio, uniform strain and elongation at fracture. A typical values for high strength steels are: ultimate-to-yield strength ratio $f_u/f_y = 1,05$, uniform strain $\varepsilon_u = 0,05$ and elongation after fracture $\varepsilon_{fr} = 15\%$. The problem is that inelastic behaviour is hidden in numerous nominally elastic resistances checks of steel structures and therefore sufficient local ductility has to be assured. The focus is set on structural elements with holes subjected to tension and to tension splices with bolts in shear. Local ductility in terms of plastic deformations has to be sufficient in order to assure bolthole elongation, so the loading transfers through all bolts. An extensive experimental research of plates with holes and tension splices made of steel grade S690 was conducted to determine maximum resistance and ductility. The reliability of the Eurocode design rules for net cross-section resistance to was statistically evaluated. The statistical analysis was substantiated by additional test results on net cross-section failure of high strength steel members available in literature. Moreover, the experiments were numerically simulated to look inside the stress state. The test results served as a guideline for the accuracy of numerical simulations. A comprehensive numerical parametrical study of tension splices and in addition, the numerical analyses of tests on tension splices found in literature were performed. The Eurocode design bearing resistance was critically assessed on the basis of the database of 266 connection results. In certain cases the Eurocode design bearing resistance formula gives inadequate results. Therefore, a new, simple design bearing resistance formula was proposed.

BIBLIOGRAFSKO-DOKUMENTACIJSKA STRAN IN IZVLEČEK

UDK:	624.014.2:624.078(043.3)
Avtor:	Primož Može
Mentor:	prof. dr. Darko Beg
Naslov:	Duktilnost in nosilnost vijachenih spojev v konstrukcijah narejenih, iz jekel visoke trdnosti
Obseg in oprema:	156 str., 29 pregl., 130 sl., 118 en., 6 pril.
Ključne besede:	jekla visoke trdnosti, duktilnost, vijacheni spoji, oslabljen prerez, preklonni spoji

Izвлеček

Jekla z napetostjo tečenja večjo od ali enako 420 MPa uvrščamo med jekla visoke trdnosti. V smislu inženirskih meril duktilnosti, imajo ta jekla nedvomno manjšo duktilnost kot običajna, mehka konstrukcijska jekla. Med inženirska merila duktilnosti, s tipičnimi vrednostmi za jekla visoke trdnosti, štejemo: razmerje med napetostjo tečenja in natezno trdnostjo $f_u/f_y = 1,05$, deformacijo pri doseženi natezni trdnosti $\varepsilon_u = 0,05$ in deformacijo po pretrgu $\varepsilon_{fr} = 15\%$. Težava je v tem, da veliko nominalno elastičnih kontrol nosilnosti jeklenih konstrukcij v sebi skriva neelastično obnašanje in je zato potrebno zagotoviti zadostno duktilnost. V ospredje so postavljeni konstrukcijski elementi z luknjami, podvrženi natezni obremenitvi in natezni preklonni spoji z vijaki v strigu. Pri spojih je lokalna duktilnost v smislu plastičnih deformacij potrebna, da se obremenitev prenese med vse vijake. Narejena je bila obsežna eksperimentalna preiskava pločevin z luknjami in preklonnih spojev v nategu z namenom določitve največje nosilnosti in duktilnosti. Za izdelavo preizkušancev je bilo uporabljeno jeklo S690. Zanesljivost evrokodovih projektnih nosilnosti oslabljenih prerezov je bila ocenjena s statistično analizo. Ta je bila dodatno podkrepljena z rezultati preiskav na nateznih preklonnih spojih iz jekel visoke trdnosti iz literature. Preiskave preklonnih spojev so bile numerično simulirane, z namenom določiti in preiskati napetostno-deformacijsko stanje. Pri tem so rezultati testov služili kot smernica za oceno pravilnosti numeričnih simulacij. Z numeričnim orodjem je bila narejena obsežna parametrična študija nateznih preklonnih spojev. Prav tako so bili numerično simulirani testi nateznih preklonnih spojev iz literature. Evrokodova projektna nosilnost na bočni pritisk je bila kritično ocenjena na podlagi baze podatkov z 266 rezultati preklonnih spojev. V določenih primerih evrokodova projektna nosilnost na bočni pritisk podaja neustrezne rezultate. Zato je v disertaciji predlagana nova metoda za izračun projektnih vrednosti bočnega pritiska na vijak, ki je enostavna za uporabo.

ZAHVALE

Ministrstvo za visoko šolstvo, znanost in tehnologijo je financiralo moje usposabljanje v okviru programa mladih raziskovalcev. Iskreno se zahvaljujem podjetju Trimco d.d. iz Trebnjega, ki je podarilo material in poskrbelo za izdelavo preizkušancev. Zahvala gre v prvi vrsti mojemu mentorju prof. dr. Darku Begu, ki me je usmerjal pri znanstvenem delu in pri raznovrstnih strokovnih projektih, kjer sem se priučil mnogo inženirskih prijemov. Za jezikovni pregled angleškega dela teksta je zaslužna Romana Hudin. Sodelavci, prijatelji, skupaj smo poskrbeli za prijetno vzdušje na katedri in preživeli nekaj nepozabnih trenutkov.

Svojci in prijatelji, vselej ste mi stali ob strani. Zaradi tebe, moja Petra, ki razumeš hrepenenje po znanju in odkrivanju neznanega, moja pot nikoli ni bila težka.

TABLE OF CONTENTS

1	Introduction	1
2	Methodology of experimental work	9
2.1	General	9
2.2	Material characteristics	9
2.3	Descriptions of specimens, measuring devices and test set-up	11
2.3.1	Experimental phase one – specimen types H, HH, B1, B2	11
2.3.2	Experimental phase two – specimen type L	15
3	Methodology of numerical models	19
3.1	General	19
3.2	Numerical model type M1	19
3.3	Numerical model type M2	20
3.4	Numerical model type M3	21
3.5	Contact interactions	22
3.6	Finite elements and meshing	23
3.7	Determination of material model	25
4	Tension members with holes – net cross section failure	29
4.1	Introduction	29
4.2	Test results	30
4.3	Statistical evaluation of results	36
4.3.1	Data for statistical evaluation of net cross-section resistance formula	40
4.4	Results of statistical evaluation and discussion	41
4.5	Summary	45
5	Tension splices with bolts in shear – failure in bearing	47
5.1	Introduction	47
5.2	Design resistance of bearing type shear connections	47
5.3	Definition of bearing resistance at bolt holes	48
5.4	Test results	50
5.4.1	One- and two-bolt shear connections – specimens B1, B2	50
5.4.2	Bolted shear connections with 3 or 4 bolts positioned in the direction of load – specimens L	58
5.5	Numerical parametrical study of bolted shear connections	70
5.5.1	Width as the varying parameter	71
5.5.2	Plate stiffness as the varying parameter	72
5.5.3	Bolt diameter as the varying parameter	76
5.5.4	Number of bolts as the varying parameter	78

5.6	Test results on bolted shear connection found in literature	78
5.7	Analysis of bearing resistances in relation to EN 1993-1-8	83
5.7.1	General.....	83
5.7.2	Single bolt connections.....	84
5.7.3	The connections with a single row of bolts positioned in the direction of load transfer	89
5.7.4	The connections included in the numerical parametric study.....	90
5.7.5	The connections with two lines of bolts in the direction of load transfer.....	91
5.8	Development of new design resistance bearing formula	93
5.8.1	General.....	93
5.8.2	Single bolt connections.....	93
5.8.3	The connections with a single row of bolts positioned in the direction of load transfer	97
5.8.4	The connections included in the numerical parametric study.....	101
5.8.5	The connections with two lines of bolts in the direction of load transfer.....	103
5.9	Comparison of new bearing resistance formula to Eurocode bearing resistance	106
5.10	Summary.....	112
6	Conclusions	117
7	Povzetek	121
	References	153
Appendix A	Specimen types H, HH – Test results	157
Appendix B	Specimen types B1, B2 – Test results	167
Appendix C	Specimen type L – Test results	175
Appendix D	Results of parametric study	189
Appendix E	Results of numerical FE analyses, replicating tests from literature	235
Appendix F	Factors used in bearing resistance formulas	251

TABLE OF FIGURES

Fig. 1: Simple tension splice with bolts in double shear	5
Fig. 2: Stress-strain diagrams of standard tensile tests	10
Fig. 3: Test rig (testing machine Instron)	11
Fig. 4: Specimen types H, HH – steel strips with holes subjected to tension	12
Fig. 5: Specimen types B1 – single bolt connection with bolt in double shear	13
Fig. 6: Specimen type B2 – two-bolt connection with bolts in double shear.....	13
Fig. 7: Specimen B2 under loading	13
Fig. 8: Testing machine with capacity of 2500 kN.....	16
Fig. 9: Specimen type L equipped with measuring devices.....	16
Fig. 10: Symbols for measured distances of specimen type L.....	17
Fig. 11: Numerical model type M1	20
Fig. 12: Numerical model type M2	21
Fig. 13: Numerical model type M3	21
Fig. 14: Pressure-overclosure relationship with possible negative pressure transmission (cohesion) and/or overclosure (SIMULIA, 2007).....	22
Fig. 15: Mesh types	24
Fig. 16: Load displacement curves for different meshes and finite elements.....	25
Fig. 17: Comparison of numerical and experimental load-displacement curves	27
Fig. 18: Numerical simulation of standard tensile test on specimen 291-1	27
Fig. 19: Reduced net cross-section.....	30
Fig. 20: Specimen H10 under loading (elastic stage 4,3 kN, maximum resistance 678 kN, just first macro crack 600 kN, failure 207 kN).....	32
Fig. 21: Load displacement curves for specimens H01 to H16 (steel grade S690)	32
Fig. 22: Load displacement curves for specimens H – comparison of materials S690 and S235.....	33
Fig. 23: Failure of specimens of equal geometry but different steel grade.....	33
Fig. 24: Normalized resistance in relation to A_{net}/A (a) or displacement D_u at maximum resistance (b) for steel grade S690 and S235.....	34
Fig. 25: Load displacement curves for specimens B1 that failed in net cross-section.....	35
Fig. 26: Load displacement curves for specimens B2 that failed in net cross-section.....	35
Fig. 27: Load-disp. curves for specimens L18s, L20 that failed in net cross-section	35
Fig. 28: Net cross-section failure of specimen B122.....	35
Fig. 29: Net cross-section failure of specimen L20	35
Fig. 30: (r_e , r_t) diagram – Model 1, data set 0.....	44
Fig. 31: Sensitivity diagram – Model 1	44
Fig. 32: (r_e , r_t) diagram – Model 2, data set 0.....	45
Fig. 33: Sensitivity diagram – Model 2	45
Fig. 34: (r_e , r_t) diagram – Model 3, data set 3.....	45
Fig. 35: (r_e , r_t) diagram – Model 3, data set 5.....	45
Fig. 36: Definition of distances	50
Fig. 37: Failure modes for specimens B1	52
Fig. 38: Comparison of experimental and numerical load-displacement curves	52
Fig. 39: Force-displacement curves for two groups of specimens with the same width.....	53
Fig. 40: Results of numerical simulation of B109 at 5,365 mm of hole elongation in the middle surface.....	54
Fig. 41: Results of numerical simulation of B111 at 6,375 mm of hole elongation in the middle surface.....	56
Fig. 42: Magnitude of plastic strain at integration points at failure – a cut through B111	56

Fig. 43: Results of numerical simulation of B101 in the middle surface (a, b, c at 2,717 mm of displacement).....	57
Fig. 44: Force-displacement curves for different boundary conditions	57
Fig. 45: Comparison of numerical and experimental resistances.....	58
Fig. 46: Mises stress plotted over the actual specimens L20 and L21 (grid of lines), respectively	59
Fig. 47: Failure types of specimens L.....	62
Fig. 48: Experimental and numerical load-displacement curves for specimen L14	62
Fig. 49: Distribution of bearing forces and friction for specimen L14	62
Fig. 50: Distribution of bearing forces and friction for specimen L14 at <i>global</i> maximum	63
Fig. 51: Distribution of bearing forces and friction for specimen L14 at <i>local</i> maximum	63
Fig. 52: Contact pressure at surface nodes for specimen L14.....	63
Fig. 53: Frictional shear stress at surface nodes for specimen L14.....	63
Fig. 54: Stress state of specimen L14 in the middle surface.....	63
Fig. 55: Stress state of specimen L03	65
Fig. 56: Experimental and numerical load-displacement curves for specimen L03	65
Fig. 57: Distribution of bearing forces and friction for specimen L03	65
Fig. 58: Distribution of bearing forces and friction for specimen L03 at <i>global</i> maximum	66
Fig. 59: Distribution of bearing forces and friction for specimen L03 at <i>local</i> maximum	66
Fig. 60: Stress state of specimen L18 in the middle surface at maximum force.....	66
Fig. 61: Experimental and numerical load-displacement curves for specimen L18	66
Fig. 62: Distribution of bearing forces and friction for specimen L18	66
Fig. 63: Distribution of bearing forces and friction for specimen L18 at <i>global</i> maximum	67
Fig. 64: Distribution of bearing forces and friction for specimen L18 at <i>local</i> maximum	67
Fig. 65: Experimental and numerical load-displacement curves for specimens L13 and L22, respectively.....	67
Fig. 66: Experimental and numerical load-displacement curves for specimens L04, L04s.....	69
Fig. 67: Experimental and numerical load-displacement curves for specimens L06, L06s.....	69
Fig. 68: Distribution of bearing forces and friction for specimen L04	69
Fig. 69: Distribution of bearing forces and friction for specimen L06	69
Fig. 70: Distribution of bearing forces and friction for specimen L04s.....	69
Fig. 71: Distribution of bearing forces and friction for specimen L06s.....	69
Fig. 72: Distribution of bearing forces and friction for specimen L04s.....	70
Fig. 73: Distribution of bearing forces and friction for specimen L06s.....	70
Fig. 74: Distribution of bearing forces and friction for specimens L04, L04s at <i>global</i> maximum.....	70
Fig. 75: Distribution of bearing forces and friction for specimens L06, L06s at <i>global</i> maximum.....	70
Fig. 76: Distribution of bearing forces and friction for specimens L04, L04s at <i>local</i> maximum	70
Fig. 77: Distribution of bearing forces and friction for specimens L06, L06s at <i>local</i> maximum.....	70
Fig. 78: Distribution of bearing forces and friction for connections with basic geometry L04	72
Fig. 79: Distribution of bearing forces and friction for connections with basic geometry L14	72
Fig. 80: Mises stress at displacement 15,29 mm for L17_1s.....	73
Fig. 81: Distribution of bearing forces and friction for connections with bolts in <i>single</i> shear and with equal plate bearing stiffness	74
Fig. 82: Distribution of bearing forces and friction for connections with bolts in <i>double</i> shear and with equal plate bearing stiffness.....	74
Fig. 83: Tension splice with bolts in double shear.....	75
Fig. 84: <i>Different</i> plate bearing stiffness.....	75
Fig. 85: The influence of thickness on the pattern of bearing forces.....	75
Fig. 86: The influence of end distance on the pattern of bearing forces	76
Fig. 87: Stress state of L06_2s_t10-20_M27_b270.....	76
Fig. 88: Distribution of bearing forces and friction for connections with bolts M27	77

Fig. 89: Distribution of bearing forces and friction for connections with bolts M27 and plate width $b = 270$ mm.....	77
Fig. 90: Distribution of bearing forces and friction for connections with 7 bolts.....	78
Fig. 91: Comparison of numerical and experimental resistances	82
Fig. 92: Comparison of numerical and experimental resistances (Kouhi, Kortessmaa, 1990)	82
Fig. 93: Connection KK E2 – Mises stress.....	82
Fig. 94: Connection KK G5 – Mises stress	82
Fig. 95: Displacement D_{EC} at which bearing resistance acc. to EN 1993-1-8 was reached in relation to end distance a) or to bearing-to-maximum resistance ratio b); c) displacement at which maximum resistance was reached.....	86
Fig. 96: Normalized Eurocode bearing resistance and experimental results B1, B2 versus normalized end distance.....	87
Fig. 97: Experimental results B1, B2 in relation to Eurocode bearing resistance function	87
Fig. 98: Experimental r_e vs. EC 3 bearing resistance F_b for single bolt connections	88
Fig. 99: Experimental r_e vs. minimum of bearing F_b and net cross-section N_u resistance for single bolt connections.....	88
Fig. 100: Bearing forces on bolts for connections with one line of bolts positioned in the direction of loading.....	89
Fig. 101: Resistance of connections with one line of bolts positioned in the direction of loading.....	90
Fig. 102: Bearing forces on bolts for connections included in the numerical parametrical study	91
Fig. 103: Resistance of connections included in the numerical parametrical study	91
Fig. 104: Bearing forces on bolts for connections with two lines of bolts parallel to loading direction	92
Fig. 105: Resistance of connections with two lines of bolts parallel to loading direction.....	92
Fig. 106: Experimental results in relation to proposed bearing resistance function	95
Fig. 107: Failure modes: a) net cross-section b) shear	95
Fig. 108: The effect of end (a) or edge (b) distance on product k_1k_2	96
Fig. 109: Experimental r_e vs. new bearing resistance F_b for single bolt connections.....	96
Fig. 110: Factor k_3 (left equation (87); right equation (88)) versus e_1/p_1 ratio	98
Fig. 111: Bearing forces on bolts for connections with one line of bolts positioned in the direction of loading.....	99
Fig. 112: Resistance of connections with one line of bolts positioned in the direction of loading.....	101
Fig. 113: Bearing forces on bolts for connections included in the numerical parametrical study	102
Fig. 114: Resistance of connections included in the numerical parametrical study	103
Fig. 115: Resistance of connections included in the numerical parametrical study without geometries L11-L13, L21-L22	103
Fig. 116: Bearing force on bolt for the connections with two bolts positioned perpendicular to load transfer ...	105
Fig. 117: Bearing forces on bolts for connections with two lines of bolts parallel to loading direction	106
Fig. 118: Resistance of connections with two lines of bolts parallel to loading direction.....	106
Fig. 119: Comparison of results for the edge bolt	107
Fig. 120: Comparison of results for the inner bolt.....	108
Fig. 121: Comparison of results for the sum of bearing forces	108
Fig. 122: Comparison of results for the minimum of sum of bearing forces, net cross-section resistance and bearing resistance	108
Fig. 123: Comparison of results for the minimum of sum of bearing forces, net cross-section resistance and bearing resistance – only results, where net cross-section or block tearing resistance is critical are shown	109
Fig. 124: Comparison of results for the minimum of sum of bearing forces, net cross-section resistance and bearing resistance – only results, where net cross-section or block tearing resistance is critical are shown – friction also is considered on the ordinate.....	109
Fig. 125: Diagrams in normalized format obtained for the edge bolt.....	110
Fig. 126: Diagrams in normalized format obtained for the inner bolt.....	110

Fig. 127: Diagrams in normalized format obtained for the group of bolts	111
Fig. 128: Diagrams in normalized format obtained for the group of bolts, where additional Eurocode checks are considered	111
Fig. 129: Diagrams in normalized format obtained for the group of bolts, where additional Eurocode checks are considered and maximum resistance (including friction) as the “experimental” value	111
Fig. 130: Bolt nomenclature	114

LIST OF TABLES

Table 1: Results of standard tensile test for plate I.....	10
Table 2: Results of standard tensile test for plate II	10
Table 3: Average material characteristics.....	10
Table 4: Geometry of specimen types H, HH.....	12
Table 5: Geometry of specimen types B1, B2.....	14
Table 6: Nominal dimensions of specimen type L	17
Table 7: Actual dimensions of specimen type L.....	17
Table 8: Comparison of the resistance and computational time for different meshes and finite elements.....	24
Table 9: Material model applied in Abaqus for plate I.....	27
Table 10: Material model applied in Abaqus for plate II	27
Table 11: Test results of specimens that failed in net cross-section (specimens H, HH, B1, B2 and L).....	31
Table 12: Geometry and maximum force of specimens from literature	41
Table 13: Results of statistical analyses of design net cross-section resistance	41
Table 14: Test results for specimens B1 and B2	51
Table 15: Test results for specimens L.....	58
Table 16: Results of numerical simulations for specimen type L.....	60
Table 17: Maximum (experimental) resistance [kN] versus connection geometry	61
Table 18: Geometry and results for the connections where width was the varying parameter.....	71
Table 19: Geometry and results for the connections where plate stiffness was the varying parameter.....	73
Table 20: Geometry and results for the connections where bolt diameter was the varying parameter.....	77
Table 21: Geometry and results for the connections where the number of bolts was the varying parameter.....	78
Table 22: Geometry and results for connections found in literature.....	80
Table 23: Material model for numerical simulations of Kim and Yura's tests.....	81
Table 24: Material model for numerical simulations of Aalberg and Larsen's tests for steel grade S1100	81
Table 25: Distribution of bearing forces on bolts for connections found in literature.....	82
Table 26: Material models for numerical simulations in Abaqus for Kouhi and Kortessmaa connections	83
Table 27: Bearing resistance of specimens B1 and B2.....	85
Table 28: Reduction factors β_1 and β_2	97
Table 29: The calculation of the sum of bearing forces	100

1 INTRODUCTION

Technological evolution began 2 million years ago when Homo habilis made the first tool from stone. From a simple spear, to steam engine and electronic microscope, tools have always been developed to survive and to serve mankind. What seemed impossible yesterday is commonly available today. Innovations are being introduced in all fields of science, including the field of materials.

All materials that have been used in structural civil engineering have one thing in common. They are available in almost infinite quantities and they are reasonably easy for exploitation. The Earth's crust is composed of about 5% of iron (MII, 2008). Therefore, it was just a matter of time when man discovered steel. Steel – an old material under never ending development. In 2007 world's crude steel production was 1344 millions of metric tons and it has doubled since 2000 (IISN, 2008). Many different types of steel have been developed, but only a fraction of them are used in structural civil engineering. Any new material has to fulfil two main conditions for its application in this branch: reliability and affordability. A fractured engine block may be replaced, but a fractured bolt may result in a collapse of an entire structural system (e.g. Kemper Arena in Kansas City, MO, USA in 1979 approx. 4000 m² of roof collapsed due to bolt fatigue failure) and take human lives. Therefore structural engineers and scientists push, pull, tear... They depend on the knowledge of materials and their properties, in order to understand how different materials support and resist loads. Hopefully, this thesis will help to encourage designers to consider high strength structural steel as very a competitive material with several advantages and to apply it in their designs.

In constructional practice across Europe structural high strength steels (HSS) are considered as steels with specified minimum yield strength (SMYS) equal to or higher than 420 MPa. In this work, mild steels are defined as steels with SMYS lower than 420 MPa. Weldable structural HSSs are delivered in the conditions: thermomechanically controlled rolled, normalised and quenched and tempered. They differ in their microstructure and accordingly in their mechanical properties. Herein quenched and tempered HSSs are considered. Such steels can reach a yield stress up to 1300 MPa (SAAB, 2005). For successful application of higher strength steels design and fabrication standards need to be accepted by the authorities responsible for safety and by industry. Eurocode 3, standard for the design of steel structures, is divided into several parts. Part EN 1993-1-1 (CEN, 2005a) includes steel grades up to S460. Additional rules for steel grades up to S700 are presented in EN 1993-1-12 (CEN, 2007) and were the lattermost addition to Eurocode 3. HSSs presented in this standard are covered in EN 10025-6 (CEN, 2004b) that maintains quality and defines steel grades for hot rolled flat product in the quenched and tempered condition. Important for fabrication was the

presentation of ENV 1090-3 (CEN, 1997a) with supplementary rules for the execution of steel structures in HSS.

Economic aspects are usually the deciding factors for the choice of the structural material, where the overall economy is of particular significance. Overall economy is based on material cost, production economy and maintenance costs during the design lifetime of the product. In general, the use of HSS is more attractive if strength is the governing factor. Accordingly, lower self weight of the final product is the primary advantage of HSS. Secondary benefits, on account of lower weight, are lower transportation and handling costs, both resulting in lower energy consumption, smaller weld metal volumes due to thinner steel plates and therefore increased production speed. The welding process can be automated due to smaller and simpler welds. In addition to all foregoing, there is also lower energy consumption that has a favourable effect on the environment.

Quenching hardens steel by introducing brittle martensite, which becomes ductile after tempering. Hence, there is always a tradeoff between ductility and brittleness. Ductility is a qualitative, subjective property of a material (Dowling, 1993). It is generally defined as the ability of a material to accommodate inelastic deformation without breaking. Ductile material tolerates the designer errors in stress calculation or the prediction of severe loads (Dieter, 1987). This definition is obsolete and refers to elastic design where maximum allowable stress should be less than yield stress. "Additional" strength is hidden in the difference between yield and ultimate tensile strength. There are several engineering measures of ductility obtained from the tension tests. The most commonly presented material ductility parameter is the ultimate-to-yield strength ratio f_u/f_y . The yield strength f_y is usually determined by offset yield strength $R_p 0,2$, which is stress corresponding to the intersection of the stress-strain curve and a line parallel to the elastic part of the curve offset by the strain of 0,002. The engineering fracture strain ε_{fr} is obtained from the length at fracture L_u of the gage section with original length L_0 . Often ε_{fr} is expressed as percentage and is called percentage total elongation after fracture A^c . Because an appreciable fraction of the plastic deformation will be concentrated in the necked region of the test specimen, the value of A^c will depend on the original gage length L_0 over which the measurement was taken. Therefore, the gage length should always be given when reporting the percentage total elongation at fracture, or geometrically proportional tension test specimens should be machined according to appropriate standard. Another measure of ductility is percent reduction in area Z . It is obtained by comparing the cross-sectional area after fracture S_u with the original gage area S_0 . Both quantities are obtained after failure by putting the specimen back together and taking the required measurements using marks placed a known distance apart prior to the tests.

$$A_t = 100\varepsilon_{fr} = \frac{L_u - L_0}{L_0} \quad (1)$$

$$Z = 100 \frac{S_0 - S_u}{S_0} \quad (2)$$

Standard for HSS EN 1993-1-12 recommends lower limits for ductility requirements than EN 1993-1-1. The recommended values for ultimate-to-yield ratio is lowered from $f_u/f_y \geq 1,10$ to $f_u/f_y \geq 1,05$, elongation at failure is lowered from $\varepsilon_{fr} \geq 15\%$ to $\varepsilon_{fr} \geq 10\%$ while the requirement for ultimate strain remains unchanged $\varepsilon_u \geq 15f_y/E$, where E is the Young's modulus. The latter requirement is stricter for higher steel grades ($\varepsilon_u \geq 1,68\%$ – for S235, $\varepsilon_u \geq 4,93\%$ – for S690, $\varepsilon_u \geq 9,29\%$ – for S1300). Very typical steel S690 has relative fracture elongation ε_{fr} more than 14% (required by EN 10025-6), uniform strain ε_u that corresponds to tensile strength f_u around 5% and ultimate-to-yield ratio around $f_u/f_y = 1,05$ (Beg, Hladnik, 1996. Fukumoto, 1996. Axhag, 1998. Kim, Yura, 1999. Langenberg et al., 2000. Aalberg, Larsen, 2001. Puthli, Fleischer, 2001. Sause, Fahnestock, 2001. Aalberg, Larsen, 2002. Clarin, Langerquist, 2005. Girão Coelho, Bijlaard, 2007. Aalberg, Larsen, March 1999). These material parameters were measured around the world on steels made by different producers. They doubtlessly prove that high strength steels have lower ductility than mild steels in terms of engineering measures of ductility. The strain hardening and the capability of large deformations have an essential role at the constitution of stress state in an element. However, according to literature HSSs have the ability of plastic resistance and enough rotation capacity to form plastic hinge (Axhag, 1998. Earls, 1999. Sause, Fahnestock, 2001. Chen, Tu, 2004. Girão Coelho et al., 2004b). Ductility is of great importance at connections to transfer the load between all fasteners and to reduce stress concentrations. In case the material does not have the ability of local plastic deformations, fractures open due to stress peaks. Additionally, EN 1993-1-12 only allows the elastic global analysis for sections classified as Class 2 or higher. The standard disallows the use HSS for applications where capacity design is required.

The use of HSS is favourable in members in tension where the strength governs. In case of compressive loading, various buckling phenomena may occur (lateral buckling, local buckling and lateral torsional buckling). The buckling is mainly governed by elastic modulus E , which is the same for all steel grades. Hence, the use of HSSs may seem unwise. However, weight savings can still be obtained if slenderness is low $\lambda < 60-80$ (Gresnigt, Steenhuis, 1997). Moreover, better buckling curve can be applied to HSS than to mild steels due to relatively lower residual stresses (Rasmussen, Hancock, 1995. Beg, Hladnik, 1996. Collin, Möller, 1998. Greco, Earls, 2003). An economic solution regarding the problem of local buckling are hybrid steel girders, where the flanges are made of higher steel grade than the web. A limitation that strength of the flanges should not exceed twice that of the web for serviceability reasons is suggested (Veljkovic, Johansson, 2004). It was also observed that significant improvements in rotational capacity can be achieved in hybrid girders (Greco, Earls, 2003). The deflections are important criteria in serviceability limit state. The area moment of inertia and Young's modulus, which are the parameters for the deflection function, are independent of steel grade, thus the stiffness needs relatively more attention for the structures in HSS.

When material weldability is discussed, it is essential that steel has a chemical composition that promotes the fusion of the base material and the filler metal, without the formation of cracks and other imperfection (Bjorhovde, 2004). In the last ten years the use of HSS has increased enormously, mainly due to contemporary welding methods (Günther, 2005). The costs of these steels are greatly reduced if preheating is omitted. With the correct choice of steel quality, welding consumables and welding process, the preheating is in many cases unnecessary (Gresnigt, Steenhuis, 1997). It can be necessary for thicker plates to avoid cold cracking. The scope of studies was also aimed at undermatched welds, which can be successfully used in HSS structures (Johansson, 2004. Collin, Johansson, 2005).

The fatigue resistance is mainly governed by stress range $\Delta\sigma$ and notch effect. The strength of steel has only a minor effect on the fatigue resistance. The use of HSS in fatigue loaded structures will result in higher stress ranges than in structures of mild steel. The important key to the fatigue resistance is the notch effect and micro cracks that usually form where large amount of energy is added (flame cutting, welding, punching, drilling). Stress concentration leads to crack propagation, resulting in macro crack and finally in a brittle fracture. The solution at HSSs can be (Günther, 2005. Kuhlmann, Bergmann, 2005) new or modified detailing, shifting of details in less stressed sections, improved welding procedures, better workmanship and post-weld improvement methods (such as grinding, Tungsten Inert Gas dressing, needle or hammer peening...). The investigations showed positive fatigue behaviour for HSS in the high load cycle $\geq 2 \times 10^6$, especially on special notch cases from mobile crane structures (Bucak, 2000), as well.

A connection connects two or more members by means of structural elements such as welds, bolts, pins, rivets, cable sockets.... Each connection type has its own particular behaviour. This thesis will focus on tension splice connections with bolts in double shear (see Fig. 1). In the sequel these connections will be referred to as bolted shear connections. In a bolted shear connection the loading can be transmitted either by bolt bearing (bearing type connections) or by friction of the surfaces (slip resistance connections), where the friction is achieved by preloading of the bolts. Only bearing type connections are considered in this work. This connection type transfers loading from one steel plate to another by the contact between the bolt and the plates. The contact is characterized by high stresses that enforce transverse shear in the bolts and high local compression stress to the plate. Concentrations of stresses are therefore unavoidable. Another characteristic of bearing type connections is initial slip due to bolthole clearance. In general, contacts between bolts and plates are not established simultaneously. A single contact may be established sooner. In such case the whole loading is transferred through this single contact. For that reason, the local ductility of the connection in terms of plastic deformations has to be sufficient in order to assure bolthole elongation, so that the remaining contacts will be established and the loading will be transferred through all bolts. If local ductility was not sufficient, the stress concentration would cause rupture of the steel plate or shear fracture of the bolt. In either case the maximum connection resistance

would be equal to the resistance of a single bolt connection. The problem is that the strength ratio in connections made of HSS is in favour of the steel plate. In the connections made of mild steel the bolt material is much stronger than the plate material. This situation can be referred to as “weak” plates and “strong” bolts, while in connections made of HSS the situation changes to “strong” plates and “weak” bolts. These “weak” bolts should be at least of material grade 8.8 or higher, which are considered as non-ductile. Therefore, assuring the ductility in bolts is not an option. In this thesis it will be shown that local ductility of bolted shear connections is sufficient to distribute the loading between all bolts evenly in four-bolt connection with the most unfavourable initial position of the bolts. But let us first summarize the work that has already been done in the field of joints made of HSS. The attention will be given to experimental testing of connections made of steel grades higher than S460.

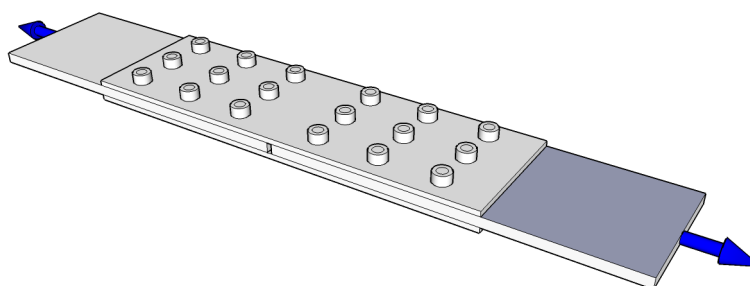


Fig. 1: Simple tension splice with bolts in double shear

The characterization of the ductility of bolted end plate beam-to-column steel connections was done by Girão Coelho (Girão Coelho, 2004. Girão Coelho et al., 2004a. Girão Coelho et al., 2004b. Girão Coelho et al., 2006b. 2006a). The connections were made of steel grade S355 and S690. A methodology for the characterization of the rotational response of a joint based on the component method was implemented and calibrated against experimental results. The methodology was restricted to joints the behaviour of which was governed by the end plate modelled as equivalent T-stubs in tension. The results of this study along with the conclusions drawn from the analysis of individual T-stubs afforded some basis for the proposal of some criteria for the verification of sufficient rotation capacity. The proposal was made in terms of a non-dimensional parameter, the joint ductility index (Girão Coelho, 2004). The research on block shear tear-out failure in gusset-plate welded connections in structural hollow sections and steel S1300 showed that design rules for block tearing resistance according to Eurocode, as well as American standard are inadequate (Ling et al., 2007). A modification of the effective net area and failure stress definitions were proposed.

Kouhi and Kortasma (1990) presented test results of multi-bolt shear connections. Steel grade with nominal yield strength of 640 MPa and nominal ultimate strength of 700 MPa was used in the test. Actual material strengths were given for 3, 4, 6 and 8 mm thick plates. Specimens were divided in four series regarding their failure. The investigation included connections with two bolts positioned in the direction of loading and a connection with four bolts in 2×2

configuration. The main deformation and failure were performed in cover plates, except for test series H which failed in net cross-section. The test results were compared to bearing, net area and block tearing resistances according to various standards.

The report on a comparative research of bolted connections in HHS and mild steel was prepared by Aalberg and Larsen (March 1999). The tests included tension splices with three bolts in double shear, block tear tests and tension tear-out test. All tension splices failed in net cross-section. The test resistance was compared to block tearing resistance according to Eurocode and AINSI standard. The conclusion was that the reduced ultimate-to-yield ratio $f_u/f_y = 1,05$ did not significantly affect the ductility.

Kim and Yura (1999) investigated shear connections with one or two bolts placed parallel to the loading. Beside mild steel grade they used steel with yield strength of $f_y = 483 \text{ N/mm}^2$ and ultimate tensile strength of 545 MPa. The specimens were connected to rigid plate so that the bolts were in single shear. The failures were characterized as splitting and shear failures with large bolthole elongations. The experimental resistance was compared to bearing resistance according to American AISC standard and to Eurocode standard in which conservatism was found.

Aalberg and Larsen (2001, 2002) duplicated Kim and Yura tests, using steel grades S690 and S1100. The steel grade S1100 is not considered in EN 1993-1-12. The value of ultimate tensile to yield ratio was equal to $f_u/f_y = 1,05$ for both steel grades. The local ductility of connections was not decreased due to the low f_u/f_y ratio. The test setup was similar to the tests in this thesis. The actual yield strength of steel S1100 was 1330 MPa. The ultimate strain was reached at $\varepsilon_u = 0,03$, while percentage total elongation after fracture was equal to $A^c = 10 \%$. With $\varepsilon_u = 0,03 \not\geq 15 f_y/E = 15 \times 1330/210000 = 0,095$ this steel did not satisfy the ductility requirements set by EN 1993-1-12. Nonetheless, large hole elongations and ductile failures were observed.

Puthli and Fleisher (2001) focused on shear connections made of steel grade S460 ($f_u/f_y = 1,23$) with two bolts placed perpendicular to loading. They also experienced block tear failure. They compared experimental resistances to resistance according to EN 1993-1-8. The focus was set on minimum end and edge distances and the result was the suggestion to reduce minimum distances and to modify bearing resistance formula.

More recent research was published by Rex and Easterling (2003). The research on the behaviour of a bolt bearing on a single plate was part of larger investigation of the behaviour of partially restrained steel and composite connections. The 6,5 mm thick plate of different high steel grades (ultimate strength from 665 to 752 MPa) was tested against bearing resistance. Due to small plate thickness and large end distance e_1 several curling failures were observed. A research on single bolt shear connection was conducted on Delft University of

technology (de Freitas et al., 2005). Ductile behaviour of the connections and the conservatism of Eurocode bearing resistance formula were reported.

The papers on the net cross-section resistance and ductility of members and connections made of HSS were presented in journals and conferences (Može, Beg, 2006. Može et al., 2006a. 2006b. Može, Beg, 2007. Može et al., 2007a. 2007b).

The application of HSS in engineering structures is increasing. Lightweighting is particularly important in commercial vehicle and mobile crane construction, where dimensions, axle loads and total weight of the vehicle are restricted by legal regulations. The development of mobile cranes for loads of up to 800 tons was only made possible by the advent of high-strength steels (ThyssenKrupp Steel AG, 2006). The highest grades of HSS are applied to heavy lifting machinery. HSS can replace forged forks for trucks and carbon fibre in boat keels (SAAB, 2008). In several bridges and high buildings HSS (AG der Dillinger Hüttenwerke, 2005. Günther, 2005) was the best solution for certain structural elements (Ilverich bridge, Øresund Viaduct, Ennëus Heerma, Car park of the Stuttgarter Trade Fair, Millau viaduct – France, Verrand viaduct – Italy, the roof of Sony Centre in Berlin – Germany, Mittadalen hybrid steel bridge girder – Sweden, Fort City Bridge – USA...).

The purpose of this thesis is to determine the local ductility members in HSS and the relation of local ductility to the resistance. The local ductility was studied on members with tension with or without holes and on tension splices with bolts in shear (see Fig. 1).

The methodology of experimental work is presented in Chapter Methodology of experimental work. The chapter gives detailed information on material testing, measuring techniques and actual, as well as nominal geometry of specimens.

The methods used in numerical modelling are presented in the Chapter Methodology of numerical models. The numerical models, used to simulate the experiments, are presented and a description of main features on contact interactions, finite elements, meshing and on determination of material model is given.

The test results of members with holes in tension with net cross-section failure are reported in Chapter Tension members with holes – net cross section failure. The (un)reliability of the design provisions for net cross-section resistance is assessed by a statistical analysis.

Local ductility and resistance of tension splices with bolts in shear is the topic of Chapter Tension splices with bolts in shear – failure in bearing. The particular attention is given to the bearing resistance and to bearing failure. The stress state of tests results is described by means of numerical simulations. The bearing resistance is presented in view of the Eurocode standard together with other results on bolted shear connections in HSS gathered from literature. A new modified approach to bearing resistance is presented and a new design formula for bearing resistance per bolt is statistically evaluated.

The summary with the main conclusions are given in Chapter Conclusions. The thesis is wrapped up with the list of references in Chapter References.

The expanded summary in Slovenian language is given in the chapter titled Povzetek.

The work is completed by several appendixes, where additional test results and results of numerical simulations are presented.

2 METHODOLOGY OF EXPERIMENTAL WORK

2.1 General

The experimental work was completed in two phases. The first phase was done from summer 2005 to winter 2006 (specimen types H, HH, B1, B2) and the second in spring 2007 (specimen type L). The material was ordered separately for each phase. The first phase of the investigation of local ductility of high strength steel was divided into two main sets. In the first set local ductility of high strength steel was studied on steel strips with holes subjected to tension. The second set of tests was dedicated to tension splices with bolts in double shear. The investigation included single bolt connections, two-bolt connections with bolts positioned perpendicular to loading. The second phase of the experimental work included tension splices with three or four bolts in double shear positioned parallel to loading. The connections were designed to impose failure in the high strength steel plate and not in the bolts. Special attention was devoted to the selection of measuring devices and techniques so that the results could be compared to numerical simulations.

2.2 Material characteristics

For each of experimental phases a separate plate was delivered; plate I and plate II. The plates were made by Belgium producer Industeel (Industeel, 2008). The marketing name of the used steel is Supralsim[®] 690, which fulfils requirements of S690 QL according to EN 10025-6 (CEN, 2004b). The dimensions of the plates were $b/l/t = 1500/6000/10$ mm. The material characteristics were obtained by standard tensile tests according to EN 10002-1 (CEN, 2001). Proportional test pieces from each plate were extracted from the plates according to EN ISO 377 (CEN, 1997b); six pieces from plate I and three from plate II. The standard tensile tests were performed in longitudinal direction of rolling, using testing machine ZWICK Z 700 Y. The displacements were measured on a defined original gauge length L_0 by sensor arm extensometers. The speed of the test was defined by the displacement of the extensometers. The measured material parameters for each plate are given in Table 1-2. The original geometry of test pieces 488.1-488.3 was not measured correctly. Therefore the average R_m and $R_{p0,2}$ were obtained only from specimens 488.4-6. Average material characteristics which are used for analyses are presented in Table 3. The engineering stress-strain curves are shown in Fig. 2.

Table 1: Results of standard tensile test for plate I

Sample name	Thickness <i>t</i> [mm]	Width <i>b</i> [mm]	<i>S</i> ₀ [mm ²]	<i>L</i> ₀ [mm]	<i>F</i> _{<i>m</i>} [kN]	<i>R</i> _{<i>p</i>0,2} [MPa]	<i>R</i> _{<i>m</i>} [MPa]	<i>A</i> _{gt} [%]	<i>A</i> ^{<i>c</i>} [%]	<i>Z</i> [%]
488.1	10	25	250	90	218,74	798	875	/	14,0	61,7
488.2	10	25	250	90	228,70	876	915	/	14,5	62,6
488.3	10	25	250	90	228,03	875	912	/	14,6	62,4
488.4	10,2	24,9	254	90,0	224,89	848	885	5,1	15,0	57,3
488.5	10,1	24,9	251,5	90,0	222,42	846	884	5,1	14,6	55,2
488.6	10,1	25,0	252,5	90,0	222,69	837	882	5,1	13,6	51,4
Sample name	Speed									
488.1	to <i>R</i> _{<i>p</i>0,2} : 0,001 after <i>R</i> _{<i>p</i>0,2} : 0,007 s ⁻¹									
488.2	to <i>R</i> _{<i>p</i>0,2} : 0,001 after <i>R</i> _{<i>p</i>0,2} : 0,007 s ⁻¹									
488.3	to <i>R</i> _{<i>p</i>0,2} : 0,001 after <i>R</i> _{<i>p</i>0,2} : 0,007 s ⁻¹									
488.4	0,001 s ⁻¹									
488.5	0,00025 s ⁻¹									
488.6	to <i>R</i> _{<i>p</i>0,2} : 0,001 after <i>R</i> _{<i>p</i>0,2} : 0,007 s ⁻¹									

Table 2: Results of standard tensile test for plate II

Sample name	Thickness <i>t</i> [mm]	Width <i>b</i> [mm]	<i>S</i> ₀ [mm ²]	<i>L</i> ₀ [mm]	<i>F</i> _{<i>m</i>} [kN]	<i>R</i> _{<i>p</i>0,2} [MPa]	<i>R</i> _{<i>m</i>} [MPa]	<i>A</i> _{gt} [%]	<i>A</i> ^{<i>c</i>} [%]	<i>Z</i> [%]
291.1	10,01	24,51	245,3	90,49	206,96	796	844	6,4	17,1	58,9
291.2	10,03	24,68	247,5	90,04	208,98	795	844	6,3	16,9	59,6
291.3	10,04	24,41	245,1	91,22	206,91	798	844	6,4	17,2	59,5
Sample name	Speed									
291.1	0,01 mm/s									
291.2	0,03 mm/s									
291.3	0,03 mm/s									

Table 3: Average material characteristics

Plate	<i>R</i> _{<i>p</i>0,2} = <i>f</i> _{<i>y</i>} [MPa]	<i>R</i> _{<i>m</i>} = <i>f</i> _{<i>u</i>} [MPa]	<i>A</i> _{gt} [%]	<i>A</i> ^{<i>c</i>} [%]	<i>Z</i> [%]
I	847	884	5,1	14,4	58,4
II	796	844	6,4	17,1	59,3

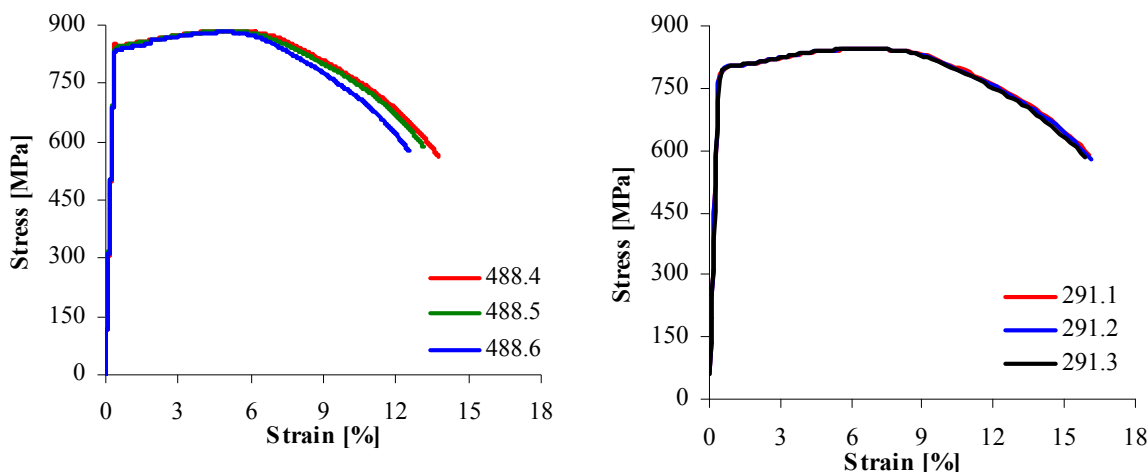


Fig. 2: Stress-strain diagrams of standard tensile tests

2.3 Descriptions of specimens, measuring devices and test set-up

2.3.1 Experimental phase one – specimen types H, HH, B1, B2

The first phase of the experiments was done in University of Ljubljana, Faculty of Civil and Geodetic Engineering, Jamova 2, Ljubljana from July 2005 to February 2006. Testing machine Instron with capacity of 1000 kN was available for the tests (Fig. 3). The displacements were measured by inductive displacement transducers (IDT) with range ± 25 mm (HBM WA50). Special extensometers were made to measure the displacements up to 5 mm. All measuring devices were connected to a universal measuring unit. Records of force and displacements were detected every 0,01s and an average of ten records was recorded. All the tests were displacement controlled through the crosshead position. The experimental work was divided into two groups of specimens: steel strips with holes subjected to tension and shear connections.



Fig. 3: Test rig (testing machine Instron)

Specimens types H and HH were strips of plates equal in geometry and with different size and position of holes. The hole diameter was varied from 0 to 50% of specimen width. In certain cases the hole was made eccentrically. Letter H in the specimen name represents *hole* and is followed by consecutive number of the specimen. Similarly, letters HH stand for *hinge hole*. All specimens (17 of type H, 6 of type HH) were manufactured from plate I (steel S690 – Table 3), except H17-H20 which were made of steel grade S235 with nominal yield strength $f_y = 235 \text{ N/mm}^2$. The actual material characteristics of steel S235 were not measured and the results were used merely for visual comparison of deformed state to evaluate ductility. The specimens were fabricated by flame cutting, in such way that the longitudinal direction

corresponded to the loading direction. The speed of the tests was about 1,5 mm/min and is given in Appendix A.

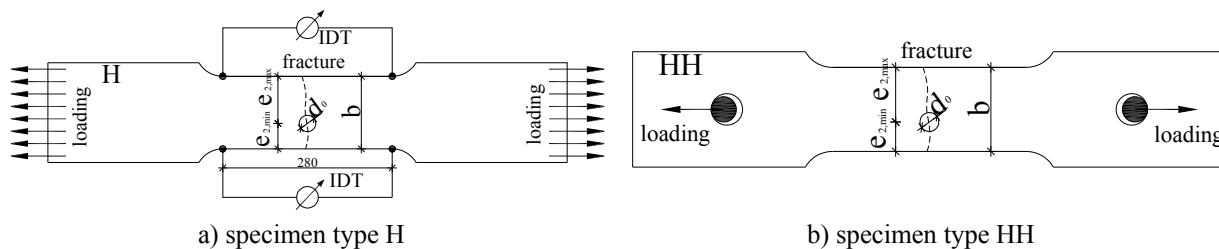


Fig. 4: Specimen types H, HH – steel strips with holes subjected to tension

Specimens H were directly attached to testing machine in such way that the rotation around strong axis of the specimen was prevented (Fig. 4a). The attachment of specimens HH allowed rotation around their strong axis (Fig. 4b). The actual and nominal geometry of specimens is presented in Table 4. At specimen type H, a relative displacement was measured between two points 280 mm apart, as shown in Fig. 4a. Displacements were measured by two inductive displacement transducers (IDTs) which were mounted on each side of the specimen. At specimen type HH, displacements were measured only from the relative displacement of the testing machine grips. The rotation of specimens did not allow installation of the IDTs.

Table 4: Geometry of specimen types H, HH

Specimen name	Eccentricity	Nominal dimensions [mm, mm ²]						Actual dimensions [mm, mm ²]					
		<i>b</i>	<i>t</i>	<i>d</i> ₀	<i>e</i> _{2,min} - <i>d</i> ₀ /2	<i>e</i> _{2,max} - <i>d</i> ₀ /2	<i>A</i> _{net}	<i>b</i>	<i>t</i>	<i>d</i> ₀	<i>e</i> _{2,min} - <i>d</i> ₀ /2	<i>e</i> _{2,max} - <i>d</i> ₀ /2	<i>A</i> _{net}
H01	No	100	10	0	50	50	1000	101,3	10,15	0			1013
H02	No	100	10	0	50	50	1000	101,5	10	0	50,0	50,0	1015
H03	No	100	10	5	47,5	47,5	950	101,9	10	5	47,7	48,8	969
H04	No	100	10	10	45	45	900	100,9	10	10	45,0	45,4	909
H05	No	100	10	10	45	45	900	101,3	10	10	45,4	45,8	913
H06	No	100	10	13	43,5	43,5	870	101,7	10	13	44,3	44,4	887
H07	No	100	10	18	41	41	820	101,3	10	18	41,7	42,0	833
H08	No	100	10	22	39	39	780	101,7	10	22	39,6	39,7	797
H09	No	100	10	22	39	39	780	102,4	10	22	39,6	40,9	804
H10	No	100	10	26	37	37	740	101,6	10	26	37,0	38,6	756
H11	No	100	10	30	35	35	700	101,6	10	30	35,1	36,4	716
H11A	No	100	10	30	35	35	700	99,9	10	30	34,8	35,1	699
H12	No	100	10	30	35	35	700	101,3	10	30	34,5	36,4	713
H13	Yes	100	10	30	28	42	700	101,4	10	30	29,4	42,0	714
H14	Yes	100	10	30	21	49	700	101,6	10	30	22,4	49,1	716
H15	No	100	10	40	30	30	600	101,8	10	40	29,2	32,5	618
H16	No	100	10	50	25	25	500	101,6	10	50	25,5	26,1	516
H17*	No	100	10	0	50	50	1000	101,3	10	0			1013
H18*	No	100	10	10	45	45	900	101,1	10	10	45,3	45,8	911
H19*	No	100	10	22	39	39	780	101,2	10	22	39,4	39,8	792
H20*	No	100	10	50	25	25	500	100,8	10	50	24,9	25,9	508
HH01	Yes	80,0	10	24	28	28	560	78,4	10	24	26,4	27,3	544
HH02	Yes	80,0	10	24	22	34	560	79,0	10	24	19,9	35,1	550
HH03	Yes	80,0	10	24	16	40	560	78,5	10	24	14,1	40,4	545
HH04	Yes	80,0	10	18	31	31	620	77,9	10	18	22,7	32,1	599
HH05	Yes	80,0	10	18	25	37	620	78,5	10	18	22,1	38,4	605
HH06	Yes	80,0	10	18	19	43	620	78,5	10	18	17,2	43,3	605

* steel S235

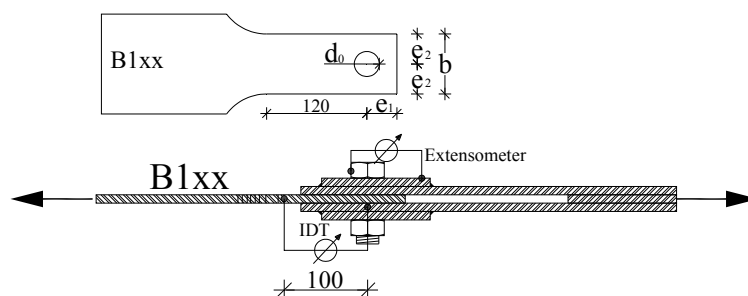


Fig. 5: Specimen types B1 – single bolt connection with bolt in double shear

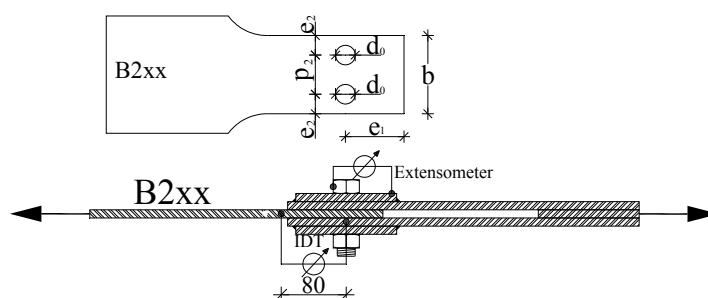


Fig. 6: Specimen type B2 – two-bolt connection with bolts in double shear

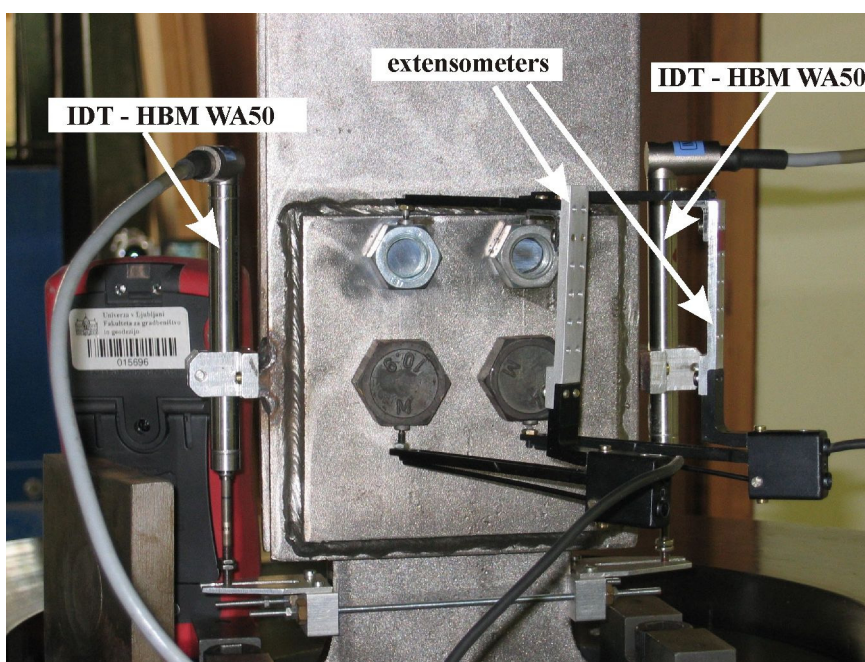


Fig. 7: Specimen B2 under loading

The second group of specimens were bolted shear connections with one bolt (25 connections) or two bolts (13 connections) positioned perpendicular to loading direction. The specimens were designated as types B1 (B1 stands for one bolt) and B2 (B2 stands for two bolts). The connection was assembled of a specimen, one or two bolts and two cover plates which were welded together to form forks. The forks were locally strengthened in bolt bearing area with another 10 mm thick plate to prevent hole elongation. All the specimens and forks were made of steel S690 – plate I with the actual material characteristics presented in Table 3. The B1

test series included 25 single bolt shear connections (Fig. 5). Bolts M27 were used in drilled standard size holes $d_0 = 30$ mm (with some exceptions – see Table 5). Some of the holes were positioned eccentrically to loading axis. The B2 test series included 13 two-bolt shear connections, with bolts positioned perpendicular to loading direction (Fig. 6). Bolts M22 in standard size holes $d_0 = 24$ mm were used. Bolts were designed to withstand resistance of the steel plate, thus grades 10.9 and 12.9 were selected to avoid bolt shear or bending. Relative displacement between the specimen and the fork was measured by IDTs. An extensometer was also mounted between the fork and the bolt to control the deformation of forks and the bending of the bolt (Fig. 7). Bolts were snug tightened to ensure that the load was transferred primarily by bearing and not by friction. Bolt shear failure and bearing failure of the plate were prevented by proper design. Geometry of specimens was selected so that for each of the selected edge distance e_2 the end distance e_1 was varied. Distance between bolts was also varied for B2 specimens. Actual and nominal geometry of all specimens is shown in Table 5. The speed of the test is presented in Appendix A.

Table 5: Geometry of specimen types B1, B2

Specimen name	Bolt	Nominal dimensions [mm, mm ²]							Actual dimensions [mm, mm ²]						
		b [mm ²]	t [mm ²]	d ₀ [mm ²]	e _{2,min} - d ₀ /2	e _{1,min} - d ₀ /2	p ₂ - d ₀	A _{net} [mm ²]	b [mm ²]	t [mm ²]	d ₀ [mm ²]	e _{2,min} - d ₀ /2	e _{1,min} - d ₀ /2	p ₂ - d ₀	A _{net} [mm ²]
B101	M27	60,0	10	30	1,00	3,00		300	61,0	10	30	0,95	3,01		310
B102	M27	72,0	10	30	1,20	1,20		420	73,2	10	30	1,20	1,21		432
B103	M27	72,0	10	30	1,20	1,50		420	71,2	10	30	1,15	1,50		412
B104	M27	72,0	10	30	1,20	2,00		420	71,7	10	30	1,19	2,01		417
B105	M27	72,0	10	30	1,20	3,00		420	72,0	10	30	1,16	2,98		420
B106	M27	81,0	10	30	1,35	2,50		510	81,0	10	30	1,33	2,52		510
B107	M27	81,0	10	30	1,35	3,00		510	80,5	10	30	1,32	3,02		505
B108*	M27	81,0	10	30	1,18	3,35		410	81,1	10	30	1,17	3,34		402
B109	M27	90,0	10	30	1,50	1,00		600	90,0	10	30	1,47	1,00		600
B110	M27	90,0	10	30	1,50	1,20		600	92,0	10	30	1,53	1,21		620
B111	M27	90,0	10	30	1,50	1,50		600	90,0	10	30	1,48	1,51		600
B112	M27	90,0	10	30	1,50	2,00		600	90,0	10	30	1,47	2,01		600
B113	M27	90,0	10	30	1,50	2,50		600	90,3	10	30	1,46	2,49		603
B114	M27	90,0	10	30	1,50	3,00		600	90,0	10	30	1,46	3,00		600
B115*	M27	90,0	10	30	1,33	3,00		500	90,3	10	30	1,30	3,00		480
B116	M27	90,0	10	30	1,50	1,50		600	87,4	10	30	1,42	1,50		574
B117	M27	90,0	10	30	1,50	1,50		600	89,2	10	30	1,48	1,50		592
B118	M27	120,0	10	30	2,00	1,50		900	118,0	10	30	1,90	1,53		880
B119	M27	120,0	10	30	2,00	2,00		900	118,2	10	30	1,93	2,06		882
B120	M27	120,0	10	30	2,00	2,50		900	119,4	10	30	1,96	2,56		894
B121	M27	120,0	10	30	2,00	3,00		900	122,1	10	30	2,02	3,06		921
B122	M27	120,0	10	30	2,00	3,50		900	118,8	10	30	1,95	3,54		888
B123	M22	80,0	10	24	1,67	4,17		560	78,7	10	24	1,61	4,22		547
B124*	M22	80,0	10	24	1,42	4,17		440	79,1	10,2	24	1,44	4,21		459
B125*	M22	80,0	10	24	1,17	4,17		320	79,1	10,15	24	1,18	4,21		333
B201	M22	96,0	10	24	1,00	3,00	2,00	480	97,2	10,15	24	0,96	2,97	2,03	499
B202	M22	115,2	10	24	1,20	1,20	2,40	672	115,9	10,15	24	1,20	1,20	2,36	689
B203	M22	115,2	10	24	1,20	2,00	2,40	672	115,9	10,15	24	1,20	2,01	2,37	689
B204	M22	115,2	10	24	1,20	3,00	2,40	672	116,0	10,15	24	1,20	2,99	2,36	690
B205	M22	122,4	10	24	1,20	3,00	2,70	744	124,1	10,15	24	1,21	2,96	2,70	772
B206	M22	129,6	10	24	1,50	1,50	2,40	816	130,3	10,15	24	1,50	1,50	2,38	835
B207	M22	136,8	10	24	1,50	3,00	2,70	888	137,0	10,15	24	1,48	3,03	2,70	903
B208	M22	144,0	10	24	1,50	1,00	3,00	960	144,0	10,15	24	1,49	1,03	3,00	974
B209	M22	144,0	10	24	1,50	1,20	3,00	960	144,1	10,15	24	1,50	1,21	3,00	975
B210	M22	144,0	10	24	1,50	1,50	3,00	960	144,0	10,15	24	1,50	1,53	2,98	975
B211	M22	144,0	10	24	1,50	2,00	3,00	960	143,7	10,15	24	1,44	2,05	3,00	971
B212	M22	144,0	10	24	1,50	3,00	3,00	960	144,4	10,15	24	1,47	3,04	3,01	978
B213	M22	122,4	10	24	1,35	2,00	2,40	744	121,0	10,15	24	1,33	2,01	2,39	741

* eccentric hole

2.3.2 *Experimental phase two – specimen type L*

The second phase of the experimental work was completed in May 2007 at the Slovenian National Building and Engineering Institute, Dimičeva 12, Ljubljana. Digitally controlled, hydraulic, multi-purpose testing machine Zwick with capacity of 2500 kN was used for the tests (Fig. 8).

Phase two included bolted shear connections with three or four bolts positioned in the loading direction. A total of 26 specimens type L (L for long connection) were tested. The specimen was fastened between two cover plates with three or four bolts M20 12.9 to form tension splice with bolts in double shear. The diameters of bolt holes were $d_0 = 22$ mm. The bearing area of the cover plates was stiffened by additional plate so that bolt bearing was transferred on 20 mm thick plate as show in Fig. 9. In this way the deformations were enforced only in the specimen while the cover plates deformed only elastically. The cover plates were welded together to form forks. Together with the bolts, they were not the subject of the investigation, thus they were designed accordingly. The forks and specimens were fabricated from plate II (steel grade 690 – Table 3). The functional fabrication tolerances were simulated at specimens coded by s (see Table 7), where the first or the last hole was shifted by 2 mm. In this way, only one bolt was carrying the bearing load for the first 2 mm of hole elongation and after that the remaining bolts were activated. The geometry of the specimens was designed to cover different types of failures. The range of pitches p_1 and end distances e_1 were selected from minimum allowed distances by EN 1993-1-8 (CEN, 2005b) to the most common ones. The edge distance e_2 was constant for all specimens and was equal to $4,5d_0$. The actual and nominal geometries of specimen type L are listed in Tables 6-7.

The tests were carried out at a prescribed displacement rate 1,5 mm/min. The records of force and displacements were recorded every 0,01s. A relative displacement between the specimen and the cover plates was measured by two inductive displacement transducers (IDT) and alternatively by sensor arm extensometers (SAE). The positions of measuring instruments are illustrated in Fig. 9. The SAEs were also used to control test speed. All measuring devices were connected to an external universal recording unit. The original gauge length of SAE was 40 mm. The reference point on the specimen for displacement measurement is illustrated in Fig. 10 and the value of distance g from the end of the specimen to the point is given in Table 7. The IDTs were fixed to the forks by a magnetic holder. The difference in displacement of SAE and IDT was in the elastic deformation of forks. The bolts were snug tightened to ensure that the load was transferred primarily by bearing and not by friction. The tests were carried out until fracture of plate in bearing or the bolt (except at L18 and L20s where the test was stopped significantly before failure).

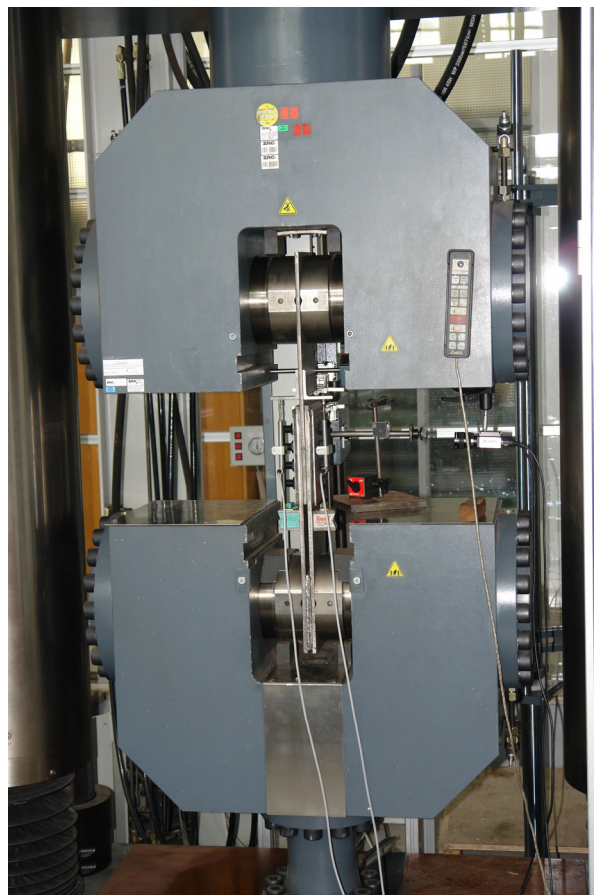


Fig. 8: Testing machine with capacity of 2500 kN

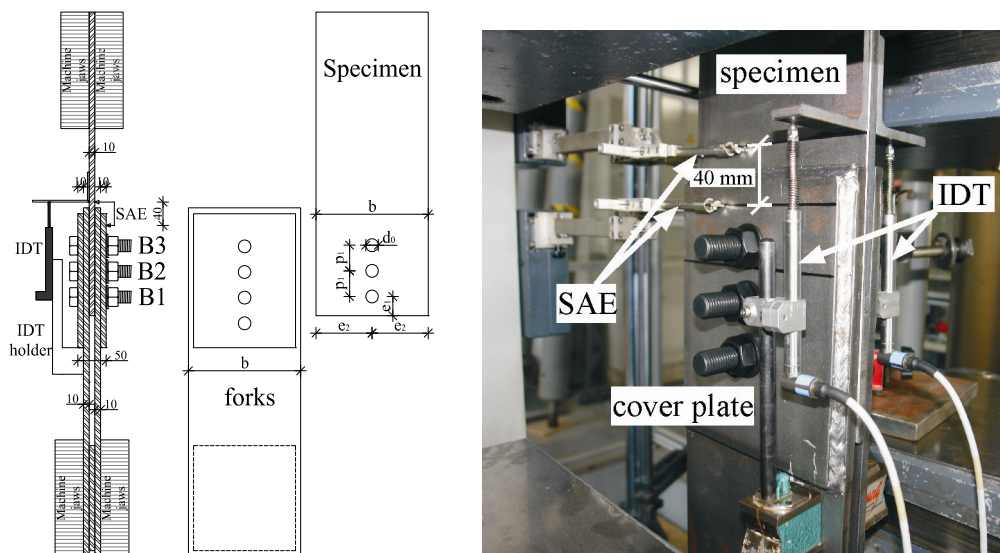


Fig. 9: Specimen type L equipped with measuring devices

Table 6: Nominal dimensions of specimen type L

Specimen name	e_1/d_0	p_1/d_0	e_2/d_0	d_0 [mm]	b [mm]	t [mm]	d [mm]	No. of bolts
L01	1,5	2,0	4,5	22	198	10	20	3
L02	2,0	2,0	4,5	22	198	10	20	3
L03	3,0	2,0	4,5	22	198	10	20	3
L04	1,5	2,0	4,5	22	198	10	20	4
L04s	1,5	2,0	4,5	22	198	10	20	4
L05	2,0	2,0	4,5	22	198	10	20	4
L06	3,0	2,0	4,5	22	198	10	20	4
L06s	3,0	2,0	4,5	22	198	10	20	4
L07	1,5	2,5	4,5	22	198	10	20	3
L08	1,5	2,5	4,5	22	198	10	20	4
L09	2,5	2,5	4,5	22	198	10	20	4
L10	3,0	2,5	4,5	22	198	10	20	4
L11	2,0	3,0	4,5	22	198	10	20	3
L12	2,5	3,0	4,5	22	198	10	20	3
L13	3,0	3,0	4,5	22	198	10	20	3
L14	1,23	3,0	4,5	22	198	10	20	4
L15	1,5	3,0	4,5	22	198	10	20	4
L16	2,0	3,0	4,5	22	198	10	20	4
L17	2,5	3,0	4,5	22	198	10	20	4
L18	3,0	3,0	4,5	22	198	10	20	4
L18s	3,0	3,0	4,5	22	198	10	20	4
L19	5,0	3,0	4,5	22	198	10	20	4
L20	2,0	3,50	4,5	22	198	10	20	4
L20s	2,0	3,50	4,5	22	198	10	20	4
L21	2,0	3,50	4,5	22	198	10	20	3
L22	2,0	3,77	4,5	22	198	10	20	3

s – hole shifted for 2 mm

(L04s, L06s, L18s – bolt B1 activates first, L20s – bolt B3 activates first)

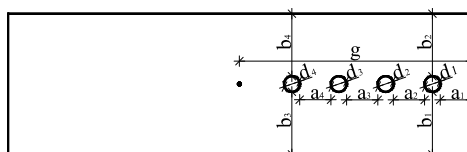


Fig. 10: Symbols for measured distances of specimen type L

Table 7: Actual dimensions of specimen type L

Specimen name	Connected to forks	a_1 [mm]	a_2 [mm]	a_3 [mm]	a_4 [mm]	b_1 [mm]	b_2 [mm]	b_3 [mm]	b_4 [mm]	d_1 [mm]	d_2 [mm]	d_3 [mm]	d_4 [mm]	t [mm]	g [mm]
L01	LF1	22,2	22,1	21,6		88,3	87,2	88,7	88,3	22,0	22,0	22,0		10,15	195,0
L02	LF1	33,7	21,6	22,1		88,3	87,6	88,3	87,6	22,0	22,0	22,0		10,20	206,0
L03	LF1	55,3	22,1	21,8		88,7	87,5	88,5	87,5	22,0	22,0	22,0		10,20	228,0
L04	LF1	22,8	21,5	21,9	21,5	88,4	87,9	88,4	87,6	22,0	22,0	22,0	22,0	10,15	239,0
L04s	LF1B	23,0	19,4	21,8	21,7	88,8	87,6	88,8	87,5	22,0	22,0	22,0	22,0	10,15	239,0
L05	LF1B	33,6	21,6	22,0	22,0	88,9	87,9	88,8	87,8	22,0	22,0	22,0	22,0	10,15	250,0
L06	LF1B	55,9	21,5	21,3	21,8	88,3	87,3	88,4	87,6	22,0	22,0	22,0	22,0	10,20	272,0
L06s	LF1B	55,0	19,4	22,2	21,8	88,2	87,6	88,0	88,0	22,0	22,0	22,0	22,0	10,15	272,0
L07	LF2B	22,0	32,7	32,7		88,5	87,5	88,7	87,3	22,0	22,0	22,0		10,15	206,0
L08	LF2A	21,8	33,6	33,0	33,0	88,9	87,0	88,3	87,0	22,0	22,0	22,0	22,0	10,15	261,0
L09	LF2A	43,9	32,7	32,9	32,8	88,6	87,4	87,9	88,2	22,0	22,0	22,0	22,0	10,20	283,0
L10	LF2A	55,1	32,7	33,3	32,9	88,0	88,1	88,4	88,7	22,0	22,0	22,0		10,15	294,0
L11	LF3E	32,8	44,2	44,0		88,5	87,7	NM	NM	22,0	22,0	22,0		10,15	250,0
L12	LF3E	44,1	44,0	43,7		88,0	88,0	88,3	88,7	22,0	22,0	22,0		10,20	261,0
L13	LF3B	55,2	43,7	44,0		88,0	88,3	87,7	88,2	22,0	22,0	22,0		10,15	272,0
L14	LF3B	16,3	43,5	43,5	43,8	88,3	87,9	88,3	87,7	22,0	22,0	22,0	22,0	10,15	299,0
L15	LF3B	22,0	43,6	44,2	43,8	88,7	87,4	88,7	87,1	22,0	22,0	22,0	22,0	10,15	305,0
L16	LF3B	32,7	43,7	44,0	43,7	88,4	87,6	88,2	88,1	22,0	22,0	22,0	22,0	10,15	316,0
L17	LF3B	43,9	43,5	44,2	43,8	88,2	88,1	88,4	87,9	22,0	22,0	22,0	22,0	10,15	327,0
L18	LF3C	55,1	43,5	44,1	43,5	87,7	88,6	88,1	87,9	22,0	22,0	22,0	22,0	10,15	338,0
L18s	LF3C	55,0	41,2	44,3	46,0	88,3	88,0	88,3	87,9	22,0	22,0	22,0	22,0	10,00	338,0
L19	LF3C	99,2	43,9	43,6	43,9	88,1	88,0	88,0	88,0	22,0	22,0	22,0	22,0	10,10	384,0
L20	LF4	33,0	54,6	54,5	55,0	88,5	87,8	88,6	87,7	22,0	22,0	22,0	22,0	10,10	360,0
L20s	LF4	33,0	54,8	55,0	56,9	88,3	87,7	88,3	87,7	22,0	22,0	22,0	22,0	10,10	362,0
L21	LF4	33,5	55,4	55,1		88,4	87,8	88,5	87,6	22,0	22,0	22,0		10,10	283,0
L22	LF5	33,3	60,9	60,9		88,3	87,8	88,5	87,6	22,0	22,0	22,0		10,10	301,0

NM not measured

3 METHODOLOGY OF NUMERICAL MODELS

3.1 General

This section deals with methodology and techniques used in numerical simulations. Each of the described numerical models was used for parametric studies of tension splices. The models differ mainly in complexity. The parameters in the study were geometry, material parameters, number of bolts and shear planes. They are described and presented in the following sections.

The finite element environment ABAQUS v6.5 to v6.7 (SIMULIA, 2007) was used to simulate shear connections. Three conceptually different numerical model types were built to describe the connections. The models were named M1, M2 and M3, where M1 was the simplest model type and M3 the most complex one. All models were three-dimensional. Deformable bodies were meshed by solid continuum finite elements. The geometry of a model was defined by parts, positioned relative to one another in an assembly. All models consisted of at least two parts: bolt(s) (either rigid or deformable) and steel plate(s). Different interactions were prescribed between parts. The full Newton solution method with nonlinear effect of large deformations and displacement was used to trace nonlinear load-displacement curve.

3.2 Numerical model type M1

This numerical model was used to simulate connections with bolts in double shear where bolts stay in their initial position and where cover plates do not restrain deformation of the plate in thickness direction. The simplification of the numerical model, described in the sequel, greatly reduces the computational time. The numerical model M1 was assembled of two separate parts. The bolt was presented by a 3D discrete rigid cylinder, while the steel plate with boltholes was modelled as a 3D deformable solid body. Bolt head, nut and washers were not modelled. The individual parts are presented in Fig. 11a-b, assembled and meshed connection is shown in Fig. 11c. An elastic-plastic material was defined for steel plate. A “hard” contact property was defined between the outer surface of the bolt and the bolthole surface. The reference point was applied to the bolt to govern the motion of the entire rigid body. A rigid body constraint was created between the leading face of the plate and a separate reference point to simplify the definition of boundary conditions. In this way boundary conditions and the outputs of results were prescribed only to the reference points. A displacement was prescribed to the plate’s reference point, while all other degrees of freedom of the reference points were prevented.

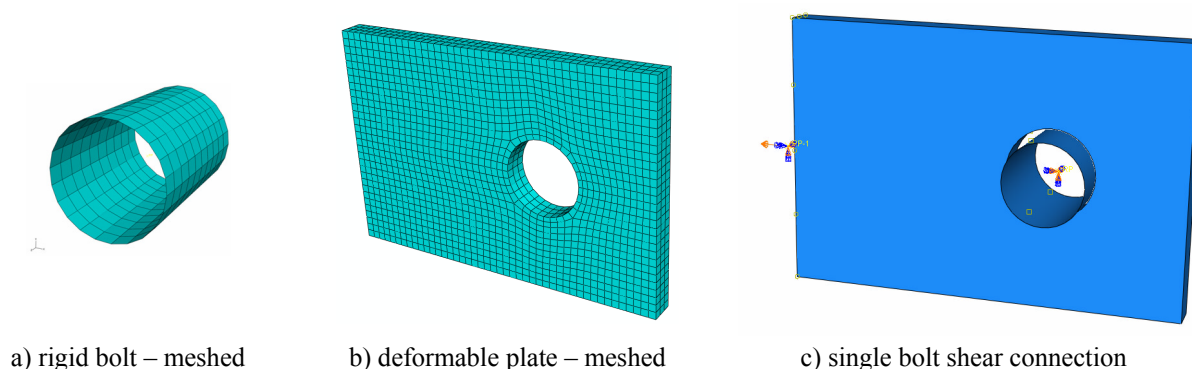


Fig. 11: Numerical model type M1

3.3 Numerical model type M2

The numerical model M2 was an upgrade of model M1. It was used to simulate shear connections with bolts in double shear, where cover plates restrain the deformation of the inner plate, while bolts remain in their initial position. Therefore bolt was modelled as 3D solid deformable body (Fig. 12a). Washers were not considered in the numerical model. In addition, cover plates (Fig. 12c) were presented as a separate part in a model. The purpose of cover plates was to obstruct the deformation of inner plate and to introduce friction between the plates. Bolt bearing was not introduced to the cover plates; therefore they did not have any boltholes. An elastic-plastic material was defined for inner steel plate, while elastic material was prescribed to the bolts and cover plates. A “hard” contact property was introduced between the following surface pairs: bolt shanks-boltholes in the inner plate, bolt head (nut)-cover plate. A “hard” contact property with penalty definition of friction was prescribed between inner and cover plate. Contact control with stabilization was prescribed to the contact bolt head (nut)-cover plate to overcome chattering between contact surfaces at the start of the analysis. Similarly as in model type M1, rigid body constraints were prescribed to the leading faces of the plates and outside surfaces of the bolt head (nut). Thus, all boundary conditions were defined on the reference points. Bolt displacements in the plane of the connection were restrained. All three rotations were also restrained. The displacement of the bolts and cover plates perpendicular to connection was unrestrained. In this way the bolts could freely deform because of the tensile force, introduced to them by transverse deformation of the inner plate. A displacement was prescribed to the inner plate’s reference point.

The friction was defined only by the coefficient of friction. The friction coefficient between steel-to-steel contact surfaces may vary from 0,05 to 0,8 (Beardmore, 2008). The value of friction coefficient used in numerical simulations was obtained through an iterative process. The value of friction was determined for one connection, so that numerical resistance matched the experimental one. The same friction coefficient was then applied to the whole series of connections. The friction coefficient influenced only the value of the resistance and had no

impact on the stiffness of load displacement curve. The values of the coefficient are given in the sequel, when describing the simulations for a specific connection series.

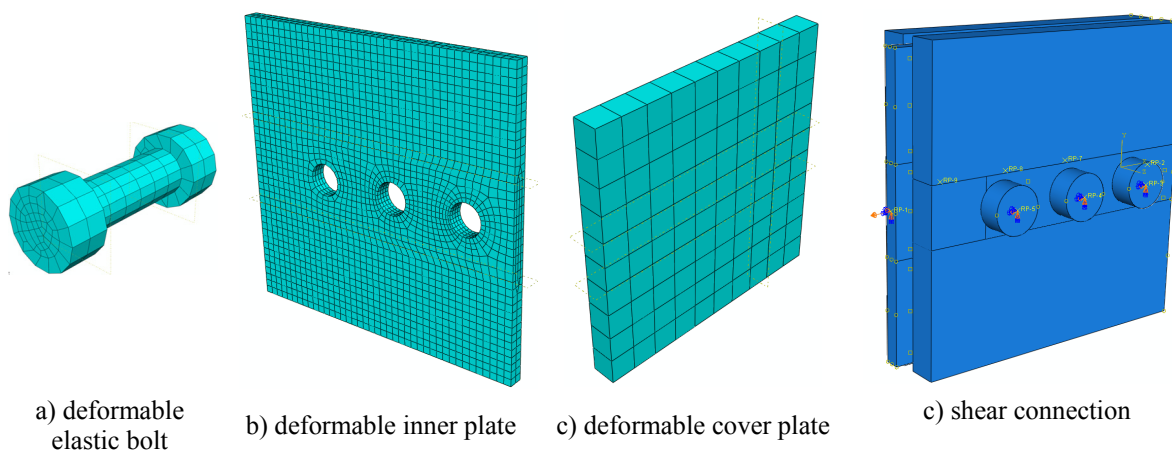


Fig. 12: Numerical model type M2

3.4 Numerical model type M3

This model type was the most realistic one. It was similar to model type M2, except that the cover plates have boltholes (Fig. 13c) and a contact was defined between the bolt shank and bolthole in the cover plate. Therefore, the loading was transmitted from the inner plate through the bolt(s) to the cover plate(s). A part of loading was also transmitted by means of friction when the inner plate deformed in thickness and introduced pressure to the cover plate. Boundary conditions were defined at the reference points that were included in rigid body constraints as in model type M2.

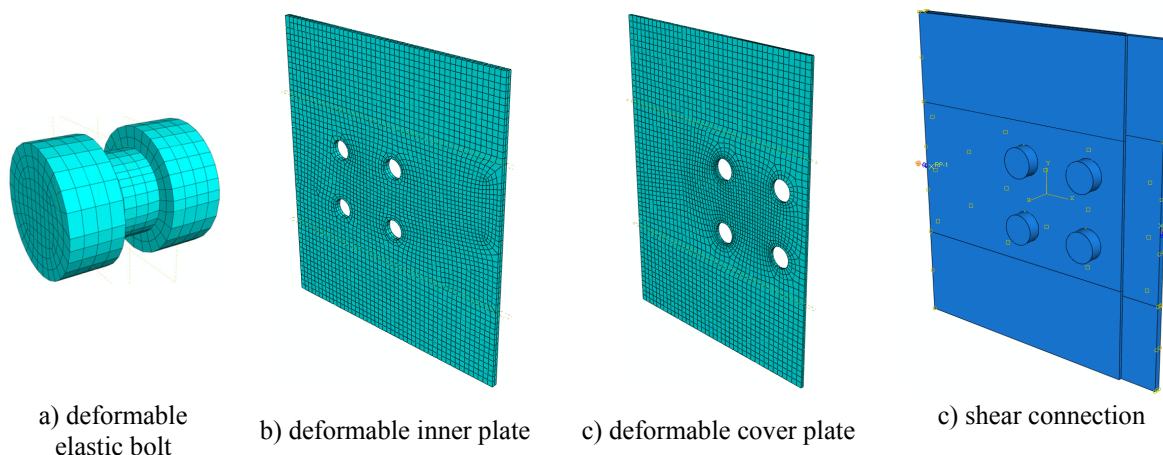


Fig. 13: Numerical model type M3

3.5 Contact interactions

A “hard” surface-to-surface contact interaction in normal direction was always defined between bolt shank and bolthole on the plate.

The contact pressure is in Abaqus defined between two surfaces at a point p , as a function of the “overclosure” h of the surfaces (the interpenetration of the surfaces). For “hard” contact it applies: $p = 0$ for $h < 0$ – the contact is opened – and: $h = 0$ for $p > 0$ – the contact is closed (see Fig. 14). The contact constraint is enforced with a Lagrange multiplier representing the contact pressure in a mixed formulation.

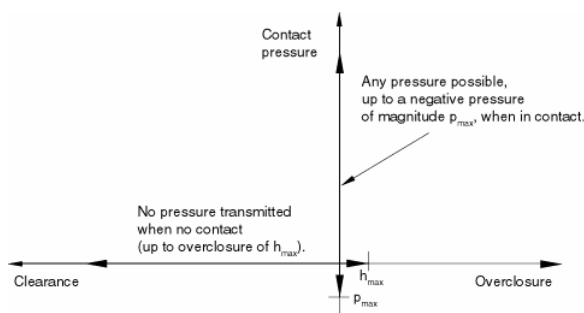


Fig. 14: Pressure-overclosure relationship with possible negative pressure transmission (cohesion) and/or overclosure (SIMULIA, 2007)

In models M2, M3 a default, penalty friction formulation of tangential contact was used. The friction was defined by coefficient of friction μ and by slip tolerance F_f .

The basic concept of the Coulomb friction model is to relate the maximum allowable frictional (shear) stress across an interface to the contact pressure between the contacting bodies. In the basic form of the Coulomb friction model, two contacting surfaces can carry shear stresses up to a certain magnitude across their interface before they start sliding relative to one another; this state is known as sticking. A critical shear stress, at which sliding of the surfaces starts, is defined as a fraction of the contact pressure between the surfaces. The stick/slip calculations determine when a point passes from sticking to slipping or from slipping to sticking. The fraction of contact pressure is known as the coefficient of friction μ . In Abaqus there are two ways to define the basic Coulomb friction model. In the default model the friction coefficient is defined as a function of the equivalent slip rate and contact pressure. The stiffness method used for friction in Abaqus/Standard is a penalty method that permits some relative motion of the surfaces (an “elastic slip”) when they should be sticking. While the surfaces are sticking, the magnitude of sliding is limited to this elastic slip. Abaqus will continually adjust the magnitude of the penalty constraint to enforce this condition. The default value of allowable elastic slip γ_i used by Abaqus/Standard generally works very well, providing a conservative balance between efficiency and accuracy. Abaqus/Standard calculates γ_i as a small fraction of the “characteristic contact surface length \bar{l}_i ”, and scans all of the facets of all the slave surfaces when calculating \bar{l}_i . The allowable elastic slip is given as $\gamma_i = F_f \bar{l}_i$, where $F_f = 0,005$ is the default value of slip tolerance.

3.6 *Finite elements and meshing*

Linear eight-noded reduced-integration brick finite elements C3D8R with hourglass control were used to mesh the numerical models. Additionally, 6-node linear triangular prisms C3D6 were used only to complete the mesh. Reduced integration reduces running time, especially in three dimensions. Hourglassing can be a problem with first-order, reduced-integration elements in stress-displacement analyses. Since the elements have only one integration point, it is possible for them to distort in such a way that the strains calculated at the integration point are all zero, which, in turn, leads to uncontrolled distortion of the mesh. First-order, reduced-integration elements in Abaqus include hourglass control, but they should be used with reasonably fine meshes. Hourglassing can also be minimized by distributing point loads and boundary conditions over a number of adjacent nodes. The option to C3D8R elements were 20-node, quadratic, brick elements with reduced integration C3D20R, but due to almost 10 times longer computational time at the same mesh size they were not selected for simulations. C3D20R behaved “softer” in post-critical region especially where necking occurred (approximately 5% difference). The difference in maximum resistance was less than 2%.

The finite element mesh was generated automatically on the basis of approximate element size for a specified cell. Cells were constructed from each part in the model. The largest finite element edge size was equal to plate thickness, if the thickness was smaller than 10 mm. At plate thickness equal to or larger than 10 mm, the edge size was 7,5 mm. There were at least two elements in thickness direction, and at 20 mm thick plates there were four elements in thickness. The mesh was generally denser in the zone of boltholes. The zone width of denser mesh was three times diameter of bolthole and there were four elements in the thickness direction. The cover plates in model type M2 were meshed very coarse. The size of finite element edge was equal to plate thickness. On one hand denser mesh gives more accurate results and on the other hand coarser mesh is more effective at contact convergence. Thus, an optimal mesh density was chosen and confirmed by mesh convergence study.

The mesh convergence study is shown on the connection B116 modelled with model type M1. Five different meshes are illustrated in Fig. 15, where *mesh1* is the coarsest with average FE edge size equal to 10 mm. Fig. 16 presents load-displacement curves for the described mesh types and different FE type. Beside the described FE types C3D8R and C3D20R, the element type C3D8I with incompatible modes was included in the study, as well. This element experienced convergence problems. Hence, it was not applied in further analyses. As can be seen in Fig. 16, the FE type C3D20R gives lower resistance in post-critical region. The difference at maximum resistance is in comparison to FE type C3D4R negligible (see also Table 8). The element type C3D20R becomes very expensive when denser mesh is used (Table 8). In some cases of model type M3 and FE type C3D4R the computational time increased to 23 hours (connection L12_t10-20_M27_b270)), thus the use of element type

C3D20R would be too expensive. Therefore, the combination of mesh types *mesh4* and *mesh5* and FE type C3D8R was used for comprehensive numerical study of tension splices.

Table 8: Comparison of the resistance and computational time for different meshes and finite elements

Mesh type	Finite element type	P_{max} [kN]	Error [%]	$P_{(u=24\text{ mm})}$ [kN]	Error [%]	Wallclock time [s]	Time ratio
mesh1	C3D4R	406	18,6	406	47,8	40	1,00
mesh2	C3D4R	356	4,1	303	10,3	84	2,10
mesh3	C3D4R	356	3,9	309	12,5	141	3,53
mesh3	C3D8I	353	3,0	N/A	NA	236	5,90
mesh3	C3D20R	344	0,5	281	2,3	936	23,40
mesh4	C3D4R	348	1,7	296	7,7	888	22,20
mesh4	C3D20R	342	0,0	275	0,0	7109	177,73
mesh5	C3D4R	356	4,0	308	12,0	337	8,43

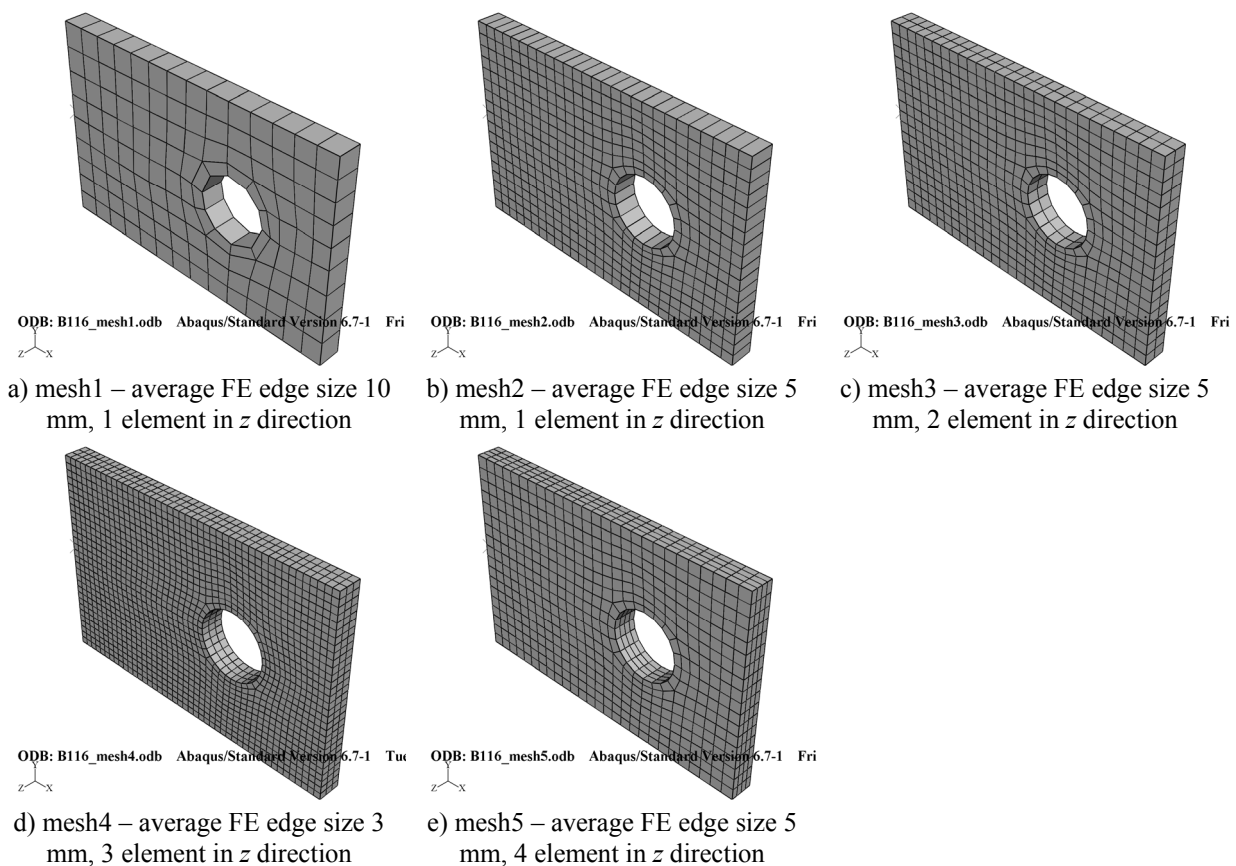


Fig. 15: Mesh types

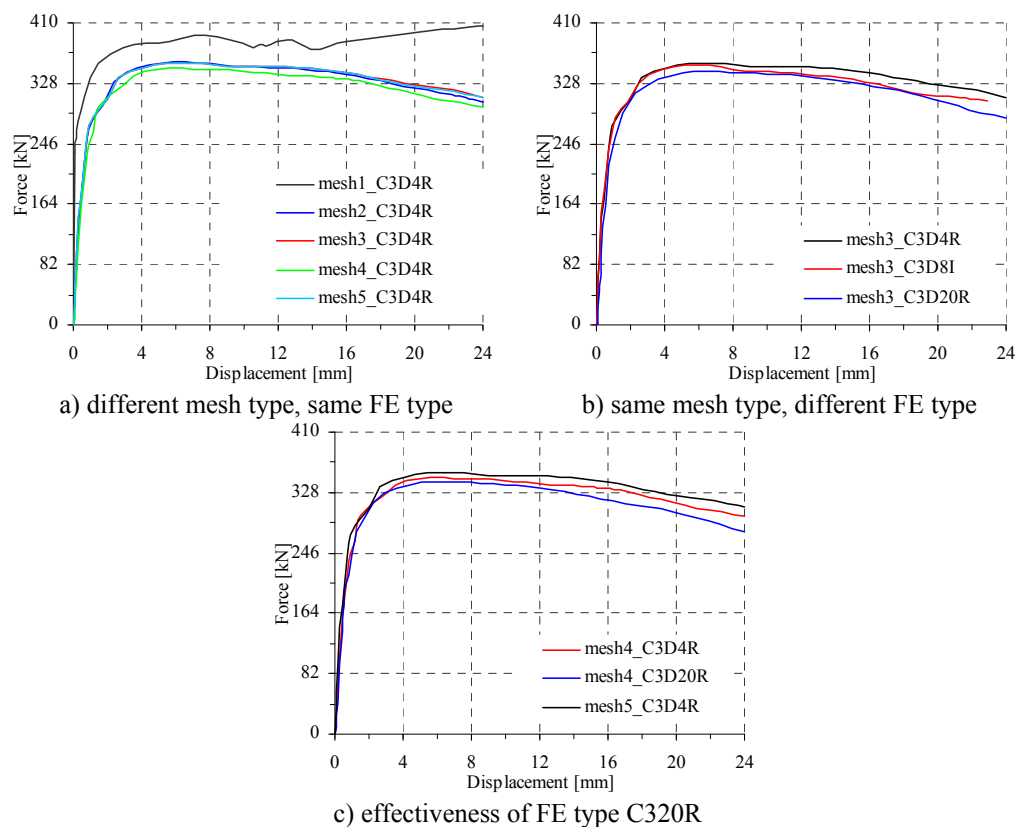


Fig. 16: Load displacement curves for different meshes and finite elements

3.7 Determination of material model

The procedure for the determination of material characteristics is standardized. On the basis of standard tensile test a number of parameters are measured. The output of this test is an engineering stress-strain diagram. The engineering stress (force per unit undeformed area) in the metal is known as the nominal stress, with the conjugate nominal strain (length change ΔL per unit undeformed length L_0). Metal deforming plastically under tensile load may experience highly localized extension and thinning, called necking, as the material fails. Thus, necking is the reason that nominal strain is not uniform through gauge length.

In Abaqus elastic and plastic behaviours are entered separately. As far as elastic part is concerned the input is trivial. Elastic modulus E and Poisson's ratio ν are sufficient parameters for stress-displacement analysis. In the case of our simulations the choice of parameters was always equal to: $E = 210$ GPa and $\nu = 0.3$. The plastic behaviour is defined by true stress and plastic part of true strain. This definition is reasonable because nominal stress-strain plots are not necessarily equal for tension and compression. A mathematical model describing the plastic behaviour of metals should be able to account for differences in the compressive and tensile behaviour independent of the structure's geometry or the nature of the applied loads. Strains in compression and tension are the same only if considered in the limit as $\Delta L \rightarrow dL \rightarrow 0$; i.e

$$d\varepsilon = \frac{dL}{L} \quad (3)$$

$$\varepsilon = \int_{L_0}^L \frac{dL}{L} = \ln\left(\frac{L}{L_0}\right), \quad (4)$$

where L is the current length, L_0 is the original length, and ε is the true strain or logarithmic strain. The stress measure that is the conjugate to the true strain is called the true stress and is defined as:

$$\sigma = \frac{F}{A} \quad (5)$$

where F is the force in the material and A is the current area. A relation between true stress σ , true strain ε , nominal stress σ_{nom} and nominal strain ε_{nom} can be easily derived:

$$\sigma = \sigma_{nom} (1 + \varepsilon_{nom}) \quad (6)$$

$$\varepsilon = \ln(1 + \varepsilon_{nom}). \quad (7)$$

Thus, traditional engineering stress-strain diagram could be easily transformed to true stress-strain diagram. But it is not so. In case of steel these formulas are valid until necking (localized deformations) occurs. That is approximately to ultimate tensile strength of the material. After necking the transformation is based on the definition of true stress and true strain. Thus, true stress at failure is force at failure divided by the measured area of test specimen at failure. True strain at failure can only be estimated. First, the length on which most necking occurred has to be measured. Then the displacement caused by necking has to be assessed. This displacement is always smaller than the difference between the displacement at failure and the displacement at maximum force. The points between maximum true stress and true stress at failure have to be calibrated through numerical simulation of standard tensile test. In this way numerical simulation may fit experimental load-displacement curve even in post-critical region.

On the basis of the described procedure the material models for numerical simulations were determined. Numerical model of standard tension specimens was build and standard tensile test was simulated to verify the material model. Comparison of experimentally and numerically obtained load-displacement curves of standard tensile tests are presented in Fig. 17. Strain and stress state of standard specimen 291.1 is illustrated in Fig. 18. The material models used for further numerical analyses are shown in Table 9 for plate I and in Table 10 for plate II.

Table 9: Material model applied in Abaqus for plate I

True stress [MPa]	850,6	854,32	876,85	912,46	922,66	928,87	970,76	1091
True plastic strain	0	0,0032	0,0142	0,0321	0,0387	0,044	0,0943	1,38

Table 10: Material model applied in Abaqus for plate II

True stress [MPa]	799	826	893	928	994
True plastic strain	0	0,009	0,053	0,090	0,700

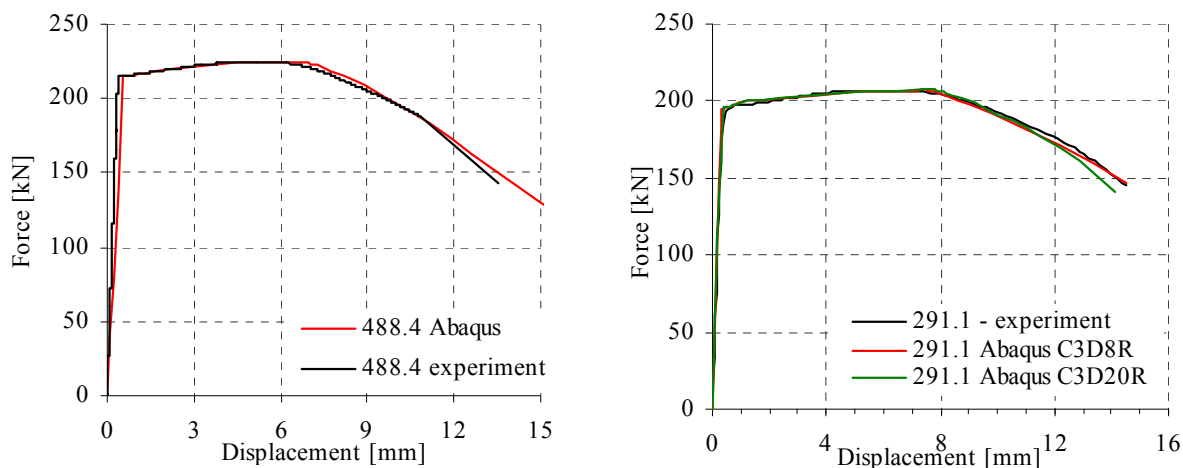


Fig. 17: Comparison of numerical and experimental load-displacement curves

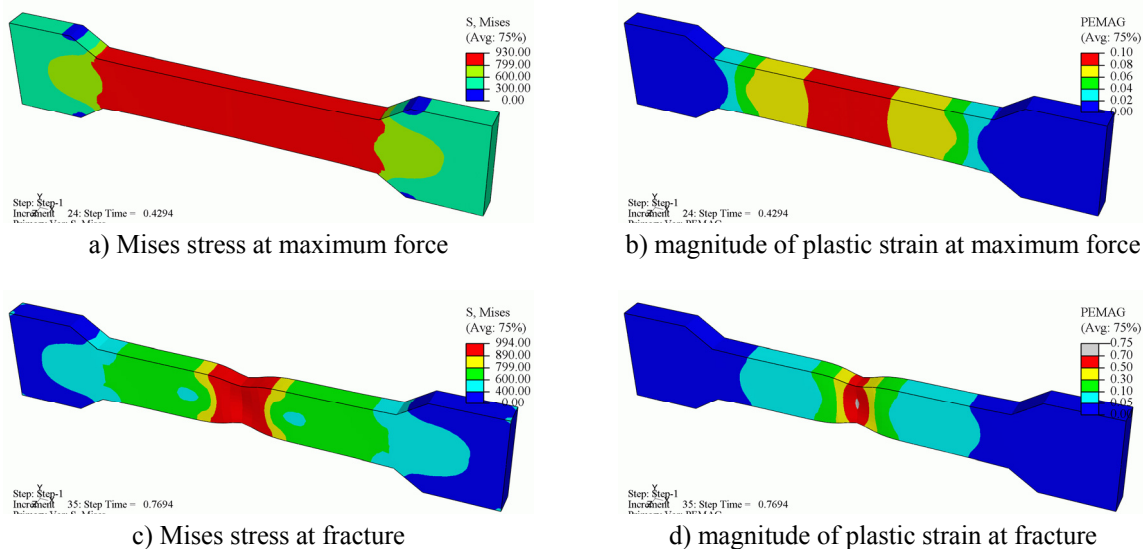


Fig. 18: Numerical simulation of standard tensile test on specimen 291-1

4 TENSION MEMBERS WITH HOLES – NET CROSS SECTION FAILURE

4.1 Introduction

Members in tension are a subject of everyday design. Usually two basic checks are required. The net cross section resistance check prevents the rupture of net cross-section, while the gross cross-section resistance check limits the excessive elongation of a whole member. Accordingly, EN 1993-1-1 (CEN, 2005a) defines that design resistance of cross-section with holes in tension should be taken as the smallest of:

- the design ultimate resistance of the net cross-section at holes for fasteners

$$N_{u,Rd} = \frac{0,9A_{net}f_u}{\gamma_{M2}} \quad (8)$$

- the design plastic resistance of the gross cross-section

$$N_{pl,Rd} = \frac{Af_y}{\gamma_{M0}} \quad (9)$$

These two rules presume that sufficient local ductility is available. The basic ductility measurements that are obtained from the standard tension tests are the engineering strain after fracture A^c (usually called the elongation) and the reduction of cross-section area at fracture Z , and last but not the least, the tensile-to-yield strength ratio f_u/f_y . For HSS this ratio is much lower than for mild steel, usually below 1,1 (see Chapter Introduction). Therefore, an additional design net cross-section resistance check was set in the draft of EN 1993-1-12, stating that it does not need to be taken smaller than:

$$N_{t,Rd} = \frac{A_{net}f_y}{\gamma_{M0}} \quad (10)$$

In the previous formulas factors γ_{Mi} are partial factors for resistance. They are defined by each country in National Annexes to relevant EN standards, but the recommended values given in EN standards are: $\gamma_{M0} = 1,00$ and $\gamma_{M2} = 1,25$. Since the limit state design method, which is adopted in Eurocodes, is semi-probabilistic in nature, the appropriate choice of partial factors should be determined on the basis of statistical analysis of experimental results. The classes of partial factors were defined in order to avoid different partial factors from one resistance function to another. In EN 1993-1-1 three resistance partial factors γ_M are defined as follows:

- resistance of cross-sections: γ_{M0} ;
- resistance of members to instability assessed by member checks: γ_{M1} ;
- resistance of cross-sections in tension to fracture: γ_{M2} .

It is easy to prove that the design resistance given by equation (10) is always critical for HSS, considering that the ultimate tensile to yield strength ratio f_u/f_y may be close to 1,0 and that the

recommended value for the partial factor γ_{M0} is 1,00. In this section it will be shown that the design resistance (10) with its partial factor $\gamma_{M0} = 1,00$ and yield strength, which is for HSS almost equal to tensile strength, is not in compliance with reliability requirements in EN 1990 (CEN, 2004a). Based on our test results, this design resistance was in the final draft of prEN 1993-1-12 (CEN, 2007) changed to (where the recommended value of partial factor equals to $\gamma_{M12} = \gamma_{M2} = 1,25$):

$$N_{t,Rd} = \frac{0,9A_{net}f_u}{\gamma_{M12}} \quad (11)$$

The design net cross-section resistance of unsymmetrically connected member with one bolt in tension is according to EN 1993-1-8 (CEN, 2005b) defined as:

$$N_{u,Rd} = \frac{2(e_2 - 0,5d_0)tf_u}{\gamma_{M2}} \quad (12)$$

where e_2 is the minimum distance to the edge of the plate and d_0 is hole diameter as shown in Fig. 19. Due to lack of test results in EN 1993-1-12 (CEN, 2007), this design resistance expression was set as not applicable for HSS. It will also be shown that this design resistance may also be used for high strength steel sections.

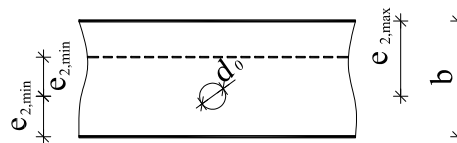


Fig. 19: Reduced net cross-section

4.2 Test results

Test results presented in this section refer only to those where rupture of net cross-section occurred. All specimen types H and HH (strips in tension) and a few specimen types B1, B2, L (bolted shear connection) failed in the net cross-section. The maximum resistance F_{max} and displacement at maximum force D_U of all specimens that failed in net cross-section are presented in Table 11.

At specimens H, HH the tensile stress flow was obstructed by a hole. Therefore, stress concentration on both edges of the hole in the net cross-section resulted in transverse contraction before maximum resistance was reached. The stress peaks were eliminated by yielding of the material. Once the maximum resistance was reached, necking in net cross-section became significant. When the member was yielding, a localized band, inclined to the specimen axis, was formed. This band was a localized neck and the process is called *localized necking* (Dieter, 1987). Macro cracks first developed at the edges of the hole in the net cross-section, where the plastic deformations were the largest. The crack started to progress along the localized neck, but it soon diverted onto the shortest path to the edge of the specimens.

The propagation was slow regardless of the hole size. The photographs of the specimens after failure are presented in Appendixes A, B and C.

Table 11: Test results of specimens that failed in net cross-section (specimens H, HH, B1, B2 and L)

Specimen name	H01	H02	H03	H04	H05	H06	H07	H08	H09	H10	H11	H11A	H12	H13*	H14*	H15	H16	H17	H18	H19	H20
F_{max} [kN]	868	886	861	811	811	789	748	717	713	679	639	627	644	636	636	542	456	492	461	403	191
D_U [mm]	11,8	12,2	6,1	3,2	3,2	3,3	3,1	3,2	3,1	2,9	3	2,9	2,8	3	2,6	2,9	2,7	38,2	16,9	10,3	8,4

Specimen name	HH01	HH02*	HH03*	HH04	HH05*	HH06*
F_{max} [kN]	499	490	470	553	544	536

Specimen name	B101	B105	B106	B107	B108*	B113	B114	B115*	B122	B123	B124*	B125*
F_{max} [kN]	262	355	445	440	370	516	510	435	788	483	400	322
D_U [mm]	2,4	3,5	5,8	5,6	4	8,5	9,1	6,2	24,3	15,9	10	5,6

Specimen name	B201	B203	B204	B205	B207	B212	B213
F_{max} [kN]	457	643	638	689	789	851	678
D_U [mm]	2,4	4,3	3,9	6,2	10,4	12,6	5,8

Specimen name	L09	L10	L16	L17	L18**	L18s	L19	L20	L20s**
F_{max} [kN]	1521	1522	1537	1539	1537	1533	1507	1527	1480**

* eccentric hole

** test stopped before failure

Deformation of specimen H10 at different load stages is presented in Fig. 20. The thickness and the total width of the plate at the location of the fracture were reduced from 21 to 41% and 32 to 58%, respectively, on average by 27% and 40%. The size of reduction depended on the size and the shape of net the cross-section. The displacement at maximum force for different hole sizes (10 to 50 mm) did not differ significantly (Fig. 21). The displacement at failure (when the macro crack was formed) was slightly increasing with bigger holes. It was observed that most of the test specimen's plastic elongation occurred in the vicinity of the hole. The similarity of load displacement curves between specimens H04 to H16 in Fig. 21 suggests that the gross cross-section was not exposed to significant plastic deformations. Specimens H17 to H20 were made of mild steel S235. The f_u/f_y ratio for such steel may be as high as 1,5. Because of large ratio, net cross-section may reach stress far above yield stress f_y and due to strain hardening, the gross cross-section of a member in tension can also yield and therefore be exposed to excessive plastic deformations. Load displacement curves of specimens H17 to H20 (steel S235) differ in shape as well as in displacements at maximum force. Although specimens H04 and H18 differ only in steel grade, the displacements at failure were 6,6 mm for H04 and 19,4 mm for H18 (Fig. 22). At these specimens the ratio A_{net}/A is equal to 0,9. Due to high f_u/f_y ratio, the design plastic resistance of gross cross-section according to equation (9) is critical for specimen H18 and generally for mild steel elements with A_{net}/A close to 1. The material strain hardening of specimen H18 allowed the gross area to yield, causing excessive deformation of the whole member in tension To prevent large member elongation the resistance is limited by equation (9). The low f_u/f_y ratio does not allow yielding of gross area of H04. Fig. 23 illustrates that the difference in the displacements of

H04 and H18 occurred on account of plastic deformation of gross cross-section of specimen H18.

Fig. 24a presents normalized resistance F/F_{max} (for specimens H) in relation to A_{net}/A , for steel grades S690 and S235. Linearly decreasing tendency is observed for both steel grades for elements with $A_{net}/A \leq 0,3$. The linear dependency continues for steel grade S690, while for steel S235 the gradient lowers. In case when $A_{net}/A = 0,5$ steel grade S690 has relatively higher resistance than S235. This may also be one explanation for factor 0,9 in resistance formula (8).

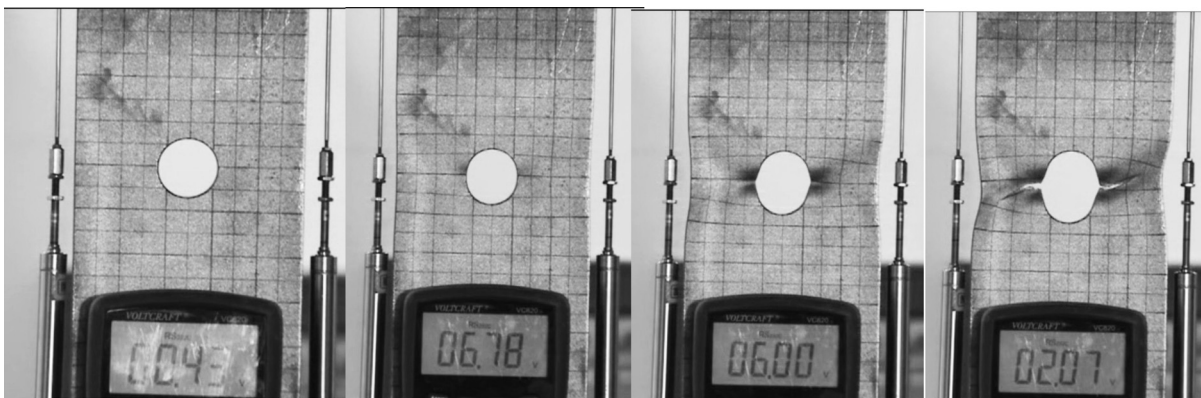


Fig. 20: Specimen H10 under loading (elastic stage 4,3 kN, maximum resistance 678 kN, just first macro crack 600 kN, failure 207 kN)

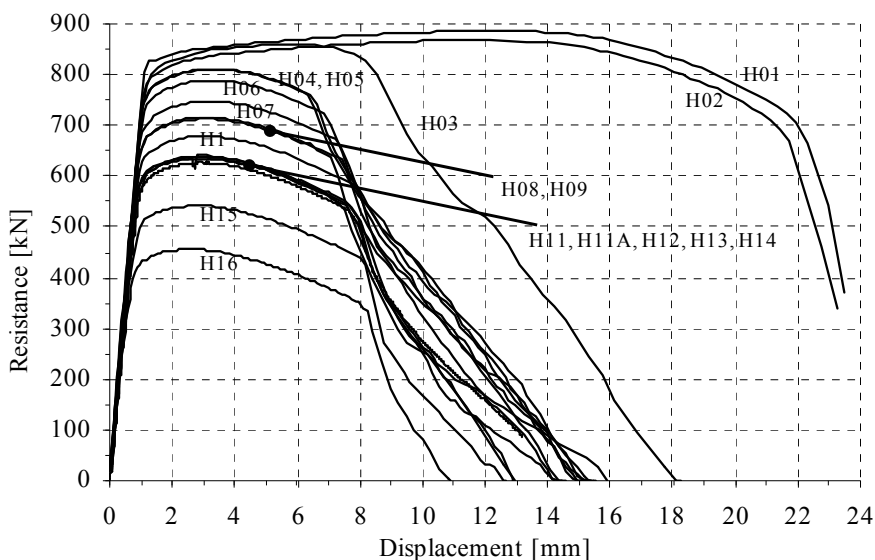


Fig. 21: Load displacement curves for specimens H01 to H16 (steel grade S690)

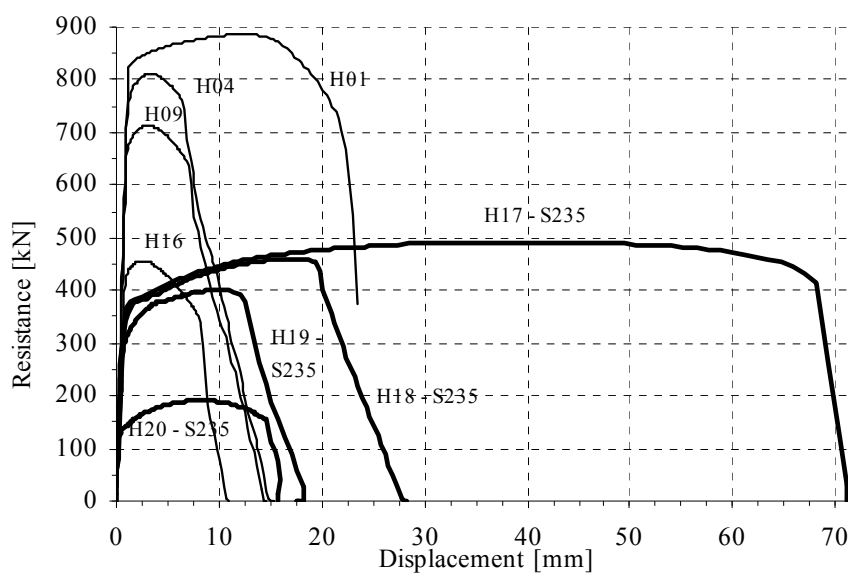


Fig. 22: Load displacement curves for specimens H – comparison of materials S690 and S235

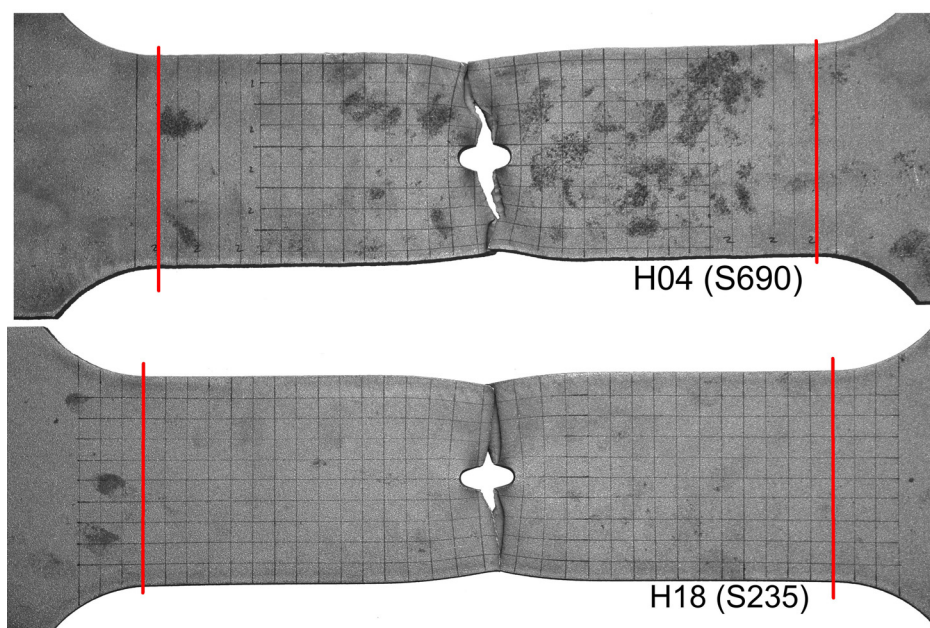


Fig. 23: Failure of specimens of equal geometry but different steel grade

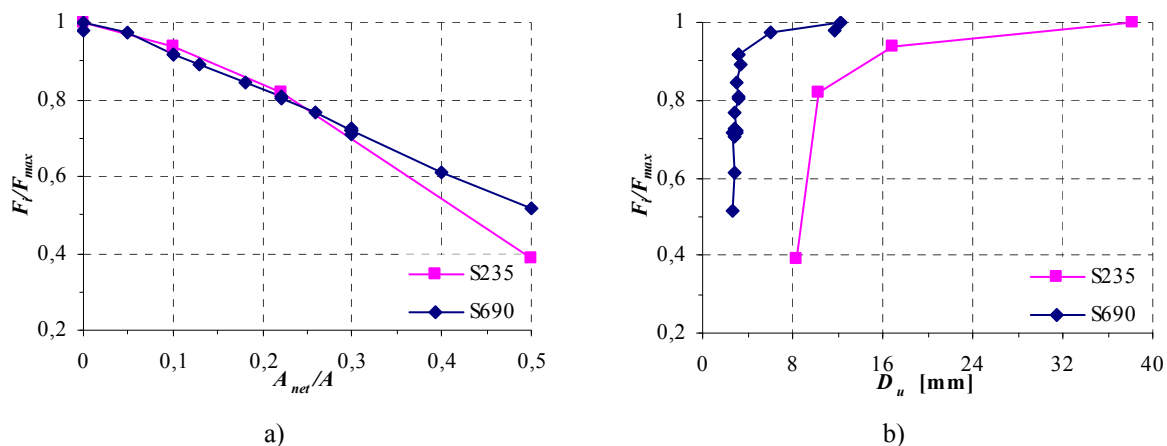


Fig. 24: Normalized resistance in relation to A_{net}/A (a) or displacement D_u at maximum resistance (b) for steel grade S690 and S235

Load transfer was different at specimens B1, B2 and L compared to specimens H and HH. At specimens B1, B2 and L the load was transferred to the plate by means of bolts. The failure mode was directed by end distances e_1 , pitch p_1 and number of bolts. If the distances and the number of bolts were large enough, the specimen would fail in net cross-section and not in some other failure mode. The load displacement curves for bolted connections (Figs. 25-27) are not as steep as of specimens H. The plateau is also not so distinctive. The additional displacement that reduced rigidity goes on account of hole elongations, which was especially large at specimen B122 (Fig. 28). At bolted connections with several bolts positioned parallel to loading the hole elongations summarize (Fig. 29). Although HSSs are considered to be less ductile and the f_u/f_y ratio was only 1,05, the thickness of specimen B122 increased locally from 10 mm to 20 mm. This deformation occurred in the vicinity of the contact between the plate and the bolt and is associated with large hole elongation. All failures were typically ductile with plastic deformations limited only to net area and to hole elongation. At connections with four bolts the loading was distributed uniformly between all bolts before net cross-section started to yield. The phenomenon of localized necking was also observed.

Specimen with eccentric holes failed in two different ways. Macro cracks at specimens H occurred in net cross-section on both sides of the hole simultaneously, regardless of the hole position. The hole eccentricity was of greater importance for specimens HH and B1, where specimens failed on the side where the edge distance was smaller. The eccentricity of the hole affected the resistance only for specimens B1, while for specimens H and HH the influence was practically negligible. No tests of unsymmetrically connected members in tension with several bolts positioned in loading direction were performed.

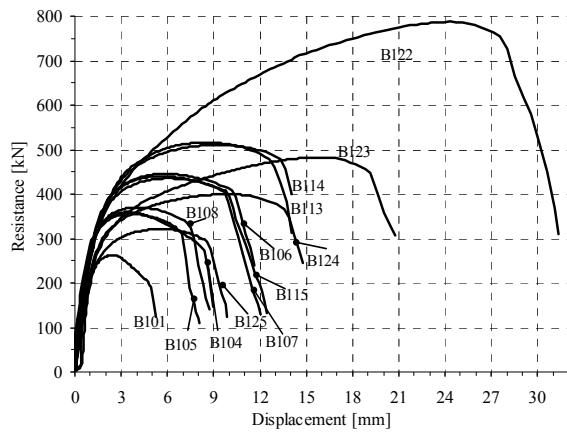


Fig. 25: Load displacement curves for specimens B1 that failed in net cross-section

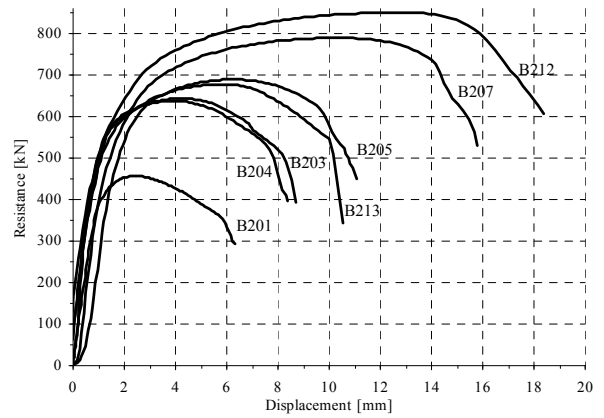


Fig. 26: Load displacement curves for specimens B2 that failed in net cross-section

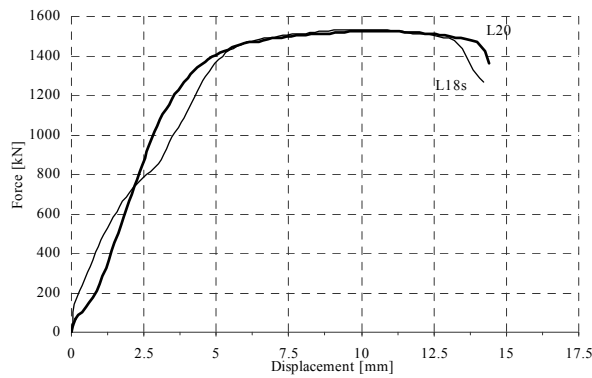


Fig. 27: Load-disp. curves for specimens L18s, L20 that failed in net cross-section

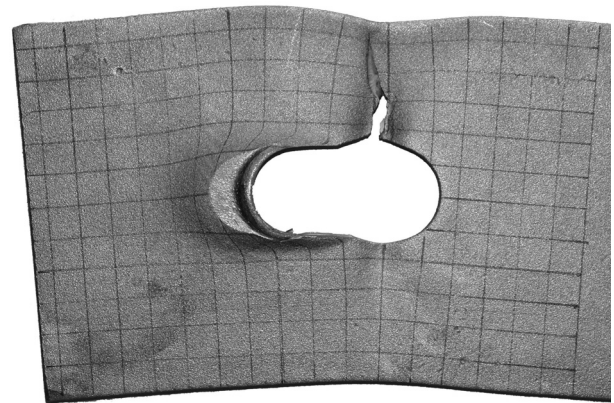


Fig. 28: Net cross-section failure of specimen B122



Fig. 29: Net cross-section failure of specimen L20

4.3 Statistical evaluation of results

Generally, the objective of the statistical analysis is the verification of the strength function and the determination of appropriate partial factor γ_M , defined as a ratio between the characteristic and the design value. The guidance for the statistical analysis is described in EN 1990, Annex D, which gives procedure for the assessment of a characteristic or design value based on the following assumptions:

- the resistance function is a function of a number of independent variables;
- a sufficient number of tests is available;
- all relevant geometrical and material properties are measured;
- there is no correlation (statistical dependence) between the variables in the resistance function;
- all variables follow either a normal or a log-normal distribution.

The characteristic value has a prescribed probability (as the 5% quantile) of not being attained in a hypothetical infinite number of tests. The probability of observing a lower value than a design value is slightly less than 0,1%.

The first step of the analysis is to establish a theoretical resistance model which corresponds to the experimental results. The theoretical resistance r_t is a function of a number of independent variables \underline{X} . For the evaluation of this function, the measured values of mechanical characteristics and geometry are used.

$$r_t = g_{rt}(\underline{X}) \quad (13)$$

To check the design resistances of net cross-section presented in EN 1993-1-1 and in the draft of EN 1993-1-12, three theoretical models or resistance models are introduced. The first resistance model for the net cross-section failure mode is based on the assumption that failure occurs if net section A_{net} is fully stressed up to tensile material strength f_u and is related to the design resistance given in equation (8).

Resistance model 1:
$$r_{t,1} = A_{net} f_u \quad (14)$$

This resistance model multiplied by 0,9 is presented in EN 1993-1-1. Factor 0,9 was proposed for mild steels only to satisfy the reliability criteria for the selected value of partial factor $\gamma_{M2} = 1,25$ (Snijder et al., 1988a).

The second resistance model assumes that the net cross-section is stressed up to yield stress f_y . This is a conservative assumption for ductile materials (e.g. mild structural steels) which have the ability of considerable strain hardening. Such approach was introduced in the draft of prEN 1993-1-12 for HSSs by equation (10).

Resistance model 2:
$$r_{t,2} = A_{net} f_y \quad (15)$$

The third resistance model suggests the use of reduced net cross-section for unsymmetrically connected member in tension. The unsymmetrical connection or hole eccentricity may reduce

resistance. The resistance model suggests that such members may be treated as concentrically loaded over an effective net section as illustrated in Fig. 19. In EN 1993-1-8, the design net cross-section resistance of unsymmetrically connected member with one bolt in tension (equation (12)) is based on this resistance model.

Resistance model 3:
$$r_{t,3} = (2e_{2,\min} - d_0) t \cdot f_u \quad (16)$$

The experimental resistances are gathered in vector r_e . Correction factor b is calculated using the least square method.

$$b = \frac{\sum_i r_{ei} r_{ti}}{\sum_i r_{ti}^2} \quad (17)$$

The estimated error δ_i of each experimental result is determined from:

$$\delta_i = \frac{r_{ei}}{b r_{ti}}. \quad (18)$$

Mean values of theoretical resistances r_m are calculated by mean values of basic variables

$$\underline{X}_m : \quad r_m = b r_t(\underline{X}_m) \delta = b g_{rt}(\underline{X}_m) \delta. \quad (19)$$

Mean values of geometry are adopted as nominal values for the calculation of the net cross-section. Mean values of material properties are equal to the measured ones. The material properties are equal for all specimens because all specimens were extracted from one steel plate.

On the basis of estimated error δ_i , the estimator of variation coefficient for scatter V_δ is determined by:

$$\Delta_i = \ln(\delta_i). \quad (20)$$

$$\bar{\Delta} = \frac{1}{n} \sum_{i=1}^n \Delta_i. \quad (21)$$

$$s_\Delta^2 = \frac{1}{n-1} \sum_{i=1}^n (\Delta_i - \bar{\Delta})^2, \quad (22)$$

where n is the number of tests.

Finally:

$$V_\delta = \sqrt{\exp(s_\Delta^2) - 1}. \quad (23)$$

To include uncertainty of steel grade and fabrication of elements, the standard deviation is increased by the coefficients of variation V_{X_i} which are determined on the basis of prior knowledge. To determine variations of independent variables V_{X_i} , the data were gathered from literature (Snijder et al., 1988a. Johansson et al., 2001). The following variations were used:

$$V_{d_0} = 0,005 \quad \text{variation coefficient for diameter of bolt hole;} \quad (24)$$

$$V_{f_y} = V_f = 0,07 \text{ variation coefficient for yield strength;} \quad (25)$$

$$V_{f_u} = V_f = 0,07 \text{ variation coefficient for tensile strength;} \quad (26)$$

$$V_t = 0,05 \text{ variation coefficient for plate thickness;} \quad (27)$$

$$V_b = 0,005 \text{ variation coefficient for width.} \quad (28)$$

$$V_{e_1} = 0,005 \text{ variation coefficient for end distance (used for evaluation of bearing resistance);} \quad (29)$$

$$V_{e_2} = 0,005 \text{ variation coefficient for edge distance (used for evaluation of bearing resistance);} \quad (30)$$

$$V_{p_1} = 0,005 \text{ variation coefficient for pitch distance (used for evaluation of bearing resistance);} \quad (31)$$

For small values V_δ^2 and $V_{X_i}^2$ it is allowed to use simplified procedure for the determination of V_r .

$$V_r^2 = V_\delta^2 + V_{rt}^2, \quad (32)$$

where

$$V_{rt}^2 = \sum_{i=1}^j V_{X_i}^2 \text{ (j – number of different variations).} \quad (33)$$

For the calculation of characteristic and design resistances, the corresponding standard deviations and coefficients are obtained from equations:

$$Q_{rt} = \sigma_{\ln(rt)} = \sqrt{\ln(V_{rt}^2 + 1)}, \quad (34)$$

$$Q_\delta = \sigma_{\ln(\delta)} = \sqrt{\ln(V_\delta^2 + 1)}, \quad (35)$$

$$Q = \sigma_{\ln(r)} = \sqrt{\ln(V_r^2 + 1)}, \quad (36)$$

$$\alpha_{rt} = \frac{Q_{rt}}{Q}, \quad (37)$$

$$\alpha_\delta = \frac{Q_\delta}{Q}. \quad (38)$$

The characteristic and design values are calculated according to formulae (39) and (40), considering the appropriate values of quantile factors k_n , $k_{d,n}$, k_∞ and $k_{d,\infty}$ according to Tables D.1 and D.2 in EN 1990 (see Table 13).

The characteristic value for a limited number of tests is given by the following expression:

$$r_k = b g_{rt}(\underline{X}_m) \exp(-k_\infty \alpha_{rt} Q_{rt} - k_n \alpha_\delta Q_\delta - 0,5 Q^2) = b g_{rt}(\underline{X}_m) \cdot R_k. \quad (39)$$

Similarly the design value for a limited number of tests is obtained as:

$$r_d = b g_{rt}(\underline{X}_m) \exp(-k_{d,\infty} \alpha_{rt} Q_{rt} - k_{d,n} \alpha_\delta Q_\delta - 0,5 Q^2) = b g_{rt}(\underline{X}_m) \cdot R_d. \quad (40)$$

If a large number of tests (e.g. $n > 100$) is available, the characteristic and design values may be obtained from:

$$r_k = bg_{rt}(\underline{X}_m) \exp(-k_{\infty} Q - 0,5Q^2) = bg_{rt}(\underline{X}_m) \cdot R_k \quad (41)$$

$$r_d = bg_{rt}(\underline{X}_m) \exp(-k_{d,\infty} Q - 0,5Q^2) = bg_{rt}(\underline{X}_m) \cdot R_d \quad (42)$$

Material partial factor γ_M covering also uncertainty in the resistance model and geometric derivations is determined in two steps directly from characteristic, design and nominal resistances.

The initial estimate for partial factor γ_M is defined as ratio between characteristic and design value.

$$\gamma_M = \frac{r_k}{r_d} = \frac{\exp(-k_{\infty} \alpha_{rt} Q_{rt} - k_n \alpha_{\delta} Q_{\delta} - 0,5Q^2)}{\exp(-k_{d,\infty} \alpha_{rt} Q_{rt} - k_{d,n} \alpha_{\delta} Q_{\delta} - 0,5Q^2)} = \frac{R_k}{R_d} \quad (43)$$

The design resistance function contains basic variables defined as nominal values \underline{X}_n . The nominal value of the material strength may be adopted as characteristic value and the nominal values for the geometrical variables may be adopted as mean values. Thus, on the basis of actual material strengths, characteristic material strengths need to be obtained. This can only be done, if additional prior knowledge is available. The deviation of the nominal material strengths of selected steel grade from actual strengths may be too large and consequently the choice of partial factor would be incorrect. To justify this step, an upper bound (conservative assumption) for coefficient of variation V_f , which is known from a significant number of previous tests, should be taken.

Therefore, the characteristic value for material strength is determined by using prior knowledge. Characteristic value of material strength is equal to:

$$r_k = \exp(-2,0V_r - 0,5V_r^2) r_{em} \quad (44)$$

where V_r is maximum variation coefficient obtained from previous tests and r_{em} is the mean value of at least three tests. This procedure is limited by:

$$|r_{ee} - r_{em}| \leq 0,1r_{em} \quad (45)$$

where r_{ee} is the extreme measured value. The variation coefficient for yield and tensile strengths given by equations (25), (26) were taken from literature. The Background documentation to EC 3 (Snijder et al., 1988a) gives coefficient for f_u independent of steel grade. Although there are also some tests with HSS, the coefficients probably apply to mild steels. The same coefficients were used in our case. Characteristic values f_{yk} and f_{uk} , calculated according to equation (44), give:

$$f_{yn}^* = f_{yk} = \exp(-2 \cdot 0,07 - 0,5 \cdot 0,07^2) f_{y,act} = 0,867 \cdot f_{y,act} \quad (46)$$

Ratio k_c between the nominal resistance r_n and the characteristic resistance r_k is written as follows:

$$k_c = \frac{r_n}{r_k}. \quad (47)$$

The corrected partial factor for the use with the nominal resistance is finally obtained from:

$$\gamma_M^* = k_c \gamma_M = \frac{r_n}{r_k} \frac{r_k}{r_d} = \frac{r_n}{r_d}. \quad (48)$$

4.3.1 Data for statistical evaluation of net cross-section resistance formula

To statistically evaluate the net cross-section resistance checks, our test results and results found in literature were used. Specimens that failed in net cross-section are evident from Table 11. Only those tests on bolted connections made of HSS found in literature with net cross-section failure mode were used in the evaluation. A series of 6 bolted shear connections that failed in net cross-section was tested in Finland (Kouhi, Korttesmaa, 1990). The connections with 4 bolts positioned rectangularly were made of steel grade equivalent to S620. Bolted connections with 3 bolts positioned parallel to loading were investigated by Aalberg and Larsen (March 1999). Two high steel grades (S460, S690) were used and 18 connections failed in net cross-section. Puthli and Fleisher (2001) tested bolted connections with two bolts positioned perpendicular to loading. Steel grade S460 was used and 4 connections failed in net cross-sections. The net cross-section, actual material parameters and maximum force of the results from literature are presented in Table 12. The specimens are denoted by authors' surname initial and specimen name used in the literature (e.g. PF 10 – Puthli, Fleischer spec. no. 10 as denoted in Puthli, Fleischer, 2001).

Experimental resistances are expressed by vector r_e . In Fig. 30 test results r_{ei} are plotted versus the theoretical resistance $r_{i,3}$. The scatter of data is small, except for the eccentric specimens where load is transferred through bolts. Sensitivity diagram in Fig. 31 suggest that the data set could be independent of bolt number and that hole eccentricity of specimens H and HH does not effect the resistance.

To exclude the effect of eccentricity, six data sets are formed. Data sets are formed as follows:

- data set 0: all results
- data set 1: only specimens with concentric holes
- data set 2: all specimens, except B1 with eccentric holes (specimens H, HH with eccentric holes are included)
- data set 3: all specimens with eccentric holes (H, HH, B1 eccentric)
- data set 4: only specimens B1 with eccentric holes
- data set 5: only specimens B1 (single bolt shear connections)

Table 12: Geometry and maximum force of specimens from literature

Specimen name	Actual A_{net} [mm ²]	Nominal A_{net} [mm ²]	Actual f_y [MPa]	Actual f_u [MPa]	F_{max} [kN]
KK H1	700,0	707,2	622	733	529,0
KK H2	936,0	915,2	622	733	679,0
KK H3	1121,0	1913,6	622	733	795,0
KK H4	851,0	832,0	622	733	652,0
KK H5	1058,0	1040,0	622	733	795,0
KK H6	1200,0	1164,8	622	733	890,0
PF 10	840,0	840,0	524	645	568,0
PF 11	997,5	997,5	524	645	630,0
PF 15	997,5	997,5	524	645	660,0
PF 16	1155,0	1155	524	645	762,0
AL 460-1	882,5	880	472	556	507,8
AL 460-2	876,4	880	472	556	506,4
AL 460-3	878,1	880	472	556	506,8
AL 460-4	845,7	840	472	556	487,8
AL 460-5	837,3	840	472	556	487,8
AL 460-6	834,8	840	472	556	492,9
AL 460-7	773,8	780	472	556	443,4
AL 460-8	776,1	780	472	556	442,4
AL 460-9	775,5	780	472	556	443,4
AL 700-1	888,8	880	820	873	768,6
AL 700-2	888,8	880	820	873	758,3
AL 700-3	884,3	880	820	873	750,0
AL 700-4	839,2	840	820	873	729,0
AL 700-5	837,8	840	820	873	727,0
AL 700-6	838,8	840	820	873	729,5
AL 700-7	786,2	780	820	873	678,7
AL 700-8	780,0	780	820	873	672,4
AL 700-9	786,2	780	820	873	673,3

4.4 Results of statistical evaluation and discussion

The results of statistical analysis are presented in Table 13. The difference in the value of partial factor γ_M^* for the data sets 1 and 2 is negligible. As mentioned above, the eccentricity of the hole at specimens H and HH did not affect the resistance.

In Figs. 30, 32, 34-35 the diagrams of experimental resistances versus theoretical resistances are plotted. If the resistance function was exact and complete, all points (r_{ti} , r_{ei}) would lie on the bisector of 1st quadrant. In general the points (r_{ti} , r_{ei}) show some scatter due to incorrect resistance model, scatter in material properties and error in geometry.

Table 13: Results of statistical analyses of design net cross-section resistance

Model	Data set	No. tests	k_n	k_d	b	V_δ	V_r	γ_M	γ_M^*
1 Eq. (14)	0	80	1,73	3,44	1,002	0,068	0,110	1,182	1,237
	1	70	1,73	3,44	1,007	0,027	0,091	1,138	1,143
	2	76	1,73	3,44	1,007	0,027	0,090	1,137	1,142
1*	0	80	1,73	3,44	1,113	0,068	0,110	1,182	1,113
	1	70	1,73	3,44	1,119	0,027	0,091	1,028	1,028
	2	76	1,73	3,44	1,118	0,027	0,090	1,137	1,027
2 Eq. (15)	0	80	1,73	3,44	1,071	0,098	0,131	1,229	1,252
	1	70	1,73	3,44	1,078	0,072	0,113	1,188	1,161
	2	76	1,73	3,44	1,077	0,070	0,111	1,185	1,157
3 Eq. (16)	3	10	1,73	3,44	1,286	0,239	0,254	1,524	1,635
	4	4	2,63	11,4	1,028	0,043	0,096	1,318	1,333
	4a	4	1,73	3,44	1,028	0,043	0,096	1,151	1,144
	5	8	2	5,07	1,020	0,031	0,092	1,156	1,151

4a – considered as large number of tests were performed (in factors k_n , k_d)

Resistance model 1, with correction factor b close to 1 and relatively small scatter, most appropriately describes the ultimate load of a net cross-section. According to Eurocode 3 partial factor γ_{M2} (with recommended value $\gamma_{M2} = 1,25$) should be assigned to this resistance model to form design resistance, since the resistance model is defined by fracture mechanism. For data set 1 it is clear that design resistance:

$$N_{t,Rd} = \frac{A_{net} f_u}{\gamma_{M2}} \quad (49)$$

meets reliability requirements of EN 1990, since partial factor $\gamma_{M2} = 1,25$ is greater than the value of $\gamma_M^* = 1,143$ (data set 1, Table 13). Moreover, design resistance (49) has also some extra safety for parameters which were not included in our analysis, like the effects of fabrication tolerances for hole position, that may be larger than assumed in V_{Xi} parameters. It was shown that additional partial factor should be approximately 1,1 (Sinur, Beg, 2008) to account for the characteristic value (as 5% quantile) of fabrication tolerance for hole position equal to ± 2 mm.

The resistance model 1 multiplied by 0,9 (further in the text referred to as resistance model 1*) and in combination with partial factor γ_{M2} forms the design net cross-section resistance as defined in EN 1993-1-1 given by equation (8). This design resistance was determined on the basis of tests (Snijder et al., 1988a. 1988b) mainly for steel grade S235. 77 tests for steel grade S235 and only a few test results for other steel grades (3 tests for A43 and 3 for StE460) were processed in that research. The estimator for variation coefficient for scatter $V_\delta = 0,139$ and correction factor $b = 1,242$ for steel S235 were high (Table I.7.3 in Snijder et al., 1988b) in comparison to the estimator for variation coefficients for scatter and correction factors in Table 13. The large scatter is the consequence of the fact that the test results came from many different sources with different test methods and different levels of accuracy. For steel grades A43 and StE460 the partial factors γ_M^* were even 1,570 and 1,554, respectively, although the estimators for variation coefficients for scatter V_δ were small, equalling 0,030 and 0,060, respectively. Due to small number of tests higher factors k_n and k_d had to be introduced, resulting in higher values γ_M^* that are higher than the value $\gamma_{M2} = 1,25$ accepted in Eurocode 3. From Table 13 it is clear that the obtained partial factor $\gamma_M^* = 1,028$ is below $\gamma_{M2} = 1,25$.

Resistance model 2 is conservative in nature. Nevertheless, the design resistance based on this resistance model and inappropriate partial factor may be too optimistic. If the design resistance of the net cross-section is based on resistance model 2, the partial safety factor should be larger than the value of $\gamma_M^* = 1,161$ (data set 1 in Table 13). Thus, partial factor $\gamma_{M0} = 1,00$ is not appropriate in equation (10). Consequently, the design resistance of the net cross-section according to the draft of EN 1993-1-12 is not consistent with EN 1990 reliability criteria. Based on these results the net cross-section design resistance was changed in the final draft of EN 1993-1-12 to be the same as in EN 1993-1-1 (equation (11) only).

According to EN 10025-6 (CEN, 2004b) a steel plate is classified as grade S690, if among several other conditions yield and tensile strengths satisfy the conditions: $f_{yn} \geq 690$ N/mm² and

$f_{un} \geq 770 \text{ N/mm}^2$. Considering the common ratio $f_u/f_y = 1,05$, which was for steel S690 and higher grades measured in several researches done around the world the nominal yield strength should not be lower than f'_{yn} to classify steel as S690:

$$f'_{yn} = \frac{f_{un}}{1,05} = \frac{770 \text{ MPa}}{1,05} = 733 \text{ MPa} . \quad (50)$$

Under the assumption $f_u/f_y = 1,05$, additional relative resistance or additional safety is present in the design resistance given by equation (10). This additional safety can be expressed as the ratio of yield strengths:

$$\gamma_{add} = \frac{f'_{yn}}{f_{yn}} = \frac{733}{690} = 1,06 . \quad (51)$$

Nevertheless, additional safety γ_{add} is smaller than the partial factor obtained in statistical analysis ($\gamma_M^* = 1,161$, see data set 1 in Table 13). This was more engineering approach to prove that design net cross section resistance (10) is not safe enough, at least for steel grade S690.

In the case of unsymmetrical members the test results showed that eccentricity of the hole was very important for specimens where loading was transferred through the bolt. For plates in tension with eccentrically drilled holes (specimens H and HH – different boundary condition) the eccentricity of the hole had almost no effect on the resistance. This fact is confirmed in Figs. 30-33, where the resistance models 1 and 2 (data set 0) are suitable for all specimens H and HH (including unsymmetrical ones). Models 1 and 2 give too optimistic values for unsymmetrically loaded specimens B1, where loading was transferred by means of the bolt. The small estimator for variation coefficient for scatter $V_\delta = 0,043$ and correction factor $b = 1,028$ indicates that data set 4 meets resistance model 3, which is appropriate for unsymmetrically connected members. Since only 4 results were available in data set 4, k_n and k_d factors are very large and consequently partial factor $\gamma_M^* = 1,333$ is large (see data set 4 in Table 13). The resistance model 4 can also be used for symmetrically connected elements with single bolt. Therefore, data set 5 was created. Now, all parameters are even more favourable and the value of partial factor drops to $\gamma_M^* = 1,151$ (see data set 5 in Table 13). If data set 4 was treated as a larger set, the k_n and k_d factors would be higher and a similar value of partial factor would be obtained (see data set 4a in Table 13). Thus, resistance model 3 could be formed with $\gamma_{M2} = 1,25$ and the design net cross-section resistance of unsymmetrically connected members in tension with one bolt (12) could also be applied to high strength steels.

Fig. 34 plots the theoretical resistances against the experimental resistance for all specimens with eccentric holes (data set 3) calculated according to resistance model 3. Because this resistance model is inappropriate for specimens H and HH with eccentric hole, the scatter of points and the value of $\gamma_M^* = 1,635$ are large (data set 3 in Table 13). The resistance of net cross-section of members with eccentric holes in tension may be verified according to equation (8) for concentric holes or conservatively also by equation (12) for eccentric holes.

Current ANSI/AISC 360-05, Specification for structural steel buildings (AISC, 2005), covers steel grades up to yield strength 690 N/mm² with some limitations. The standard gives two distinct methods: Load and Resistance Factor Design (LRFD) and Allowable Strength Design (ASD). LRFD is in principle equal to design approach according to Eurocodes. Under the assumption that the definition of the characteristic and the design value is equal to Eurocode, safety factors can be directly compared. In AISC 360-05 the design tensile strength of tension members should be the lower value obtained according to the limit states of tensile yielding in the gross cross section and tensile rupture in the net section. The yielding in the gross cross section for HSSs is almost never or never decisive because of very low f_u/f_y ratio. Hence, design tensile strength is

$$P_{n,u} = \phi f_u A_{net}, \quad \phi = 0,75. \tag{52}$$

Equation (53) is consistent with resistance formula (8) and resistance model 1*:

$$P_{n,u} = \phi A_{net} f_u = \frac{0,9 A_{net} f_u}{\gamma_{M,AISC}} \Rightarrow \gamma_{M,AISC} = \frac{0,9}{\phi} = 1,20. \tag{53}$$

Partial factor $\gamma_{M,AISC}$ is larger than $\gamma_M^* = 1,028$ for data set 1 in Table 13. Then it follows that equation (53) is acceptable according to reliability criteria of EN 1990. Furthermore, the design resistance function according to AISC 360-05 gives slightly less conservative values than equation (8) in EN 1993-1-1, where the recommended partial factor is $\gamma_{M2} = 1,25$.

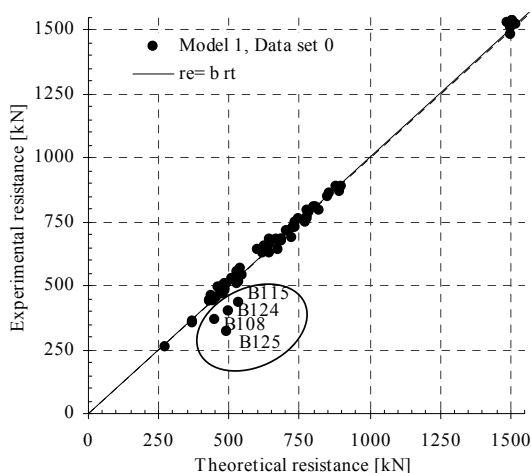


Fig. 30: (r_e, r_t) diagram – Model 1, data set 0

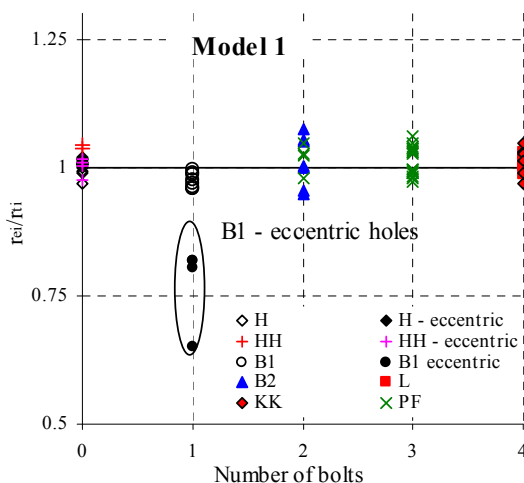


Fig. 31: Sensitivity diagram – Model 1

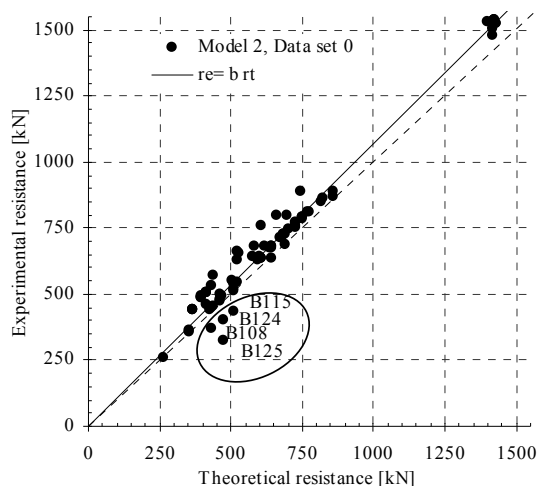


Fig. 32: (r_e, r_t) diagram – Model 2, data set 0

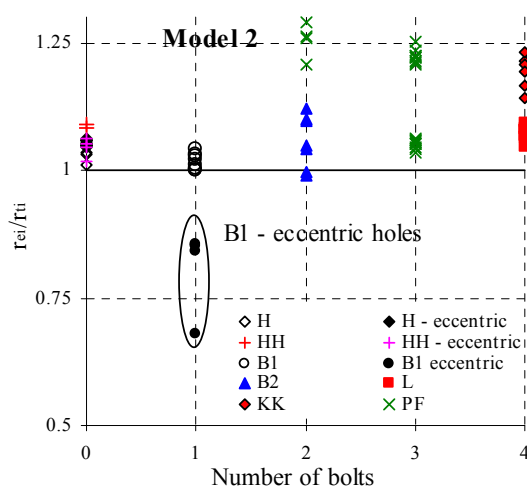


Fig. 33: Sensitivity diagram – Model 2

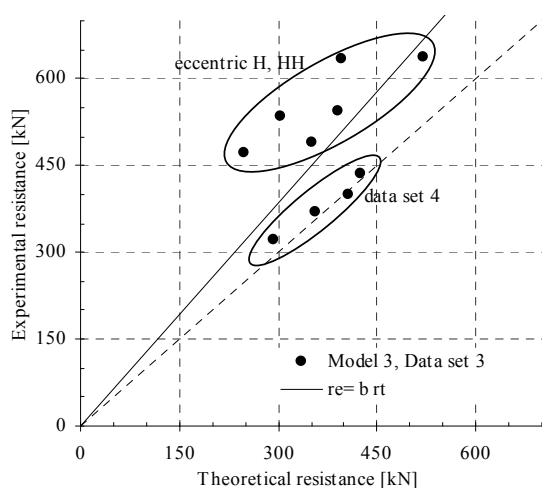


Fig. 34: (r_e, r_t) diagram – Model 3, data set 3

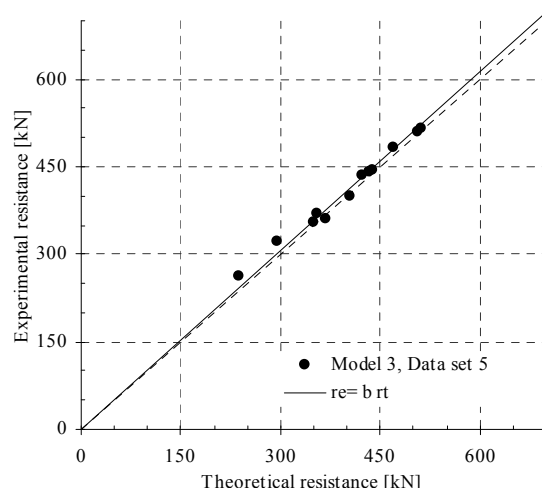


Fig. 35: (r_e, r_t) diagram – Model 3, data set 5

4.5 Summary

High strength steels, with a typical f_u/f_y ratio of 1,05, are considered to be less ductile than mild structural steel. Therefore it is believed that they are suitable only for elastic analysis. The problem is that inelastic behaviour is hidden in numerous nominally elastic resistance checks of steel structures and therefore sufficient local ductility has to be assured. In this chapter the net cross-section design resistance as it was defined in draft of EN 1993-1-12 was discussed. An extensive experimental research of plates with holes and bolted connections made of steel grade S690 (nominal yield strength $f_{yn} = 690 \text{ N/mm}^2$) was conducted to determine maximum resistance and ductility of the net section area. It was confirmed that a low f_u/f_y ratio does not affect local ductility significantly. All net section failures were ductile and comparable to failures of mild steels. However, a low f_u/f_y ratio does not allow yielding of gross cross-section and therefore net section check gains its importance.

The primary goal of this research work was the validation of design provisions for elements in tension by statistical analysis of experimental results. Local ductility and failure mechanisms of elements in tension were quantitatively and qualitatively assessed. Additionally, high strength steel net cross-section test resistances were gathered from literature to include different steel grades in the statistical evaluation. By statistical analysis of the test results according to Annex D of EN 1990 the following results were obtained:

- Net cross-section design resistance for high strength steels:

$$N_{t,Rd} = \frac{0,9A_{net}f_u}{\gamma_{M2}} \quad (54)$$

is with $\gamma_{M2} = 1,25$ safe. Moreover, it was established that this design resistance is very conservative for high strength steel sections. The partial factor needed is only 1,03 (data set 1 in Table 13). This design resistance has some extra safety for cases of accidental eccentric hole position and is safe even without factor 0,9.

- Additional rule for lower bound of net cross-section design resistance for high strength steels as was defined in the draft of EN 1993-1-12:

$$N_{t,Rd} = \frac{A_{net}f_y}{\gamma_{M0}} \quad (55)$$

(with $\gamma_{M0} = 1,00$) may not be safe enough. Based on our test results, the design resistance according to equation (55) was in the final draft of EN 1993-1-12 changed to equation (54).

- It was established that the design net cross-section resistance of unsymmetrically connected member in tension with one bolt may also be used for high strength steel sections, although EN 1993-1-12 disallows its use:

$$N_{u,Rd} = \frac{2(e_2 - 0,5d_0)tf_u}{\gamma_{M2}} \quad (56)$$

There are, however, two possibly arguable issues in our statistical analysis. The first relates to variation coefficients for material properties. Due to lack of more precise data, the same variation coefficients were used as for the evaluation of the design rules for bearing resistances and net cross-section resistances in ENV 1993-1-1 (Snijder et al., 1988b) where also some specimens made of S460 and S690 were included. The second relates to members in tension with staggered holes configuration. The tests for such members were not performed. In case of net cross-section failure a localized band, inclined to the specimen axis, was observed. The high local ductility was observed, as well. These facts indicate that the failure in a member with staggered holes could be formed in the plane connecting the staggered holes if the stag was not too large. In case the stag was very large, the fracture line would lay perpendicular to loading direction.

5 TENSION SPLICES WITH BOLTS IN SHEAR – FAILURE IN BEARING

5.1 Introduction

This chapter deals with tension splices with bolts in double shear. In these connections loads are transferred from one structural element to another through bolts by a bearing on the connected parts. Thus, the tension splices are also referred to as bearing type shear connections. In these connections the load enforces transverse shear in the bolts and high local compression stresses to the plate. The disadvantages of this bearing connection are initial sliding, low initial stiffness in shear and poor fatigue performance. On the other hand bolted shear connections with preloaded bolts are stiff in shear and offer good fatigue resistance, but are expensive mainly due to surface preparation and installing. In the connections with preloaded bolts, the bolts are preloaded so that compressive force is exerted on the connected parts. This gives rise to high frictional resistance which enables the load to be transferred between the connected parts. When the applied load exceeds the frictional resistance that can be developed between the plates, they will slip relative to each other, allowing the bolts to act in bearing. Only the first connection type with bearing bolts is discussed in this chapter.

This chapter presents the results of experimental work. The bearing resistance is presented in view of the Eurocode standard together with other results on bolted shear connections in HSS gathered from literature. A new modified approach to bearing resistance is presented and a new design formula for bearing resistance per bolt is statistically evaluated.

5.2 Design resistance of bearing type shear connections

According to EN 1993-1-12 (CEN, 2007) bearing type shear connections (category A acc. to EN 1993-1-8) should be checked against:

- *Gross and net cross-section design resistance*
Net cross-section resistance prevents rupture of net area in tension, while plastic resistance of gross cross-section prevents excessive deformations of whole member in tension. The resistances are defined in Chapter 4.1.
- *Design bearing resistance of individual fastener*
The definition of bearing resistance is given in Section 5.3. Considering that bearing resistance in Eurocode is limited by an average bearing stress to control deformation, the sum of bearing resistances should always be less than or at least equal to resistance to rupture, supposing that fasteners are strong enough. Therefore, sufficient material ductility is required.

- *Design shear resistance of fastener(s)*

The design ultimate shear load on each bolt should not exceed the design shear resistance of the fastener. Therefore, the distribution of bearing forces has to be predicted. The design shear resistance of all fasteners should be reduced by a reduction factor β_{Lf} when the distance L_j between the centres of the end fasteners in a joint, measured from the direction of force transfer, is more than $15d$. The reduction factor is given by (see 3.8 in (CEN, 2005b)):

$$\beta_{Lf} = 1 - \frac{L_j - 15d}{200d}; \quad 0,75 \leq \beta_{Lf} \leq 1,0 \quad (57)$$

This reduction does not apply where there is uniform distribution of force transfer over the length of a joint (e.g. the transfer of shear force between the web and the flange of a section).

- *Design resistance of group of fasteners*

The design resistance of a group of fasteners may be taken as the sum of the design bearing resistances of the individual fasteners provided that the design shear resistance of each individual fastener is greater than or equal to the design bearing resistance. Otherwise the design resistance of a group of fasteners should be taken as the number of fasteners multiplied by the smallest design resistance of any of the individual fasteners.

- *Design block tearing resistance*

Block tearing consists of failure in shear at a row of bolts along the shear face of the hole group accompanied by tensile rupture along the line of bolt holes on the tension face of the bolt group (see 3.10.2 in CEN, 2005b). For a symmetric group subject to concentric loading the design block tearing resistance $V_{eff,1,Rd}$ is given by:

$$V_{eff,1,Rd} = \frac{f_u A_{nt}}{\gamma_{M2}} + \frac{f_y A_{nv}}{\gamma_{M0} \sqrt{3}} \quad (58)$$

where A_{nt} and A_{nv} are net areas subjected to tension and shear, respectively. In case of eccentric loading only half of net area subjected to tension is considered.

- *Design shear resistance of bolt*

Another component in the bearing type shear connections is bolt exposed to transverse shear. The design shear resistance of the bolt is based on pure shear strength of the bolt material and is dependent of material grade and whether the shear plane passes through threads of the bolt. Throughout the thesis it is assumed that bolts can withstand bearing pressure.

5.3 Definition of bearing resistance at bolt holes

Bearing pressure between the bolt and the plate will cause elongation of the hole under increasing load until the weakest connection component fails. The failure may occur either as

bolt shear failure or as failure of the plate in net cross-section or bolt(s) tearout (block tearout). Therefore, the sum of ultimate bearing pressures between all bolts and plate should be less than or equal to the ultimate resistance of the connection. Thus, material bearing strength may be limited either by bearing deformation of the hole or by tearout of the material upon which the bolt(s) bear(s). American standard ANS/AISC 360-05 (AISC, 2005) defines bearing resistance separately in serviceability limit state (SLS) and in ultimate limit state (ULS). In SLS the bearing strength is defined by hole elongation equal to 6.35 mm (¼ in.) and in ULS an upper bound anticipates hole ovalization at maximum bearing strength. On the other hand, Eurocode gives a limit for mean bearing stress to control deformation. This limit stress was originally set to $3f_y$ (Snijder et al., 1988a).

In EN 1993-1-8 (CEN, 2005b) the design bearing resistance per bolt is defined as:

$$F_{b,Rd} = \frac{k_1 \alpha_b f_u d t}{\gamma_{M2}}, \quad (59)$$

where f_u is nominal ultimate tensile strength of the plate, d is bolt diameter, t is plate thickness and partial factor γ_{M2} with the recommended value of 1,25. Parameters α_b and k_1 are defined as given below and take into account mainly geometrical parameters:

- in the direction of load transfer

$$\alpha_b = \min\left(\alpha_d; \frac{f_{ub}}{f_u}; 1\right) \quad (60)$$

$$\alpha_d = \frac{e_1}{3d_0} \quad \text{for end bolts} \quad (61)$$

$$\alpha_d = \frac{p_1}{3d_0} - \frac{1}{4} \quad \text{for inner bolts} \quad (62)$$

- perpendicular to the direction of load transfer

$$k_1 = \min\left(2,8 \frac{e_2}{d_0} - 1,7; 2,5\right) \quad \text{for edge bolts} \quad (63)$$

$$k_1 = \min\left(1,4 \frac{p_2}{d_0} - 1,7; 2,5\right) \quad \text{for inner bolts} \quad (64)$$

In the previous definitions f_{ub} is nominal ultimate tensile strength of the bolt and d_0 is a bolt hole diameter. End distance e_1 , edge distance e_2 and pitches p_1 and p_2 are defined in Fig. 36. Maximum and minimum end and edge distances and pitches are limited in EN 1993-1-8, as well. Maximum dimensions are also related to the exposure of steel to corrosion and local buckling of plate in compression. Minimum dimensions set lower limit for the resistance and are indirectly related also to tolerances. Minimum distances are: end distance $e_1 \geq 1.2 d_0$, edge distance $e_2 \geq 1.2 d_0$, pitch $p_1 \geq 2.2 d_0$ and pitch $p_2 \geq 2.4 d_0$. Standard EN 1993-1-12 (CEN, 2007) gives no additions to any of these rules. Ratio f_{ub}/f_u in factor α_b considers cases where bolts have lower strength than plates in order to control deformations. Additional rules apply for non-standard bolt holes.

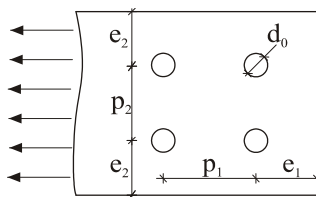


Fig. 36: Definition of distances

For a group of bolts the following statement is given in 3.7(1), EN 1993-1-8: “The design resistance of a group of fasteners may be taken as the sum of the design bearing resistances $F_{b,Rd}$ of the individual fasteners provided that the design shear resistance $F_{v,Rd}$ of each individual fastener is greater than or equal to the design bearing resistance $F_{b,Rd}$. Otherwise the design resistance of a group of fasteners should be taken as the number of fasteners multiplied by the smallest design resistance of any of the individual fasteners.” This paragraph was commented by Bijlaard (Bijlaard, 2006): “This statement is meant to persuade the designer to choose a balanced bolt pattern and to avoid having a relatively small end distance in combination with a relatively large pitch. A wrong design may lead to premature failure of the end bolts before the inner bolts reach their capacities. The capacity of the group of bolts will be overestimated in such cases.” In order to correctly predict a balanced bolt pattern and consequently the desired ductility and failure, the bearing resistance formula should accurately describe the phenomena and should also be supported by experimental results.

ANS/AISC 360-05 (AISC, 2005) defines the available design bearing strength ϕR_n at bolt holes as follows (resistance factor $\phi = 0,75$):

- When deformation at the bolt hole at service load is a design consideration

$$R_n = 1,2L_c t f_u \leq 2,4d t f_u . \quad (65)$$

- When deformation at the bolt hole at service load is not a design consideration

$$R_n = 1,5L_c t f_u \leq 3,0d t f_u . \quad (66)$$

In equations (65)-(66) parameter L_c is clear end distance in the direction of the force, between the edge of the hole and the edge of the adjacent hole or edge of the material ($p_1 - d_0/2$ or $e_1 - d_0/2$). For connections, the bearing resistance shall be taken as the sum of the bearing resistances of the individual bolts. Additional rules apply for long-slotted holes with the slot perpendicular to the direction of force.

5.4 Test results

5.4.1 One- and two-bolt shear connections – specimens B1, B2

Several failure modes were observed among 25 single bolt shear connections (specimens B1) and 13 two-bolt shear connections (specimens B2). Nominal and actual geometry of specimens is presented in Table 5, while the failure mode and maximum resistance are shown

in Table 14. In Table 14 failure mode, maximum force F_{max} and displacement at maximum force D_U for specimens B1 and B2 are displayed.

The experiment was also numerically simulated to obtain the stress state and to develop an effective numerical model for later simulations. Specimens that failed in different ways (B101 – net cross-section failure, B109 – plate shear failure, B111, B112 – splitting failure – see Fig. 37) were numerically simulated. Numerical model type M1 was applied for the simulation (see Chapter 3.2). Material model in terms of true stress – true plastic strain curve, applied in the simulation, is presented in Table 9 (see also Chapter 3.7). Additionally, numerical model M2 (see Chapter 3.3) was applied for the numerical simulation of B112. Friction coefficient $\mu = 0,25$ was used in the model. The choice of friction coefficient is explained in Chapter 3.3. The comparison of numerically and experimentally obtained load-displacement curves is presented in Fig. 38. The agreement of both (experimental and numerical) curves is outstanding. Numerical model M1 gave very satisfactory results for the determination of maximum resistance, while stiffness was in good agreement with the test only for specimens where deformations in thickness direction were not too large. The disadvantage of model M1 was corrected by model M2.

Table 14: Test results for specimens B1 and B2

Specimen name	Failure mode ^a	F_{max} [kN]	D_U [mm]	Specimen name	Failure mode ^a	F_{max} [kN]	D_U [mm]
B101	3	262	2,4	B201	3	457	2,4
B102	1	273	5,1	B202	1	471	5,8
B103	1	342	6,1	B203	3	643	4,3
B104	1	360	3,5	B204	3	638	3,9
B105	3	355	3,5	B205	3	689	6,2
B106	3	445	5,8	B206	1	596	6,7
B107	3	440	5,6	B207	3	789	10,4
B108*	3	370	4,0	B208	1	398	3,9
B109	1	228	5,2	B209	1	491	4,9
B110	1	286	5,8	B210	1	603	5,6
B111	1	363	6,4	B211	1,3	776	10,2
B112	1	483	8,9	B212	3	851	12,6
B113	3	516	8,5	B213	3	678	5,8
B114	3	510	9,1				
B115*	3	435	6,2				
B116	1	371	5,8				
B117	1	362	6,6				
B118	1	392	9,8				
B119	1	530	12,0				
B120	1	629	19,5				
B121	1,3	763	24,8				
B122	3	788	24,3				
B123	3	483	15,9				
B124*	3	400	10,0				
B125*	3	322	5,6				

* eccentric hole

- a 1 fracture in the specimen between hole and free edge perpendicular to the direction of load
 2 fracture in the specimen between bolt holes
 3 net cross-section failure

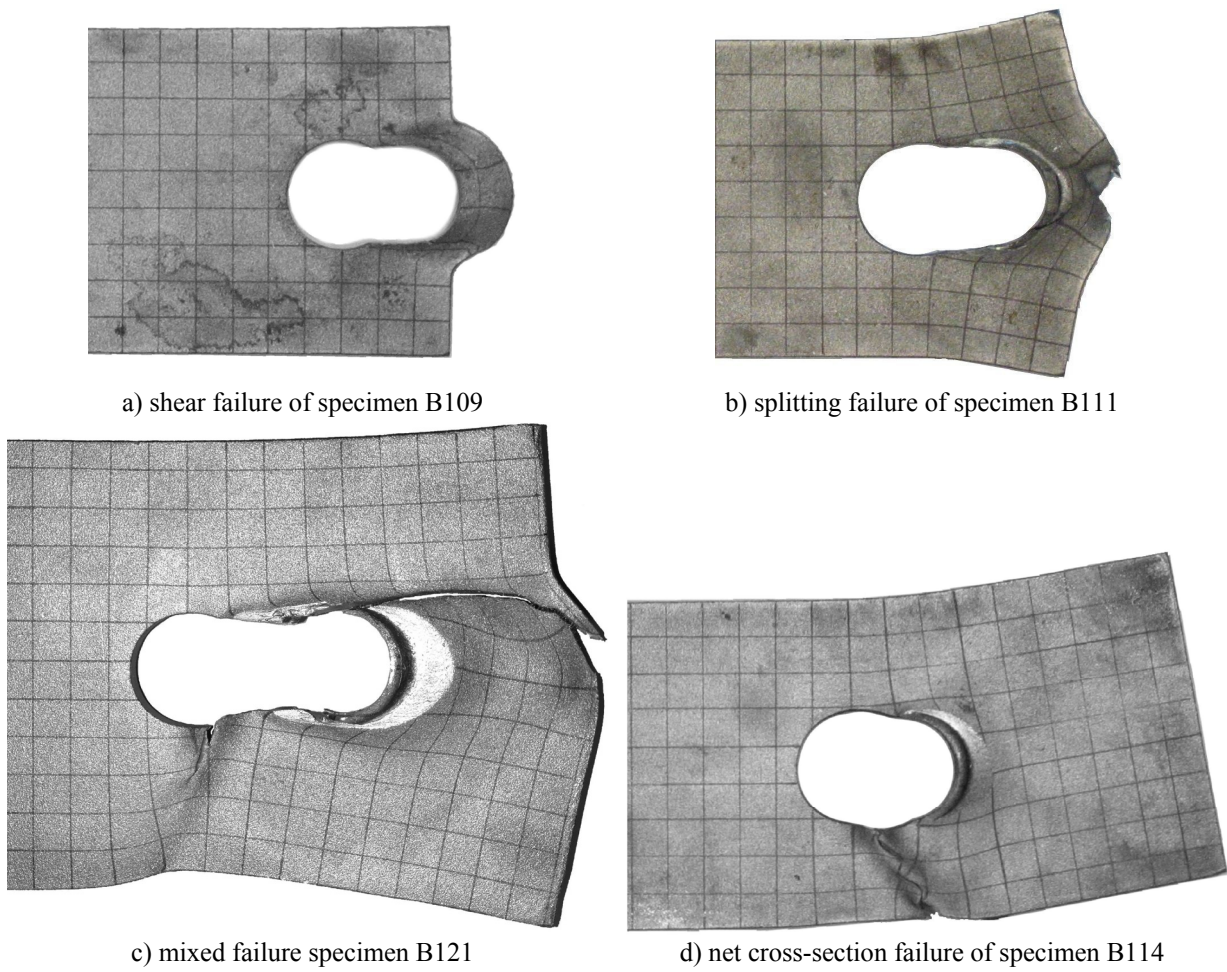


Fig. 37: Failure modes for specimens B1

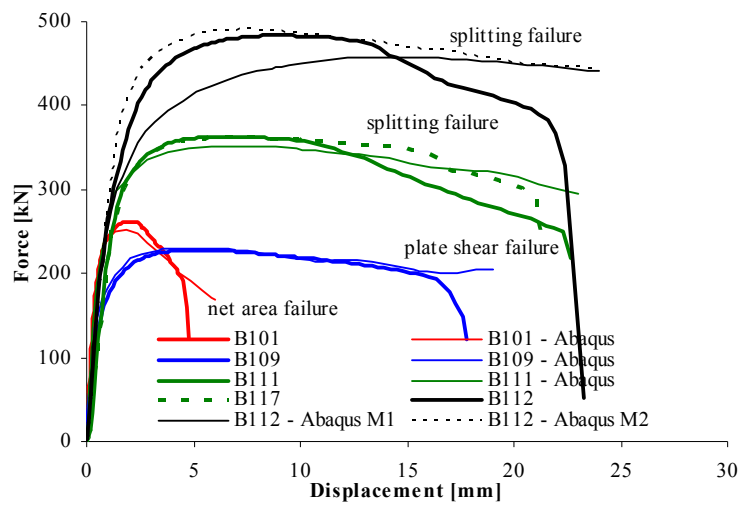


Fig. 38: Comparison of experimental and numerical load-displacement curves

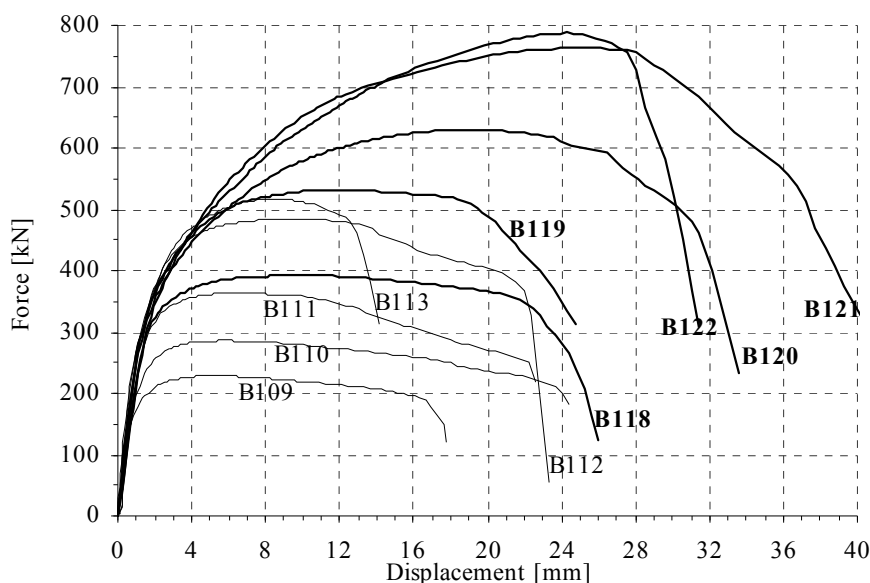


Fig. 39: Force-displacement curves for two groups of specimens with the same width

Fig. 39 illustrates load displacement curves for two groups of specimens. The first group includes B109 to B114 and the second group includes B118 to B122. The widths of specimens in the first and second groups were 90 mm ($e_2 = 1,5d_0$) and 120 mm ($e_2 = 2d_0$), respectively. End distance e_1 was the varying parameter. B109 (see Fig. 39a) and B118 *failed in shear*. The displacements at failure were approximately equal to clear end distance ($e_1 - 0,5d_0$). *Splitting failure* was observed at specimens B110, B111 (see Fig. 39b), B119 and B120 due to transverse tensile stress on a free edge perpendicular to load direction. Specimens B112, B121 (see Fig. 39c) almost reached net cross-section resistance. The necking appeared on the edge of the hole in the net cross-section, but splitting failure occurred sooner than the fracture in the net cross-section. These failures could also be characterized as *mixed failures*. Specimens B113, B114 (see Fig. 39d) and B122 *failed in the net cross-section* after hole elongation. The fractures were characterized as ductile failures (necking of net cross-section, reduction of thickness). The load displacement curves of all the remaining specimens are shown in Appendix B as well as in photographs of deformed specimens.

Shear failure of the plate due to bolt bearing occurred when the absolute and relative values of end distance e_1 were small enough compared to the edge distance e_2 (see Fig. 37a). This type of failure only occurred if the specimens were sufficiently wide for the net section not to yield. The fractures were instantaneous after excessive local plastic deformations of the specimen. The stress state of B109 at maximum resistance is shown in Fig. 40. Maximum principal stresses (Fig. 40c) were not able to hold back the steel in front of the bolt due to high shear (Fig. 40d) that caused the fracture (bolt tearout). It followed the path of high shear in a straight line. These kinds of failures were very ductile where load displacement curves were characterized by a long yield plateau (exp. as curve B109 in Fig. 39).

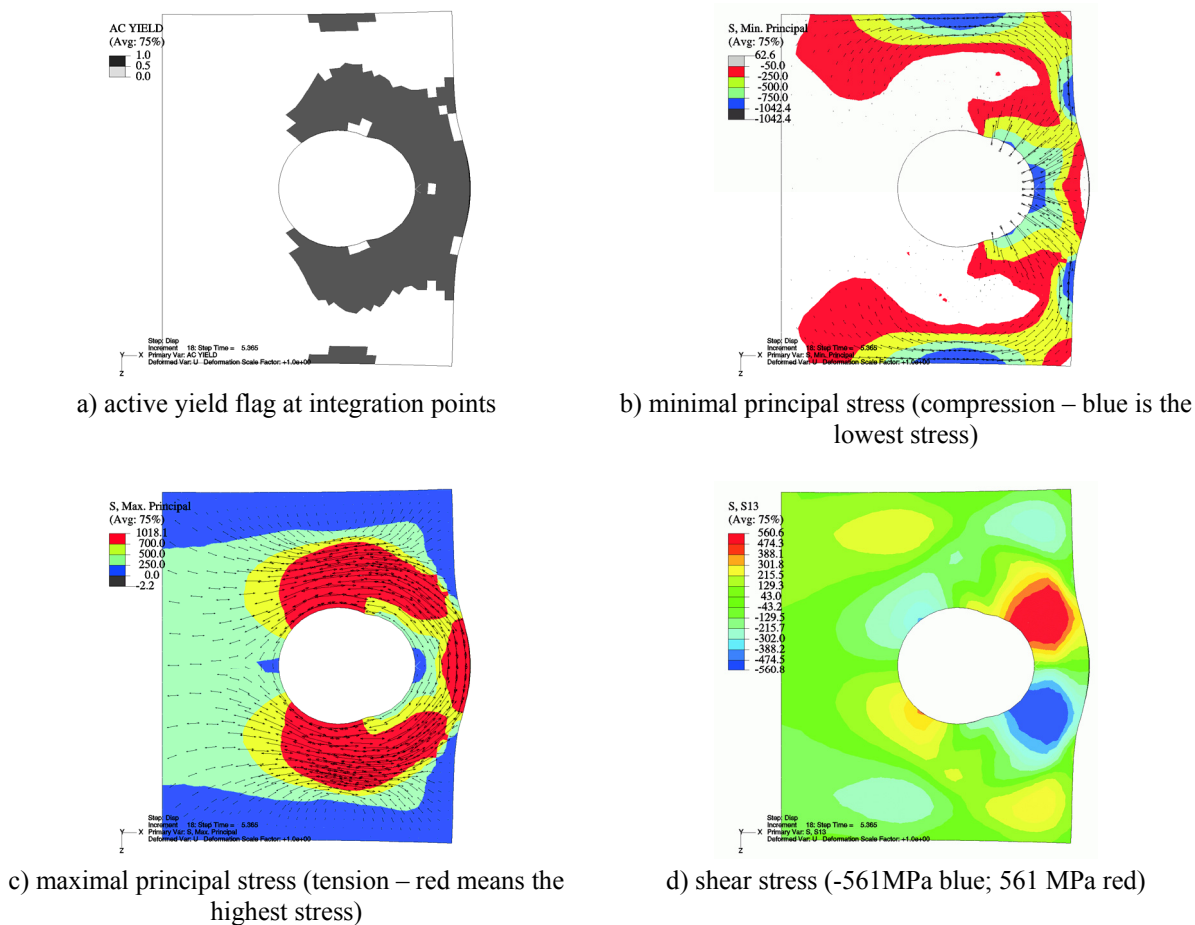


Fig. 40: Results of numerical simulation of B109 at 5,365 mm of hole elongation in the middle surface

If end distance e_1 was increased (at a constant edge distance e_2), specimens failed as shown in Fig. 37b – *splitting failure*. Numerical simulation of specimen B111 revealed that stress redistribution resulted in yielding of the area shown in Fig. 41a. Maximal principal stresses shown in Fig. 41c formed an arc of high tensile stresses that contained the bursting action. The free edge of the plate perpendicular to loading direction was subjected to high tensile stress which caused necking, followed by fracture which progressed to the area with the highest shear stress (see Fig. 41d) in a curved pattern, as shown in Fig. 37b. Minimal principal stress – mostly in compression – (Fig. 41b) forced the specimen to deform in thickness direction. These kinds of failures were characterized by higher resistance and larger displacement at maximum resistance than pure shear failures. The magnitude of plastic strain at integration points higher than 1 shown in Fig. 42 should be interpreted as rupture of the material.

At even larger end distances e_1 (narrow specimens) *net cross-section failure* prevailed (see Fig. 37d). The fracture formed after necking of the net area and after large bolthole elongation. The net cross-section resistance was also the maximum resistance possible for specimens of equal widths. The stress state of specimen B101 just after reaching the maximum resistance is illustrated in Fig. 43. Maximum principal stresses concentrated in the

net cross-section causing failure. It seems that load (ec)centricity is of vital importance at single bolt connections. Experimentally (Fig. 37d) as well as numerically (Fig. 43d) the necking and failure were observed only on one (the weakest) side of the specimen.

At certain end distance e_1 a *mixed failure* was observed, where splitting failure occurred simultaneously with net cross section failure (see Fig. 37c). Excessive plastic deformations of net section and plate in bearing were typical for this kind of failure. All types of failures were denoted by severe plastic deformations, especially in front of the bolt where steel literally flowed into the hole between the bolt and the bolthole in the adjacent plates. The specimens tended to deform in thickness direction. This caused pressure on adjacent plates and therefore introduced tension into the bolts. The bolts acted like a spring, which reduced the out of plane deformations.

The effect of restraining in thickness deformations on stiffness of load-displacement curves was observed in the test and in numerical simulation. This deficiency of model M1 was effectively suppressed by model type M3 which gave excellent results for specimen B112. To study different boundary conditions three specimens of equal geometry with different tightening force were tested. Specimens B111 and B116 were snug tightened, but to B116 additional half a turn of the nut was given. At specimen B117 a gap between adjacent plates was left for specimen to freely deform in thickness. The load displacement curves (see Fig. 44) and failures of all three specimens were very similar. Slightly larger maximum resistance of B116 went on account of friction between specimen and forks. Fracture in the tensile area opened later at unrestrained specimen B117 and therefore B117 developed higher resistance in the post-critical region. Therefore, the choice of numerical model M1, M2 or M3 is dependent on boundary conditions. It has to be considered that model type M1 shortens the computational time by 4,5 times.

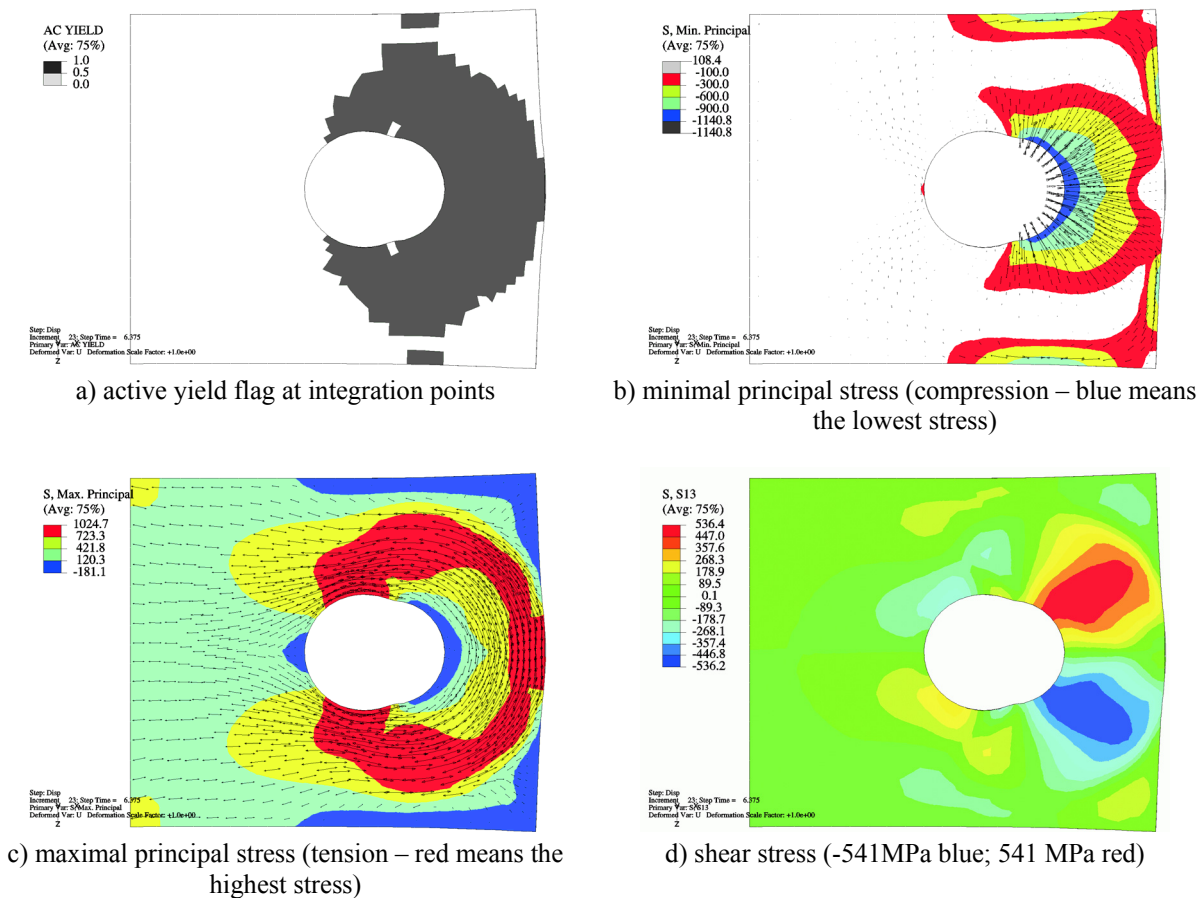


Fig. 41: Results of numerical simulation of B111 at 6,375 mm of hole elongation in the middle surface

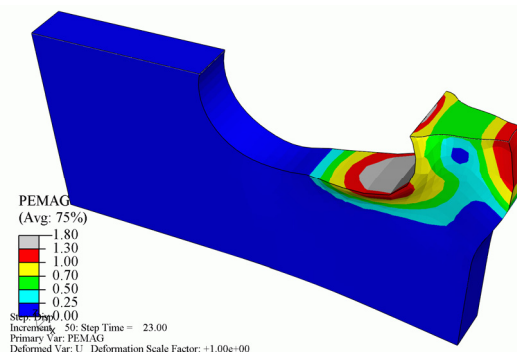
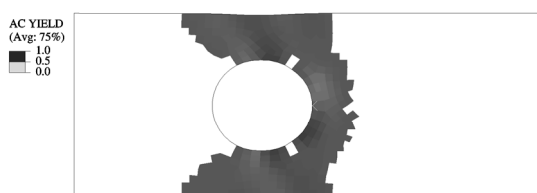
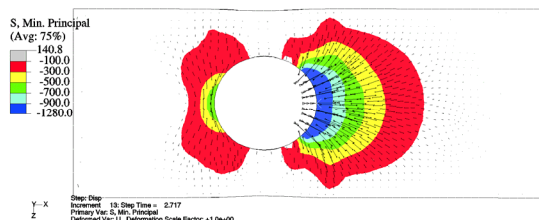


Fig. 42: Magnitude of plastic strain at integration points at failure – a cut through B111

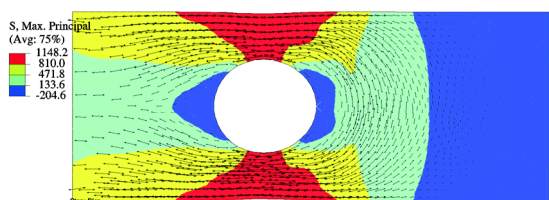
Larger geometry of single bolt connection in terms of end, edge distances results in large hole elongation at maximum resistance. The stiffness of load-displacement curves was equal to the point of yielding of the material (see Fig. 39). If the hole elongation was considered as a limit state, then the bearing resistance should be limited for connection with larger geometry (as e.g. B120-B122). The gradually decreasing stiffness of these geometries resulted in large hole elongations, long before maximum resistance was reached. On the other side, the stiffness of connections with smaller geometries decreased quickly. Thus, hole elongation at e.g. $0,8P_{max}$ was much lower than at maximum resistance P_{max} .



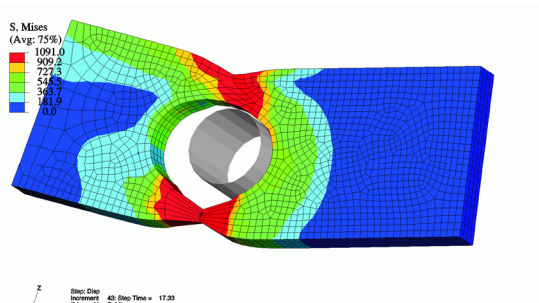
a) active yield flag at integration points



b) minimal principal stress (compression – blue means the lowest stress)



c) maximal principal stress (tension – red means the highest stress)



d) Mises stresses at 17,33mm of displacement

Fig. 43: Results of numerical simulation of B101 in the middle surface (a, b, c at 2,717 mm of displacement)

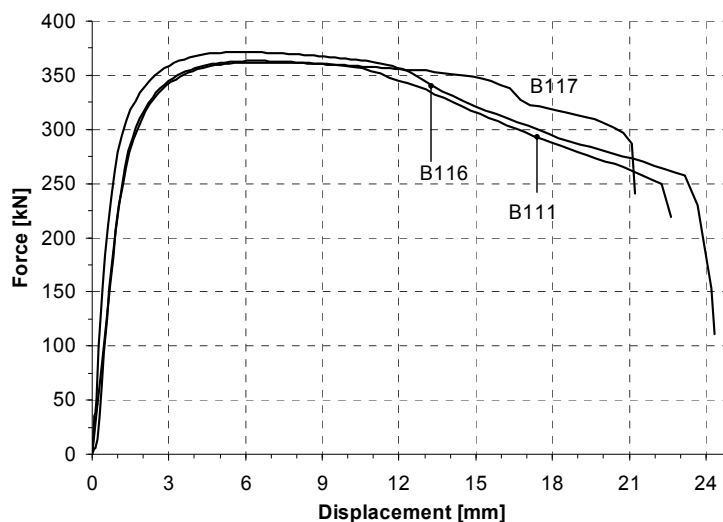


Fig. 44: Force-displacement curves for different boundary conditions

The failure modes of specimens B2 were similar to failure modes of specimens B1. Although, ratio $2e_2/p_2$ was varied from 0,89 to 1,25, the pitch p_2 had only a slight effect on the stress state. For these connections it is obvious that the bearing forces on both bolts are equal. Therefore, the results of specimens B2 can be directly compared to the results of specimens B1.

5.4.2 Bolted shear connections with 3 or 4 bolts positioned in the direction of load – specimens L

In the second experimental phase 9 three-bolt and 17 four-bolt shear connections were tested. All tests were numerically simulated in order to observe stress-deformation state and to obtain the distribution of bearing forces between bolts. Model type M2 (see chapter 3.3) with nominal geometry was applied in numerical simulations. Material model (see chapter 3.7) was based on material characteristics obtained from standard tensile test for plate II – S690 (see Table 3) since specimens were fabricated from that plate. The true stress – true plastic strain values are presented in Table 10. Friction coefficient $\mu = 0,25$ was used in the numerical simulations. The choice of friction coefficient is explained in Chapter 3.3. In Table 15 failure modes and maximum force F_{max} for specimens L are displayed.

Table 15: Test results for specimens L

Specimen name	Failure mode ^a	F_{max} [kN]
L01	1	778
L02	1	908
L03	2	1088
L04	1	1066
L04s	1	1057
L05	1	1185
L06	2	1386
L06s	2	1374
L07	1	945
L08	1	1294
L09	3	1521
L10	3	1522
L11	1	1155
L12	1	1268
L13	4	1329
L14	1	1425
L15	1	1501
L16	3	1537
L17	3	1539
L18**	3	1537
L18s	3	1533
L19	3	1507
L20	3	1527
L20s**	3	1480**
L21	1,4	1271
L22	1,4	1250

- a
- 1 fracture in the specimen between hole and free edge perpendicular to the direction of load
 - 2 fracture in the specimen between bolt holes
 - 3 net cross-section failure
 - 4 shear failure of the bolt
- ** test stopped before failure

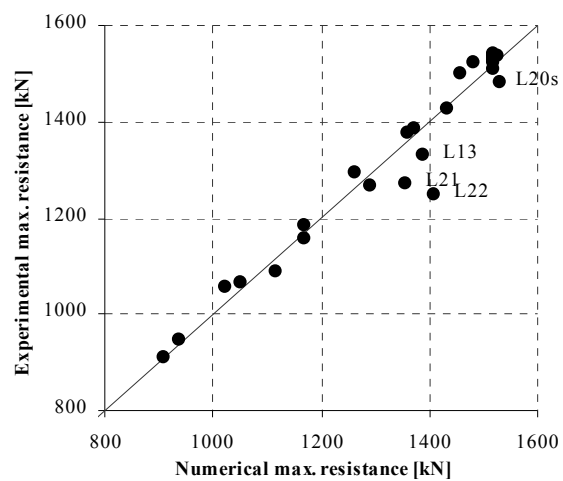


Fig. 45: Comparison of numerical and experimental resistances

The numerical response curves agree with the experimental ones in resistance (Fig. 45), stiffness and in deformation state (Fig. 46) for all kinds of failures. The only exceptions are the connections where bolt shear failure was observed (see Table 15 – L13, L21, L22) or where the test was stopped before reaching the maximum resistance (L20s). The numerical and experimental load displacement curves for all specimens are presented in Appendix C.

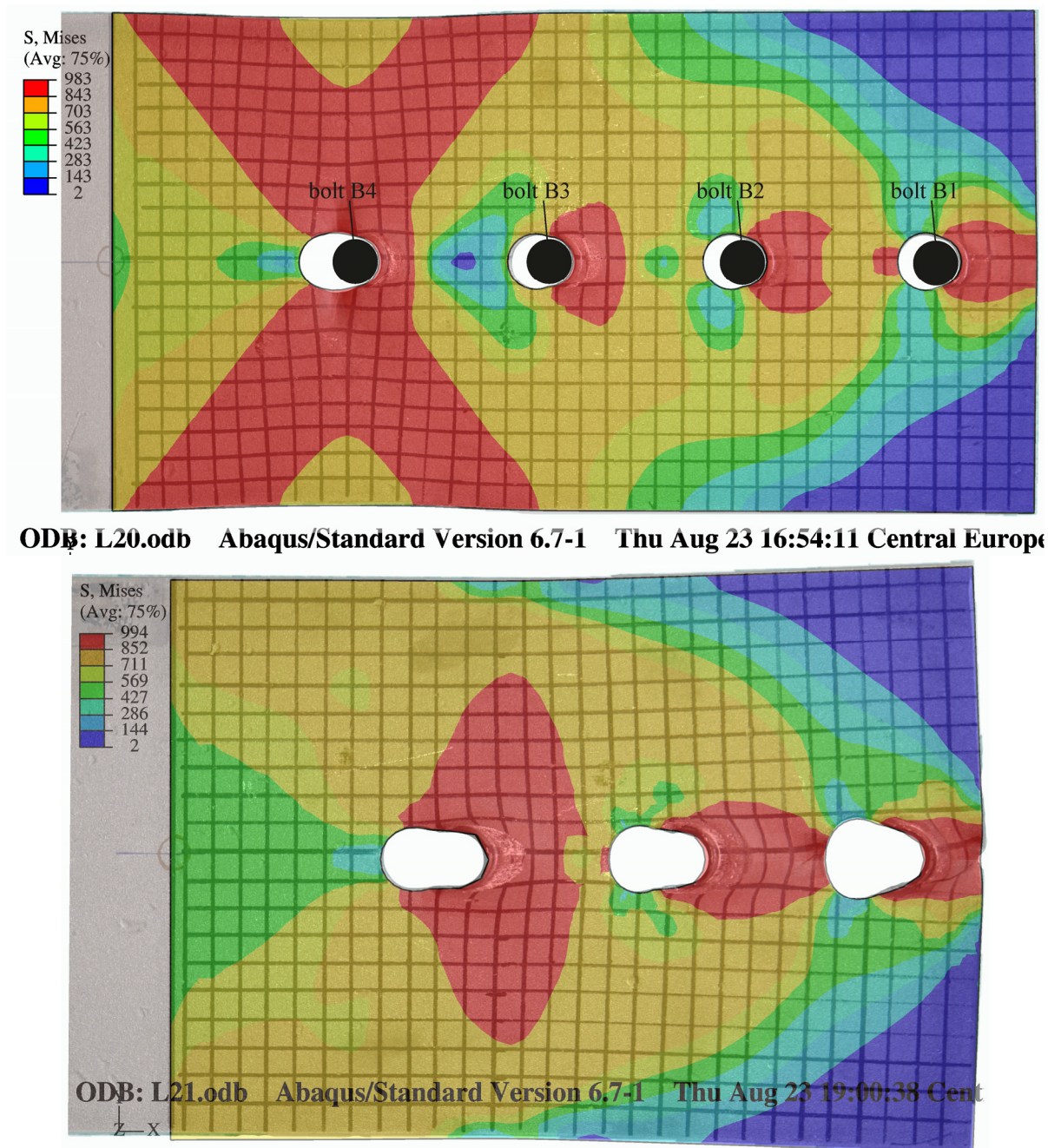


Fig. 46: Mises stress plotted over the actual specimens L20 and L21 (grid of lines), respectively

The bolts are denoted as B1, B2, B3 and B4, where bolt B1 is the closest to specimen's free edge (see Fig. 46). Similar notification is considered for holes. Hole H1 on the specimen is paired with bolt B1 and is considered as the first hole.

Bearing forces per bolts, friction, maximum resistance P_{max} and displacement at P_{max} for two sets of maximums are shown in Table 16. *Global maximums* refer to maximum resistance and *local maximums* refer to the resistance, where the first among all bolts reached its maximum resistance. The bolt that first reached the maximum resistance is printed in bold. *Local* and *global* maximums are also graphically presented in the sequel.

Table 16: Results of numerical simulations for specimen type L

Specimen name	Global maximums								Local maximums								
	U [mm]	P_{max} [kN]	B1 [kN]	B2 [kN]	B3 [kN]	B4 [kN]	Friction [kN]	ΣBi [kN]	U [mm]	P_{max} [kN]	B1 [kN]	B2 [kN]	B3 [kN]	B4 [kN]	Friction [kN]	ΣBi [kN]	
L01	5,7	813	176	241	278			117	696	2,9	771	178	227	271		94	676
L02	5,9	912	214	261	284			152	760	3,8	891	220	256	282		133	758
L03	8,7	1115	289	276	287			263	852	5,1	1088	294	282	290		222	866
L04	4,7	1052	159	210	265	279	138	913		2,3	988	169	201	242	261	115	873
L04s	7,3	1023	161	198	256	277	130	893		2,6	543	231	51	90	110	61	482
L05	5,1	1169	198	234	272	284	181	988		2,3	1061	209	214	241	260	137	924
L06	7,2	1374	273	261	281	281	277	1097		3,7	1309	285	260	273	280	211	1098
L06s	9,4	1360	275	247	277	281	279	1081		3,3	1000	320	154	188	200	138	862
L07	6,8	937	182	265	323			167	770	3,2	893	192	262	301		138	755
L08	5,9	1265	176	235	304	320	230	1035		2,9	1190	185	242	285	292	186	1004
L09	11,0	1481	225	279	319	323	333	1148		3,5	1372	256	275	298	299	244	1129
L10	11,0	1520	282	301	327	282	327	1193		4,0	1433	293	285	304	291	259	1174
L11	11,4	1172	207	308	364			293	879	3,2	1047	247	298	317		184	862
L12	12,2	1293	234	321	375			354	929	3,4	1127	279	306	322		211	907
L13	14,0	1390	263	338	380			408	982	4,2	1225	308	324	333		260	965
L14	15,3	1434	143	224	342	383	342	1092		3,7	1316	180	276	315	316	229	1087
L15	11,7	1458	183	243	344	349	339	1119		4,0	1365	206	279	319	316	246	1120
L16	10,4	1528	241	324	354	300	310	1219		4,1	1449	246	305	332	306	261	1189
L17	10,0	1519	277	313	338	273	318	1201		3,1	1395	275	289	299	293	239	1155
L18	8,6	1518	308	314	327	263	306	1211		3,1	1416	292	289	300	288	246	1170
L18s	10,0	1519	325	289	311	277	317	1202		3,7	1292	324	195	215	324	233	1058
L19	9,1	1518	324	312	323	258	301	1217		2,8	1388	286	283	294	290	235	1153
L20	10,4	1520	261	320	340	279	318	1200		3,4	1405	257	297	308	297	243	1158
L20s	12,0	1529	268	314	330	300	315	1212		4,2	1292	234	249	247	335	220	1066
L21	18,4	1357	203	336	459			350	998	4,3	1154	267	321	346		211	934
L22	18,0	1408	207	334	422			437	964	4,8	1212	274	330	345		255	948

Table 17 presents the dependency between connection geometry and maximum resistances. The nominal width of specimens in Table 17 is equal. The resistance of the connection was generally increasing if pitches p_1 , end distance e_1 or the number of bolts were higher. The upper limit of the resistance was net cross-section resistance (approx. 1537 kN). If the distances were even larger or the number of bolts was lower, the resistance was lower due to bolt shear failure. The connection geometry also dictated the type of failure.

If the end distance was small ($e_1 \leq 2d_0$) and smaller than the pitch p_1 ($e_1 < p_1$), a longitudinal crack was formed between hole H1 and a free edge perpendicular to load direction (see Fig. 47a). The crack was initiated primarily by transverse tension, which formed at the edge trying to contain the bursting action, as the specimen tended to splay out. This kind of failure was defined as a *splitting failure*. In several cases (L04, L04s, L07, L08, L14, L15, L21) a splitting failure between the hole H1 and the edge was simultaneously followed by another fracture between holes H1 and H2. The secondary fracture was also of a splitting type. The first crack opened in a curved pattern starting from a point on the free edge with the highest tension and ending on the edge of the hole with the highest shear stress, similar with at single bolt connection described earlier. The second crack just initiated at the back edge of hole H1. The test was stopped before it could progress. At specimen L21 bolt shear failure was followed immediately after the fractures. Shear failure of plate was surprisingly not observed

even at the smallest end distance $e_1 = 27$ mm combined with large pitch $p_1 = 66$ mm (specimen L14).

Table 17: Maximum (experimental) resistance [kN] versus connection geometry

3 bolt connections					4 bolt connections								
		e_1/d_0						e_1/d_0					
		1,5	2	2,5	3			1,2	1,5	2	2,5	3	5
p_1/d_0	2	778	908		1088	p_1/d_0	2		1066	1185		1386	
	2						2		1057			1374	
	2,5	945					2,5		1294		1521	1522	
	3		1155	1268	1329		3	1425	1501	1537	1539	1537	1507
	3						3					1533	
	3,5		1271				3,5			1527			
	3,5						3,5			1480			
3,77		1250				3,77							

Fig. 48 compares experimental and numerical load-displacement curves for specimen L14. The experimental curve was shifted due to initial position of the bolts in the experiment. The decrease in stiffness and the resistance were very accurately fitted by numerical model. Fig. 49 illustrates load-displacement curves of bearing forces on bolts. Its distribution became unequal at a small displacement (2,5 mm). The maximum resistance of bearing force on bolts B1 and B2 was reached at 4,4 mm of displacement (*local* maximum). The linear patterns of bearing forces at *global* and *local* maximums are shown in Figs. 50-51, respectively. Although the contact surfaces were small (Fig. 52), friction significantly influenced the connection resistance. Bolts restrained the deformation of specimen in thickness direction, while plate thickness increased due to high compression stress introduced by the bolts. The thickness of the plate increased only locally at the bolt. Therefore the frictional contact was formed only in the vicinity of the holes (Fig. 53). This can also be seen on the specimen surface as the shiny surface at holes (see Fig. 54a). In Fig. 54a the contours of Mises stress were plotted over the deformed specimen L14. The calculated deformation state accurately fits to the real one.

Figs. 54b-d show that the load was distributed over the whole specimen. Net cross-section yielded and due to small end distance e_1 the failure of net cross-section did not occur. The area of high compression stress (Fig. 54d) spread in width approximately $3d_0$.

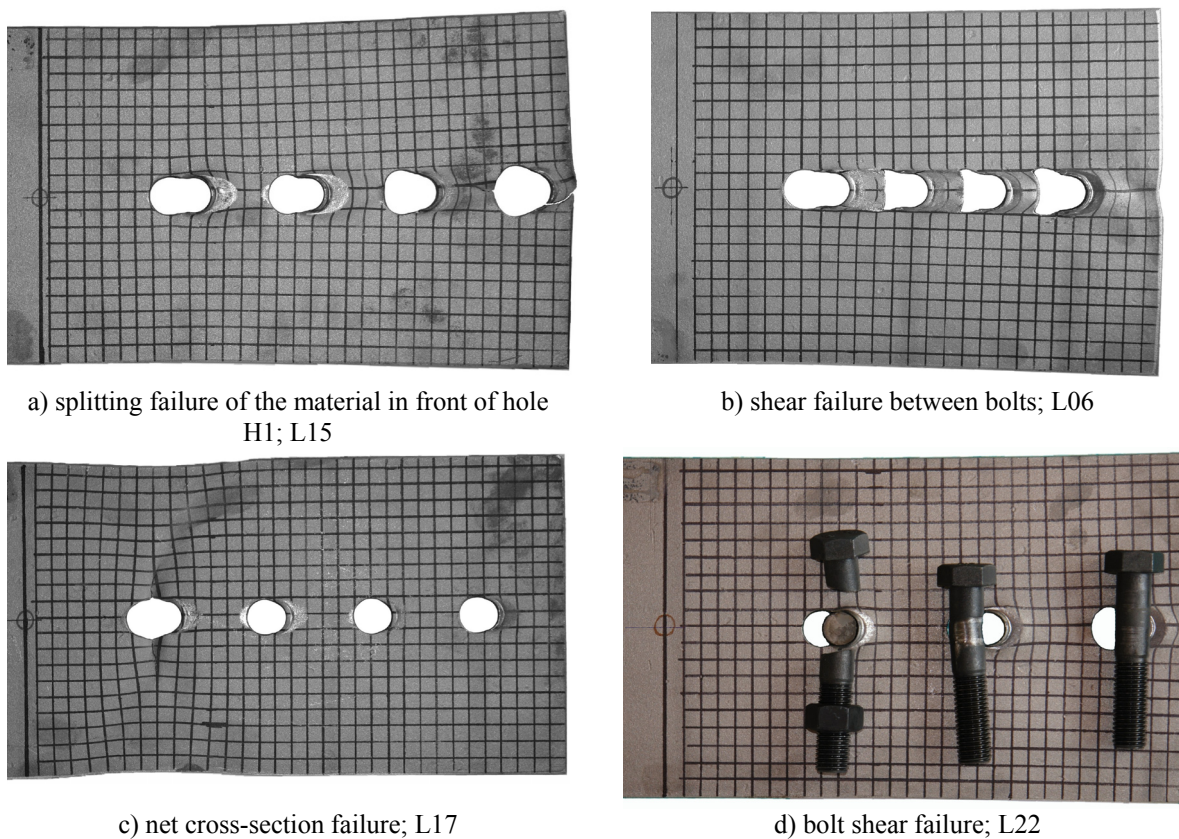


Fig. 47: Failure types of specimens L

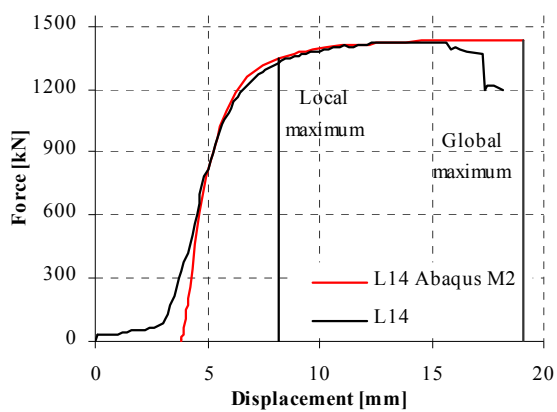


Fig. 48: Experimental and numerical load-displacement curves for specimen L14

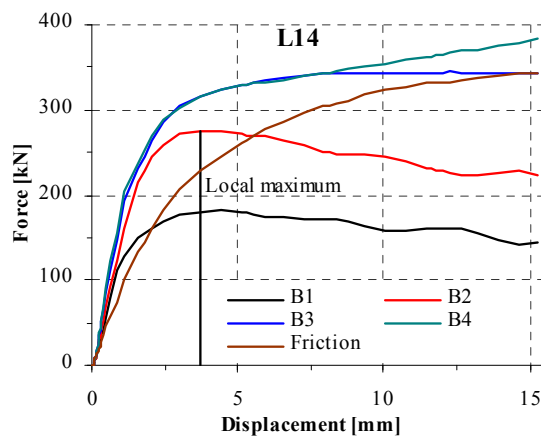


Fig. 49: Distribution of bearing forces and friction for specimen L14

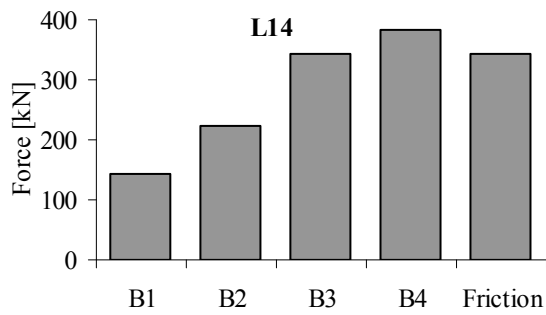


Fig. 50: Distribution of bearing forces and friction for specimen L14 at global maximum

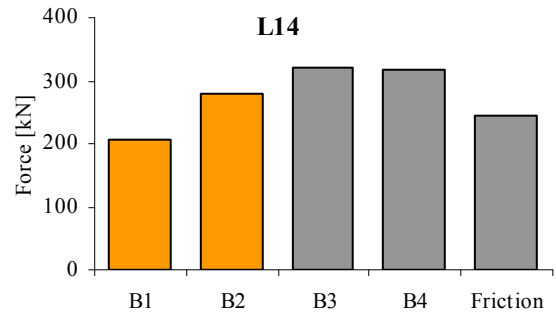


Fig. 51: Distribution of bearing forces and friction for specimen L14 at local maximum

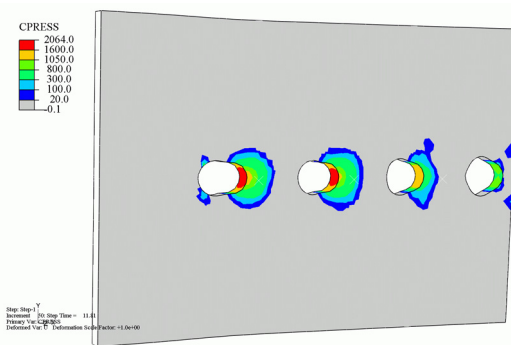


Fig. 52: Contact pressure at surface nodes for specimen L14

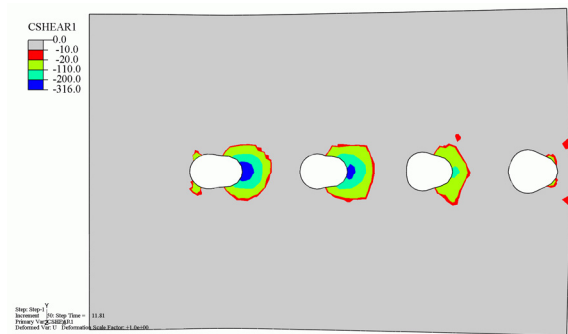
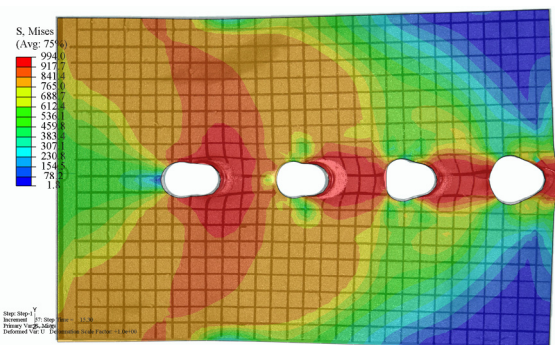
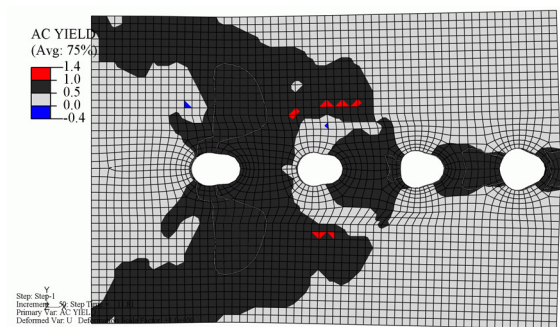


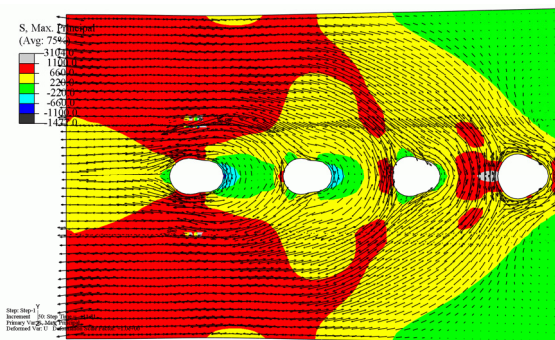
Fig. 53: Frictional shear stress at surface nodes for specimen L14



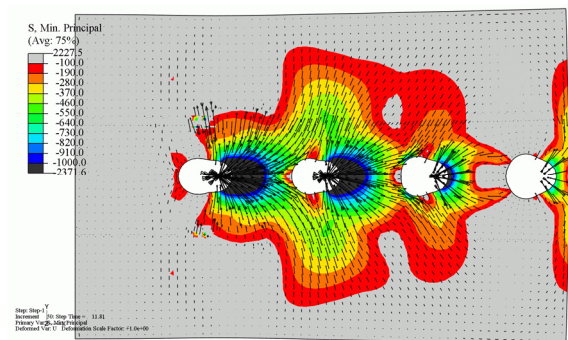
a) Mises stress plotted over actual specimen (grid of lines) L14 after failure



b) yield flag at displacement 11,8 mm



c) maximum principal stress at displacement 11,8 mm



d) minimum principal stress at displacement 11,8 mm

Fig. 54: Stress state of specimen L14 in the middle surface

If the end distance e_1 was large ($e_1 \geq 3d_0$) and the pitch p_1 was small ($p_1 \approx 2d_0$), the capacity of the material between holes was exhausted (see Fig. 47b, Fig. 55a). Two fractures usually formed symmetrically to the bolt line. The direction of the fractures coincided with maximum shear stresses in the plate (Fig. 55e) and they usually opened between all holes simultaneously. Transverse tension in the area between free edge and hole H1 (Fig. 55c) caused necking of the material, while pitches p_1 were too small for the development of transverse tension. High ductility (Fig. 56) and equal distribution of bearing forces (Figs. 57-59) characterized this failure mode. This second type of failure can be considered as a *shear failure*.

The third type of failure was a typical *net cross-section failure* (Fig. 47c) with two types of tensile flow instabilities. The diffuse necking as the first unstable flow was followed by localized necking, where the neck was a narrow band about equal to the plate thickness inclined at an angle to the specimen axis, across the width of the specimen (Fig. 46, Fig. 60a,c). This kind of failure is distinctive for a sheet tensile specimen, where width is much greater than thickness. Failure was ductile due to bolthole elongations and necking. The experimental load-displacement curve (Fig. 61) was characterized by initial sliding and several plateaus before reaching its true stiffness. This was due to bolthole clearance and geometrical tolerances of the forks to which specimen L18 was attached. Distribution of bearing forces between bolts was balanced equally, although bearing force on bolts B4 decreased when net cross-section yielded (Figs. 62-64). The pattern of bearing forces is also noticeable from minimum principal stresses in Fig. 60d. Friction had significant impact on resistance (Fig. 62), as well. Its magnitude at maximum resistance was equal to bearing force of one bolt (see Fig. 63).

The shear failure of the bolt was observed at specimens L13, L21, L22. In all three cases the last bolt B3 failed. Shear deformation of the bolt (Fig. 47d) was small due to high steel grade of the bolts 12.9. In these cases the numerical load-displacement curves deviate from the experimental ones, because the bolts were modelled elastically (Fig. 65).

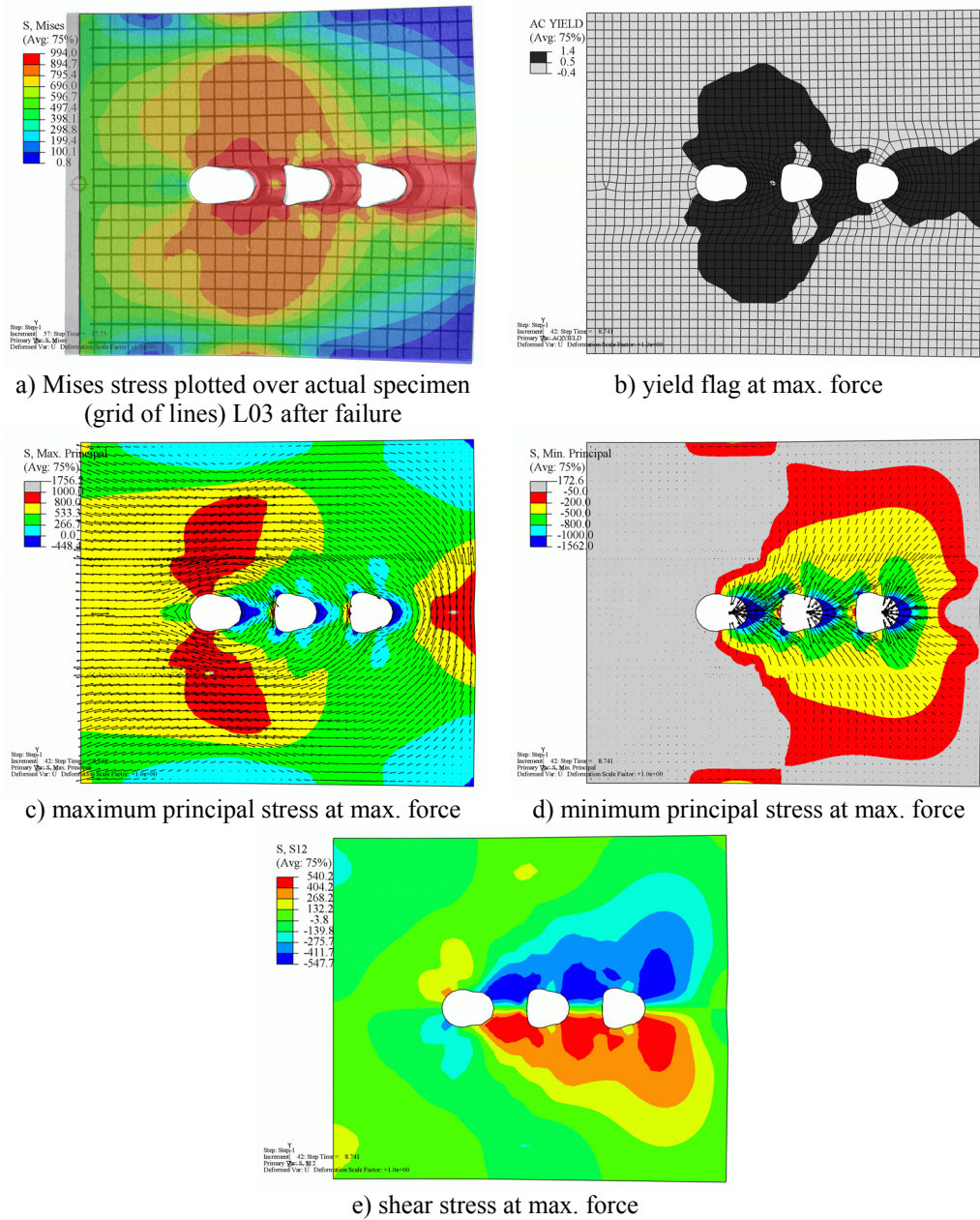


Fig. 55: Stress state of specimen L03

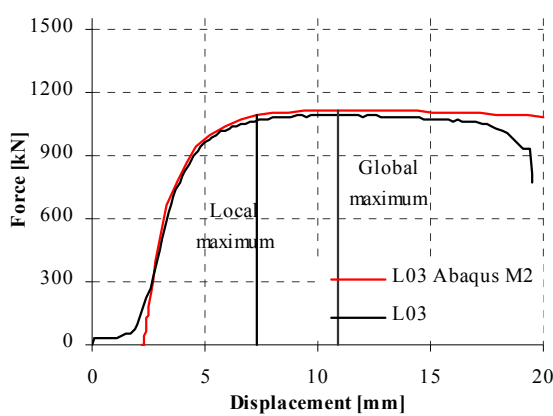


Fig. 56: Experimental and numerical load-displacement curves for specimen L03

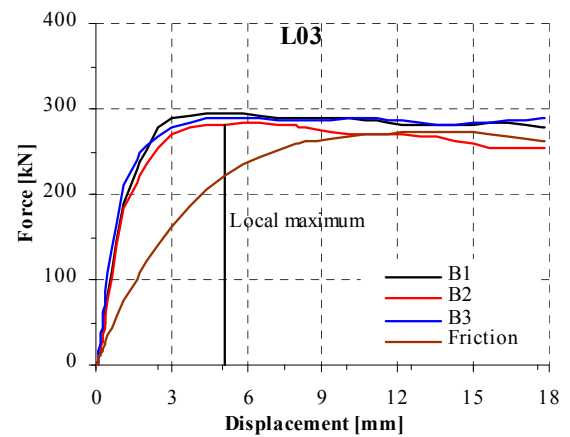


Fig. 57: Distribution of bearing forces and friction for specimen L03

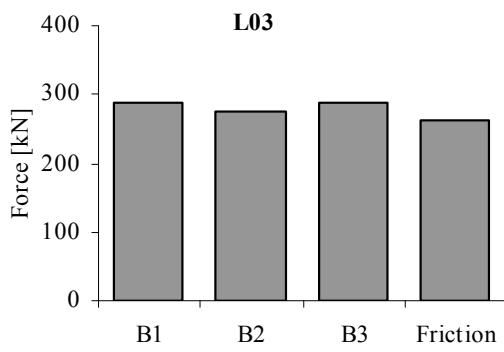


Fig. 58: Distribution of bearing forces and friction for specimen L03 at global maximum

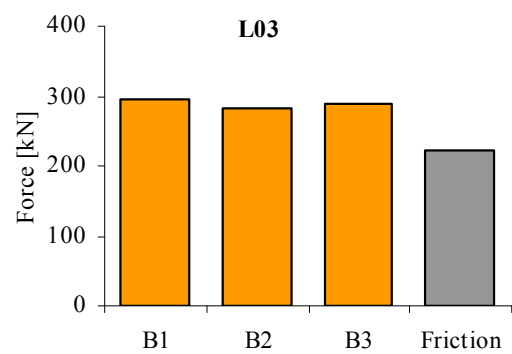
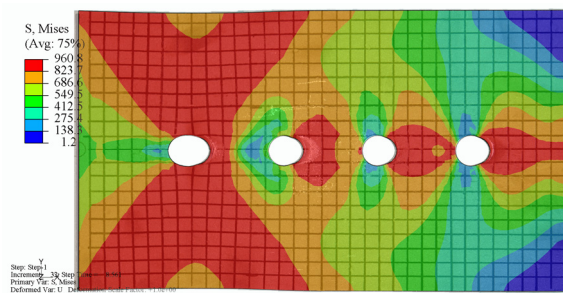
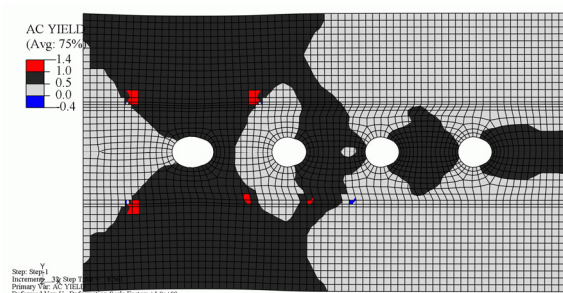


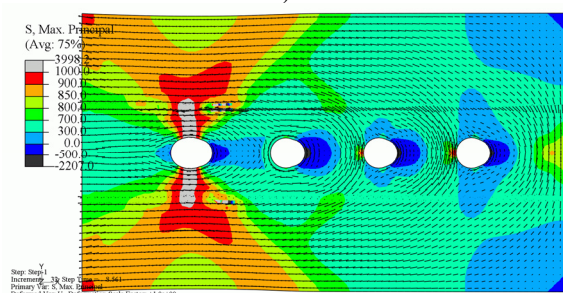
Fig. 59: Distribution of bearing forces and friction for specimen L03 at local maximum



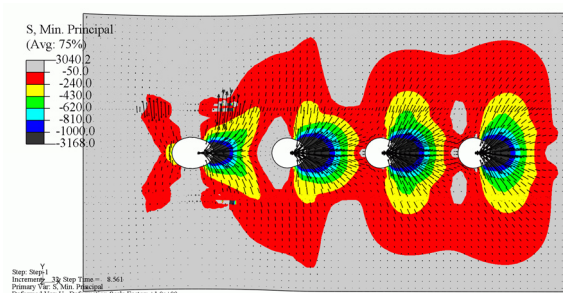
a) Mises stress plotted over actual specimen (grid of lines) L18



b) yield flag



c) maximum principal stress



d) minimum principal stress

Fig. 60: Stress state of specimen L18 in the middle surface at maximum force

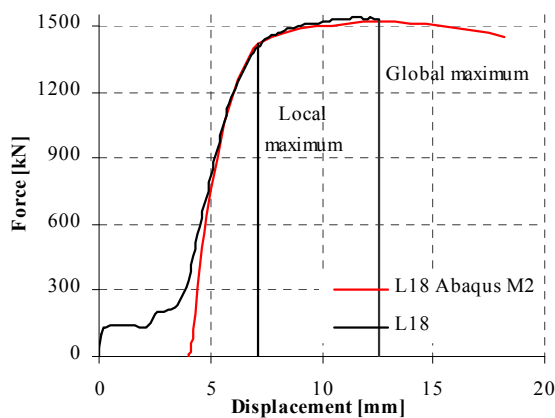


Fig. 61: Experimental and numerical load-displacement curves for specimen L18

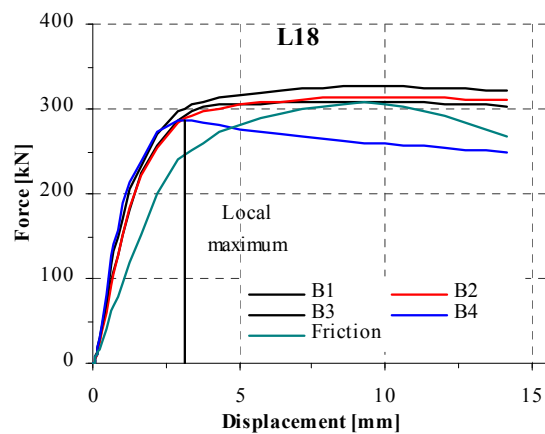


Fig. 62: Distribution of bearing forces and friction for specimen L18

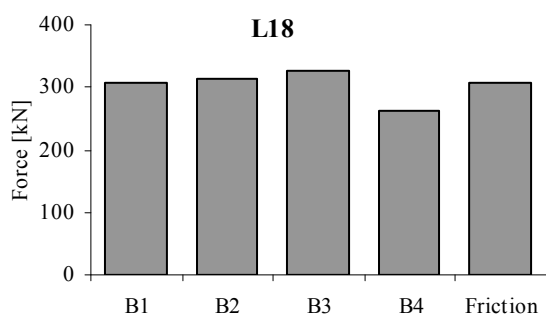


Fig. 63: Distribution of bearing forces and friction for specimen L18 at *global* maximum

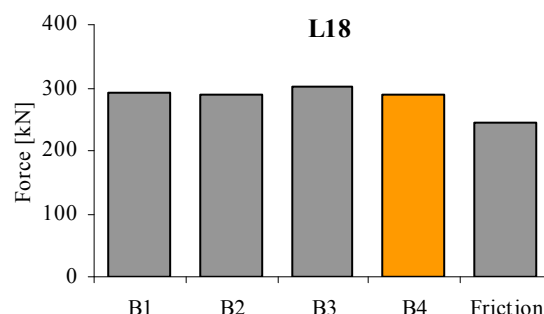


Fig. 64: Distribution of bearing forces and friction for specimen L18 at *local* maximum

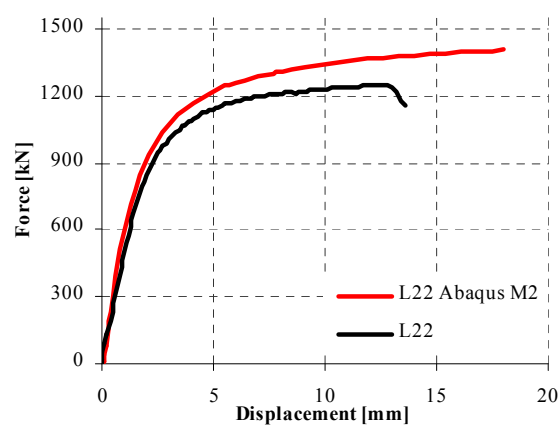
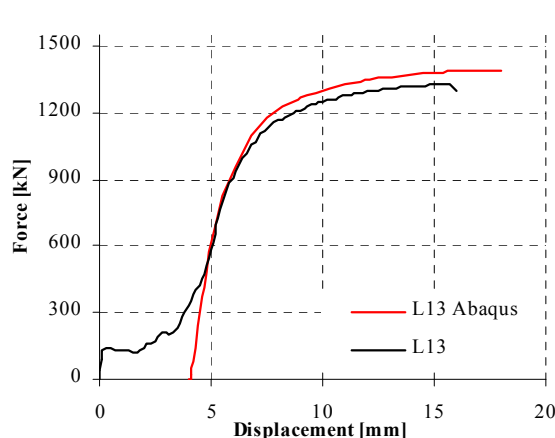


Fig. 65: Experimental and numerical load-displacement curves for specimens L13 and L22, respectively

It has been presented that distribution and magnitude of bearing forces depend mainly on the geometry, number of bolts and on the stiffness of the plates.

The average ratio between *local* connection resistance and *global* maximum connection resistance is 0,9 (see Table 16). Nevertheless, the displacement at which *local* resistance was reached was up to four times lower than the displacement at maximum global resistance. This indicates a long yield plateau for certain geometries (see Fig. 48). There are two extreme distributions of bearing forces. On one hand there is unequal distribution of bearing forces, where bolt B1 transfers the smallest load and the last bolt the highest load (Fig. 51). This force pattern is typical for specimens with end distances smaller than the pitches, where the fracture formed on the free edge. On the other hand, equal distribution of bearing forces was observed at specimens with pitch larger than end distance (Figs. 58, 63). This distribution led to failure of the material between bolt holes (Fig. 47b) or to the net cross section failure (Fig. 47c). If the failure occurred between boltholes, the distribution remained equal at *local* and *global* maximums (Figs. 58-59). At net cross-section failure the distribution of forces remained equal to the *local* maximum (Fig. 64) and after that the force on the last bolt (B4) decreased (Fig. 63). Thus, at the global resistance the load on the last bolt was the smallest, whereas the load on the remaining bolts remained more or less equally distributed.

The stiffness of the connections with several bolts in the direction of loading was larger than the stiffness of single bolt connections. The displacements at maximum resistances for specimens L were from 5 to 18 mm (Table 16). These caused average hole elongations up to 6 mm. Therefore, the limitation of hole elongations is not necessary.

Surprisingly, friction had significant impact on resistance and also on failure mode. Its magnitude at maximum resistance was equal to bearing force of one bolt (see Figs. 50, 58, 63). Although the bolts were only snug tightened, the friction developed due to high bearing pressure. The stress peaks were eliminated by yielding of the material. Therefore, the plate plastically deformed in thickness creating pressure on the cover plates. The deformation was restricted by bolts that acted as elastic springs. The contact area generating the friction was actually quite small (see Fig. 52), located in the bearing (stressed) edge of bolt holes. Due to large friction force, net cross-section failure could develop instead of some other failure mode. Moreover, this friction force is hard to estimate and should therefore be interpreted with caution.

The effect of functional tolerances the distribution of bearing forces

The functional fabrication tolerances had almost no effect on the connection resistance. As expected, the distribution of bearing forces between bolts was affected. Load displacement curves for connections with perfect (L04, L06) and shifted (L04s, L06s) geometry are plotted in Figs. 66-71. In both connections with shifted holes (L04s, L06s) the hole closest to the free edge was shifted by 2 mm (equal to bolthole clearance), thus bolt B1 was activated before all the remaining bolts. The connections behaved as single bolt shear connections for the first 2 mm of deformation (bolthole clearance). Figs. 72, 73 illustrate Mises stress just before bolts B2-B4 were activated. The red area indicates stress higher than yield stress. After that the remaining bolts were activated and the distribution of bearing forces tended to become equal to the connection with perfect geometry (see Figs. 66-67, 74-75). In the previous tests of single bolt shear connections it was shown that the maximum resistance of the connection was developed at a displacement much larger than 2 mm (Table 15, Fig. 39). Therefore, the significant decrease of bearing force on bolt B1 (Figs. 70, 71) was merely load redistribution and not connection component failure. At L06 and L06s the bearing force reached *local* maximum on bolt B1 at 285 and 320 kN (Fig. 77), respectively. Bearing forces on the remaining bolts were always lower than 285 kN (Figs. 75, 77). In case of specimen L06s, the maximum bearing force on the bolt increased by 12% due to fabrication tolerances. This increased bearing force should be accounted for especially in case of slotted holes with the slot parallel to the direction of the bearing force, otherwise bolt shear failure might be critical.

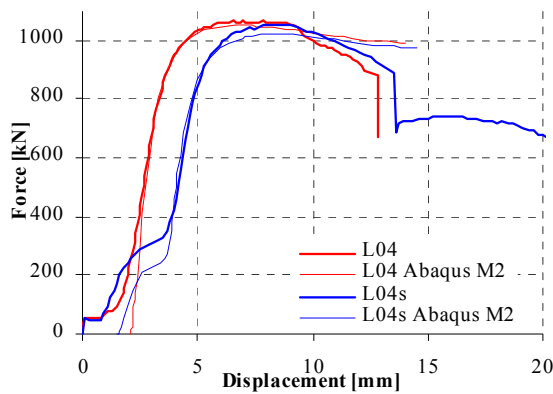


Fig. 66: Experimental and numerical load-displacement curves for specimens L04, L04s

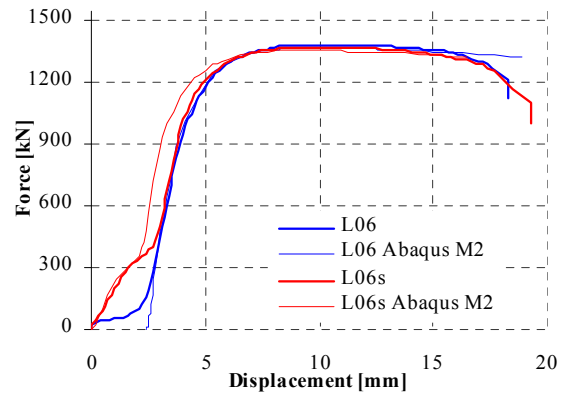


Fig. 67: Experimental and numerical load-displacement curves for specimens L06, L06s

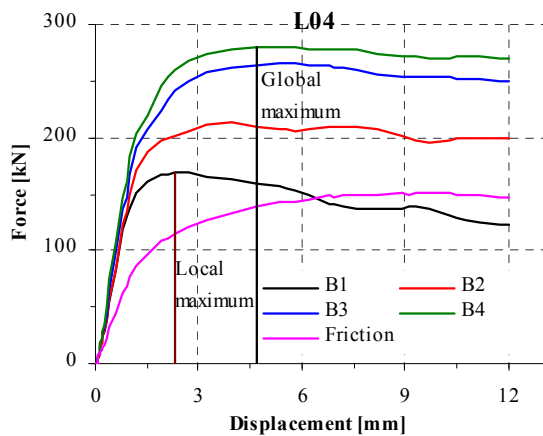


Fig. 68: Distribution of bearing forces and friction for specimen L04

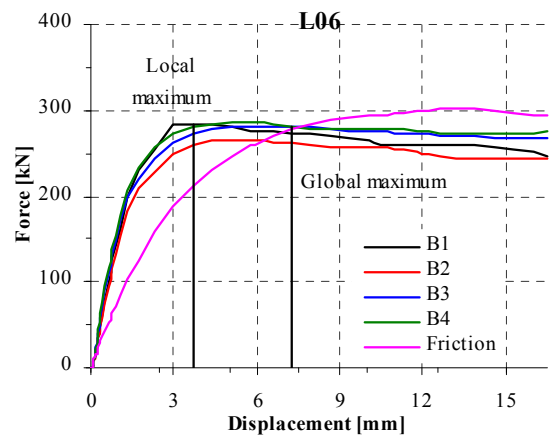


Fig. 69: Distribution of bearing forces and friction for specimen L06

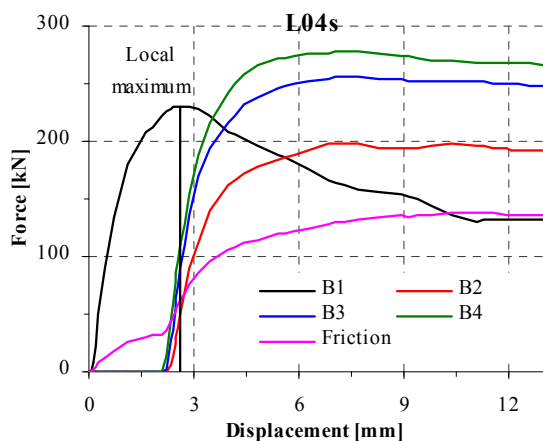


Fig. 70: Distribution of bearing forces and friction for specimen L04s

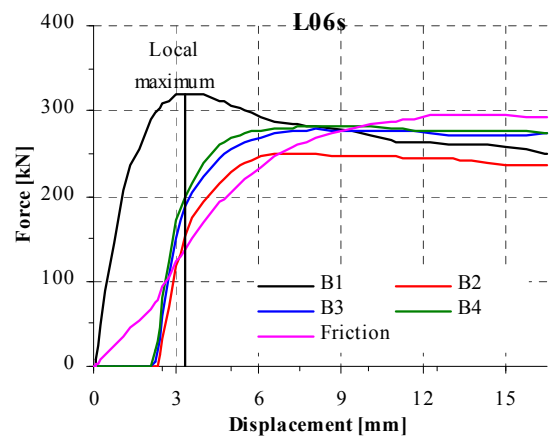


Fig. 71: Distribution of bearing forces and friction for specimen L06s

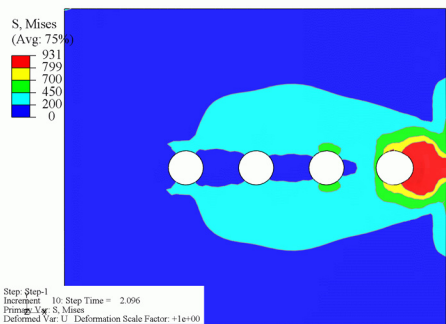


Fig. 72: Distribution of bearing forces and friction for specimen L04s

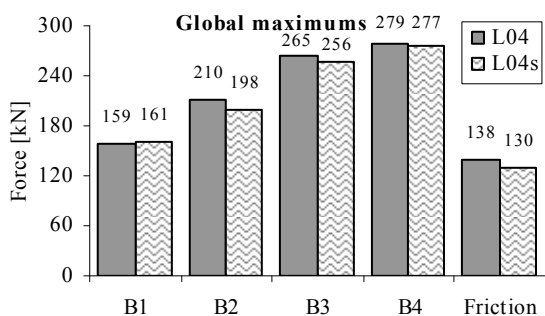


Fig. 74: Distribution of bearing forces and friction for specimens L04, L04s at global maximum

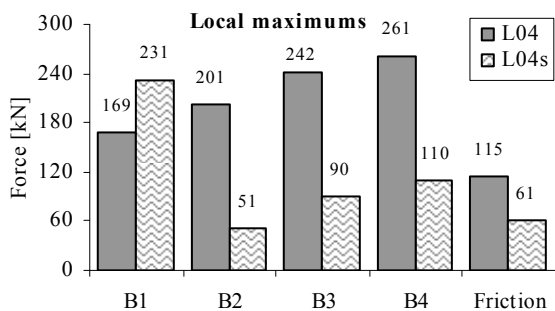


Fig. 76: Distribution of bearing forces and friction for specimens L04, L04s at local maximum

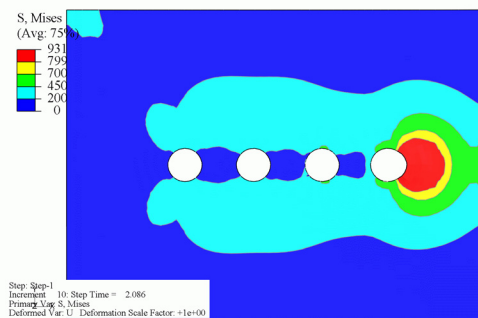


Fig. 73: Distribution of bearing forces and friction for specimen L06s

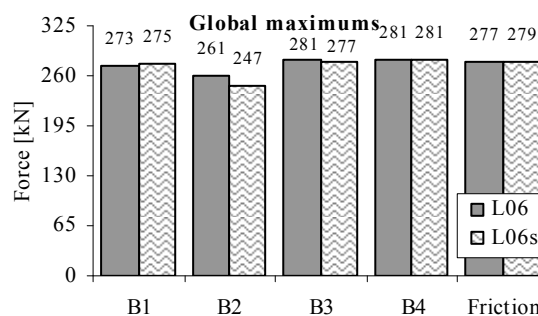


Fig. 75: Distribution of bearing forces and friction for specimens L06, L06s at global maximum

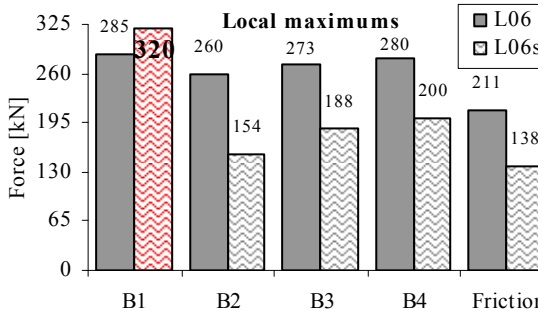


Fig. 77: Distribution of bearing forces and friction for specimens L06, L06s at local maximum

5.5 Numerical parametrical study of bolted shear connections

The comparison of test results and numerical simulations for specimens B1 and L showed that numerical simulations followed the experimental load-displacement curves with a desired accuracy (see Figs. 48, 56, 61, 66, 67). Furthermore, the comparison of the specimens after failure to the deformation state of the specimen as a result of numerical simulation revealed an excellent resemblance (see Figs. 46, 54, 55, 60). Hence, the numerical simulations of the connections present a reliable tool for the analyses of stress-strain state.

A comprehensive numerical parametric study was done in order to obtain the influence of different parameters on bearing resistance. The results were used for the evaluation of bearing resistance (59) according to Eurocode standard and for the development of a new formula for

bearing resistance. Numerical model types M2 and M3 (see Chapters 3.3, 3.4) were used in the analyses. Material model was adopted from the second phase of experiment (see Table 10). Geometry and results of parametrical study are presented in Tables 18-21. Distribution of bearing forces on bolts are printed at their maximum sum $\max(\Sigma Bi)$, neglecting the friction. Displacement U and resistances P_b of connections at $\max(\Sigma Bi)$ are also presented in Tables 18-21. The maximum resistance P_{max} of the connection was reached at displacement equal to or larger than displacement U .

Detailed results of this parametrical study are presented in Appendix D.

5.5.1 Width as the varying parameter

This group includes 19 numerical simulations. The geometry of the connections was based on specimen type L. The geometry of specimens L04, L06, L10, L14, L16 and L19 was taken as the basic geometry. The only variable was width b . The coding e.g. L04_b100 stands for specimen geometry L04, where width b of the connection is equal to 100 mm. The philosophy was to obtain the resistance and distribution of bearing forces for very narrow (net cross-section failure is critical) and very wide (shear failure of the plate is critical) connections with small and large pitches p_1 and end distance e_1 . The geometry of the series is presented in Table 18.

Table 18: Geometry and results for the connections where width was the varying parameter

Specimen name	Model type	Basic geometry	b [mm]	U [mm]	P_b [kN]	B1 [kN]	B2 [kN]	B3 [kN]	B4 [kN]	Friction [kN]	$\max \Sigma Bi$ [kN]
L04_b100	M2	L04	100	4,1	680	135	145	158	177	65	615
L04_b150	M2	L04	150	4,6	1054	162	213	266	277	136	919
L04_b175	M2	L04	175	3,8	1048	164	214	262	276	132	916
L04_b242	M2	L04	242	4,7	1057	165	214	264	277	137	920
L06_b150	M2	L06	150	6,1	1107	257	225	248	231	147	960
L06_b175	M2	L06	175	6,8	1310	295	262	272	258	222	1088
L06_b242	M2	L06	242	5,0	1355	271	266	282	288	247	1107
L10_b132	M2	L10	132	5,3	954	206	206	223	206	115	840
L10_b260	M2	L10	260	6,8	1601	263	299	330	336	373	1228
L14_b154	M2	L14	154	6,5	1143	175	273	292	249	154	988
L14_b230	M2	L14	230	16,0	1422	158	227	345	399	281	1129
L14_b330	M2	L14	330	16,0	1489	167	260	350	393	287	1169
L16_b160	M2	L16	160	6,1	1194	232	261	281	235	184	1010
L16_b242	M2	L16	242	7,2	1581	228	286	343	352	371	1210
L16_b286	M2	L16	286	7,5	1584	229	283	341	354	377	1207
L16_b330	M2	L16	330	7,4	1584	234	284	339	353	375	1210
L19_b154	M2	L19	154	6,0	1142	243	240	259	235	164	977
L19_b330	M2	L19	330	30,0	2489	356	424	459	553	698	1791
L19_b440	M2	L19	440	30,0	2542	394	438	466	555	689	1853

These simulations revealed that the resistance of the connection becomes constant at a certain width of the plate, regardless of end distance and pitch (see Figs. 78-79). The work of bolt bearing exhausts the material between bolts of before the first bolt. Therefore the stress cannot activate the unstressed area of the connection. The net cross-section failure is distinctive for narrow plate width (e.g. L04_b100, L19_b154). The magnitude of friction for L19_b330 and L19_b440 is unrealistic (Fig. 79). In the actual connection the bolts would yield and therefore elongate, decreasing the friction force. Due to large bearing forces, the bolts would fail in shear. The point of these geometries was to show the magnitude of bearing force that arises if

bolts remain elastic. Very stiff cover plates (if compared to the inner plate) result in the linearly increasing, unsymmetrical distribution of bearing forces.

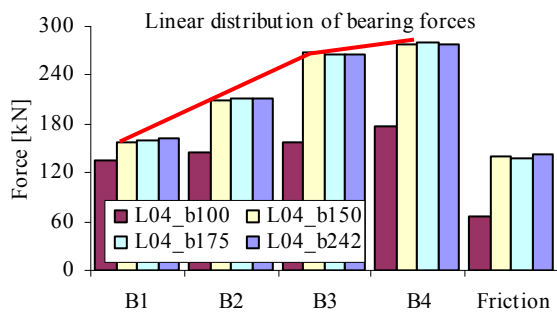


Fig. 78: Distribution of bearing forces and friction for connections with basic geometry L04

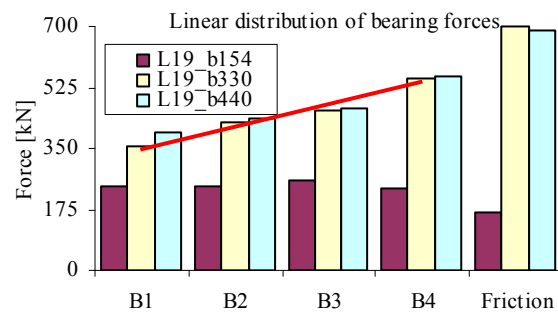


Fig. 79: Distribution of bearing forces and friction for connections with basic geometry L19

5.5.2 Plate stiffness as the varying parameter

The cover plates in the experiment were designed to deform only elastically. The thickness and end distance of the cover plates affect the distribution of bearing forces. In total 43 connections with two configurations were analysed. The geometry of the connections was equal to the geometry of specimens L. The first group included bolted shear connections with bolts in single shear, where both connected plates are equal in geometry. The coding e.g. L08_1s stands for connection geometry L08 with bolts in single shear (1s). The second group of connections were the connections with bolt in double shear. The geometry of inner plate and cover plates was equal, except in thickness. The thickness of cover plate (10 mm) was equal to half of the thickness of inner plate (20 mm). The coding e.g. L03_2s_t10-20 stands for connection geometry L03 with bolts in double shear (2s), where cover plates and inner plate were 10 mm and 20 mm thick, respectively. Numerical model type M3 (see chapter 3.4) was selected for the analyses.

The connections with bolts in single shear were loaded eccentrically and therefore a moment was introduced which resulted in bolt rotation (see Fig. 80). The rotated bolts acted like a wedge, increasing the resistance of the connection. Therefore, the sum of bearing forces on bolts and friction is lower than P_b in Table 19. At a displacement around 15 mm most of the calculations did not converge due to bolt rotations and contact difficulties. Nevertheless, most of the the load-displacement curves reached their maximum (see Appendix D). Bolts in the initial and rotated position are shown in Fig. 80. The force on the first bolt was equal to the force on the last bolt (Figs. 81-82). The symmetrical distribution of bearing forces was also observed at the connections with bolts in double shear (Fig. 82). Therefore, stiffness of cover plates has significant influence on the distribution of load between bolts. Moreover, in the ultimate limit state the friction forces are relatively lower if plates have equal bearing stiffness.

Table 19: Geometry and results for the connections where plate stiffness was the varying parameter

Specimen name	Model type	Basic geometry	t_i [mm]	t_c [mm]	U [mm]	P_b [kN]	B1 [kN]	B2 [kN]	B3 [kN]	B4 [kN]	Friction [kN]	max Σ Bi [kN]
L01_1s	M3	L01	10	10	11,2	753	225	244	225		51	694
L02_1s	M3	L02	10	10	14,0	858	252	263	261		56	777
L03_1s	M3	L03	10	10	9,1	986	283	274	287		92	845
L04_1s	M3	L04	10	10	8,7	964	207	229	230	208	78	874
L05_1s	M3	L05	10	10	10,6	1089	238	246	248	238	95	970
L06_1s	M3	L06	10	10	8,8	1258	275	264	265	272	124	1077
L07_1s	M3	L07	10	10	12,2	836	236	277	244		60	758
L08_1s	M3	L08	10	10	13,8	1109	222	267	268	231	85	988
L09_1s	M3	L09	10	10	14,7	1362	286	299	304	283	117	1172
L10_1s	M3	L10	10	10	12,2	1391	297	300	300	291	124	1188
L11_1s	M3	L11	10	10	14,6	1030	286	305	295		78	886
L12_1s	M3	L12	10	10	13,7	1119	315	322	315		93	951
L13_1s	M3	L13	10	10	13,9	1178	324	325	327		96	975
L14_1s	M3	L14	10	10	13,0	1149	202	299	301	198	97	1001
L15_1s	M3	L15	10	10	12,9	1234	238	295	298	240	111	1071
L16_1s	M3	L16	10	10	15,1	1367	275	311	310	277	112	1173
L17_1s	M3	L17	10	10	15,2	1439	296	319	320	290	115	1225
L18_1s	M3	L18	10	10	14,5	1456	301	320	319	296	127	1235
L19_1s	M3	L19	10	10	14,5	1442	302	316	315	293	115	1226
L20_1s	M3	L20	10	10	14,6	1433	287	324	325	286	121	1221
L21_1s	M3	L21	10	10	14,8	1085	297	322	306		83	925
L22_1s	M3	L22	10	10	14,7	1113	302	324	312		86	938
L01_2s_t10-20	M3	L01	20	10	8,4	1485	460	499	472		82	1432
L02_2s_t10-20	M3	L02	20	10	12,7	1684	532	545	534		109	1612
L03_2s_t10-20	M3	L03	20	10	13,9	2107	638	609	656		245	1903
L04_2s_t10-20	M3	L04	20	10	8,5	1883	424	468	484	434	95	1810
L05_2s_t10-20	M3	L05	20	10	9,1	2127	483	509	517	497	146	2006
L06_2s_t10-20	M3	L06	20	10	13,7	2635	601	598	601	598	268	2398
L07_2s_t10-20	M3	L07	20	10	13,4	1637	483	586	499		100	1568
L08_2s_t10-20	M3	L08	20	10	13,9	2144	460	556	556	480	130	2051
L09_2s_t10-20	M3	L09	20	10	12,6	2681	588	634	623	583	280	2429
L10_2s_t10-20	M3	L10	20	10	14,7	2890	634	667	671	635	323	2607
L11_2s_t10-20	M3	L11	20	10	13,8	2026	602	647	603		209	1852
L12_2s_t10-20	M3	L12	20	10	13,8	2245	657	683	660		290	2001
L13_2s_t10-20	M3	L13	20	10	13,7	2429	700	716	698		353	2114
L14_2s_t10-20	M3	L14	20	10	13,7	2227	415	636	642	391	178	2084
L15_2s_t10-20	M3	L15	20	10	14,7	2395	469	639	636	487	200	2231
L16_2s_t10-20	M3	L16	20	10	14,1	2705	573	660	657	569	281	2458
L17_2s_t10-20	M3	L17	20	10	14,7	2904	612	695	694	611	327	2612
L18_2s_t10-20	M3	L18	20	10	14,6	2968	625	696	695	649	336	2665
L19_2s_t10-20	M3	L19	20	10	14,2	2962	636	689	692	656	328	2673
L20_2s_t10-20	M3	L20	20	10	14,6	2878	594	703	695	597	326	2589
L21_2s_t10-20	M3	L21	20	10	13,8	2151	630	683	635		251	1948

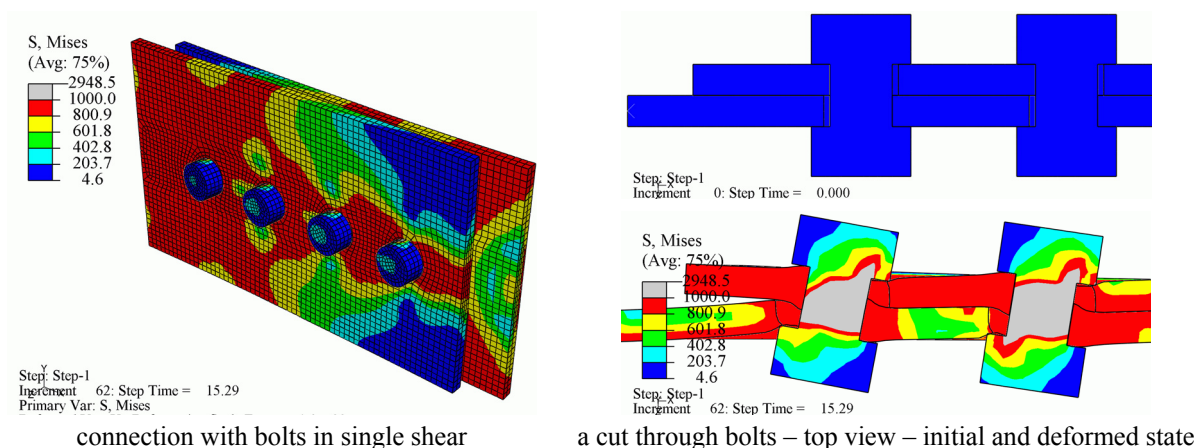


Fig. 80: Mises stress at displacement 15,29 mm for L17_1s

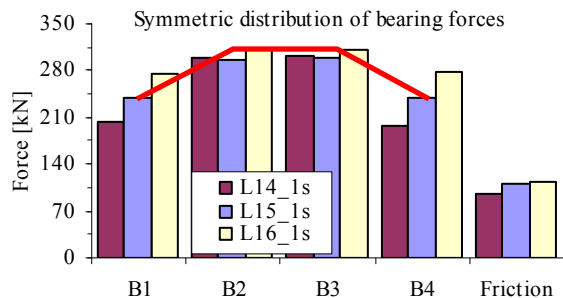


Fig. 81: Distribution of bearing forces and friction for connections with bolts in *single* shear and with equal plate bearing stiffness

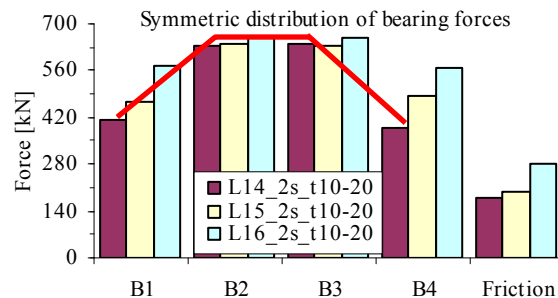


Fig. 82: Distribution of bearing forces and friction for connections with bolts in *double* shear and with equal plate bearing stiffness

Definition of equal or different plate bearing stiffness

It was shown that the pattern of bearing forces between bolts is also dependent on plate bearing stiffness. In this section a relative distinction between *different* and *equal* bearing stiffness of the connection plates is drawn. The results of the FE analyses presented in this section also prove the validity of numerical model M2. Further on, the FE analyses are presented for specimen L14 with different geometries of the cover plates. It is also defined when it may be considered that the cover plates have *equal* or *different* bearing stiffness than the specimen (inner plate).

The bearing stiffness of plates is *equal* if end distance e_1 on all plates (inner and cover plates – Fig. 83) is equal and if the thickness of inner plate is equal to the sum of plate thicknesses of outer plates (see Fig. 83). Otherwise, the bearing stiffness of plates is *different*. In the sequel, the term “the connections with *different* plate bearing stiffness” is used for the connections, where the difference in plate stiffness causes linear pattern of bearing forces as illustrated in Fig. 79. The difference is considered to be large enough, if the thickness of the inner plate is at least equal to (or smaller than) the thickness of the cover plate in the connections with two cover plates (see Fig. 84 – upper drawing). Similar applies to the connections with bolts in single shear. In case that the sum of cover plate thicknesses is equal to the thickness of the inner plate, the difference is large enough to cause linear pattern of bearing forces, if the end distance e_1 of the cover or inner plate is at least three times larger than the end distance on the opposite plate (see Fig. 84 – middle drawing).

The influence of plate thickness on the pattern of bearing forces is presented in Fig. 85. Additional numerical simulations on specimen L14 were performed, where the thickness of a single cover plate equalled to 5 and 10 mm, respectively. If the thickness of the cover plate was equal to 10 mm, the pattern of bearing forces was similar as if the cover plates were rigid.

The influence of end distance on the pattern of bearing forces is presented in Fig. 86. Additional numerical simulations on specimen L14 were performed, where the thickness of a single cover plate equalled 5 mm. The end distance of the cover plate was larger than the end distance of the inner plate by factor 1,5 and 3 (see Fig. 84 – middle drawing), respectively. The linearly increasing pattern of bearing forces was observed, if the end distance of the cover plate was at least 3 times larger than the end distance of the inner plate.

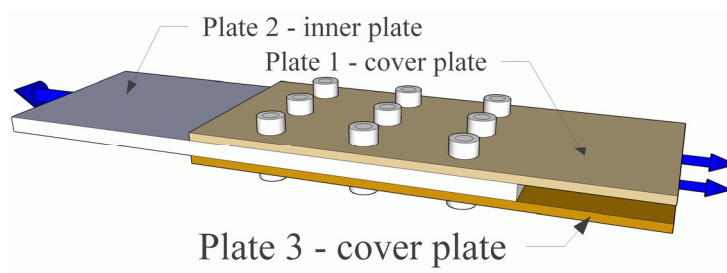


Fig. 83: Tension splice with bolts in double shear

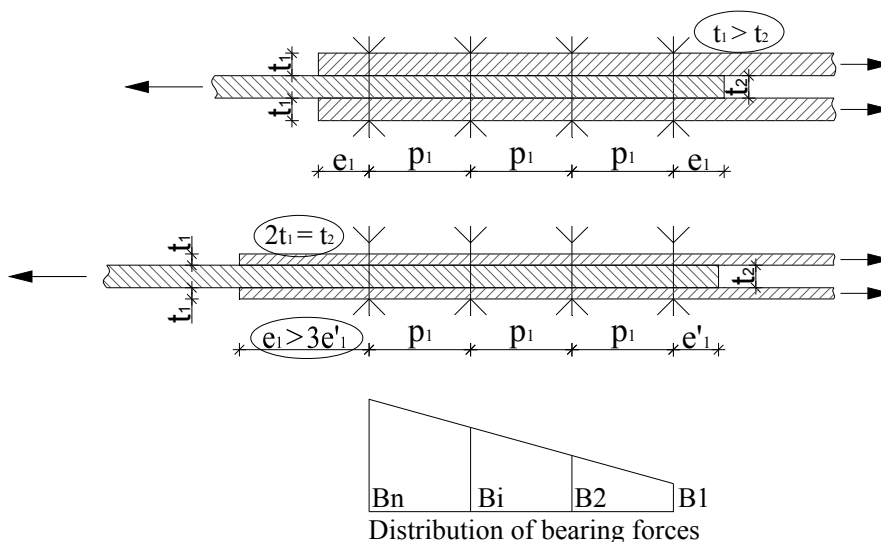


Fig. 84: Different plate bearing stiffness

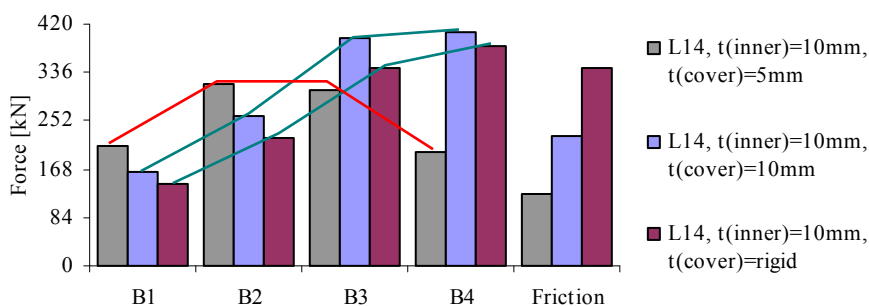


Fig. 85: The influence of thickness on the pattern of bearing forces

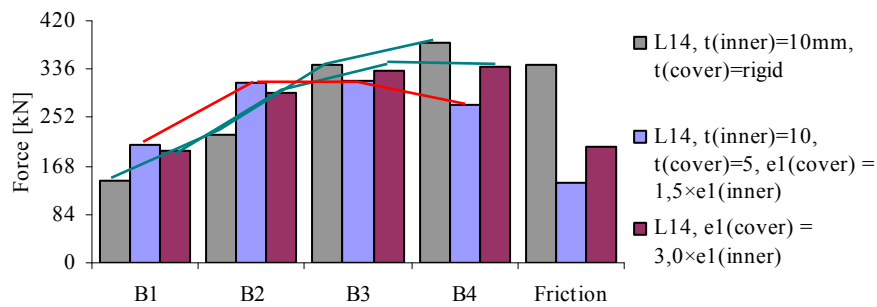


Fig. 86: The influence of end distance on the pattern of bearing forces

5.5.3 Bolt diameter as the varying parameter

This series of numerical simulations includes two groups. The only difference to the second group of previous series (see Section 5.5.2) is bigger bolts. The bolthole clearance for bolts M27 is 3 mm. The first group of connections (coded e.g. L03_2s_t10-20_M27) is based on the geometry of specimen type L, so that ratios e_1/d_0 , p_1/d_0 and absolute value of width b remained equal to the base geometry. The second group of connections (coded e.g. L03_2s_t10-20_M27_b270) is also based on the geometry of specimen type L, but in this case ratios e_1/d_0 , p_1/d_0 and e_2/d_0 remained equal to the base geometry. Thus, the width was equal to $b = 270$ mm.

Another type of failure was observed in this series. Curling of outer (cover) plates developed due to stress gradient in thickness direction and a large area of high compression introduced by bolt bearing (Fig. 87). This type of failure is typical for bolted sheet steel connections and is known as curling failure (Rogers, Hancock, 2000. Rex, Easterling, 2003). The main parameter for curling failure is plate thickness and end distance e_1 .

The symmetrical pattern of bearing forces with large difference among minimum and maximum bearing force is distinctive of these connections (Figs. 88-89). Thus, in certain cases bolt shear failure would be critical.

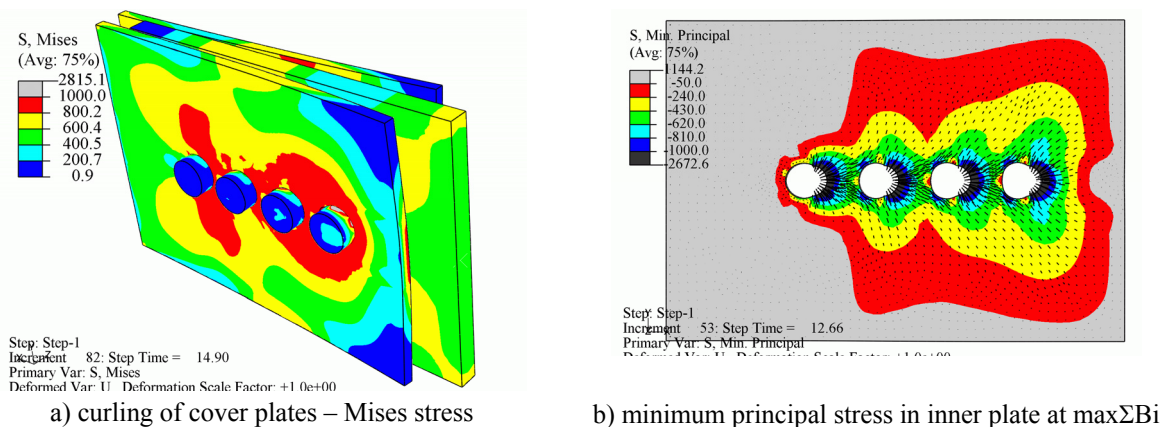


Fig. 87: Stress state of L06_2s_t10-20_M27_b270

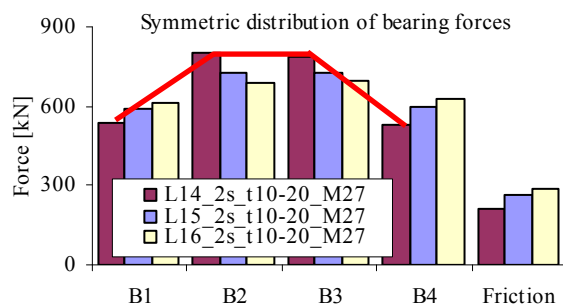


Fig. 88: Distribution of bearing forces and friction for connections with bolts M27

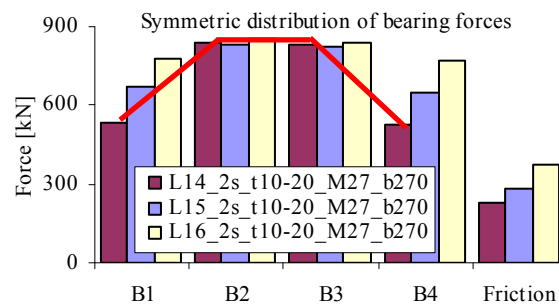


Fig. 89: Distribution of bearing forces and friction for connections with bolts M27 and plate width $b = 270$ mm

Table 20: Geometry and results for the connections where bolt diameter was the varying parameter

Specimen name	Model type	e_1/d_0	p_1/d_0	e_2/d_0	d_0 [mm]	b [mm]	t [mm]	d [mm]	U [mm]	B1 [kN]	B2 [kN]	B3 [kN]	B4 [kN]	Friction [kN]	P_b [kN]	$\max \Sigma B_i$ [kN]
L01_2s_t10-20_M27	M3	1,5	2,0	3,3	30	198	20	27	11,5	592	644	590		77	1890	1826
L02_2s_t10-20_M27	M3	2,0	2,0	3,3	30	198	20	27	11,9	701	716	680		144	2226	2109
L03_2s_t10-20_M27	M3	3,0	2,0	3,3	30	198	20	27	12,4	812	768	787		221	2568	2367
L04_2s_t10-20_M27	M3	1,5	2,0	3,3	30	198	20	27	8,8	541	638	639	556	148	2508	2374
L05_2s_t10-20_M27	M3	2,0	2,0	3,3	30	198	20	27	13,3	644	701	689	647	185	2850	2681
L06_2s_t10-20_M27	M3	3,0	2,0	3,3	30	198	20	27	13,3	660	664	665	676	236	2887	2665
L07_2s_t10-20_M27	M3	1,5	2,5	3,3	30	198	20	27	12,8	641	737	627		117	2107	2005
L08_2s_t10-20_M27	M3	1,5	2,5	3,3	30	198	20	27	14,4	599	735	729	596	197	2838	2659
L09_2s_t10-20_M27	M3	2,5	2,5	3,3	30	198	20	27	11,6	626	678	682	636	279	2889	2622
L10_2s_t10-20_M27	M3	3,0	2,5	3,3	30	198	20	27	12,2	622	686	681	639	276	2891	2628
L11_2s_t10-20_M27	M3	2,0	3,0	3,3	30	198	20	27	13,3	787	838	779		244	2626	2404
L12_2s_t10-20_M27	M3	2,5	3,0	3,3	30	198	20	27	13,5	815	869	824		271	2757	2508
L13_2s_t10-20_M27	M3	3,0	3,0	3,3	30	198	20	27	13,4	834	858	830		269	2768	2522
L14_2s_t10-20_M27	M3	1,2	3,0	3,3	30	198	20	27	14,7	540	801	788	529	215	2856	2658
L15_2s_t10-20_M27	M3	1,5	3,0	3,3	30	198	20	27	13,2	590	725	728	595	266	2891	2638
L16_2s_t10-20_M27	M3	2,0	3,0	3,3	30	198	20	27	12,1	611	685	692	628	286	2891	2617
L17_2s_t10-20_M27	M3	2,5	3,0	3,3	30	198	20	27	11,7	618	682	686	632	285	2890	2617
L18_2s_t10-20_M27	M3	3,0	3,0	3,3	30	198	20	27	12,3	613	685	683	639	285	2892	2620
L19_2s_t10-20_M27	M3	5,0	3,0	3,3	30	198	20	27	12,0	614	686	682	631	290	2890	2613
L20_2s_t10-20_M27	M3	2,0	3,5	3,3	30	198	20	27	12,1	611	684	687	629	291	2890	2611
L21_2s_t10-20_M27	M3	2,0	3,5	3,3	30	198	20	27	13,4	799	868	802		257	2699	2469
L01_2s_t10-20_M27_b270	M3	1,5	2,0	4,5	30	270	20	27	12,9	621	670	616		72	1965	1906
L02_2s_t10-20_M27_b270	M3	2,0	2,0	4,5	30	270	20	27	13,0	715	720	692		138	2249	2127
L03_2s_t10-20_M27_b270	M3	3,0	2,0	4,5	30	270	20	27	10,3	823	785	783		278	2650	2391
L04_2s_t10-20_M27_b270	M3	1,5	2,0	4,5	30	270	20	27	11,7	571	626	625	576	114	2495	2397
L05_2s_t10-20_M27_b270	M3	2,0	2,0	4,5	30	270	20	27	11,9	654	682	686	655	185	2845	2677
L06_2s_t10-20_M27_b270	M3	3,0	2,0	4,5	30	270	20	27	12,7	794	773	768	776	322	3410	3111
L07_2s_t10-20_M27_b270	M3	1,5	2,5	4,5	30	270	20	27	13,2	661	757	645		135	2182	2063
L08_2s_t10-20_M27_b270	M3	1,5	2,5	4,5	30	270	20	27	13,4	620	732	728	621	180	2861	2701
L09_2s_t10-20_M27_b270	M3	2,5	2,5	4,5	30	270	20	27	13,6	796	824	817	789	348	3550	3225
L10_2s_t10-20_M27_b270	M3	3,0	2,5	4,5	30	270	20	27	13,3	838	844	845	823	402	3729	3350
L11_2s_t10-20_M27_b270	M3	2,0	3,0	4,5	30	270	20	27	13,1	800	828	787		267	2659	2415
L12_2s_t10-20_M27_b270	M3	2,5	3,0	4,5	30	270	20	27	13,1	856	876	843		352	2905	2574
L13_2s_t10-20_M27_b270	M3	3,0	3,0	4,5	30	270	20	27	13,1	909	895	865		395	3039	2669
L14_2s_t10-20_M27_b270	M3	1,2	3,0	4,5	30	270	20	27	14,0	537	840	829	525	227	2939	2730
L15_2s_t10-20_M27_b270	M3	1,5	3,0	4,5	30	270	20	27	13,3	673	829	822	651	281	3238	2975
L16_2s_t10-20_M27_b270	M3	2,0	3,0	4,5	30	270	20	27	13,4	781	853	837	768	376	3597	3239
L17_2s_t10-20_M27_b270	M3	2,5	3,0	4,5	30	270	20	27	13,3	831	879	876	807	448	3825	3394
L18_2s_t10-20_M27_b270	M3	3,0	3,0	4,5	30	270	20	27	13,3	847	887	873	836	441	3864	3443
L19_2s_t10-20_M27_b270	M3	5,0	3,0	4,5	30	270	20	27	13,4	845	890	875	837	451	3880	3447
L20_2s_t10-20_M27_b270	M3	2,0	3,5	4,5	30	270	20	27	13,3	811	897	887	795	416	3784	3389
L21_2s_t10-20_M27_b270	M3	2,0	3,5	4,5	30	270	20	27	13,1	909	895	865		395	3039	2669

5.5.4 Number of bolts as the varying parameter

Large number of bolts in the direction of load and narrow connection plates lead to net cross-section failure. The elongation of holes might be very small in these cases. The distribution of bearing forces on bolts was determined on connection geometries of L06, L14 and L19 with seven bolts in single shear, where the variable was the width of connections plates. Numerical model type M3 was applied to analyses.

Uniform pattern of bearing forces is distinctive of net cross-section failure. Even in case of connection with small end distance e_1 (see Table 21), bearing forces are more or less equally balanced between inner bolts (see Fig. 90). However, linearly increasing pattern of forces is proposed for their summation (dotted lines in Fig. 90).

Table 21: Geometry and results for the connections where the number of bolts was the varying parameter

Specimen name	Model type	No. bolts	Basic geometry	b [mm]	e_1/d_0	p_1/d_0	e_2/d_0	d_0 [mm]	t [mm]	d [mm]
L06_7bolts_1s_b150	M3	7	L06	150	3,00	2,00	3,41	22	10	20
L14_7bolts_1s_b150	M3	7	L14	150	1,23	3,00	3,41	22	10	20
L14_7bolts_1s_b250	M3	7	L14	250	1,23	3,00	5,68	22	10	20
L14_7bolts_1s_b300	M3	7	L14	300	1,23	3,00	6,82	22	10	20
L19_7bolts_1s_b150	M3	7	L19	150	5,00	3,00	3,41	22	10	20

Specimen name	U [mm]	P_b [kN]	B1 [kN]	B2 [kN]	B3 [kN]	B4 [kN]	B5 [kN]	B6 [kN]	B7 [kN]	Friction [kN]	max(ΣB_i) [kN]
L06_7bolts_1s_b150	10,0	1106	134	155	148	143	150	153	136	88	1020
L14_7bolts_1s_b150	10,2	1107	129	158	149	145	149	156	131	90	1018
L14_7bolts_1s_b250	14,2	1949	184	263	275	270	269	260	187	192	1709
L14_7bolts_1s_b300	14,0	2186	193	276	301	310	307	283	198	188	1868
L19_7bolts_1s_b150	10,1	1107	134	154	147	143	145	155	143	88	1021

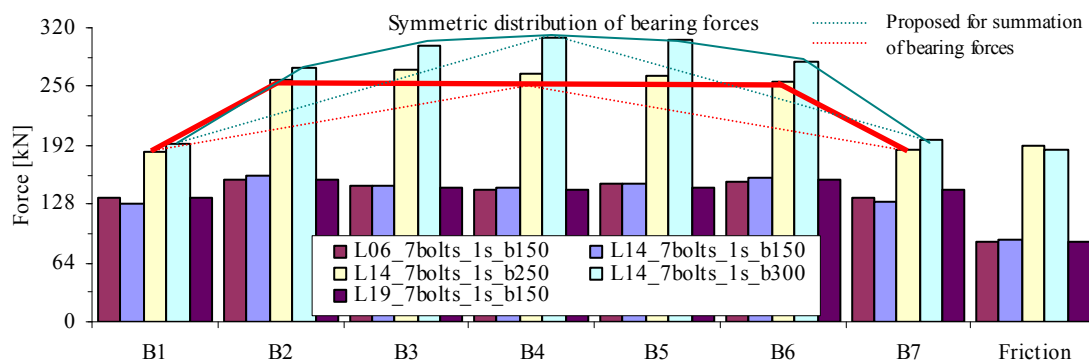


Fig. 90: Distribution of bearing forces and friction for connections with 7 bolts

5.6 Test results on bolted shear connection found in literature

Test results found in literature and presented in this section will be used in the following chapters (see Chapters 5.8 and 5.9) for the evaluation of design bearing resistance formula according to Eurocode and for the development and evaluation of a proposed design bearing resistance. The geometry and test results of connection found in literature are presented in Table 22. The failure mode given in the last column is cited from the original source, therefore the failure definition should be looked up in there. The coding of connection name is

assembled from authors' initials and the specimen name used in the specified source (e.g. KY BO050 stands for - Kim, Yura, 1999 - specimen BO050).

Kim and Yura (1999) investigated shear connections with one or two bolts placed parallel to the loading. Beside mild steel grade they used steel with yield strength of $f_y = 483 \text{ N/mm}^2$ and ultimate tensile strength of 545 MPa. The specimens were connected to rigid plate so that bolt was in single shear. The failures were characterized as splitting and shear failures.

Aalberg and Larsen (2001. 2002) duplicated Kim and Yura tests, using steel grades S690 and S1100. The value of ultimate tensile to yield ratio was equal to $f_u/f_y = 1,05$ for both steel grades. The local ductility of connections was not decreased due to the low f_u/f_y ratio. The test setup was similar to ours.

The tests done by Kim, Yura (1999) and Alberg, Larsen (2001. 2002) were replicated by numerical simulations in order to obtain the distribution of bearing forces between bolts. The detailed results of our numerical simulations are presented in Appendix E. Model type M1 was adopted for the numerical analysis. The data for material model were based on material parameters given in the literature and according to our experience. The material model for Kim and Yura's tests is presented in Table 23. The material characteristic of steel grade S690 used in Aalberg and Larsen's tests were very similar to our steel, thus material model presented in Table 9 was used. For steel grade S1100 model in Table 24 was adopted. Numerical resistance is compared to experimental one in Fig. 91, where the average error is equal to 3,6%. The distribution of bearing forces as a result of numerical simulation is given in Table 25.

Puthli and Fleisher (2001) focused on shear connections made of steel grade S460 ($f_u/f_y = 1,23$) with two bolts placed perpendicular to loading. They also experienced block tear failure. They compared experimental resistances to resistance according to EN 1993-1-8. The focus was on minimum end and edge distances.

Kouhi and Korteesma (1990) presented test results of multi-bolt shear connections. Steel grade with nominal yield strength of 640 MPa and nominal ultimate strength of 700 MPa was used in the test. Actual material strengths are given for 3, 4, 6 and 8 mm thick plates. Specimens were divided in four series according to their failure. The investigation included connections with two bolts positioned in the direction of loading (Fig. 93) and connections with four bolts in 2x2 configuration (Fig. 94). The connections were assembled of bolts, inner plate and two cover plates. The inner plate was twice as thick as the cover plate and its end distance was large ($e_1 = 5d_0$) compared to the cover plate. Therefore, the main deformation and failure were performed in cover plates, except for test series H which failed in net cross-section. Thoughtfully presented experiment and data in the report (Kouhi, Korteesmaa, 1990) allowed us to numerically simulate the tests. The numerical model was based on model type M3 and on nominal geometry. The coefficient of friction between steel plates used in numerical

analyses was equal to 0,37. The information about steel surfaces was not available. Hence, the friction coefficient was determined according to the procedure described in Chapter 3.3. The material model is presented in Table 26. The comparison of experimental and numerical results is carried out in Fig. 92. The average error of numerical results is 2,6% and maximum/minimum errors are 12,5/-7,2%. There could be several reasons for the deviations, the main reasons being the deviation from actual geometry, varying material characteristics and engineering presumption of friction which was based on general data. Otherwise the scatter of points in Fig. 92 is small. The numerical deformation state of connections shown in Figs. 93-94 and the remaining ones are very similar to experimental ones shown in Kouhi's report (1990).

More recent research was published by Rex and Easterling (2003). The research on the behaviour of a bolt bearing on a single plate was part of larger investigation of the behaviour of partially restrained steel and composite connections. The 6,5 mm thick plate of different high steel grades was tested against bearing resistance. The test plate was not restrained by cover plates. Due to small plate thickness and large end distance e_1 several curling failures were observed.

Table 22: Geometry and results for connections found in literature

Connection name	e_1/d_0	p_1/d_0	e_2/d_0	p_2/d_0	d_0 [mm]	b [mm]	t [mm]	d [mm]	f_y [MPa]	f_u [MPa]	P_{max} [MPa]	Failure mode
KY BO050	0,93		2,12		21	89	4,75	19	483	545	49	N/A
KY BO0100	1,40		2,12		21	89	4,8	19	483	545	80	N/A
KY BO150	1,86		2,12		21	89	4,78	19	483	545	108	N/A
KY BO200	2,33		2,12		21	89	4,75	19	483	545	133	N/A
KY BT510	0,92	1,91	3,57		21	150	4,75	19	483	545	146	N/A
KY BT520	0,93	2,58	3,57		21	150	4,78	19	483	545	171	N/A
KY BT530	0,87	3,65	3,57		21	150	4,75	19	483	545	191	N/A
KY BT1510	1,82	1,90	3,57		21	150	4,78	19	483	545	199	N/A
KY BT1520	1,82	2,58	3,57		21	150	4,78	19	483	545	226	N/A
KY BT1530	1,91	3,66	3,57		21	150	4,75	19	483	545	254	N/A
AL W700-1	0,98		2,12		21	89	4,84	20	820	861	79	shear
AL W700-2	1,43		2,12		21	89	4,84	20	820	861	122	shear
AL W700-3	1,87		2,12		21	89	4,84	20	820	861	156	splitting
AL W700-4	2,31		2,12		21	89	4,84	20	820	861	188	splitting
AL W700-5	1,01	1,89	3,57		21	150	4,92	20	820	861	220	N/A
AL W700-6	0,99	2,81	3,57		21	150	4,93	20	820	861	272	N/A
AL W700-7	0,95	3,75	3,57		21	150	4,96	20	820	861	304	N/A
AL W700-8	1,86	1,89	3,57		21	150	4,92	20	820	861	281	splitting
AL W700-9	1,87	2,82	3,57		21	150	4,95	20	820	861	331	N/A
AL W700-10	1,88	3,71	3,57		21	150	4,98	20	820	861	375	N/A
AL W1000-1	0,99		2,12		21	89	5,21	20	1330	1430	138	N/A
AL W1000-2	1,40		2,12		21	89	5,21	20	1330	1430	211	N/A
AL W1000-3	1,88		2,12		21	89	5,23	20	1330	1430	279	N/A
AL W1000-4	2,32		2,12		21	89	5,22	20	1330	1430	337	N/A
AL W1000-5	0,98	1,88	3,57		21	150	5,2	20	1330	1430	353	N/A
AL W1000-6	1,02	2,77	3,57		21	150	5,18	20	1330	1430	444	N/A
AL W1000-7	0,97	3,70	3,57		21	150	5,16	20	1330	1430	498	N/A
AL W1000-8	1,89	1,89	3,57		21	150	5,2	20	1330	1430	478	N/A
AL W1000-9	1,89	2,81	3,57		21	150	5,19	20	1330	1430	567	N/A
AL W1000-10	1,89	3,70	3,57		21	150	5,17	20	1330	1430	613	N/A
PF1	1,20		1,20	2,40	30	144	17,50	27	524	645	817	bearing
PF2	1,20		1,35	2,40	30	153	17,50	27	524	645	774	bearing
PF3	1,20		1,50	2,40	30	162	17,50	27	524	645	785	bearing
PF4	1,20		1,20	2,70	30	153	17,50	27	524	645	755	bearing
PF5	1,20		1,35	2,70	30	162	17,50	27	524	645	772	bearing
PF6	1,20		1,50	2,70	30	171	17,50	27	524	645	771	bearing
PF7	1,20		1,20	3,00	30	162	17,50	27	524	645	811	bearing
PF8	1,20		1,35	3,00	30	171	17,50	27	524	645	801	bearing
PF9	1,20		1,50	3,00	30	180	17,50	27	524	645	813	bearing
PF10	1,20		0,90	1,80	30	108	17,50	27	524	645	568	net cross-section

Connection name	e_1/d_0	p_1/d_0	e_2/d_0	p_2/d_0	d_0 [mm]	b [mm]	t [mm]	d [mm]	f_y [MPa]	f_u [MPa]	P_{max} [MPa]	Failure mode
PF11	1,20		1,05	1,80	30	117	17,50	27	524	645	630	net cross-section
PF12	1,20		1,20	1,80	30	126	17,50	27	524	645	644	mixed
PF13	1,20		1,35	1,80	30	135	17,50	27	524	645	643	mixed
PF14	1,20		1,50	1,80	30	144	17,50	27	524	645	662	mixed
PF15	1,20		0,90	2,10	30	117	17,50	27	524	645	660	net cross-section
PF16	1,20		1,05	2,10	30	126	17,50	27	524	645	762	net cross-section
PF17	1,20		1,20	2,10	30	135	17,50	27	524	645	779	mixed
PF18	1,20		1,35	2,10	30	144	17,50	27	524	645	794	mixed
PF19	1,20		1,50	2,10	30	153	17,50	27	524	645	783	mixed
PF20	1,20		0,90	2,40	30	126	17,50	27	524	645	683	mixed
PF21	1,20		1,05	2,40	30	135	17,50	27	524	645	793	mixed
PF22	1,20		0,90	2,70	30	135	17,50	27	524	645	656	mixed
PF23	1,20		1,05	2,70	30	144	17,50	27	524	645	781	mixed
PF24	1,20		0,90	3,00	30	144	17,50	27	524	645	666	mixed
PF25	1,20		1,05	3,00	30	153	17,50	27	524	645	785	mixed
KK E1	1,2	2,2	3,85		26	200	4	24	660	759	450	bearing
KK E2	1,2	2,8	3,85		26	200	4	24	660	759	490	bearing
KK E3	1,2	3	3,85		26	200	4	24	660	759	510	bearing
KK E4	1,5	2,2	3,85		26	200	4	24	660	759	520	bearing
KK E5	1,5	2,8	3,85		26	200	4	24	660	759	515	bearing
KK E6	1,5	3	3,85		26	200	4	24	660	759	623	bearing
KK F1	1,35	2,6	3,75	7	22	319	3	22	623	724	697	bearing
KK F2	1,35	3,3	3,75	7	22	319	3	22	623	724	725	bearing
KK F4	1,4	3,5	3,75	7	22	319	3	22	623	724	685	bearing
KK F5	1,75	3,5	3,75	7	22	319	3	22	623	724	740	bearing
KK G1	1,4	3,5	5,75	3	22	319	3	22	623	724	640	block shear
KK G2	1,4	2,6	5,75	3	22	319	3	22	623	724	563	block shear
KK G4	1,75	2,6	5,75	3	22	319	3	22	623	724	677	block shear
KK G5	1,75	3,3	5,75	3	22	319	3	22	623	724	635	block shear
KK H1	3	3	1,5	2,4	26	140,4	4	24	660	759	529	net cross-section
KK H2	3	3	2	2,4	26	166,4	4	24	660	759	679	net cross-section
KK H3	3	3	2,4	2,4	26	187,2	4	24	660	759	795	net cross-section
KK H4	3	3	1,5	3	26	156	4	24	660	759	652	net cross-section
KK H5	3	3	2	3	26	182	4	24	660	759	795	net cross-section
KK H6	3	3	2,3	3	26	197,6	4	24	660	759	890	net cross-section
RE 1	0,93		2,11		27	114	6,5	25	414	690	108	bearing
RE 2	0,93		2,11		27	114	6,5	25	414	690	99	tearout
RE 3	1,41		2,11		27	114	6,5	25	414	690	152	splitting
RE 4	1,41		2,11		27	114	6,5	25	414	690	150	bearing
RE 5	1,89		2,11		27	114	6,5	25	414	690	193	bearing
RE 6	1,89		2,11		27	114	6,5	25	414	690	203	curling
RE 7	2,37		2,11		27	114	6,5	25	507	752	186	curling
RE 8	2,37		2,11		27	114	6,5	25	407	655	188	curling
RE 9	2,81		2,11		27	114	6,5	25	414	690	186	curling
RE 10	2,81		2,11		27	114	6,5	25	414	690	180	curling
RE 11	0,93		2,11		27	114	6,5	25	407	665	106	splitting
RE 12	0,93		2,11		27	114	6,5	25	407	665	98	splitting
RE 13	1,89		2,11		27	114	6,5	25	407	665	184	curling
RE 14	1,89		2,11		27	114	6,5	25	407	665	191	curling
RE 17	1,89		2,54		27	137	6,5	25	507	752	190	curling
RE 18	1,89		2,54		27	137	6,5	25	507	752	196	curling
RE 19	1,89		1,65		27	89	6,5	25	507	752	169	curling
RE 20	1,89		1,65		27	89	6,5	25	507	752	159	curling

Table 23: Material model for numerical simulations of Kim and Yura's tests

True stress [MPa]	483	500	520	600	650	700	900
True plastic strain	0	0,003	0,03	0,095	0,12	0,25	1

Table 24: Material model for numerical simulations of Aalberg and Larsen's tests for steel grade S1100

True stress [MPa]	1330	1450	1550	2100
True plastic strain	0	0,03	0,045	1

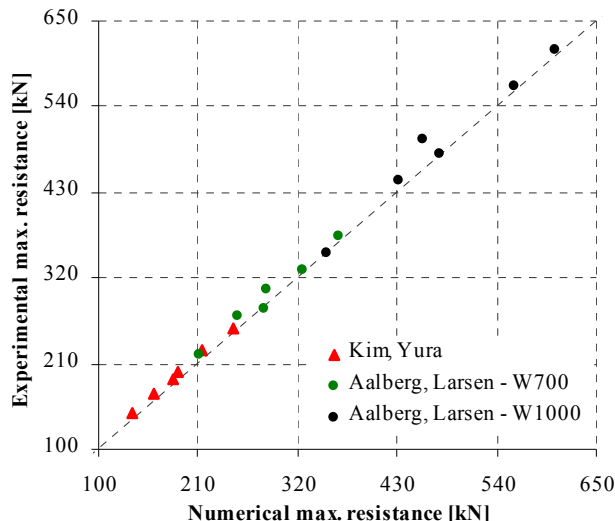


Fig. 91: Comparison of numerical and experimental resistances

Table 25: Distribution of bearing forces on bolts for connections found in literature

Specimen name	B1 [kN]	B2 [kN]	P_{max} [kN]	Specimen name	B1 [kN]	B2 [kN]	B3 [kN]	B4 [kN]	Friction [kN]	$\max(\Sigma B)_i$ [kN]	P_b [kN]	P_{max} [kN]
KY BT0510	42	95	137	KK E1	153	242			48	396	437	462
KY BT0520	36	124	160	KK E2	168	233			98	401	493	493
KY BT0530	39	143	182	KK E3	168	240			102	408	504	506
KY BT1510	86	100	186	KK E4	191	233			76	425	493	508
KY BT1520	77	136	214	KK E5	197	244			93	441	526	552
KY BT1530	91	158	249	KK E6	200	246			90	446	528	561
AL W700-5	68	143	211	KK F1	125	147	125	148	141	546	674	677
AL W700-6	60	195	255	KK F2	127	148	130	150	154	555	695	697
AL W700-7	71	215	285	KK F4	128	147	127	147	125	549	660	679
AL W700-8	133	150	282	KK F5	137	151	136	148	170	572	727	737
AL W700-9	135	190	325	KK G1	120	144	116	147	86	527	599	624
AL W700-10	148	219	366	KK G2	115	127	115	128	74	486	549	563
AL W1000-5	110	242	352	KK G4	123	125	123	126	98	497	584	592
AL W1000-6	101	331	432	KK G5	115	146	113	146	81	521	590	617
AL W1000-7	125	334	458	KK H1	110	115	107	119	76	452	522	522
AL W1000-8	221	256	477	KK H2	129	147	128	141	120	546	658	660
AL W1000-9	220	338	559	KK H3	147	166	145	167	148	626	766	766
AL W1000-10	257	348	606	KK H4	118	142	120	139	107	519	621	621
				KK H5	141	167	141	166	146	616	755	756
				KK H6	153	181	153	183	176	671	837	837

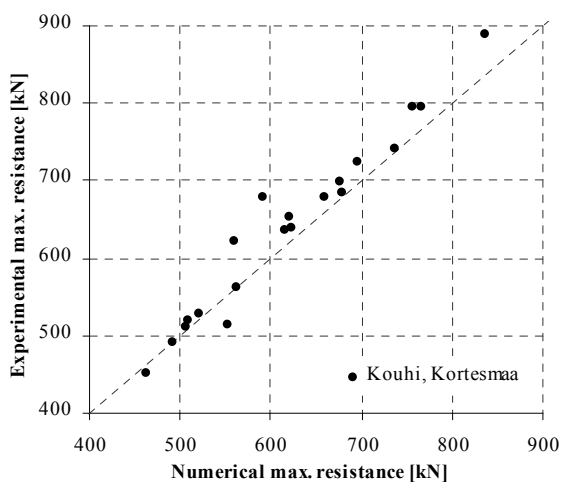


Fig. 92: Comparison of numerical and experimental resistances (Kouhi, Kortoesmaa, 1990)

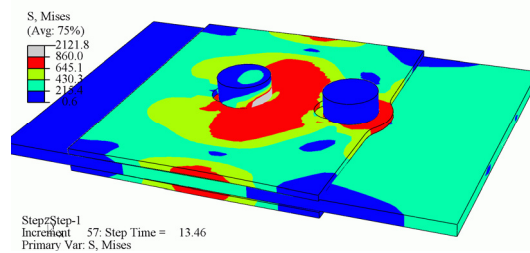


Fig. 93: Connection KK E2 – Mises stress

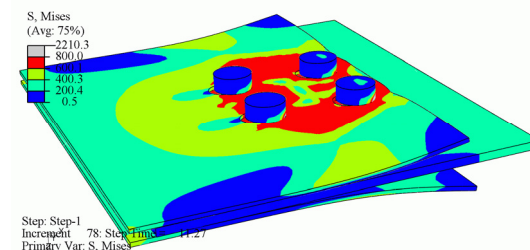


Fig. 94: Connection KK G5 – Mises stress

Table 26: Material models for numerical simulations in Abaqus for Kouhi and Korteesmaa connections

	3 mm thick plate				4 mm thick plate				6 mm thick plate				8 mm thick plate			
True yield stress	623	725	750	810	660	760	790	860	604	712	730	790	622	735	771	830
True plastic strain	0	0,085	0,13	1	0	0,085	0,13	1	0	0,085	0,13	1	0	0,085	0,13	1

5.7 Analysis of bearing resistances in relation to EN 1993-1-8

5.7.1 General

Design bearing resistance per bolt (59) in EN 1993-1-8 was evaluated on the basis of 167 tests of plates in bearing (Snijder et al., 1988a. 1988b). There was only one test result available for more than one bolt. 137 tests results were for S235 and 30 results for higher steel grades with StE690 as the highest grade (equivalent to S690). The resistance model studied did not account for the reduction of resistance for edge distances between $1,2 d_0 \leq e_2 \leq 1,5 d_0$. This reduction is considered in the k_1 factor (equation (63), (64)). However, there were a few test results for edge distances $e_2 \leq 1,5 d_0$ and all these results were on the safe side, even without reduction of bearing capacity. Similar conclusion was made for the pitch p_2 . Moreover, there were no test results where f_{ub}/f_u governed.

It is very important to stress that the bearing resistance is according to Eurocode defined by mean bearing stress in order to limit deformations, but the limit deformation is not prescribed by Eurocode. Therefore, it is difficult to compare experimental values of force to the Eurocode bearing resistance. The value of experimental force that the definition of bearing resistance refers to is simply not defined. If the maximum experimental resistance was compared to the Eurocode bearing resistance, then the statistical evaluation (according to EN 1990) of a design function would not give satisfying results. According to the definition, the results would be scattered on the safe side. This seems to be the case in the background documentation to Eurocode (Snijder et al., 1988a. 1988b), where the scatter of the results was significant ($V_\delta = 0,201$) and the mean correction factor b for bearing resistance model was equal to 1,561 in order to obtain partial factor lower than γ_{M2} of bearing resistance.

Comparison of theoretically and numerically (experimentally) determined resistance is plotted in Figs. 98-105. The theoretical resistance is referred to the bearing resistance according to Eurocode. Besides our experimental results, the results of different researchers are also shown (Kouhi, Korteesmaa, 1990. Kim, Yura, 1999. Aalberg, Larsen, 2001. Puthli, Fleischer, 2001. Aalberg, Larsen, 2002. Rex, Easterling, 2003). The abscissas were defined by theoretical resistances. Bearing resistance $F_{b,EC}$ of an edge and inner bolt, net cross-section N_u and block tearing $V_{eff,1}$ resistances were calculated by equations (59), (8) and (58), respectively, without partial factor γ_{M2} . Moreover, actual geometry and material parameters were used. The resistance of the connection was considered in two ways. On one hand, the resistance of the connection was expressed as the sum of bearing resistances per bolt ΣF_b and on the other

hand it was phrased as the minimum of the sum of bearing resistances ΣF_b , net cross-section resistance N_u and block tearing $V_{eff,1}$ resistance ($\min(\Sigma F_b, N_u, V_{eff,1})$). The block tearing resistance is considered only for connections with several bolts positioned perpendicular to loading direction. The sum of bearing resistances per bolt ΣF_b was calculated differently, for two types of connections. At the connections with symmetric distribution of bearing forces (see Section 5.5.2) the first and the last bolt are considered as the edge bolts, therefore the sum is given by (the connections with *equal* bearing stiffness):

$$\sum F_b = (2F_b^{edge} + (n-2)F_b^{inner})m \quad (67)$$

The distribution of bearing forces was increasing linearly at the connections where the stiffness of the plates was *different*. In this case the sum is given by:

$$\sum F_b = (F_b^{edge} + (n-1)F_b^{inner})m. \quad (68)$$

In equations (67)-(68) n is the number of bolts in a single row parallel to the direction of loading and m is the number of bolt in a single column perpendicular to loading direction.

The ordinates in Figs. 98-105 were defined by numerical or experimental resistances. The numerical resistance of the edge bolt was the value of bearing force on the first bolt denoted as B1. The resistance of the inner bolt was taken as the maximum bearing resistance on all except the edge bolt. The results of numerical simulations are given in Tables 16-21, 25 and experimental results in Tables 14-15, 22.

The results in Figs. 98-105 were statistically analyzed in order to evaluate the partial factor for the determination of design resistances. The analyses were done according to the procedure described in EN 1990, Annex D (CEN, 2004a) and have already been described and applied in Chapter 4.3.

5.7.2 Single bolt connections

In this section the bearing resistance of single bolt connections are discussed. Specimens B2 (two-bolt connections) are presented in the diagrams in the sequel. Since pitch p_2 did not have any visible effect on the resistance, specimens B2 are also included in the diagrams. The comparison of bearing resistance to Eurocode formula is presented in Section 5.7.5.

In order to compare our experimental results to Eurocode, the bearing resistance formula (59) is used without partial factor γ_{M2} and with actual material and geometric parameters as follows (all other parameters are defined with formula (59)):

$$F_{b,EC} = k_1 \alpha_b f_u dt. \quad (69)$$

Numerical presentation of experimental results and Eurocode bearing resistance are shown in Table 27.

Normalized bearing resistance per bolt is defined as:

$$\bar{F}_{b,EC} = \frac{F_{b,EC}}{f_u dt} = k_1 \alpha_b \quad - \text{in terms of Eurocode formula} \quad (70)$$

$$\bar{F}_b = \frac{P_{max}}{f_u dt} \quad \text{-- in terms of experimental results} \quad (71)$$

Table 27: Bearing resistance of specimens B1 and B2

Specimen name	k_1	α_b	$\bar{F}_{b,EC} = k_1 \alpha_b$	$F_{b,EC}$ [kN]	\bar{F}_b	P_{max} [kN]
B101	0,96	1,00	0,96	229	1,10	262
B102	1,65	0,40	0,66	159	1,14	273
B103	1,51	0,50	0,75	180	1,43	342
B104	1,64	0,67	1,10	263	1,50	360
B105	1,55	0,99	1,54	367	1,49	355
B106	2,01	0,84	1,69	404	1,86	445
B107	1,99	1,00	1,99	475	1,84	440
B108*	1,58	1,00	1,58	377	1,55	370
B109	2,41	0,33	0,80	192	0,96	228
B110	2,50	0,40	1,01	242	1,20	286
B111	2,44	0,50	1,23	293	1,52	363
B112	2,43	0,67	1,62	388	2,02	483
B113	2,40	0,83	1,99	475	2,16	516
B114	2,38	1,00	2,38	568	2,14	510
B115*	1,94	1,00	1,94	464	1,82	435
B116	2,29	0,50	1,14	273	1,55	371
B117	2,44	0,50	1,22	292	1,52	362
B118	2,50	0,51	1,28	305	1,64	392
B119	2,50	0,69	1,72	410	2,22	530
B120	2,50	0,85	2,13	510	2,63	629
B121	2,50	1,00	2,50	597	3,20	763
B122	2,50	1,00	2,50	597	3,30	788
B123	2,50	1,00	2,50	487	2,48	483
B124*	2,33	1,00	2,33	462	2,01	400
B125*	1,61	1,00	1,61	319	1,63	322
B201	1,00	0,99	0,99	389	2,31	457
B202	1,61	0,40	0,65	255	2,38	471
B203	1,61	0,67	1,08	427	3,25	643
B204	1,60	1,00	1,60	631	3,23	638
B205	1,68	0,99	1,66	656	3,49	689
B206	1,63	0,50	0,82	322	3,02	596
B207	2,09	1,00	2,09	824	3,99	789
B208	2,48	0,34	0,85	334	2,01	398
B209	2,49	0,40	1,01	398	2,48	491
B210	2,48	0,51	1,26	498	3,05	603
B211	2,34	0,68	1,60	632	3,93	776
B212	2,42	1,00	2,42	956	4,31	851
B213	1,64	0,67	1,10	435	3,43	678

In Fig. 95a,b the displacement D_{EC} at which the bearing resistance (69) was reached is plotted on abscissa. On ordinate either the normalized end distance e_1/d_0 or ratio of maximum resistance is plotted. The displacement D_{EC} was in a range from 0,7 to 8,5 mm for specimens B1 and B2. In cases when D_{EC} was equal to 0, failure occurred before the prescribed resistance could be reached. In all these cases the net cross-section failure was observed. Moreover, at the displacement equal to D_{EC} , the resistance was ranging from 0,5 to 1,0 P_{max} (see Fig. 95b). Considering these results, the bearing resistance $F_{b,EC}$ does not assure an effective deformation control, since D_{EC} is scattered over a large range. Fig. 95c shows that limitation of hole elongation was in certain cases successful, while the displacements at P_{max} were larger than 20 mm.

Fig. 96 presents normalized bearing resistances versus normalized end distance e_1/d_0 . The test results (presented as symbols) are grouped in curves according to similar normalized edge distance. In thin lines the normalized resistance according to Eurocode (equation (70)) for different normalized edge distances e_2/d_0 is presented. The lower and the upper limits of

Eurocode bearing resistance are defined by minimum distances and by maximum value of the product $k_1 \alpha_b$. Considering formula (69) the resistance is linearly increasing by increasing the end distance e_1 until it is equal to $3d_0$. From that point on, the resistance is constant. Although the upper limit of bearing resistance is set to control deformations, this limitation indirectly includes net cross-section resistance check (at least for single bolt connections). The test results in Fig. 96 show similarity to Eurocode formula only in terms of the shape of the curves. The bearing failures of the plate with large displacements are typical for linear part and net cross-section failures for a constant part of the curve. In order to compare bearing resistances per bolt, only half of the experimental resistances of B2 specimens (with two bolts) is considered in Figs. 96, 97. The pitch p_2 had no visible effect on the resistance.

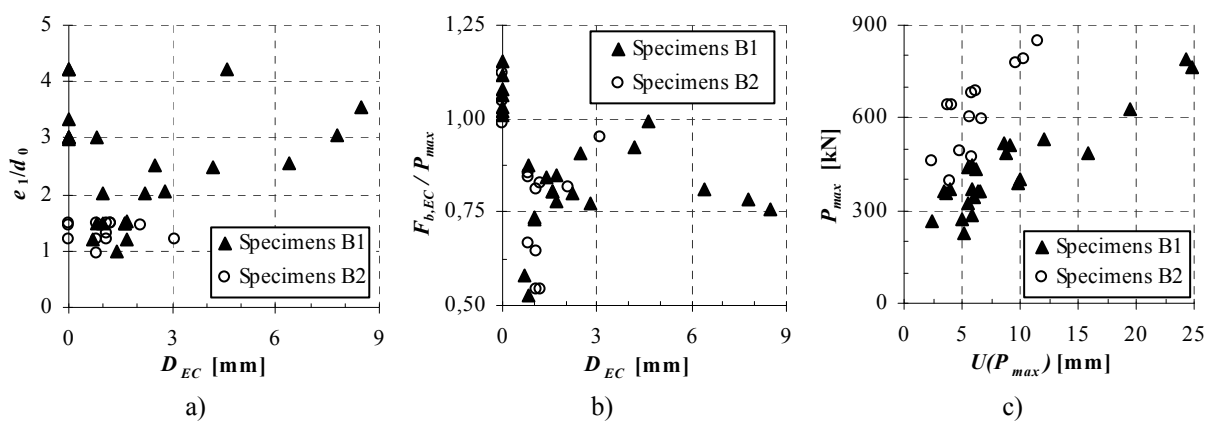


Fig. 95: Displacement D_{EC} at which bearing resistance acc. to EN 1993-1-8 was reached in relation to end distance a) or to bearing-to-maximum resistance ratio b); c) displacement at which maximum resistance was reached

A disagreement between the test results and the Eurocode formula is shown also in Fig. 97. The plot Fig. 97 presents the end-to-edge distance ratio e_1/e_2 versus normalized resistance. The graph suggests that a transition between increasing and constant part of the curve (bearing and net cross-section failures) is a function of e_1/e_2 ratio. Although the transition happens gradually, a transition line is constructed. The line separates net cross-section failures from other kinds of failures and lies between $1,4 - 1,5 e_1/e_2$. In Eurocode's bearing formula (69) this transition is for HSS not accounted correctly. Correct resistance model is vital for correct assumption of failure mode in a connection with more than one bolt. Furthermore, Eurocode underestimates bearing resistances for HSS for any kind of geometry. Moreover, it underestimates maximum bearing resistance per bolt (where net cross-section is critical) for large edge distances $e_2 \geq 1,5 d_0$ and overestimates the resistance for smaller edge distances. Fortunately, a separate net cross-section resistance check is also required.

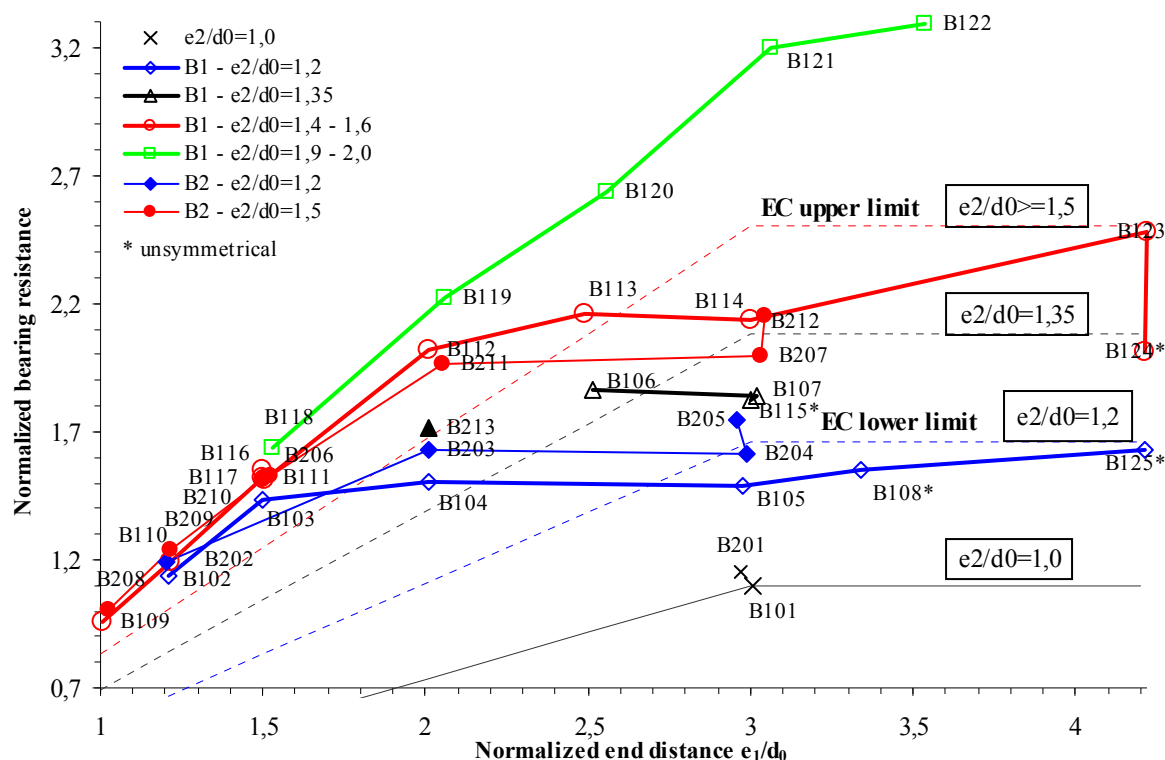


Fig. 96: Normalized Eurocode bearing resistance and experimental results B1, B2 versus normalized end distance

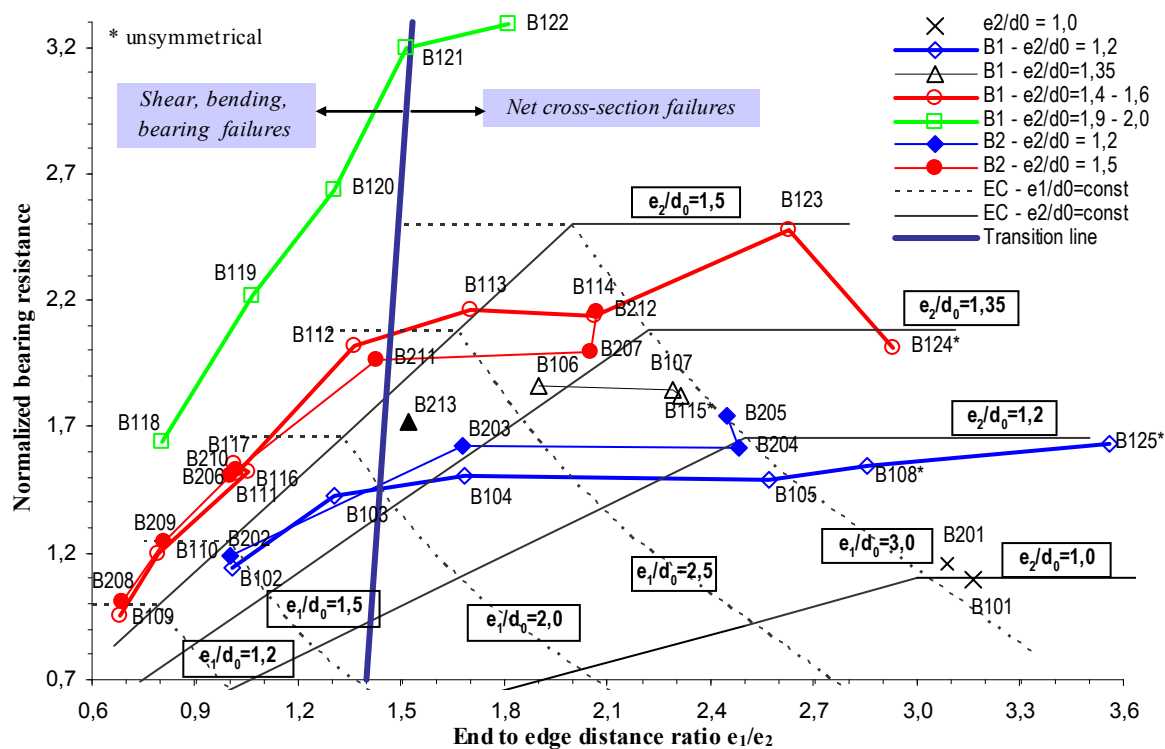


Fig. 97: Experimental results B1, B2 in relation to Eurocode bearing resistance function

Figs. 98-99 illustrate experimental result for single bolt connections. Several B1 and Rex, Easterling results fall below the dotted diagonal line (danger side) in Fig. 98a. For these results the bearing resistance (69) according to EC 3 gives too optimistic results. As it has already been established, the results B1 failed in net cross-section, while the results Rex, Easterling failed in curling. Partial factor $\gamma_M^* = 1,631$ should be chosen for the design formula, if all the results were considered. The results with curling failures were removed from the Fig. 98b. Consequently the scatter and the required partial factor lowered ($V_\delta = 0,152$; $\gamma_M^* = 1,396$). If a minimum of the net cross-section formula N_u and bearing resistance formula had been considered on the x -axis, only the results with net area failures moved above the dotted diagonal. For several results the bearing resistance (69) is too safe and therefore the scatter of points is enlarged. The partial factor equal to $\gamma_M^* = 1,166$ should be applied for the calculation of design values in Fig. 99b.

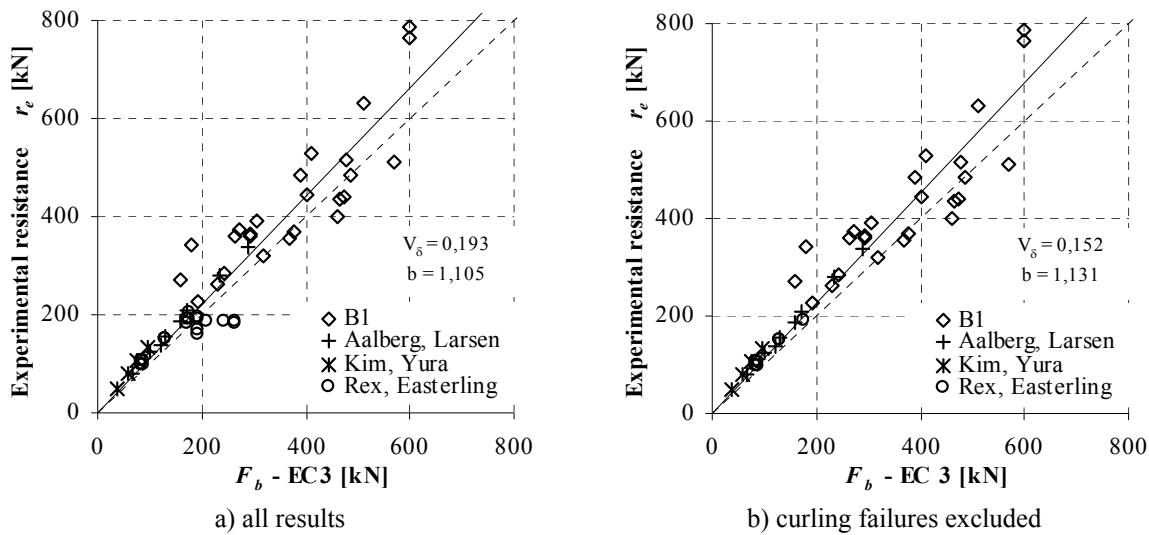


Fig. 98: Experimental r_e vs. EC 3 bearing resistance F_b for single bolt connections

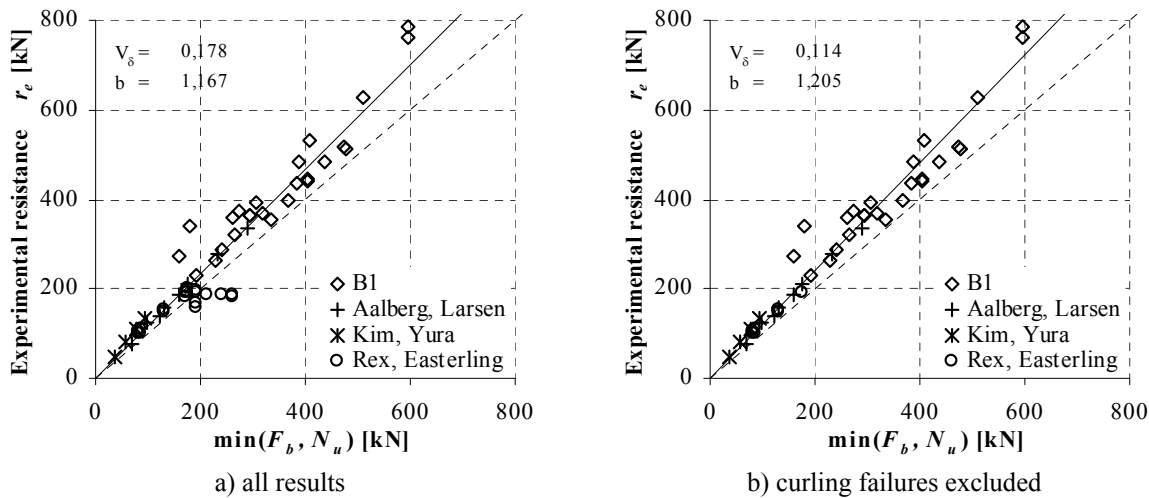


Fig. 99: Experimental r_e vs. minimum of bearing F_b and net cross-section N_u resistance for single bolt connections

5.7.3 The connections with a single row of bolts positioned in the direction of load transfer

Figs. 100-101 show the results for connections with one line of bolts positioned in the direction of loading. The experimental load-displacement curves were traced by numerical simulation in order to obtain the distribution of bearing forces between bolts. The accuracy of numerical results was additionally proved by comparison of experimentally and numerically deformed specimens in section 5.4.2. Bearing resistance formula (69) estimates the bearing force on the edge bolt (Fig. 100a) too bravely, especially for three or four bolt connections. Considering the bearing force on the inner bolts (Fig. 100b), the situation is the opposite. The bearing force was underestimated only for connections that failed in the net area that had large end and pitch distances. If the bearing resistances were summed according to equation (68) and compared to the maximum sum of numerically obtained bearing resistances (Fig. 101a), the scatter of points became smaller. The negative error at the estimation of bearing force on the edge bolt and positive error on the inner bolt were summed approximately to zero. Therefore the numerically obtained maximum resistance of the connection P_{max} was compared to the minimum of the net cross-section N_u and bearing resistance formula. Maximum resistance P_{max} besides bearing forces also accounts for friction forces. Some connections failed in bolt shear, thus numerical and not experimental P_{max} was considered on ordinate in Fig. 101b. Due to friction, all points moved considerably above the dotted diagonal line – on the safe side. The net area check was critical only for the results marked in Fig. 101a. The choice of the partial factor to form design resistances should be equal to 2,472 for bearing resistance on the edge bolt (Fig. 100a), 2,122 for the resistance on the inner bolt (Fig. 100b), 1,689 for the resistance of group of bolts (Fig. 101a) and 1,133 for the resistance of group of bolts together with net area check (Fig. 101b).

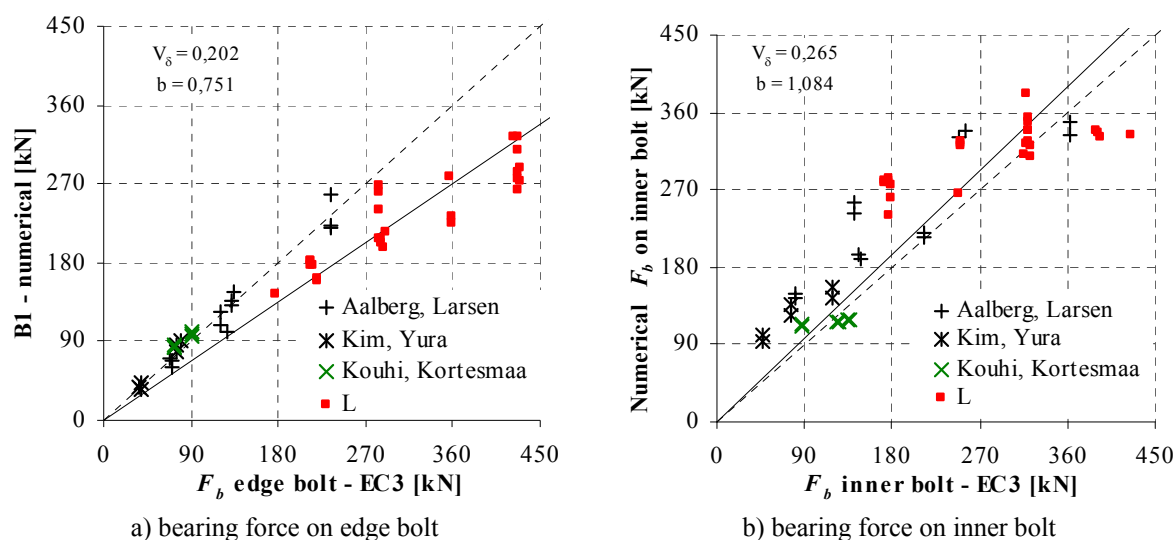


Fig. 100: Bearing forces on bolts for connections with one line of bolts positioned in the direction of loading

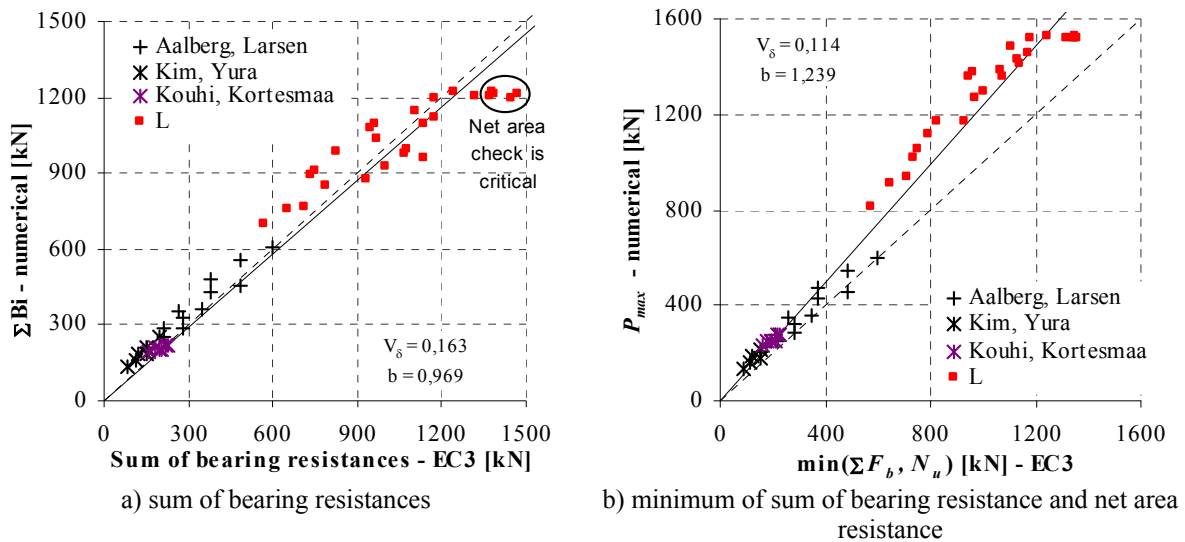


Fig. 101: Resistance of connections with one line of bolts positioned in the direction of loading

5.7.4 The connections included in the numerical parametric study

The results from numerical parametrical study are gathered in Figs. 102-103. In Fig. 102a the Eurocode's bearing resistance on the edge bolt was higher than numerically obtained bearing force (danger side). On one hand, the resistance function (69) does not consider important parameters that influence the bearing force on the edge bolt. For this reason the points are grouped in vertical lines. On the other hand, the bearing force was constant but the function (69) gave higher resistance (horizontal line of points). Function (69) also does not consider the net cross-section failure as the maximum resistance of the connection for connections with equal net cross-sections. Similar story goes for the bearing force on the inner bolt, except that in more cases function (69) gives the results that are on the safe side (Fig. 102b).

The resistance of group of bolts was calculated according to equation (67) or (68), depending on the connection type in terms of plate stiffness. The positive and negative errors were summed approximately to zero, thus most of the points in Fig. 103a lie near the dotted diagonal. There are several points that deviate from the diagonal. These points present the connections where net area fully yielded. If minimum of the net area and sum of bearing resistances is taken as theoretical resistance on x-axis and friction is accounted for on y-axis (Fig. 103b), then the scatter of points is small with $V_{\delta} = 0,098$ and all point move close to the dotted diagonal. There are two results on very safe side. L19_b330 and L19_b440 are connections with 4 bolts, large pitch, end and edge distances, where stiff cover plates enforced large friction forces. The choice of the partial factor to form design resistances should be equal to 2,109 for bearing resistance on the edge bolt (Fig. 102a), 1,729 for the resistance on the inner bolt (Fig. 102b), 1,571 for the resistance of group of bolts (Fig. 103a) and 1,164 for the resistance of group of bolts together with net area check (Fig. 103b). The design values were calculated by equation (42) for large number of tests.

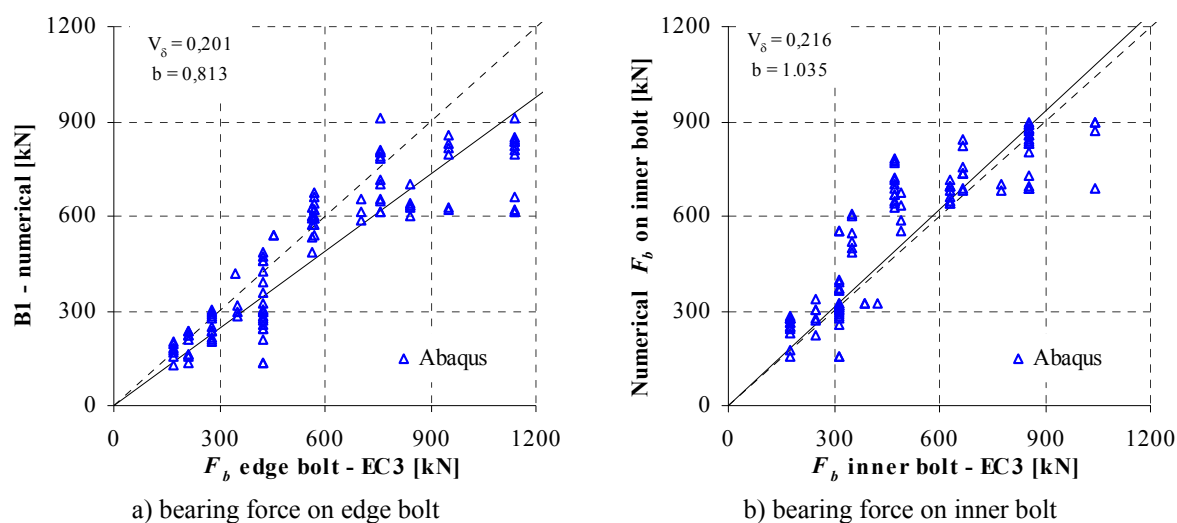


Fig. 102: Bearing forces on bolts for connections included in the numerical parametrical study

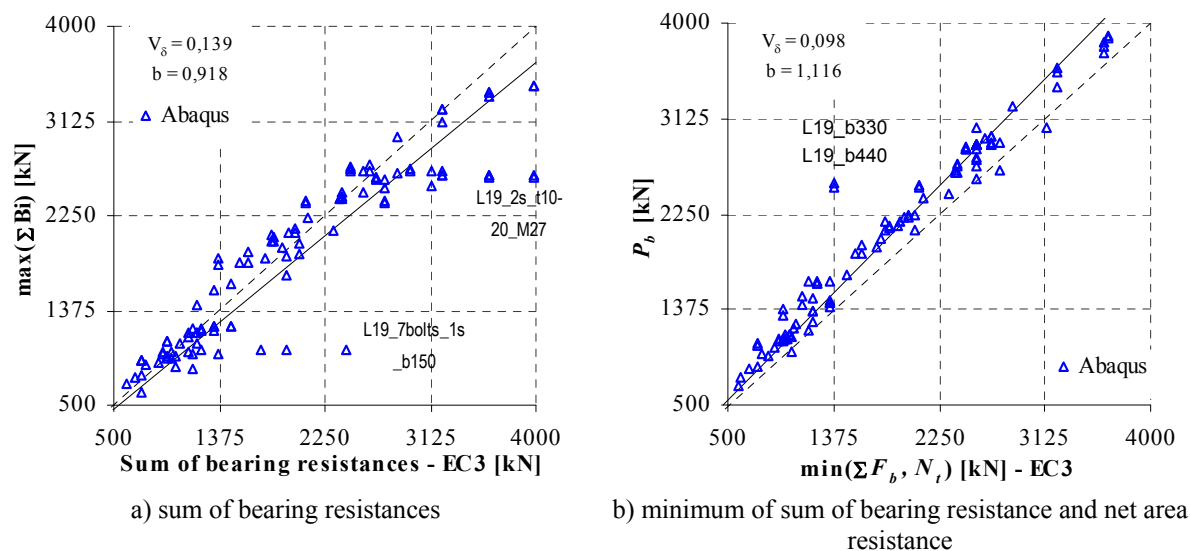


Fig. 103: Resistance of connections included in the numerical parametrical study

5.7.5 The connections with two lines of bolts in the direction of load transfer

The connections with two lines of bolts in the direction of bearing forces remain. The connections B2 and Puthli, Fleischer (2001) are with two bolts positioned perpendicular to loading, while Kouhi, Kortessmaa (1990) are connection with bolt configurations in a 2x2 pattern as described previously. In Fig. 104a the abscissa is defined by equation (69). The reduction due to $p_2 < 3d_0$ (eq. (64)) was considered. The bearing force on the ordinate applies to numerical results for Kouhi, Kortessmaa connections and to experimental results for B2 and Puthli, Fleischer connections, where half of the experimental resistance was considered. Eurocode formula gives much lower values for bearing force on the edge bolts than the experiment for Puthli, Fleischer connections, regardless of the failure mode (see Fig. 104a). The Eurocode bearing formula (63) is conservative due to resistance reduction for small edge distances and pitches p_2 . The bearing force on the edge bolt was overestimated by about 4

times in Eurocode for Kouhi, Korteesmaa connections that failed in net area. Similar conclusions are drawn for B2 connections. Eurocode formula also overestimated the bearing force on the inner bolt for any kind of failure (Fig. 104b). The sum of bearing resistances was calculated according to equation (68). In this case the points are scattered over whole diagram (Fig. 105a). If beside the sum of bearing resistances also net area and block tearing checks are considered on the abscissa and maximum experimental resistance is considered on the ordinate in Fig. 105b, all points are pushed above the dotted diagonal on the safe side. In the latter case (Fig. 105b) the partial factor for the determination of design values should be at least 2,708. This large partial factor is unrealistic. The group of results for which the conservativeness of the Eurocode formula is known should be eliminated from the evaluation. This would decrease the scatter of points and result in realistic partial factor. The problem is identifying the mentioned group of results.

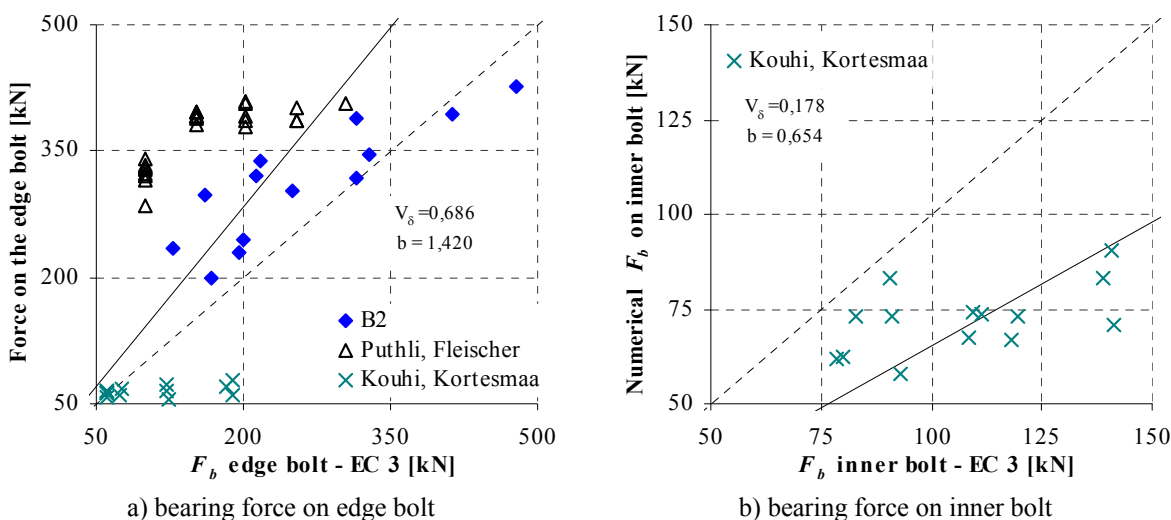


Fig. 104: Bearing forces on bolts for connections with two lines of bolts parallel to loading direction

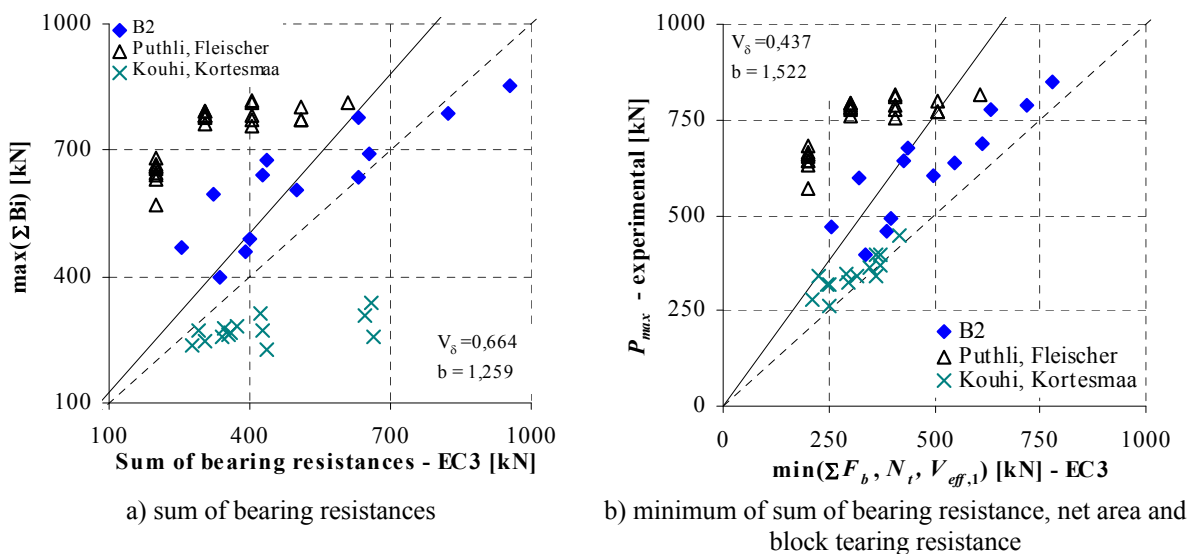


Fig. 105: Resistance of connections with two lines of bolts parallel to loading direction

5.8 Development of new design resistance bearing formula

5.8.1 General

The modern standards for structural design (like the group of Eurocode standards) introduce the limit state design method. The ultimate limit state typically represents the collapse of the structure due to loss of structural stiffness and strength, while serviceability limit state conventionally represents failure states for normal operations due to deterioration of routine functionality. Although Eurocode standard defines the bearing resistance by hole elongation (see Section 5.3), the design bearing resistance is an ultimate limit state check. Therefore it is proposed that the bearing resistance is defined by the maximum strength of plate caused by the bearing pressure. In view of the proposed definition, the sum of bearing resistances of the individual fasteners would be equal to the maximum resistance of a shear connection – like net section failure, block shear, rupture of one bolt... In general bearing resistance of the single bolt shear connection with infinite end and edge distances is limited by bolt shear failure. Nevertheless, hole elongation could be easily limited by a prescribed reduction factor. A new formula that would anticipate the bearing resistance of the plate in ultimate limit state is suggested in this section. The new formula is applicable only to high strength steel and is supported by the results of our tests, the results of other tests on similar bolted shear connection found in literature and by numerical simulations for additional connection configurations, totalling of 266 results. A design function will be determined by the procedure given in EN 1990, Annex D (CEN, 2004a), described and used on a practical case in chapter 4.3.

Identically as in Eurocode, the new bearing formula should be expressed by the mean bearing stress and various factors k_i as geometry parameters.

5.8.2 Single bolt connections

Let us first consider single bolt connections. Factors k_1 and k_2 are linear functions of end to edge distance ratio e_1/e_2 and of absolute value of normalized edge distance e_2/d_0 , respectively. In case of unsymmetrically connected member the minimum edge distance $e_{2,min}$ is considered (Fig. 19). Written in mathematical language, it follows:

$$F_{b,new} = k_1 k_2 \cdot d \cdot t \cdot f_u \quad (72)$$

$$k_1 = \min \left(k_{11} \frac{e'_1}{e'_2}; k_{12} \right) = \min \left(1,3 \frac{e'_1}{e'_2}; 1,9 \right), \quad (73)$$

$$k_2 = k_{21} \frac{e_2}{d_0} + k_{22} = 0,9 \frac{e'_2}{d_0} - \frac{1}{4} \quad (74)$$

$$e'_1 = e_1 \quad (75)$$

$$e'_2 = e_2 \text{ or in case of unsymmetrically connected member } e'_2 = e_{2,min} \quad (76)$$

Coefficients k_{ij} are determined by the following procedure. According to EN 1990, Annex D (CEN, 2004a) the estimator for the coefficient of variation of the error, term V_δ is calculated. Term V_δ is the measure for scatter of points in the $r_e - r_t$ diagram (scatter diagram), where r_e is a vector of test results (measured resistances) and r_t is a vector of theoretical resistances calculated by a prescribed expression (e.g. (72)). Coefficients k_{ij} are evaluated by minimizing V_δ . The preferred solution is the one with correction coefficient $b > 1$ (b is the slope of regression line obtained by the least square method) and that the design resistance could be formed by partial factor $\gamma_{M2} = 1,25$. In addition, the coefficients should also have some theoretical explanation. Considering all these demands, coefficients k_{ij} were evaluated through nonlinear optimization by Microsoft Excel Solver.

Function (72) is plotted in thin lines in Fig. 106. The slope and the position of the curves are defined by both coefficient k_1 and k_2 , while k_1 defines the transition between shear and net cross-section failure which occurs at (see equation (73)):

$$\frac{e_1}{e_2} = \frac{k_{12}}{k_{11}} = \frac{1,9}{1,3} = 1,46. \quad (77)$$

The transition can also be simply theoretically derived. The main assumption is that shear resistance is equal to net cross-section resistance (Fig. 107). Such failure was observed at specimen B121 (Fig. 37c). It follows:

$$F_{net} = F_{shear} \quad (78)$$

$$(2e_2 - d_0)tf_u = 2\left(e_1 - \frac{d_0}{2}\right)t\frac{f_u}{\sqrt{3}} \quad (79)$$

$$\frac{e_1}{e_2} = \sqrt{3} - \left(\frac{\sqrt{3}-1}{2}\right)\frac{d_0}{e_2} \quad (80)$$

$$\frac{e_1}{e_2} \doteq \begin{cases} 1,7 \dots e_2 \gg d_0 \\ 1,46 \dots \frac{e_2}{d_0} = 1,35 \\ 1,43 \dots \frac{e_2}{d_0} = 1,2 \end{cases} \quad (81)$$

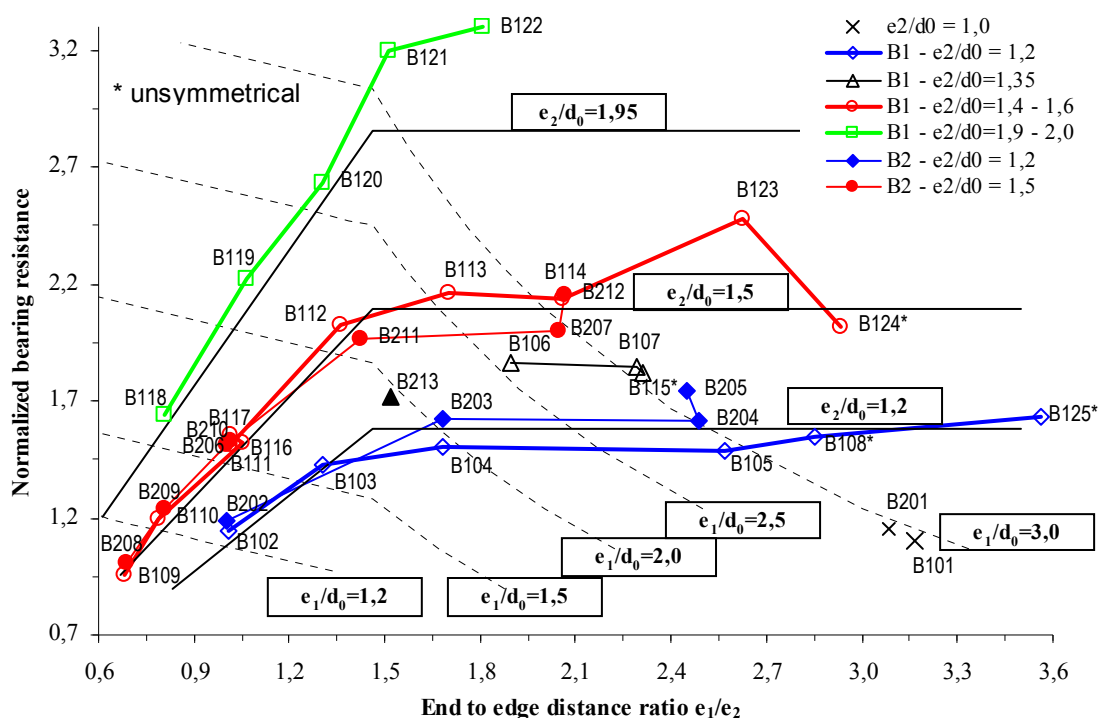


Fig. 106: Experimental results in relation to proposed bearing resistance function

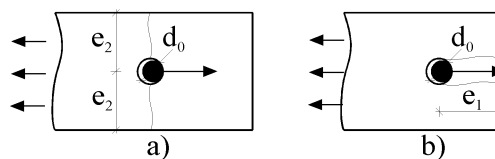


Fig. 107: Failure modes: a) net cross-section b) shear

Theoretically, the transition between shear failure and net cross-section failure occurs when end-to-edge distance ratio is from 1,4 to 1,7. This agrees with experimental results in Fig. 97, where the transition line separates splitting failure from the net cross-section failure. There are two extreme possibilities that are also considered in the new formula. On one hand it gives an upper limit for plates with a constant width and increasing end distance e_1 (see Fig. 108a). In this case the net cross-section becomes the critical failure. On the other hand it also limits the resistance of very wide plates with a constant end distance e_1 , where shear failure of the plate is the limiting resistance (see Fig. 108b).

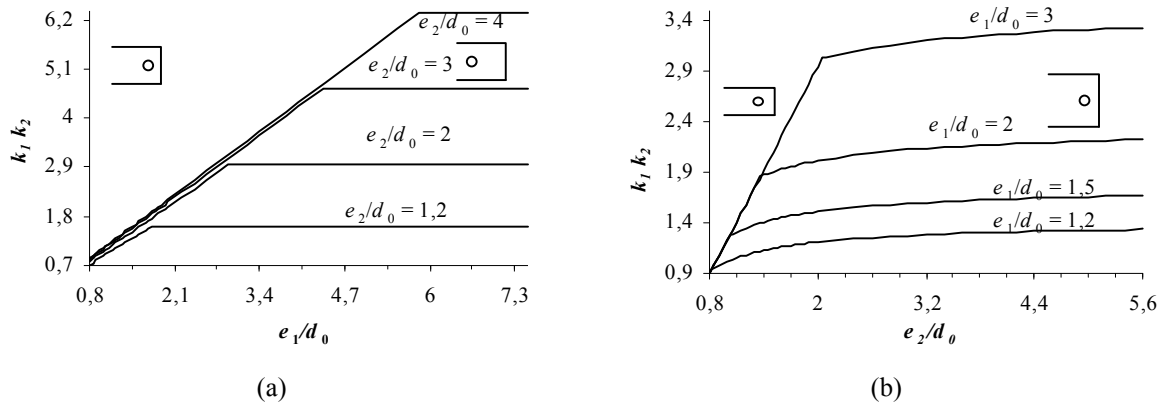


Fig. 108: The effect of end (a) or edge (b) distance on product k_1k_2

As can be seen in Fig. 106, function (72) matches with experimental results very well. The function becomes slightly conservative only for large e_1/e_2 ratios with larger edge distance (for instance $e_2 > 1,9d_0$). For such cases bolt shear is usually relevant.

In Fig. 109 the new bearing resistance function is compared to experimentally determined bearing forces of single bolt shear connections, where besides our results also the results found in literature are included. There is a group of points in Fig. 109a that deviate from the dotted diagonal. These are the connections with thinner plate thickness that failed in curling (Rex, Easterling, 2003). The resistance of these connections was reduced due to the curling of the plates. Therefore an additional reduction factor should be prescribed in the formula (72). The results with curling failures were excluded in Fig. 109b. Now, the theoretical function (72) describes the experiment with satisfying accuracy. The scatter of point is outstandingly low $V_\delta = 0,061$, so the design bearing resistance for single bolt shear connections may be defined by γ_{M2} ($\gamma_M = 1,165 < \gamma_{M2} = 1,25$), having some extra safety for parameters which were not included in our analysis, like the effects of fabrication tolerances, that may be larger than assumed in (29) to (30), especially for small end and edge distances.

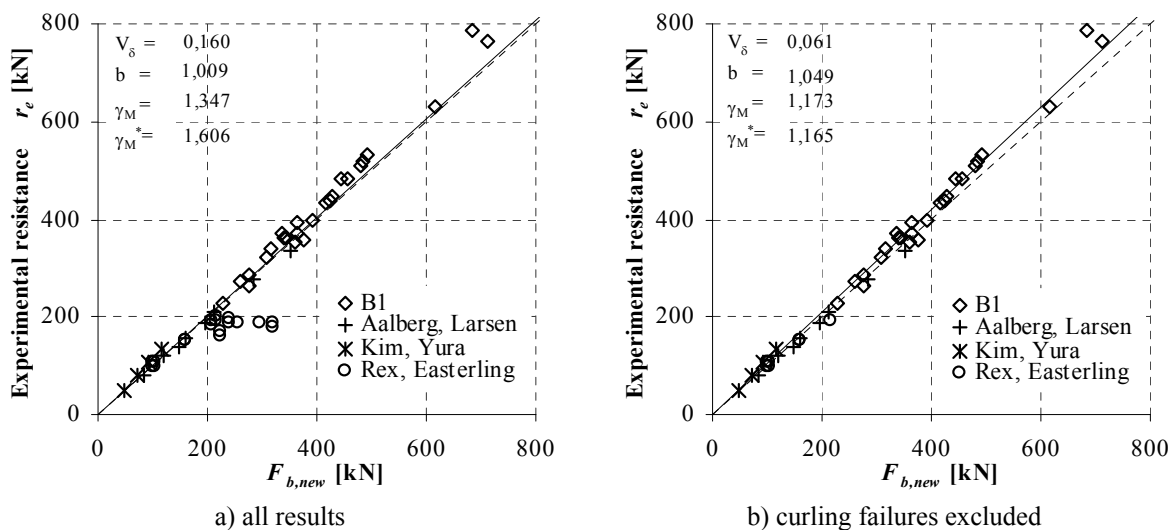


Fig. 109: Experimental r_e vs. new bearing resistance F_b for single bolt connections

5.8.3 The connections with a single row of bolts positioned in the direction of load transfer

Let us consider the connections with several bolts positioned in the direction of load transfer. Factor k_1 that divides net area failures from other kinds of failures remains equal as in equation (73), while e'_2 is defined by an effective width b_{eff} which is equal to connection width. Parameter e'_1 is expanded to include pitch p_1 and the number of bolts n . The analysis of experimental and numerical work revealed that the bearing force on the edge bolt decreased, if another bolt was put behind it. Hence, another factor k_3 was introduced in the bearing formula to reduce the force on the edge bolt. Furthermore, the pattern of force distribution between bolts was dictated by plate bearing stiffness. Coefficient k_3 also controls the bearing force pattern. The description of the choice of factor k_3 is given in the sequel. In view of all, the bearing resistance formula is rewritten:

$$F_{b, new} = k_1 k_2 k_3 \cdot d \cdot t \cdot f_u \quad (82)$$

$$k_2 = \left(0,9 \frac{e'_2}{d_0} - \frac{1}{4} \right) \cdot \frac{1}{n} \quad (83)$$

$$b_{eff} = 2e_2 \quad (84)$$

$$e'_1 = e_1 + (n-1)(p_1 - d_0) \quad (85)$$

$$e'_2 = \frac{b_{eff}}{2} \quad (86)$$

- for edge bolt

$$k_3 = \min \left(\frac{2}{3} \frac{e_1}{p_1} + \frac{1}{2}; 1 \right) \quad \text{for plates with equal bearing stiffness} \quad (87)$$

$$k_3 = \min \left(\frac{2}{3} \frac{e_1/d_0}{(p_1/d_0)^2} + \frac{1}{2}; 1 \right) = \min \left(\frac{2}{3} \frac{e_1}{p_1^2} d_0 + \frac{1}{2}; 1 \right) \quad \text{for plates with different bearing stiffness} \quad (88)$$

- for inner bolt or $n = 1$

$$k_3 = 1 \quad (89)$$

In case of unsymmetrically connected member, the effective width should be considered as:

$$b_{eff} = \beta_i \frac{A_{net}}{t}, \quad (90)$$

where β_i are the same factors β_1 and β_2 as defined in section 3.10.3 of EN 1993-1-8 (CEN, 2005b).

Table 28: Reduction factors β_1 and β_2

Pitch	p_1	$\leq 2,5 d_0$	$\geq 5,0 d_0$
2 bolts	β_2	0,4	0,7
3 bolts or more	β_3	0,5	0,7

Coefficient k_3 in equations (87)-(88) controls the bearing force pattern. The relation of factor k_3 to the e_1/p_1 ratio is illustrated in Fig. 110. It was shown that the difference between minimum and maximum value of bearing force is primarily dependent on ratio e_1/p_1 . The coefficients in equation (87) were evaluated on the bases of results of parametric study. The difference between minimum and maximum value of bearing force is larger if the plate in a connection have different bearing stiffness. To achieve larger reduction on bearing force on the edge bolt in case of different plate bearing stiffness, the normalized pitch p_1/d_0 was raised to the second power. The negative effect of this reduction is that for equal ratios e_1/p_1 , the reduction is larger at larger pitches p_1 (see the right diagram in Fig. 110). The positive effect is that designers are forced to choose a balanced bolt pattern in order to avoid the reduction of bearing resistance. Moreover, in case of large pitches and insufficient number of bolts, the bolt shear failure is usually critical.

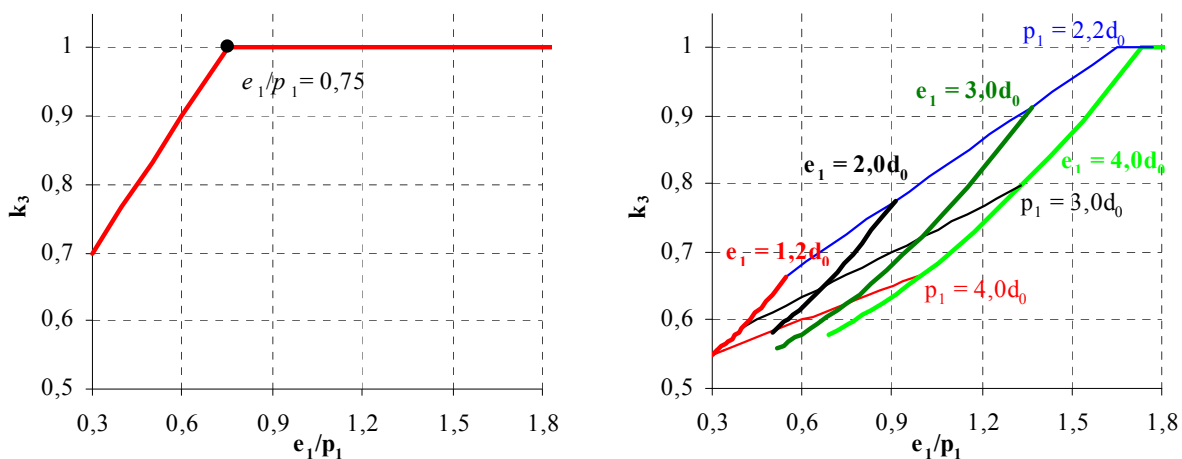


Fig. 110: Factor k_3 (left equation (87); right equation (88)) versus e_1/p_1 ratio

Fig. 111 compares the bearing force on the edge and inner bolt calculated according to equation (82) and to the result of numerical simulation, presented in Sections 5.4.2 and 5.6. Numerical resistance on the inner bolt is the largest bearing force among all except the edge bolt. For the edge bolt, the points are scattered about the dotted diagonal ($b = 1,057$, $V_d = 0,191$ – Fig. 111a). The deviation of points above the dotted diagonal (safe side) is due to factor k_3 . For larger pitch distances equation (88) gives larger reduction than for smaller pitch p_1 at the same e_1/p_1 ratio. Just the opposite is true for the points below the dotted diagonal. The situation is more favourable for the resistance on the inner bolt. In general all points are moved slightly to the safe side (Fig. 111b). The required partial factors are quite high ($\gamma_M^* = 1,697$ for edge bolts; $\gamma_M^* = 1,533$ for inner bolts), but still low compared to Eurocode bearing resistance formula (see section 5.7.3). The quantile factors for 30 tests were used for its calculation. If lower values of quantile factors were used, the required partial factors would lower for about 0,1 (to 1,4).

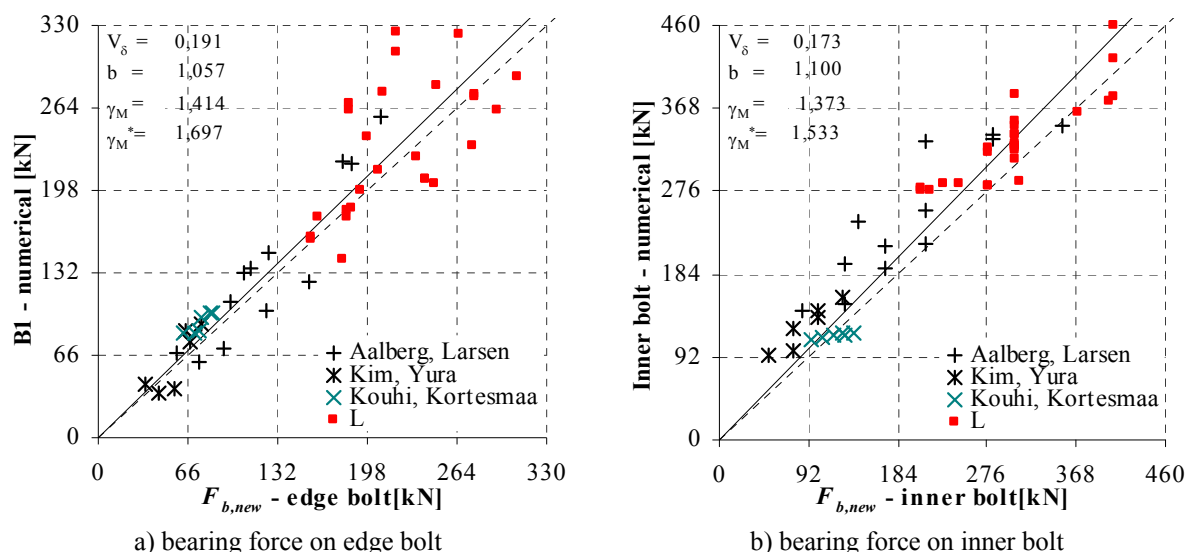


Fig. 111: Bearing forces on bolts for connections with one line of bolts positioned in the direction of loading

The calculation of the sum of bearing forces on individual bolt $\Sigma F_{b,new}$ was done under the assumption that the pattern of bearing forces depends on plate bearing stiffness. The pattern of bearing forces for the connections with *different* plate bearing stiffness is more or less increasing linearly (see Figs. 50, 58, 63, 74, 75, 78, 79). Thus, the sum is given by:

$$\sum F_{b,new} = \frac{m \cdot n (F_{b,new}^{edge} + F_{b,new}^{inner})}{2} \quad (91)$$

For the connections with *equal* plate bearing stiffness the pattern of bearing forces is symmetrical (see Figs. 81-82, 88-90). A conservative approach is proposed for the summation of bearing forces. The symmetrical pattern is simplified to the symmetrical linearly increasing pattern as shown by dotted lines in Fig. 90. Therefore, the sum of bearing forces on individual bolt $\Sigma F_{b,new}$ for the connections with *equal* plate bearing stiffness, with *odd number of bolts* positioned in the direction of load transfer in one line, is given by the following equation.

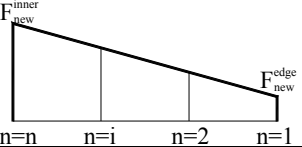
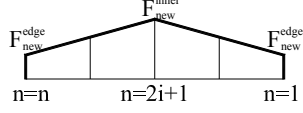
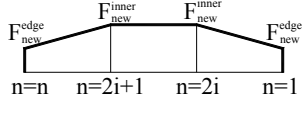
$$\sum F_{b,new} = m \left(\frac{(n+1)(F_{b,new}^{edge} + F_{b,new}^{inner})}{2} - F_{b,new}^{inner} \right) \quad (92)$$

For the connections with *even number of bolts* positioned in the direction of load transfer in one line the equation (91) applies. In equations (91)-(92) parameter m is the number of bolts in a single column positioned in the direction of load transfer.

In cases when $m > 1$, the equations (91)-(92) assume constant distribution of bearing forces in the direction perpendicular to bearing force. In the sequel, the equations will be evaluated only for $m \leq 2$.

The application of equations (91)-(92) is presented in Table 29. Equations (91)-(92) are nothing less than the sum of arithmetic series.

Table 29: The calculation of the sum of bearing forces

	Different plate bearing stiffness	Equal plate bearing stiffness	
Distribution of bearing forces			
Equation	(91)	$n - \text{odd number}$ (91)	$n - \text{even number}$ (92)

In Fig. 112a the sum $\Sigma F_{b,new}$ is compared to the numerically obtained sum of bearing forces at maximum resistance (without friction). The sum $\Sigma F_{b,new}$ was calculated according to equation (91). Relatively small scatter ($V_\delta = 0,119$) of points indicates that the bearing resistance function covers all cases of plate failure. The mean correction factor $b = 1,090$ signifies a suitable correlation between theoretical and “experimental” values. The required partial factor is larger than γ_{M2} ($\gamma_M^* = 1,307$). Additional analysis with lower values of quantile factors was performed. In this case, the required partial factors would decrease to 1,26. In Fig. 112b the ordinate was defined by maximum (numerical) resistance of the connection P_{max} . Due to high friction forces of the connections with more than 2 bolts, the points moved higher from the dotted diagonal. This resulted in lower scatter ($V_\delta = 0,098$), higher mean correction factor $b = 1,367$ and consequently to low required partial factor $\gamma_M^* = 0,981$.

It was established that friction forces increased the maximum resistance of the connections with more than two bolts. The friction forces developed due to the restraining in thickness deformation of the plates by the bolts, even if the bolts were only snug tightened. To obtain the ultimate connection resistance, friction forces should be considered. This can be done by multiplying the sum of bearing resistances $\Sigma F_{b,new}$ by additional factor k_{fric} .

$$P_{max} = k_{fric} \Sigma F_{b,new} \quad (93)$$

This can only be done, if the sum $\Sigma F_{b,new}$ is function that gives reliable results. The maximum value of factor k_{fric} could be determined from the ratio between mean correction factor b in Fig. 112b and b in Fig. 112a.

$$k_{fric,max} = \frac{1,367}{1,090} = 1,25 \quad (94)$$

It was shown that the friction forces had a greater influence in the connections with very stiff cover plates than in the connections, where the stiffness of cover plates was equal. Large friction forces are present only if the bolt elastically deforms. If the bolt elongations are plastic, than the friction forces decrease. Therefore, the value of $k_{fric,max}$ is reduced to:

$$k_{fric} = 1,1 \quad (95)$$

In case the friction is considered, sufficient reliability of the design resistance would still be achieved by partial factor γ_{M2} , since the required partial factor in Fig. 112b multiplied by k_{fric} is smaller than partial factor γ_{M2} , as follows:

$$\gamma_{M2} = 1,25 \leq \gamma_M^* k_{fric} = 0,981 \cdot 1,1 = 1,08. \quad (96)$$

It has to be stressed that coefficient k_{fric} applies only to the connections with more than two bolts. In Section 5.4.1 it was shown, that the friction forces insignificantly increased the resistance of single bolt connection.

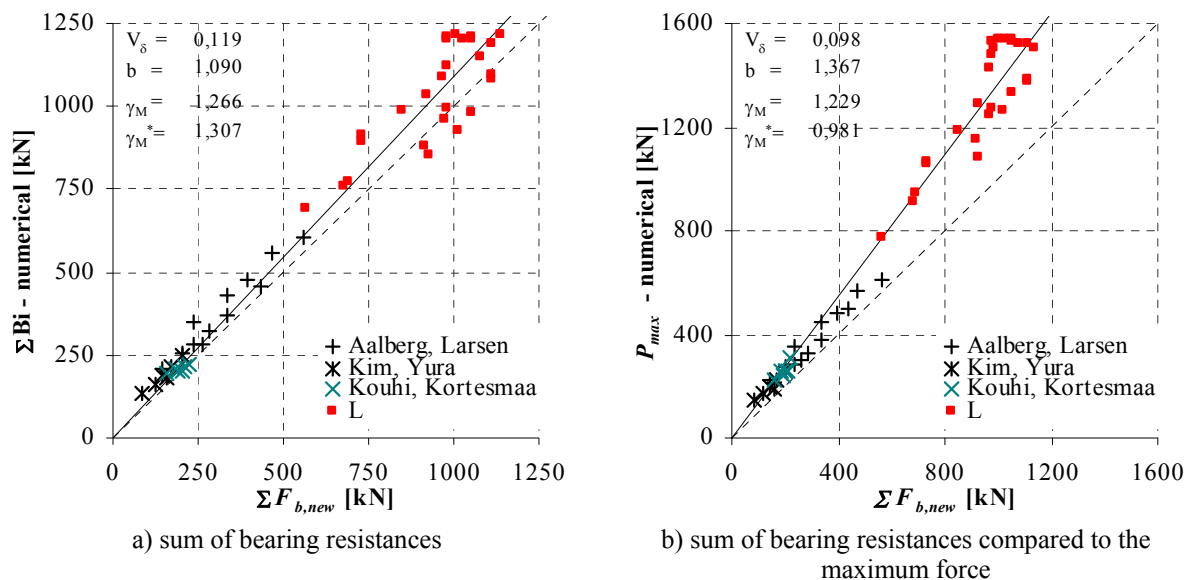


Fig. 112: Resistance of connections with one line of bolts positioned in the direction of loading

5.8.4 The connections included in the numerical parametric study

The largest data set deals with connections included in the numerical parametrical study (see Section 5.5). Two groups of connections were considered: connections with plates of equal bearing stiffness resulted in symmetric distribution of bearing forces and connections with plates of different bearing stiffness that resulted in linear distribution of bearing forces. Therefore different equations for the calculation of factor k_3 and the sum of bearing forces had to be considered. In Fig. 113a the bearing forces on the edge bolt are plotted. The scatter of points is not so large ($V_\delta = 0,120$), but there appears to be a group of results that deviate below the dotted diagonal. Otherwise, the new bearing formula successfully describes the force on the edge bolt. This group of points is recognizable in Fig. 113b that illustrates the results for inner bolt. These points refer to the connections codes as L11_1s, L12_1s, L13_1s, L21_1s, L22_1s, L11_2s_t10-20, L12_2s_t10-20, L13_2s_t10-20, L21_2s_t10-20, L11_2s_t10-20_M27_b270, L12_2s_t10-20_M27_b270, L13_2s_t10-20_M27_b270, L21_2s_t10-20_M27_b270. The basic geometry of these connections are L11, L12, L13, L21 and L22, which are all 3 bolt connections with large pitches $p_1 \geq 3d_0$ and end distance $e_1 \geq 2d_0$. For such large distances the maximum resistance developed at larger displacement or hole elongations. The problem was that the numerical calculations were stopped at displacements around 14 mm due to convergence difficulties; before the maximum resistance of the connection was not reached. The other thing was that high bearing forces led to curling of the plates. Thus, the resistance was not as high as it would be, if the plates were restrained. When analyzing of single bolt connections, it was established that the new bearing resistance formula does not account for curling. Moreover, for these geometries bolt shear is usually

critical. This is also indicated by large friction forces that result in high tension stress in the bolt, which causes yielding of the bolt. The yielding causes plastic elongations, which consequently decrease the friction forces. Therefore the high friction for the mentioned geometries as a result of numerical simulations is not realistic. If these results were removed from the analysis, the scatter as well as the required partial factor to form design values would decrease ($V_\delta = 0,109$, $\gamma_M^* = 1,309$ for edge bolt; $V_\delta = 0,087$, $\gamma_M^* = 1,175$ for inner bolt).

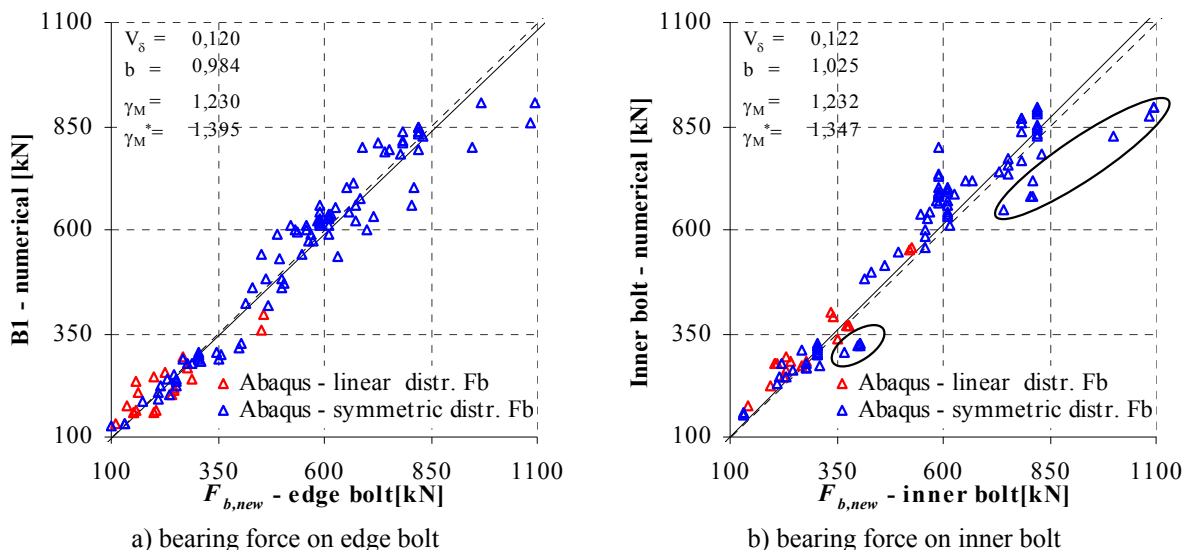


Fig. 113: Bearing forces on bolts for connections included in the numerical parametrical study

The sum of bearing resistances on individual bolt $\Sigma F_{b,new}$ was calculated according to equations (91)-(92) and compared either to maximum sum of bearing forces $\max(\Sigma Bi)$ (see Fig. 114a) from numerical analyses or to connection resistance P_b at $\max(\Sigma Bi)$ which also includes friction (see Fig. 114b). In both cases the scatter of points is quite low. If geometries L11-L13, L21-L22 are removed from the analysis, the scatter becomes even lower and the design formula could be formed by partial factor γ_{M2} in both cases. The connection maximum resistance could be estimated according to formulas (93), (95). Adequate design reliability would also be achieved by γ_{M2} .

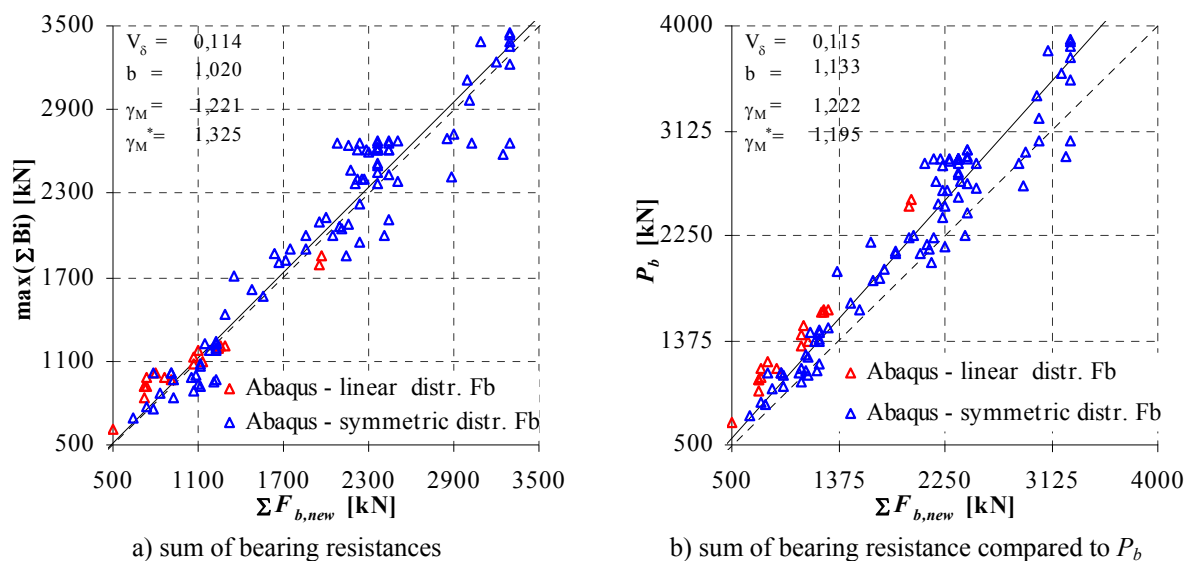


Fig. 114: Resistance of connections included in the numerical parametrical study

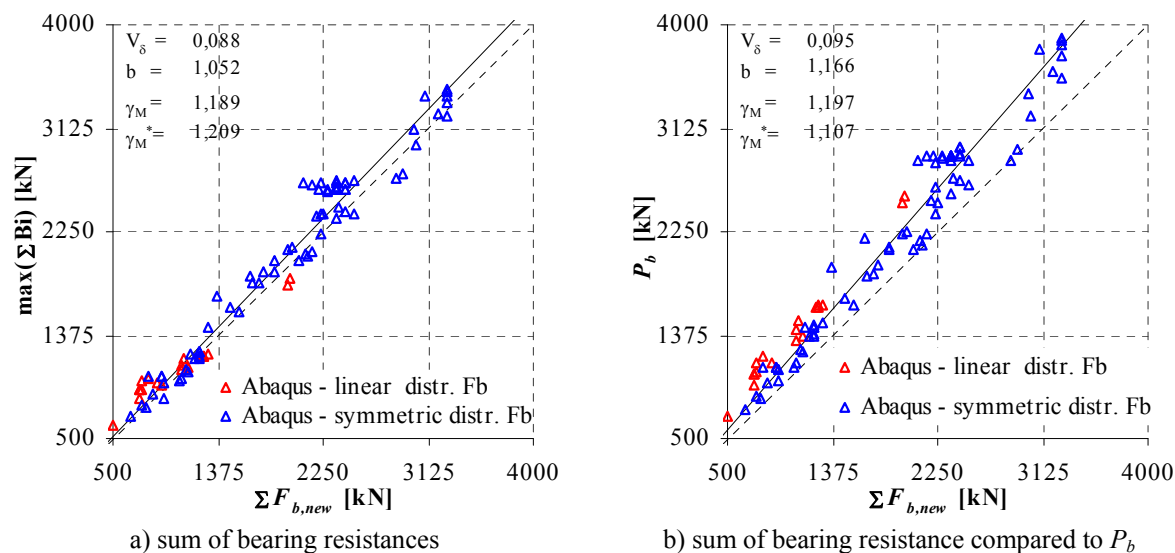


Fig. 115: Resistance of connections included in the numerical parametrical study without geometries L11-L13, L21-L22

5.8.5 The connections with two lines of bolts in the direction of load transfer

The new bearing resistance formula can be expanded to its general form for $n \times m$ bolt connections, where n is the number of bolts in a single row positioned parallel to load transfer and m is the number of bolts in a single column positioned perpendicular to load transfer. The main assumption is that the elongation of all bolt holes positioned in a column perpendicular to loading is equal. Therefore, the bearing forces on all bolts are equal. Coefficients k_1 and k_2 remain equal as for $n \times 1$ bolt connections and are calculated according to equations (73) and (83), respectively. Accordingly, the number of bolts m positioned perpendicular to loading is included in parameter e'_2 and in the effective width b_{eff} . Additionally, two factors k_4, k_5 are introduced in order to reduce resistance due to block tearing. Both factors are applied only to inner bolts in case where $m > 1$. Coefficient k_3 does not change (see equations (87)-(88)). The

equations are rewritten in the most general form, but are valid only for $m \leq 2$, since no results for $m > 2$ were available:

$$F_{b, new} = k_1 k_2 k_3 k_4 k_5 \cdot dtf_u \quad (97)$$

$$b_{eff} = 2e_2 + (m-1)(p_2 - d_0) \quad (98)$$

$$e'_2 = \frac{b_{eff}}{2m} \quad (99)$$

- for edge bolt or when $m = 1$

$$k_4 = 1 \quad (100)$$

$$k_5 = 1 \quad (101)$$

- for inner bolt

$$k_4 = \min\left(\frac{1}{2} \frac{p_1}{p_2} + \frac{1}{2}; 1\right) \quad (102)$$

$$k_5 = \min\left(\frac{1}{2} \frac{p_2}{e_2} + \frac{1}{2}; 1\right) \quad (103)$$

The case of block tearing, where bolt holes are put very close together and far away from the edge of the plate ($e_2 \gg p_2$), is considered directly in coefficient (103) and indirectly in (102). The $m \times 1$ bolt connection geometries that lead to block tearing failures result in hyperbolic decrease of k_1 factor and linear increase of k_2 factor, thus the product $k_1 k_2$ tends to stabilize, similarly as in Fig. 108b. The experimental results support the statement. Therefore, coefficients k_4, k_5 should not be applied to $m \times 1$ bolt connections.

In the case of proposed approach, the new bearing resistance function (97) for $m \times n = 2 \times 1$ bolt connections gives much better results than the Eurocode bearing resistance function (69). Again, the scatter of the results is for modified function very small ($V_\delta = 0,089$, $b = 1,252$ – Fig. 116). Our experimental results B2 and Puthli and Fleisher's (2001) results show very good agreement with a proposed bearing function. It is important to stress that different types of failures are covered in presented experimental results. Besides shear, bearing and net cross-section failures in our experimental results, Puthli and Fleisher also experienced block tearing (Puthli and Fleisher defined block tearing failure as a mixed failure in their paper). The required partial factor for modified bearing resistance for two-bolt connection is $\gamma_M^* = 1,044$. Therefore, the design resistance can be formed with partial factor γ_{M2} . The mean correction factor $b = 1,252$ is large, probably due to friction forces. Numerical simulations were not performed for these series of test, thus friction could not be estimated. Previous results showed that friction forces were smaller if net area failure developed. In Fig. 116 the points that are the closest to the dotted diagonal present net area failures with the lowest friction forces. Higher friction developed at the connections with significant hole elongation which resulted in shear, splitting or bolt tearing failures. These points are positioned further from the dotted diagonal. Therefore it is reasonable to assume that friction increased the connection

resistance in case of B2 and Puthli, Fleisher results. Moreover, the maximum connection resistance (93) could be established by factor k_{fric} equal to 1,1 (95).

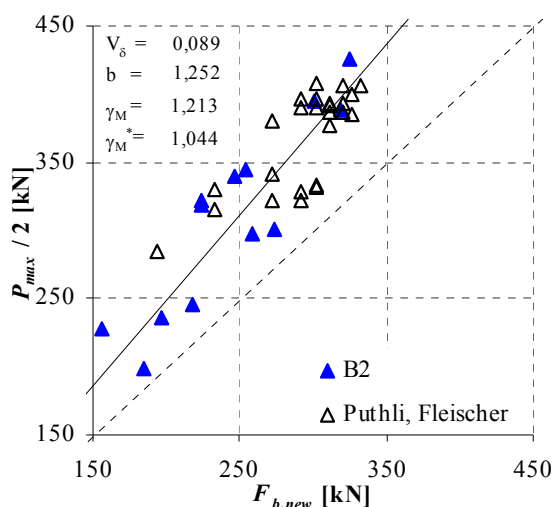


Fig. 116: Bearing force on bolt for the connections with two bolts positioned perpendicular to load transfer

The last data set includes connections with bolts configured in a pattern 2×2 . The numerical simulation for this data set was based on experiments performed by Kouhi and Kortessmaa (1990). The new bearing resistance formula (97) estimated the bearing force on the edge bolt satisfactory with mean bearing ratio $b = 1,182$. Reasonably low scatter of point ($V_{\delta} = 0,119$) allows partial factor $\gamma_M^* = 1,229$ smaller than γ_{M2} even if quantile factors for 20 tests were applied (see Fig. 117a). At first sight it seems that the estimation of the bearing force on the inner bolt was a missed approach. A detailed review discovered that the new formula gives good results for the connections that failed in net cross-section (coded as KK H; black crosses in Fig. 117b). The failures of test series coded as KK F and KK G were recognized as bearing and block tearing by authors of the report (Kouhi, Kortessmaa, 1990). The photographs in the report as well as our numerical simulations (see Fig. 94) evidently testify that the failures were primarily curling, which is a typical failure for thin plates. The thickness of the plates of KK F and KK H were only 3 mm. Coefficients k_4 and k_5 reduced the resistance of inner bolt, so only three results fell below the dotted diagonal, while one result was explicitly on the safe side. These four results increased the scatter ($V_{\delta} = 0,130$), thus the required partial factor is $\gamma_M^* = 1,459$. In Fig. 118a the sum of bearing forces calculated according to the new function is compared to the sum of forces from the numerical simulation. The required partial factor $\gamma_M^* = 1,316$ is slightly larger than γ_{M2} . Considering that only one point lies considerably below the dotted diagonal and even for this point the error $(\sum B_i - \sum F_{b,new}) / \sum B_i = -10\%$ is low and that all other points lie either on the safe side or close to the dotted diagonal, sufficient reliability could be achieved by recommended value of $\gamma_{M2} = 1,25$. Beside that, several connections failed primarily in curling, which is not covered by the new bearing function. On top of all, the friction forces in these connections were around 30% of bearing forces. If friction is also considered (Fig. 118b), the required partial factor drops to 1,036. The

estimation of maximum connection resistance could be performed according to equations (93), (95). Large friction forces are the consequence of the large friction coefficient used in the numerical simulations ($k = 0,37$).

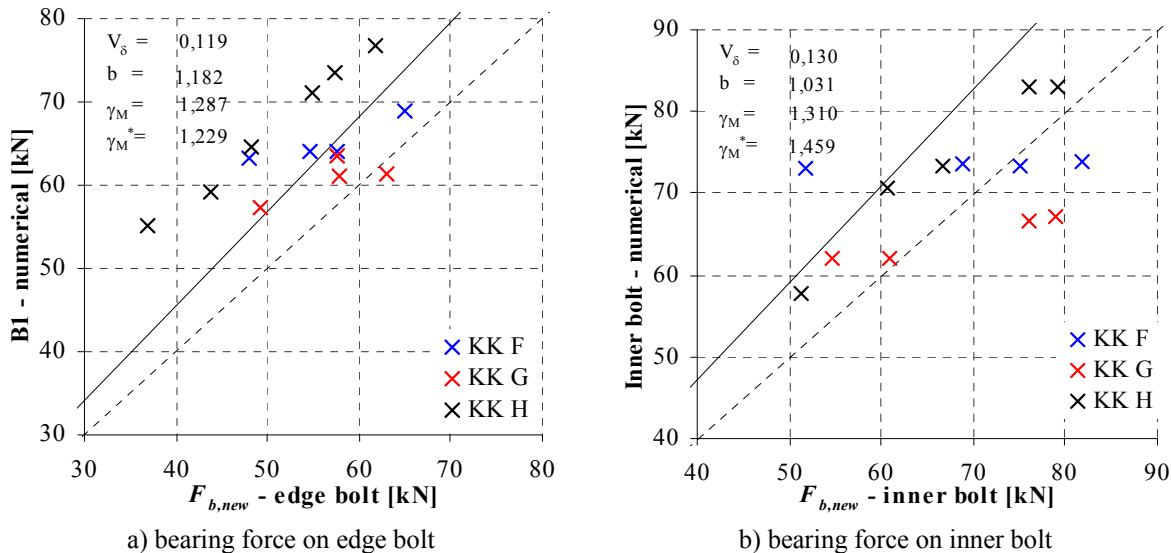


Fig. 117: Bearing forces on bolts for connections with two lines of bolts parallel to loading direction

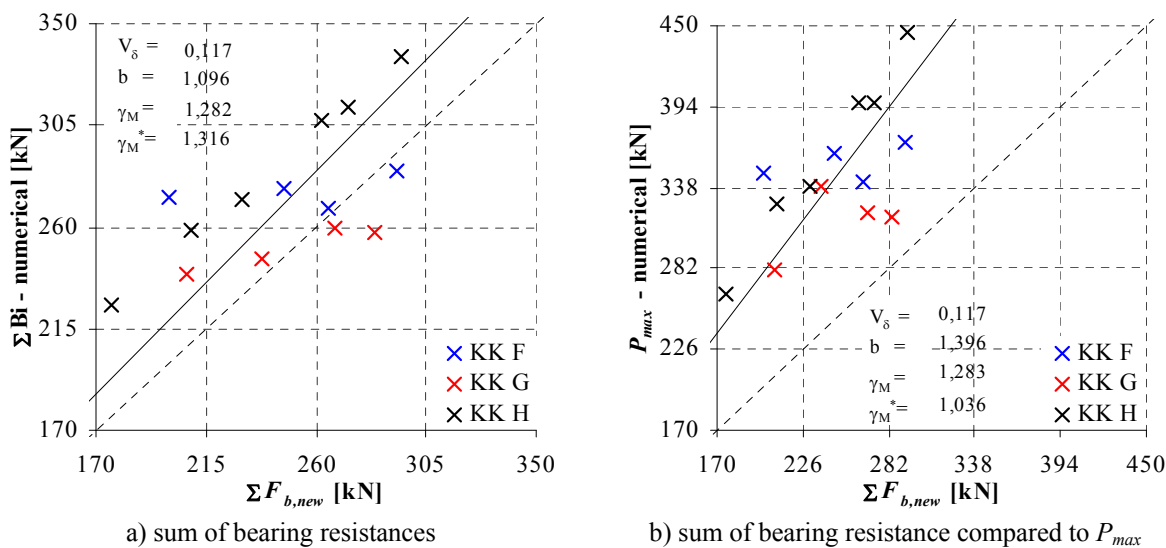


Fig. 118: Resistance of connections with two lines of bolts parallel to loading direction

5.9 Comparison of new bearing resistance formula to Eurocode bearing resistance

Figs. 119-121 compare the bearing resistance according to EN 1993-1-8 to the bearing resistance formula developed in this chapter. The Eurocode formula is plotted on the abscissa and the new formula is plotted on the ordinate. In Fig. 119 the resistances on the edge bolt are compared. In all cases of specimens L, the new formula gives lower values. In the cases of specimens B1 and B2 the new formula gives lower values if net cross-section failure was observed. Higher values of bearing resistances were obtained by new formula for Puthli, Fleisher connections, where edge distances and pitch p_2 were small. The new formula also

gives lower values in most cases of the connections from the numerical parametric study. Similarly is true for the resistance on the inner bolt in Fig. 120 for these results. In several cases of specimens L, the new formula gives higher values. If the resistance of the whole connection is considered (Fig. 121), then the sum of bearing forces according to Eurocode gives higher values than the sum of bearing forces according to new formula, mainly in cases of net cross-section failure.

In Fig. 122 the minimum of bearing resistance, net cross-section failure and block tearing resistance according to Eurocode is compared to the sum of bearing forces according to new formula as presented in this chapter. The scatter of points around dotted diagonal is much lower than in previous case in Fig. 121. Fig. 123 shows the same as Fig. 122, but only the results, where net cross-section or block tearing resistance is critical are shown. It is presented in this figure that new formula successfully accounts for net cross-section and block tearing resistance check. There are some results for specimen L for which the new formula gives lower results than Eurocode (safe side!). The reason for this is that the friction increased the resistance of the connection. If the friction forces were considered for the connections with more than two bolts by factor $k_{fric} = 1,1$ (see Fig. 124), all point moved even closer to the dotted diagonal, but not above it.

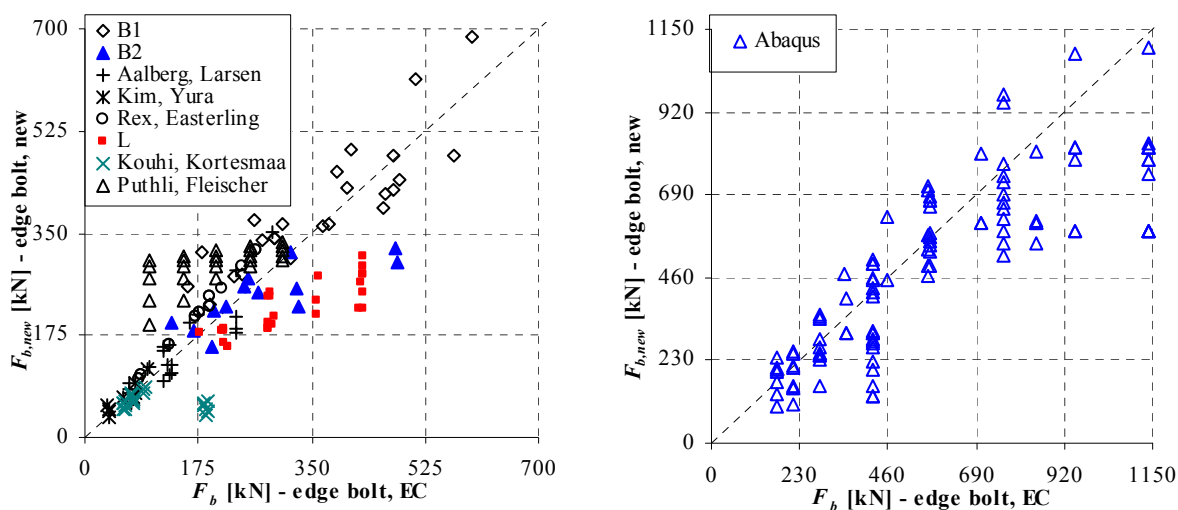


Fig. 119: Comparison of results for the edge bolt

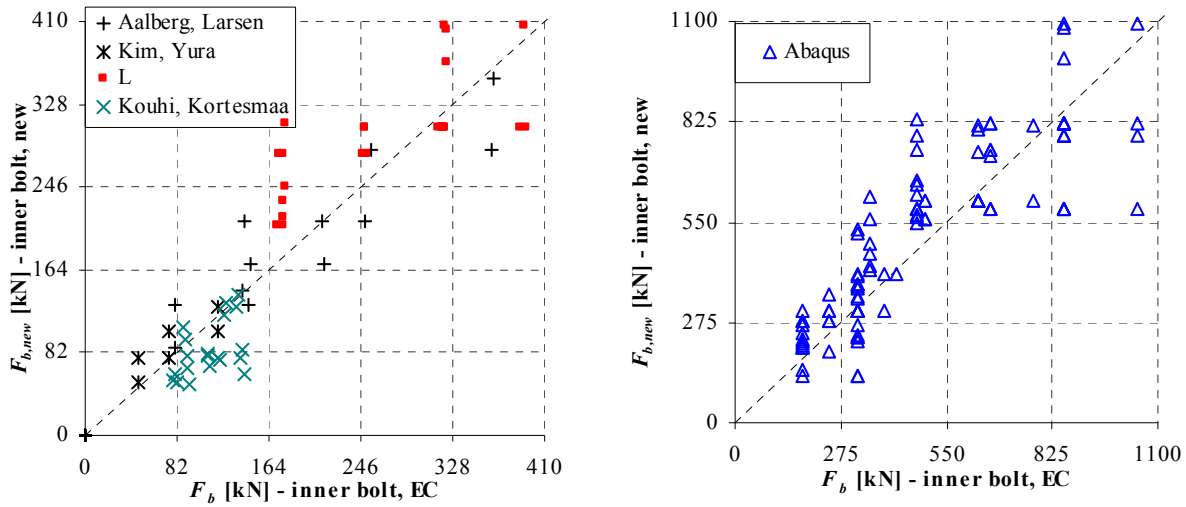


Fig. 120: Comparison of results for the inner bolt

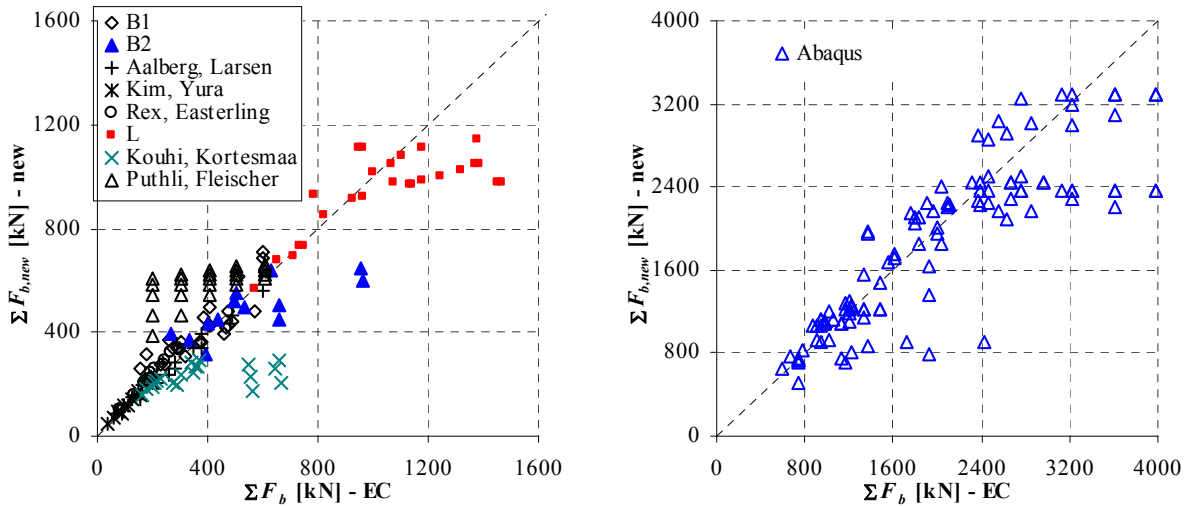


Fig. 121: Comparison of results for the sum of bearing forces

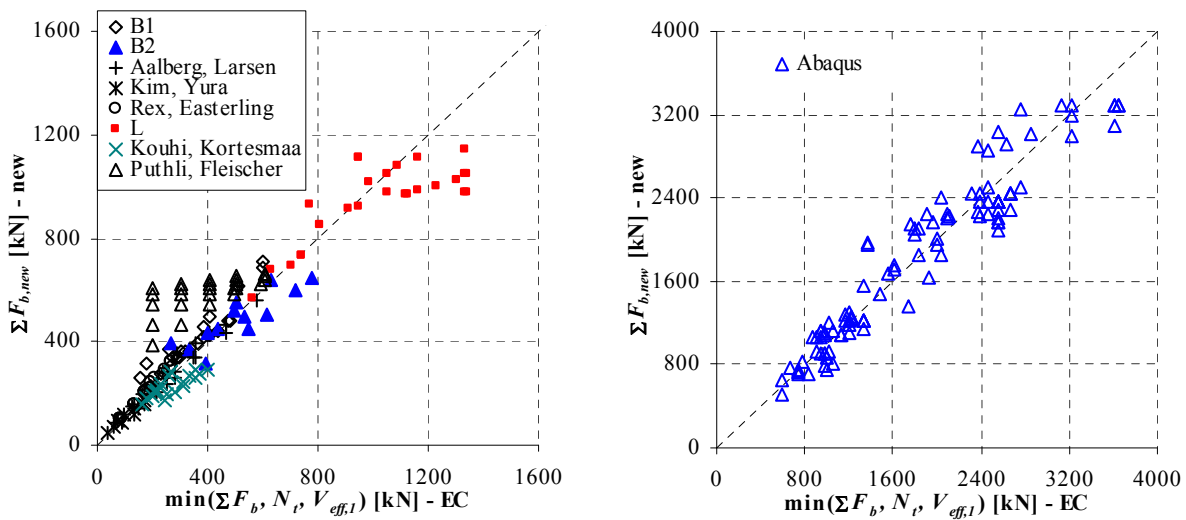


Fig. 122: Comparison of results for the minimum of sum of bearing forces, net cross-section resistance and bearing resistance

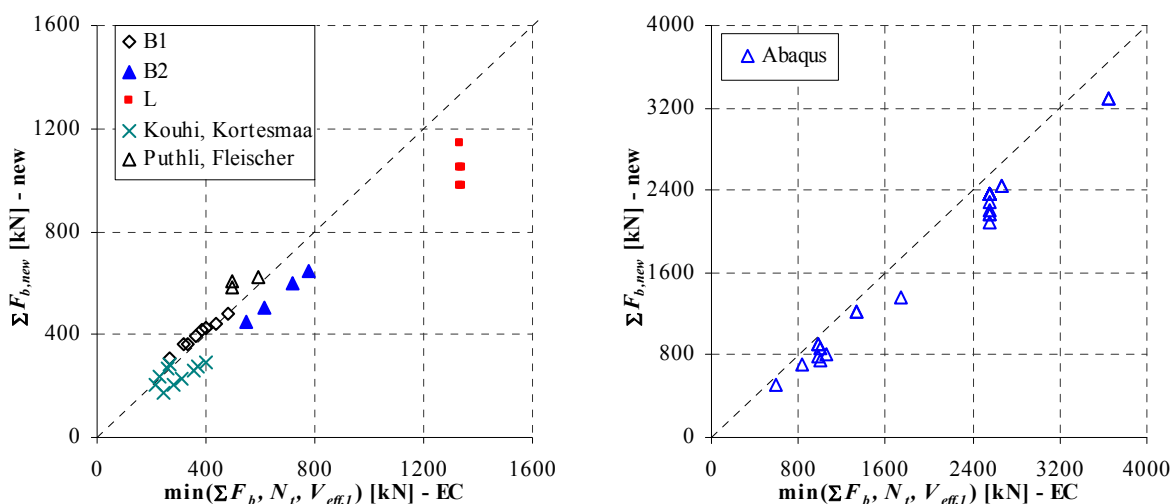


Fig. 123: Comparison of results for the minimum of sum of bearing forces, net cross-section resistance and bearing resistance – only results, where net cross-section or block tearing resistance is critical are shown

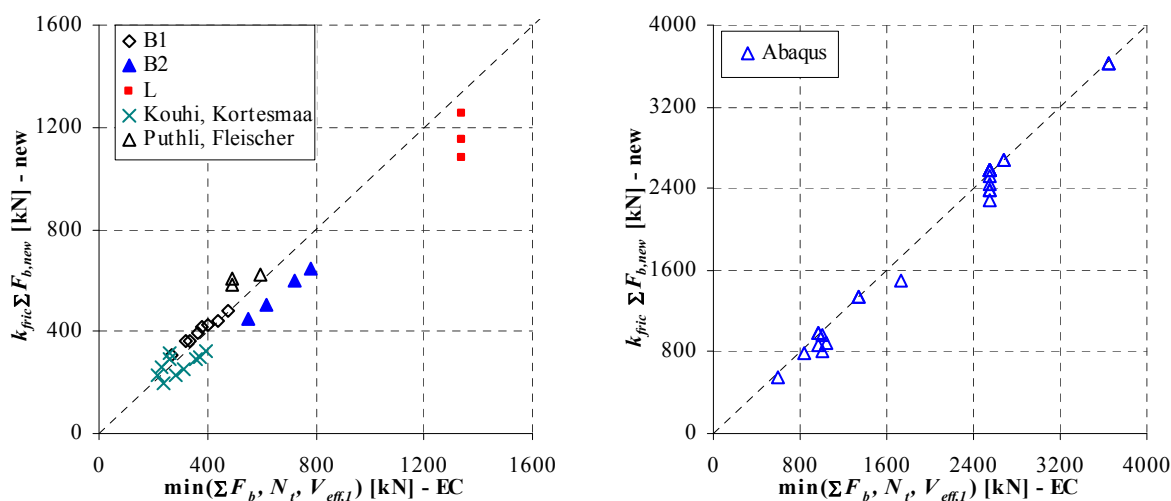


Fig. 124: Comparison of results for the minimum of sum of bearing forces, net cross-section resistance and bearing resistance – only results, where net cross-section or block tearing resistance is critical are shown – friction also is considered on the ordinate

The comparison of resistances in normalized format obtained as ratios theoretical/experimental values is shown in Figs. 125-129. In these figures the results for geometries L11-L13, L21-L22 and Rex, Easterling results with curling failures are excluded. The reasons for the exclusion of the results for geometries L11-L13, L21-L22 were convergence difficulties of numerical simulations before reaching the maximum resistance of the connections. The Eurocode and new bearing resistance formula do not account for curling failures, therefore and Rex, Easterling results with curling failures are excluded. The abscissas in Figs. 125-129 present the ratio between Eurocode bearing resistance formula and numerical (or experimental) resistance. The ordinates in these figures present the ratio between new bearing resistance formula and numerical (or experimental) resistance. The values lower than 1 are on the safe side. The thick black lines (horizontal and vertical) in the mentioned figures present unity, where theoretical and experimental results are equal. In these cases the dotted diagonal presents the equality of Eurocode and new bearing resistance formula.

In Fig. 125 the normalized resistance for the edge bolt is shown. Eurocode bearing resistance formula gives in certain cases very unrealistic results that are for more than three times on the unsafe side. There are also a lot of larger than 1,2 (danger side). The new formula much better estimates the values on the edge bolt. There are only a few results above the unity line, where one Kim, Yura result strikes the eye. Due to the rigid cover plates the distribution of bearing forces is very unequal. The new model does not account for such inequality. The new model gives the range of values between 0,7 and 1,1 for most of the results.

Fig. 126 depicts the normalized resistances on the inner bolt. The Eurocode formula scatters the values from 0,48 to 2,05. The most results are scattered approximately between 0,6 to 1,2. This is another confirmation of inaccurate resistance model of Eurocode function. On the other hand the new formula scatters the results between 0,55 to 1,18. The majority of results are placed in range of 0,75 to 1,1. The range of the results is significantly reduced by the new bearing resistance formula.

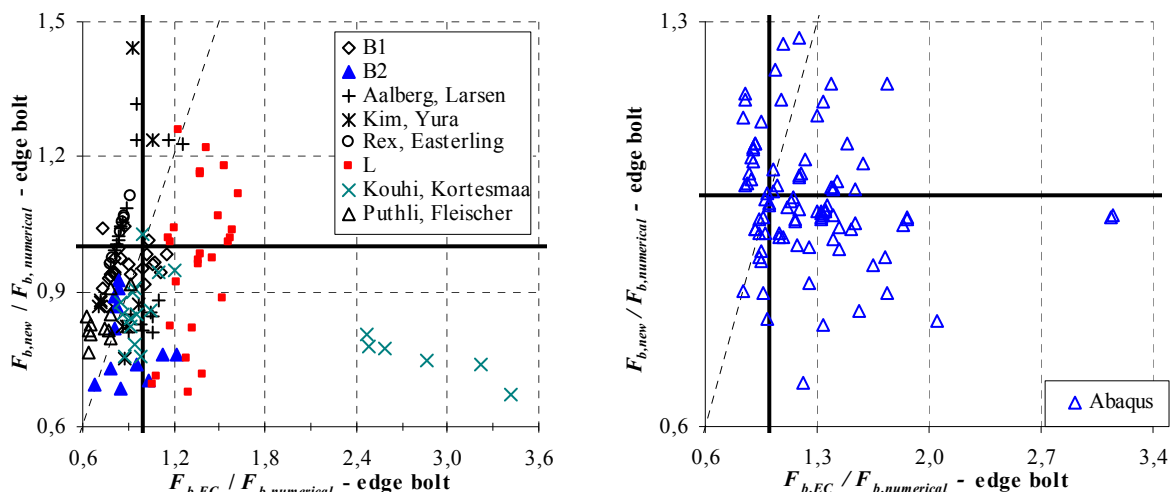


Fig. 125: Diagrams in normalized format obtained for the edge bolt

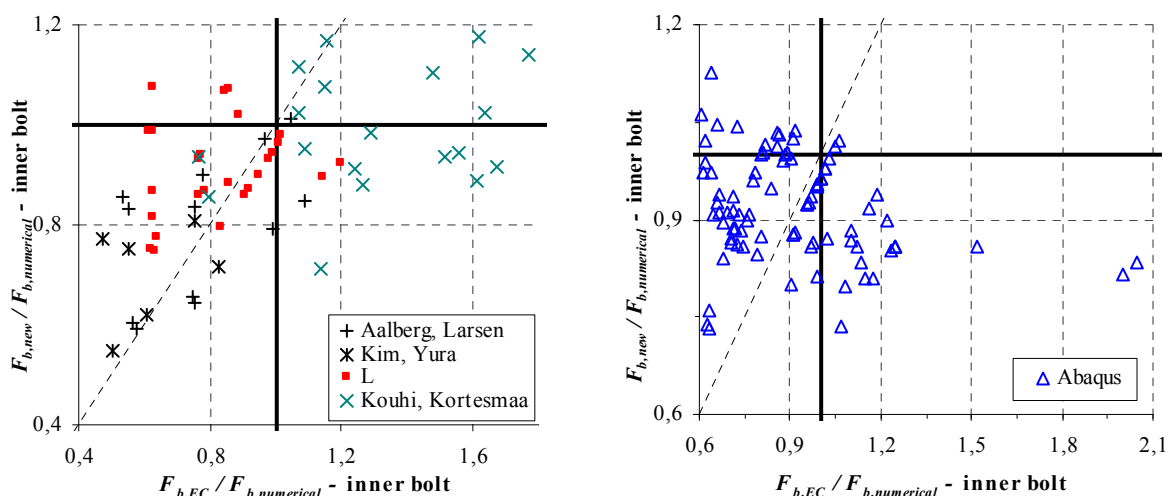


Fig. 126: Diagrams in normalized format obtained for the inner bolt

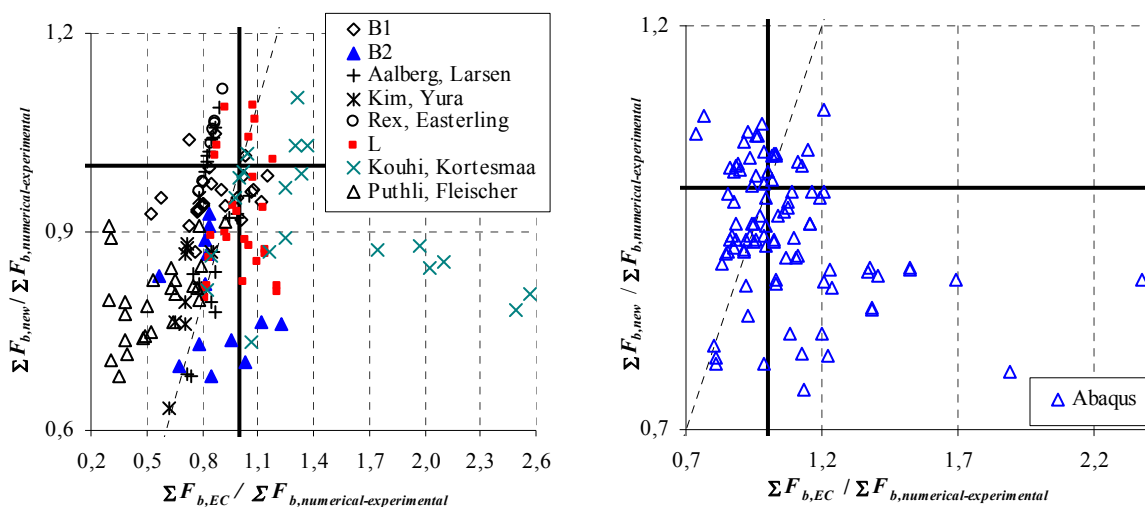


Fig. 127: Diagrams in normalized format obtained for the group of bolts

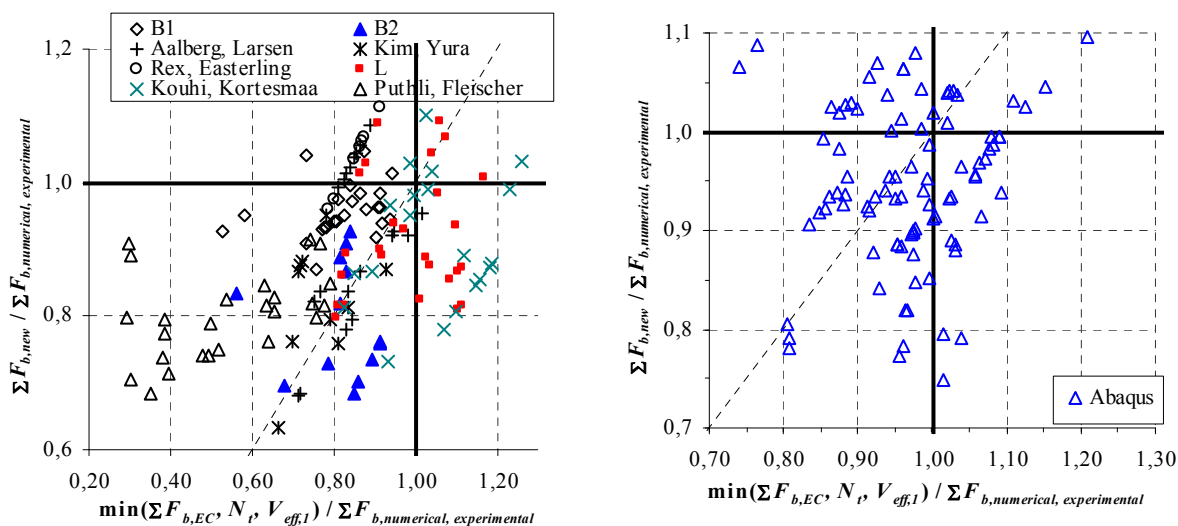


Fig. 128: Diagrams in normalized format obtained for the group of bolts, where additional Eurocode checks are considered

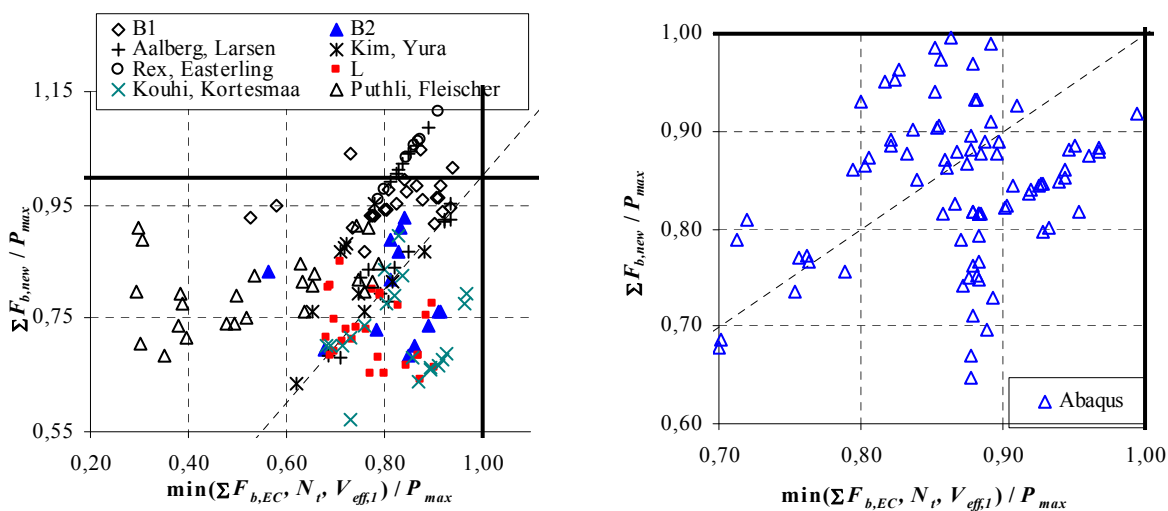


Fig. 129: Diagrams in normalized format obtained for the group of bolts, where additional Eurocode checks are considered and maximum resistance (including friction) as the “experimental” value

The normalized resistance of group of bolts is presented in Fig. 127, where the theoretical resistance is compared to the numerically obtained sum of bearing resistance (without friction). Again Eurocode formula scatters the values in the range between 0,29 to 2,57. If the net cross-section resistance and block-tearing checks are also considered on the abscissa (see Fig. 128), the upper boundary lowers to 1,26. The new bearing resistance formula estimates the resistance of group of bolts very well. The results lay in the range between 0,6 to 1,1, where the majority of the results are larger than 0,75 (see Figs. 127-128). If the theoretical resistances from Fig. 128 are normalized by the maximum resistance of the connection (friction included), all results with several bolts (where the friction plays an important role) move below unity line, for both Eurocode and new formula.

5.10 Summary

The stress and deformation state of steel plates loaded by bearing pressure, which is imposed by the fasteners, is a complicated phenomenon that can only be determined by numerical simulation. Notwithstanding, the increasing capability of computers, detailed numerical simulations remain expensive in everyday design. Hence, designers have to rely on simple formulas that present complex phenomena. This chapter has dealt with the transfer of load in bolted bearing type connections, which is one of such phenomena. There are many checks against different failure types regarding bolted bearing connections, prescribed in Eurocode standard. However, there is only one formula, called bearing resistance formula, which estimates the distribution of bearing forces between bolts. The bearing resistance formula is considered as an ultimate limit state check, but it is defined to limit hole elongations. The definition of this of formula is inconsistent with its application in Eurocode. Herein it was presented that the bearing resistance formula according to Eurocode gives in certain cases much too safe results, while in case of net cross-section failures it is too optimistic. Therefore, the net cross-section check has to be performed. Furthermore, on the basis of tests it has been shown that the formula poorly controls the hole elongation for single bolt connections. The connections with several bolts positioned in the direction of bearing force were characterized by average hole elongation equalling up to 6 mm, which is not a significant hole elongation. In addition, the distribution of bearing forces between bolts is a missed approach by Eurocode bearing resistance formula. The resistance of group of bolts is defined by the sum of bearing resistances of the individual bolt. It is merely a game of errors that the resistance of group of bolts is comparable to experimental results (the positive and negative errors summed to zero). Despite all, the design bearing resistance check of the group of bolts meets the reliability demands according to Eurocode only when all the required design checks are satisfied (design net cross-section check, design bolt tearing check...).

The thesis put the bearing resistance in a new light. The new definition follows. The bearing resistance on individual fastener is the maximum strength of the plate loaded by the bearing pressure of the fastener. A simple bearing resistance formula for high strength steel was

derived and is supported by our test results, the results found of other tests on bolted bearing shear connections found in literature and by numerical simulations of additional connection configurations. In total 266 results of bolted shear connections made of high steel grade were processed and statistically analysed. The new bearing function estimates the distribution of bearing force on individual bolt with statistically satisfying accuracy. The sum of bearing resistances correctly estimates the bearing resistance of the connection and anticipates the failure type. The design reliability of the new bearing resistance function was met by the recommended value of partial factor $\gamma_{M2} = 1,25$. The new function was evaluated only for $m \leq 2$. The new design bearing resistance on individual fastener is given by:

$$F_{b,new,Rd} = k_1 k_2 k_3 k_4 k_5 \cdot \frac{df_u}{\gamma_{M2}} \quad (104)$$

$$k_1 = \min\left(1,3 \frac{e'_1}{e'_2}; 1,9\right) \text{ if } k_1 = 1,9, \text{ the net cross-section fully yields,} \quad (105)$$

$$k_2 = \left(0,9 \frac{e'_2}{d_0} - \frac{1}{4}\right) \cdot \frac{1}{n} \quad (106)$$

$$b_{eff} = 2e_2 + (m-1)(p_2 - d_0) \quad (107)$$

$$e'_2 = \frac{b_{eff}}{2m} \quad (108)$$

- for edge bolt

$$k_3 = \min\left(\frac{2}{3} \frac{e_1}{p_1} + \frac{1}{2}; 1\right) \quad \text{for plates with equal bearing stiffness} \quad (109)$$

$$k_3 = \min\left(\frac{2}{3} \frac{e_1}{p_1^2} d_0 + \frac{1}{2}; 1\right) \quad \text{for plates with different bearing stiffness} \quad (110)$$

$$k_4 = 1 \quad \text{– also when } m = 1 \quad (111)$$

$$k_5 = 1 \quad \text{– also when } m = 1 \quad (112)$$

- for inner bolts

$$k_3 = 1 \quad \text{– also when } n = 1 \quad (113)$$

$$k_4 = \min\left(\frac{1}{2} \frac{p_1}{p_2} + \frac{1}{2}; 1\right) \quad (114)$$

$$k_5 = \min\left(\frac{1}{2} \frac{p_2}{e_2} + \frac{1}{2}; 1\right) \quad \text{if } k_5 < 1, \text{ the block tearing failure is possible} \quad (115)$$

d nominal bolt diameter

d_0 bolthole diameter

e_1 the end distance from the centre of the fastener hole to the adjacent end of any part, measured in the direction of load transfer

e_2 edge distance from the centre of the fastener hole to the adjacent end of any part, measured at right angles to the direction of load transfer

m number of bolts in a single column positioned perpendicular to load transfer

- n number of bolts in a single row positioned parallel to load transfer
- p_1 spacing between centres of the fasteners in a line of the direction of load transfer
- p_2 spacing measured perpendicular to the load transfer direction between adjacent lines of fasteners
- t thickness of the plate

Bolt nomenclature is illustrated in Fig. 130. The distribution of bearing resistances depends also on bearing stiffness of the connected plates. The plate bearing stiffness is defined in Section 5.5.2, while the distribution of bearing forces is shown in Table 29. Linear distribution of forces between fasteners was presumed, where force $F_{b,new,Rd}^{inner}$ is the maximum force on an inner bolt. The sum of design resistances for connections with *different* plate bearing stiffness, is given by

$$\sum F_{b,new,Rd} = \frac{m \cdot n (F_{b,new,Rd}^{edge} + F_{b,new,Rd}^{inner})}{2} \tag{116}$$

For the connections with *equal* plate bearing stiffness, with *odd number of bolts* in a single row positioned in the direction of load transfer, the sum of design bearing forces of individual bolt is given by the following equation.

$$\sum F_{b,new,Rd} = m \left(\frac{(n+1)(F_{b,new,Rd}^{edge} + F_{b,new,Rd}^{inner})}{2} - F_{b,new,Rd}^{inner} \right) \tag{117}$$

For the connections with *even number of bolts* a single row positioned in the direction of load transfer in equation (116) applies.

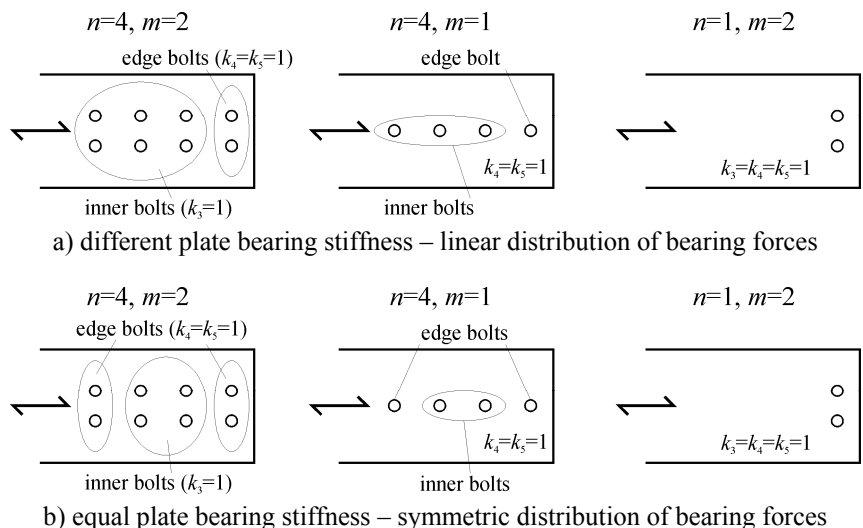


Fig. 130: Bolt nomenclature

Although the bolts are not preloaded in the bearing type connections, noteworthy friction forces develop in ultimate limit state. Bolts restrain the thickness deformation of the plates, which generates high pressure between them. The value of friction forces is dependent of the plate surface. The friction forces can be conservatively estimated by coefficient k_{fric} equal to

1,1. Therefore, the maximum design resistance of the bearing connection more than two bolts can be given by the equation:

$$P_{max,Rd} = k_{fric} \sum F_{b,new,Rd} \cdot \quad (118)$$

It is important to stress out that friction forces induce tension stress to the bolt. The friction forces are limited by yielding of the bolt, which may be caused by the combination of tension stress and shear stress induced by bearing. Plastic deformations in terms of bolt elongation decrease the friction forces. The magnitude of the tension stress in the bolts is not discussed in the thesis, but it may be obtained directly from the friction. The cases, where the friction is “out of range” are unrealistic. In these cases the yielding of the bolt would reduce the friction forces and probably slightly redistribute the distribution of bearing forces. The meaning of these cases was to obtain the resistance of the steel plate if the bolts withstand the high bearing pressures. The large magnitude of friction is therefore the consequence of very stiff bolts.

6 CONCLUSIONS

One of basic problems of structural high strength steels is that they are considered to be less ductile than mild structural steel. High strength steels undoubtedly have lower ductility than mild steels in terms of engineering measures of ductility, such as ultimate-to-yield strength ratio, uniform strain and elongation at fracture. Typical values for high strength steels are: ultimate-to-yield strength ratio $f_u/f_y = 1,05$, uniform strain $\epsilon_u = 0,05$ and percentage elongation after fracture $A^e = 15\%$, and are much lower than for mild steels. Therefore it is believed that they are suitable only for elastic analysis. Often forgotten measure of ductility is reduction of area at fracture Z , which is obtained by comparing the cross-sectional area after fracture. For high strength steel this measure indicates that the fractures can be characterized as ductile with large inelastic deformations. Inelastic behaviour is hidden in numerous nominally elastic resistance checks of steel structures and therefore sufficient local ductility has to be assured.

The primary goal of this thesis was to establish whether local ductility of bolted connections made of high strength steel can assure sufficient ductility for the transfer of loading between all bolts. The bolts impose high bearing pressure to the plates. Their position is due to bolthole clearance never perfect. Therefore stress concentration in the plate can cause fracture in the steel plate. If sufficient local ductility was assured, the inelastic deformations in the vicinity of bolthole would eliminate stress concentration and redistribute stress among fasteners. The scope of the research was restricted to tension splices with bolts in shear for which the failure occurred in the steel plate and not in the bolts.

This goal was achieved firstly by conducting extensive experimental test programme of 23 members with holes of different sizes in tension. These gave us the information on ductile behaviour of net cross-section. The experimental work was continued by monotonic tests of tension splices with bolts in double shear. Steel grade S690 was used in the experimental work. Beside single bolt connections (25 tests), and the connections with two bolts positioned perpendicular to the direction of bearing force (13 tests), the connections with three or four bolts positioned in the direction of bearing force (26 tests) were tested. The research of the latter assembly of the connections has not yet been documented in technical nor in scientific literature. The experimental programme was supplemented by FE analysis. The influence of bolthole clearance was also considered in the research. Additionally, the researches of similar connections were gathered from literature (93 tests) and most of them were simulated by FE analysis (38 tests). The tests showed that the connections made of high strength steel have sufficient local ductility to redistribute the loading. Sufficient ductility was assured even when the position of the bolts was unfavourable. Due to bolthole clearance all bolts except one were shifted to the back surface of the bolthole, thus only a single bolt was transferring whole

bearing force until the remaining bolts were activated. This occurred at a displacement equal to bolthole clearance or in our case to the displacement of 2 mm.

The original contribution of this work was the validation of design provisions for elements in tension by statistical analysis of experimental results. A reliable database of net cross-section resistances was created from our test results and also from results found in literature that include different high steel grades. A total of 80 results of net cross-section resistances were presented. By statistical analysis of test results according to Annex D of EN 1990 the following results were obtained:

- Net cross-section design resistance for high strength steels:

$$N_{t,Rd} = \frac{0,9 A_{net} f_u}{\gamma_{M2}}$$

is with $\gamma_{M2} = 1,25$ safe. Moreover, it was established that this design resistance is very conservative for high strength steel sections. The partial factor needed is only 1,03 (data set 1 in Table 13).

- Additional rule for lower bound of net cross-section design resistance for high strength steels as was defined in the draft of EN 1993-1-12:

$$N_{t,Rd} = \frac{A_{net} f_y}{\gamma_{M0}}$$

(with $\gamma_{M0} = 1,00$) may not be safe enough. Based on our test results, the design resistance as written above was in the final draft of EN 1993-1-12 changed to be equal to the design net cross-section resistance as defined in EN 1993-1-1. This is very important original contribution.

- It was established that the design net cross-section resistance of unsymmetrically connected member in tension with one bolt may also be used for high strength steel sections, although EN 1993-1-12 disallows its use:

$$N_{u,Rd} = \frac{2(e_2 - 0,5d_0) t f_u}{\gamma_{M2}} .$$

Another important result and also an original contribution was presented in this work. An extensive parametrical FE study of the connections was performed in order to obtain the distribution of bearing forces between bolts. The parameters are presented in Chapter 5.5. The study included 173 connection assemblies, of which 64 were based on full scale tests. Additionally, the database was supplemented by 93 one-bolt and two-bolt connections (two bolts positioned perpendicular to the direction of bearing force) for which the bearing force on individual bolt was known. Hence, a database included 266 connections. Based on this database the reliability of design bearing resistance formula as defined in EN 1993-1-8 was performed according to the procedure described in Annex D, En 1990. The bearing resistance formula is considered as an ultimate limit state check, but it is defined to limit hole

elongations. The definition of this of formula is inconsistent with its application in Eurocode. It was presented that the bearing resistance formula gives in certain cases much too safe results, while in case of net cross-section failures it is too optimistic. This two-faced character of the formula implies large scatter of results when compared to the experimental values and therefore large partial factors are required to form a design formula. It was established that the design bearing resistance is according to the definition of the reliability in EN 1990 not statistically reliable. The design bearing resistance of a group of fasteners cannot be considered as reliable if used as a stand-alone check in the connection design, as well. Despite all this, the design bearing resistance check of group of bolts meets the reliability demands, however only when all of the required design checks are satisfied (design net cross-section check, design bolt tearing check...).

Another important original contribution was the description of complex stress-strain state of tension splices with bolts in shear by means of numerical simulations. The results of numerical simulations were graphically and numerically compared to the experiment. To achieve the perfect fit of the state-of-the art numerical methods were used.

The most important original contribution of this thesis is the proposition of new design bearing resistance formula. Different definition of the bearing resistance is proposed, consistent with ultimate limit state. The new bearing resistance formula was on a basis of theoretical background and large database of experimental results developed for a single bolt connection and successfully applied to any kind of connection with bolts in bearing by additional factors. The summation of bearing forces was proposed with regards to the distribution of forces between fasteners. The design formulas, the bearing resistance on individual fastener as well as its summation, were evaluated by the procedure in EN 1990 and are in a compact form presented in Chapter 5.10. The main advantages of the new design bearing resistance formula are:

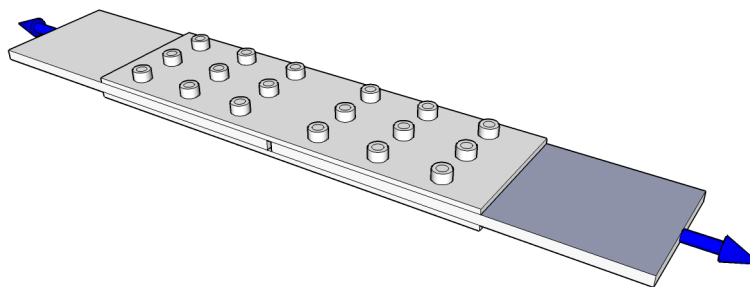
- it is simple to use, because it consists of five coefficients which are linear functions of geometric parameters, and is therefore appropriate for the use in practise,
- it is able to distinguish between several failure type; thus a connection can be designed to fail in a desired failure mode,
- inductile failure of bolts can be prevented, since high strength bolts should be used in the bearing type connections made of high strength steel,
- the bearing resistance of group of fasteners can be used as a stand-alone check (although this is not recommended) it can therefore can be directly compared to other resistance checks that are required and it consequently also minimizes the collapse risk if the other required checks were not performed,
- the maximum connection resistance consists of the bearing and frictional part of the resistance – the frictional resistance part can be conservatively taken into account,
- the geometry of the connections can be optimized for peak performance.

7 POVZETEK

UVOD

Med jekla visoke trdnosti (JVT) štejemo tista z napetostjo tečenja višjo ali enako od $f_y \geq 420$ MPa. Zaradi sodobnih postopkov izdelave in nizke vsebnosti ogljika so jekla visoke trdnosti dobro variva. Ugodno razmerje med ceno in nosilnostjo povečuje zanimanje za njihovo uporabo. Glede na običajno konstrukcijsko jeklo imajo JVT višjo trdnost in običajno tudi višjo žilavost, vendar manjšo duktilnost.

Projektiranje jeklenih konstrukcij je usmerjeno k duktilnemu odzivu celotne konstrukcije. Pri tem je pomemben prenos obtežbe med elementi, saj lahko pri prenosu nastanejo koncentracije napetosti. Prav tako je za globalno duktilnost pomemben izbor materiala. Znano je, da so JVT manj duktilna od običajnih jekel. Njihova uporaba v konstrukcijskih elementih je bila v preteklosti omejena pretežno na elastično globalno analizo. Standard Evrokod 3 za projektiranje jeklenih konstrukcij EN 1993-1-1 (CEN, 2005a) dovoljuje uporabo jekel do S460, čeprav se v konstrukcijski praksi uporabljajo jekla do trdnosti S1300. V ta namen je bil k Evrokodu 3 v zadnjem trenutku dodan standard EN 1993-1-12 (CEN, 2007), ki obravnava jekla do S700. V tem standardu so določeni nižji kriteriji glede duktilnosti kot v EN 1993-1-1. Priporočene vrednosti so $f_u/f_y \geq 1,05$, deformacija pri poružitvi $\varepsilon_{fr} \geq 10\%$ in $\varepsilon_u \geq 15 f_y/E$ (f_y – napetost tečenja, E – elastični modul). Tipično jeklo S690 ima deformacijo pri natezni trdnosti ε_u okoli 5% (Može et al., 2007a), deformacija pri poružitvi pa se giblje okoli 15%.



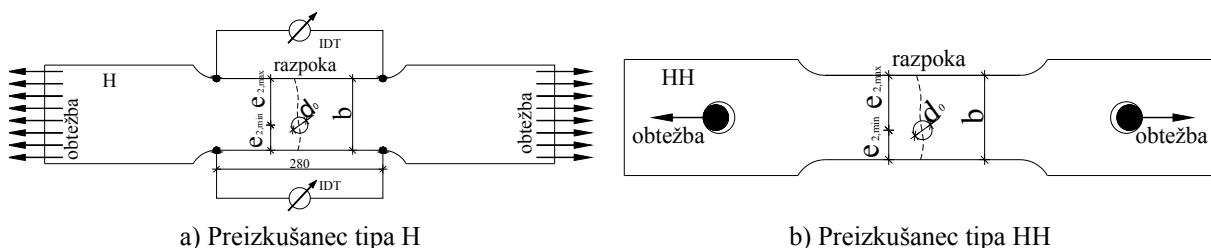
Slika 1: Enostavno natezni preklopni spoj

Namen doktorskega dela je bila ocena lokalne duktilnosti in z njo povezane nosilnosti vijachenih spojev narejenih iz JVT z nizkim razmerjem f_u/f_y . Težišče disertacije temelji na obsežnih eksperimentalnih testih, ki so osnova za razvoj novih in enostavnih metod za projektiranje vijachenih spojev iz JVT. Osredotočili smo se na teste jeklenih trakov z luknjo in nateznih preklopnih spojev z vijaki v dvojnem strigu (glej sliko 1).

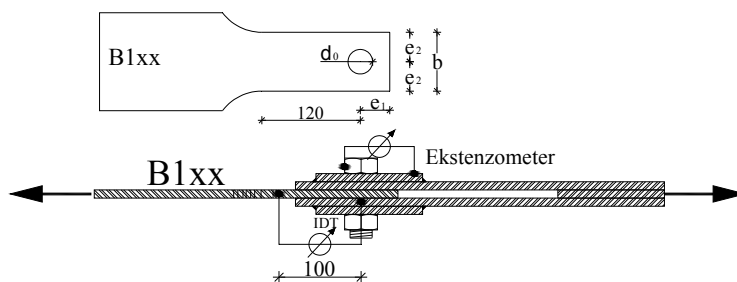
Obravnavana tema je bila predstavljena slovenski in tuji strokovni javnosti (Može, Beg, 2006. Može et al., 2006a. 2006b. Može, Beg, 2007. Može et al., 2007a. 2007b).

TESTNI PROGRAM

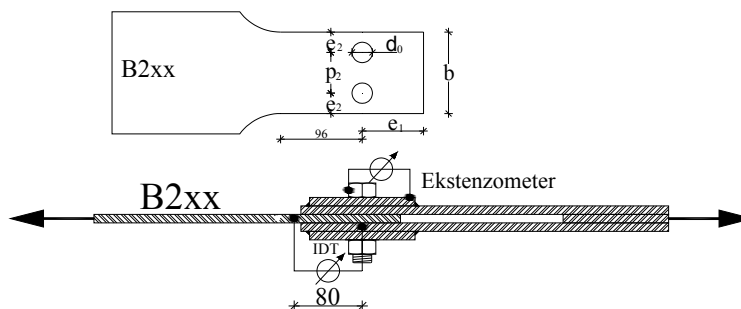
Eksperimentalno delo smo izvršili v dveh fazah. V prvi fazi smo izvedli serijo testov na nateznih trakovih z luknjo, kjer je luknja predstavljala oslabitev prereza. Preizkušanci tipa H (glej sliko 2a) so bili togo vpeti v preizkuševalno napravo, preizkušanci tipa HH pa členkasto (glej sliko 2b). V tej fazi smo testirali tudi natezne spoje z enim vijakom B1 (slika 3) ali dvema vijakoma B2 (slika 4) postavljenima pravokotno na smer obremenitve. Predmet druge faze so bili izključno spoji s tremi ali štirimi vijaki v dvojnem strigu, postavljenim v smeri prenosa obtežbe, ki smo jih poimenovali preizkušance tipa L. (slika 5). Geometrija posameznih preizkušancev je prikazana v preglednicah 1-3. Simboli uporabljeni v preglednici 3 so prikazani na sliki 6.



Slika 2: Preizkušanci tipa H, HH – jekleni trakovi z luknjami podvrženi nategu

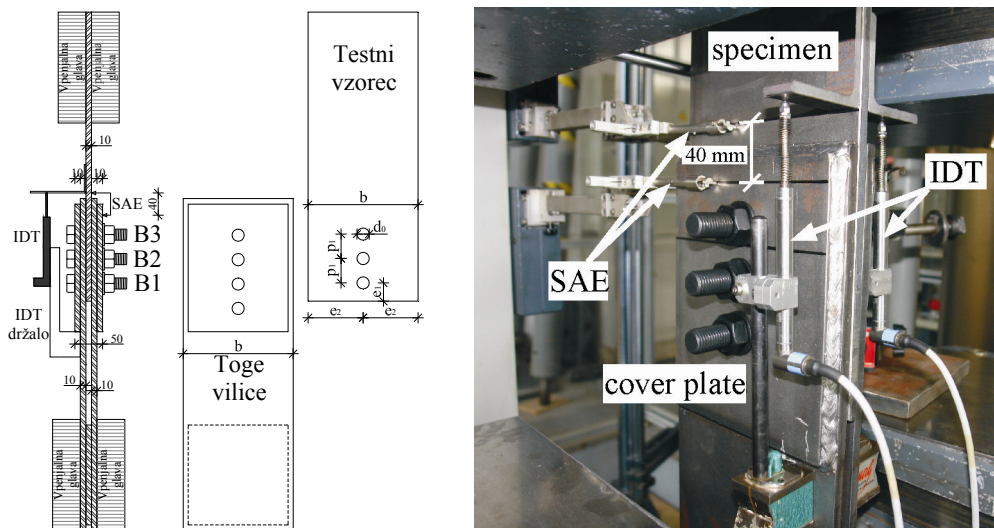


Slika 3: Preizkušalec tipa B1 – spoj z enim vijakom

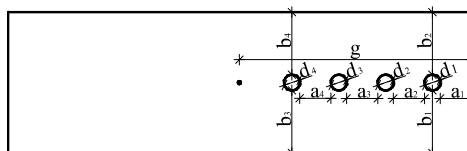


Slika 4: Preizkušalec tipa B2 – spoj z dvema vijakoma

Za izdelavo preizkušancev smo v vsaki izmed faz uporabili po eno jekleno ploščo z nominalno debelino $t = 10$ mm in kvaliteto jekla S690 QL (z nominalno napetostjo tečenja $f_{yn} = 690$ MPa in nominalno natezno trdnostjo $f_{un} = 770$ MPa). Dejanske materialne karakteristike smo izmerili v skladu z merodajnimi standardi. Povprečne izmerjene materialne karakteristike so prikazane v preglednici 4.



Slika 5: Preizkušanci tipa L opremljeni z merilnimi napravami



Slika 6: Simboli izmerjenih dolžin pri preizkušancih tipa

Preglednica 1: Geometrija preizkušancev tipa H, HH

Ime preizkušanca	Ekscen-tričnost	Nominalne dimenzije [mm, mm ²]						Dejanske dimenzije [mm, mm ²]					
		<i>b</i>	<i>t</i>	<i>d</i> ₀	<i>e</i> _{2,min} - <i>d</i> ₀ /2	<i>e</i> _{2,max} - <i>d</i> ₀ /2	<i>A</i> _{net}	<i>b</i>	<i>t</i>	<i>d</i> ₀	<i>e</i> _{2,min} - <i>d</i> ₀ /2	<i>e</i> _{2,max} - <i>d</i> ₀ /2	<i>A</i> _{net}
H01	Ne	100	10	0	50	50	1000	101,3	10,15	0			1013
H02	Ne	100	10	0	50	50	1000	101,5	10	0	50,0	50,0	1015
H03	Ne	100	10	5	47,5	47,5	950	101,9	10	5	47,7	48,8	969
H04	Ne	100	10	10	45	45	900	100,9	10	10	45,0	45,4	909
H05	Ne	100	10	10	45	45	900	101,3	10	10	45,4	45,8	913
H06	Ne	100	10	13	43,5	43,5	870	101,7	10	13	44,3	44,4	887
H07	Ne	100	10	18	41	41	820	101,3	10	18	41,7	42,0	833
H08	Ne	100	10	22	39	39	780	101,7	10	22	39,6	39,7	797
H09	Ne	100	10	22	39	39	780	102,4	10	22	39,6	40,9	804
H10	Ne	100	10	26	37	37	740	101,6	10	26	37,0	38,6	756
H11	Ne	100	10	30	35	35	700	101,6	10	30	35,1	36,4	716
H11A	Ne	100	10	30	35	35	700	99,9	10	30	34,8	35,1	699
H12	Ne	100	10	30	35	35	700	101,3	10	30	34,5	36,4	713
H13	Da	100	10	30	28	42	700	101,4	10	30	29,4	42,0	714
H14	Da	100	10	30	21	49	700	101,6	10	30	22,4	49,1	716
H15	Ne	100	10	40	30	30	600	101,8	10	40	29,2	32,5	618
H16	Ne	100	10	50	25	25	500	101,6	10	50	25,5	26,1	516
H17*	Ne	100	10	0	50	50	1000	101,3	10	0			1013
H18*	Ne	100	10	10	45	45	900	101,1	10	10	45,3	45,8	911
H19*	Ne	100	10	22	39	39	780	101,2	10	22	39,4	39,8	792
H20*	Ne	100	10	50	25	25	500	100,8	10	50	24,9	25,9	508
HH01	Da	80,0	10	24	28	28	560	78,4	10	24	26,4	27,3	544
HH02	Da	80,0	10	24	22	34	560	79,0	10	24	19,9	35,1	550
HH03	Da	80,0	10	24	16	40	560	78,5	10	24	14,1	40,4	545
HH04	Da	80,0	10	18	31	31	620	77,9	10	18	22,7	32,1	599
HH05	Da	80,0	10	18	25	37	620	78,5	10	18	22,1	38,4	605
HH06	Da	80,0	10	18	19	43	620	78,5	10	18	17,2	43,3	605

* jeklo S235

Preglednica 4: Povprečne materialne karakteristike

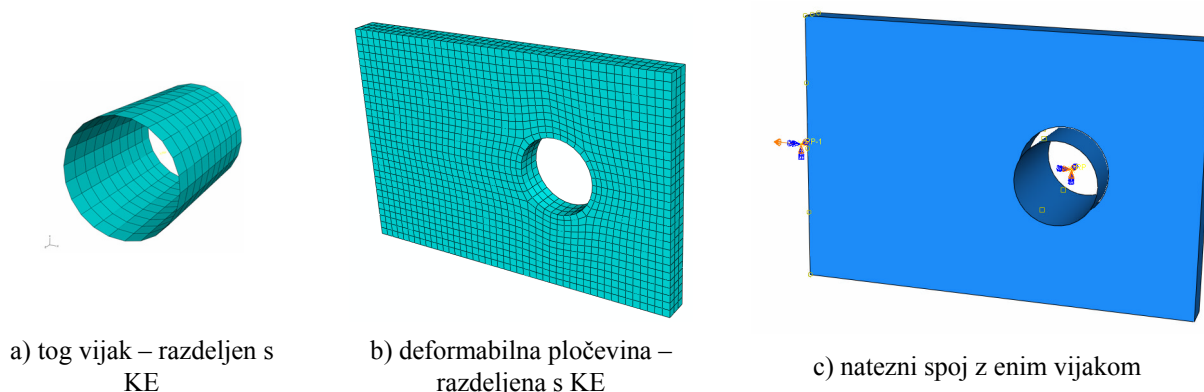
Pločevina	$R_{p0,2} = f_y$ [MPa]	$R_m = f_u$ [MPa]	A_{gt} [%]	A^c [%]	Z [%]
I	847	884	5,1	14,4	58,4
II	796	844	6,4	17,1	59,3

METODOLOGIJA NUMERIČNIH MODELOV

Z numeričnimi simulacijami smo določili veličine, ki jih v preiskavi nismo mogli izmeriti. Preizkus smo numerično modelirali končnimi elementi (KE) v okolju ABAQUS v6.5-v6.7 (SIMULIA, 2007). Uporabili smo tri konceptualno različne numerične modele nateznih spojev z vijaki v strigu, ki smo jih poimenovali numerični model tipa M1, M2 in M3.

Numerični model tip M1

Numerični model tipa M1 je najbolj preprost model. Spoj sestavljata tog vijak (modeliran kot tego telo) in deformabilna pločevina oziroma preizkušanelec, ki bil bila modelirana s tridimenzionalnimi osem-vozliščnimi KE z reducirano integracijo z imenom C3D8R. Med vijakom in pločevino je bil definiran kontakt v normalni smeri. Posamezni deli numeričnega modela in celoten spoj je prikazan na sliki 7. Model M1 smo uporabili v primeru, ko se pozicija vijakov ni spremenila in kadar preklonni pločevini nista ovirali deformacije preizkušanca v smeri debeline.

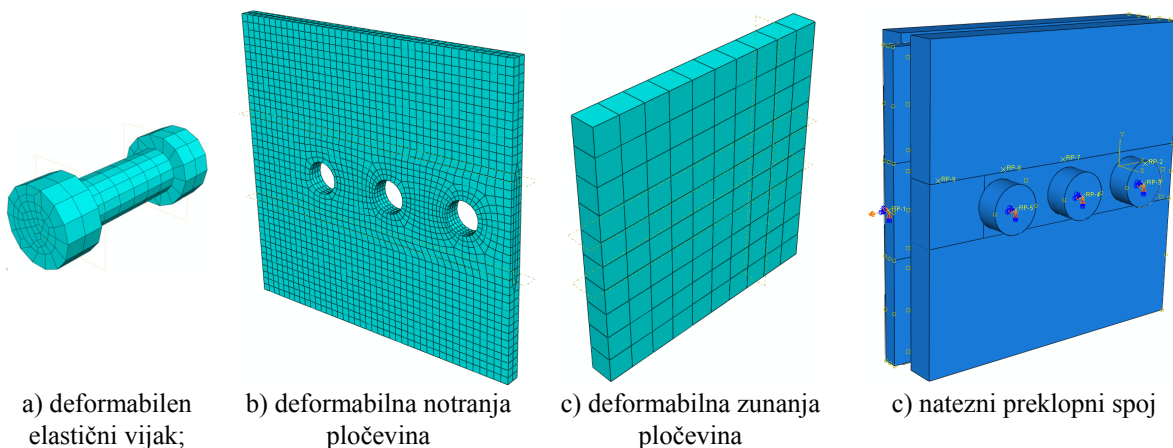


Slika 7: Numerični model tip M1

Numerični model tip M2

Ta numerični model je nadgradnja modela M1. Dodatno sta bili vpeljani preklonni oziroma zunanji pločevini. Vijaki so bili modelirani kot deformabilno telo z glavo in matico. Zunanji pločevinama in vijakom je bil predpisan elastični material. Med preizkušancem in zunanji pločevinama je bil definiran kontakt v normalni in tangencialni smeri s trenjem. Prav tako je bil definiran kontakt med stebлом vijaka in luknjo za vijak na preizkušancu. Kontakt med zunanji pločevinama in vijaki ni bil zajet. Vpeljan je bil samo kontakt med glavo oziroma matico vijaka in pripadajočo površino na zunanji pločevini. Glava in matica sta bili podprti v vseh smereh razen v osi pravokotni na ravnino pločevin. Podobno sta bili podprti zunanji pločevini, kar je omogočilo, da je deformacija preizkušanca v smeri debeline povzročila natezno silo v vijakih, ki so delovali kot elastična vzmet. Pogoj za nastanek sile

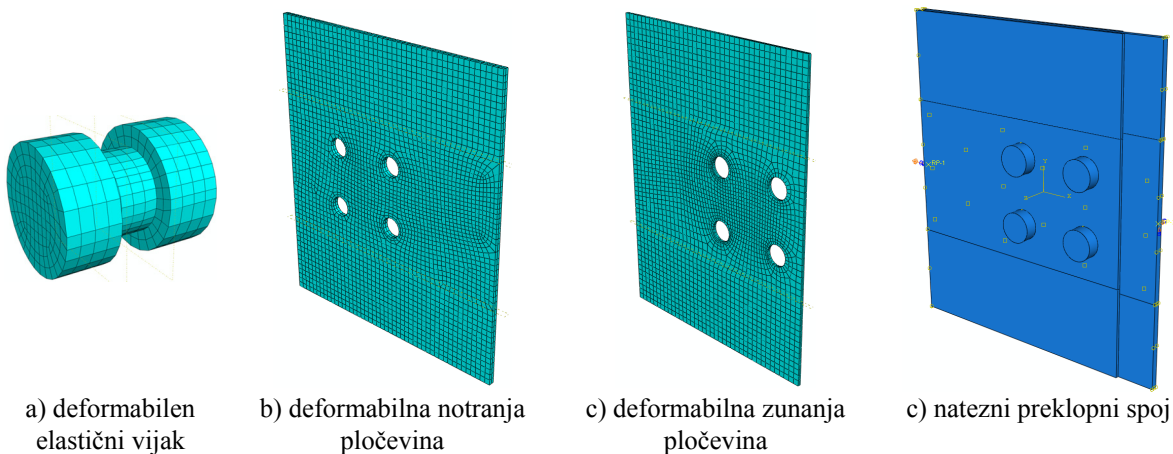
trenja je bil pritisk med zunanjo pločevino in preizkušancem. Numerični model tipa M2 je predstavljen na sliki 8. Numerični model tipa M2 smo uporabili za simulacijo spojev, kjer so bile zunanje pločevine bistveno bolj toge od preizkušanca in so hkrati ovirale deformacijo debeline preizkušanca ter s tem v spoj vnesle trenje. Zaradi velike togosti zunanjih pločevin se pozicija vijakov med obremenjevanjem ni spremenila.



Slika 8: Numerični model tip M2

Numerični model tip M3

Numerični model tipa M3 je najbolj splošno opisoval natezni preklopni spoj z vijaki v dvojnem strigu. Razlika z modelom tipa M2 je le v vpeljavi kontakta med stblom vijaka in zunanjsima pločevinama. Model je prikazan na sliki 9. Pri tem modelu je bila pozicija vijakov med obremenitvijo odvisna od deformacij lukenj na zunanjsih pločevinah.



Slika 9: Numerični model tip M3

ELEMENTI Z LUKNJAMI V NATEGU – PORUŠITEV PO OSLABLJENEM PREREZU

Splošno o projektih nosilnostih

Standard EN 1993-1-1 (CEN, 2005a) navaja, da se pri prečnih prerezih z luknjami za natezno nosilnost vzame manjša izmed naslednjih dveh vrednosti:

- projektne nosilnosti oslabiljenega prereza v območju lukenj za vezna sredstva, ki preprečuje pretrganje oslabiljenega prereza A_{net}

$$N_{u,Rd} = \frac{0,9A_{net}f_u}{\gamma_{M2}} \quad (E1)$$

- oziroma projektne plastične nosilnosti polnega prereza, ki preprečuje prekomerno podaljševanje nateznega elementa zaradi tečenja polnega prereza A

$$N_{pl,Rd} = \frac{Af_y}{\gamma_{M0}} \quad (E2)$$

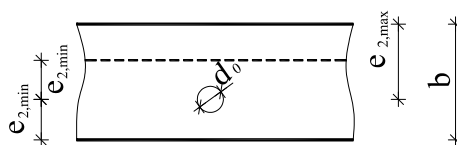
Za JVT je bila v predlogu standarda prEN 1993-1-12 navedena dodatna zahteva, ki je določila spodnjo mejo nosilnosti oslabiljenega prereza.

$$N_{t,Rd} = \frac{A_{net}f_y}{\gamma_{M0}} \quad (E3)$$

Nesimetrično priključen element v nategu se lahko v skladu z EN 1993-1-8 (CEN, 2005b) obravnava kot centrično obremenjen v sodelujočem oslabiljenem prerezu. Projektna nosilnost takega elementa, priključenega z enim vijakom, je podana z enačbo:

$$N_{u,Rd} = \frac{2(e_2 - 0,5d_0)tf_u}{\gamma_{M2}} \quad (E4)$$

kjer je e_2 minimalna robna razdalja, d_0 premer luknje in t debelina pločevine, kot je prikazano na sliki 10. V EN 1993-1-12 je določeno, da zaradi pomanjkanja eksperimentalnih rezultatov uporaba enačbe (E4) za JVT ni dovoljena.



Slika 10: Reducirana velikost oslabiljenega prereza

V prejšnjih enačbah koeficienti γ_{Mi} predstavljajo delne faktorje odpornosti, ki se uporabljajo skupaj z različnimi karakterističnimi vrednostmi odpornosti. Določeni so s pomočjo statistične analize eksperimentalnih rezultatov, saj je metoda mejnih stanj, ki je uporabljena v evrokodih, semiprobabilistična metoda. V izogib prevelikim številom faktorjev odpornosti so v EN 1993-1-1 definirani trije razredi γ_M faktorjev:

- γ_{M0} nosilnost prečnih prerezov,
- γ_{M1} odpornost elementov na nestabilnost,
- γ_{M2} odpornost natezno obremenjenih neto prečnih prerezov na pretrg, vezna sredstva.

Slovenski Nacionalni dodatek k EN 1993-1-1 za delne faktorje odpornosti privzema priporočene vrednosti in sicer $\gamma_{M0} = \gamma_{M1} = 1,0$ in $\gamma_{M2} = 1,25$.

Za JVT je projektna nosilnost določena z enačbo (E3) vedno merodajna, saj je vedno večja od projektne nosilnosti določene z enačbo (E1). Ob predpostavki, da za JVT velja $f_u/f_y \leq 1,10$, je dokaz trditve enostaven. Sedaj se ob upoštevanju priporočene vrednosti delnega faktorja odpornosti $\gamma_{M0} = 1,0$ in razmerja med natezno trdnostjo in napetostjo tečenja za JVT postavlja vprašanje, ali je projektna nosilnost (E3) v skladu s kriteriji zanesljivosti kot je to določeno v standardu EN 1990 (CEN, 2004a), ki določa osnove za projektiranje konstrukcij.

Rezultati testov

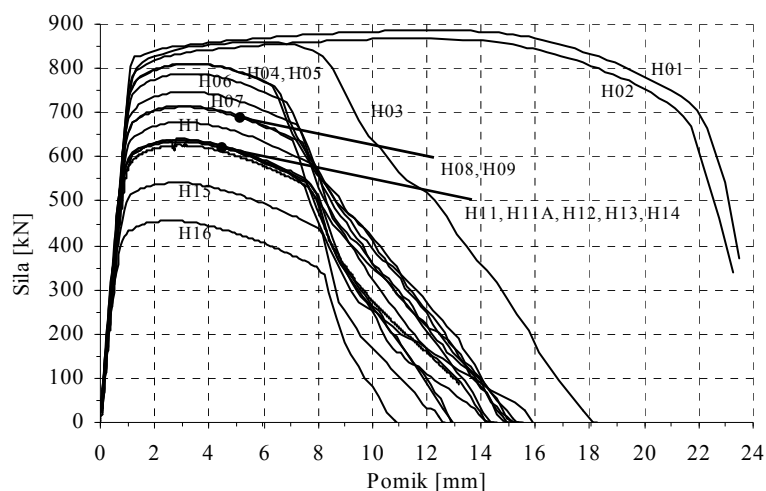
Pri preizkušancih H in HH (jeklo S690) se je pojavilo lokalno tanjšanje pločevin (prečna kontrakcija) na robovih luknje oslabiljenega prereza preden je bila dosežena največja odpornost preizkušancev. Prečna kontrakcija celotnega oslabiljenega prereza je postala opazna šele po vnosu največje sile. Plastične deformacije so bile največje na robovih luknje oslabiljenega prereza, kjer je nastala vidna razpoka. Le ta je počasi napredovala proti zunanjemu robu preizkušanca. Hitrost napredovanja razpoke je bila neodvisna od velikosti luknje. Opisana obtežna stanja za preizkušane H10 so prikazana na sliki 11.



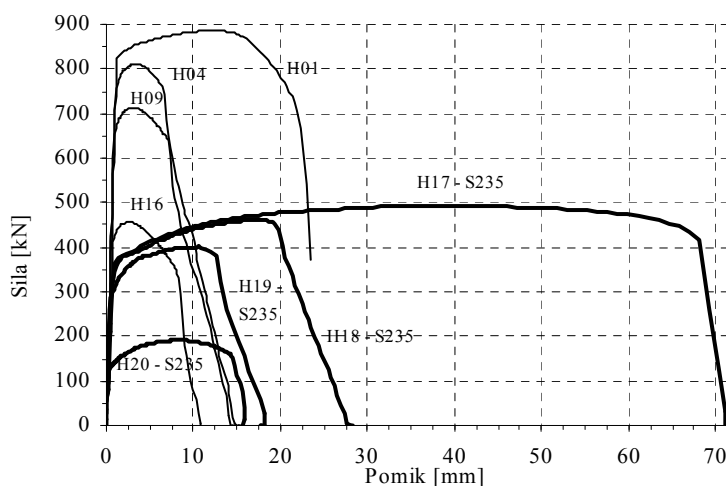
Slika 11: Preizkušane H10 med testom (elastično območje 4,3 kN, največja odpornost 678 kN, trenutek pred prvo razpoko 600 kN, prelom 207 kN)

O duktilnosti same porušitve priča dejstvo, da se je debelina pločevine na mestu preloma v povprečju zmanjšala za 27%. Prav tako se je zmanjšala celotna širina preizkušanca za povprečno 40%. Ne glede na dimenzijo luknje se pomik pri največji sili ni bistveno razlikoval (glej sliko 12– vidna razpoka nastopi pri strmem padcu krivulje). Pomik pri porušitvi, ko je nastala vidna razpoka, se je malenkostno povečal z večjo dimenzije luknje. Z optično primerjavo preizkušancev H04 do H16 smo opazili, da poln (bruto) prerez ni bil izpostavljen plastičnim deformacijam in da se je večina plastičnih deformacij izvršila v bližini oslabiljenega prereza. Preizkušanci H17 do H20 so bili narejeni iz jekla S235. Takšno jeklo ima lahko razmerje natezne trdnosti in napetosti tečenja f_u/f_y tudi preko 1,5. Zaradi tako visokega razmerja f_u/f_y lahko napetost v oslabiljenem prerezu naraste zelo preko napetosti tečenja f_y , hkrati pa utrjevanje povzroči tečenje polnega prereza nateznega elementa in s tem tudi velike plastične deformacije ob predpogoju, da luknja ni prevelika. V nasprotju s preizkušanci H04 do H16 (jeklo S690) se krivulje preizkušancev H18 do H20 razlikujejo po obliki in po velikosti pomika pri največji obremenitvi (glej sliko 13). Preizkušanca H04 in

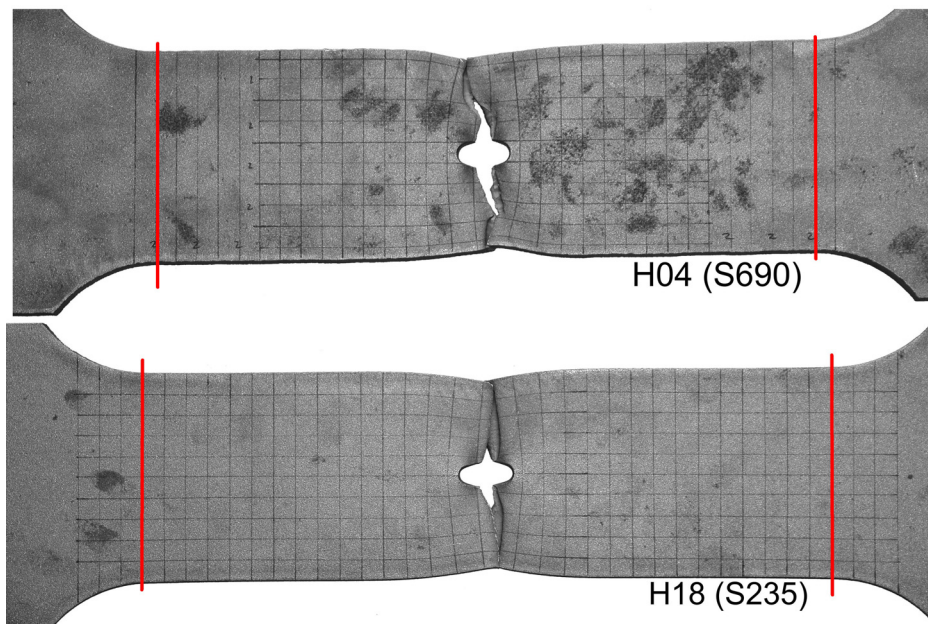
H18 imata enako geometrijo, z razmerjem prerezov $A_{net}/A = 0,9$, in se razlikujeta samo v kvaliteti jekla. Pomik pri porušitvi za H04 je bil 6,6 mm in 19,4 mm pri H18 (slika 13). Za preizkušane H18, in tudi v splošnem za običajna jekla, je zaradi visokih razmerij A_{net}/A in f_u/f_y kritična projektna odpornost polnega prereza določena z enačbo (E2). Zaradi utrditve materiala v oslabiljenem prerezu se je plastificiral polni prerez celotnega elementa, kjer so se pojavile velike plastične deformacije, ki so povzročile velik pomik pri porušitvi. Zaradi omejitve le teh, je projektna nosilnost nateznega elementa omejena z enačbo (E2). Nizko razmerje f_u/f_y preizkušancu H04 in dovolilo tečenja polnega prereza, zato so se plastične deformacije, ki so povzročile večji del pomika, izvršile le v oslabiljenem prerezu. Slika 14 prikazuje oba preizkušanca po porušitvi.



Slika 12: Diagram sila-pomik za H01 do H16 (jeklo S690)

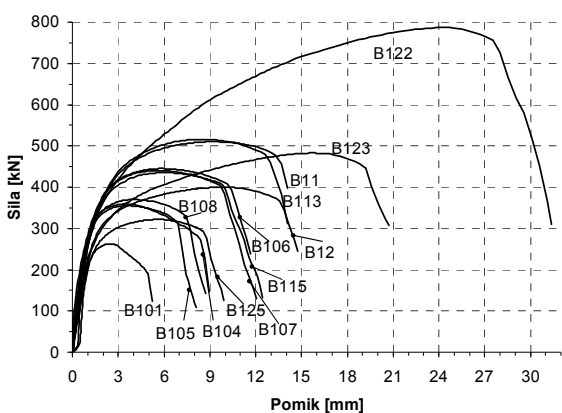


Slika 13: Diagram sila-pomik za preizkušance H – primerjava med S690 in S235

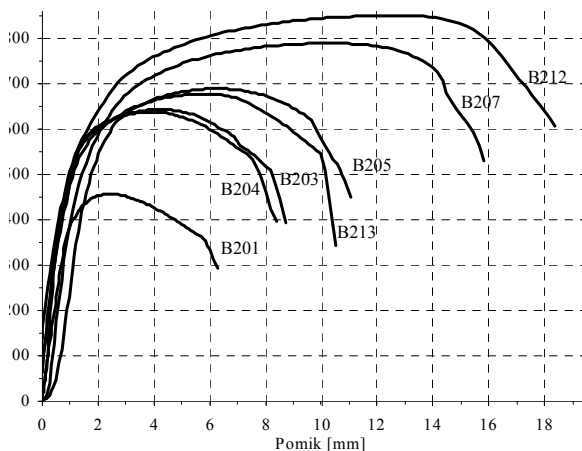


Slika 14: Prelom preizkušancev enake geometrije z različnim materialom

Preizkušanci H in HH so predstavljali element z oslavitvijo v nategu, kjer je napetostni tok ovirala luknja, medtem ko so bili preizkušanci B1 in B2 vijачeni spoji, pri katerih se je obtežba prenesla na sosednji pločevini preko vijaka. Robna razdalja v smeri obtežbe e_1 je bila zadosti velika, da so se preizkušanci B1 in B2 porušili v oslabiljenem prerezu in ne npr. v strigu. Plastične deformacije so bile omejene na oslabiljen prerez in njegovo okolico. Oblika krivulj *sila-pomik* za B1 in B2 je podobna krivuljam H. Razlika je najbolj očitna v začetni togosti. Pri B1 in B2 pride do koncentracije napetosti pri bočnem pritisku vijaka na pločevino. Tečenje jekla na mestu koncentracije napetosti povzroči manjši naklon krivulje (sliki 15-16) v začetnem delu obtežne poti. Čeprav se JVT zaradi nizkega razmerja f_{ult}/f_y pripisuje nizko duktilnost, se je izkazalo nasprotno. Pri preizkušancu B122 (slika 17) se je zaradi nastanka plastičnih deformacij pri bočnem pritisku vijaka na pločevino debelina pločevine povečala iz 10 mm na 20 mm. Nastanek velikih pomikov pri B122 je posledica ovalizacije luknje.

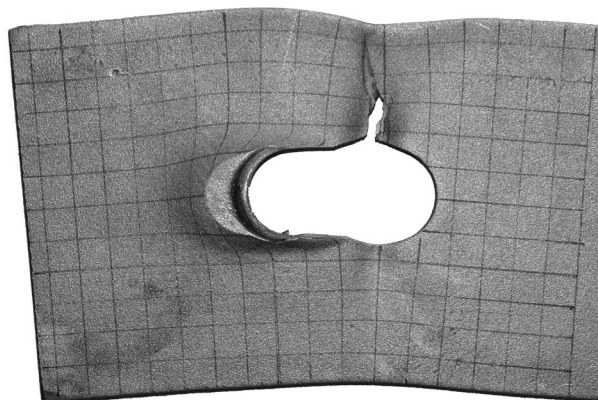


Slika 15: Diagram sila-pomik za preizkušance B1, ki so se porušili v oslabiljenem prerezu



Slika 16: Diagram sila-pomik za preizkušance B2, ki so se porušili v oslabiljenem prerezu

Preizkušanci z ekscentrično luknjo so se porušili na dva načina. Pri preizkušancih H je razpoka nastala istočasno na obeh robovih luknje v oslavljenem prerezu, ne glede na položaj luknje. Pri HH in B1 pa je razpoka nastala na strani z manjšo robno razdaljo. Ekscentričnost luknje je na nosilnost bistveno vplivala samo pri preizkušancih B1, medtem ko pri H in HH nosilnost ni bila bistveno zmanjšana. Odpornost in geometrija vseh preizkušancev je podana v preglednici 5.



Slika 17: Porušitev v oslavljenem prerezu preizkušanca B122

Preglednica 5: Rezultati testov za preizkušance, ki so se porušili v oslavljenem prerezu (preizkušanci H, HH, B1, B2 in L)

Ime	H01	H02	H03	H04	H05	H06	H07	H08	H09	H10	H11	H11A	H12	H13*	H14*	H15	H16	H17	H18	H19	H20
F_{max} [kN]	868	886	861	811	811	789	748	717	713	679	639	627	644	636	636	542	456	492	461	403	191
D_U [mm]	11,8	12,2	6,1	3,2	3,2	3,3	3,1	3,2	3,1	2,9	3	2,9	2,8	3	2,6	2,9	2,7	38,2	16,9	10,3	8,4

Ime	HH01	HH02*	HH03*	HH04	HH05*	HH06*
F_{max} [kN]	499	490	470	553	544	536

Ime	B101	B105	B106	B107	B108*	B113	B114	B115*	B122	B123	B124*	B125*
F_{max} [kN]	262	355	445	440	370	516	510	435	788	483	400	322
D_U [mm]	2,4	3,5	5,8	5,6	4	8,5	9,1	6,2	24,3	15,9	10	5,6

Specimen name	B201	B203	B204	B205	B207	B212	B213
F_{max} [kN]	457	643	638	689	789	851	678
D_U [mm]	2,4	4,3	3,9	6,2	10,4	12,6	5,8

Ime	L09	L10	L16	L17	L18**	L18s	L19	L20	L20s**
F_{max} [kN]	1521	1522	1537	1539	1537	1533	1507	1527	1480**

* ekscentrična luknja

** test je bil ustavljen pred prelomom

Statistično ovrednotenje rezultatov

Namen statistične analize je bila določitev ustreznosti različnih modelov odpornosti in delnega faktorja γ_M , ki je definiran kot količnik med karakteristično in projektno vrednostjo. V Aneksu D standarda EN 1990 je postopek za izračun karakteristične oziroma projektne vrednosti podrobno opisan. Postopek smo avtorji že podrobno opisali v Gradbenem vestniku (Može et al., 2007b), zato tu navajamo le modele odpornosti, skupine podatkov in rezultate.

V analizi smo obravnavali tri modele odpornosti. Prvi model je osnovan na predpostavki, da se celoten oslavljen prerez polno plastificira do natezne trdnosti f_u . Ker je model definiran s porušitvijo, je projektna vrednost povezana z delnim faktorjem $\gamma_{M2} = 1,25$.

$$\text{Model odpornosti 1:} \quad r_{t,1} = A_{net} f_u \quad (\text{E5})$$

Model odpornosti 1, pomnožen s koeficientom 0,9 je uporabljen v EN 1993-1-1. Predlagan je bil za mehka jekla (Snijder et al., 1988a) in je bil izbran tako, da projektna funkcija zadovoljuje varnostne kriterije z izbranim delnim faktorjem $\gamma_{M2} = 1,25$.

Drugi model odpornosti predvideva, da je oslavljen prerez obremenjen samo do napetosti tečenja f_y . Za duktilne materiale kot je npr. mehko jeklo, ki imajo sposobnost utrjevanja, je to konzervativna predpostavka. Tak pristop je bil uporabljen tudi v osnutku prEN 1993-1-12.

$$\text{Model odpornosti 2:} \quad r_{t,2} = A_{net} f_y \quad (\text{E6})$$

Nesimetrična natezna obremenitev ali ekscentričnost luknje povzroči nižjo nosilnost. Tretji model odpornosti predvideva, da se takšni elementi obravnavajo kot centrično obremenjeni elementi na sodelujočem prerezu (glej sliko 10). Projektna nosilnost nesimetrično obremenjenega elementa priključenega z enim vijakom v standardu EN 1993-1-8 izhaja iz naslednje funkcije.

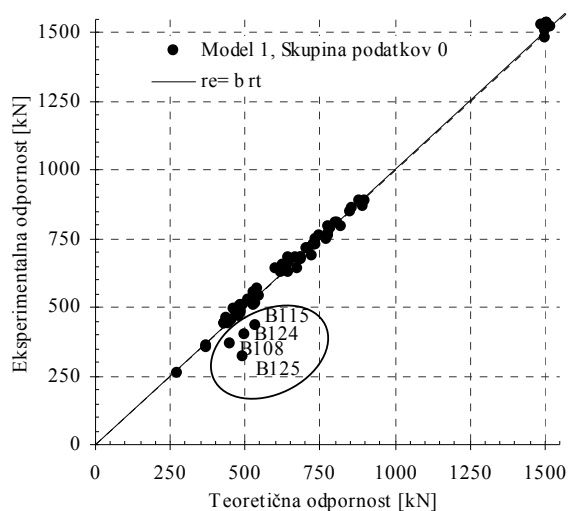
$$\text{Model odpornosti 3:} \quad r_{t,3} = (2e_{2,\min} - d_0) t \cdot f_u \quad (\text{E7})$$

V analizo podatkov smo vključili tudi rezultate preiskav na nateznih spojih iz JVT, ki smo jih našli v literaturi. V literaturnih podatkih so zajeti tudi nekateri ostali materialni razredi JVT in drugačne konfiguracije spojev z različnim številom vijakov (Kouhi, Kortessmaa, 1990. Puthli, Fleischer, 2001. Aalberg, Larsen, March 1999).

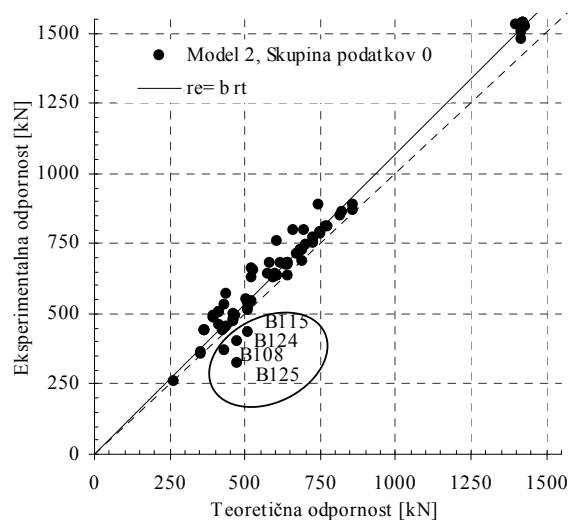
Rezultate smo razvrstili v več skupin z namenom, da bi izločili vpliv ekscentrične obremenitve. Podatke smo razdelili v naslednje skupine:

- skupina 0: vsi rezultati;
- skupina 1: samo rezultati s centrično postavljeno luknjo;
- skupina 2: vsi rezultati, razen B1 z ekscentrično postavljeno luknjo (vključno s preizkušanci tipa H in HH z ekscentrično postavljeno luknjo);
- skupina 3: vsi rezultati, ki imajo ekscentrično postavljeno luknjo;
- skupina 4: samo B1 rezultati, ki imajo ekscentrično postavljeno luknjo;
- skupina 5: vsi B1 rezultati (natezni spoji z enim vijakom);

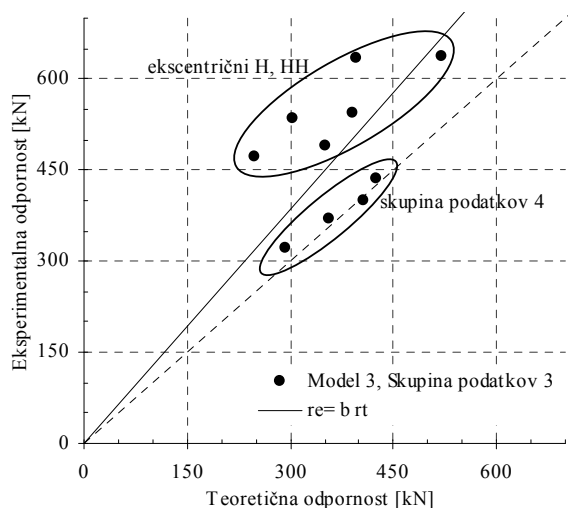
Rezultate statistične analize smo za vse modele in skupine podatkov predstavili v preglednici 6. Diagrami na slikah 18-21 so prikazane eksperimentalne odpornosti v odvisnosti od teoretičnih za različne modele odpornosti on skupine podatkov.



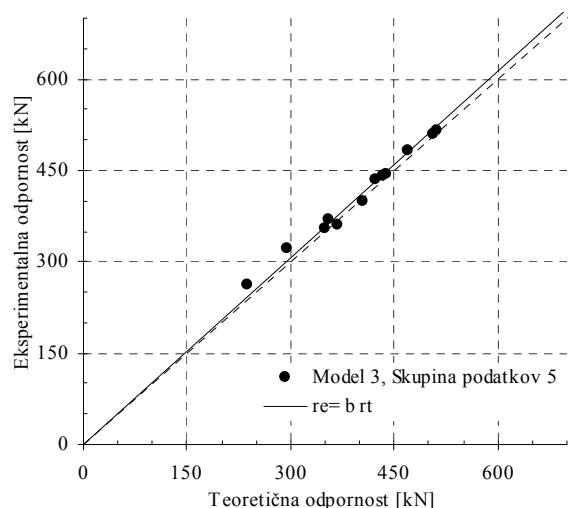
Slika 18: Diagram r_e-r_t za model odpornosti 1, skupina podatkov 0



Slika 19: Diagram r_e-r_t za model odpornosti 2, skupina podatkov 0



Slika 20: Diagram r_e-r_t za model odpornosti 3, skupina podatkov 3



Slika 21: Diagram r_e-r_t za model odpornosti 3, skupina podatkov 5

Preglednica 6: Rezultati statistične analize za projektno vrednost nosilnosti oslabiljenega prereza

Model odpornosti	Skupina podatkov	Št. testov	k_n	k_d	b	V_δ	V_r	γ_M	γ_M^*
1 Eq. (14)	0	80	1,73	3,44	1,002	0,068	0,110	1,182	1,237
	1	70	1,73	3,44	1,007	0,027	0,091	1,138	1,143
	2	76	1,73	3,44	1,007	0,027	0,090	1,137	1,142
1*	0	80	1,73	3,44	1,113	0,068	0,110	1,182	1,113
	1	70	1,73	3,44	1,119	0,027	0,091	1,028	1,028
	2	76	1,73	3,44	1,118	0,027	0,090	1,137	1,027
2 Eq. (15)	0	80	1,73	3,44	1,071	0,098	0,131	1,229	1,252
	1	70	1,73	3,44	1,078	0,072	0,113	1,188	1,161
	2	76	1,73	3,44	1,077	0,070	0,111	1,185	1,157
3 Eq. (16)	3	10	1,73	3,44	1,286	0,239	0,254	1,524	1,635
	4	4	2,63	11,4	1,028	0,043	0,096	1,318	1,333
	4a	4	1,73	3,44	1,028	0,043	0,096	1,151	1,144
	5	8	2	5,07	1,020	0,031	0,092	1,156	1,151

4a – s faktorji k_n , in k_d je upoštevano kot da je bilo narejeno veliko število testov

Model odpornosti 1 s korekcijskim koeficientom $b = 1,007$ in relativno majhnim raztrosom točk najboljše opisuje mejno nosilnost oslabiljenega prereza. Projektni nosilnosti se predpiše delni faktor γ_{M2} , ker je model definiran s poružitvijo Torej, projektna nosilnost

$$N_{t,Rd} = \frac{A_{net} f_u}{\gamma_{M2}} \quad (E8)$$

za skupino podatkov 1 izpolnjuje zahteve zanesljivosti po standardu EN 1990, saj je zahtevani delni faktor odpornosti $\gamma_M^* = 1,143$ manjši od $\gamma_{M2} = 1,25$.

Model odpornosti 1, pomnožen s koeficientom 0,9 (v nadaljevanju model odpornosti 1^{*}), in delni faktor γ_{M2} tvorita projektno nosilnost oslabiljenega prereza (E1), ki je definirana v EN 1993-1-1. Iz preglednice 6 je očitno, da je vrednost zahtevanega delnega faktorja $\gamma_M^* = 1,028$ krepko pod $\gamma_{M2} = 1,25$. Iz navedenega sledi, da je projektna nosilnost (E1) za JVT konzervativna.

Definicija *modela odpornosti 2* je po svoji filozofiji konzervativna. Projektna odpornost osnovana na neprimernem delnem faktorju je lahko premalo zanesljiva. Zahtevani delni faktor za *model odpornosti 2* je $\gamma_M^* = 1,161 > \gamma_{M0} = 1,00$. Potemtakem sledi, da projektna nosilnost oslabiljenega prereza (enačba (E2)), kot je bila definirana v osnutku predloga standarda prEN 1993-1-12, ni v skladu s kriterijem zanesljivosti po EN 1990. Na podlagi teh rezultatov je bil člen, ki določa spodnjo mejo projektne nosilnosti oslabiljenega prereza JVT v zadnjem osnutku predloga standarda prEN 1993-1-12 umaknjen. Nov člen predvideva, da je projektna nosilnost oslabiljenega prereza za JVT enaka kot za običajna jekla (model odpornosti 1^{*}).

Ekscentričnost luknje se je izkazala za pomembno pri preizkušancih B1, medtem ko pri preizkušancih H in HH ni imela vpliva na nosilnost. V prid trditvi govorijo rezultati na sliki 20, kjer samo preizkušanci B1 z ekscentrično luknjo odstopajo od ostalih rezultatov. Zaradi samo štirih testov projektna odpornost določena z enačbo (E4) ni sprejemljiva, saj je zahtevani delni faktor $\gamma_M^* = 1,333$ večji od γ_{M2} , kljub majhnemu raztrosu točk za to skupino $V_\delta = 0,043$ in nizkemu korekcijskemu faktorju $b = 1,028$ (glej preglednico 6). Zato smo vpeljali skupino podatkov 5. Na sliki 21 je predstavljen diagram eksperimentalnih vrednosti v odvisnosti od *modela odpornosti 3* za skupino podatkov 5. Že pri samo 10 rezultatih se izkaže, da je zanesljivost projektne odpornosti (E4) sprejemljiva tudi za JVT (glej preglednico 6). Potreben varnostni faktor je $\gamma_M^* = 1,151$. Podobne rezultat smo dobili, ko smo pri skupini podatkov 4 povečali faktorja kvantile (skupina 4a v preglednici 6). S tem smo predpostavili, da je število rezultatov večje. Ponovno se izkaže, da je zanesljivost projektne odpornosti določene z enačbo (E4) sprejemljiva.

PREKLOPNI NATEZNI SPOJI Z VIJAKI V STRIGU – PORUŠITEV ZARADI BOČNEGA PRITISKA

Splošno o nosilnosti na bočni pritisk

Bočni pritisk vijaka na pločevino povzroči podaljšanje luknje, ki se lahko izvrši le v primeru duktilnega materiala. Obtežba lahko narašča vse do poružitve šibkejše komponente, ki je lahko pločevina ali vijak. Pločevina se lahko poruši na različne načine: z iztrgom vijaka ali skupine vijakov, poružitvijo oslabiljenega prereza in poružitvijo materiala med vijaki, medtem ko se vijak lahko poruši v strižni ravnini. Ameriški standard (AISC, 2005) definira bočni

pritisak vijaka ločeno za mejno stanje uporabnosti (MSU) in mejno stanje nosilnosti (MSN). V MSU je bočna nosilnost vijaka definirana kot nosilnost pločevine pri podaljšanju luknje za 6,35 mm. V MSN pa je določena zgornja meja bočnega pritiska. Evrokod v nasprotju poda zgornjo mejo bočnega pritiska z namenom, da se omeji podaljšanje luknje.

V standardu EN 1993-1-8 je nosilnost na bočni pritisak definirana z naslednjo enačbo, ki velja tudi za JVT:

$$F_{b,Rd} = \frac{k_1 \alpha_b f_u d t}{\gamma_{M2}}, \quad (E9)$$

kjer je d premer vijaka, t debelina pločevine, f_u natezna trdnost pločevine, k_1 in α_b pa sta odvisna od pozicije vijaka:

$$\alpha_b = \min\left(\alpha_d; \frac{f_{ub}}{f_u}; 1\right) \quad (E10)$$

- v smeri prenašanja obtežbe

$$\alpha_d = \frac{e_1}{3d_0} \quad \text{za zunanje vijake} \quad (E11)$$

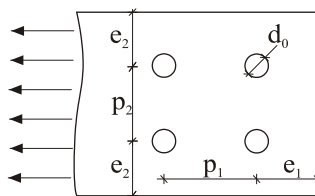
$$\alpha_d = \frac{p_1}{3d_0} - \frac{1}{4} \quad \text{za notranje vijake} \quad (E12)$$

- v smeri pravokotno na obtežbo

$$k_1 = \min\left(2, 8 \frac{e_2}{d_0} - 1, 7; 2, 5\right) \quad \text{za zunanje vijake} \quad (E13)$$

$$k_1 = \min\left(1, 4 \frac{p_2}{d_0} - 1, 7; 2, 5\right) \quad \text{za notranje vijake} \quad (E14)$$

V prejšnjih enačbah so f_{ub} nominalna natezna trdnost vijaka, d_0 premer luknje, razdalje e_1 , e_2 , p_1 in p_2 pa so definirane na sliki 22. Vrednost materialnega varnostnega faktorja γ_{M2} je enaka 1,25.



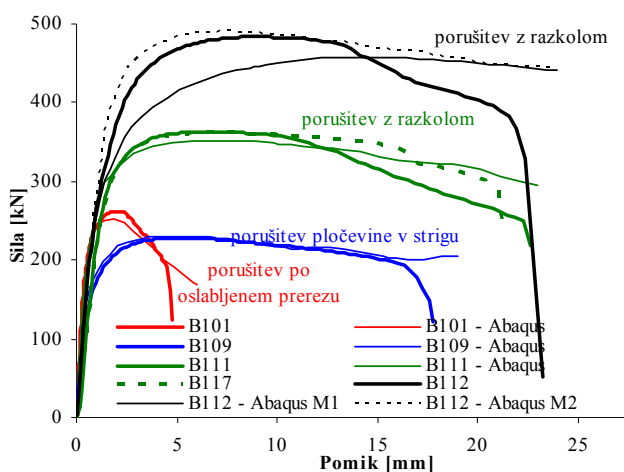
Slika 22: Definicija razdalj

Rezultati testov

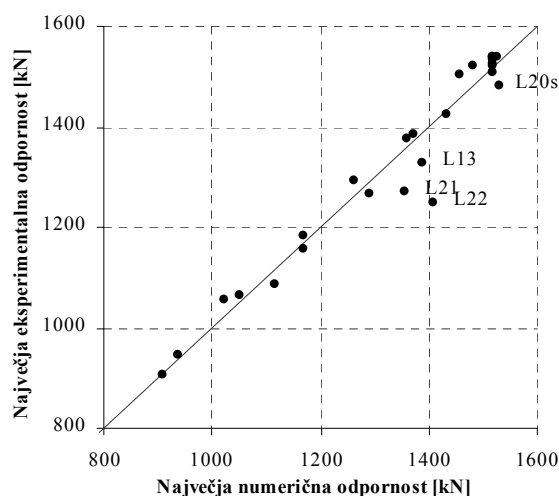
Zaradi lažjega navajanja je potrebno definirati označbo vijakov. Vijake označujemo prvi, drugi, itn. do zadnjega vijaka. Prvi vijak je poimenovan B1, drugi B2 itn. Pri tem je prvi vijak (oziroma vijak B1) tisti, ki je najbližje prostemu robu pločevine in je pravokoten na smer obremenitve.

V tem delu se bomo omejili samo na opis napetostno deformacijskega stanja spojev s tremi ali štirimi vijaki postavljenimi v smeri obremenitve (preizkušanci tipa L). Spoji z enim ali dvema vijakoma (preizkušanci tipa B1, B2) so se obnašali podobno.

Nekatere izmed spojev tipa B1 in vse spoje tipa L smo numerično simulirali. Rezultati analiz so v obliki diagramov *sila-pomik* prikazani na sliki 23. Pri simulaciji smo uporabili numerični model tipa M1 za spoje tipa B1 in model tipa M2 za spoje tipa L. Ujemanje eksperimentalno zabeleženih in numerično izračunanih krivulj je za inženirsko primerjavo popolno. Primerjava največjih nosilnosti izmerjenih v testu in izračunani z MKE je za spoje tipa L prikazana na diagramu 24. Manjše odstopanje se opazi le v primerih, kjer se je v testu porušil vijak. Ker vijaki niso predmet študije, smo jih v numerični analizi modelirali elastično.



Slika 23: Primerjava eksperimentalno in numerično določenih krivulj odziva sila-pomik



Slika 24: Primerjava numeričnih in eksperimentalno določenih nosilnosti

Zabeležili smo več tipov porušitev. Načini porušitve in eksperimentalne nosilnosti so prikazane v preglednicah 7 in 8. Če je bila razdalja do roba pločevine e_1 majhna ($e_1 \leq 2d_0$) in manjša od razdalj med vijaki p_1 , se je iztrgal vijak B1 (slika 24). Ta porušitev je nastala prvotno zaradi nateznih napetosti v smeri pravokotno na obtežbo in ne izključno zaradi strižnih napetosti (glej sliko 26). Zato smo to porušitev poimenovali porušitev z razkolom (glej sliko 27). Takšen fenomen se pojavi, ko v večjem delu oslabiljenega prereza napetosti presežejo napetost tečenja in se v bližini prostega roba tvorijo prečne natezne napetosti, ki zadržujejo poševni razkol preizkušanca (glej sliki 27, 28). Pri spojih tipa L nismo opazili iztrga vijaka B1 zaradi strižnih napetosti, tudi pri preizkušancih z najmanjšo razdaljo e_1 ne. V primeru, ko je bila razdalja med vijaki p_1 večja od razdalje do roba pločevine e_1 , je prišlo do strižne porušitve preizkušanca med vijaki (slika 29). V tem primeru so prečne natezne napetosti ob prostem robu povzročile zmanjšanje debeline preizkušanca (slika 30). Pri večjih razdaljah je prišlo do porušitve oslabiljenega prereza (slika 31). Kljub nizkemu razmerju natezne trdnosti in meje tečenja ($f_u/f_y = 1,06$) so bile vse porušitve značilno duktilne. Velike deformacije smo zaznali v bližini lukenj za vijake in v oslabiljenem prerezu.

Preglednica 7: Rezultati testov za preizkušance B1 in B2

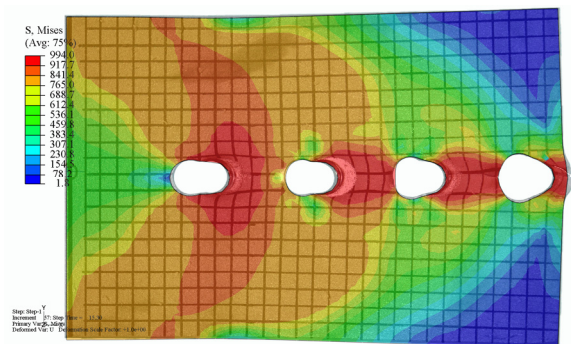
Ime	Tip porušitve ^a	F_{max} [kN]	D_U [mm]	Ime	Tip porušitve ^a	F_{max} [kN]	D_U [mm]
B101	3	262	2,4	B201	3	457	2,4
B102	1	273	5,1	B202	1	471	5,8
B103	1	342	6,1	B203	3	643	4,3
B104	1	360	3,5	B204	3	638	3,9
B105	3	355	3,5	B205	3	689	6,2
B106	3	445	5,8	B206	1	596	6,7
B107	3	440	5,6	B207	3	789	10,4
B108*	3	370	4,0	B208	1	398	3,9
B109	1	228	5,2	B209	1	491	4,9
B110	1	286	5,8	B210	1	603	5,6
B111	1	363	6,4	B211	1,3	776	10,2
B112	1	483	8,9	B212	3	851	12,6
B113	3	516	8,5	B213	3	678	5,8
B114	3	510	9,1				
B115*	3	435	6,2				
B116	1	371	5,8				
B117	1	362	6,6				
B118	1	392	9,8				
B119	1	530	12,0				
B120	1	629	19,5				
B121	1,3	763	24,8				
B122	3	788	24,3				
B123	3	483	15,9				
B124*	3	400	10,0				
B125*	3	322	5,6				

Preglednica 8: Rezultati testov za preizkušance L

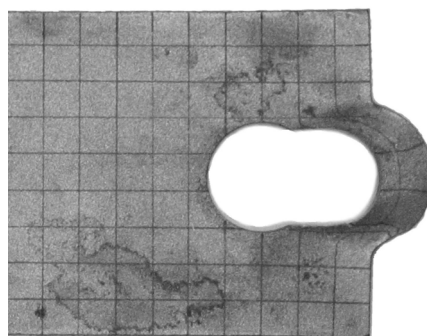
Ime	Tip porušitve ^a	F_{max} [kN]
L01	1	778
L02	1	908
L03	2	1088
L04	1	1066
L04s	1	1057
L05	1	1185
L06	2	1386
L06s	2	1374
L07	1	945
L08	1	1294
L09	3	1521
L10	3	1522
L11	1	1155
L12	1	1268
L13	4	1329
L14	1	1425
L15	1	1501
L16	3	1537
L17	3	1539
L18**	3	1537
L18s	3	1533
L19	3	1507
L20	3	1527
L20s**	3	1480**
L21	1, 4	1271
L22	1, 4	1250

- a
- 1 porušitev vzorca med luknjo in prostim pobom, ki je pravokoten na prenos obtežbe
 - 2 porušitev vzorca med luknjami
 - 3 porušitev oslabiljenega prereza
 - 4 strižna porušitev vijaka
- * ekscentrična luknja
 ** test ustavljen pred prelomom

Kadar govorimo o razporeditvi sil na vijake, moramo upoštevati rezultate numeričnih analiz, saj bočnega pritiska vijaka na pločevino v testu nismo merili. Ugotovili smo, da razpored sil na vijake ni konstanten. Če je robna razdalja e_1 manjša od razdalje med vijaki p_1 , potem je razpored sil na vijake linearen in pri tem najmanjša obtežba odpade na vijak B1. Tak razpored sil na vijake je za preizkušanec L04 prikazan na sliki 32. V primeru, ko robna razdalja e_1 postane večja od razdalje med vijaki p_1 , se razpored obtežbe na vijake uravnoteži kot na primer pri L06 na sliki 33. V preglednici 9 so izpisane sile na vijakih v trenutku, ko je dosežena največja nosilnost celotnega spoja. Pomembno je, da je najvišja nosilnost spoja dosežena, ko je nivo obtežbe na prvem vijaku že v padajočem trendu. To je zaznati na primer pri L04 na sliki 32, ko je največja nosilnost spoja dosežena pri 4,7 mm, vijak B1 pa doseže svojo največjo nosilnost že pri 2,3 mm. Nosilnost spoja L04 pri 2,3 mm je 94% celotne nosilnosti tako, da v tem primeru pojav padajočega trenda sile na prvem vijaku ni zaskrbljivoč.



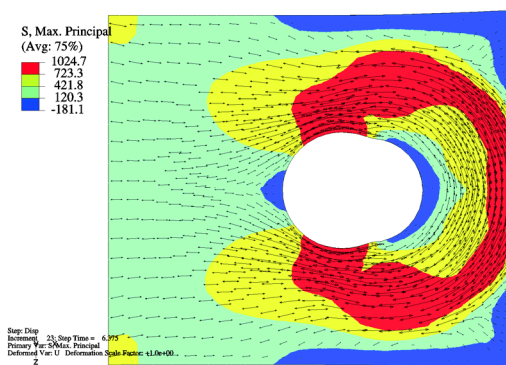
Slika 25: Polje Misesovih napetosti napeto preko dejanskega porušenega preizkušanca L14 (mreža črt)



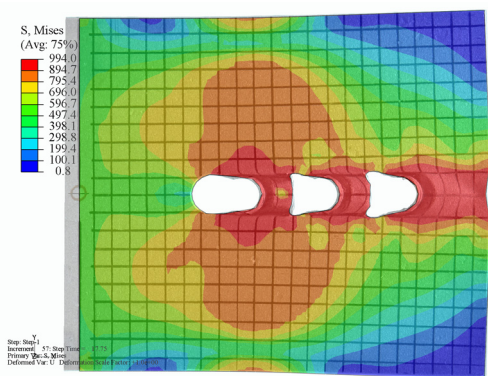
Slika 26: Strižna porušitev pločevine preizkušanca B109



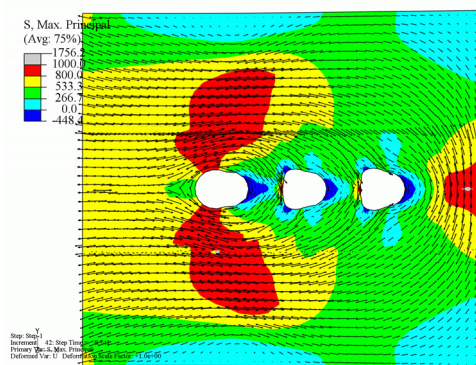
Slika 27: porušitev z razkolom preizkušanca B111



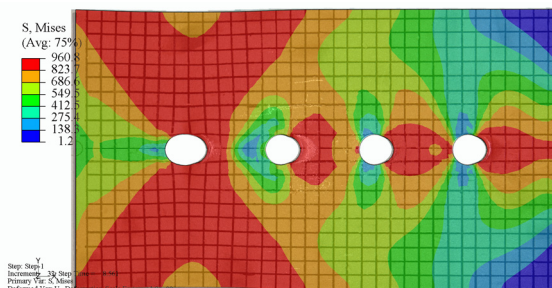
Slika 28: Polje in smeri največjih glavnih napetosti v srednji ravnini pri podaljšanju luknje za 6,375mm za preizkušavec B111



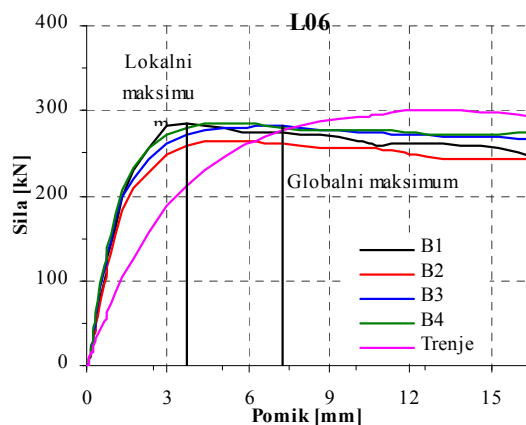
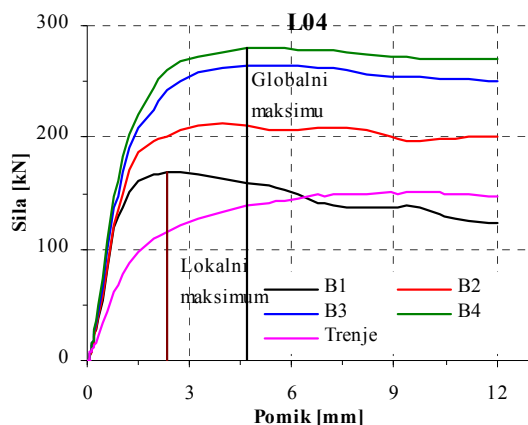
Slika 29: Polje Misesovih napetosti napeto preko dejanskega porušenega preizkušanca L03 (mreža črt)



Slika 30: Polje in smeri največjih glavnih napetosti pri največji obremenitvi za preizkušavec L03



Slika 31: Polje Misesovih napetosti napeto preko dejanskega porušenega preizkušanca L18 (mreža črt)



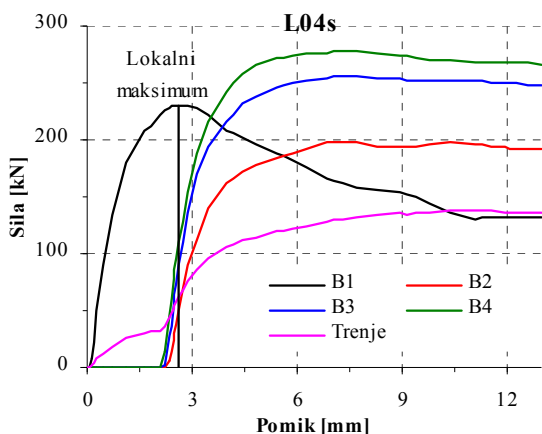
Slika 32: Razporeditev sil in trenja za preizkušane L04

Slika 33: Razporeditev sil in trenja za preizkušane L06

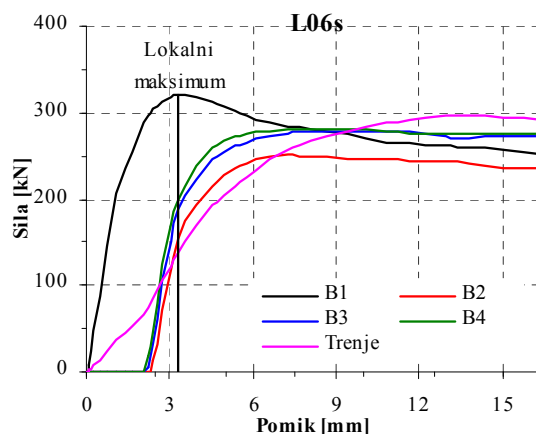
Preglednica 9: Rezultati numeričnih simulacij za spoje tipa L

Ime	Globalni maksimumi								Lokalni maksimumi							
	U [mm]	P_{max} [kN]	B1 [kN]	B2 [kN]	B3 [kN]	B4 [kN]	Friction [kN]	ΣBi [kN]	U [mm]	P_{max} [kN]	B1 [kN]	B2 [kN]	B3 [kN]	B4 [kN]	Friction [kN]	ΣBi [kN]
L01	5,7	813	176	241	278		117	696	2,9	771	178	227	271		94	676
L02	5,9	912	214	261	284		152	760	3,8	891	220	256	282		133	758
L03	8,7	1115	289	276	287		263	852	5,1	1088	294	282	290		222	866
L04	4,7	1052	159	210	265	279	138	913	2,3	988	169	201	242	261	115	873
L04s	7,3	1023	161	198	256	277	130	893	2,6	543	231	51	90	110	61	482
L05	5,1	1169	198	234	272	284	181	988	2,3	1061	209	214	241	260	137	924
L06	7,2	1374	273	261	281	281	277	1097	3,7	1309	285	260	273	280	211	1098
L06s	9,4	1360	275	247	277	281	279	1081	3,3	1000	320	154	188	200	138	862
L07	6,8	937	182	265	323		167	770	3,2	893	192	262	301		138	755
L08	5,9	1265	176	235	304	320	230	1035	2,9	1190	185	242	285	292	186	1004
L09	11,0	1481	225	279	319	323	333	1148	3,5	1372	256	275	298	299	244	1129
L10	11,0	1520	282	301	327	282	327	1193	4,0	1433	293	285	304	291	259	1174
L11	11,4	1172	207	308	364		293	879	3,2	1047	247	298	317		184	862
L12	12,2	1293	234	321	375		354	929	3,4	1127	279	306	322		211	907
L13	14,0	1390	263	338	380		408	982	4,2	1225	308	324	333		260	965
L14	15,3	1434	143	224	342	383	342	1092	3,7	1316	180	276	315	316	229	1087
L15	11,7	1458	183	243	344	349	339	1119	4,0	1365	206	279	319	316	246	1120
L16	10,4	1528	241	324	354	300	310	1219	4,1	1449	246	305	332	306	261	1189
L17	10,0	1519	277	313	338	273	318	1201	3,1	1395	275	289	299	293	239	1155
L18	8,6	1518	308	314	327	263	306	1211	3,1	1416	292	289	300	288	246	1170
L18s	10,0	1519	325	289	311	277	317	1202	3,7	1292	324	195	215	324	233	1058
L19	9,1	1518	324	312	323	258	301	1217	2,8	1388	286	283	294	290	235	1153
L20	10,4	1520	261	320	340	279	318	1200	3,4	1405	257	297	308	297	243	1158
L20s	12,0	1529	268	314	330	300	315	1212	4,2	1292	234	249	247	335	220	1066
L21	18,4	1357	203	336	459		350	998	4,3	1154	267	321	346		211	934
L22	18,0	1408	207	334	422		437	964	4,8	1212	274	330	345		255	948

Pri preizkušancih L04s in L06s smo upoštevali tolerance zaradi izdelave tako, da je bila prva luknja na preizkušancu pomaknjena 2 mm proti drugi luknji. Tako je celotno obtežbo najprej prevzel vijak B1 in šele po izvršeni deformaciji 2 mm, ki se je večinoma izvršila v podaljšanje luknje, so obtežbo prevzeli ostali vijaki. Kljub temu se največje nosilnosti preizkušancev med L04 in L04s razlikujeta samo za 3% in med L06 ter L06s le za 1% in sta doseženi pri pomiku 7,3 mm (L04s) in 9,4 mm (L06s). Na globalni ravni torej ni bistvenih sprememb. Če opazujemo razporeditve sil na vijake na slikah 34 in 35 pa opazimo, da vijak B1 doseže svojo največjo nosilnost pri pomiku 2,6 mm za preizkušane L04s in pri pomiku 3,3 mm za L06s. Nato pa sila na vijaku B1 začne padati in pade na 53% (L04s) oziroma na 74% (L06s) celotne sile na vijak. Izpostaviti je potrebno tudi dejstvo, da je največja sila na vijaku B1 za 37% večja pri geometriji L04s kot pri L04. Podobno 12% večja sila na vijaku B1 je tudi pri L06s v primerjavi z L06. Od tod lahko sklepamo, da padec sile na vijaku B1 ni posledica porušitve pločevine, temveč le običajna prerazporeditev obtežbe, zaradi aktiviranja ostalih vijakov. Pomembno je, da zaradi toleranc lahko pride do preobremenitve katerega izmed vijakov, saj se strižna sila na vijaku lahko bistveno poveča. Omenjeno je potrebno upoštevati pri projektiranju. JVT so sposobna razviti zadostno lokalno duktilnost, ki otopi napetostne konice in s podaljšanjem luknje omogoči prerazporedi prevzem obremenitve tudi na ostale vijake.



Slika 34: Razporeditev sil in trenja za preizkušane L04s



Slika 35: Razporeditev sil in trenja za preizkušane L06s

V okolici pritiska vijaka na pločevino se napetosti zaradi točkovne obremenitve v pločevini povzpnejo čez napetost tečenja ob zelo majhni obtežbi. Na ta način se napetostne konice utopijo, pločevina pa se začne plastično preoblikovati. Preoblikovanje v smeri debeline ovirajo prekrivne pločevine, ki z odporom povzročijo trenje. Izkazalo se je, da je bila velikost trenja v naši preiskavi približno enakovredna velikosti sile na vijak. Velikost ustvarjenega trenja je odvisna od mnogih parametrov, ki so slabo definirani, zato ga je v izračunu nosilnosti spoja potrebno pravilno upoštevati.

Pomembno je tudi poudariti, da je razporeditev obtežbe na vijake odvisna tudi od deformabilnosti oziroma od debeline priklopnih pločevin. V testu smo obravnavali zgolj pločevino, ki je priklopljena na zelo debelo pločevino, ki se je obnašala skoraj kot togo telo. To smo potrdili z numeričnimi simulacijami, kjer smo lahko zaradi tega upoštevali določene poenostavitve.

Numerična parametrična študija nateznih preklopnih spojev z vijaki v strigu

Primerjava numeričnih simulacij z eksperimentalnimi rezultati je pokazala, da postavljeni numerični modeli dobro ponazarjajo obnašanje preklopnih spojev z vijaki v strigu. To nam je omogočilo izvedbo obsežne parametrične študije spojev z namenom, da bi določili vpliv različnim parametrov na nosilnost na bočni pritisk. V analizah smo uporabili numerične modele tipa M2 in M3. Materialni model smo privzeli enak kot v analizi spojev tipa L. Izhajali smo iz geometrij preizkušancev L. Tem geometrijam smo spreminjali različne parametre kot so: širina pločevine, togost priklopnih pločevin (eno-strižni spoji, dvo-strižni spoji z enako togostjo pločevin), dimenzije in število vijakov. Na ta način smo tvorili 109 spojev.

Testi nateznih preklopnih spojev z vijaki v strigu iz literature

Kot dopolnitev naših eksperimentalnih in numeričnih analiz, smo v iz literature zbrali rezultate testov na nateznih preklopnih spojev z vijaki v strigu (93 testov) in jih vključili v našo bazo rezultatov (Kouhi, Kortessmaa, 1990. Kim, Yura, 1999. Aalberg, Larsen, 2001. Puthli, Fleischer, 2001. Aalberg, Larsen, 2002. Rex, Easterling, 2003). Določene izmed teh spojev smo tudi numerično simulirali (38 testov) z namenom določitve razporeda sil med vijaki.

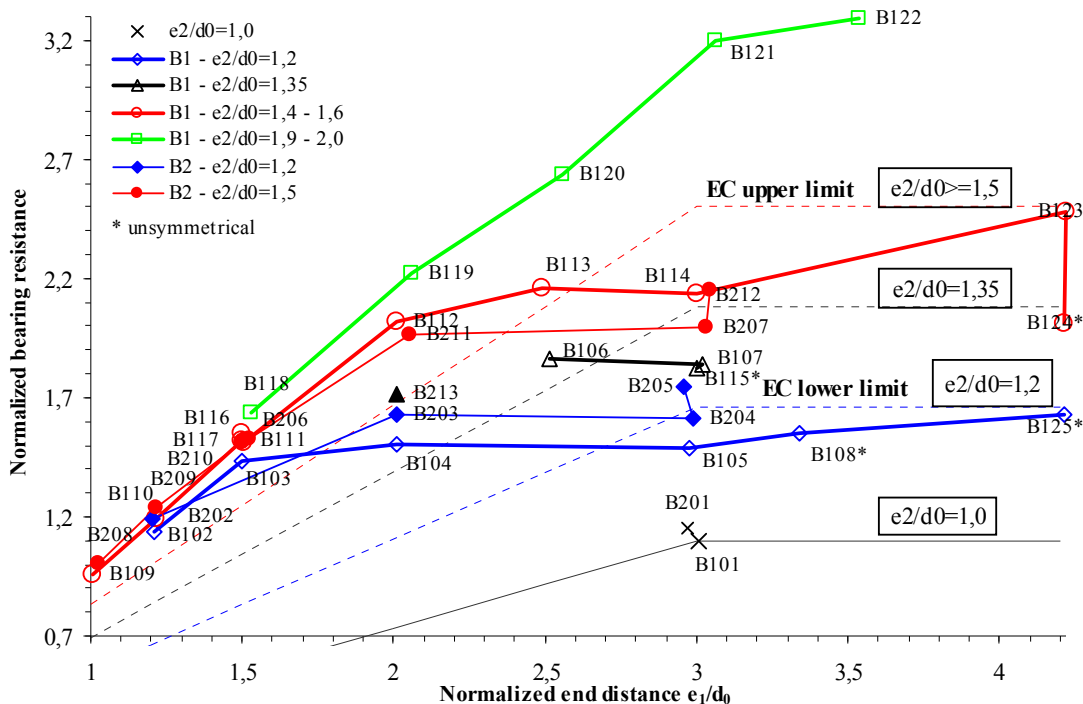
Analiza nosilnosti na bočni pritisk glede na EN 1993-1-8

V tem poglavju primerjamo nosilnost posameznega vijaka na bočni pritisk izračunano po Evrokodovi enačbi (E9) z silo, ki se je dejansko (kot rezultat numerične simulacije) razvila na posameznem vijaku. Ker primerjamo dejansko stanje, je enačba (E9) uporabljena z dejanskimi, izmerjenimi parametri in z vrednostjo $\gamma_{M2} = 1$. Predpostavili smo, da je v vseh primerih strižna nosilnost vijaka večja od nosilnosti pločevine. Pri sklicevanju na nosilnost skupine vijakov, upoštevamo vsoto nosilnosti na bočni pritisk na posameznem vijaku. Kontrola nosilnosti oslabiljenega prereza in strižnega iztrga vijakov se nanaša na kontrole v Evrokodu EN 1993-1-8.

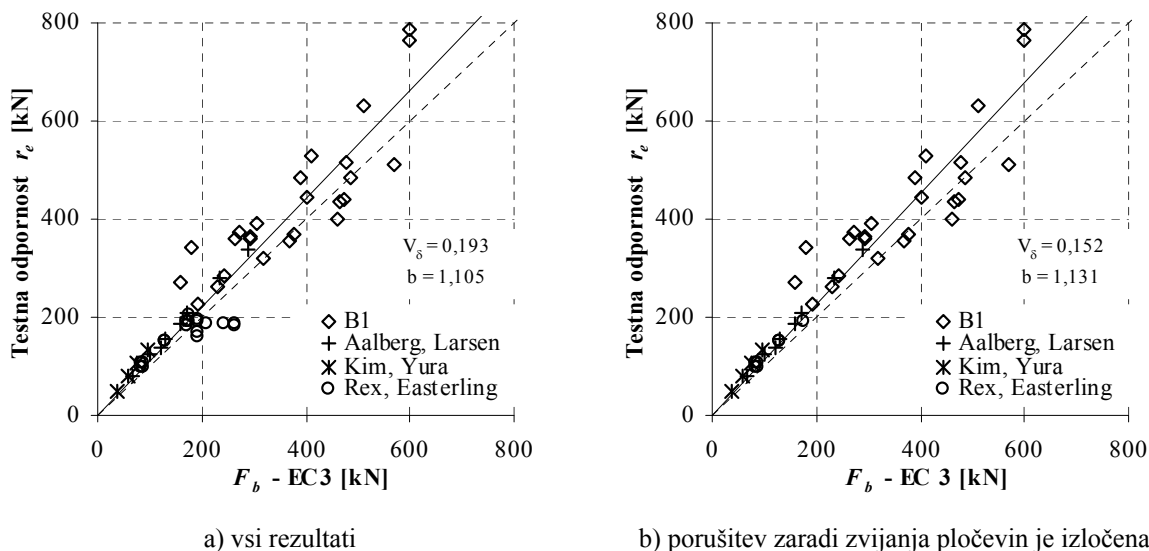
Spoji z enim vijakom

Diagram na sliki 36 prikazuje normirano nosilnost na bočni pritisk (faktor $k_1 \alpha_b$) v razmerju do normirane robne razdalje e_1/d_0 . Tanke črte predstavljajo nosilnost po Evrokodu 3 (enačba (E9)) za različne normirane robne razdalje e_2/d_0 . Ta nosilnost je omejena z zgornjo in s spodnjo mejo. Pri konstantnem razmerju e_2/d_0 nosilnost linearno narašča do vrednosti $e_1/d_0 = 3$, ko postane konstantna. Ta omejitev nosilnosti posredno vsebuje kontrolo nosilnosti oslabiljenega prereza. Simboli prikazujejo rezultate testov in so z debelejšimi črtami povezani v krivulje. Različne oblike simbolov pomenijo približno enake robne razdalje e_2/d_0 . Nosilnost se linearno povečuje (porušitev pločevine v strigu), nato se naklon krivulje hitro zmanjša (mešana porušitev) dokler nosilnost ne postane konstantna (porušitev po oslabiljenem prerezu). Prehod iz porušitve pločevine v strigu na porušitev po oslabiljenem prerezu se odvije v majhnem območju normiranih robnih razdalj e_1/d_0 in je močno odvisen od robne razdalje e_2 . Porušitev po oslabiljenem prerezu pri preizkušancih z robno razdaljo $e_2 = 1,2 d_0$ se zgodi, če je

$e_1 = 1,5 d_0$, pri preizkušancih z robno razdaljo $e_2 = 2,0 d_0$ pa, če je $e_1 = 3,3 d_0$ in ne pri konstantni razdalji $e_1 = 3 d_0$ kot to predvideva Evrokod 3.



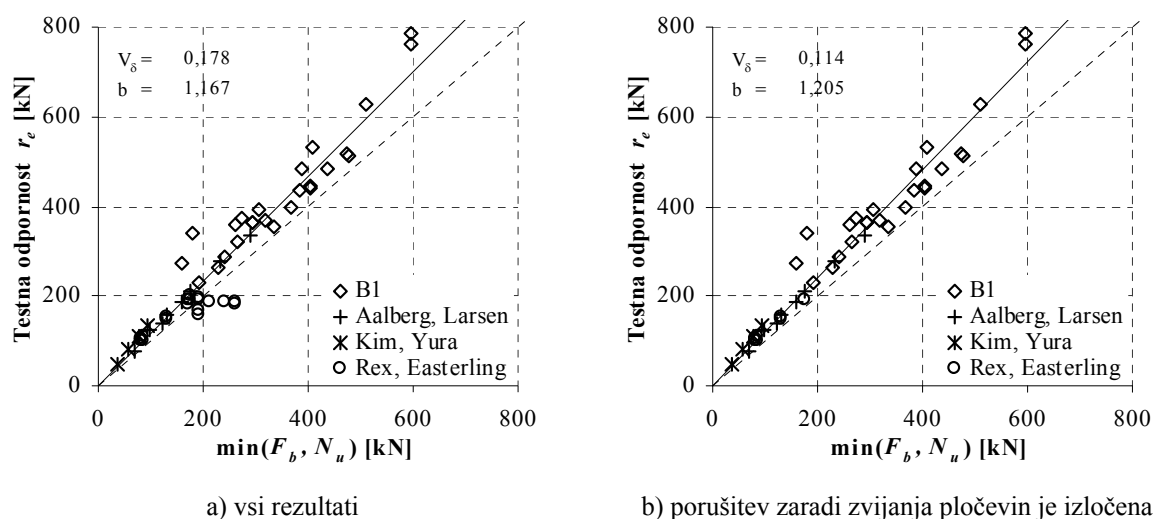
Slika 36: Normalizirana evrokodova nosilnost na bočni pritisk ter rezultati testov za spoje B1, B2 proti normalizirani robni razdalji



Slika 37: Primerjava eksperimentalnih rezultatov in nosilnosti na bočni pritisk po EC 3 za spoj z enim vijakom

Na sliki 37 so poleg naših rezultatov zbrani še rezultati testov iz literature. Večinoma so rezultati na varni strani (nad črtkano diagonalo). Formula za nosilnost na bočni pritisk po EC 3 oceni porušitve po oslabiljenem prerezu in porušitve zaradi zvijanja pločevin preveč optimistično. V primeru, da poleg kontrole za nosilnost na bočni pritisk preverimo še nosilnost oslabiljenega prereza, se vse točke na diagramu pomaknejo na varno stran (nad

črtkano diagonalno) (slika 38). S tem je tudi dosežena zanesljivost projektnih vrednosti z $\gamma_{M2} = 1,25$.



Slika 38: Primerjava eksperimentalnih rezultatov in manjše izmed nosilnosti za bočni pritisk in oslabljen prerez po EC 3 za spoj z enim vijakom

Spoji z vijaki v eni vrsti postavljeni v smeri obremenitve

Na diagramih 39 je prikazana primerjava med silo na vijaku izračunana z MKE in po Evrokodovi enačbi (E9) za bočni pritisk. Raztros točk za robni in notranji vijak je velik. Za robni vijak Evrokod povsem nadceni nosilnost, medtem ko jo na notranjem vijaku podceni. V primeru seštevka nosilnosti, dobimo nosilnost na bočni pritisk za skupino vijakov, pri tem pa se napake bolj ali manj izničijo, zato je na sliki 40. Pri upoštevanju sil zaradi bočnega pritiska in trenja na ordinati ter na abscisi manjšo izmed nosilnosti skupine vijakov in nosilnosti oslabljenega prereza se točke pomaknejo precej na varno stran. S tem je dosežena ustrezna zanesljivost z vrednostjo delnega faktorja $\gamma_{M2} = 1,25$. Upoštevati moramo, da so že v osnovi rezultati na varni strani v povprečju faktor za $b = 1,239$.

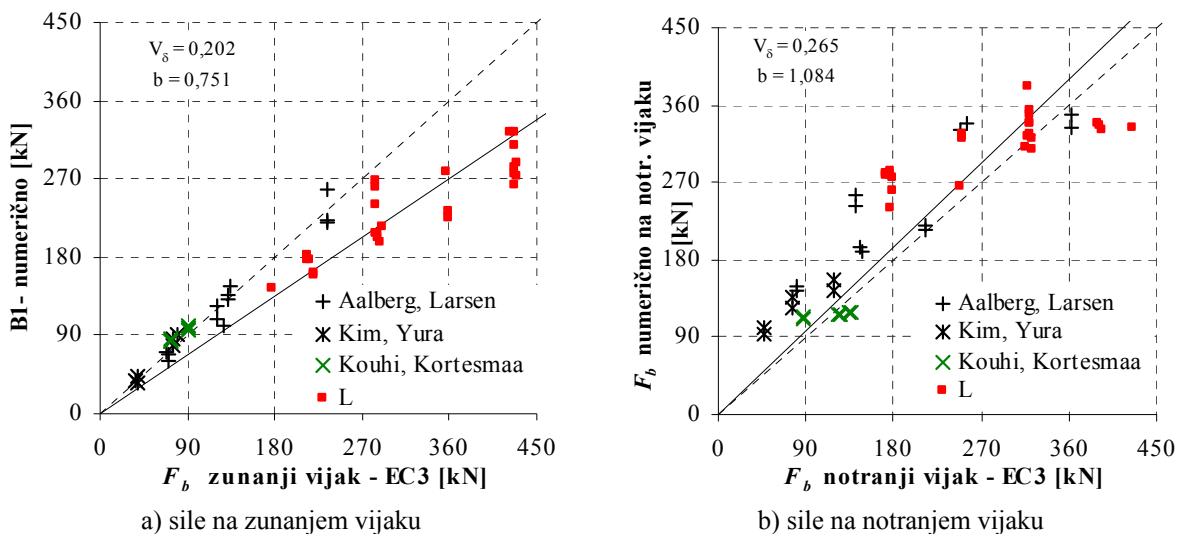
Spoji z vijaki v eni vrsti postavljeni v smeri obremenitve – rezultati parametrične študije

Zaključki so podobni kot v prejšnjem poglavju (glej zaključke v prejšnjem poglavju).

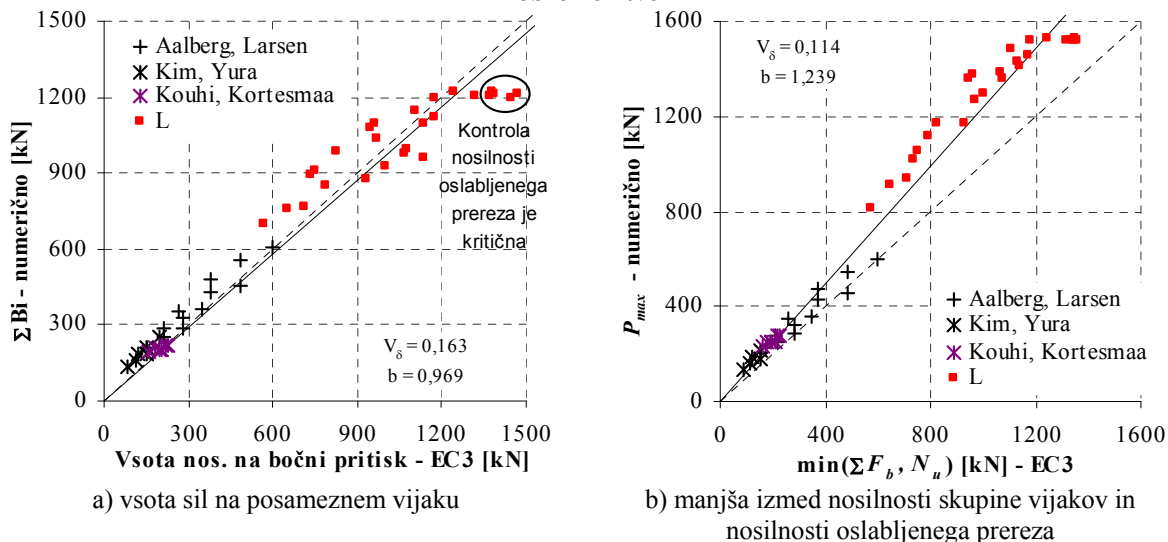
Spoji z dvema vrstama vijakov postavljenima v smeri obremenitve

V primeru, ko ima spoj prečno na obremenitev postavljenih več vijakov, enačba (E9) za določitev nosilnosti na bočni pritisk na vijak zelo slabo oceni dejansko silo, ki se razvije na vijaku (slika 41). Enačba (E9) v nekaterih primerih strižnega iztrga vijakov in vseh primerih porušitve po oslabljenem prerezu preceni dejansko nosilnost tudi do štirikrat (nevarna stran), medtem ko je nosilnost močno podceni v primerih, ko so bile prečne razdalje blizu ali manjše dovoljenim (glej sliko 41). Tudi pri nosilnosti skupine vijakov je raztros točk zelo velik in na nevarni strani (glej sliko 42a). Nad črtkasto diagonalno točke potisneta šele dve dodatni kontroli in sicer: kontrola nosilnosti po oslabljenem prerezu in strižnega iztrga

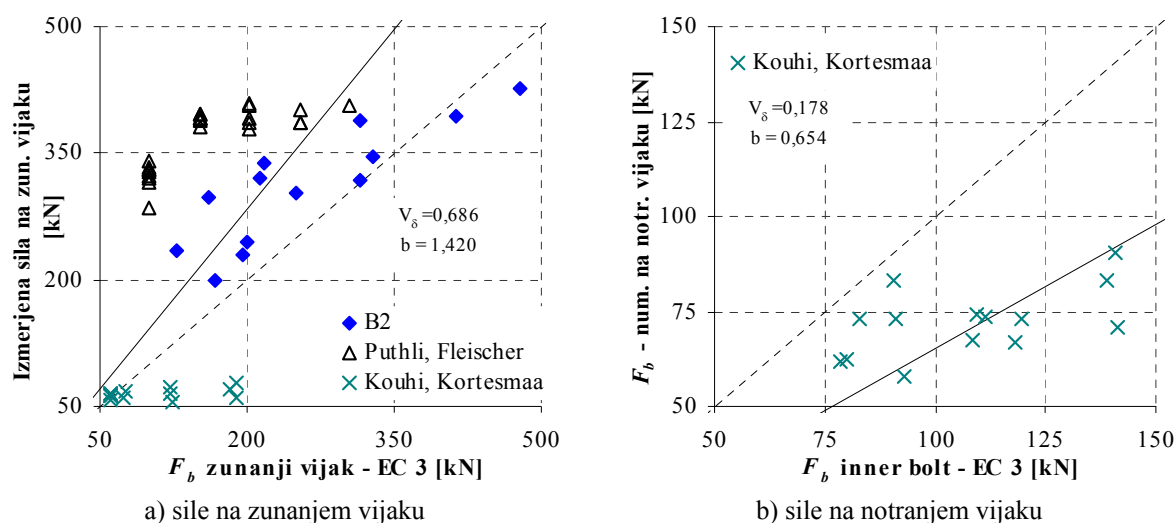
vijakov. Kljub temu potrebni delni varnostni faktor znaša 2,354 (slika 42b). Še vedno je problem, velika razpršenost točk pa čeprav točke gravitirajo na varno stran.



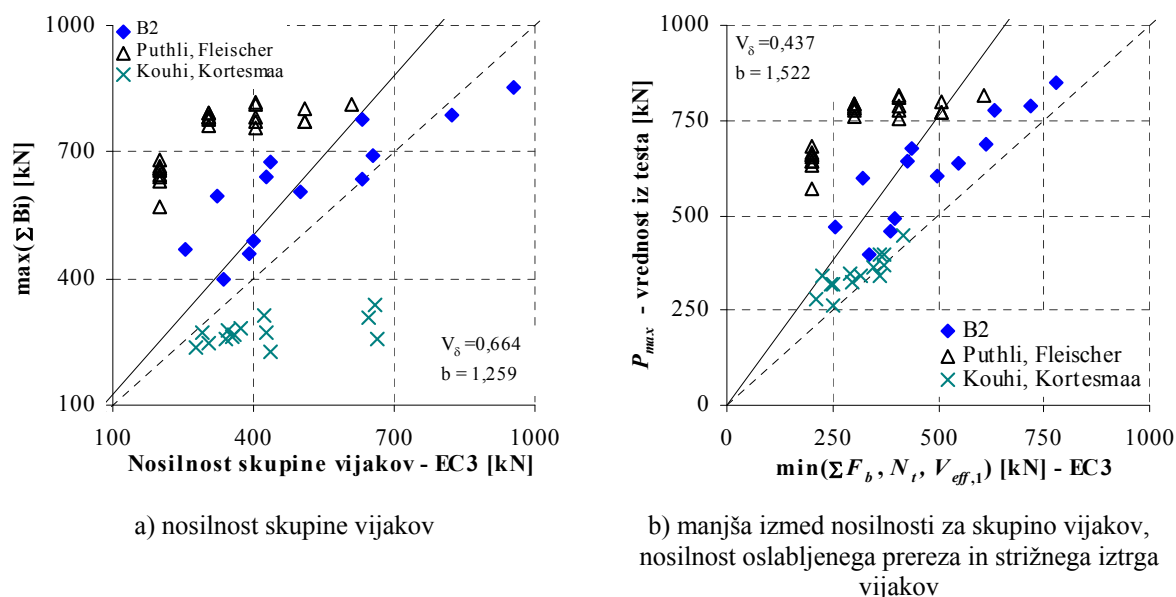
Slika 39: Sila zaradi bočnega pritiska na vijaku za spoje z vijaki v eni vrsti postavljeni v smeri obremenitve



Slika 40: Nosilnost skupine vijakov za spoje z vijaki v eni vrsti postavljeni v smeri obremenitve



Slika 41: Sila zaradi bočnega pritiska na vijaku za spoje z dvema vrstama vijakov postavljenima v smeri obremenitve



Slika 42: Nosilnost spojev z dvema linijama vijakov postavljenima v smeri obtežbe

Razvoj nove enačbe za nosilnost na bočni pritisk

Predpogoj za razvoj nove enačbe za nosilnost na bočni pritisk je bila ustrezna definicija bočne nosilnosti. Nova definicija je osnovana za mejno stanje nosilnosti, kar je skladno z Evrokodovo filozofijo. Definirali smo, da naj vsota posamezni bočnih pritiskov na pločevino (oziroma vijak) predstavlja največjo nosilnost pločevine. To omogoča, da z eno enačbo določimo razpored sil med vijaki in ocenimo nosilnost spoja. Model je bil razvit za spoje z enim vijakom in je bil nato razširjen na splošno konfiguracijo spoja.

$$F_{b,new,Rd} = k_1 k_2 k_3 k_4 k_5 \cdot \frac{df_u}{\gamma_{M2}} \quad (E15)$$

$$k_1 = \min\left(1,3 \frac{e'_1}{e'_2}; 1,9\right) \text{ če } k_1 = 1,9, \text{ se oslabiljen prerez polno plastificira,} \quad (E16)$$

$$k_2 = \left(0,9 \frac{e'_2}{d_0} - \frac{1}{4} \right) \cdot \frac{1}{n} \quad (\text{E17})$$

$$b_{eff} = 2e_2 + (m-1)(p_2 - d_0) \quad (\text{E18})$$

$$e'_2 = \frac{b_{eff}}{2m} \quad (\text{E19})$$

- za zunanje vijake v smeri obremenitve

$$k_3 = \min \left(\frac{2}{3} \frac{e_1}{p_1} + \frac{1}{2}; 1 \right) \quad \text{za pločevine enakih togosti} \quad (\text{E20})$$

$$k_3 = \min \left(\frac{2}{3} \frac{e_1}{p_1^2} d_0 + \frac{1}{2}; 1 \right) \quad \text{za pločevine različnih togosti} \quad (\text{E21})$$

$$k_4 = 1 \quad (\text{E22})$$

$$k_5 = 1 \quad (\text{E23})$$

- za notranje vijake v smeri obremenitve

$$k_3 = 1 \quad (\text{E24})$$

$$k_4 = \min \left(\frac{1}{2} \frac{p_1}{p_2} + \frac{1}{2}; 1 \right) \quad (\text{E25})$$

$$k_5 = \min \left(\frac{1}{2} \frac{p_2}{e_2} + \frac{1}{2}; 1 \right) \quad \text{če } k_5 < 1, \text{ je možen iztrg vijakov} \quad (\text{E26})$$

m število vijakov v enem stolpcu, postavljenemu prečno na smer obremenitve

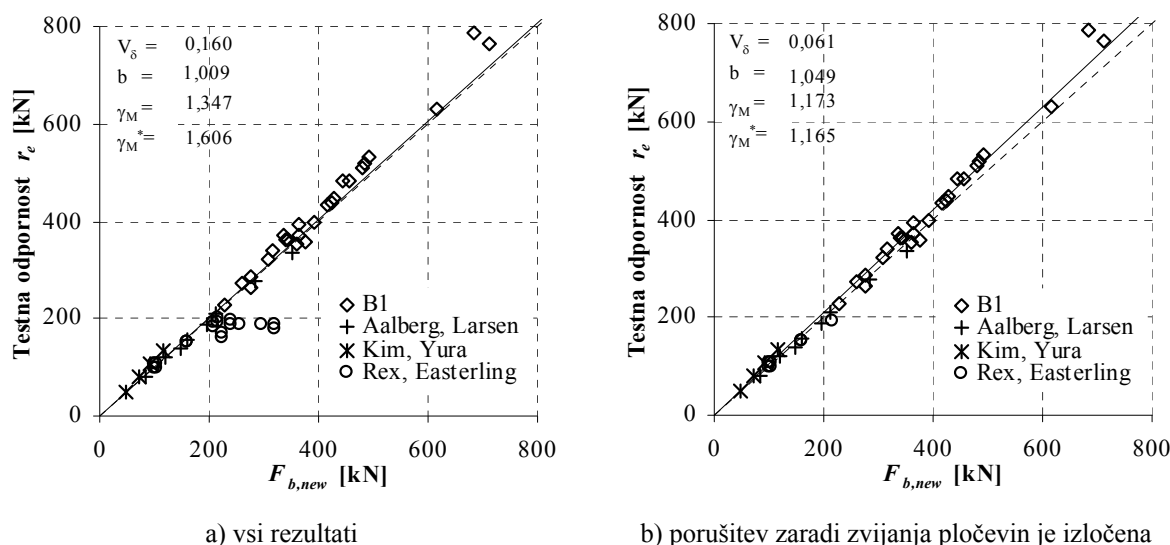
n število vijakov v eni vrsti, postavljeni v smeri obremenitve

Koeficienti k_i so bili določeni s pomočjo optimizacijskega procesa in so delno podkrepljeni s teoretično razlago.

Nosilnost skupine vijakov določimo s seštevanjem posameznih nosilnosti na vijaku glede na obliko razporeda sil (nosilnosti na vmesnih vijakih linearno interpoliramo). Zaradi pomanjkanja eksperimentalnih rezultatov je bila enačba (E15) preverjena samo za $m = 2$.

Spoji z enim vijakom

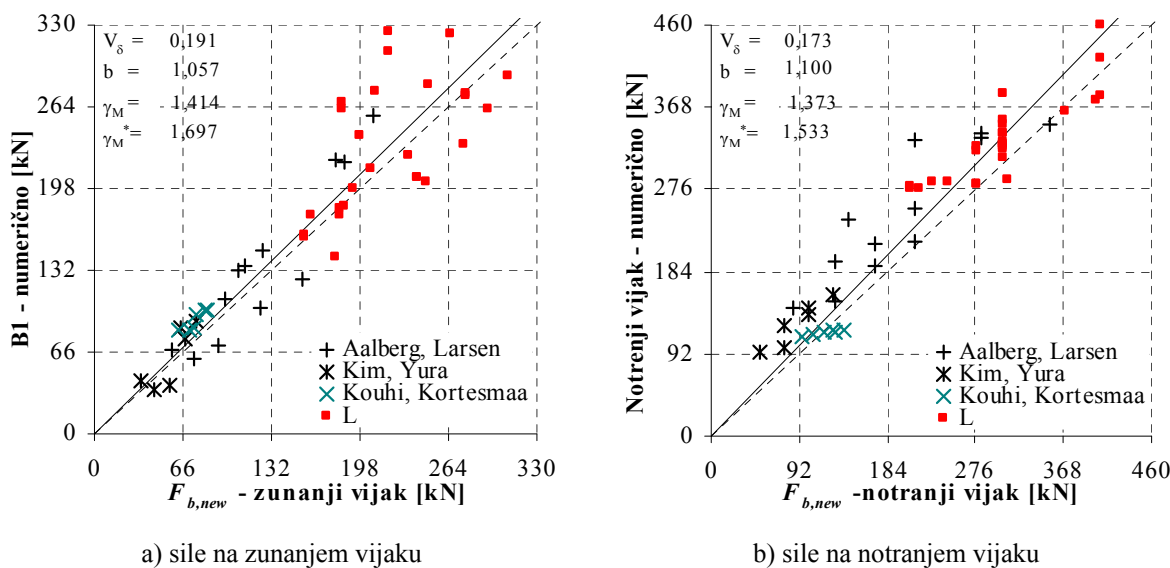
Novi model zelo dobro popisuje nosilnost na bočni pritisk za spoje z enim vijakom, brez uporabe dodatnih kontrol (slika 43).



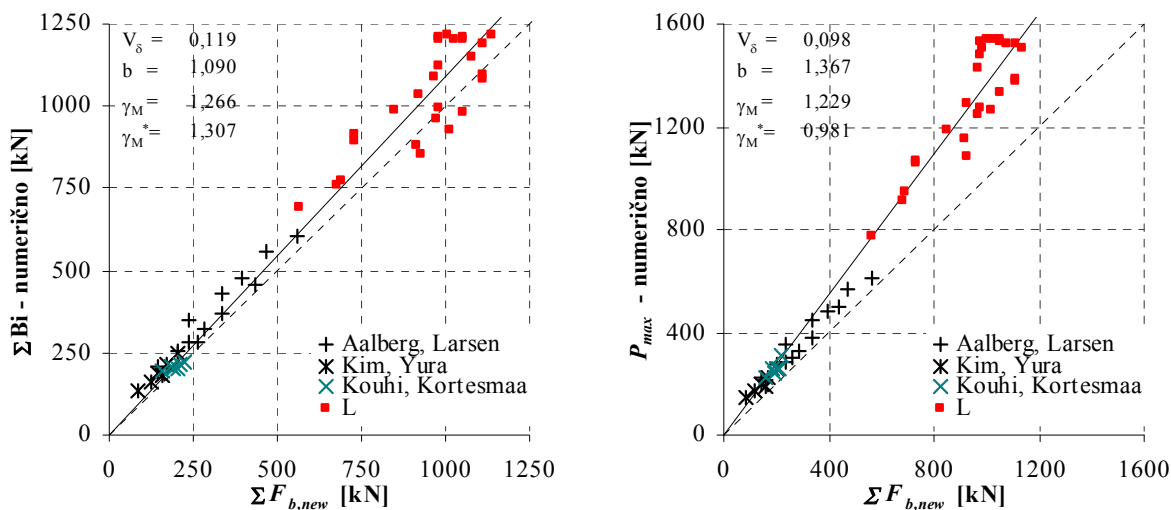
Slika 43: Primerjava eksperimentalnih rezultatov in nove formule za nosilnost na bočni pritisk po EC 3 za spoj z enim vijakom

Spoji z vijaki v eni vrsti postavljeni v smeri obremenitve

V primeru takšnih spojev je različna togost preklopnih pločevin povzročila nižjo silo na prvem vijaku. Zato je nosilnost na prvem oziroma zunanjem vijaku zmanjšana s faktorjem k_3 (slika 44). Rezultati, ki na sliki 44a bistveno odstopajo navzgor od črtkane diagonale, so imeli veliko robno razdaljo so se porušili po oslabiljenem prerezu. Za takšen primer je definicija faktorja k_3 nekoliko konzervativna. Za rezultate, ki bistveno odstopajo navzdol od črtkane diagonale, pa je značilna strižna porušitev vijaka. V teh primerih numerična simulacija tudi ni dosegla največje nosilnosti spoja. V teh primerih bi bila zaradi velikih razdalj torej merodajna strižna nosilnost vijaka. Pri nosilnosti skupine vijakov lahko z delnim faktorjem $\gamma_{M2} = 1,25$ dosežemo zahtevano zanesljivost (slika 45).



Slika 44: Sila zaradi bočnega pritiska na vijaku za spoje z vijaki v eni vrsti, postavljeni v smeri obremenitve



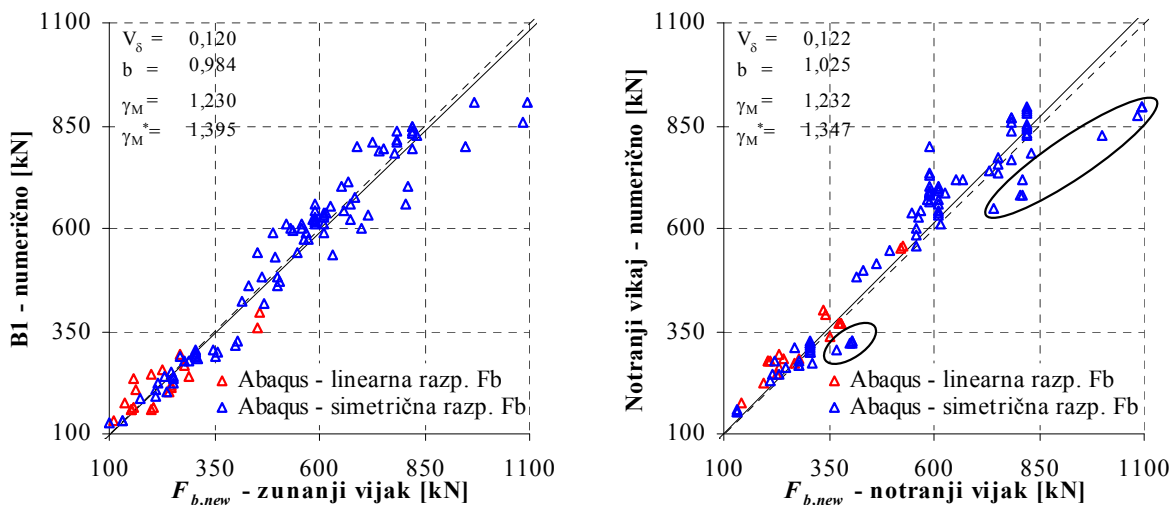
a) vsota sil na posameznem vijaku

b) primerjava z največjo odpornostjo

Slika 45: Nosilnost skupine vijakov za spoje z vijaki v eni vrsti postavljeni v smeri obremenitve

Spoji z vijaki v eni vrsti postavljeni v smeri obremenitve – rezultati parametrične študije

Zaključki so podobni kot v prejšnjem poglavju, le da se tu odstopanje na nevarno stran izrazi na notranjem vijaku (slika 46).



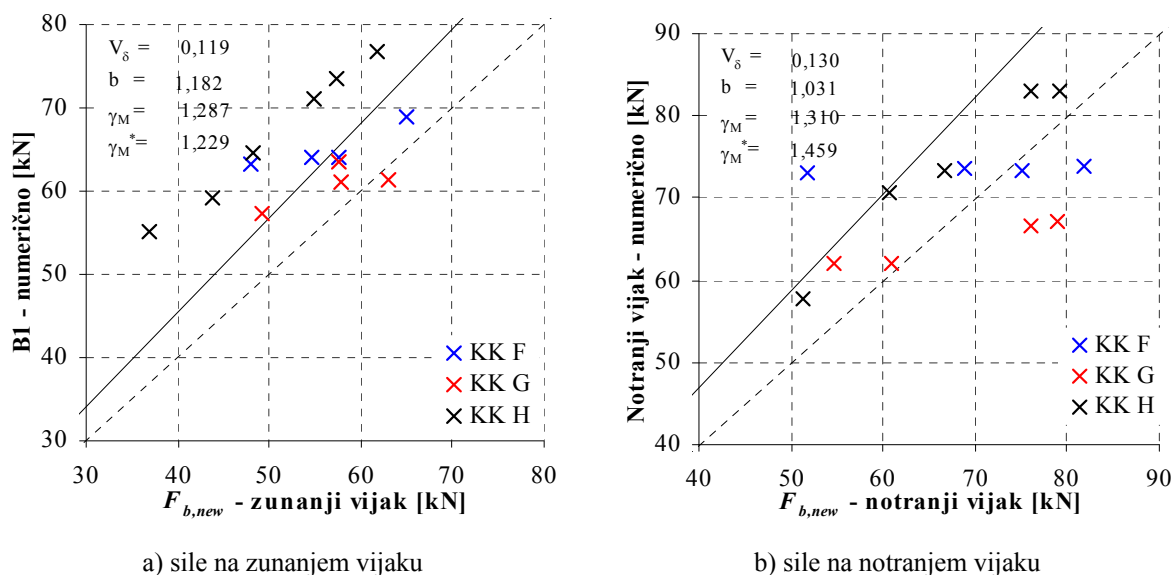
a) sile na zunanjem vijaku

b) sile na notranjem vijaku

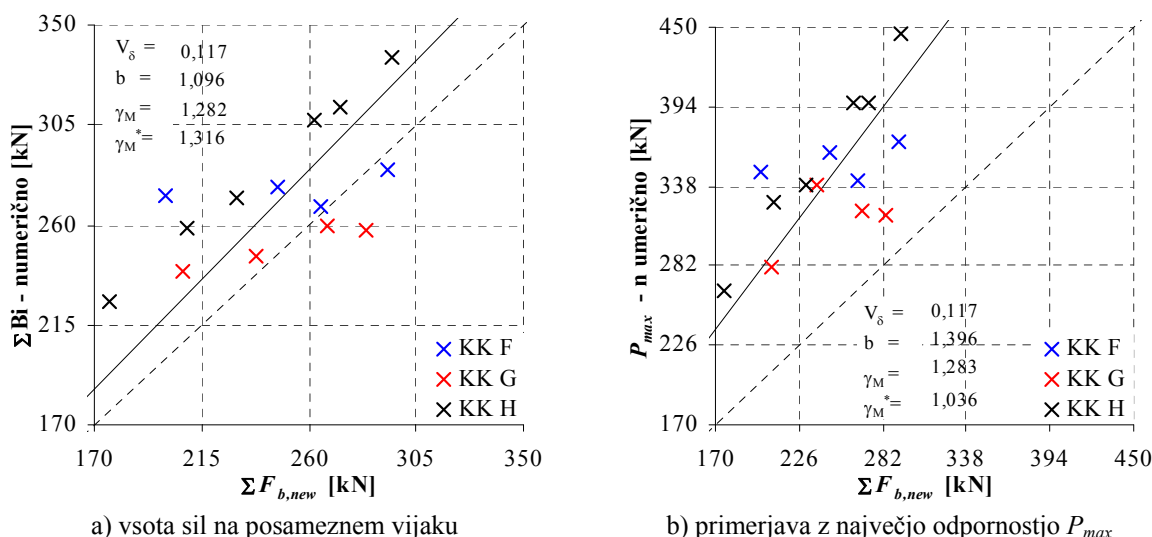
Slika 46: Sila zaradi bočnega pritiska na vijaku za spoje vključene v parametrično študijo

Spoji z dvema vrstama vijakov, postavljenima v smeri obremenitve

Koeficienta k_4 in k_5 uspešno zmanjšata nosilnosti na notranjem vijaku oziroma kontrolirata primere v katerih je prišlo do iztrga vijakov (slika 47). Pri teh je potrebno poudariti, da je bila v primeru tankih pločevin ($t = 3$ mm) prvotno merodajna porušitev zaradi zvižanja pločevin, ki jo naš model ne zajame. Pri nosilnosti skupine vijakov lahko z delnim faktorjem $\gamma_{M2} = 1,25$ dosežemo zahtevano zanesljivost tudi v tem primeru (slika 48).



Slika 47: Sila zaradi bočnega pritiska na vijaku za spoje z dvema vrstama vijakov, postavljenima v smeri obremenitve



Slika 48: Nosilnost skupine vijakov za spoje z dvema vrstama vijakov, postavljenima v smeri obremenitve

ZAKLJUČEK

Veljavnost projektčnih formul za elemente v nategu smo preverili s statistično analizo eksperimentalnih rezultatov po dodatku D standarda EN 1990, v katero smo poleg rezultatov naših testov zajeli tudi rezultate testov iz literature. Dobili smo naslednje rezultate:

- Dodatno pravilo za spodnjo mejo projektne nosilnosti oslabiljenega prereza za jekla visoke trdnosti, ki je bilo definirano v osnutku predloga standarda prEN 1993-1-12,

$$N_{t,Rd} = \frac{A_{net} f_y}{\gamma_{M0}}$$

z $\gamma_{M0} = 1,00$ ni bilo zadosti varno in je bilo na osnovi naših rezultatov umaknjeno. Projektna nosilnost oslabiljenega prereza iz jekla visoke trdnosti je v končni različici enaka kot za običajna jekla.

- Ugotovili smo tudi, da je natezna projektna nosilnost nesimetričnega oslabiljenega prereza z enim vijakom varna tudi za jekla visoke trdnosti:

$$N_{u,Rd} = \frac{2(e_2 - 0,5d_0)tf_u}{\gamma_{M2}}$$

Zato je omejitev v prEN 1993-1-12, ki ne dovoljuje uporabe te kontrole, nepotrebna.

S testi nateznih preklonih spojev z vijaki v strigu smo dokazali, da je lokalna duktilnost jekel visoke trdnosti kljub nizkemu razmerju $f_u/f_y = 1,05$ zadostna, da se v območjih napetostnih konic material plastificira in z tem otopi konice. Lokalne plastične deformacije so zadostne, da se tudi pri najbolj neugodnem začetnem položaju vijakov, ki je posledica neugodne kombinacije toleranc, obremenitev lahko prenese med vse vijake. Na osnovi podatkovne baze z 266 spoji smo ocenili zanesljivost nosilnosti na bočni pritisk glede na Evrokod EN 1993-1-8. Postavili smo novo definicijo nosilnosti na bočni pritisk in na njeni podlagi razvili nov model za določitev projektne nosilnosti na bočni pritisk. Z novim modelom je mogoče določiti tip porušitve, zato lahko predvidimo želen tip porušitve v mejnem stanju nosilnosti. Prav tako pa je nov model enostaven za aplikacijo v stroki, ker z njim pokrijemo vse tipe porušitev in ga načelno lahko uporabimo kot edino kontrolo nosilnosti.

REFERENCE

- Aalberg, A., Larsen, P. K. 2001. Bearing strength of bolted connections in high strength steel. In: P. Mäkeläinen, J. Kesti, A. Jutila, O. Kaitila, (eds.). Nordic Steel Construction Conference 2001 - NSCC 2001: proceedings. Helsinki, NSCC: 859-866.
- Aalberg, A., Larsen, P. K. 2002. The effect of steel strength and ductility on bearing failure of bolted connections. In: A. Lamas, L. S. d. Silva, (eds.). The Third European Conference on Steel Structures: Proceedings of the 3rd European conference on steel structures. Coimbra, Universidade de Coimbra: 869-878.
- Aalberg, A., Larsen, P. K. March 1999. Strength and ductility of bolted connections in normal and high strength steels. In, Norwegian University of Science and Technology.
- AISC. 2005. Specifications for Structural Steel Buildings. ANS/AISC 360-05, Chicago, American Institute of Steel Construction, Inc
- CEN. 2004. Eurocode - Basis of structural design. EN 1990, Brussels, European Committee for Standardisation
- CEN. 2005a. Eurocode 3: Design of steel structures - Part 1-1: General rules and rules for buildings. EN 1993-1-1, Brussels, European Committee for Standardisation
- CEN. 2005b. Eurocode 3: Design of steel structures - Part 1-8: Design of joints. EN 1993-1-8, Brussels, European Committee for Standardisation
- CEN. 2007. Eurocode 3: Design of steel structures - Part 1-12: Additional rules for the extension of EN 1993 up to steel grades S 700. EN 1993-1-12, Brussels, European Committee for Standardisation
- Kim, H. J., Yura, J. A. 1999. The effect of ultimate-to-yield ratio on the bearing strength of bolted connections. Journal of Constructional Steel Research, 49, 3: 255-270.
- Kouhi, J., Kortessmaa, M. 1990. Strength tests on bolted connections using high-strength steels (HSS steels) as a base material. Research notes 1185, In. 1185. Espoo, Technical Research Centre of Finland.
- Može, P., Beg, D. 2006. Preklonni strižni spoji iz jekel visoke trdnosti. In: F. Saje, J. Lopatič, (eds.). Zbornik 28. zborovanja gradbenih konstruktorjev Slovenije. Bled, Slovenija, Slovensko društvo gradbenih konstruktorjev: 115-124.

- Može, P., Beg, D. 2007. Testi na preklopnih vijachenih strižnih spojih iz jekla visoke trdnosti. In: F. Saje, J. Lopatič, (eds.). Zbornik 29. zborovanja gradbenih konstruktorjev Slovenije. Bled, Slovenija, Slovensko društvo gradbenih konstruktorjev: 233-240.
- Može, P., Beg, D., Lopatič, J. 2006a. Ductility and strength of bolted connections made of high strength steel. In: D. Dubina, V. Ungureanu, (eds.). Steel - a new and traditional material for building: proceedings of the International Conference in Metal Structures. Poiana Brasov, Romania, London; New York: Taylor & Francis: 323-330.
- Može, P., Beg, D., Lopatič, J. 2006b. Local ductility of structures made of high strength steel. In: F. M. Mazzolan, A. Wada, (eds.). STESSA 2006: proceedings of the fifth International conference on behaviour of steel structures in seismic areas. Yokohama, Japan, Leiden: Taylor & Francis: 169-174.
- Može, P., Beg, D., Lopatič, J. 2007a. Net cross-section design resistance and local ductility of elements made of high strength steel. *Journal of Constructional Steel Research*, 63, 11: 1431-1441.
- Može, P., Beg, D., Lopatič, J. 2007b. Projektna nosilnost oslabljenih prerezov elementov iz jekel visoke trdnosti. *Gradbeni vestnik*, 56, maj 2007: 124-134.
- Puthli, R., Fleischer, O. 2001. Investigations on bolted connections for high strength steel members. *Journal of Constructional Steel Research*, 57, 3: 313-326.
- Rex, C. O., Easterling, W. S. 2003. Behavior and modeling of a bolt bearing on a single plate. *Journal of Structural Engineering-Asce*, 129, 6: 792-800.
- SIMULIA. 2007. Abaqus Online Documentation: Version 6.7. Dassault Systèmes.
- Snijder, H. H., Ungermann, D., Stark, J. W. B., Sedlacek, G., Bijlaard, F. S. K., Hemmert-Halswick, A. 1988. Evaluation of test results on bolted connections in order to obtain strength functions and suitable model factors - Part A: Results. In: Eurocode No.3 - Part 1 - Background documentation, Chapter 6. Document 6.01. Brussels, Commission of the European Communities.

REFERENCES

- Aalberg, A., Larsen, P. K. 2001. Bearing strength of bolted connections in high strength steel. In: P. Mäkeläinen, J. Kesti, A. Jutila, O. Kaitila, (eds.). Nordic Steel Construction Conference 2001 - NSCC 2001: proceedings. Helsinki, NSCC: 859-866.
- Aalberg, A., Larsen, P. K. 2002. The effect of steel strength and ductility on bearing failure of bolted connections. In: A. Lamas, L. S. d. Silva, (eds.). The Third European Conference on Steel Structures: Proceedings of the 3rd European conference on steel structures. Coimbra, Universidade de Coimbra: 869-878.
- Aalberg, A., Larsen, P. K. March 1999. Strength and ductility of bolted connections in normal and high strength steels. In, Norwegian University of Science and Technology.
- AG der Dillinger Hüttenwerke. 2005. "Overview - Steel construction."
<http://www.dillinger.de/dh/referenzen/stahlbau/index.shtml.en>.
- AISC. 2005. Specifications for Structural Steel Buildings. ANS/AISC 360-05, Chicago, American Institute of Steel Construction, Inc
- Axhag, F. 1998. Plastic design of slender steel bridge girders. Doctoral thesis, Luleå, Luleå University of technology.
- Beardmore, R. 2008. "Friction factors." http://www.roymech.co.uk/Useful_Tables/Tribology/co_of_friect.htm.
- Beg, D., Hladnik, L. 1996. Slenderness Limit of Class 3 I Cross-sections Made of High Strength Steel. Journal of Constructional Steel Research, 38, 3: 201-218.
- Bijlaard, F. 2006. Eurocode 3, a basis for further development in joint design. Journal of Constructional Steel Research, 62, 11: 1060-1067.
- Bjorhovde, R. 2004. Development and use of high performance steel. Journal of Constructional Steel Research, 60, 3-5: 393-400.
- Bucak, Ö. 2000. Zum Ermüdungsverhalten von hoch- und höchstfesten Stählen. Stahlbau, 69, 4: 311-316.
- CEN. 1997a. Execution of steel structures - Part 3: Supplementary rules for high yield strength steels ENV 1090-3, Brussels, European Committee for Standardisation
- CEN. 1997b. Steel and steel products - Location and preparation of samples and test pieces for mechanical testing. EN ISO 377, Brussels, European Committee for Standardisation
- CEN. 2001. Metallic materials - Tensile testing - Part 1: Method of test at ambient temperature. EN 10002-1, Brussels, European Committee for Standardisation
- CEN. 2004a. Eurocode - Basis of structural design. EN 1990, Brussels, European Committee for Standardisation
- CEN. 2004b. Hot rolled products of structural steels - Part 6: Technical delivery conditions for flat products of high yield strength structural steels in the quenched and tempered condition. EN 10025-6, Brussels, European Committee for Standardisation

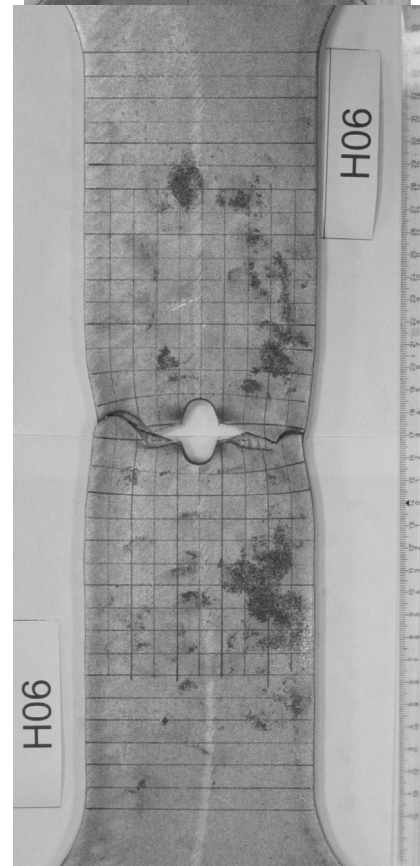
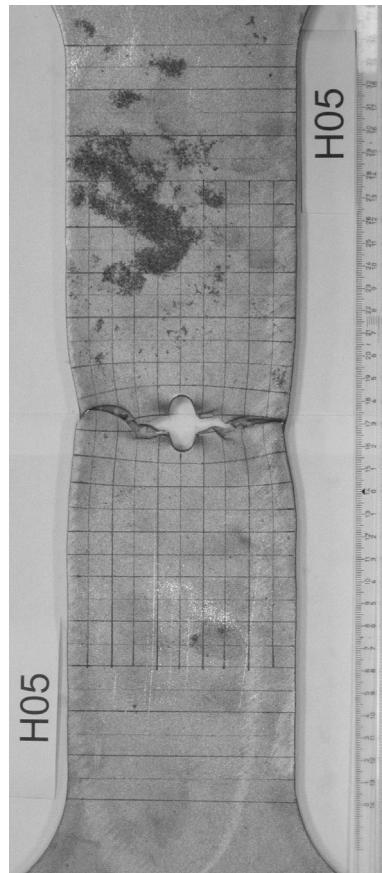
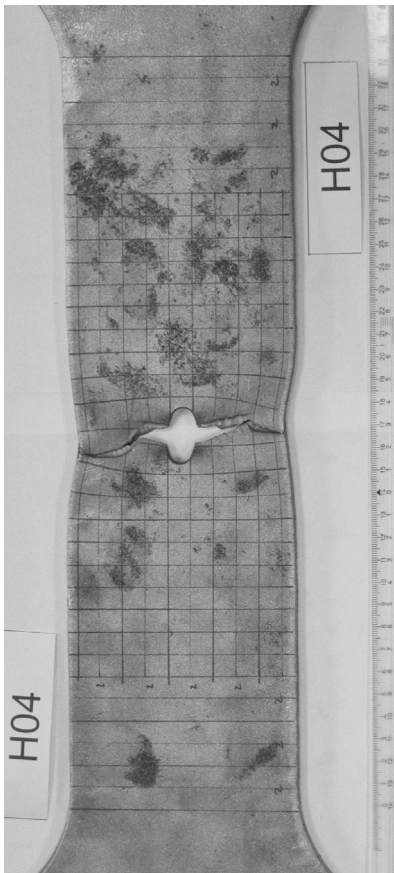
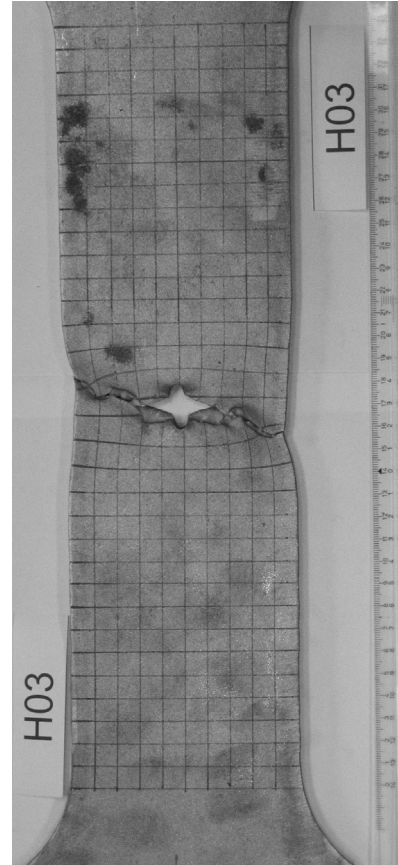
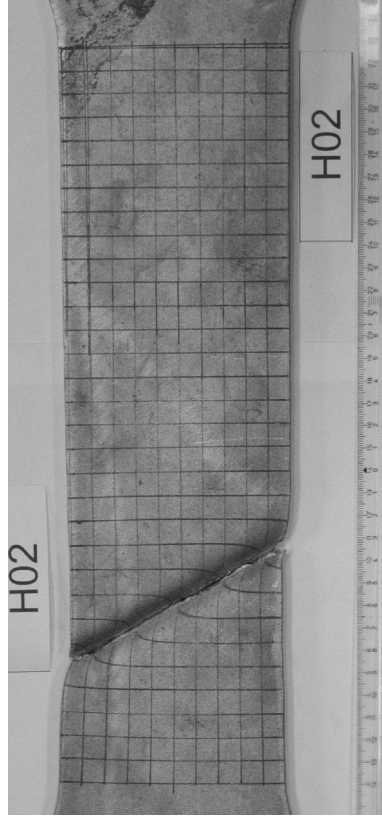
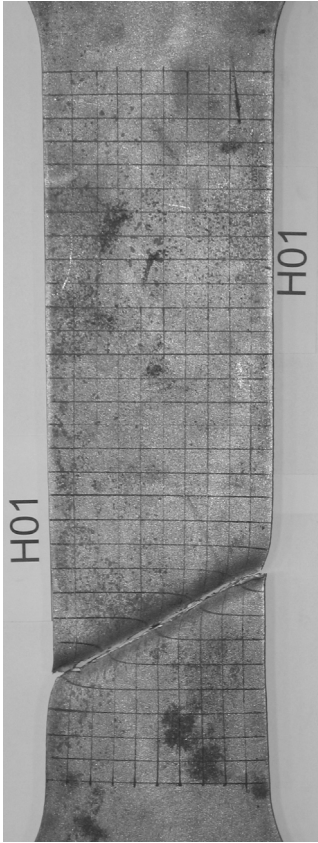
- CEN. 2005a. Eurocode 3: Design of steel structures - Part 1-1: General rules and rules for buildings. EN 1993-1-1, Brussels, European Committee for Standardisation
- CEN. 2005b. Eurocode 3: Design of steel structures - Part 1-8: Design of joints. EN 1993-1-8, Brussels, European Committee for Standardisation
- CEN. 2007. Eurocode 3: Design of steel structures - Part 1-12: Additional rules for the extension of EN 1993 up to steel grades S 700. EN 1993-1-12, Brussels, European Committee for Standardisation
- Chen, S.-J., Tu, C.-T. 2004. Experimental Study of Jumbo Size Reduced Beam Section Connections Using High-Strength Steel. *Journal of Structural Engineering*, 130, 4: 582-587.
- Clarín, M., Langerquist, O. 2005. Plate buckling of high strength steel. 4th European Conference on Steel and Composite Structures, Eurosteel 2005, B. Hoffmeister, (ed.), Druck und Verlagshaus Mainz, Maastricht.
- Collin, P., Johansson, B. 2005. Design of welds in high strength steel. In: B. Hoffmeister, (ed.). Eurosteel 2005: 4th European Conference on Steel and Composite Structures. Maastricht, Druck und Verlagshaus Mainz.
- Collin, P., Möller, M. 1998. Structural application for high strength steel. In. Nordic Steel Construction Conference 98: proceedings. Bergen, Norway, Oslo, Norsk Stalforbund: 67-77.
- de Freitas, S. T., de Vries, P., Bijlaard, F. S. K. 2005. Experimental research on single bolt connections for high strength steel S690. ECCS_TC10-05-579, In. ECCS_TC10-05-579, ECCS TC10.
- Dieter, G. E. 1987. Tension test. In: S. Rao, (ed.). *Mechanical Metallurgy*. New York [ect.], McGraw-Hill Book Company.
- Dowling, N. E. 1993. Mechanical testing: Tension test and other basic tests. In. *Mechanical behavior of materials: Engineering methods for derormation, fracture and fatigue*. New Jersey, Prentice-Hall International International.
- Earls, C. J. 1999. On the inelastic failure of high strength steel I-shaped beams. *Journal of Constructional Steel Research*, 49, 1: 1-24.
- Fukumoto, Y. 1996. New constructional steels and structural stability. *Engineering Structures*, 18, 10: 786-791.
- Girão Coelho, A. M. 2004. Characterization of the ductility of bolted end plate beam-to-column steel connections. Doctoral dissertation, Coimbra, Universidade de Coimbrap.
- Girão Coelho, A. M., Bijlaard, F. S. K. 2007. Experimental behaviour of high strength steel end-plate connections. *Journal of Constructional Steel Research*, 63, 9: 1228-1240.
- Girão Coelho, A. M., Bijlaard, F. S. K., Gresnigt, N., Simoes da Silva, L. 2004a. Experimental assessment of the behaviour of bolted T-stub connections made up of welded plates. *Journal of Constructional Steel Research*, 60, 2: 269-311.
- Girão Coelho, A. M., Bijlaard, F. S. K., Simoes da Silva, L. 2004b. Experimental assessment of the ductility of extended end plate connections. *Engineering Structures*, 26, 9: 1185-1206.
- Girão Coelho, A. M., da Silva, L. S., Bijlaard, F. S. K. 2006a. Ductility analysis of bolted extended end plate beam-to-column connections in the framework of the component method. *Steel and Composite Structures*, 6, 1: 33-53.
- Girão Coelho, A. M., da Silva, L. S., Bijlaard, F. S. K. 2006b. Finite-element modeling of the nonlinear behavior of bolted T-stub connections. *Journal of Structural Engineering-Asce*, 132, 6: 918-928.

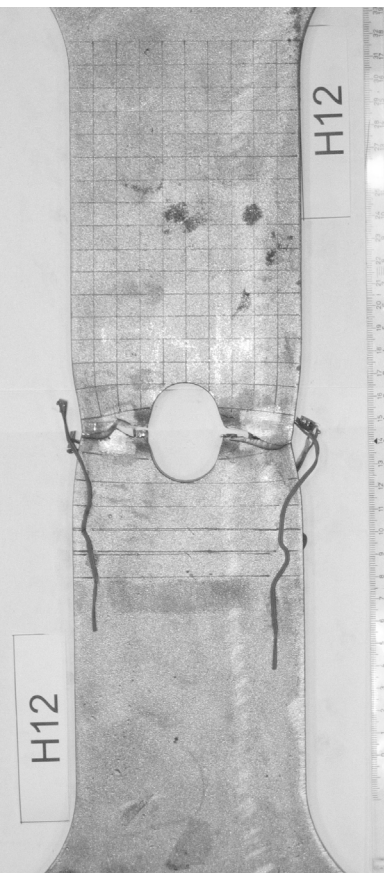
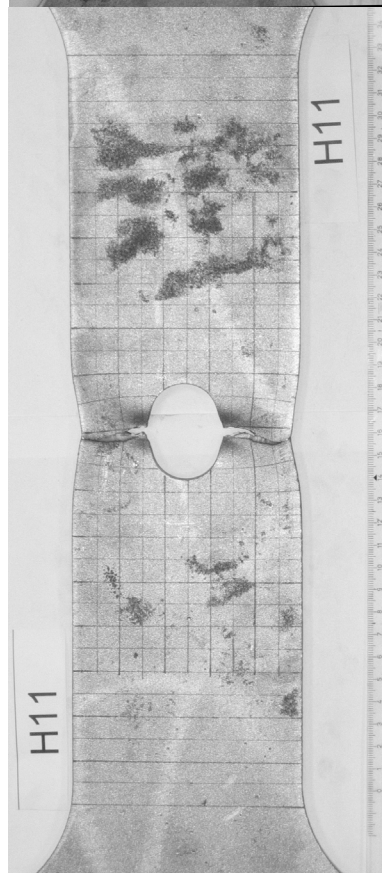
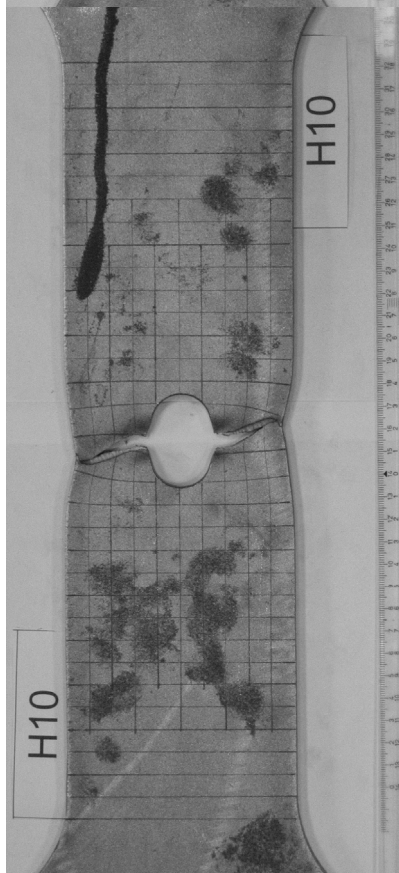
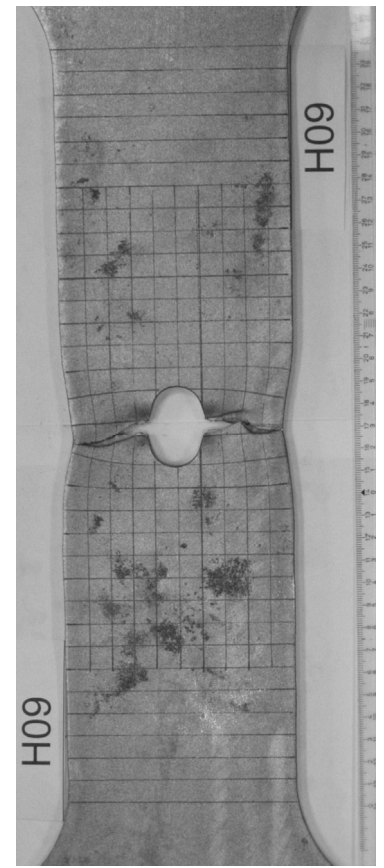
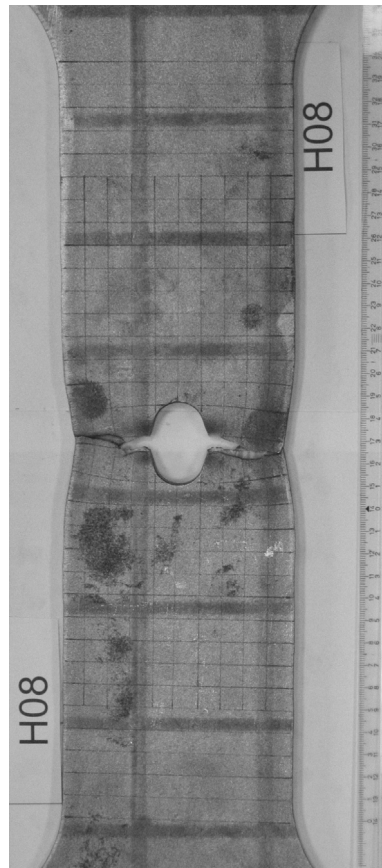
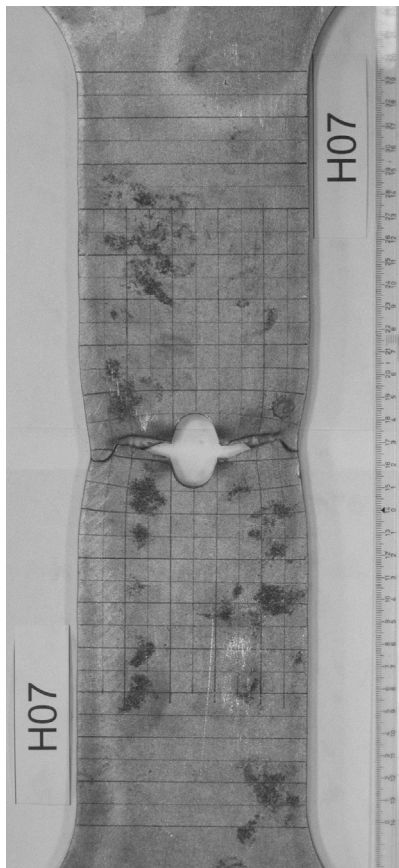
- Greco, N., Earls, C. J. 2003. Structural ductility in hybrid high performance steel beams. *Journal of Structural Engineering-Asce*, 129, 12: 1584-1595.
- Gresnigt, A. M., Steenhuis, C. M. 1997. High strength steels. *Progress in Structural Engineering and Materials*, 1, 1: 31-41.
- Günther, H.-P., Raoul, J., Kuhlmann, U., Lwin, M., Mistry, V.C., Driver, R.G., Grondin, G.Y., Macdougall, C., Miki, C., Kawabata, F., Suegana, K., Watanabe, Y., Takemura, M., Tominaga, T., Samuelsson, A., Schröter, F., Sedlacek, G., Müller, C., Nussabaumer, A., Johansson, B., Höglund, T., Collin, P., Miazzon, A. . 2005. Use and Application of High-Performance Steels for Steel Structures. In: H.-P. Günther, (ed.). *Structural engineering documents 8*. Zürich, IABSE, International Association for Bridge and Structural Engineering.
- IISN. 2008. "Crude Steel statistics." <http://www.worldsteel.org/>.
- Industeel. 2008. "Welcome to Industeel." <http://www.industeel.info/>.
- Johansson, B. 2004. Design of fillet welds with under- or overmatching electrodes. CEN/TC250/SC3/WG S690, In. CEN/TC250/SC3/WG S690, CEN.
- Johansson, B., Maquoi, R., Sedlacek, G. 2001. New design rules for plated structures in Eurocode 3. *Journal of Constructional Steel Research*, 57, 3: 279-311.
- Kim, H. J., Yura, J. A. 1996. The effect of end distance on the bearing strength of bolted connections 96-1, In. 96-1, The University of Texas at Austin.
- Kim, H. J., Yura, J. A. 1999. The effect of ultimate-to-yield ratio on the bearing strength of bolted connections. *Journal of Constructional Steel Research*, 49, 3: 255-270.
- Kouhi, J., Kortessmä, M. 1990. Strength tests on bolted connections using high-strength steels (HSS steels) as a base material. *Research notes 1185*, In. 1185. Espoo, Technical Research Centre of Finland.
- Kuhlmann, U., Bergmann, J. 2005. Effective use of high strength steels in welded structures under fatigue loading. 4th European Conference on Steel and Composite Structures, Eurosteel 2005, B. Hoffmeister, (ed.), Druck und Verlagshaus Mainz, Maastricht.
- Langenberg, P., Nießen, T., Dahl, W. 2000. Bruch- und Verformungsverhalten von hochfesten Stählen mit Streckgrenzen von 690 bis 890 MPa. *Stahlbau*, 69, 4: 283-291.
- Ling, T. W., Zhao, X. L., Al-Mahaidi, R., Packer, J. A. 2007. Investigation of block shear tear-out failure in gusset-plate welded connections in structural steel hollow sections and very high strength tubes. *Engineering Structures*, 29, 4: 469-482.
- MII. 2008. "IRON ORE Hematite, Magnetite & Taconite " <http://www.mii.org/Minerals/photoiron.html>.
- Može, P., Beg, D. 2006. Preklopni strižni spoji iz jekel visoke trdnosti. In: F. Saje, J. Lopatič, (eds.). *Zbornik 28. zborovanja gradbenih konstruktorjev Slovenije*. Bled, Slovenija, Slovensko društvo gradbenih konstruktorjev: 115-124.
- Može, P., Beg, D. 2007. Testi na preklopnih vijachenih strižnih spojih iz jekla visoke trdnosti. In: F. Saje, J. Lopatič, (eds.). *Zbornik 29. zborovanja gradbenih konstruktorjev Slovenije*. Bled, Slovenija, Slovensko društvo gradbenih konstruktorjev: 233-240.
- Može, P., Beg, D., Lopatič, J. 2006a. Ductility and strength of bolted connections made of high strength steel. In: D. Dubina, V. Ungureanu, (eds.). *Steel - a new and traditional material for building: proceedings of the International Conference in Metal Structures*. Poiana Brasov, Romania, London; New York: Taylor & Francis: 323-330.

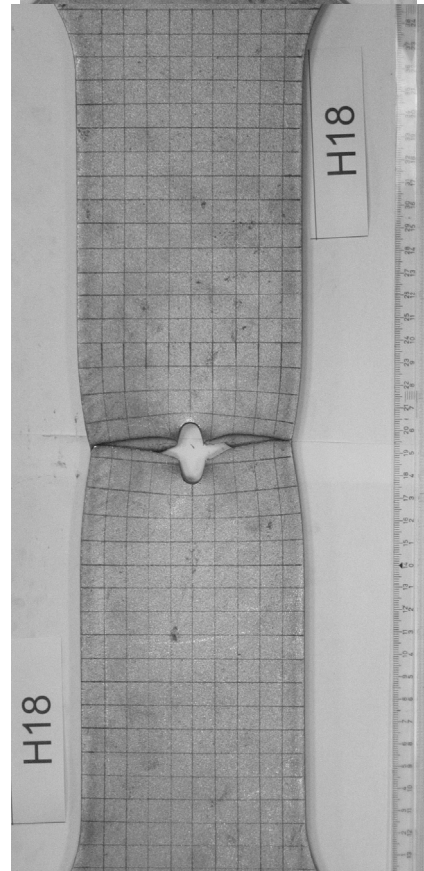
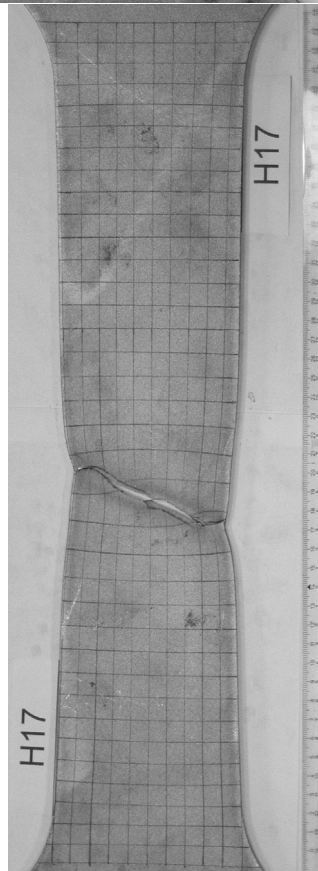
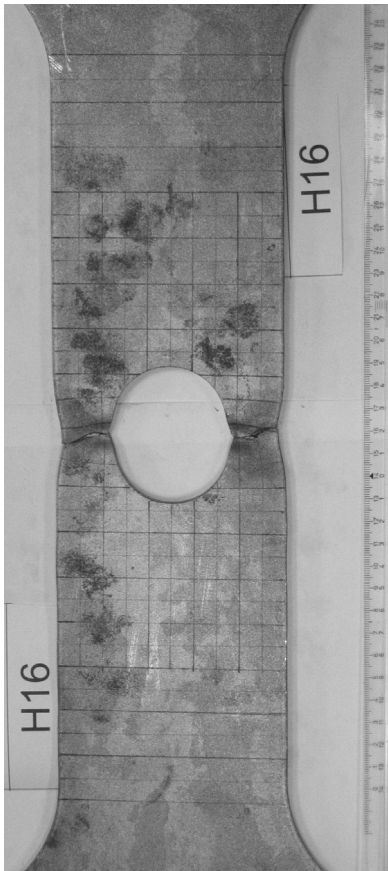
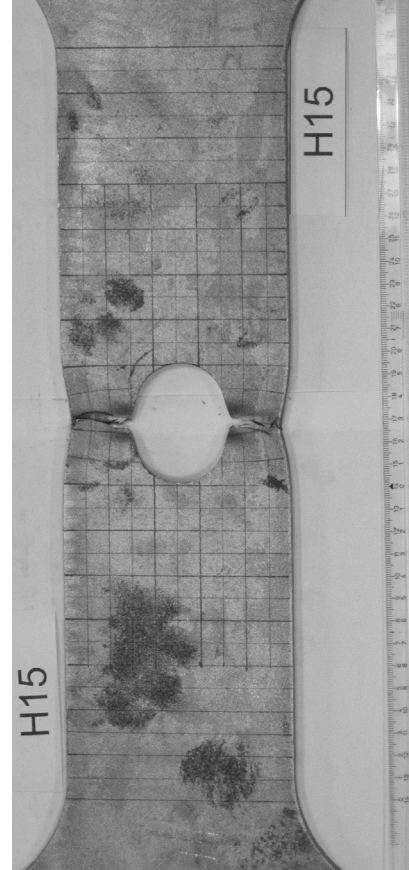
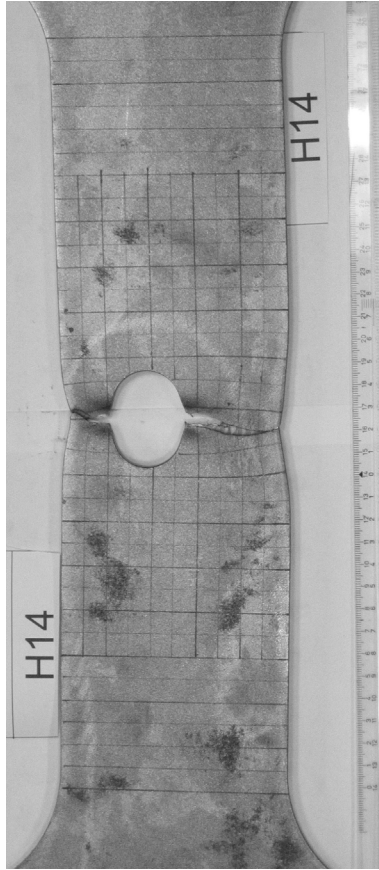
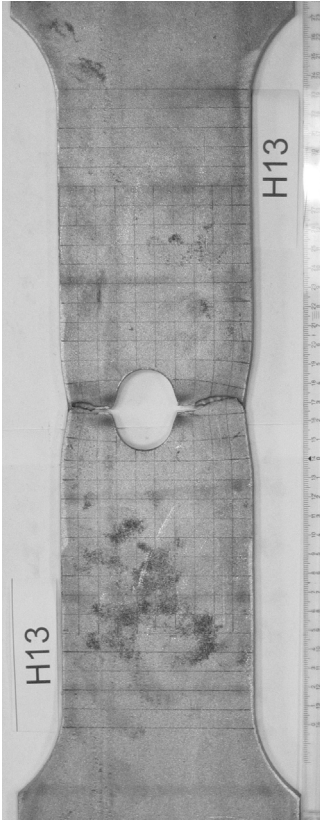
- Može, P., Beg, D., Lopatič, J. 2006b. Local ductility of structures made of high strength steel. In: F. M. Mazzolan, A. Wada, (eds.). STESSA 2006: proceedings of the fifth International conference on behaviour of steel structures in seismic areas. Yokohama, Japan, Leiden: Taylor & Francis: 169-174.
- Može, P., Beg, D., Lopatič, J. 2007a. Net cross-section design resistance and local ductility of elements made of high strength steel. *Journal of Constructional Steel Research*, 63, 11: 1431-1441.
- Može, P., Beg, D., Lopatič, J. 2007b. Projektna nosilnost oslabljenih prerezov elementov iz jekel visoke trdnosti. *Gradbeni vestnik*, 56, maj 2007: 124-134.
- Puthli, R., Fleischer, O. 2001. Investigations on bolted connections for high strength steel members. *Journal of Constructional Steel Research*, 57, 3: 313-326.
- Rasmussen, K. J. R., Hancock, G. J. 1995. Tests of High-Strength Steel Columns. *Journal of Constructional Steel Research*, 34, 1: 27-52.
- Rex, C. O., Easterling, W. S. 2003. Behavior and modeling of a bolt bearing on a single plate. *Journal of Structural Engineering-Asce*, 129, 6: 792-800.
- Rogers, C. A., Hancock, G. J. 2000. Failure modes of bolted-sheet-steel connections loaded in shear. *Journal of Structural Engineering-Asce*, 126, 3: 288-296.
- SAAB. 2005. "Weldox 1300 Special data sheet."
<http://www.weldox.com/upload/Documents/Products/Datasheets/Preliminärt%20datablad%20WELDOX%201300.pdf>.
- SAAB. 2008. "Instead of carbon fibre and aluminium." <http://www.weldox.com/templates/Page.aspx?id=11758>.
- Sause, R., Fahnestock, L. A. 2001. Strength and ductility of HPS-100W I-girders in negative flexure. *Journal of Bridge Engineering*, 6, 5: 316-323.
- SIMULIA. 2007. Abaqus Online Documentation: Version 6.7. Dassault Systèmes.
- Sinur, F., Beg, D. 2008. Partial factors for resistance of net cross-sections with accidental eccentric holes. In. to be published at Eurosteel 2008.
- Snijder, H. H., Ungermann, D., Stark, J. W. B., Sedlacek, G., Bijlaard, F. S. K., Hemmert-Halswick, A. 1988a. Evaluation of test results on bolted connections in order to obtain strength functions and suitable model factors - Part A: Results. In: Eurocode No.3 - Part 1 - Background documentation, Chapter 6. Document 6.01. Brussels, Commission of the European Communities.
- Snijder, H. H., Ungermann, D., Stark, J. W. B., Sedlacek, G., Bijlaard, F. S. K., Hemmert-Halswick, A. 1988b. Evaluation of test results on bolted connections in order to obtain strength functions and suitable model factors - Part B: Evaluations. In: Eurocode No.3 - Part 1 - Background documentation, Chapter 6. Document 6.02. Brussels, Commission of the European Communities.
- ThyssenKrupp Steel AG. 2006. "N-A-XTRA® and XABO® high-strength steels. For lighter living."
http://www.thyssenkrupp-steel.com/upload/binarydata_tkcsd4cms/56/56/00/00/00/00/5656/n-a-xtra_xabo_flyer_en_2006.pdf.
- Veljkovic, M., Johansson, B. 2004. Design of hybrid steel girders. *Journal of Constructional Steel Research*, 60, 3-5: 535-547.

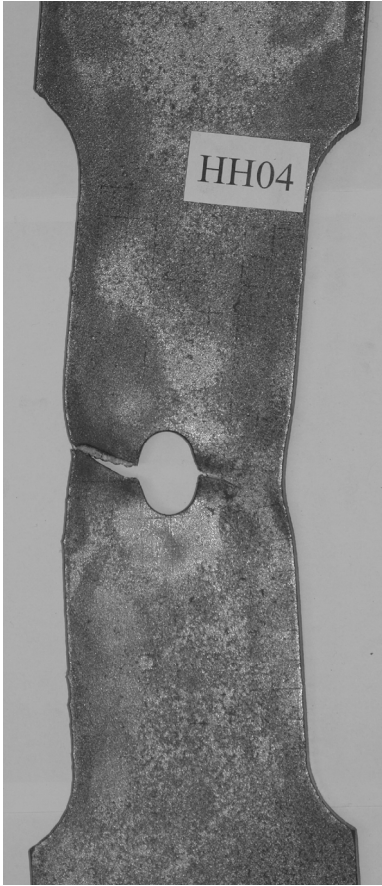
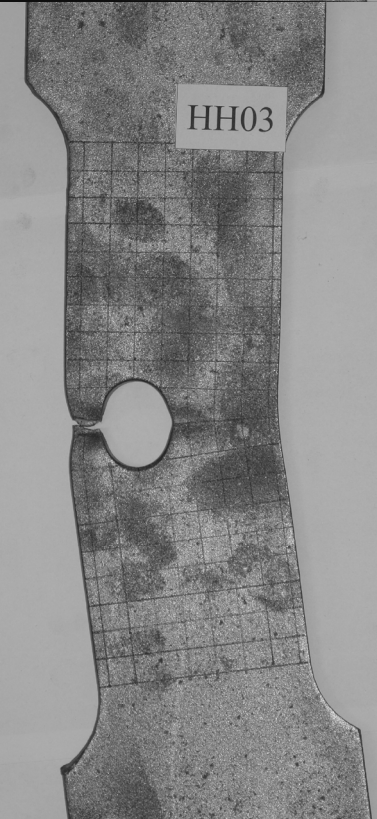
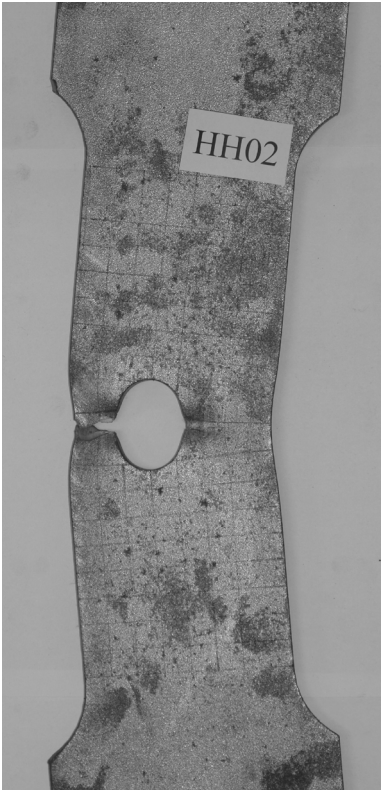
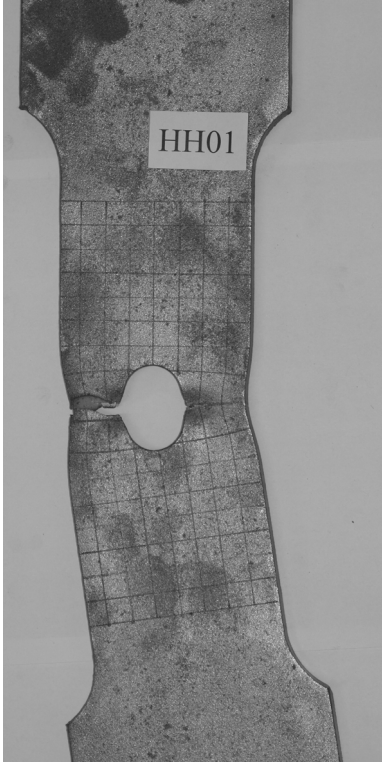
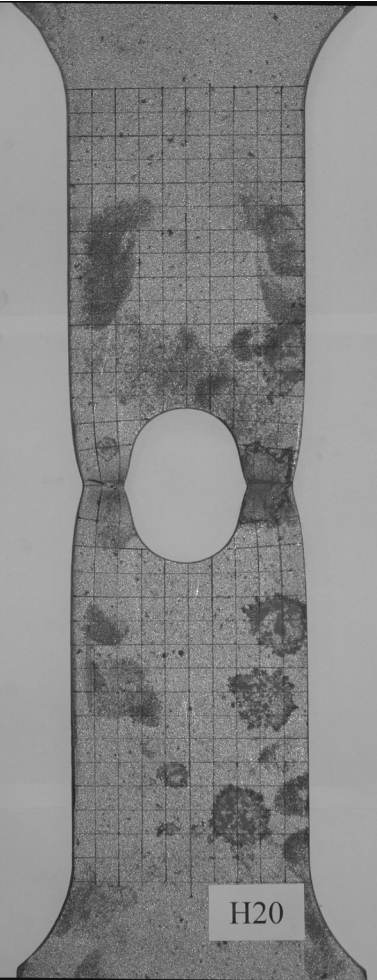
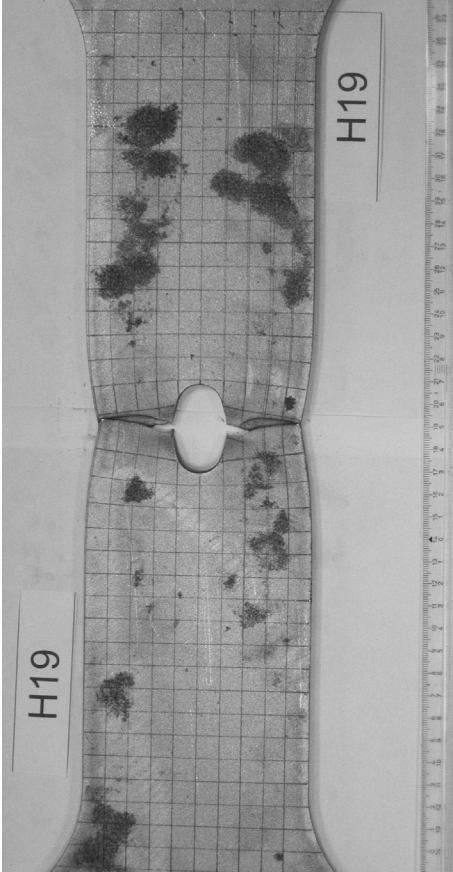
Appendix A SPECIMEN TYPES H, HH – TEST RESULTS

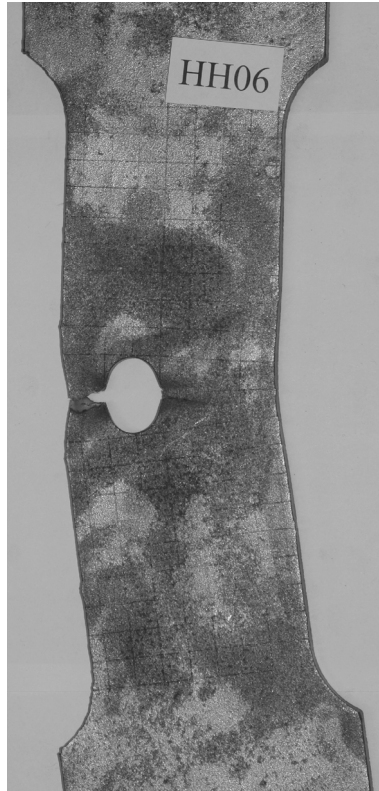
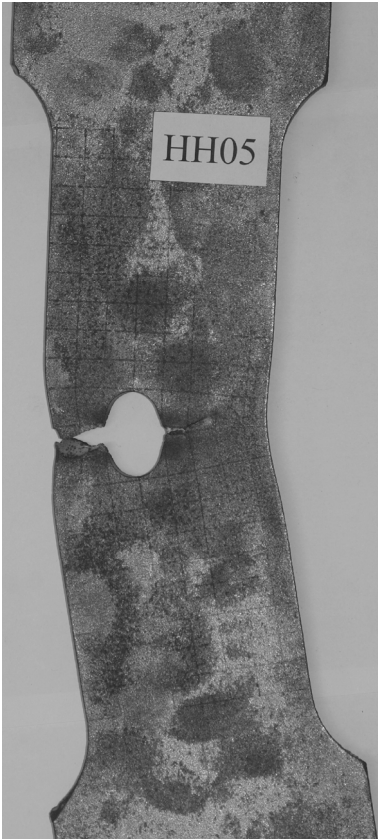
Specimen name	Speed to yielding [mm/s]	Speed after yielding or after P_{max} [mm/s]	Date of the test	Remark
H01	0,071	0,071	12.7.2005	some irregularity in speed
H02	0,071	0,071	12.7.2005	the cores of IND 101 and IND 102 switched by mistake
H03	0,042	0,042	12.7.2005	the test was stopped by mistake after macro crack was formed
H04	0,033	0,033	12.7.2005	
H05	0,025	0,025	12.7.2005	
H06	0,025	0,025	12.7.2005	
H07	0,017	0,017	12.7.2005	
H08	0,017	0,017	13.7.2005	
H09	0,014	0,029	13.7.2005	
H10	0,014	0,014	13.7.2005	
H11	0,014	0,014	13.7.2005	
H11A	0,143	0,143	10.2.2006	
H12	0,020	0,020	13.7.2005	
H13	0,014	0,014	13.7.2005	
H14	0,014	0,029	13.7.2005	
H15	0,014	0,014	13.7.2005	
H16	0,014	0,029	13.7.2005	
H17	0,071	0,143	13.7.2005	the cores of IDTs fell out due to displacement larger than 50 mm
H18	0,071	0,071	13.7.2005	
H19	0,014	0,029	13.7.2005	possible error (small) of displacements on IDTs due to motion of IDT holders. Contraction of specimen.
H20	0,014	0,029	10.2.2006	
HH01	0,020	0,040	27.1.2006	no IDTs mounted
HH02	0,020	0,040	27.1.2006	due to excessive rotation of specimens IDT almost damaged
HH03	0,020	0,040	27.1.2006	no IDTs mounted
HH04	0,020	0,040	27.1.2006	no IDTs mounted
HH05	0,020	0,040	27.1.2006	no IDTs mounted
HH06	0,020	0,040	27.1.2006	no IDTs mounted
B101	0,017	0,017	8.9.2005	
B102	0,020	0,040	8.9.2005	
B103	0,020	0,040	8.9.2005	
B104	0,020	0,040	8.9.2005	
B105	0,020	0,020	8.9.2005	
B106	0,020	0,040	8.9.2005	
B107	0,020	0,040	8.9.2005	
B108	0,025	0,050	8.9.2005	
B109	0,025	0,050	8.9.2005	
B110	0,025	0,050	8.9.2005	
B111	0,025	0,050	8.9.2005	
B112	0,025	0,050	8.9.2005	
B113	0,025	0,050	8.9.2005	
B114	0,025	0,050	8.9.2005	
B115	0,025	0,025	8.9.2005	
B116	0,025	0,050	4.10.2005	bolt tightened to approx. 150 Nm of torque
B117	0,025	0,050	4.10.2005	space between specimen and forks. B117 could deform in transverse direction
B118	0,025	0,050	10.2.2006	
B119	0,025	0,050	10.2.2006	
B120	0,025	0,050	10.2.2006	
B121	0,025	0,050	10.2.2006	
B122	0,025	0,050	10.2.2006	
B123	0,025	0,050	27.1.2006	
B124	0,025	0,050	27.1.2006	
B125	0,025	0,050	10.2.2006	
B201	0,020	0,020	13.9.2005	missing approx. 10s of records
B202	0,025	0,050	13.9.2005	
B203	0,025	0,025	13.9.2005	
B204	0,025	0,025	13.9.2005	
B205	0,025	0,025	13.9.2005	
B206	0,025	0,050	13.9.2005	
B207	0,025	0,025	13.9.2005	
B208	0,025	0,050	13.9.2005	
B209	0,025	0,050	13.9.2005	
B210	0,025	0,050	13.9.2005	ind 102 fell off the specimen
B211	0,025	0,050	13.9.2005	ind 102 fell off the specimen
B212	0,025	0,025	13.9.2005	ind 102 not fixed properly, IND 102 rotated around fixed point
B213	0,025	0,050	4.10.2005	same bolts were used previously on B208

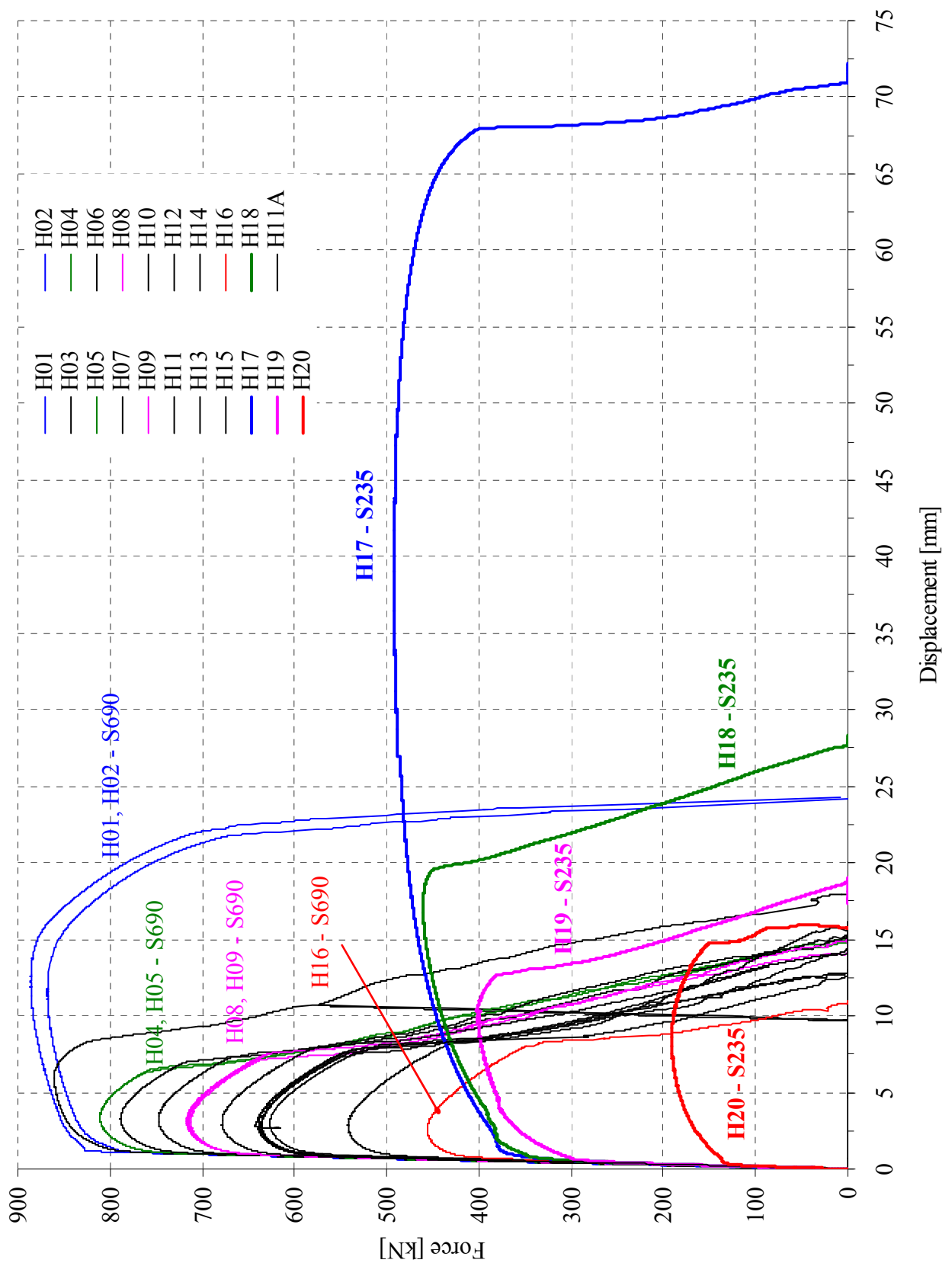




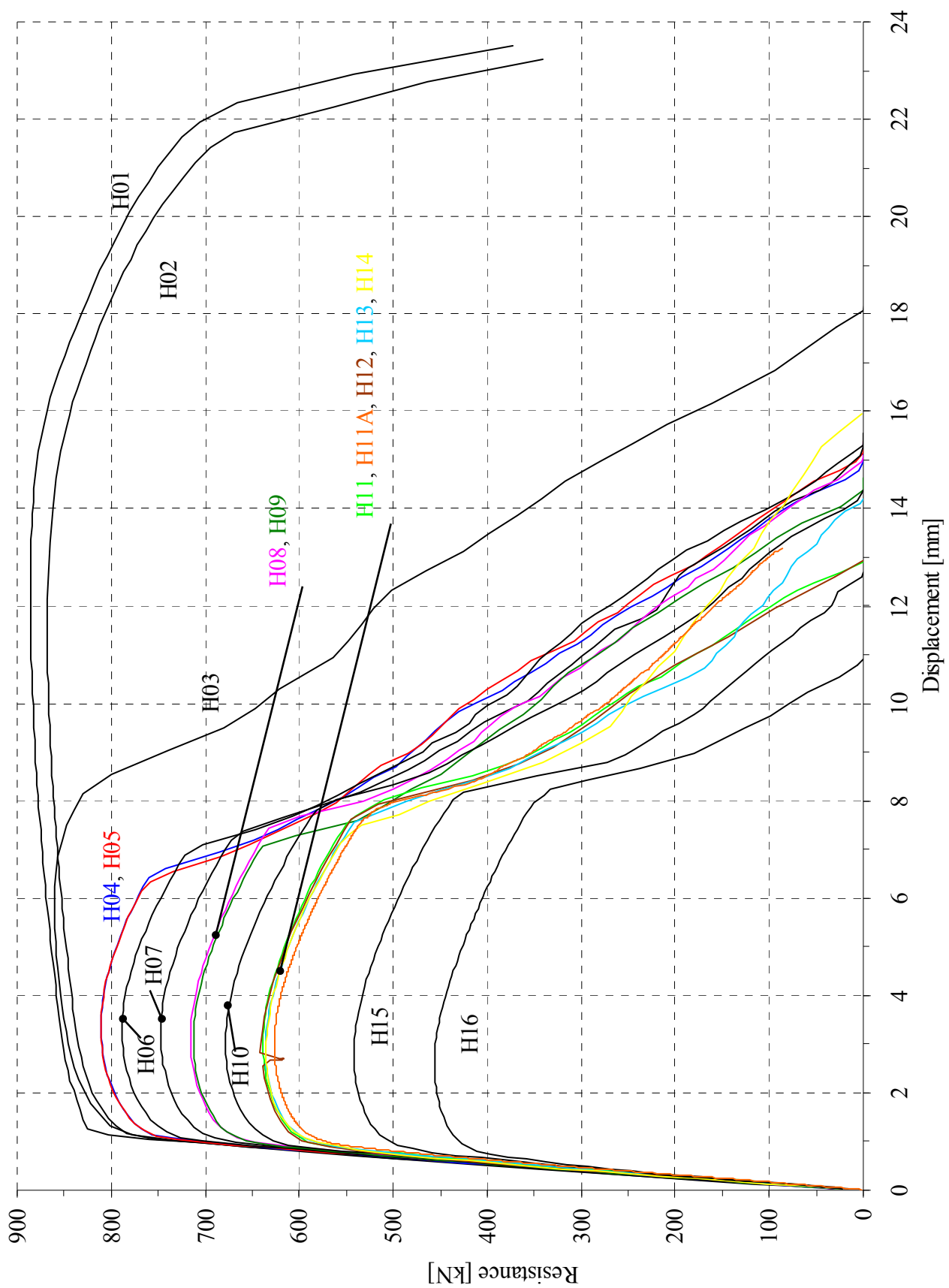




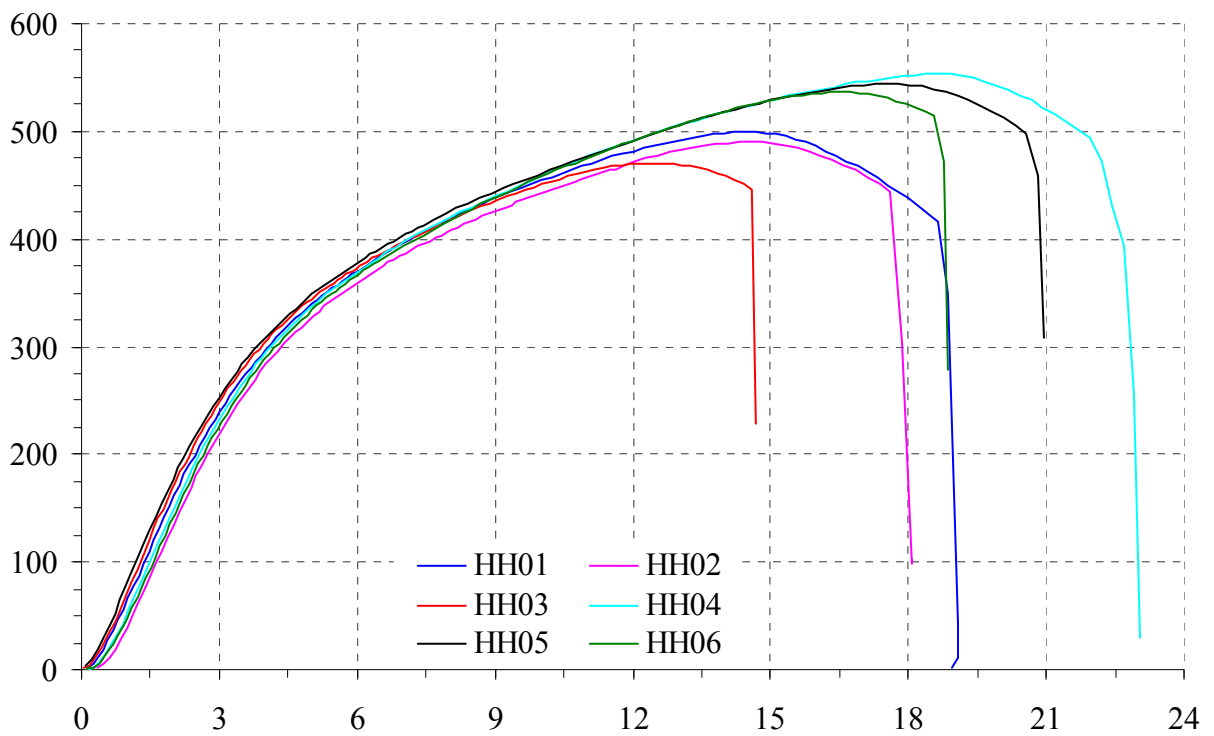




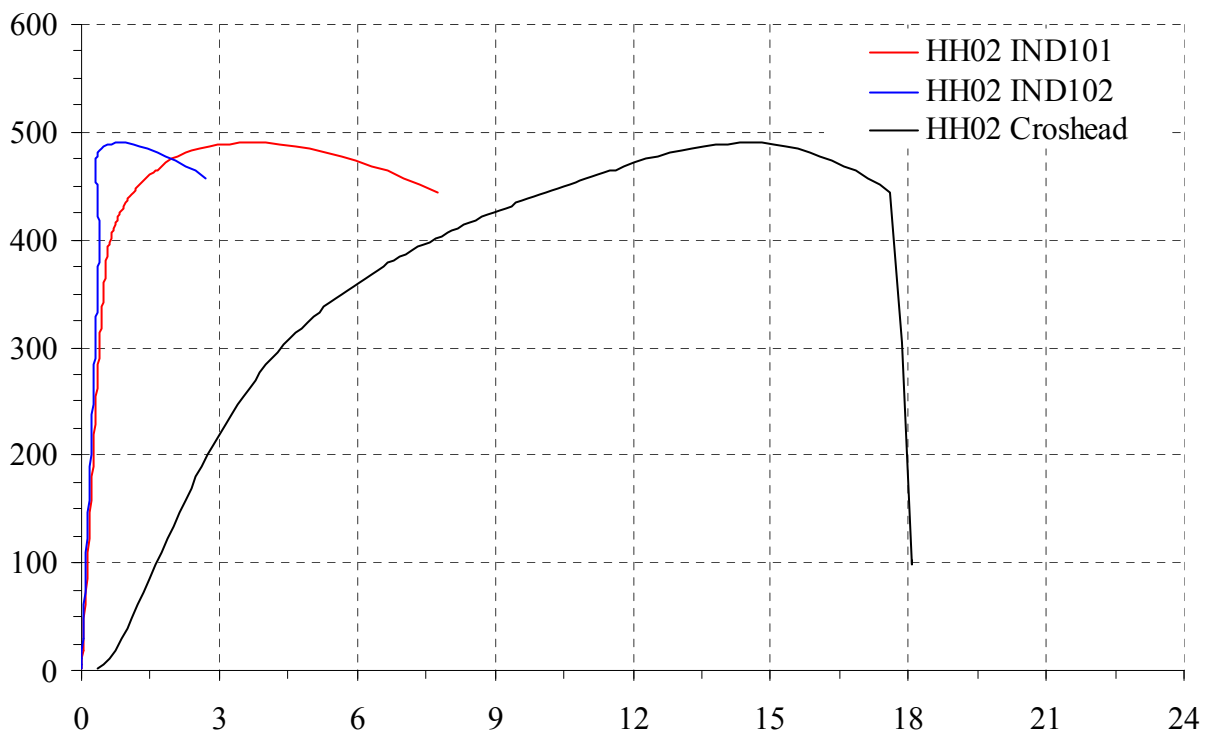
Load-displacement curves for specimens H – comparison of steel grades S235 and S690



Load-displacement curves for specimens H01-H16 (steel grade S690)

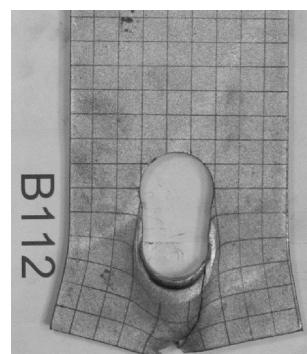
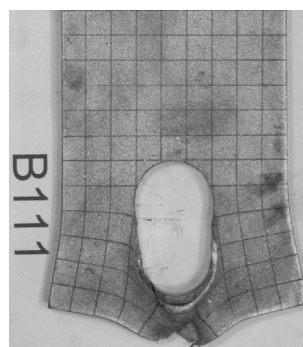
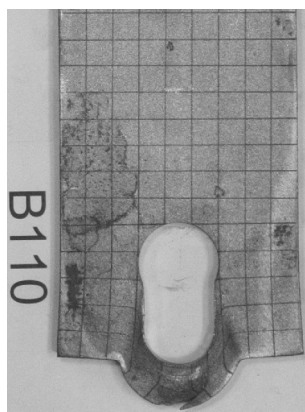
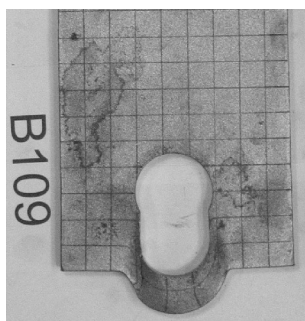
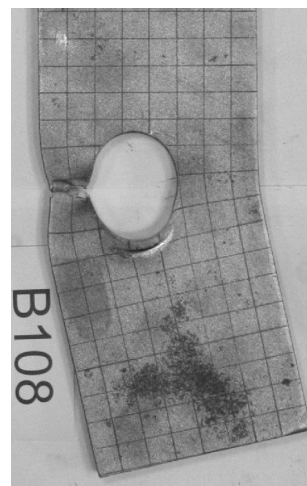
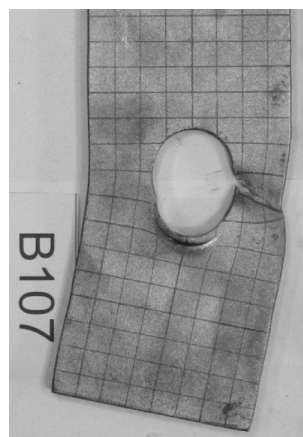
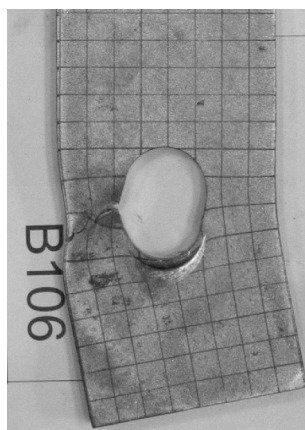
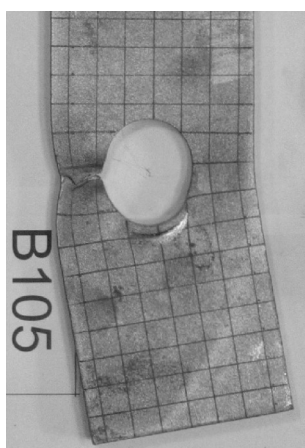
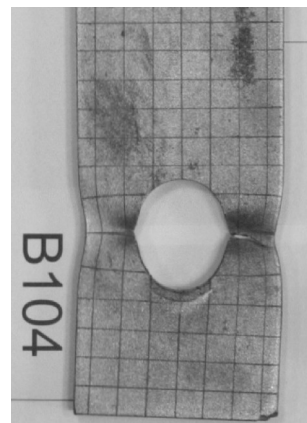
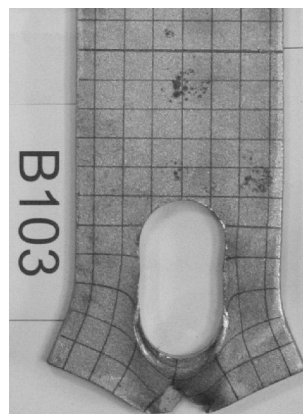
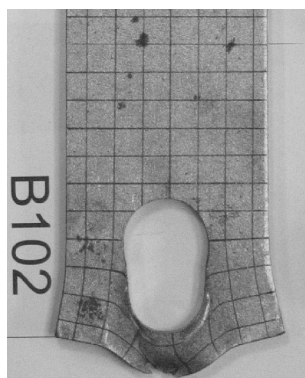
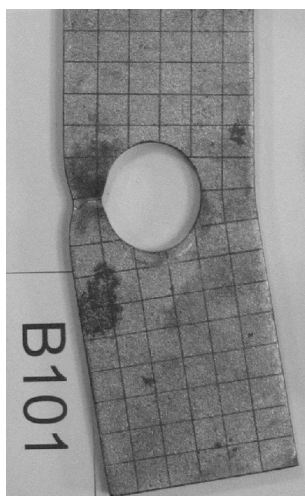


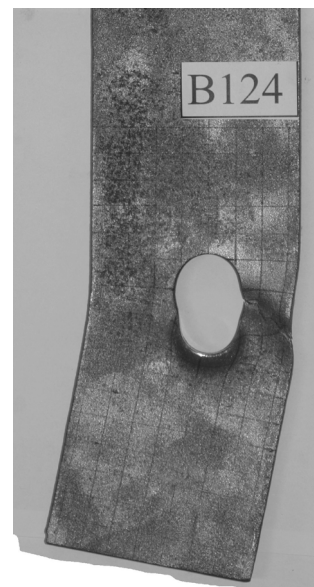
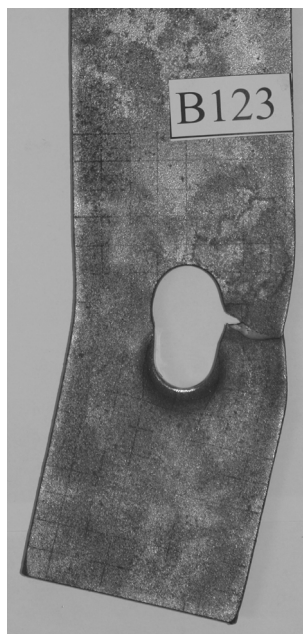
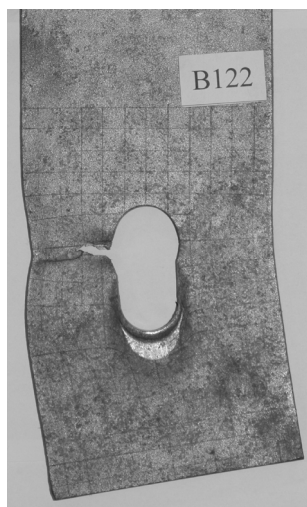
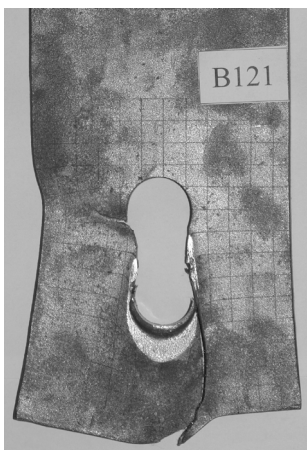
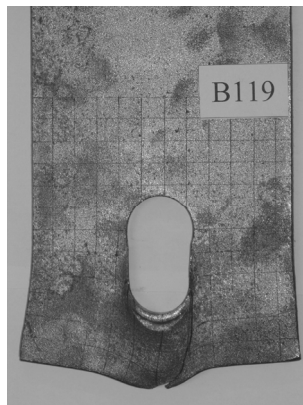
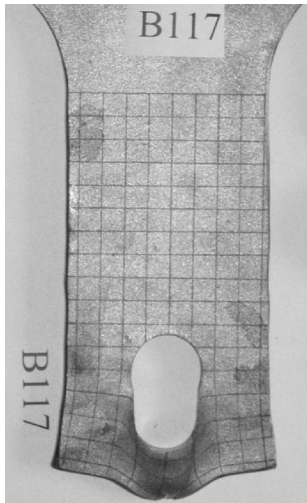
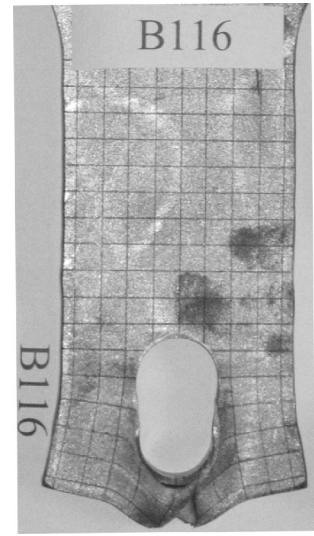
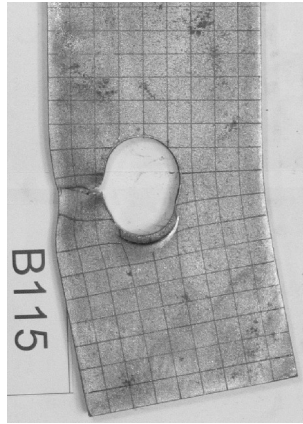
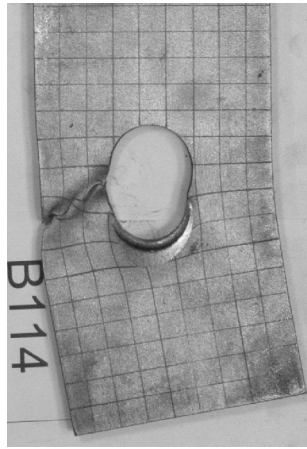
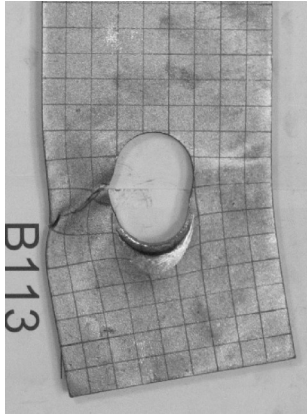
Load-displacement curves for specimens HH. The displacements were measured on the crosshead of the testing machine

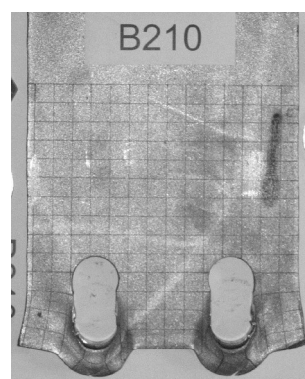
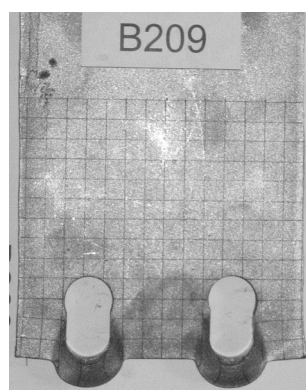
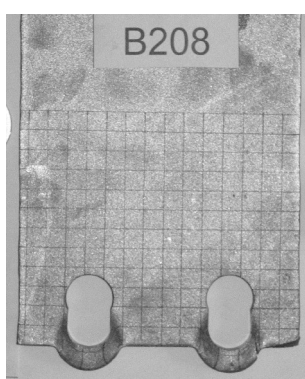
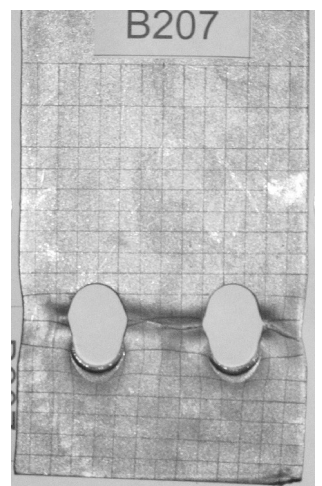
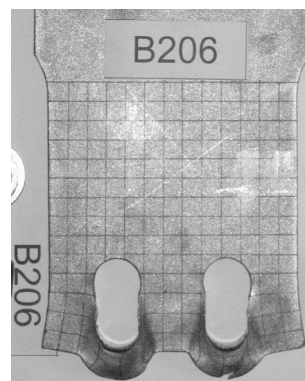
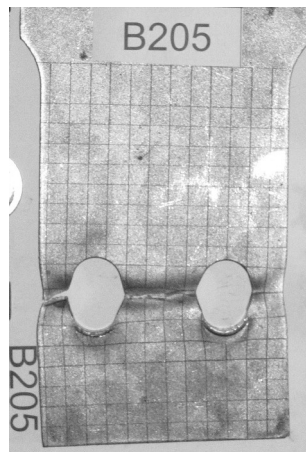
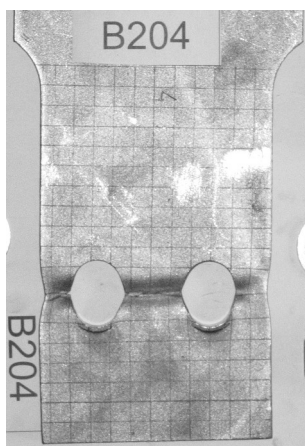
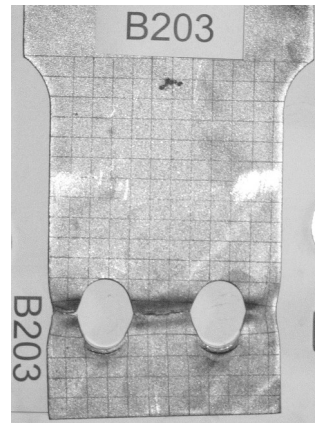
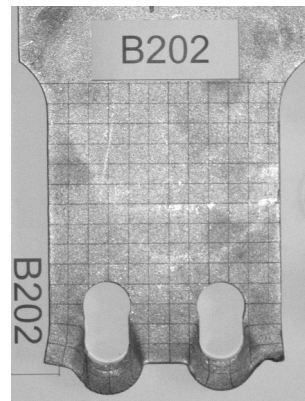
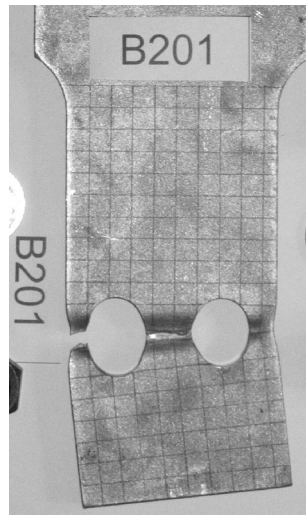
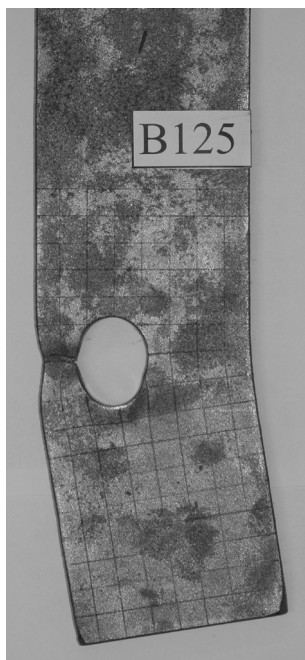


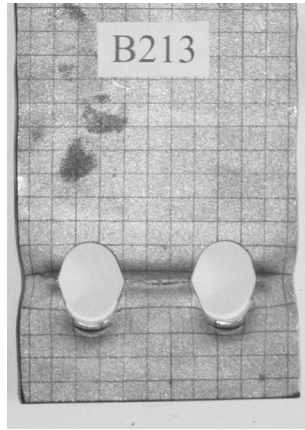
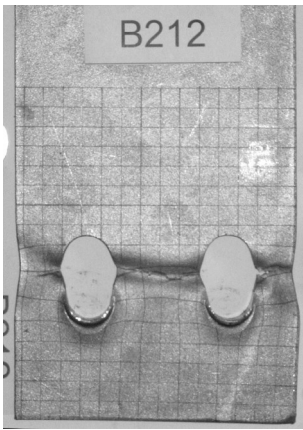
Load-displacement curves for specimens HH02. The displacements were measured on the crosshead of the testing machine and on inductive displacement trasducers (IND 101, IND 102)

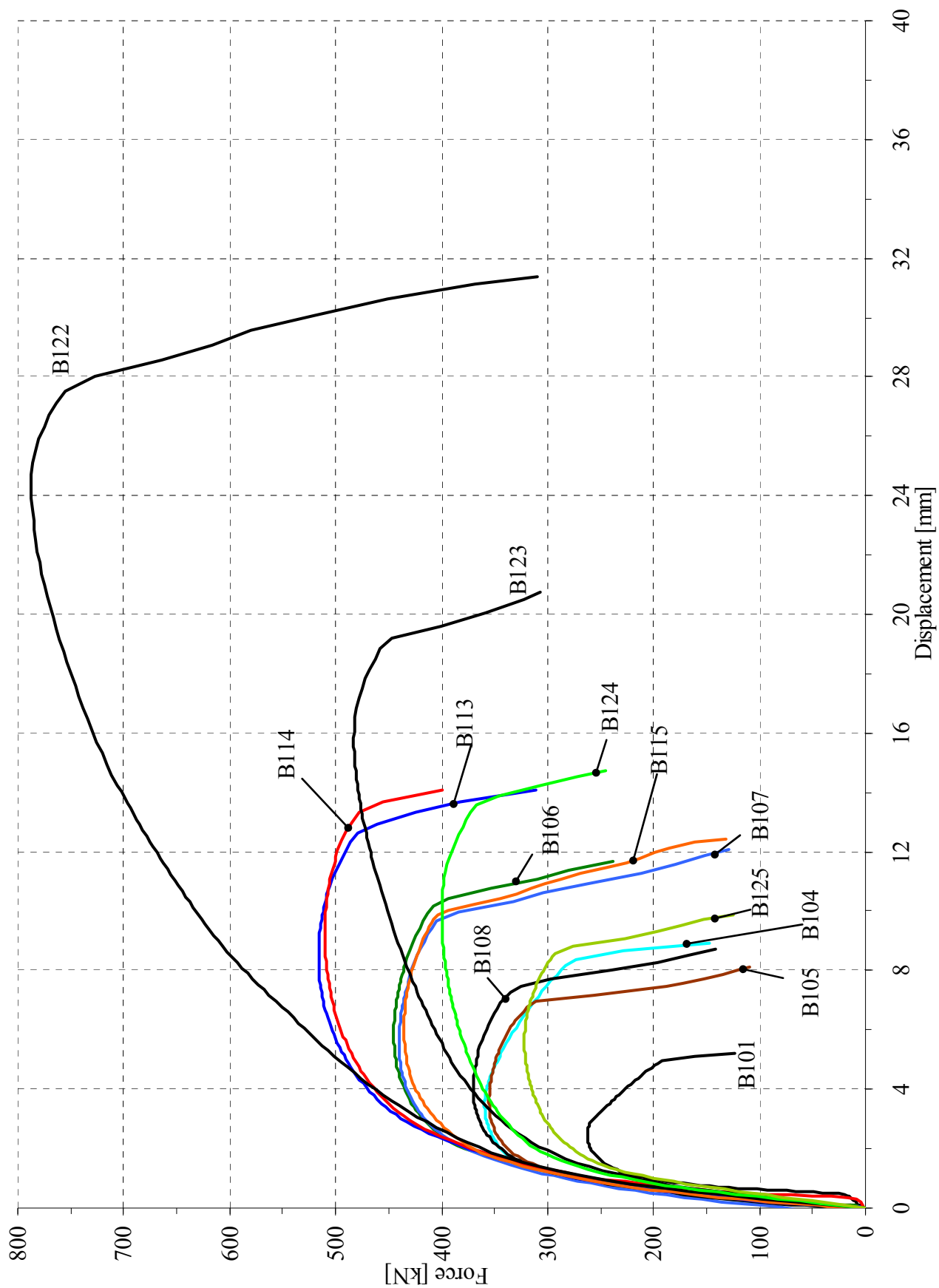
Appendix B SPECIMEN TYPES B1, B2 – TEST RESULTS



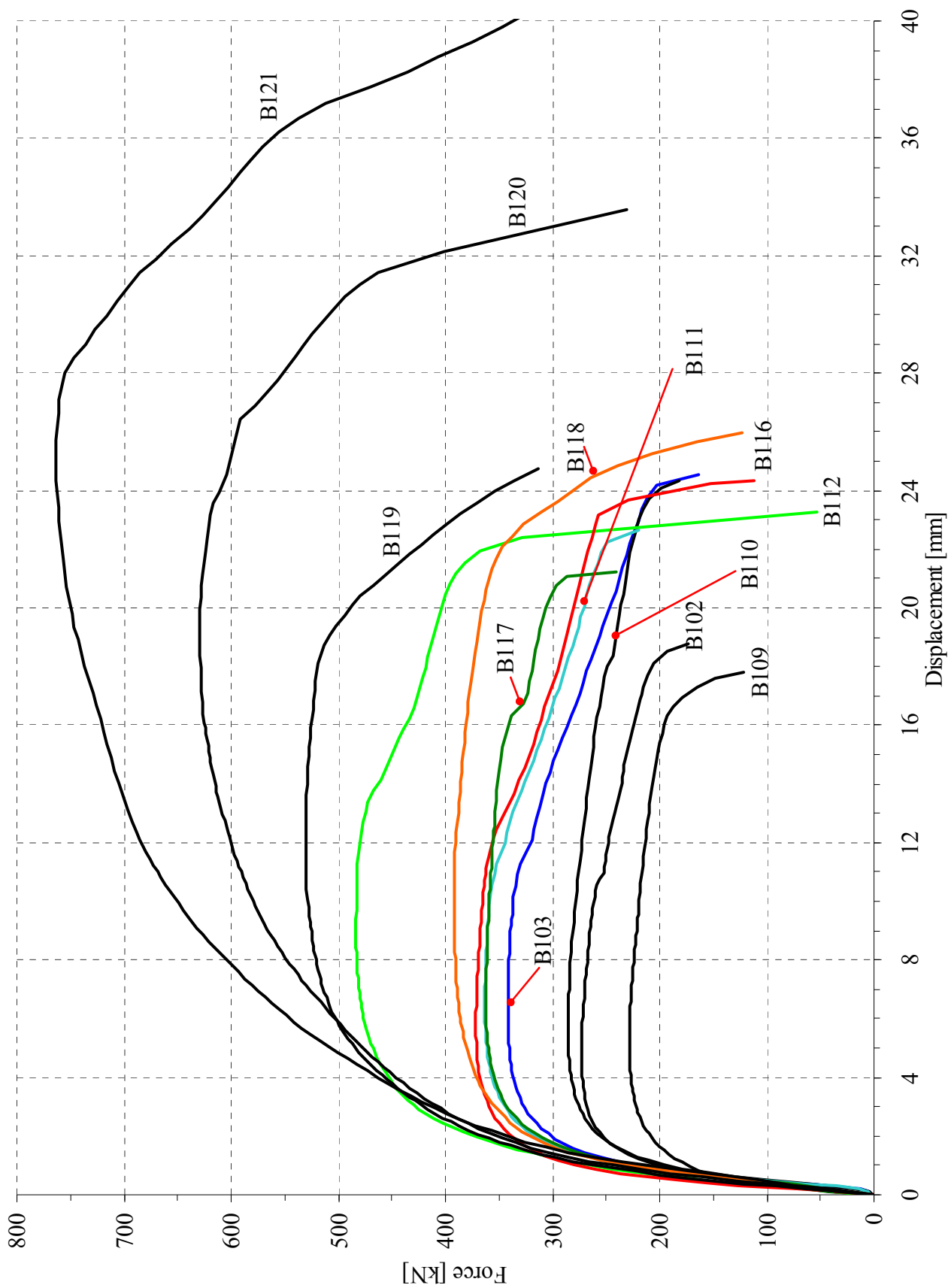




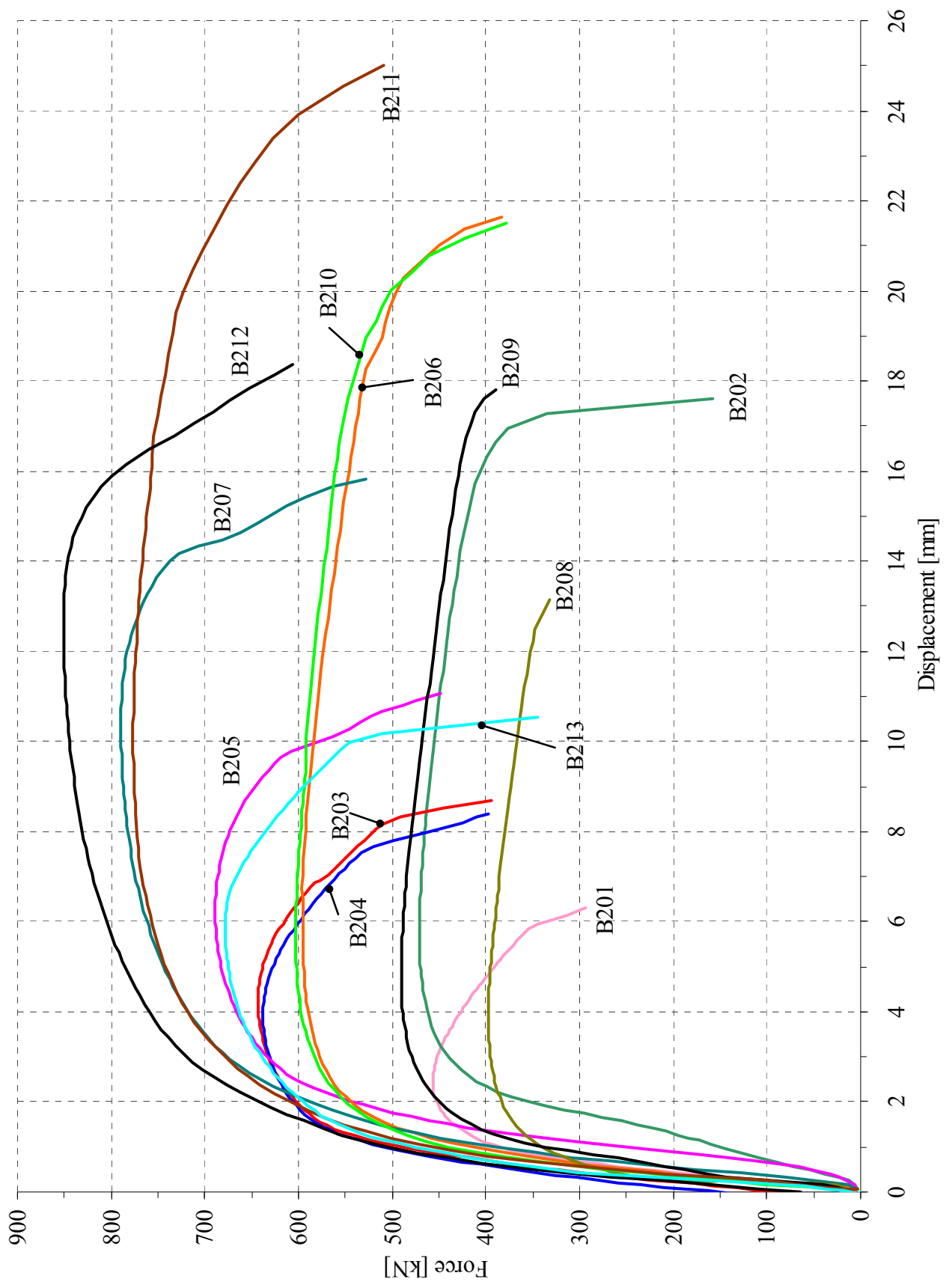




Load-displacement curves for specimens B1 that failed in net cross-section



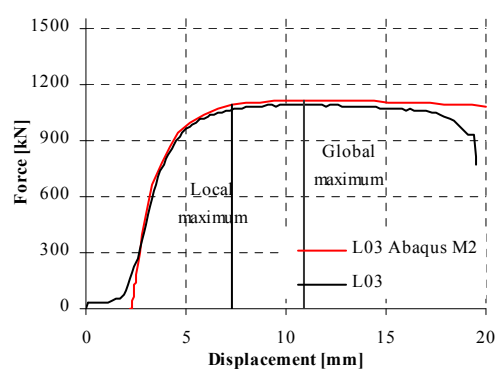
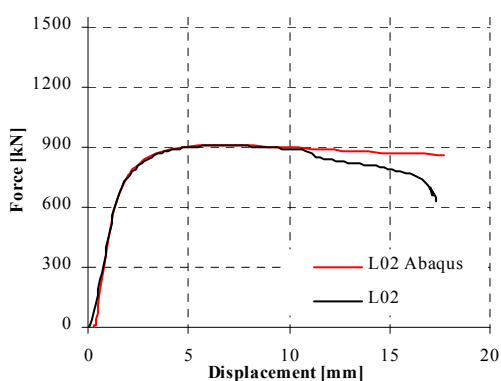
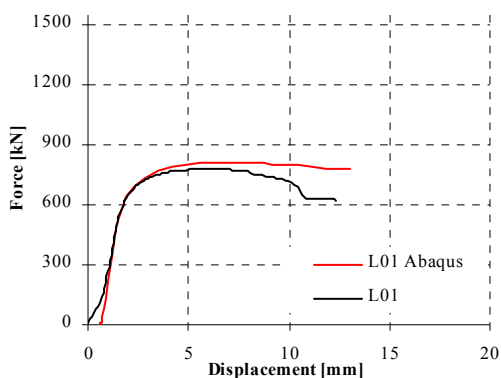
Load-displacement curves for specimens B1 that failed in shear or splitting



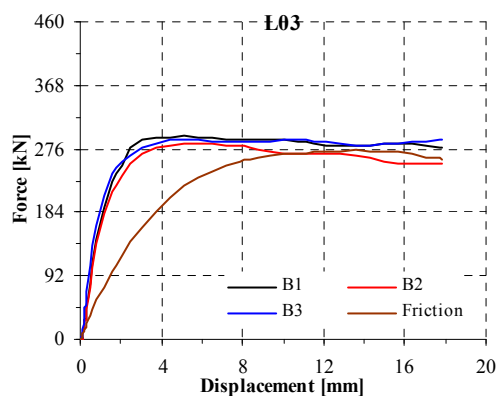
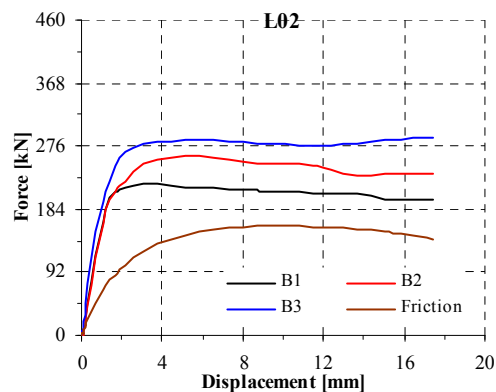
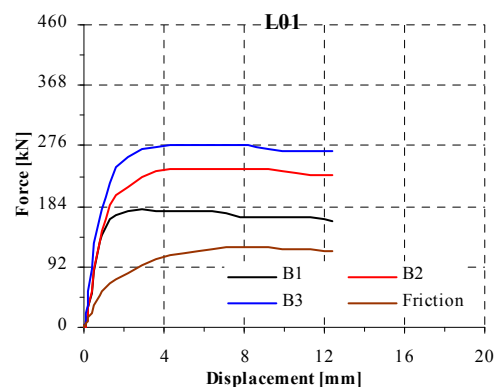
Load-displacement curves for specimens B2

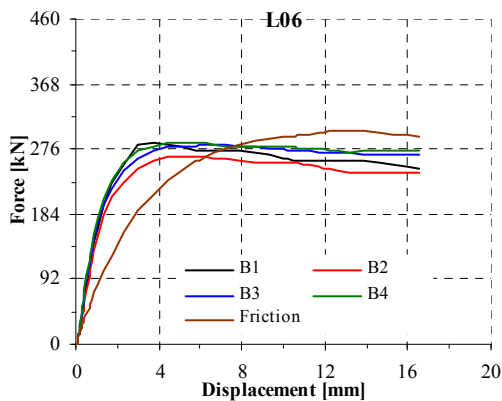
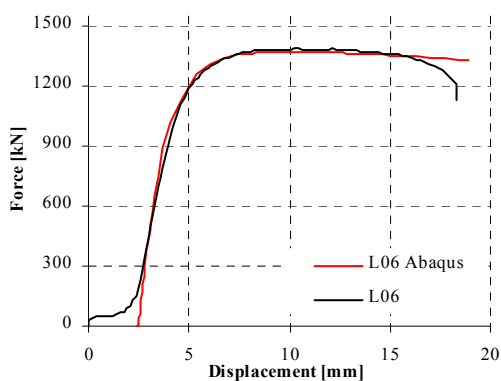
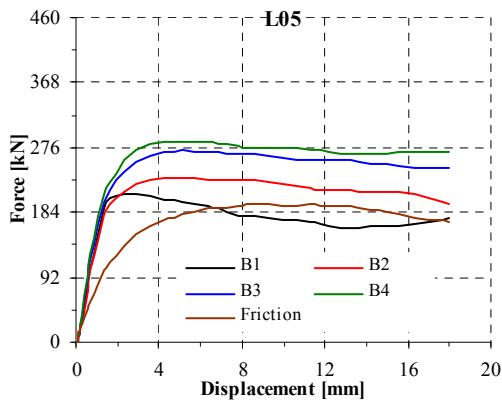
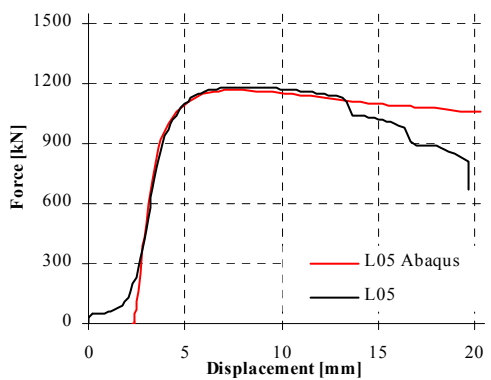
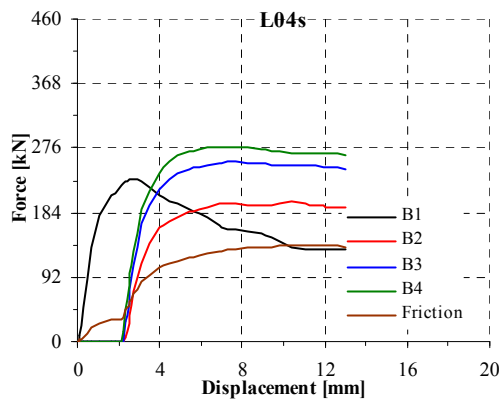
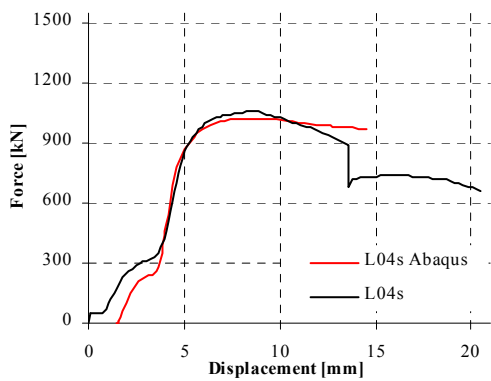
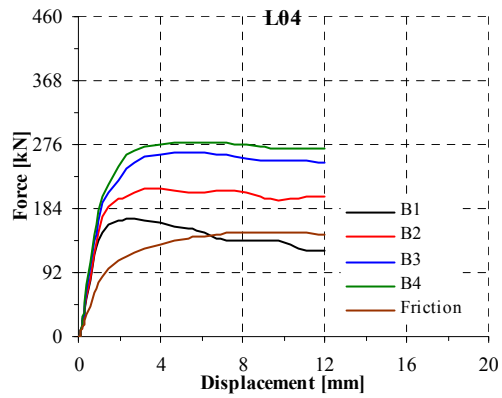
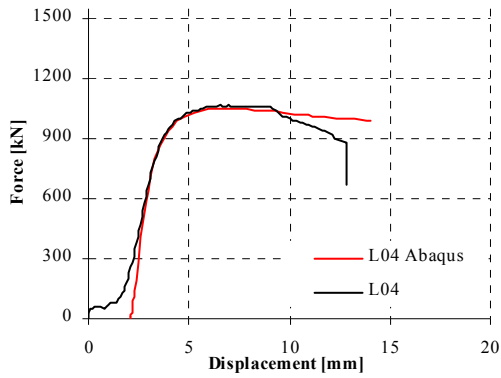
Appendix C SPECIMEN TYPE L – TEST RESULTS

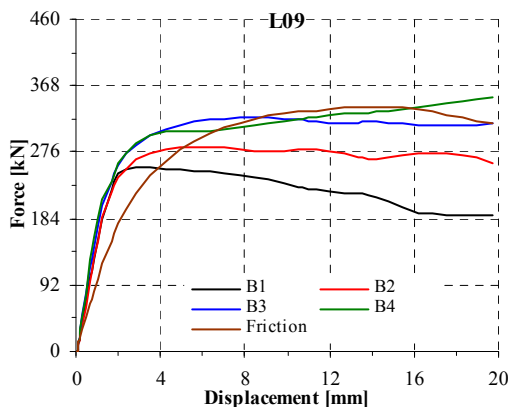
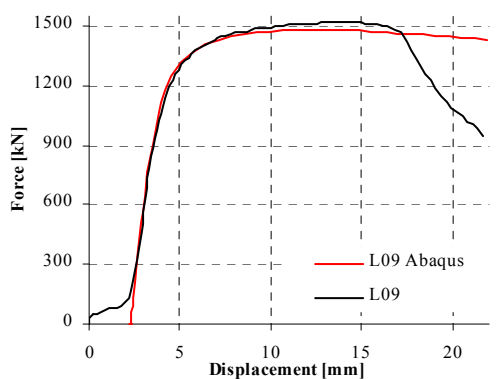
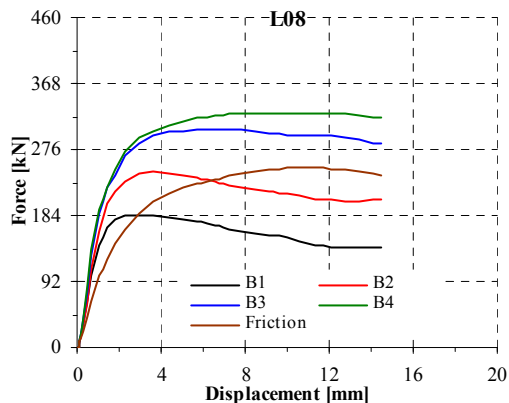
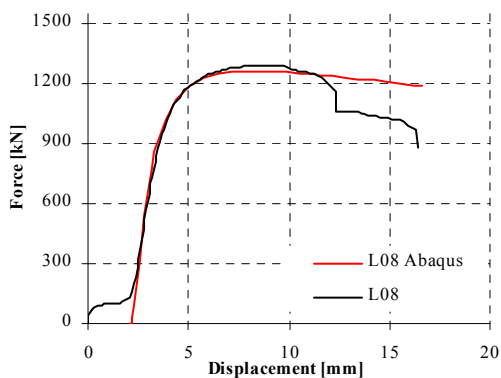
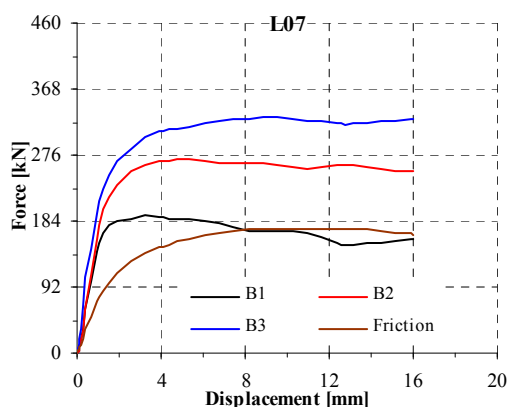
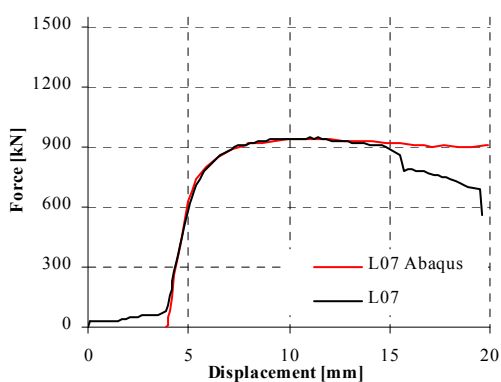
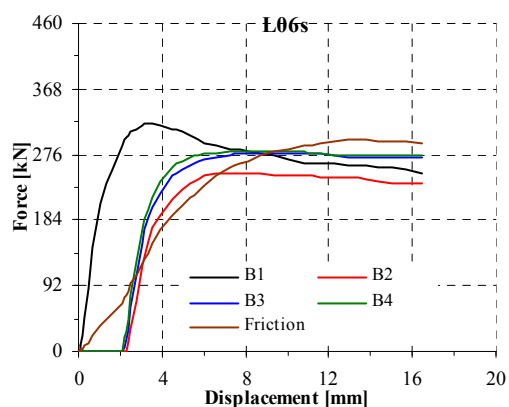
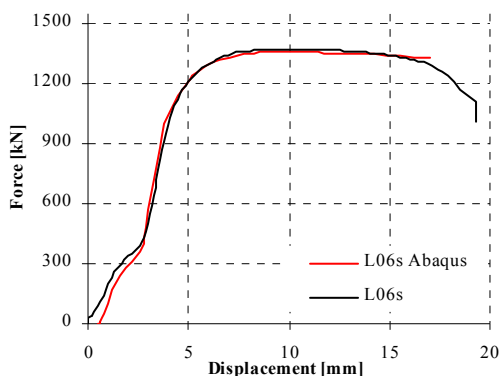
Experimental and numerical load-displacement curves

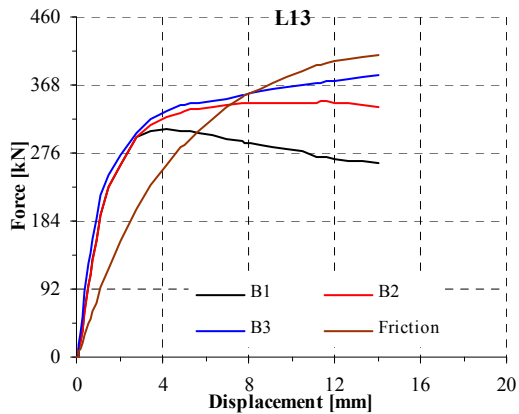
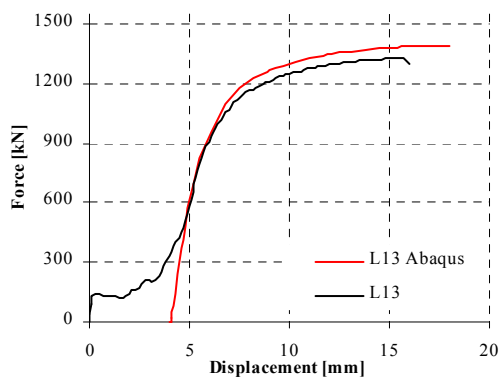
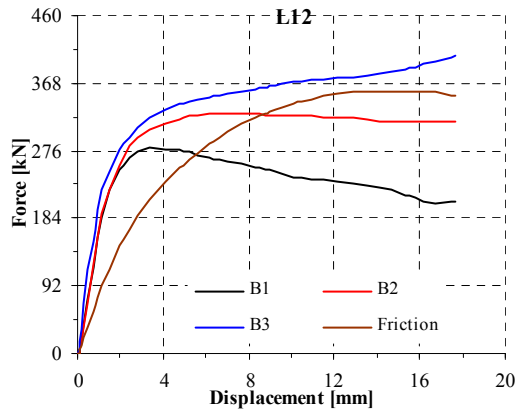
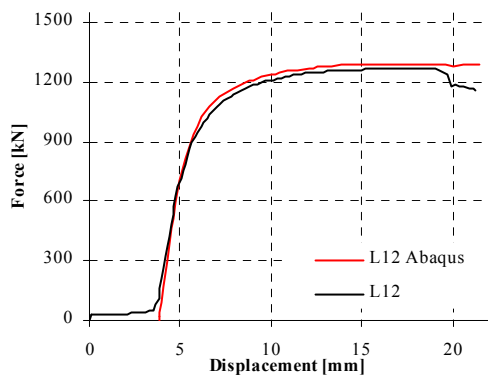
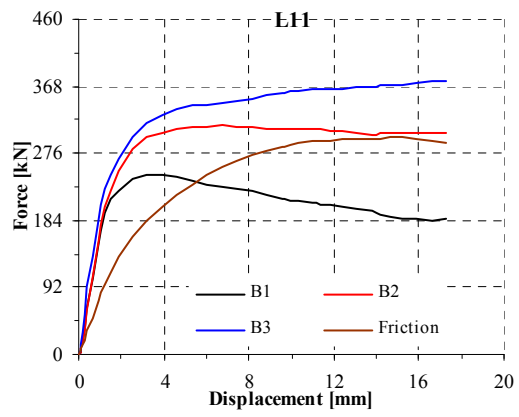
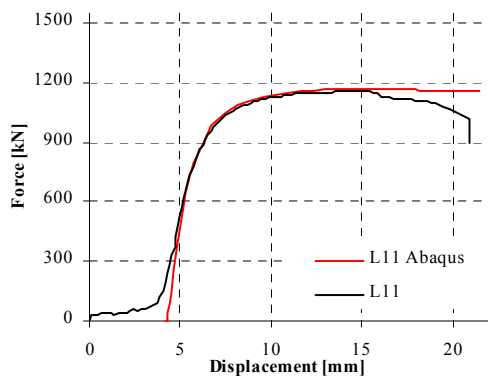
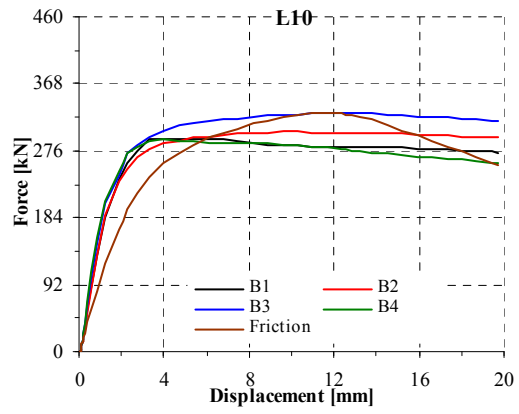
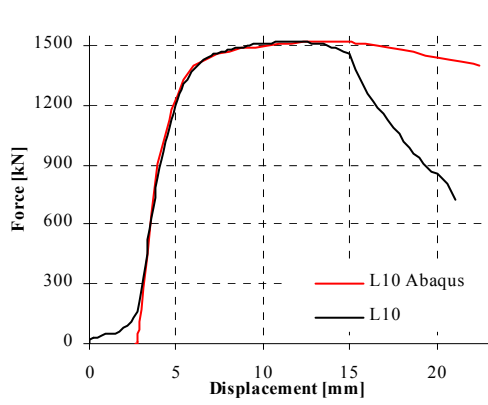


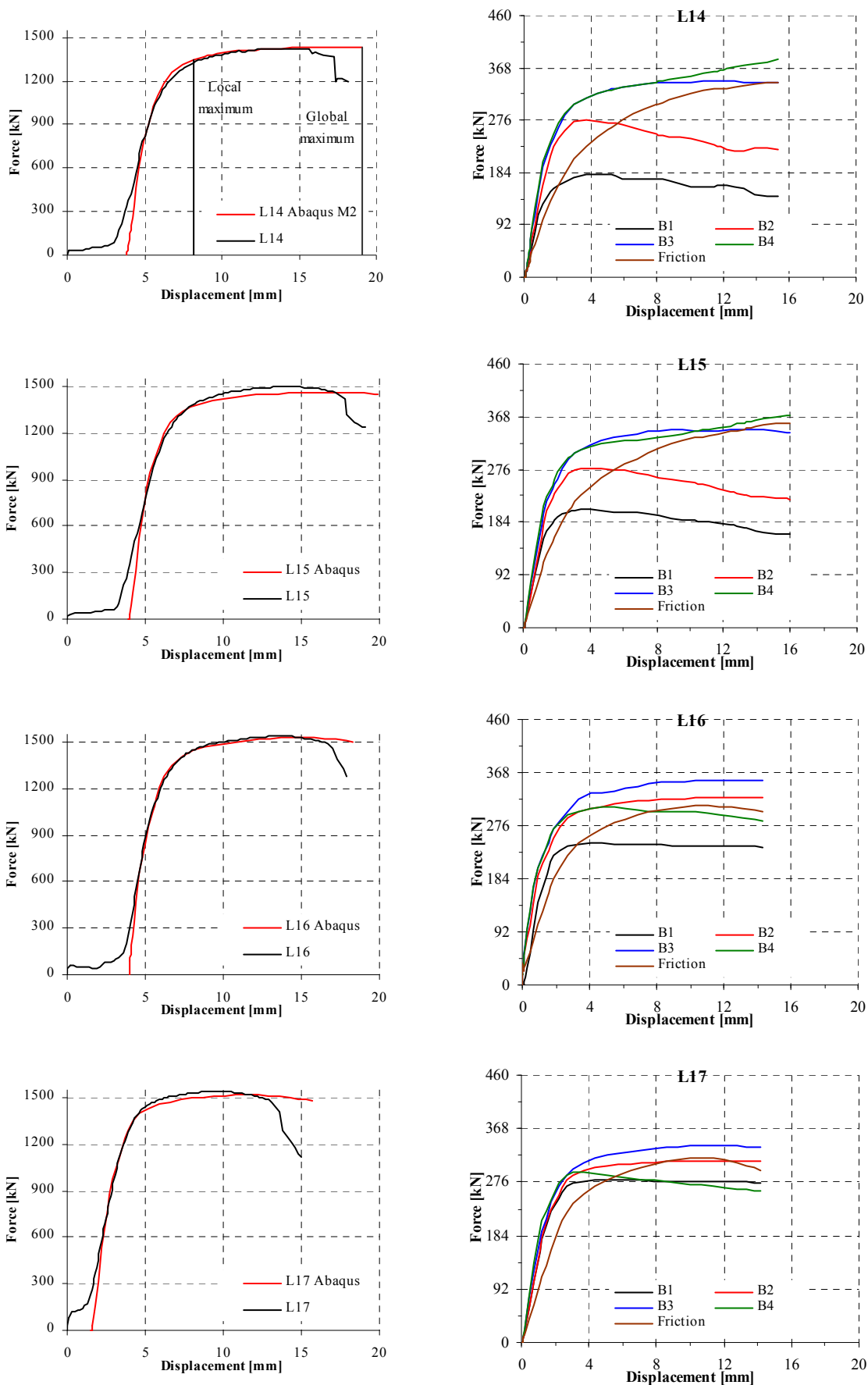
Distribution of forces between bolts and the friction force

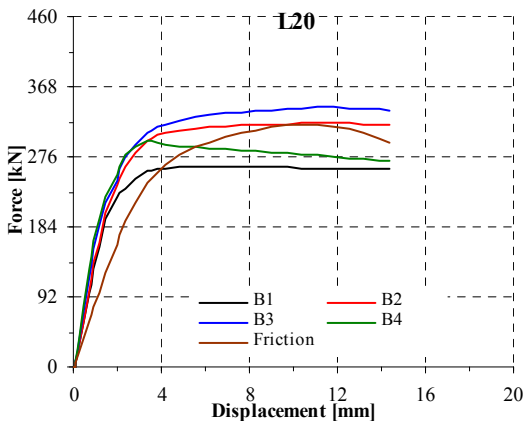
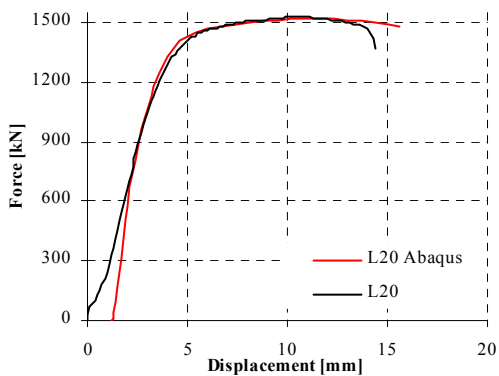
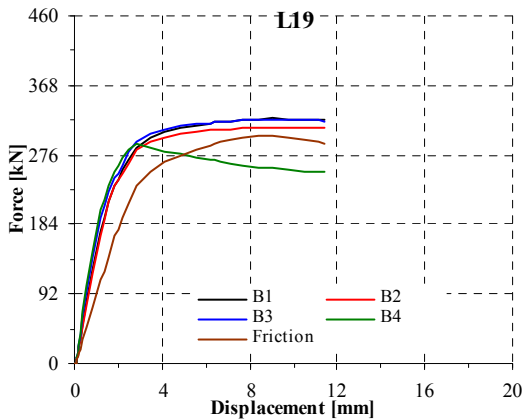
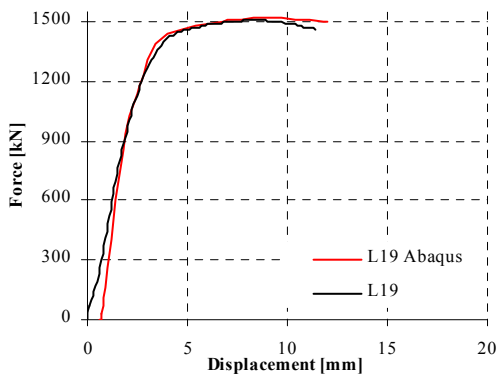
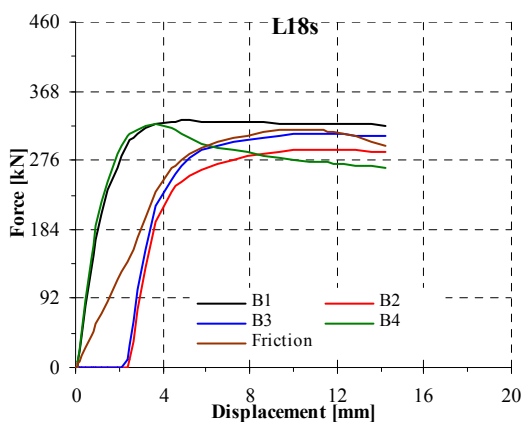
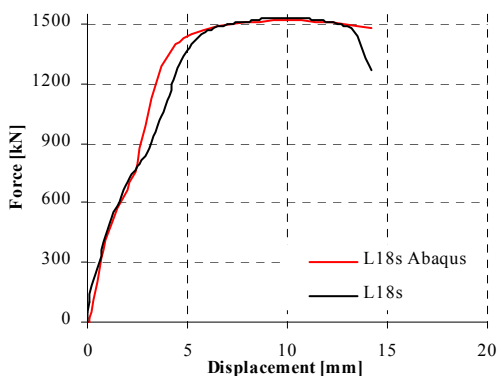
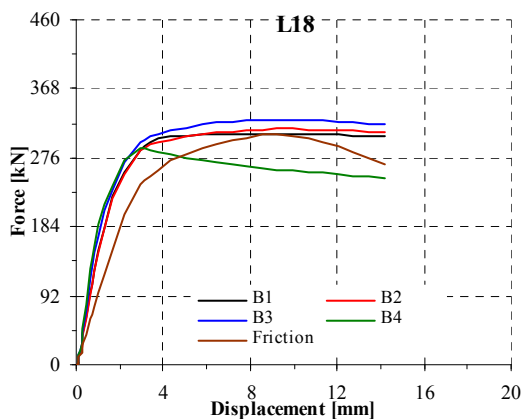
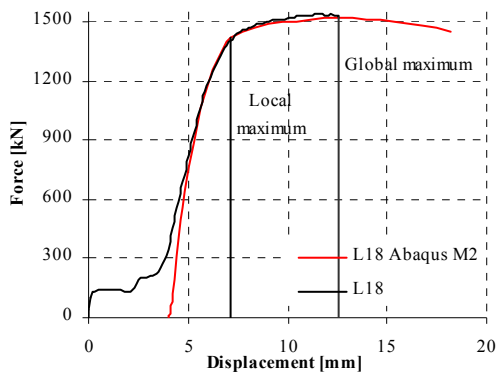


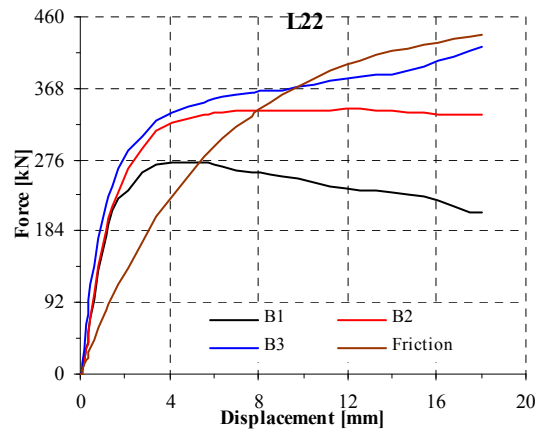
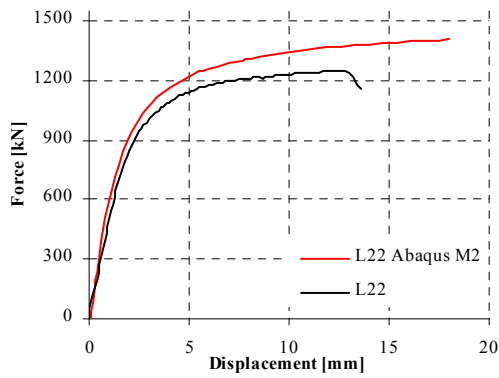
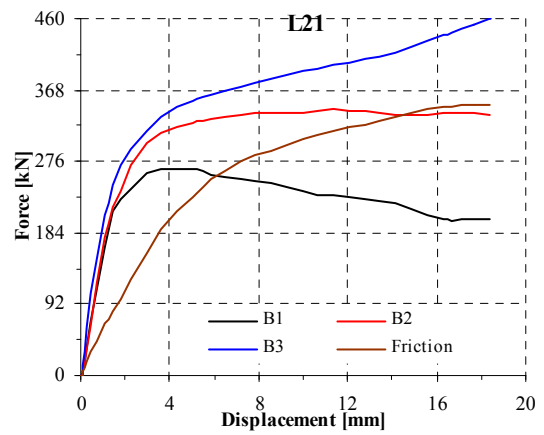
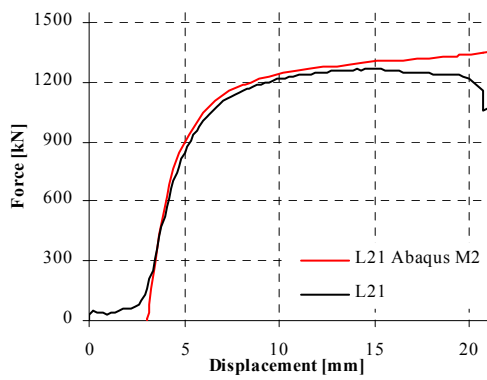
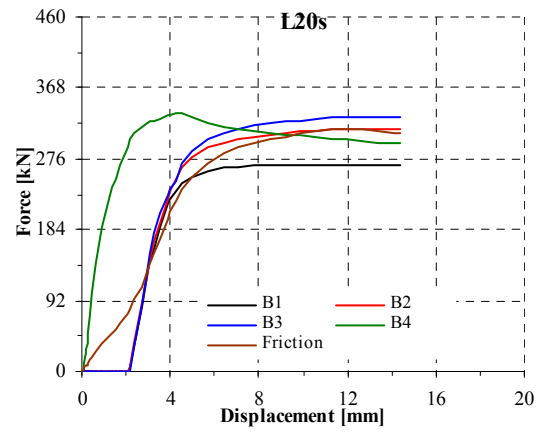
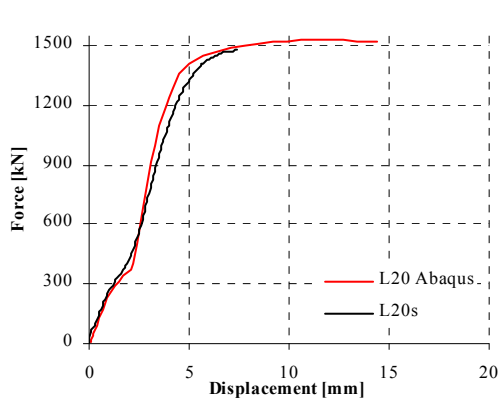






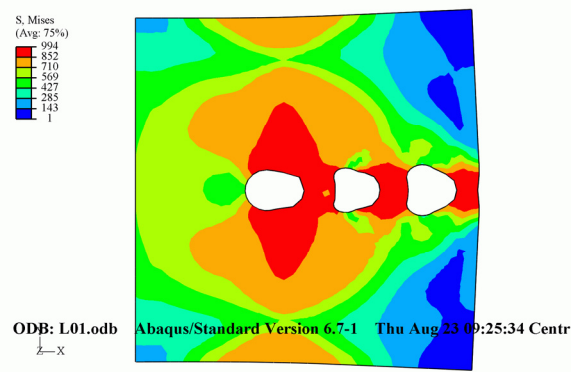




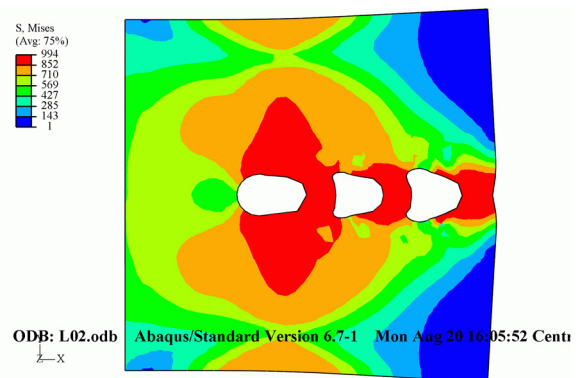
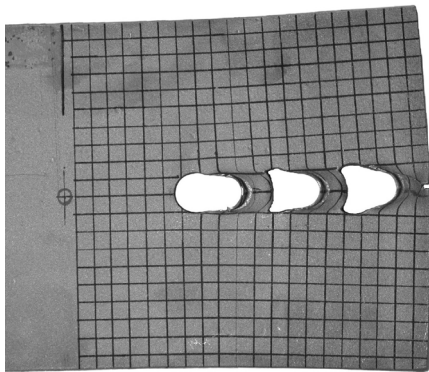


Specimens type L after failure

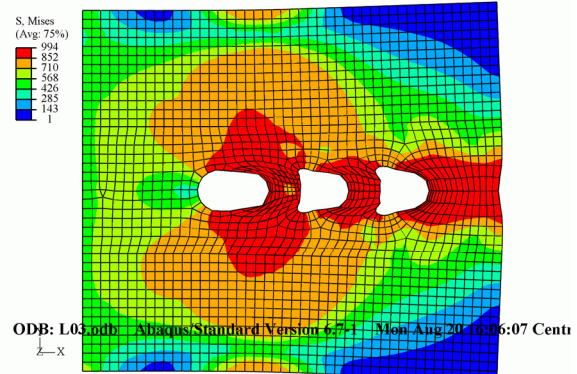
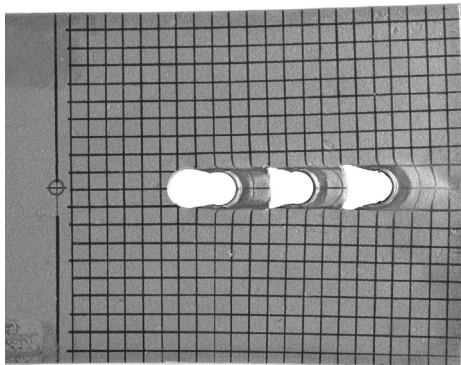
L01



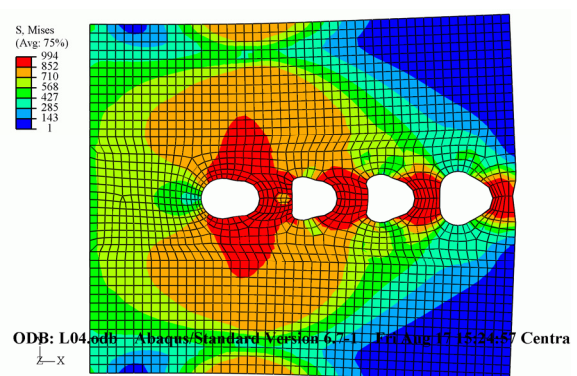
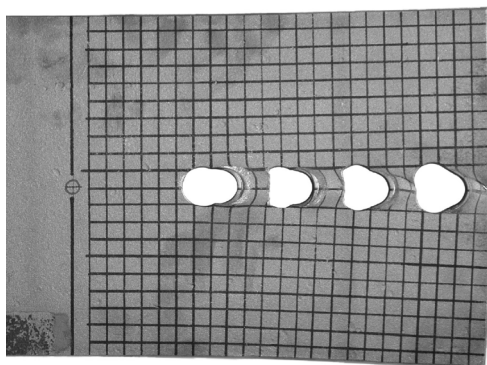
L02



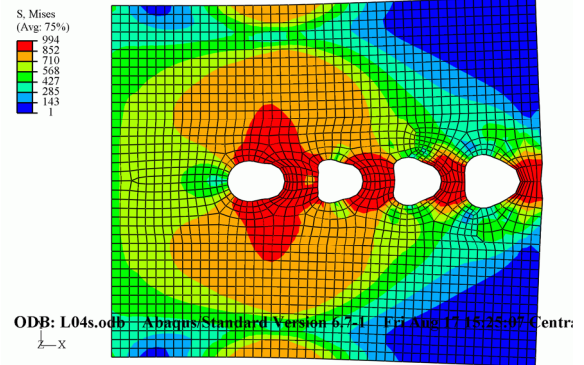
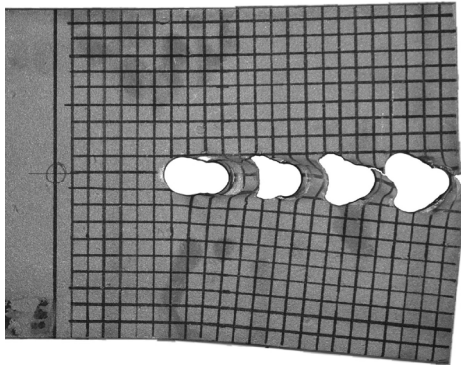
L03



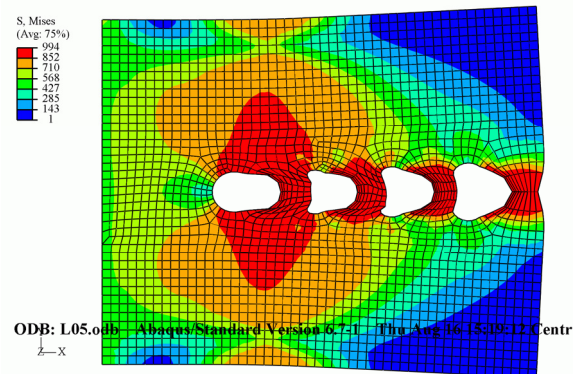
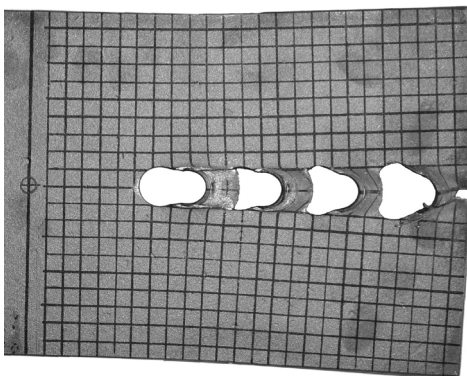
L04



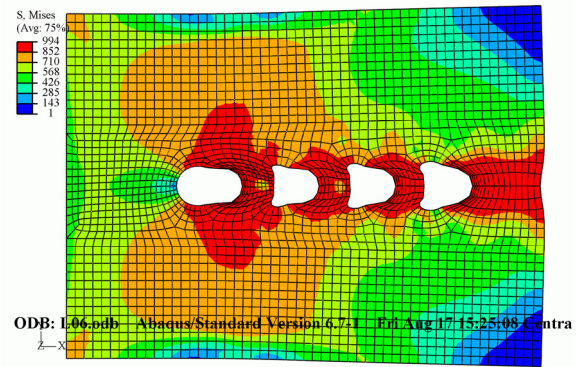
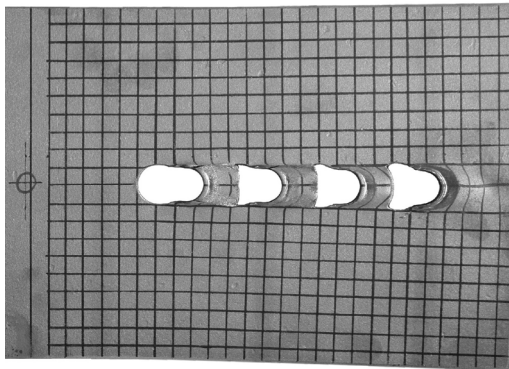
L04s



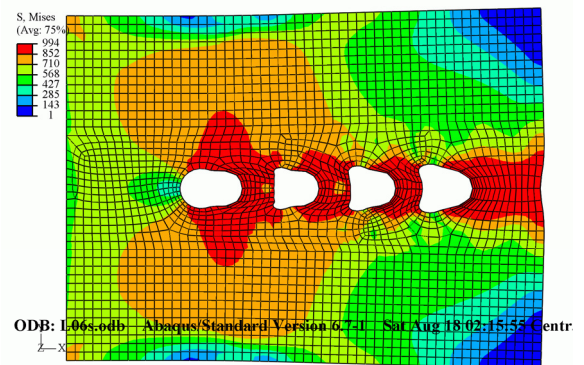
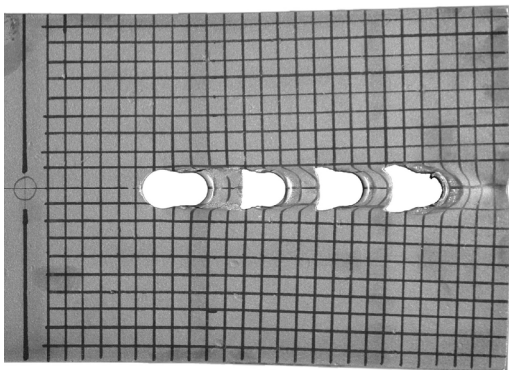
L05



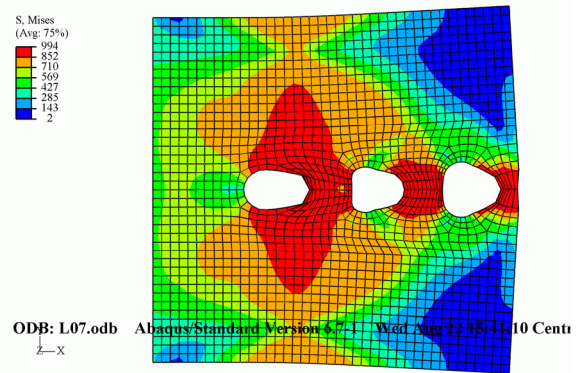
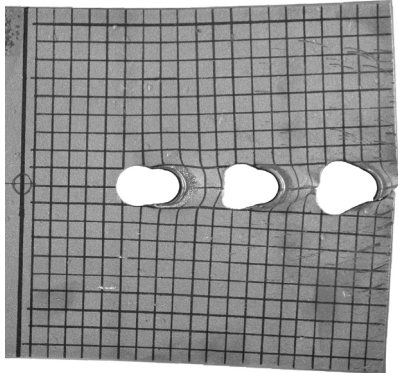
L06



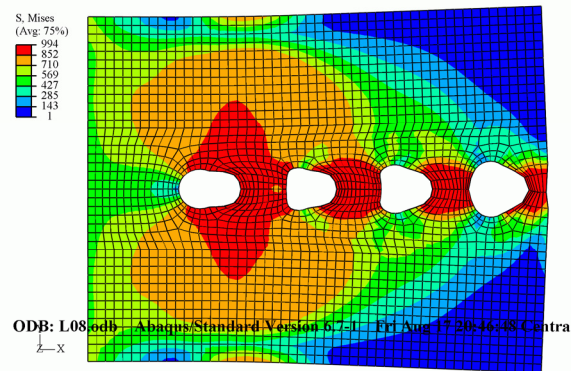
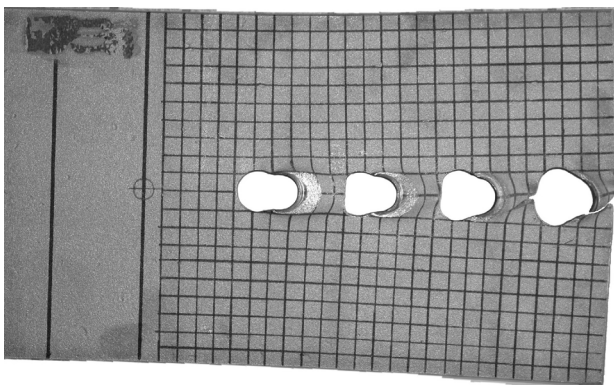
L06s



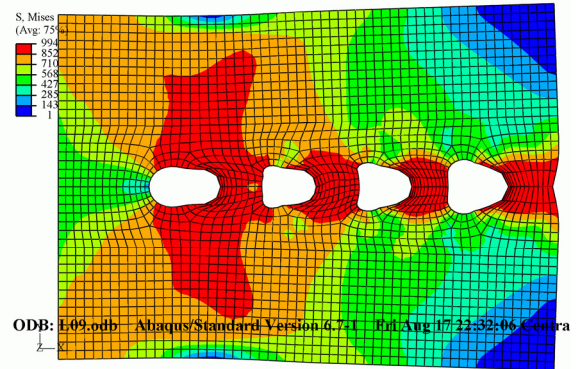
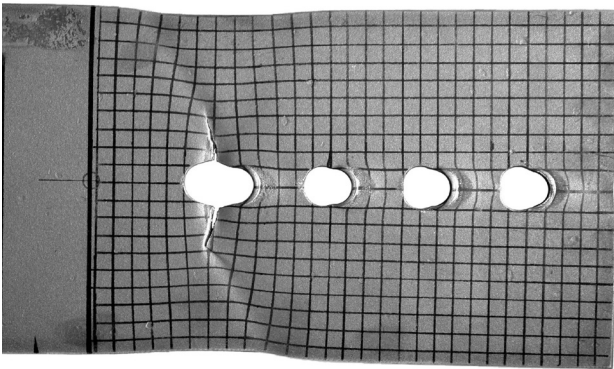
L07



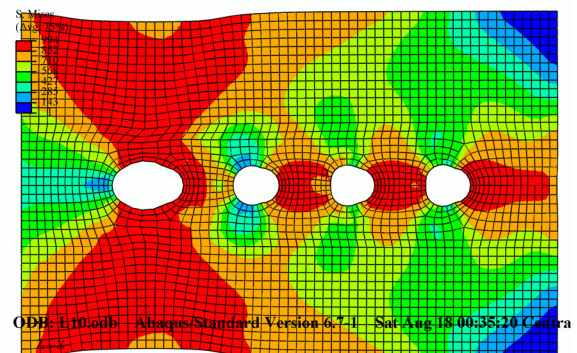
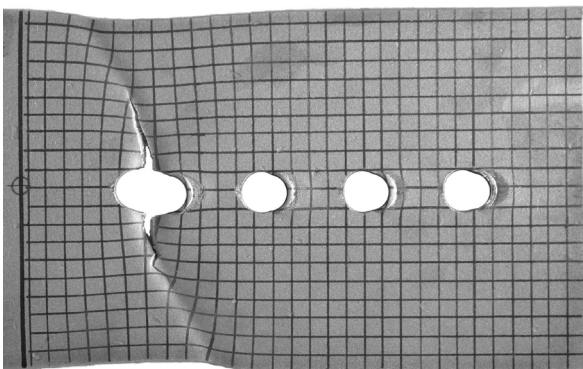
L08



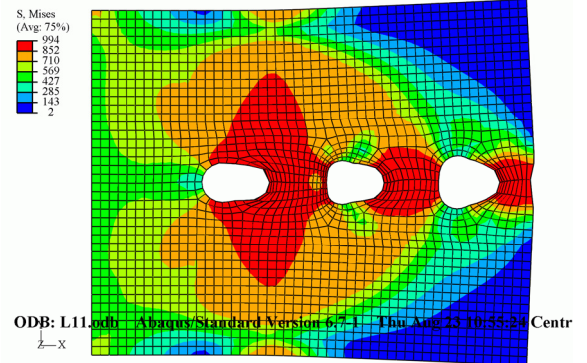
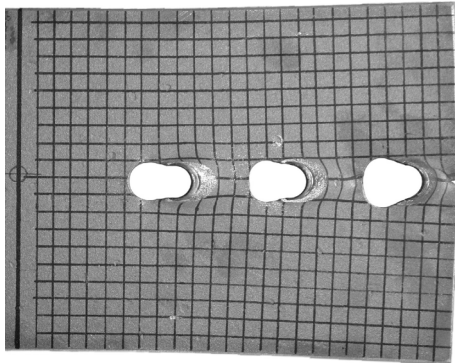
L09



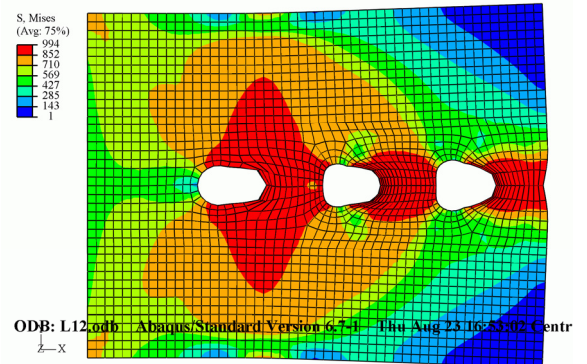
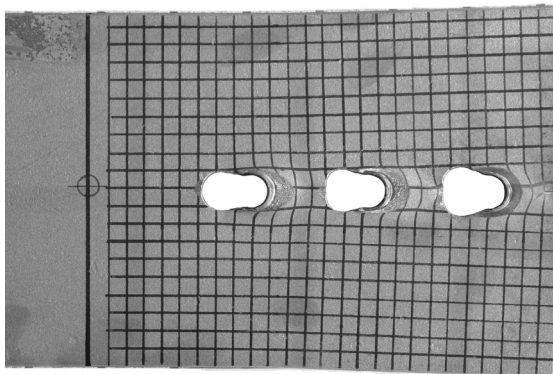
L10



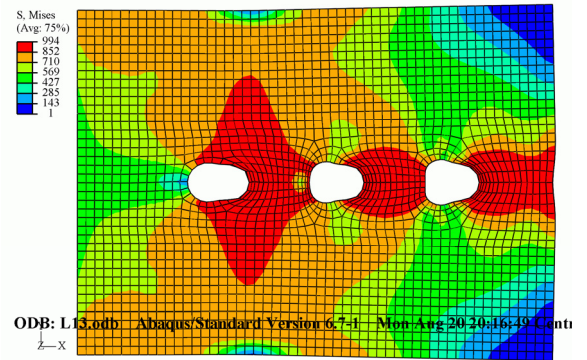
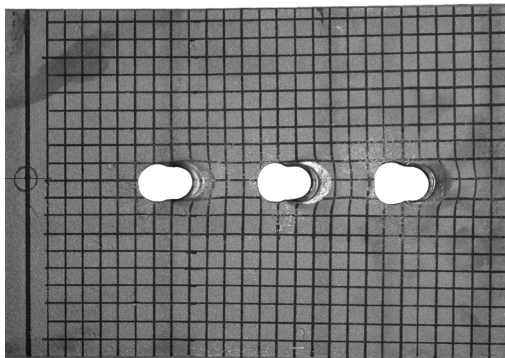
L11



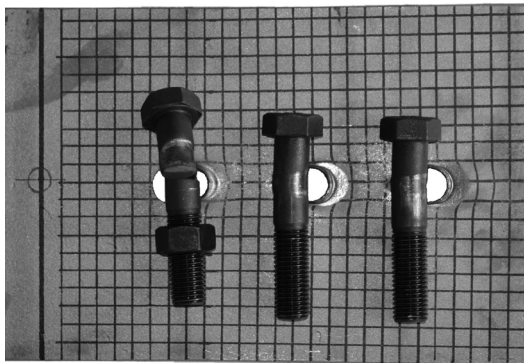
L12



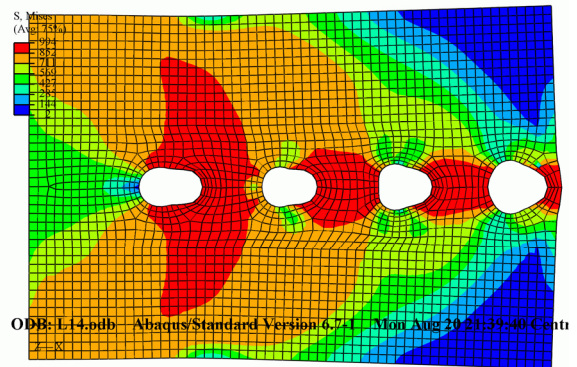
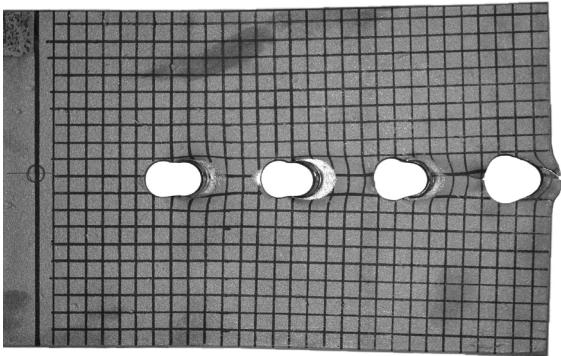
L13



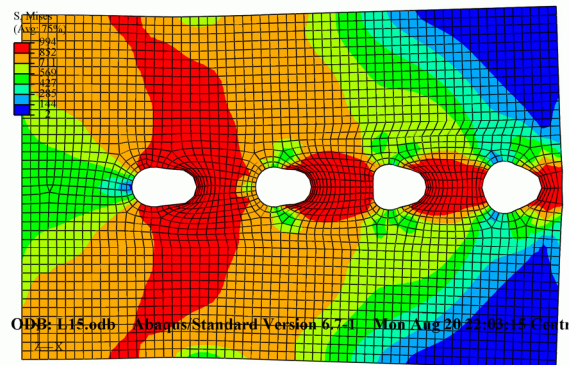
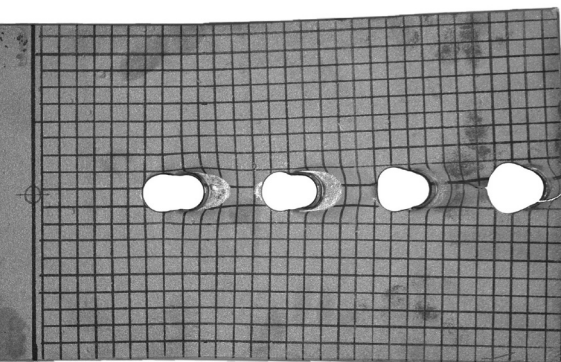
L13



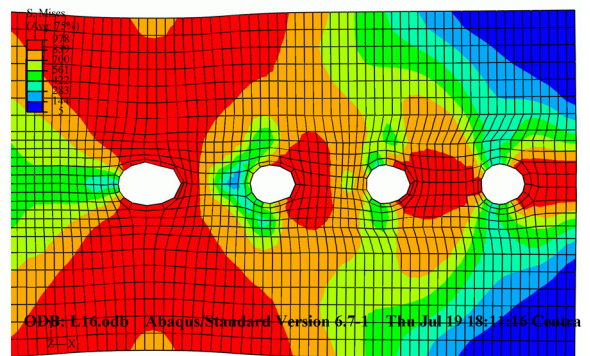
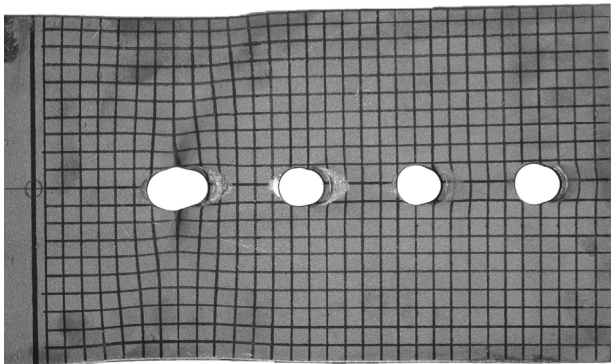
L14



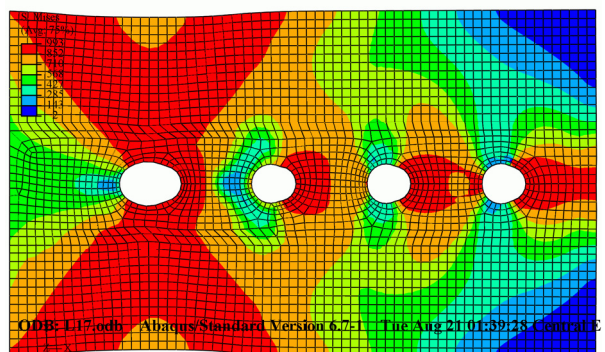
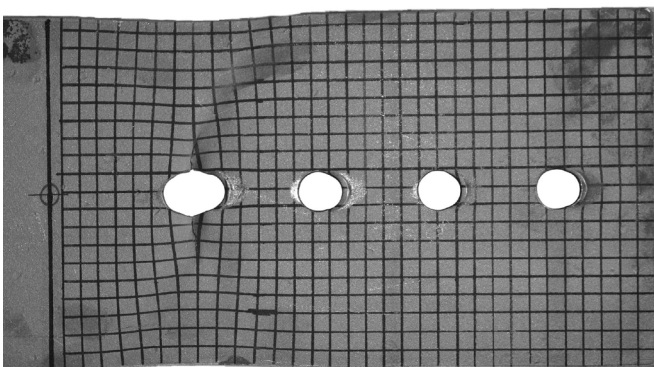
L15



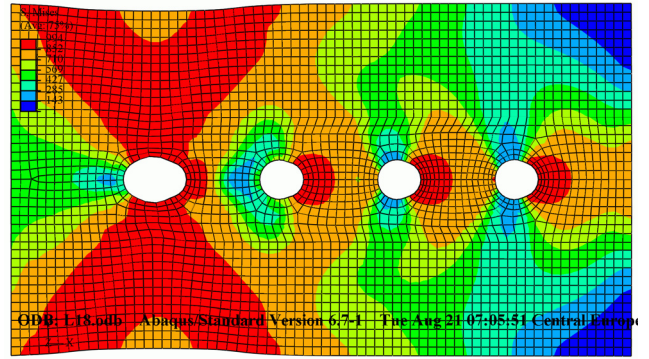
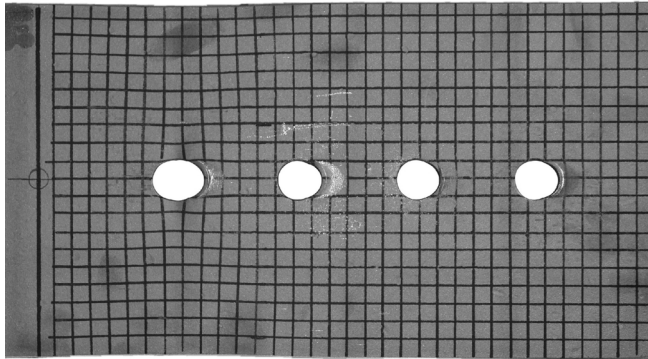
L16



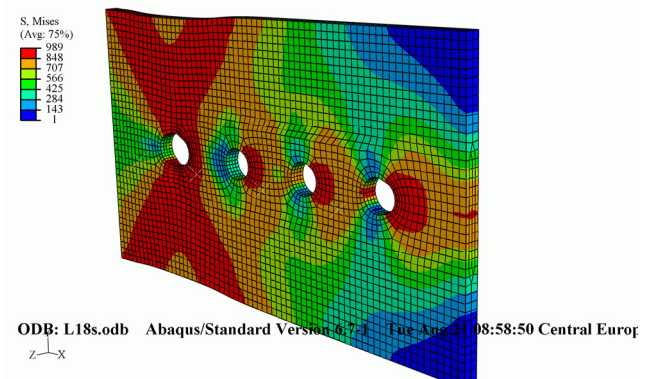
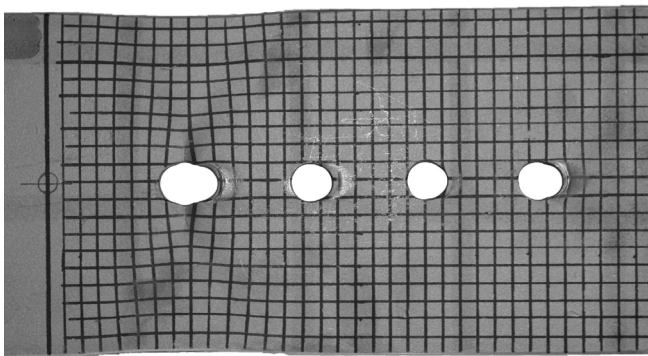
L17



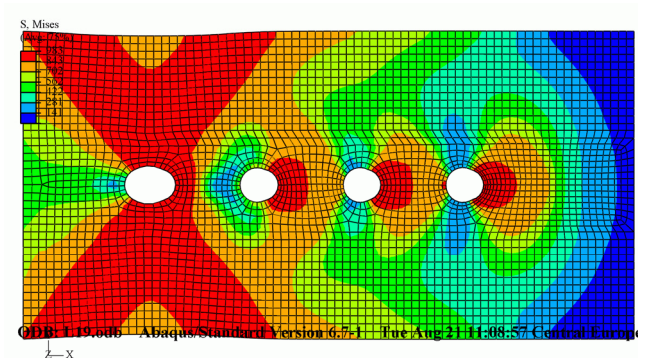
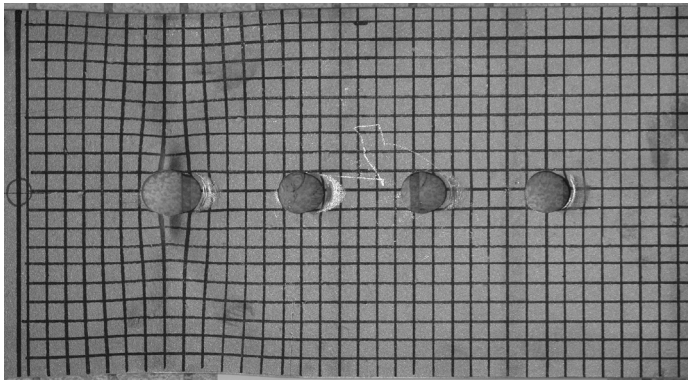
L18



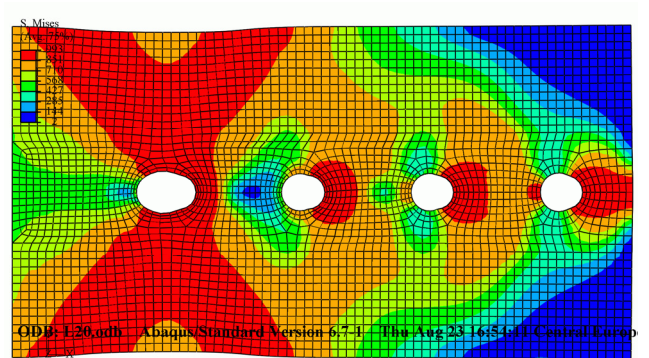
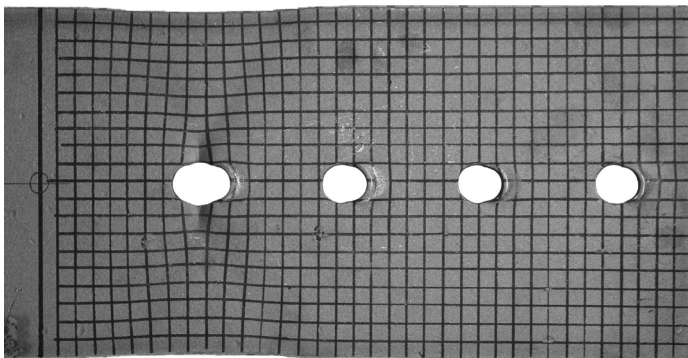
L18s



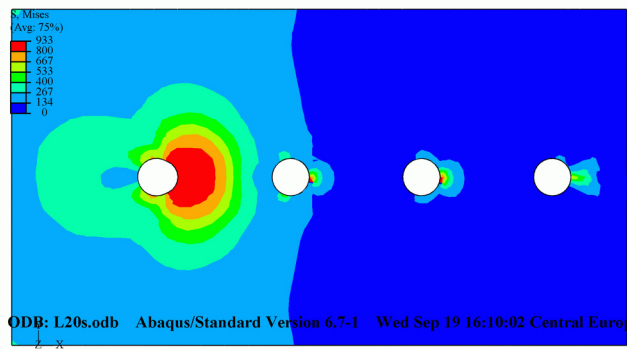
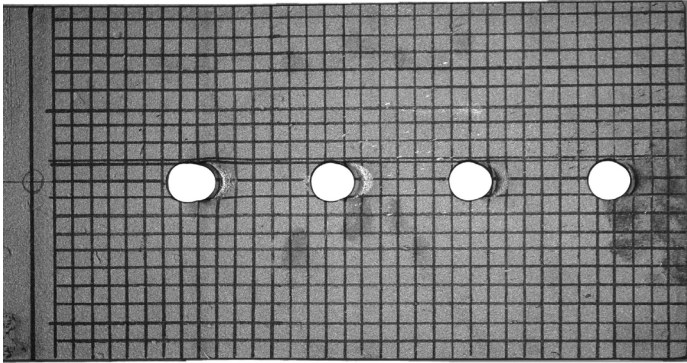
L19



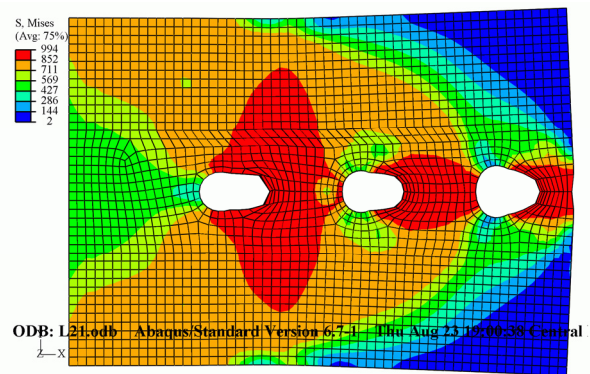
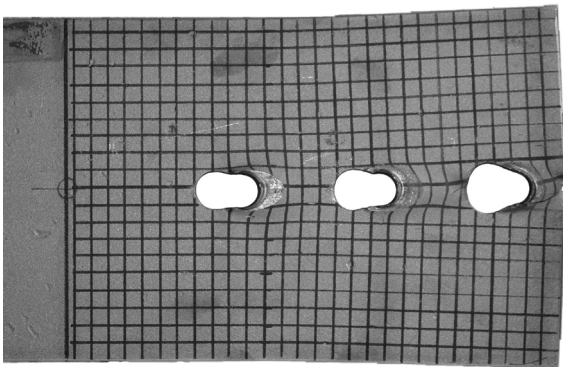
L20



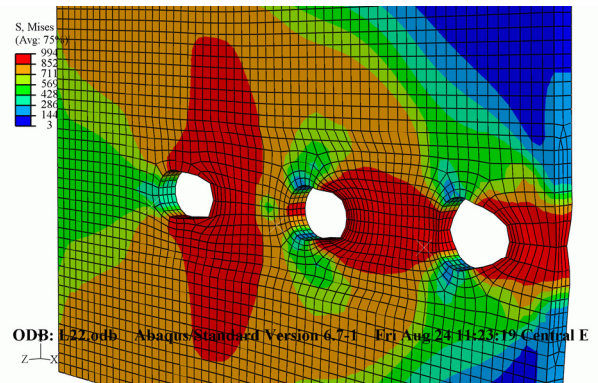
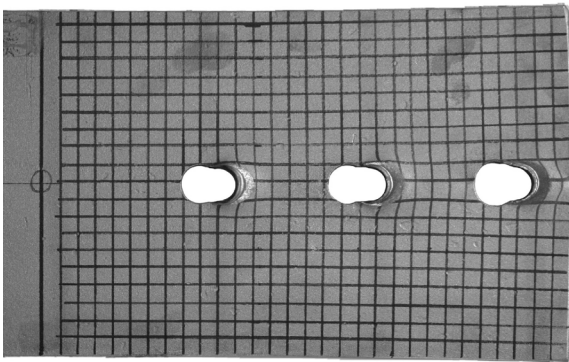
L20s



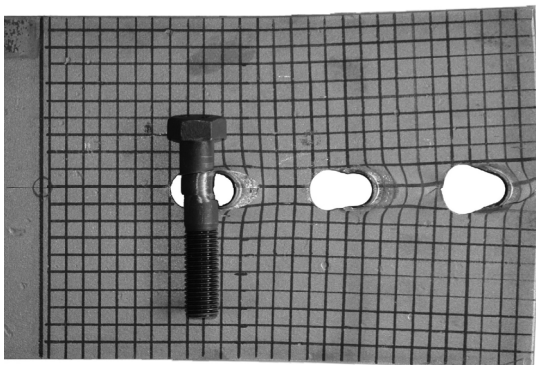
L21



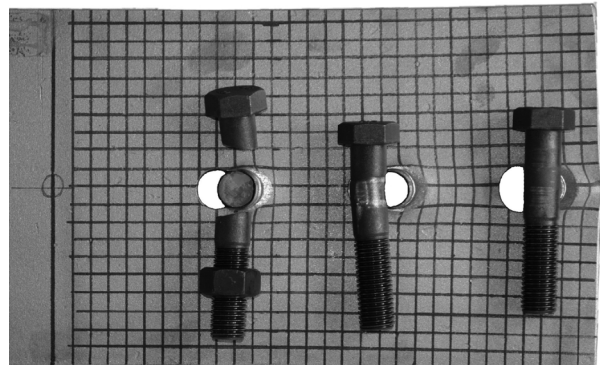
L22



L21



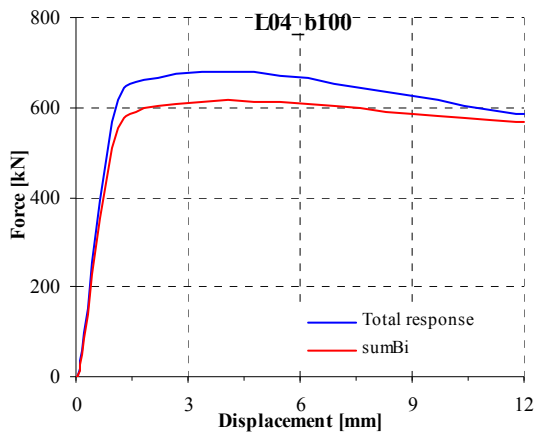
L22



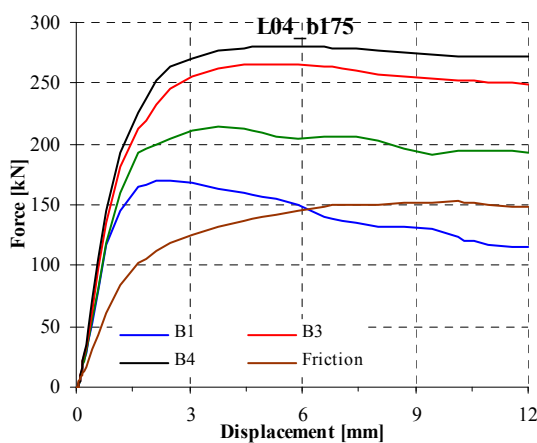
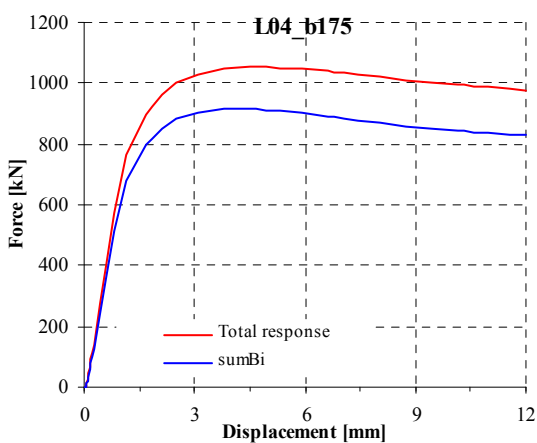
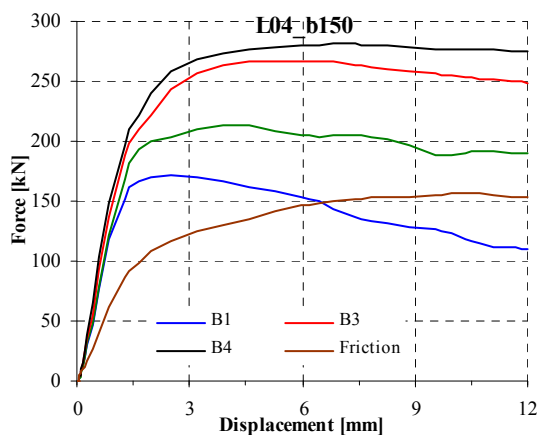
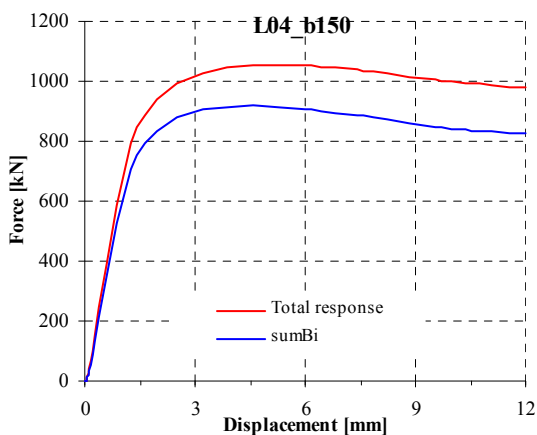
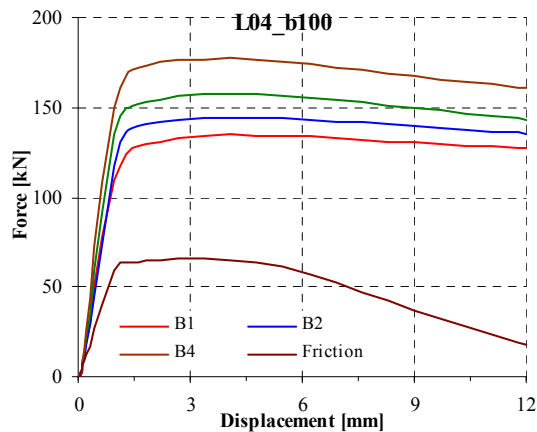
Appendix D RESULTS OF PARAMETRIC STUDY

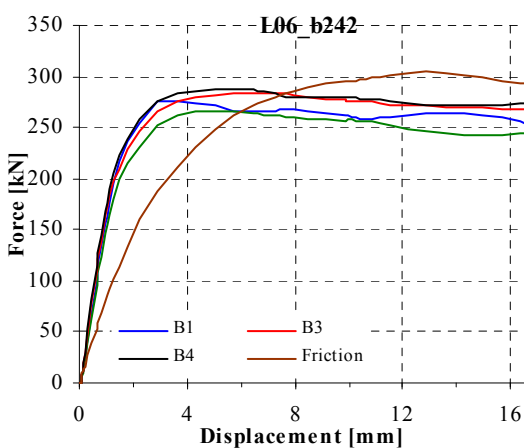
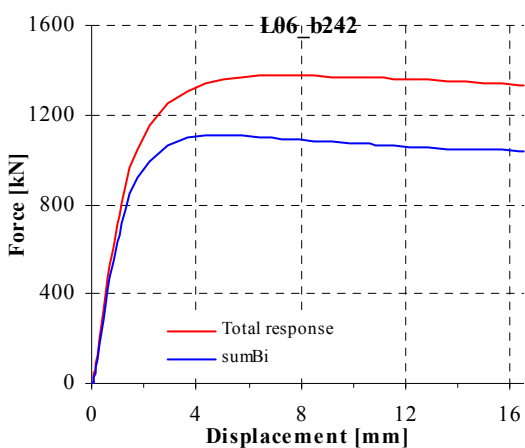
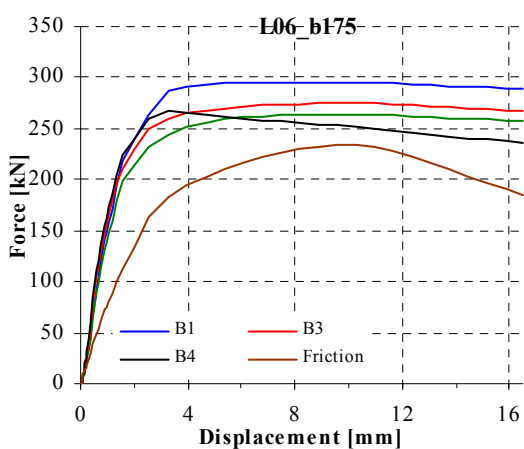
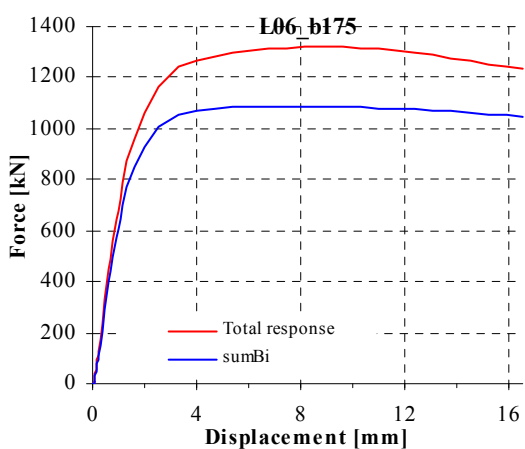
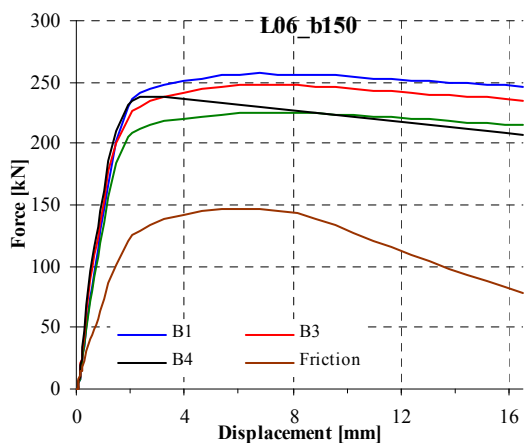
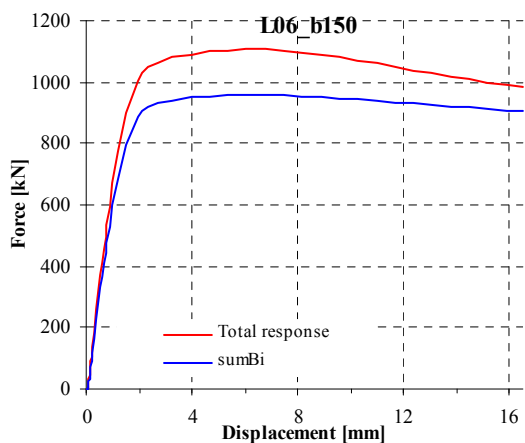
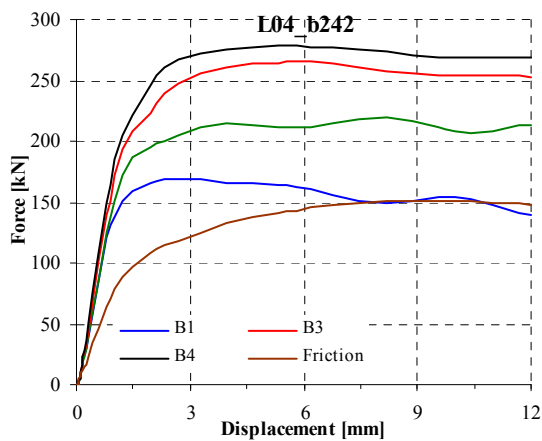
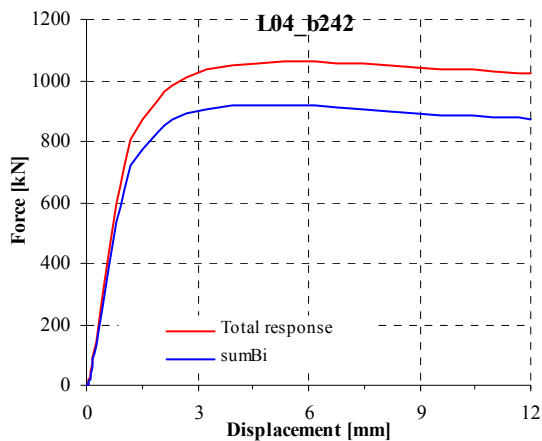
Lxx_bxxx; Numerical model type M2; 19 FE analyses

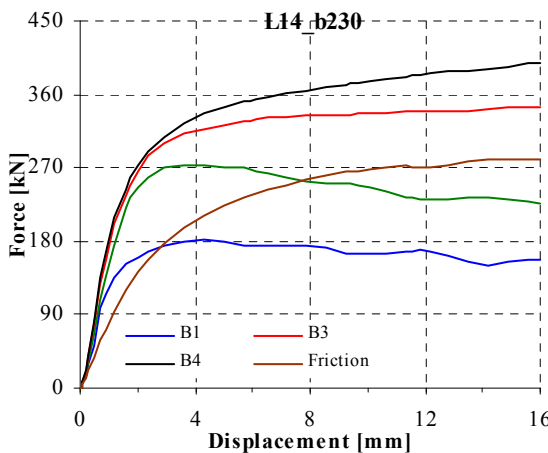
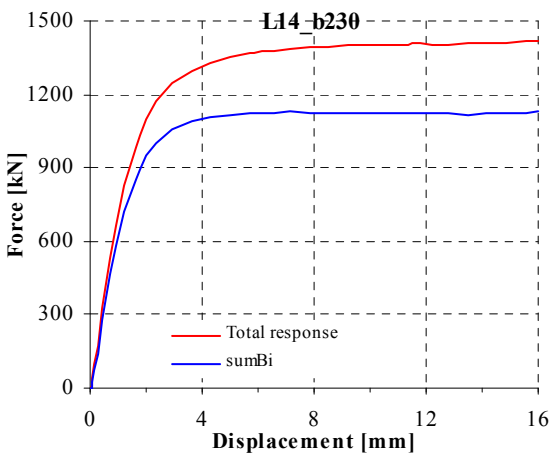
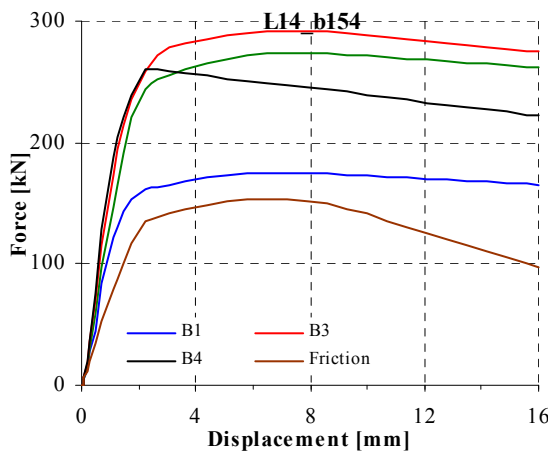
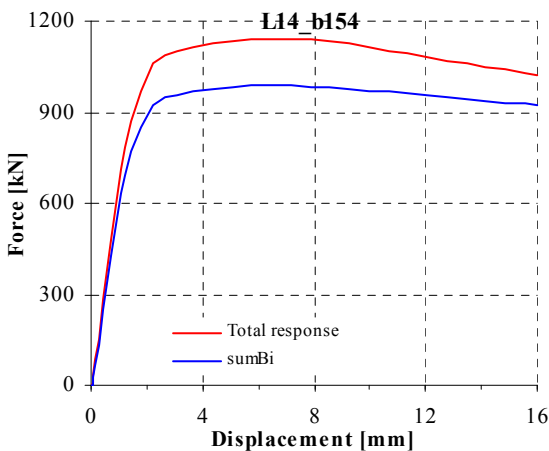
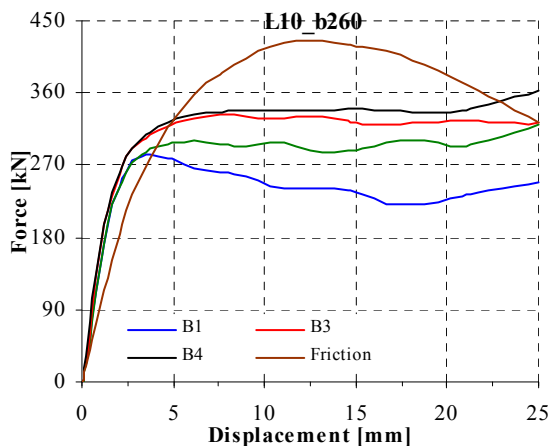
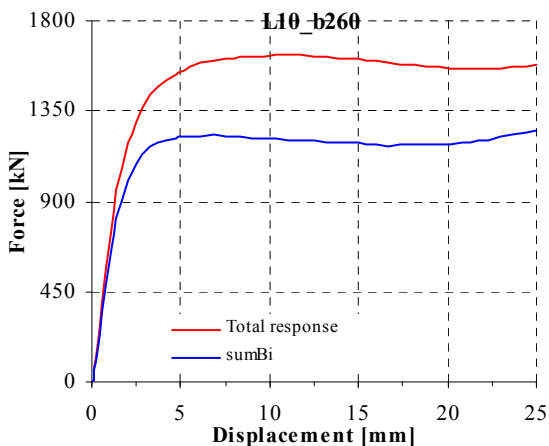
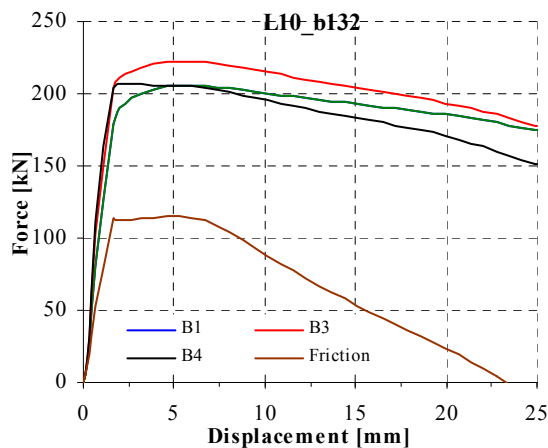
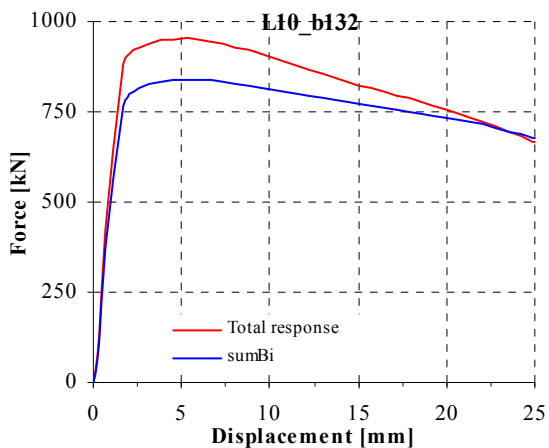
Experimental and numerical load-displacement curves

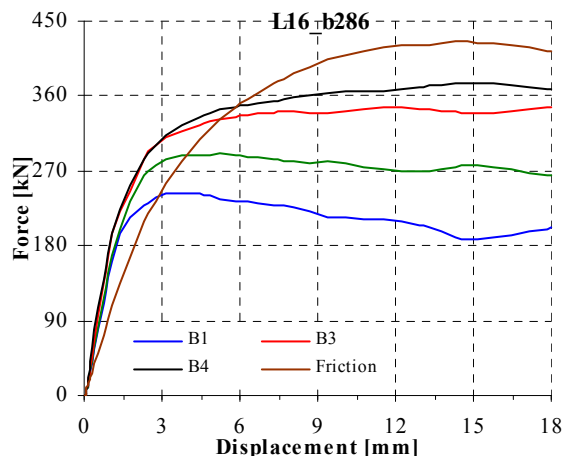
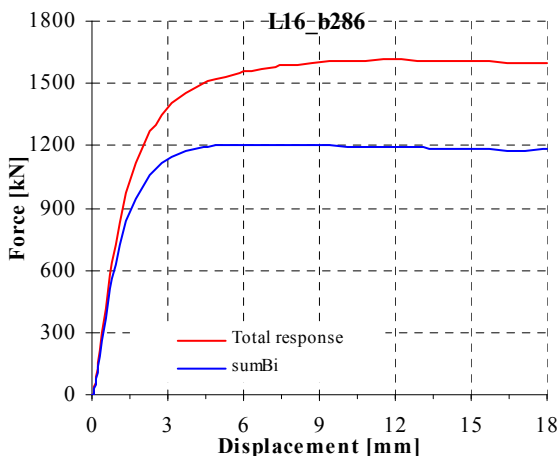
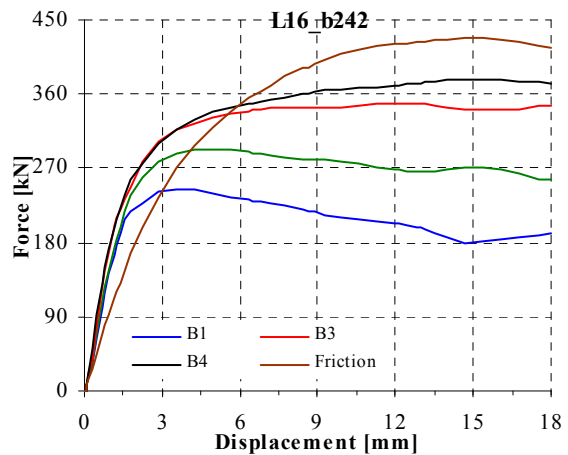
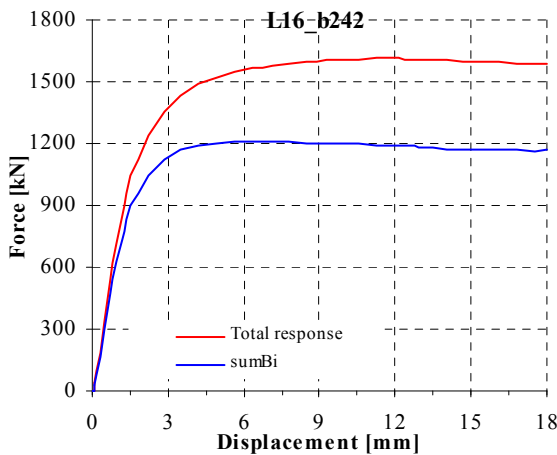
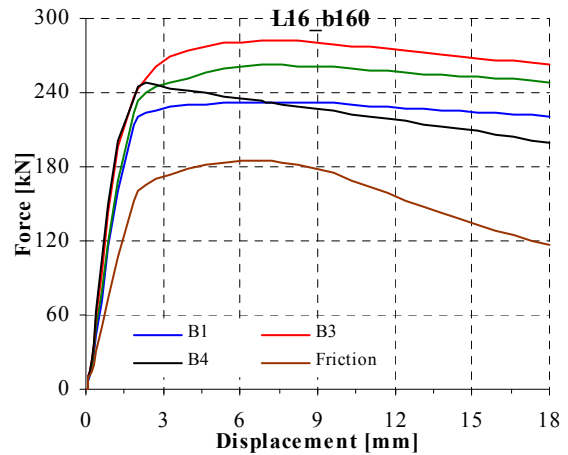
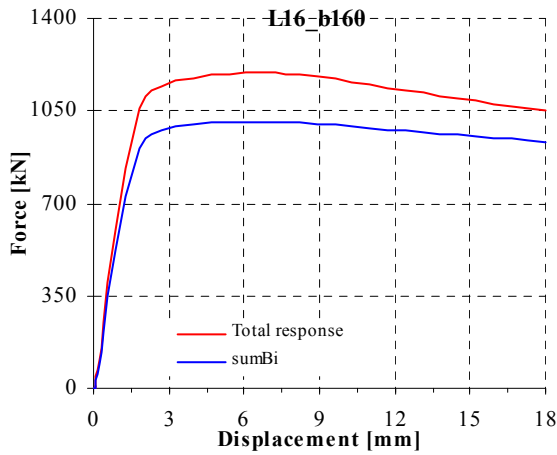
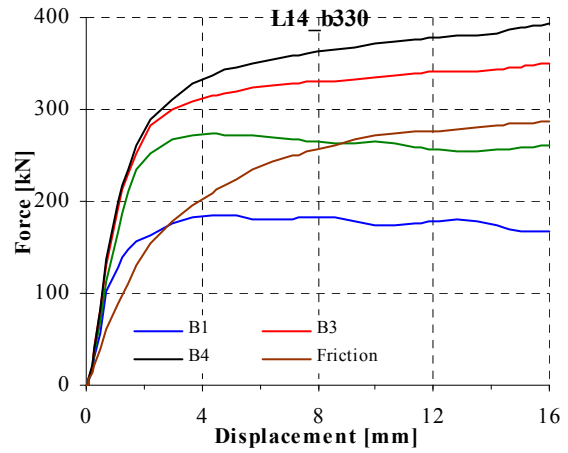
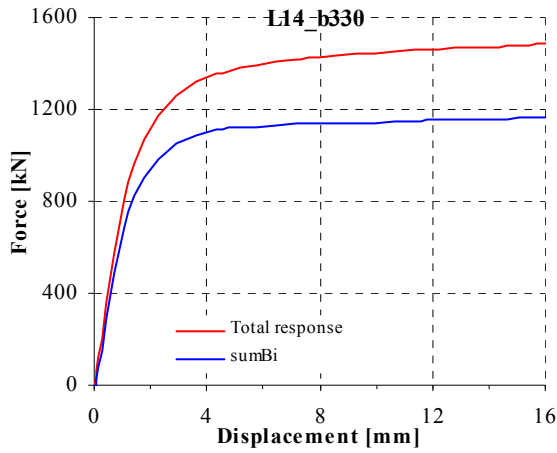


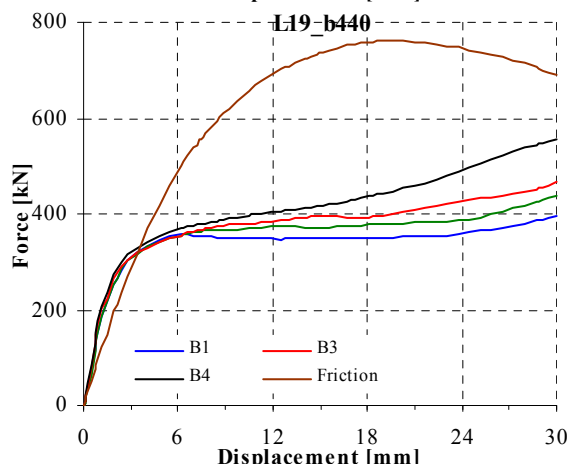
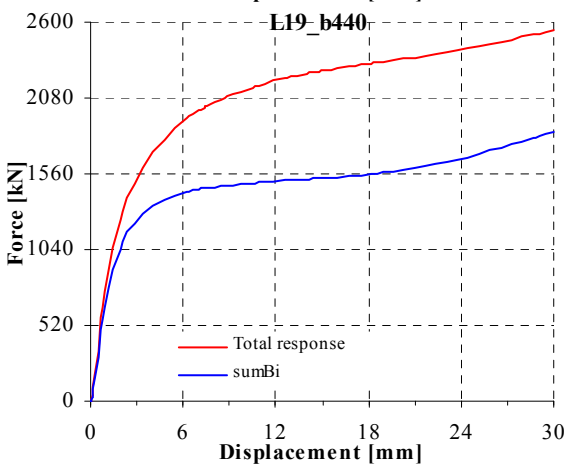
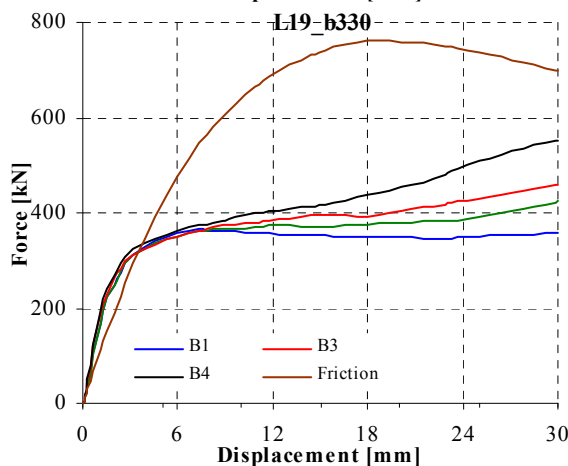
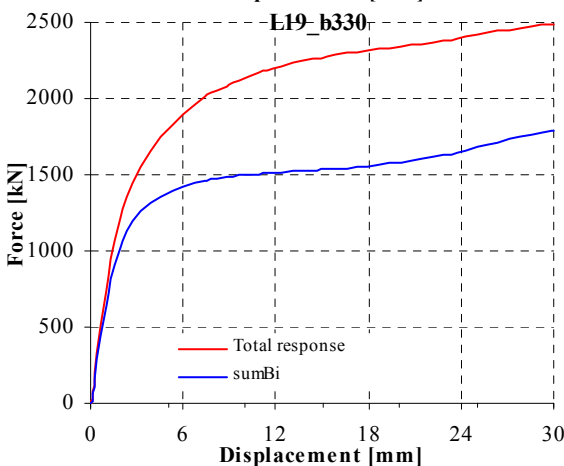
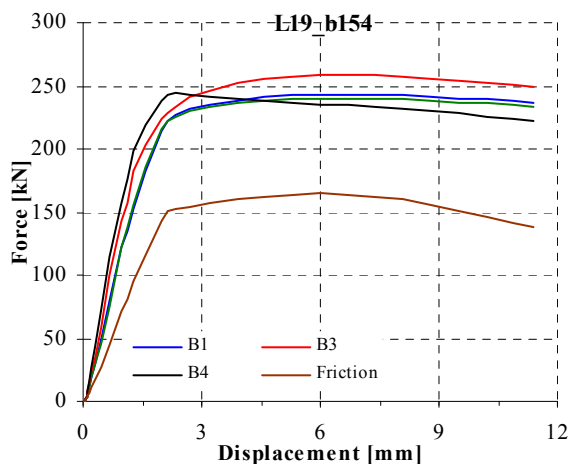
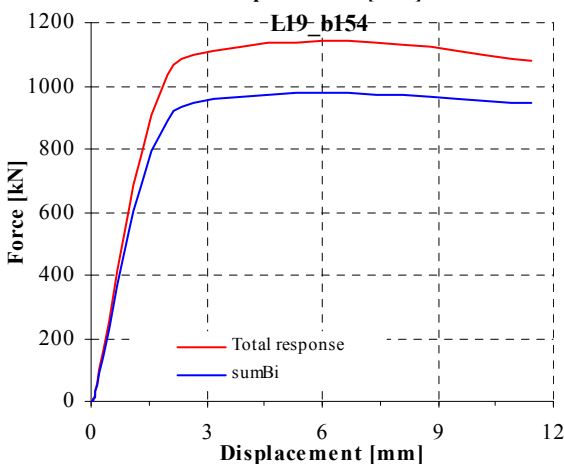
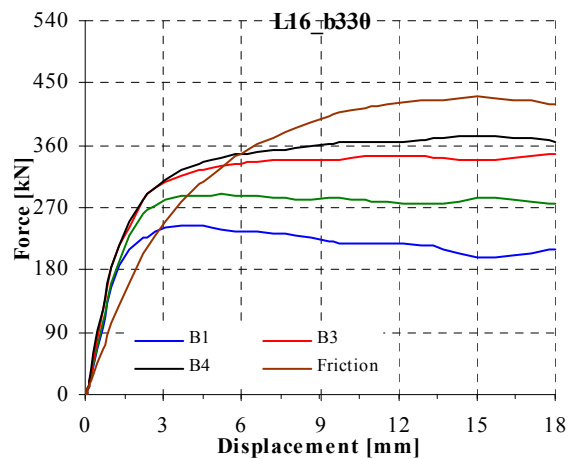
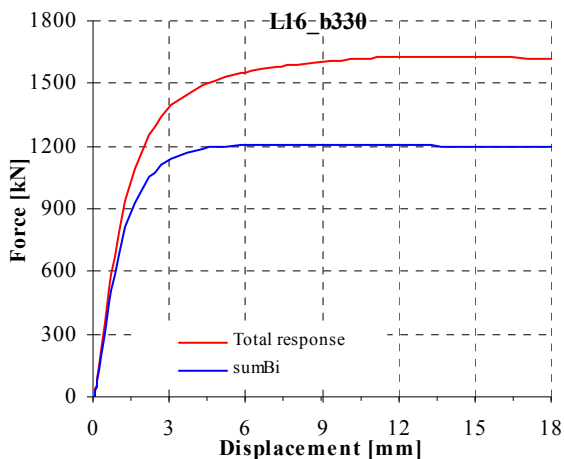
Distribution of forces between bolts and the friction force



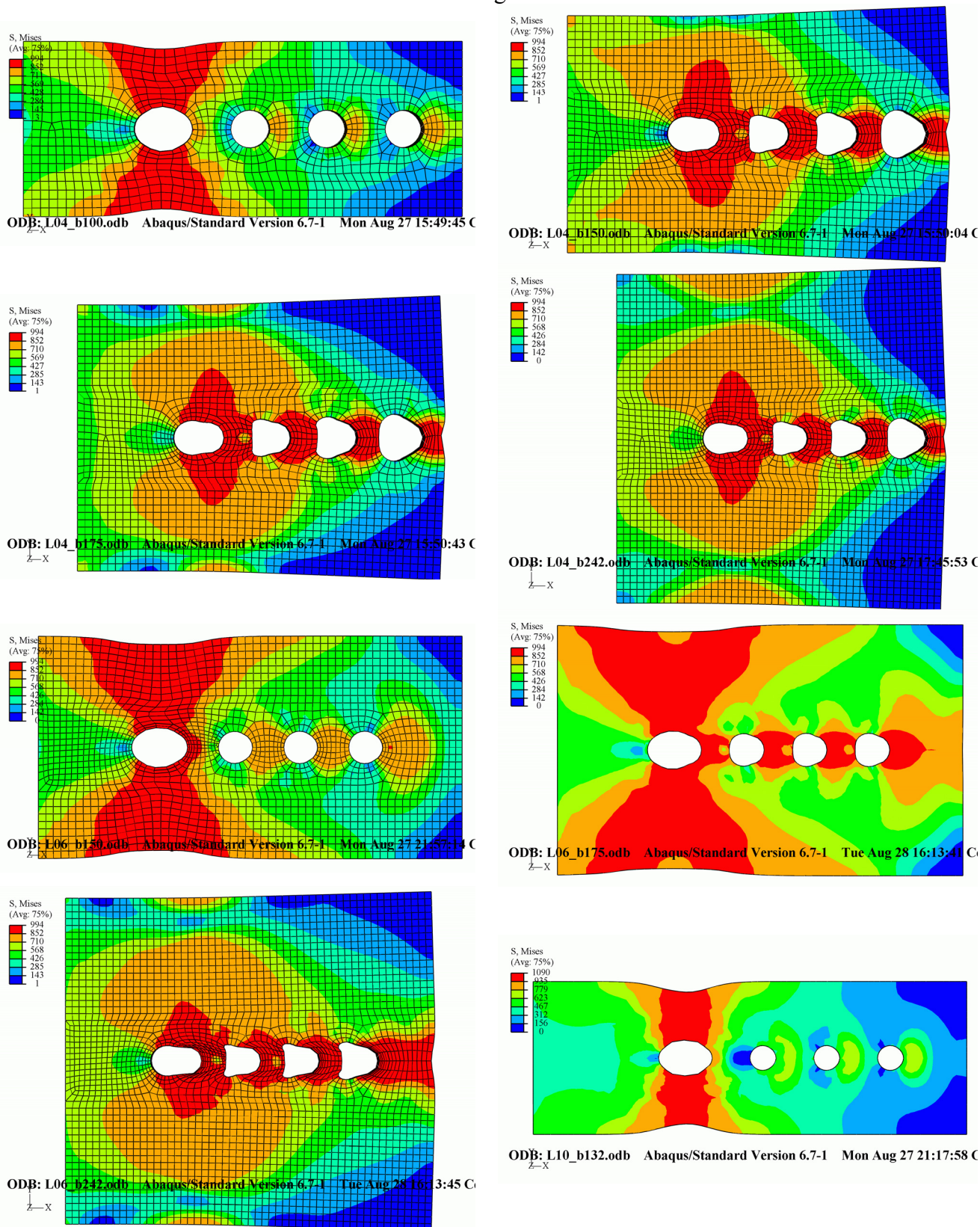


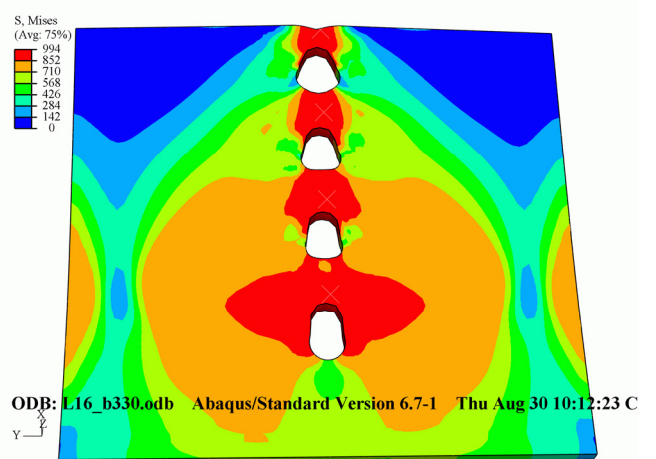
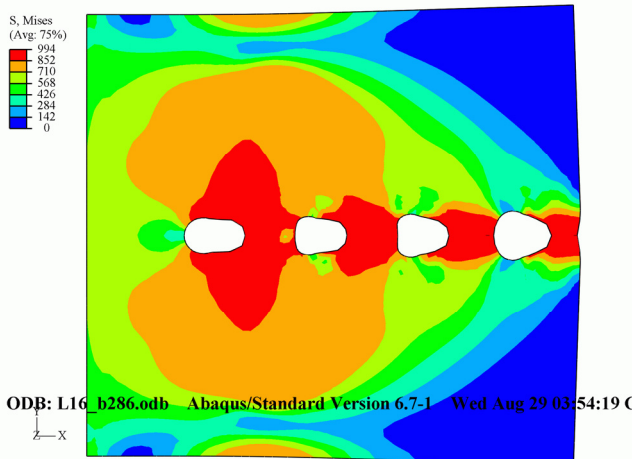
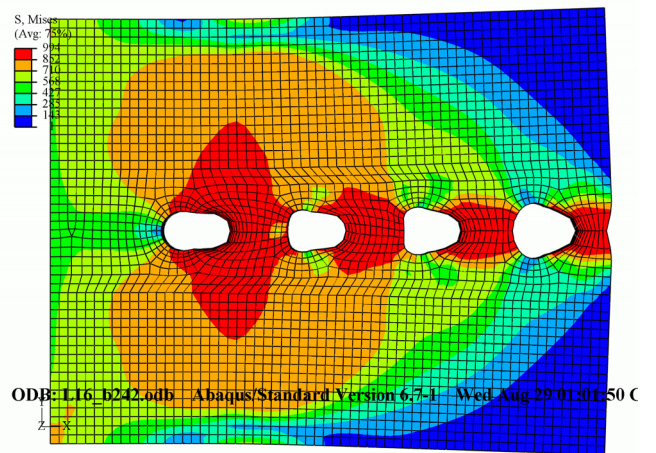
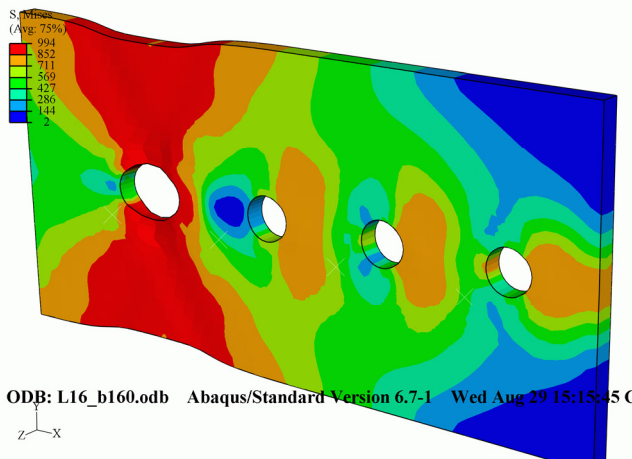
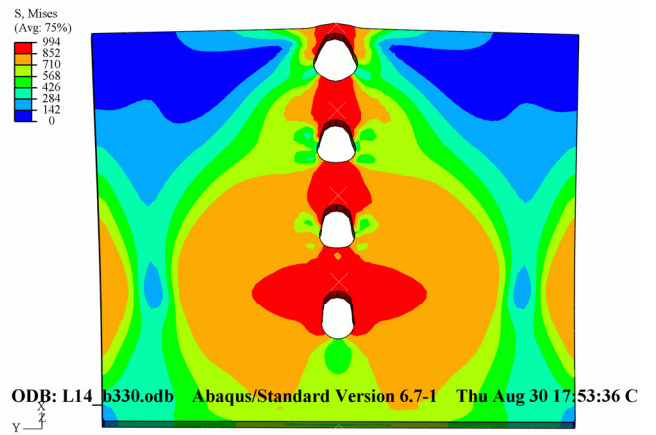
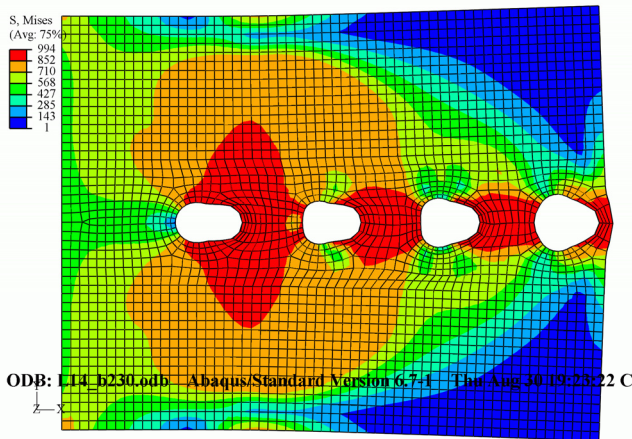
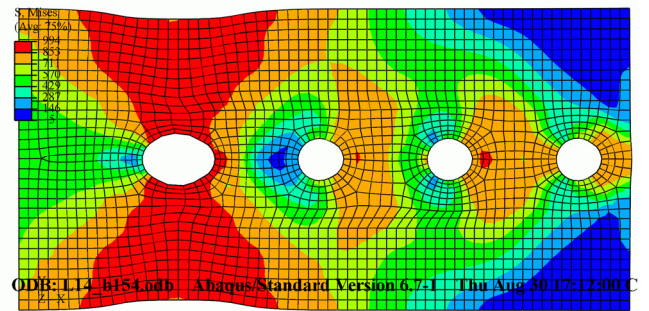
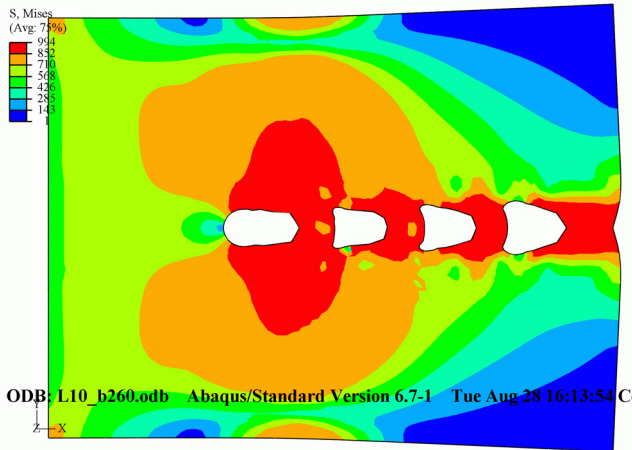


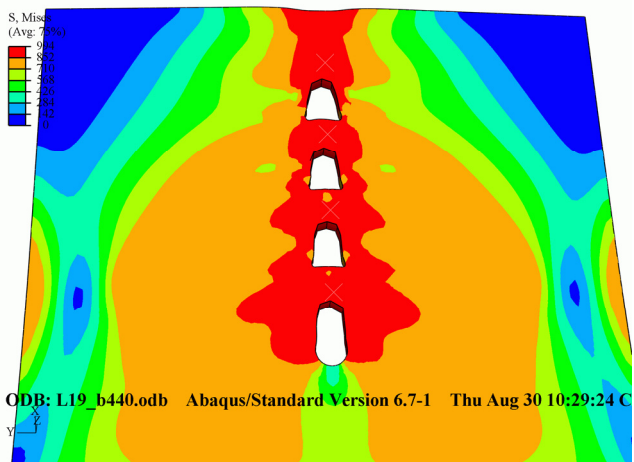
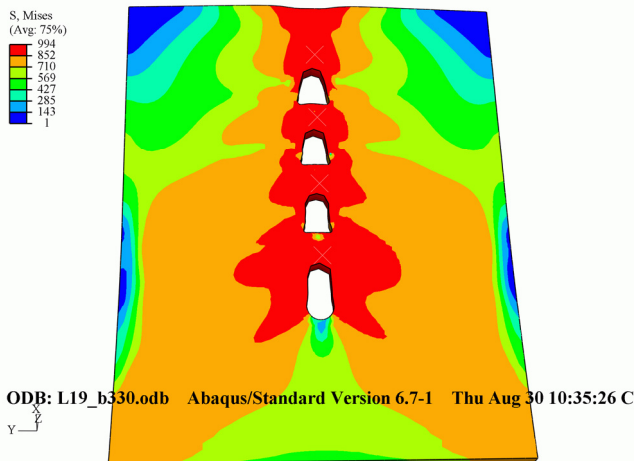
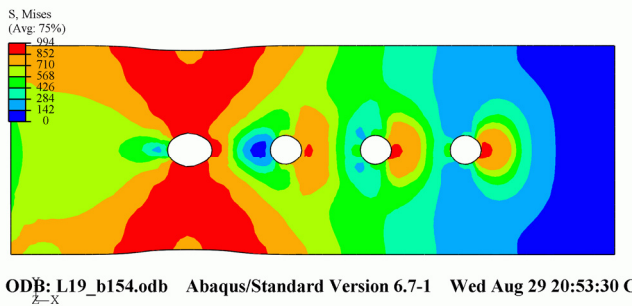




Mises stress on a deformed connection. The connection name is displayed on the bottom left side of the figure

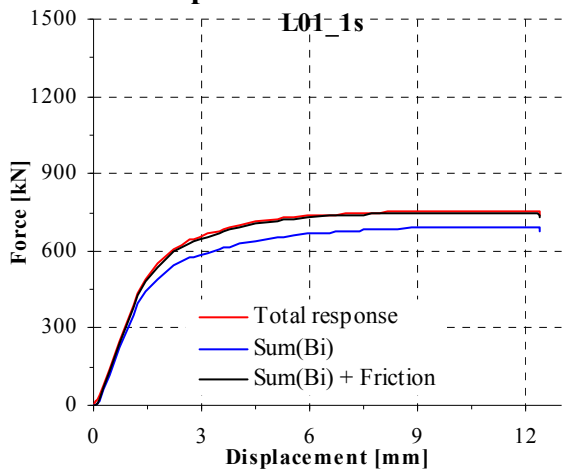




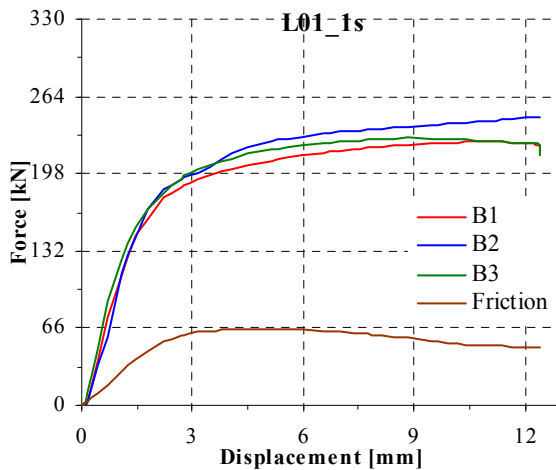


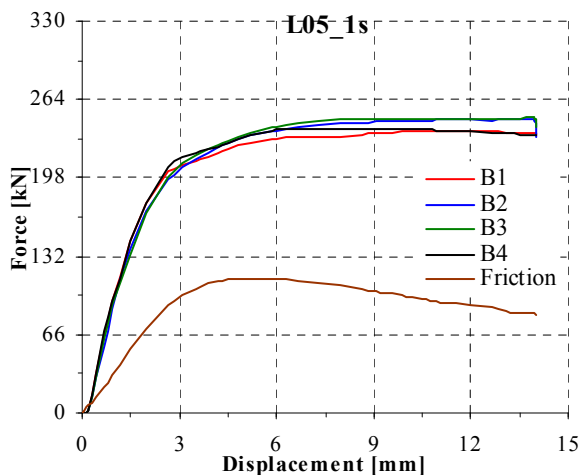
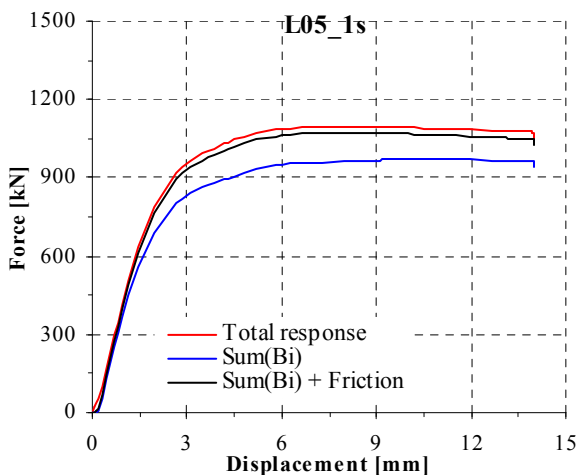
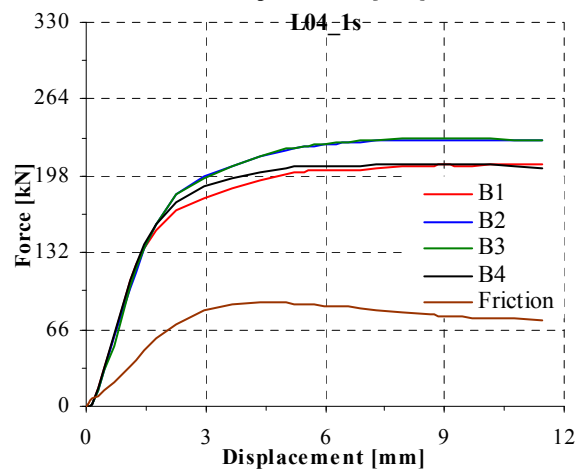
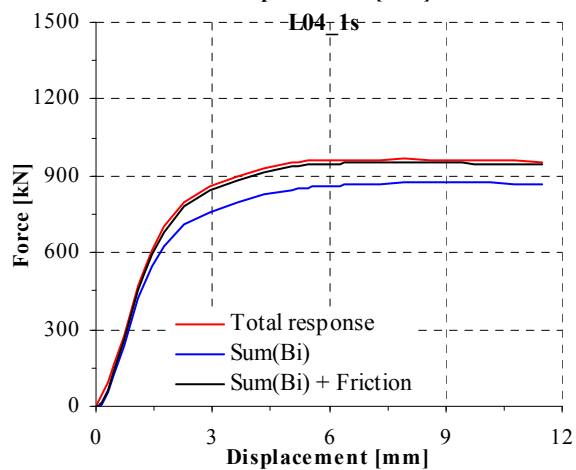
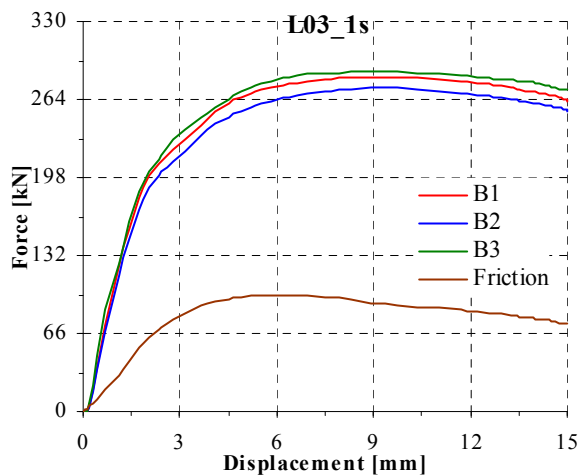
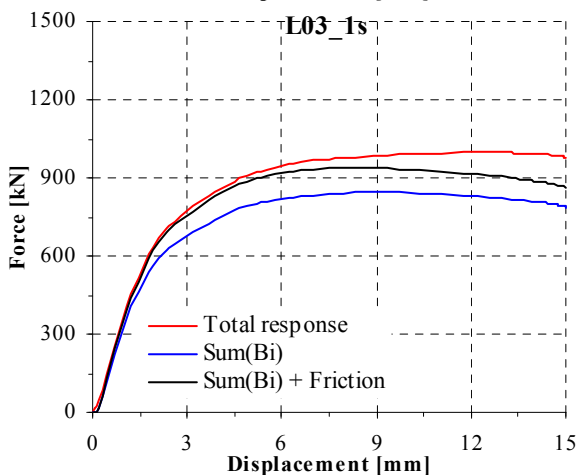
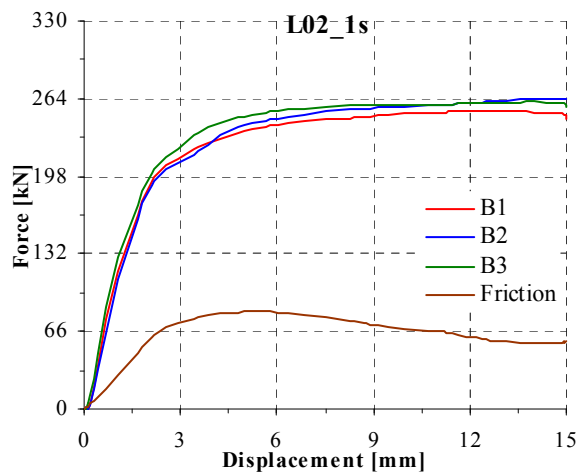
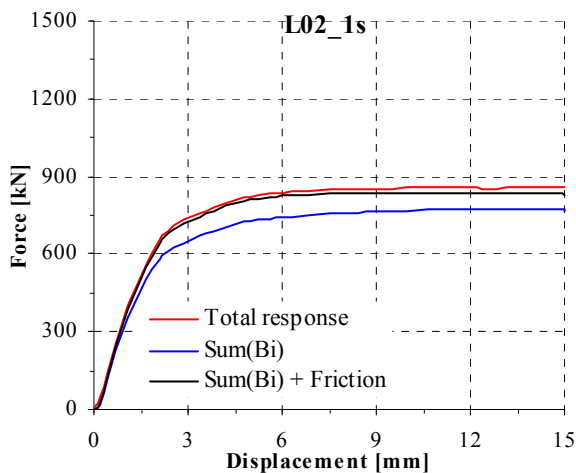
Lxx_1s; Numerical model type M3; 22 FE analyses

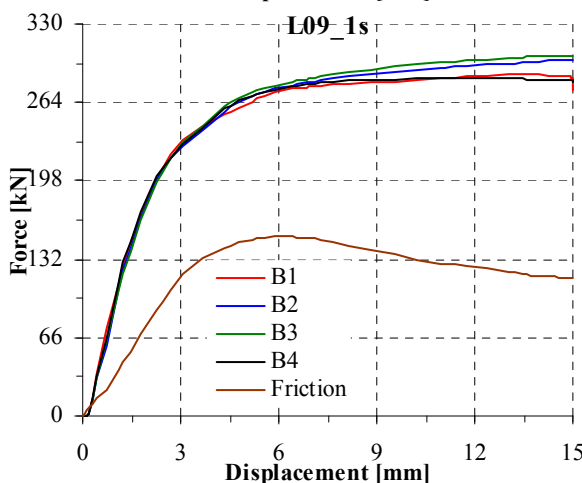
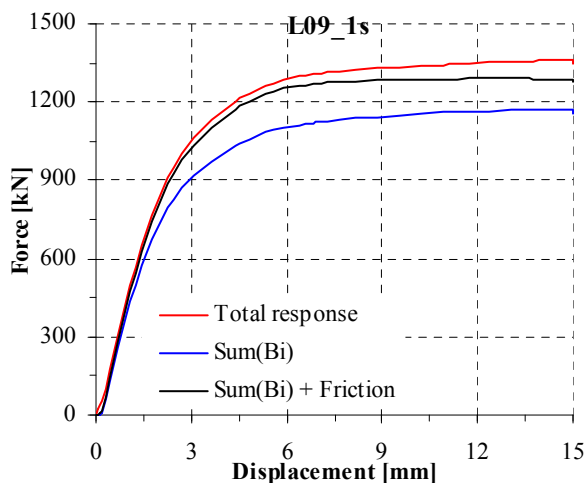
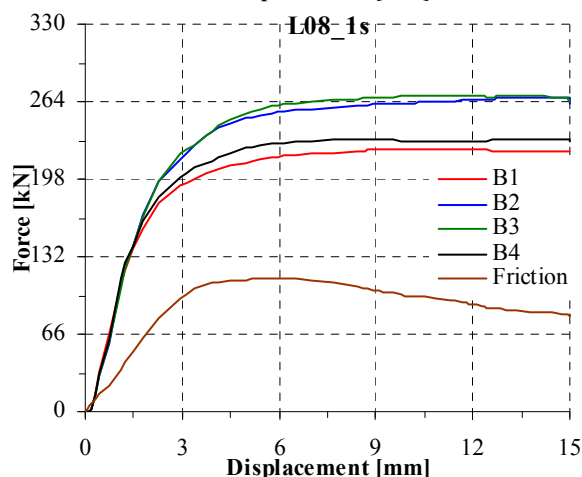
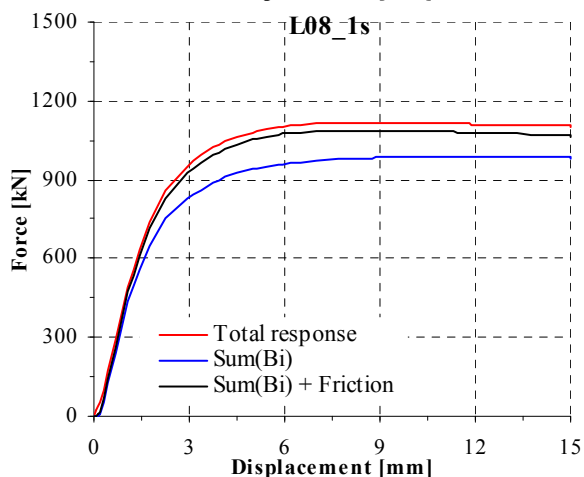
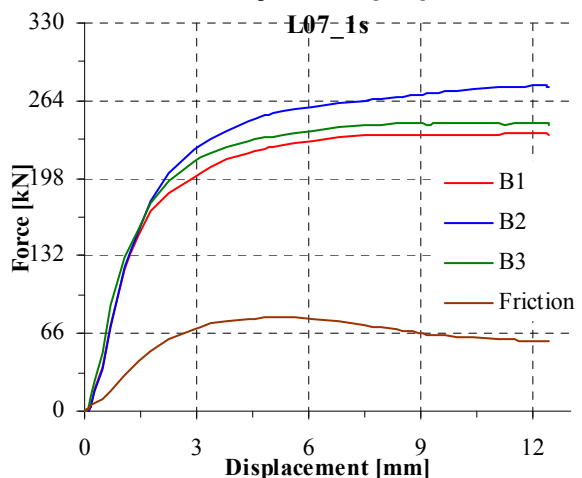
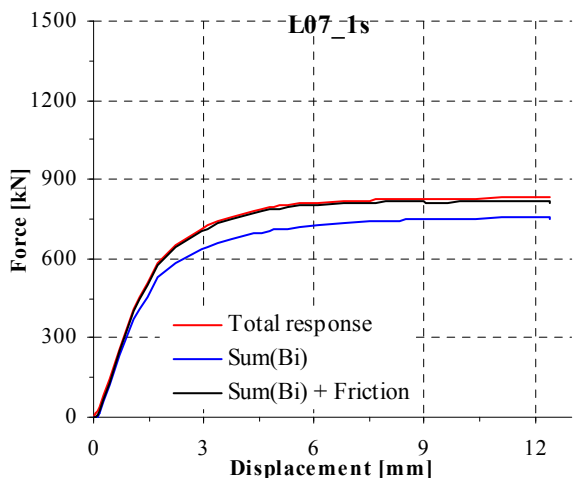
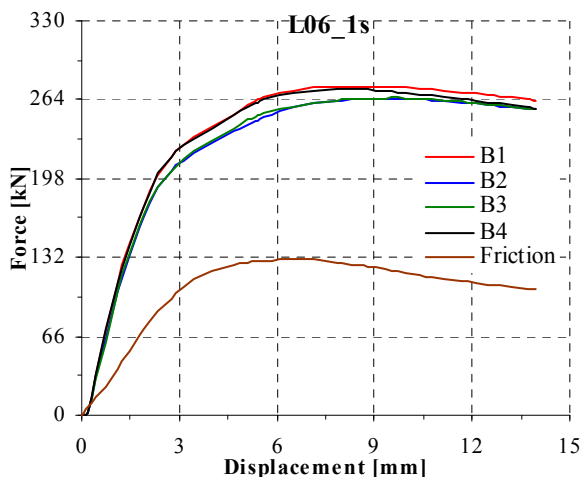
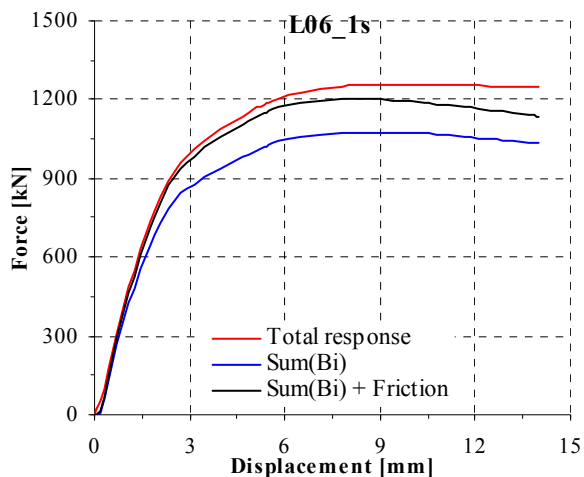
Experimental and numerical load-displacement curves

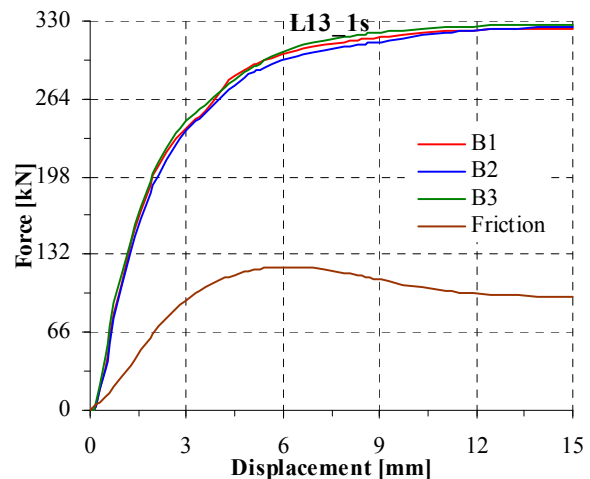
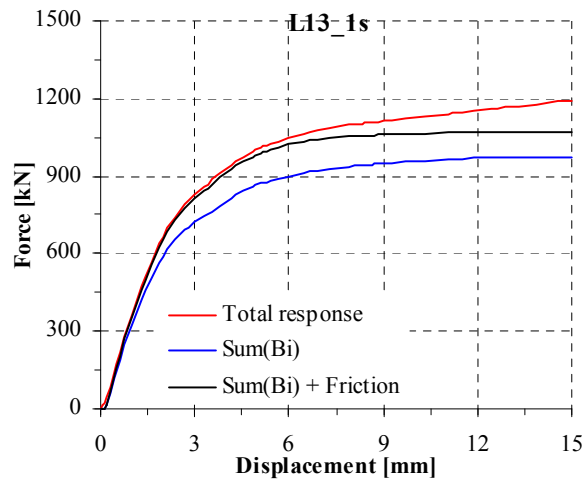
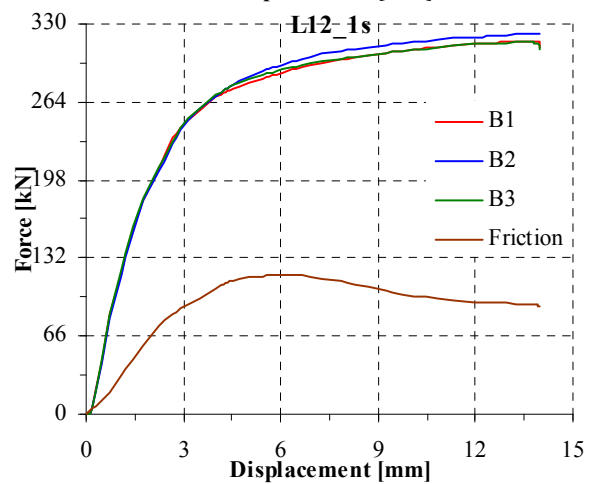
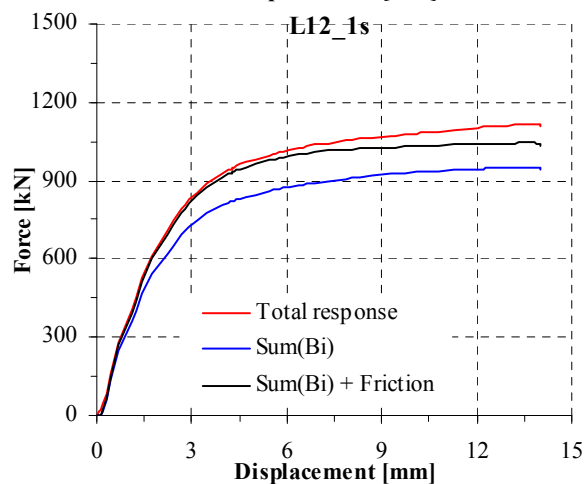
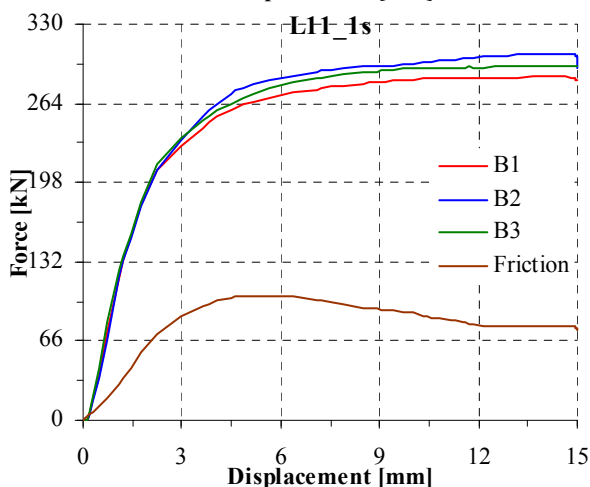
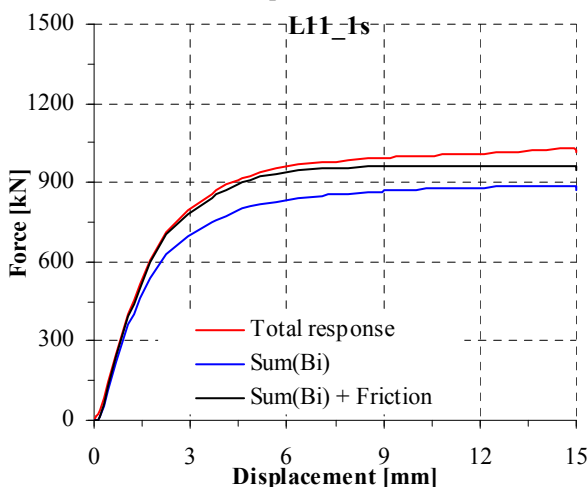
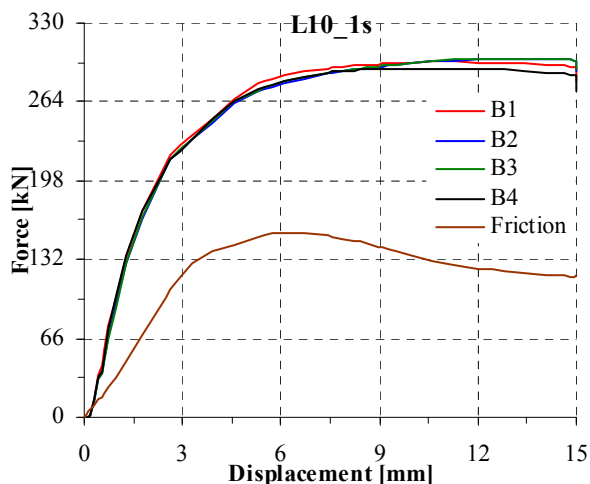
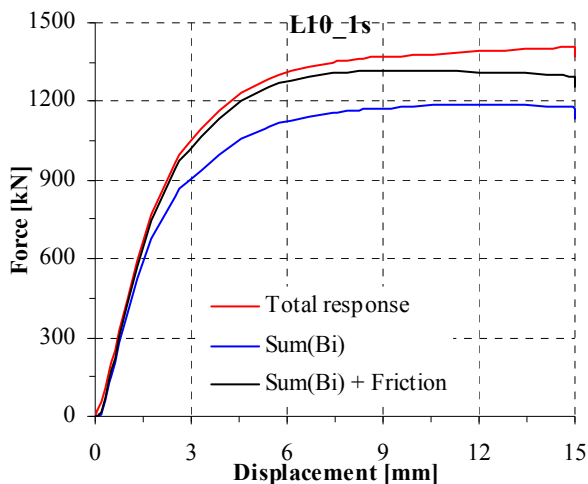


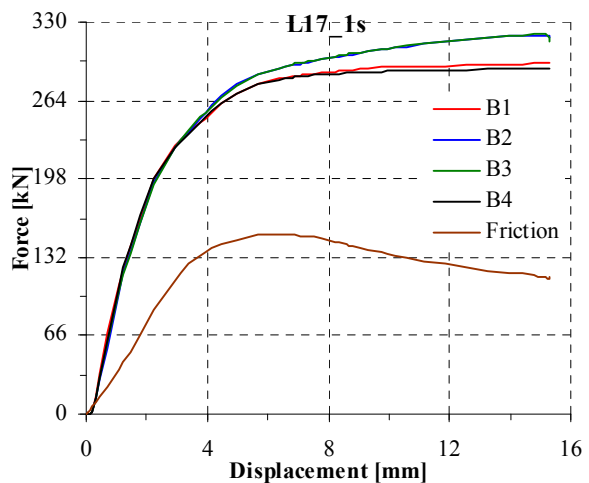
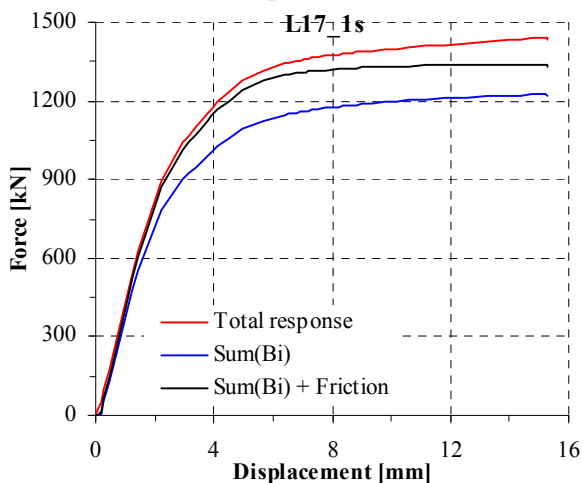
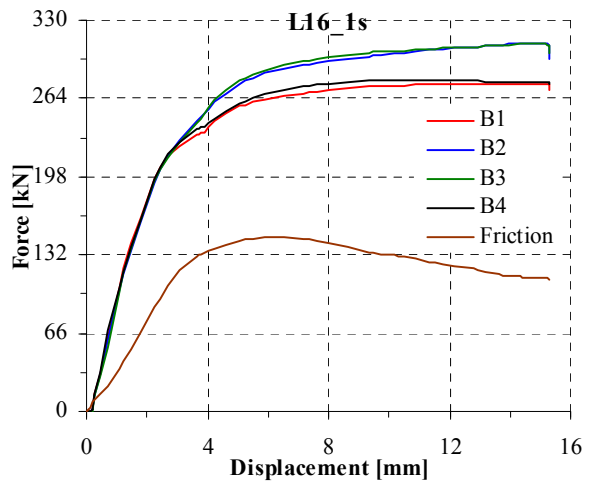
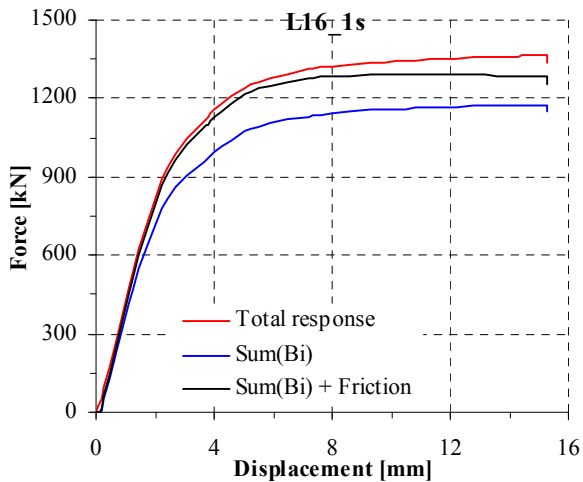
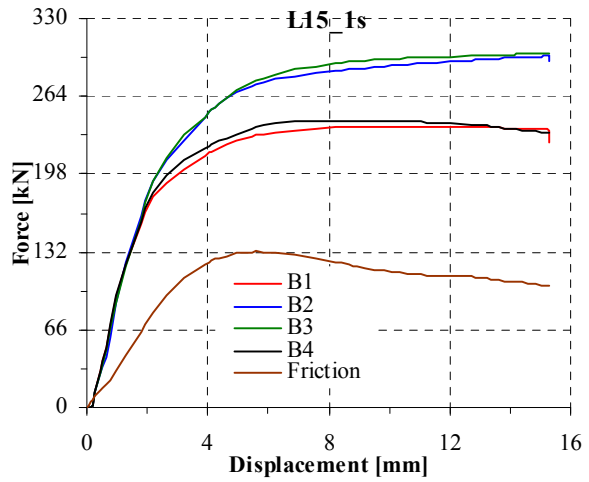
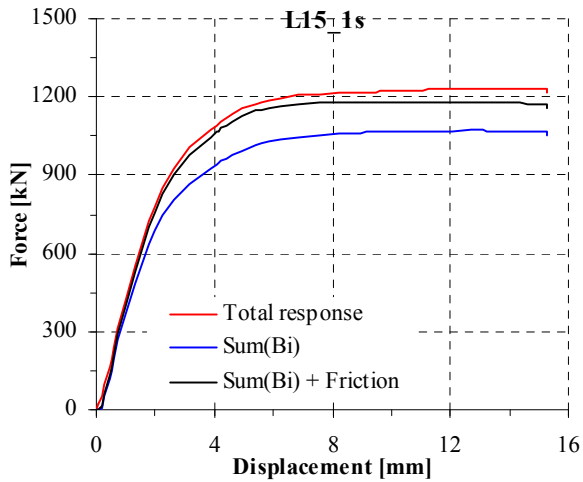
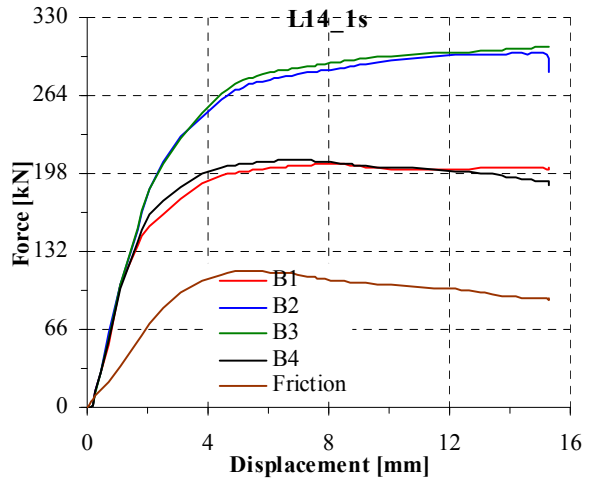
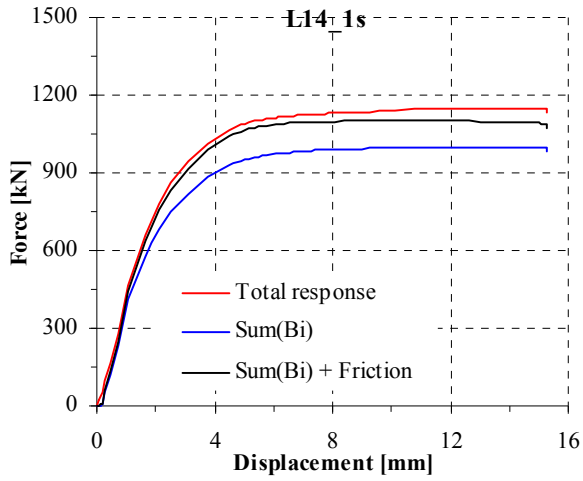
Distribution of forces between bolts and the friction force

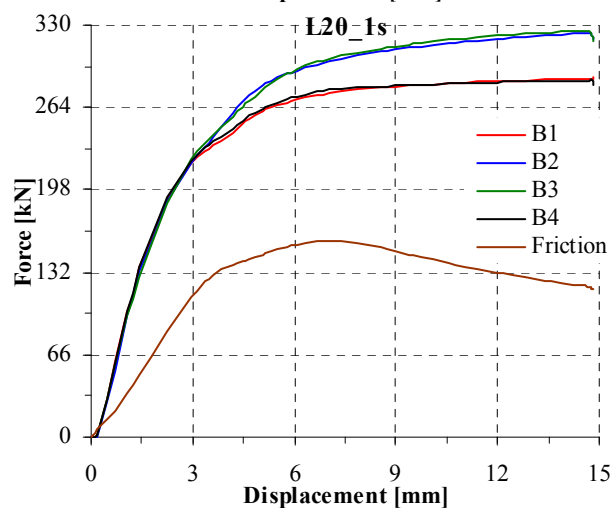
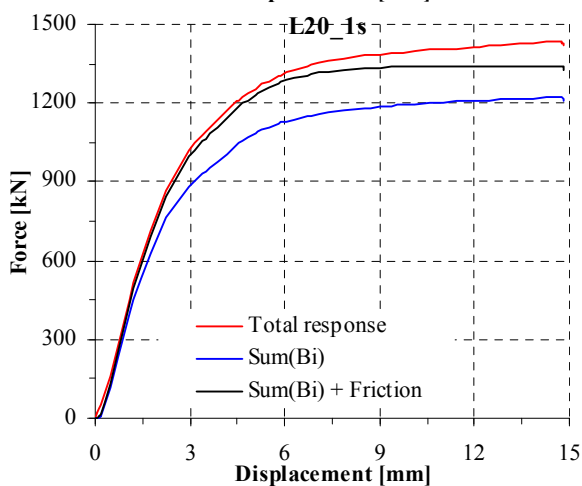
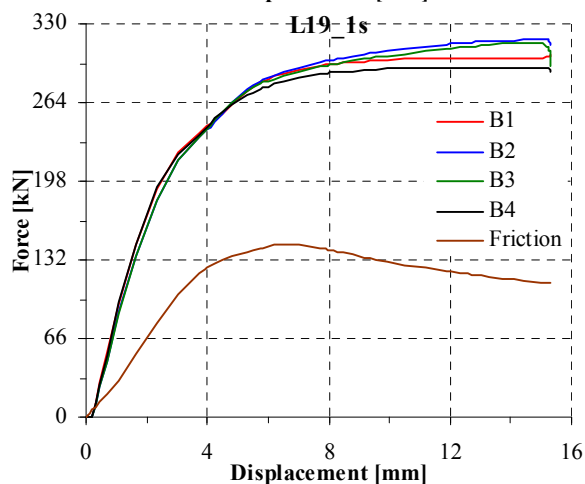
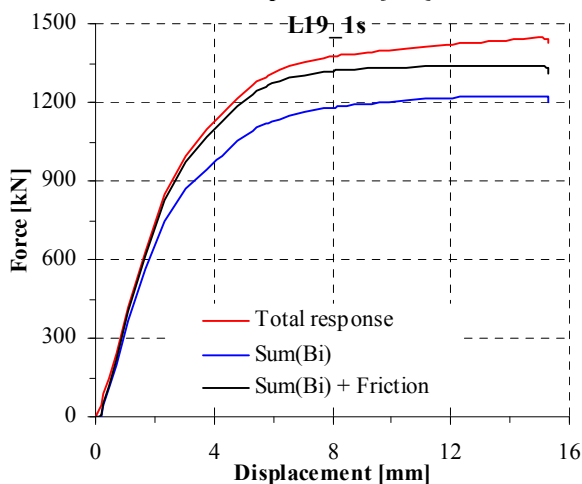
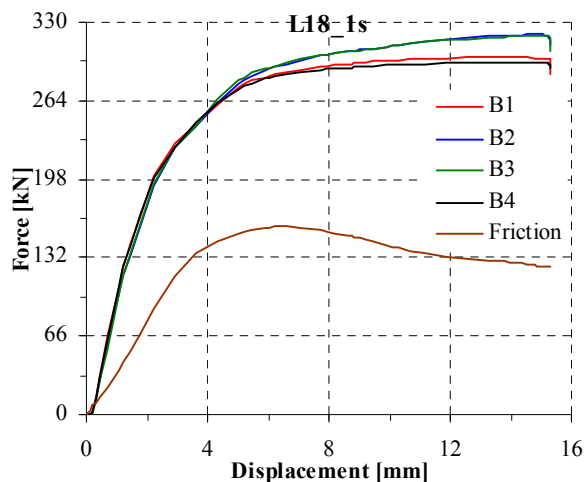
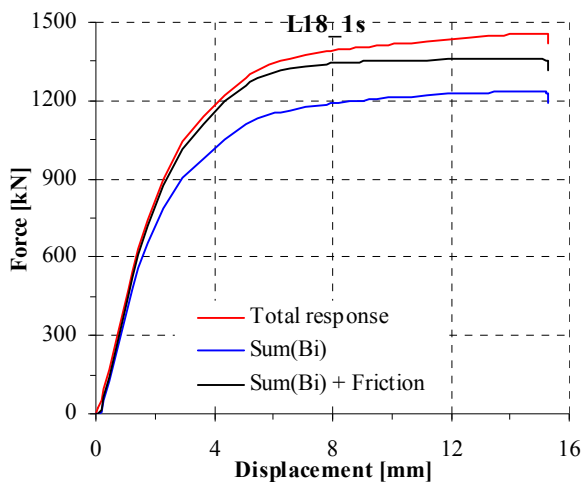


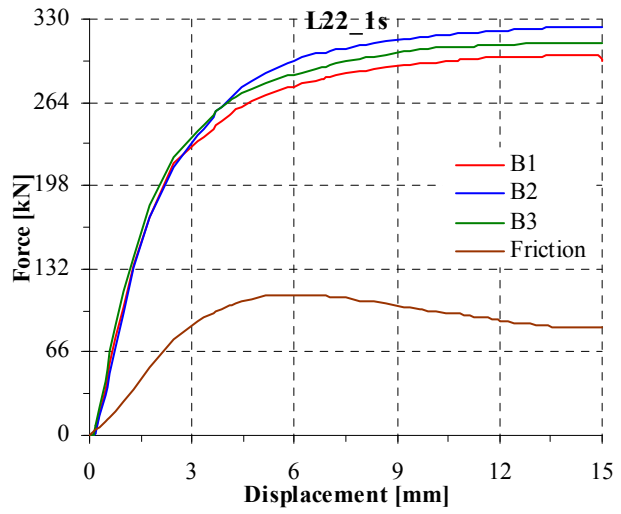
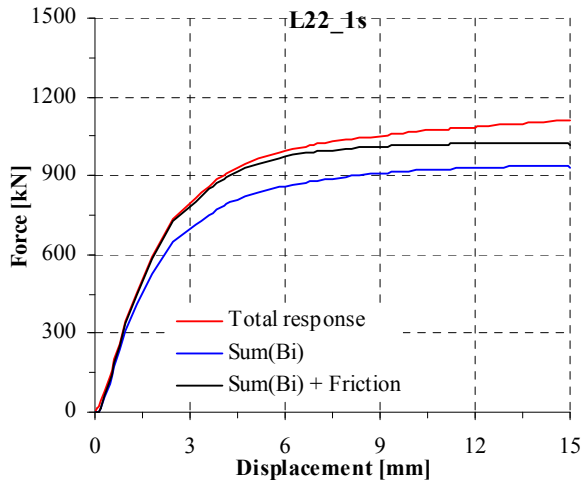
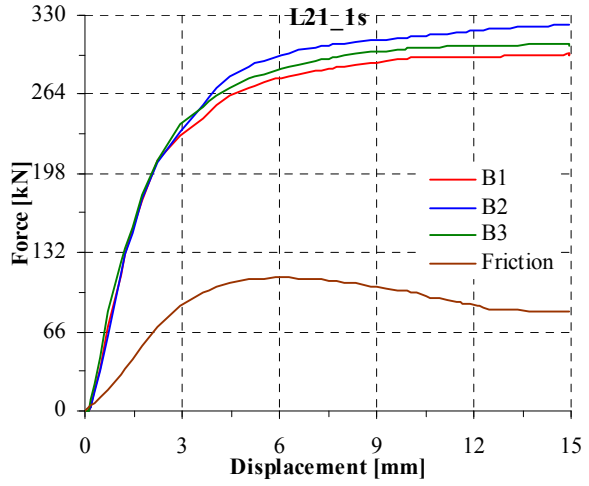
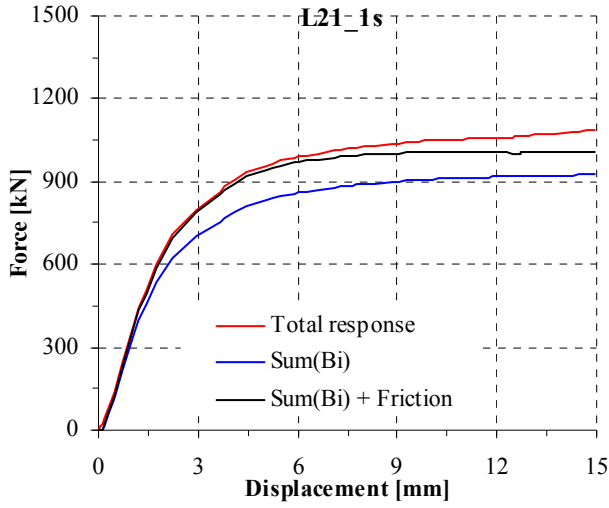




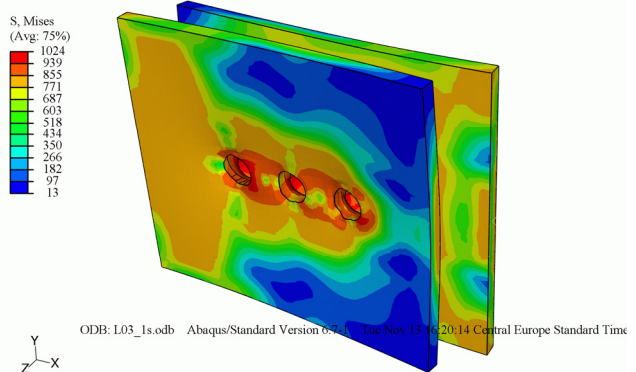
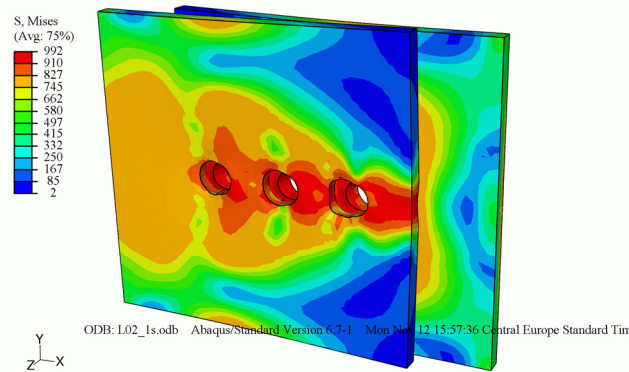
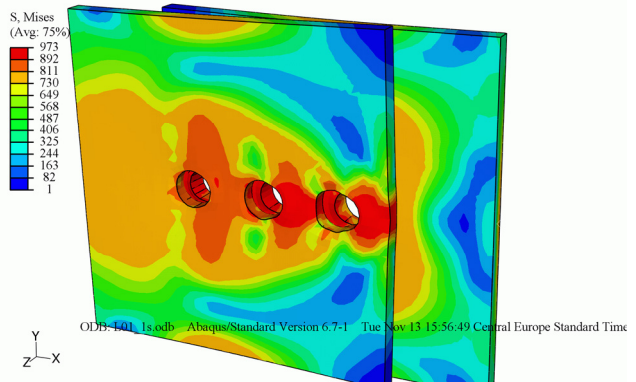
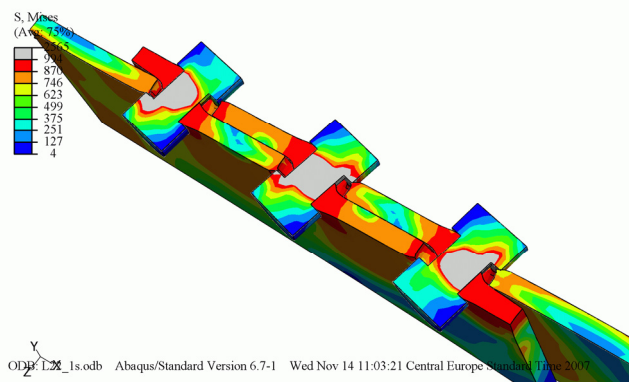


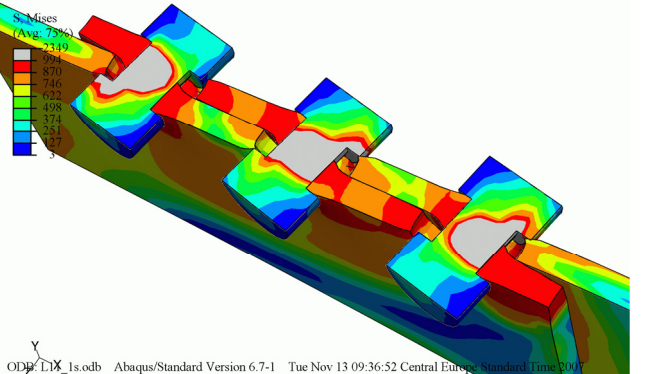
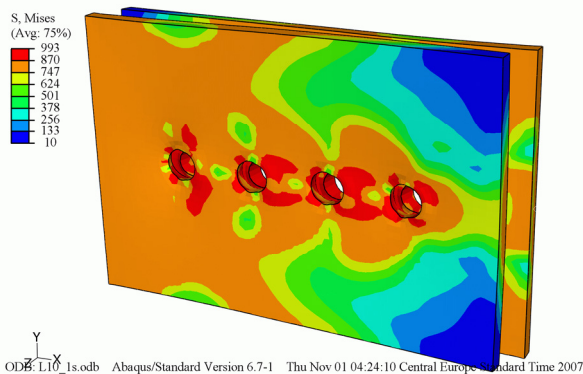
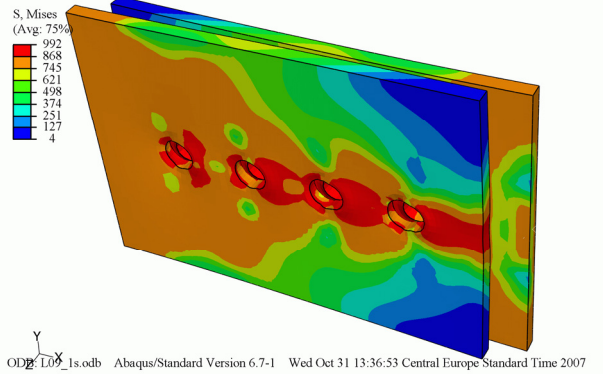
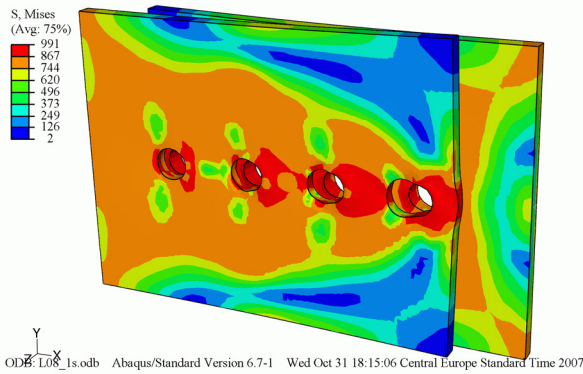
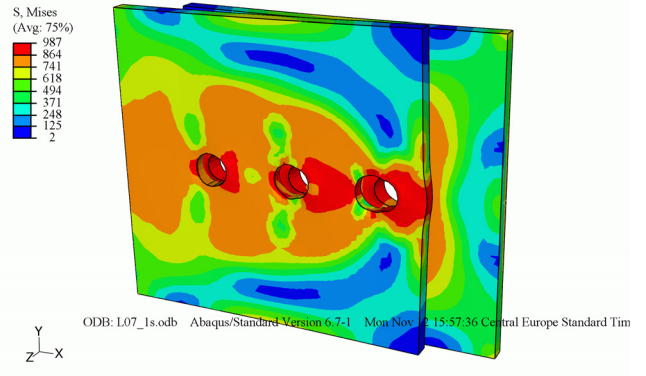
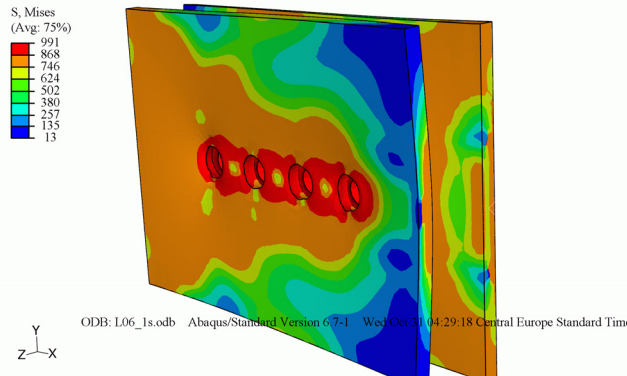
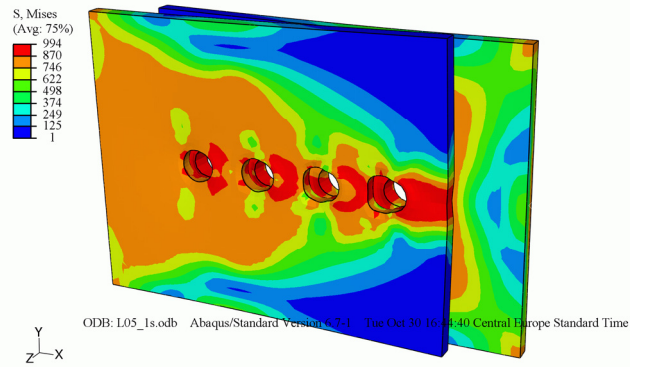
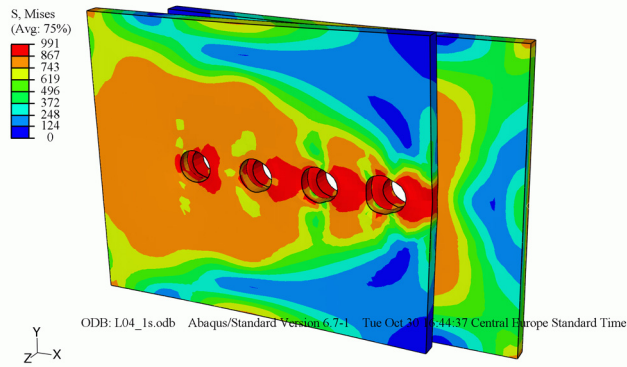


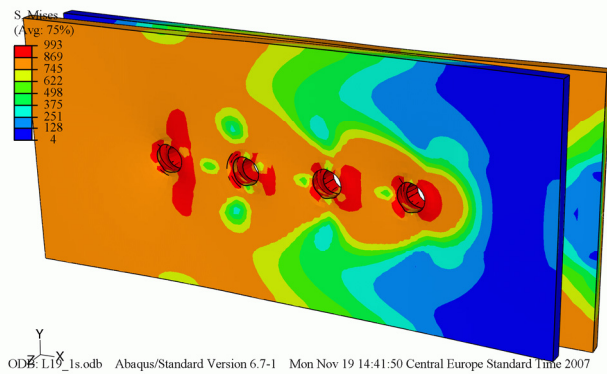
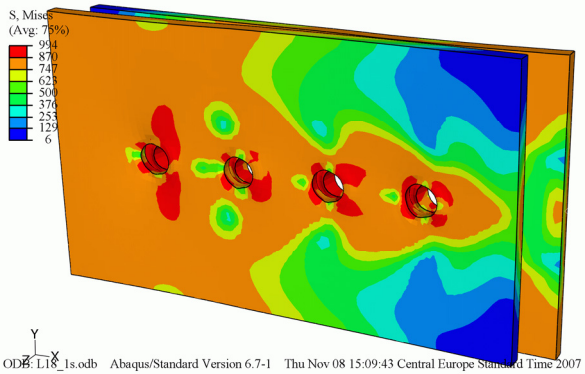
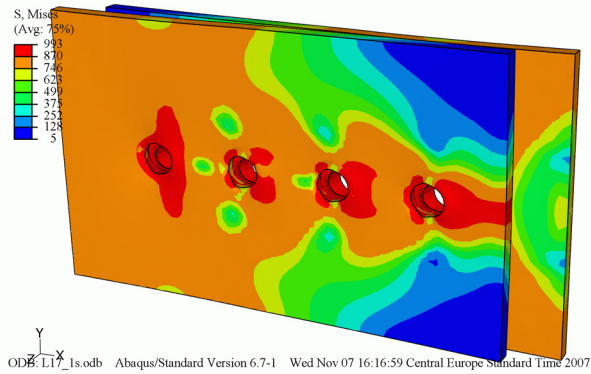
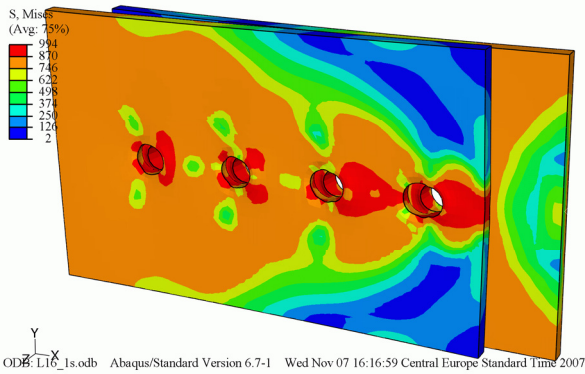
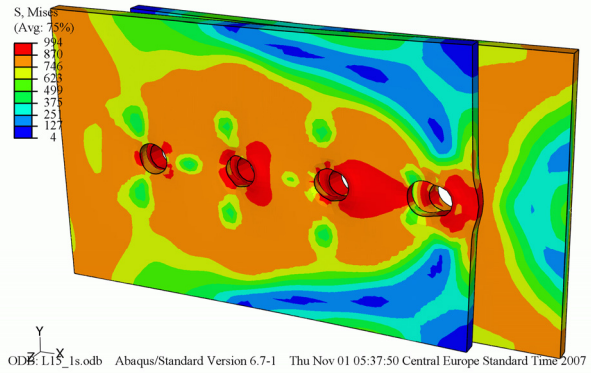
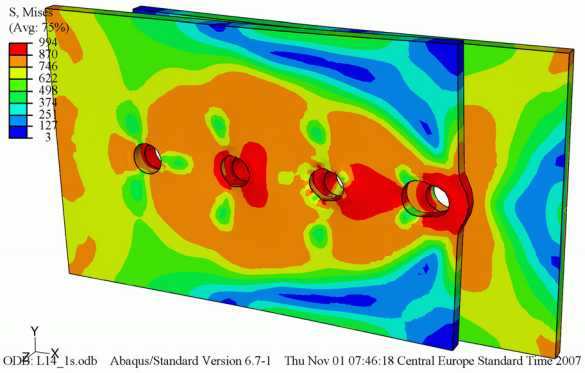
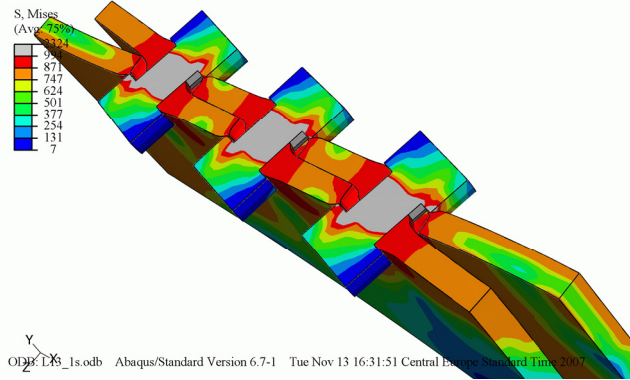
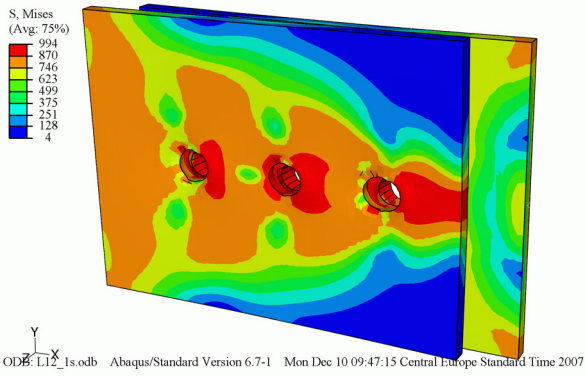


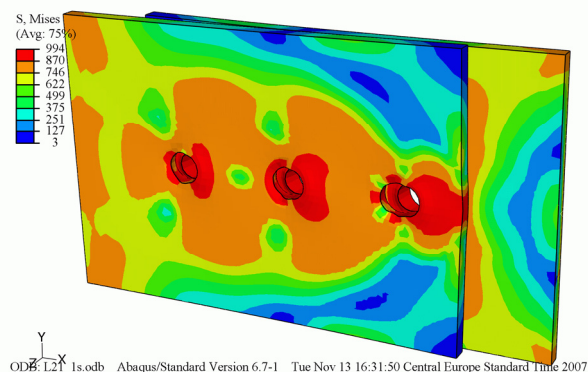
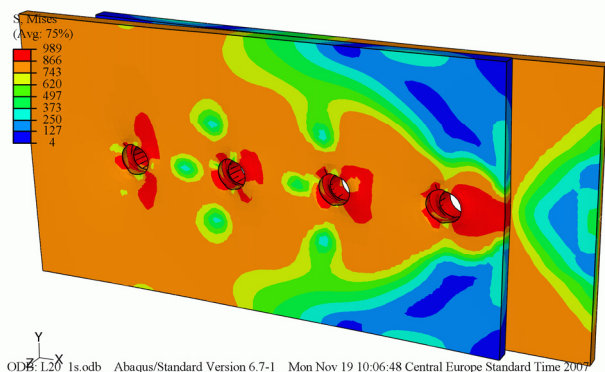


Mises stress on a deformed conbnection. The connection name is displayed on the bottom left side of the figure





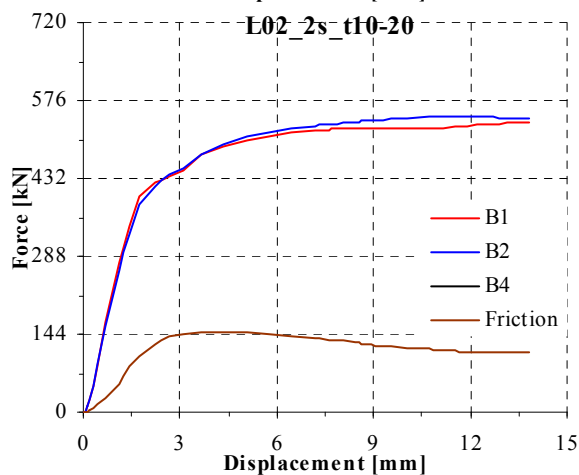
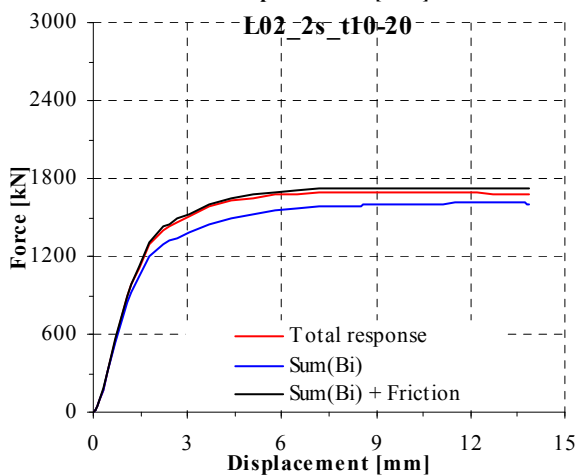
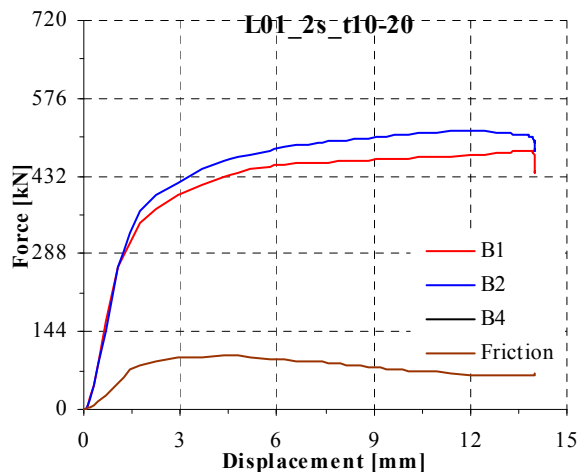
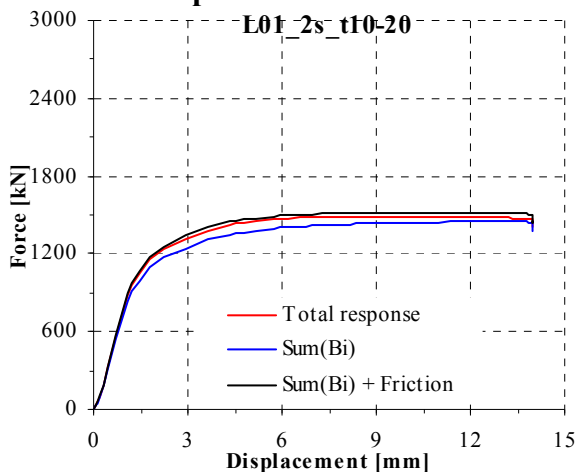


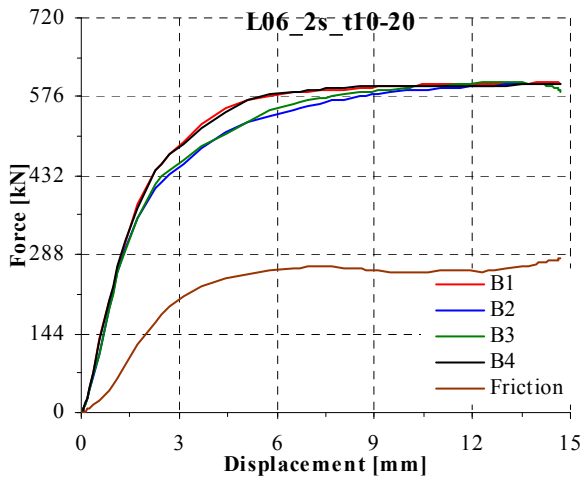
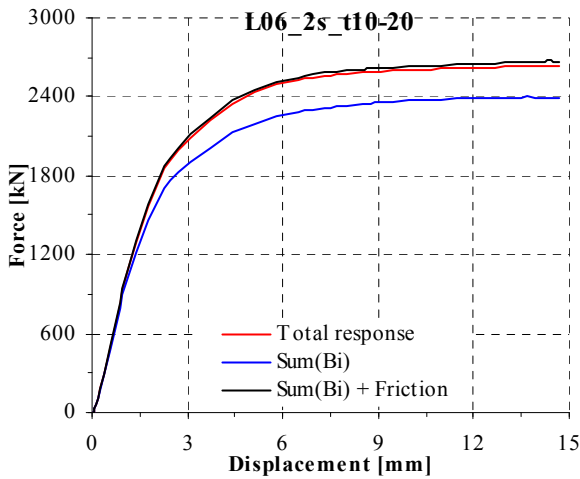
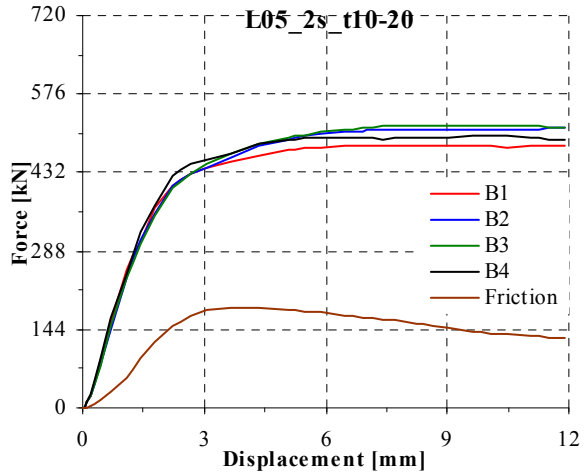
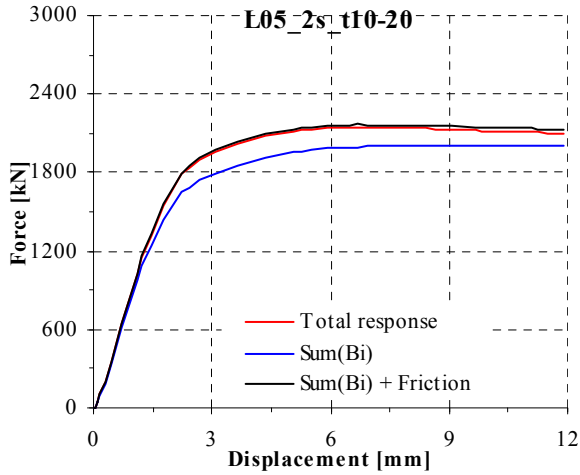
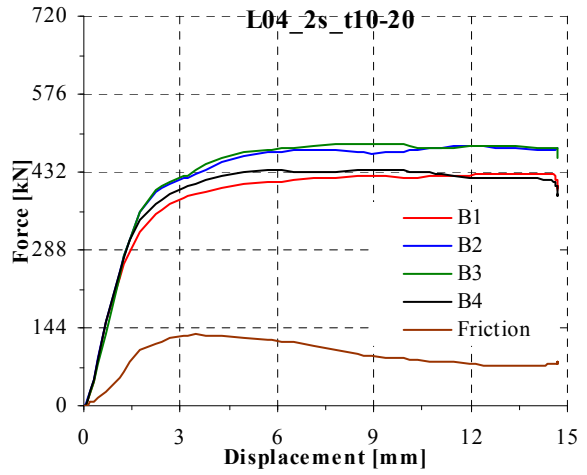
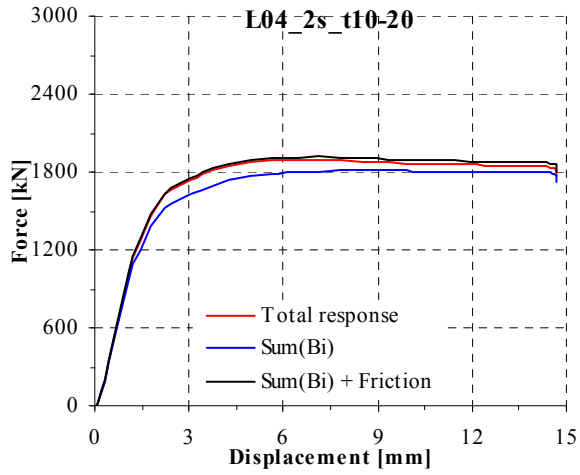
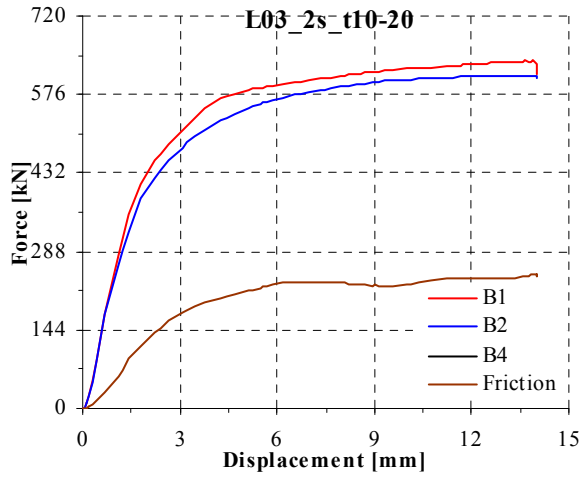
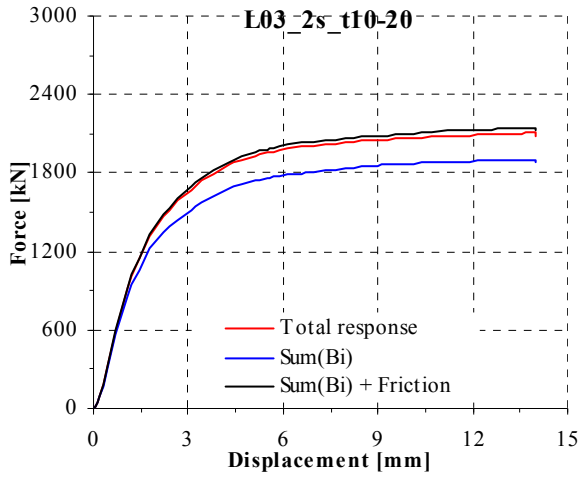


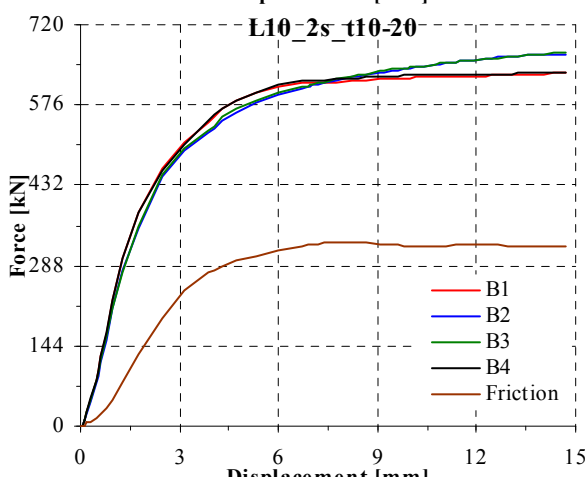
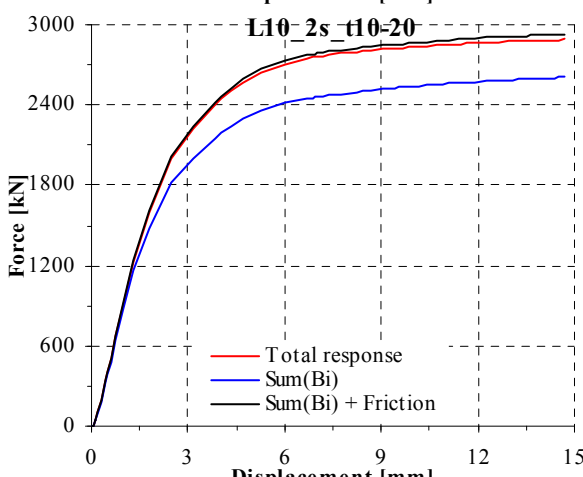
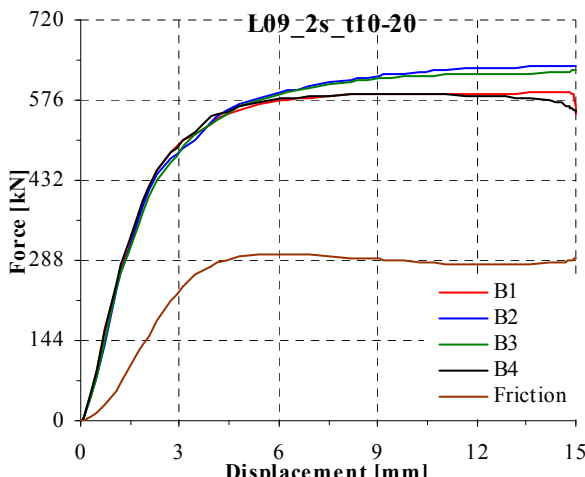
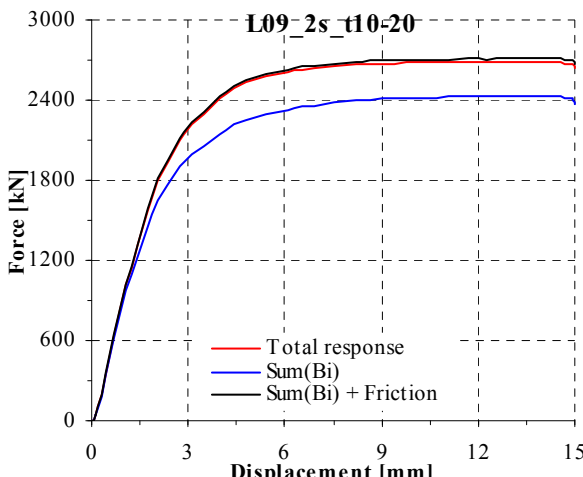
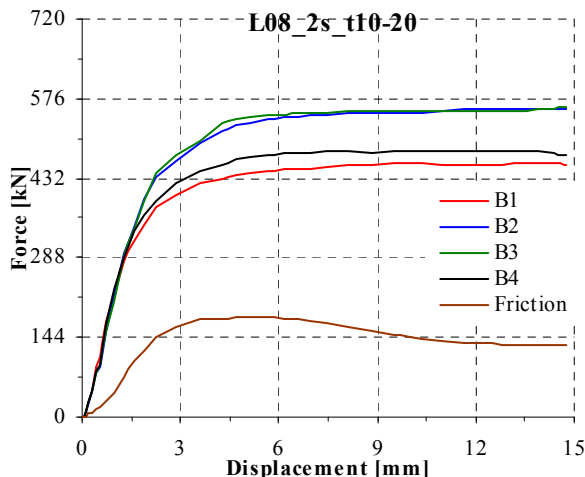
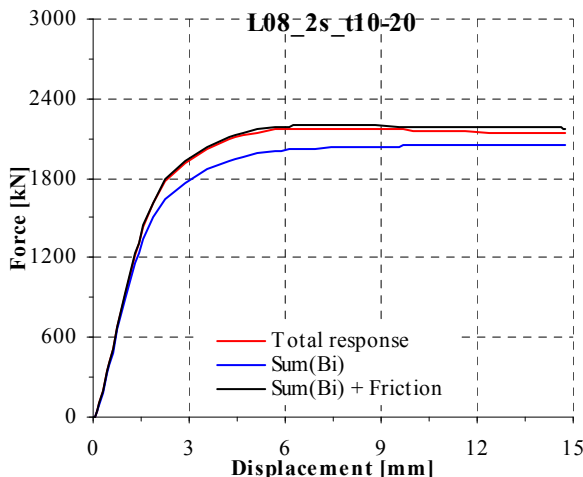
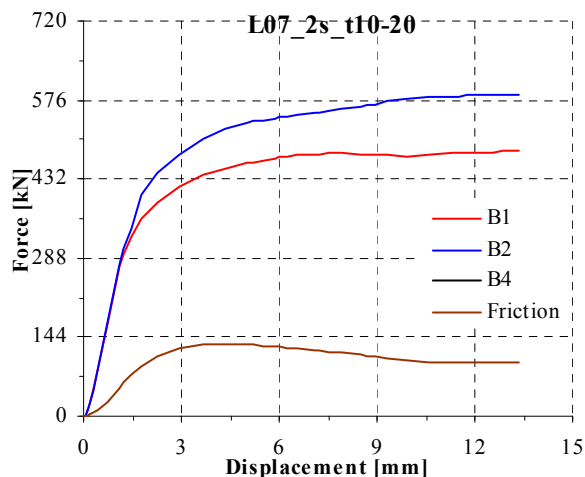
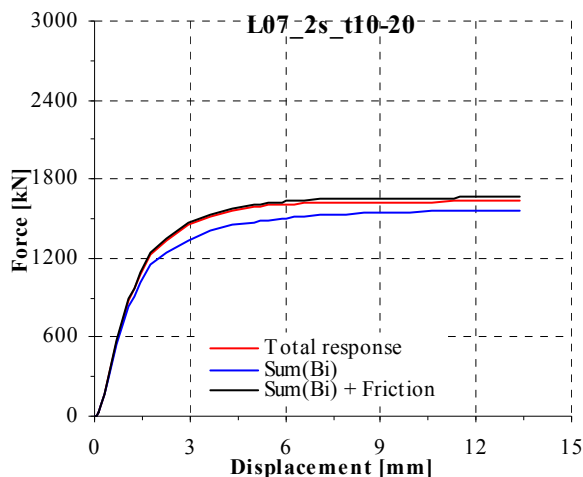
Lxx_2s_t10-20; Numerical model type M3; 21 FE analyses

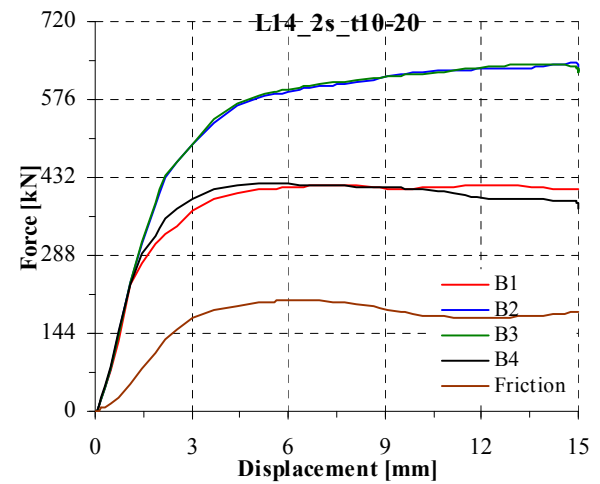
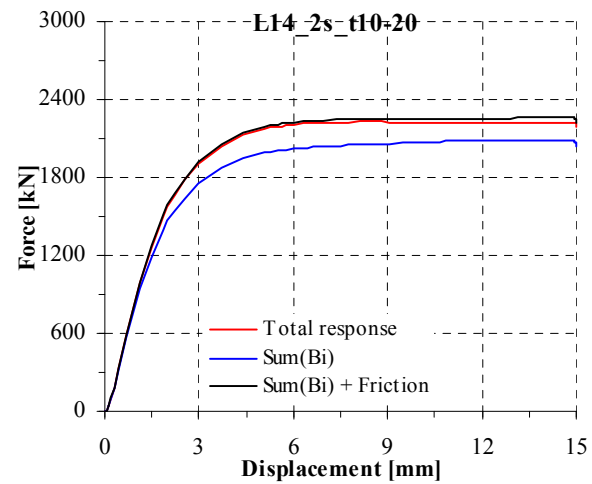
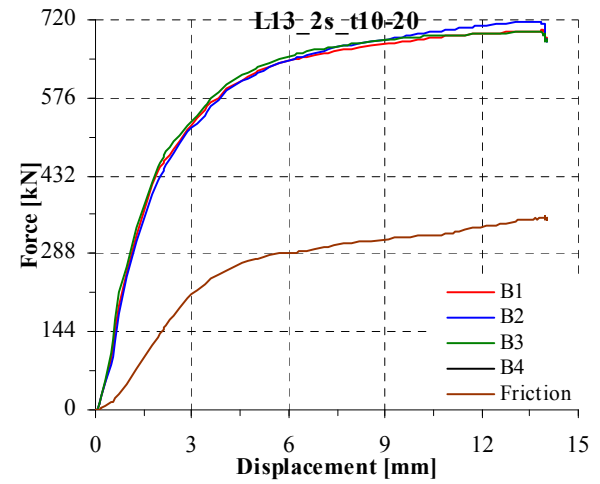
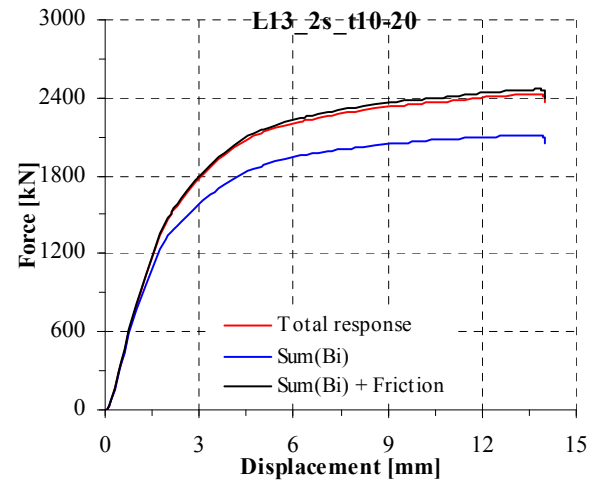
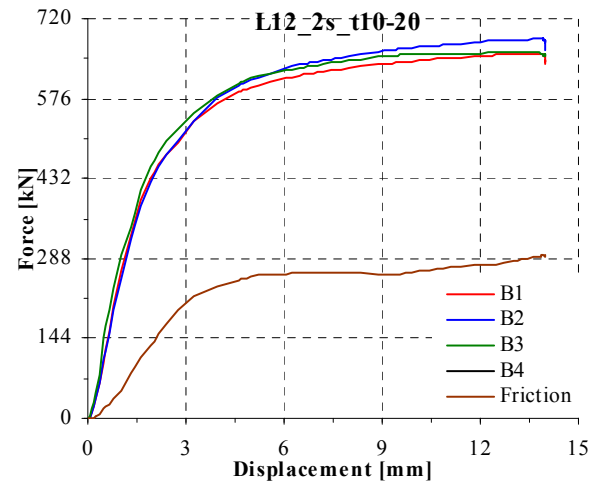
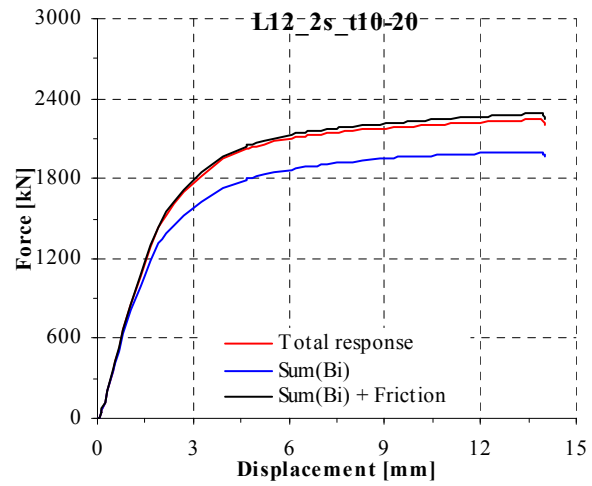
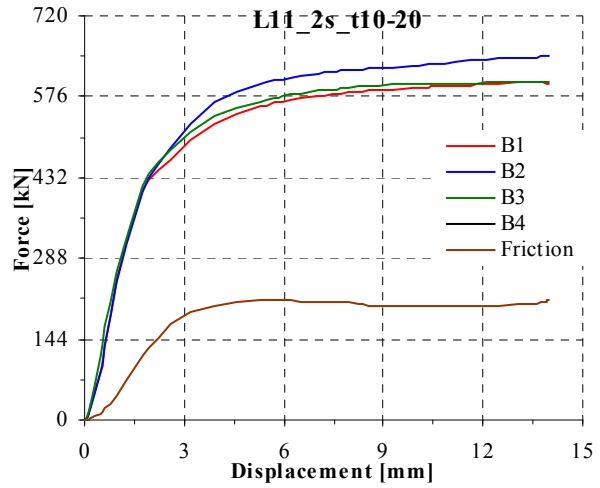
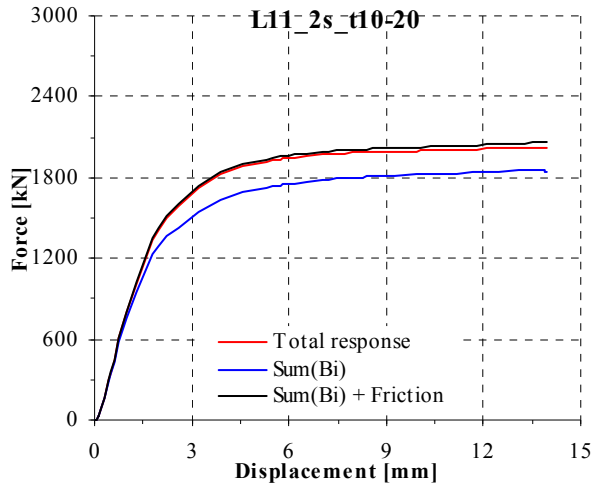
Experimental and numerical load-displacement curves

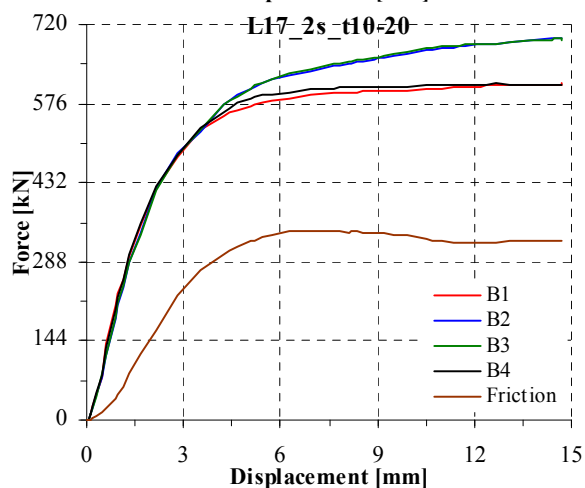
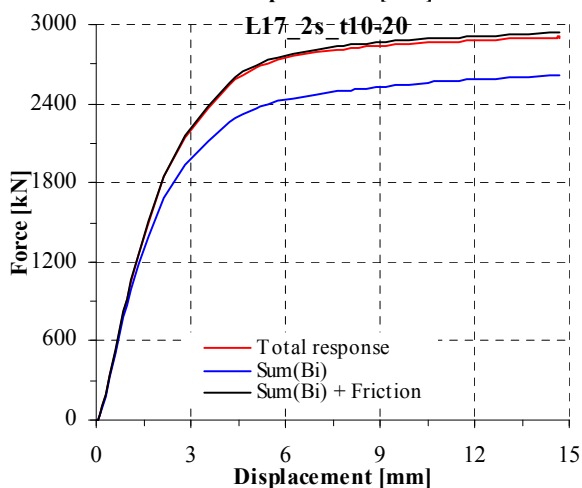
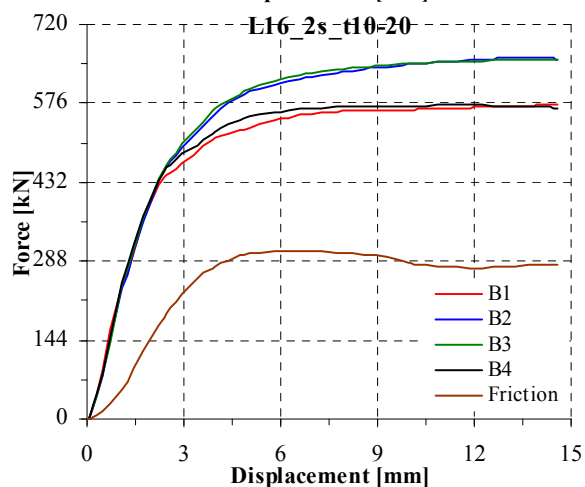
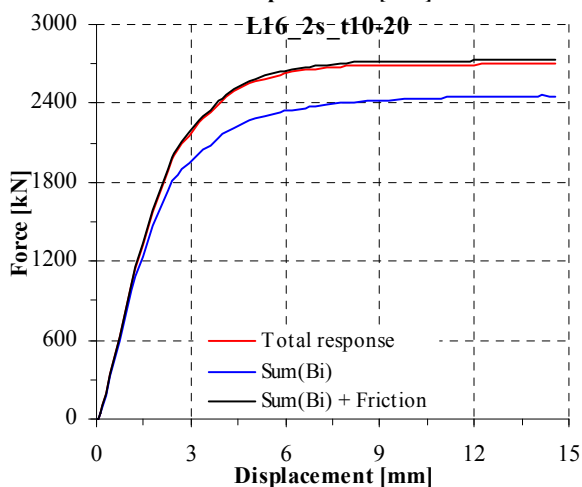
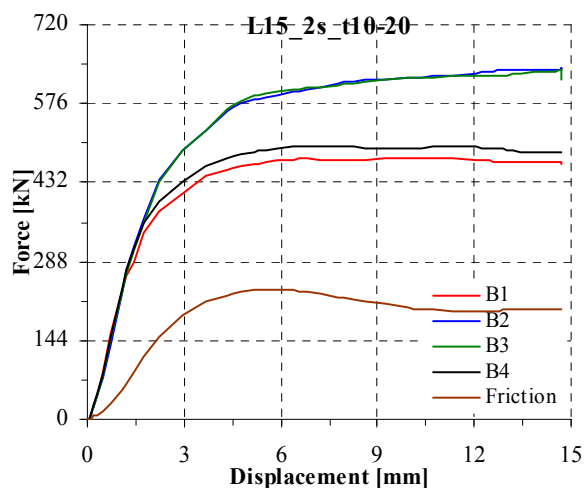
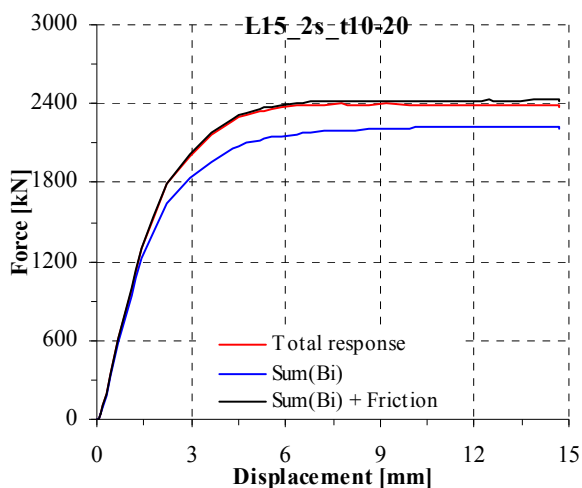
Distribution of forces between bolts and the friction force

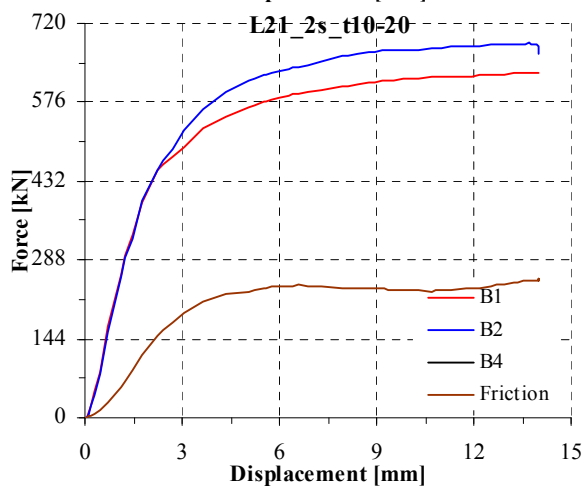
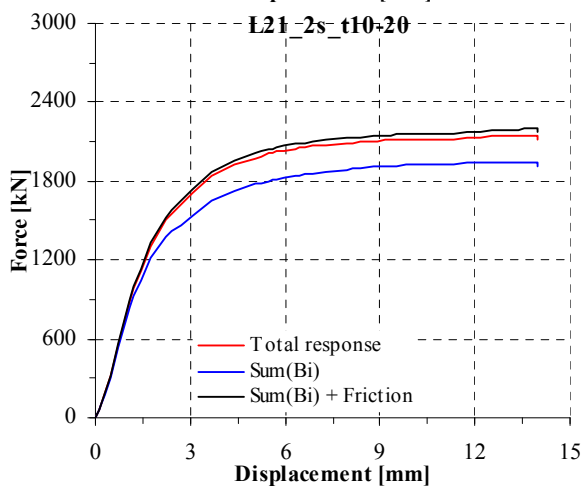
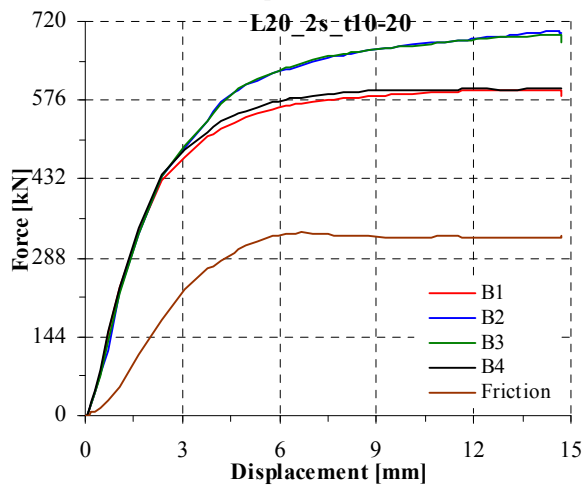
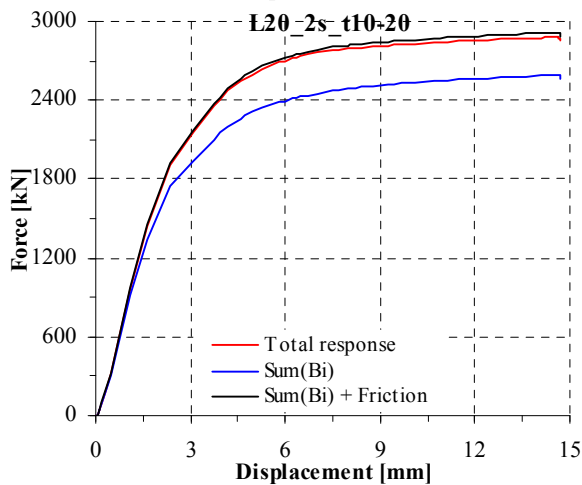
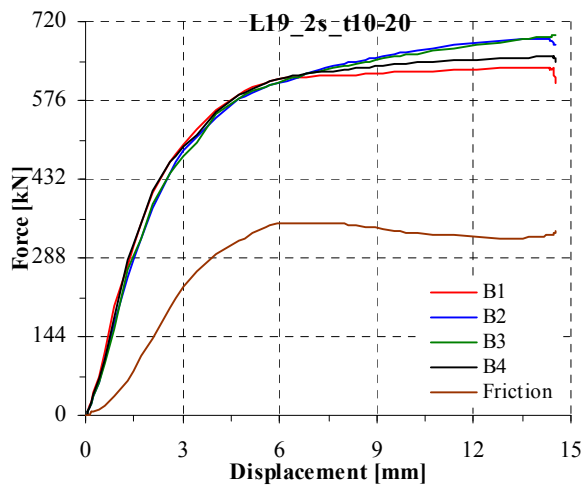
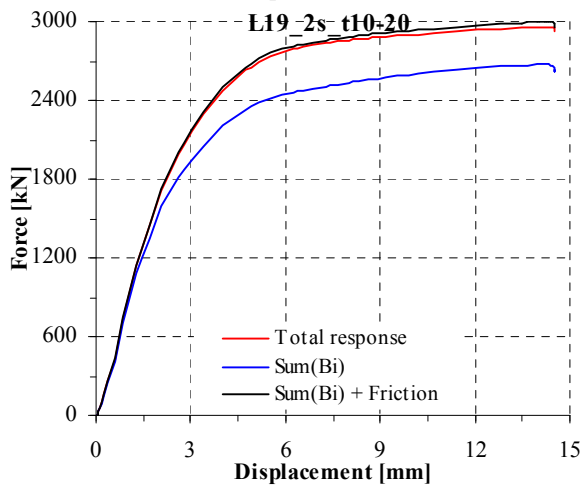
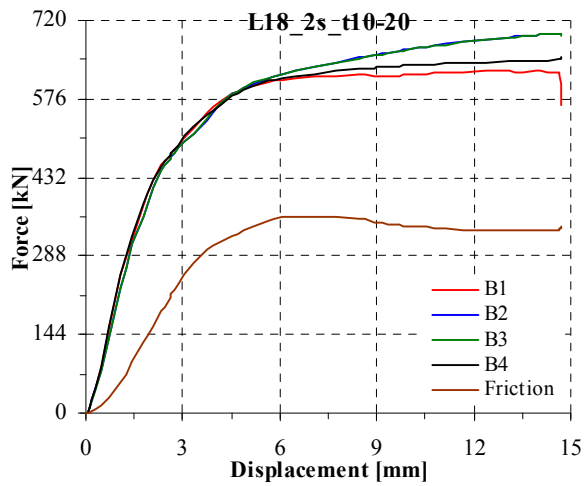
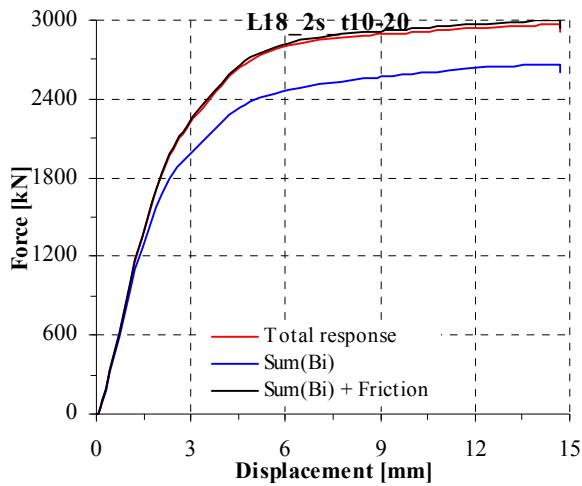




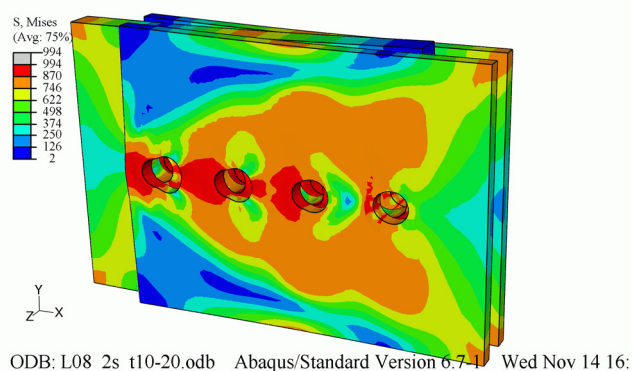
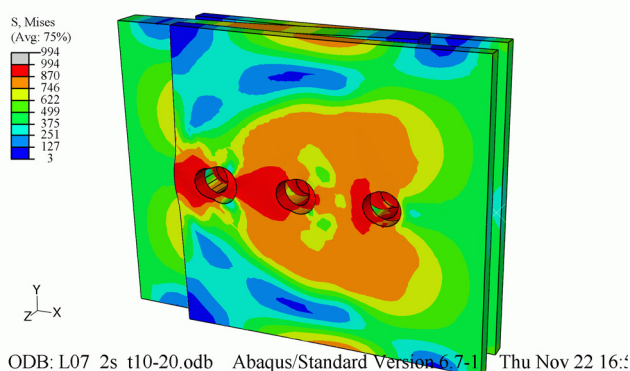
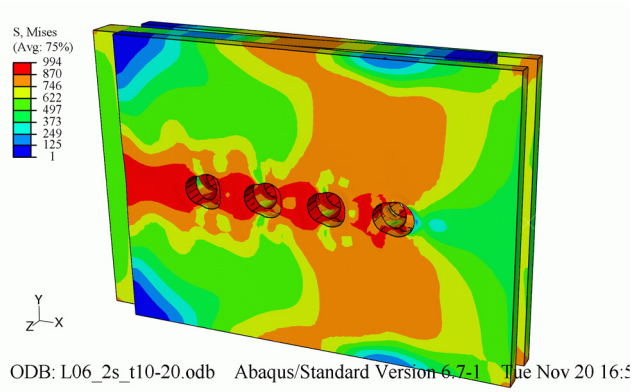
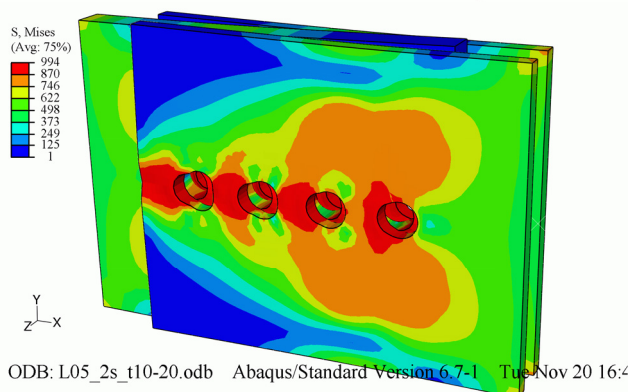
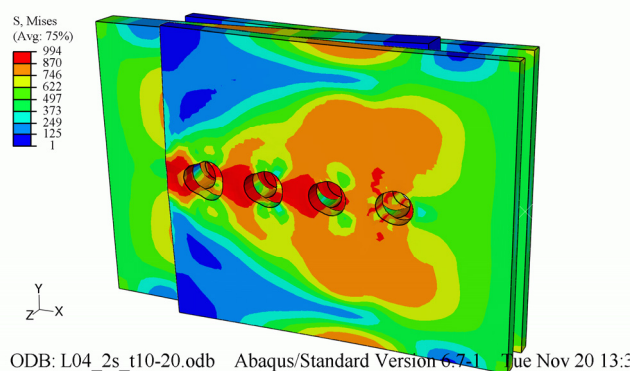
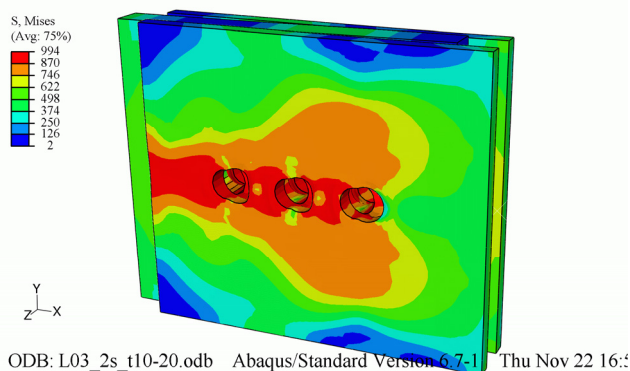
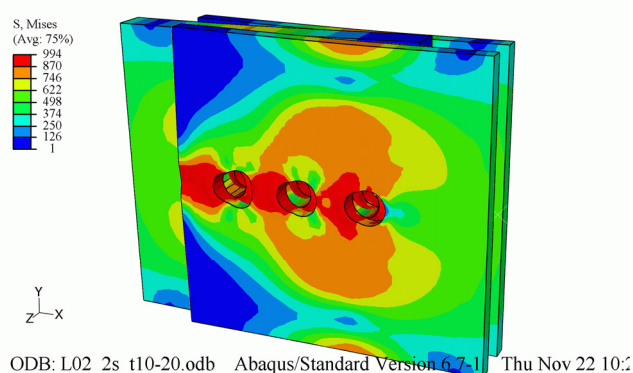
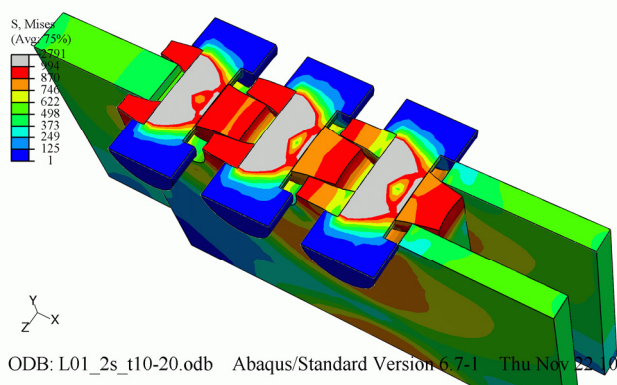


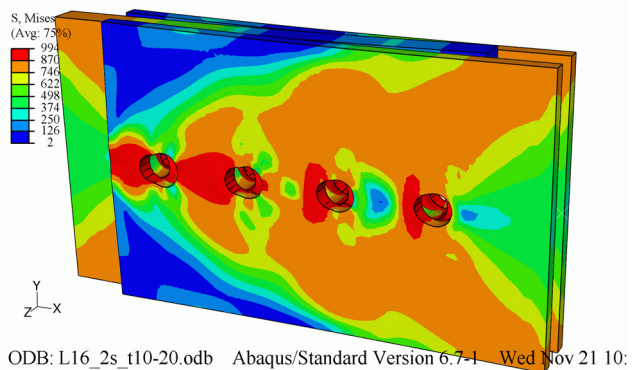
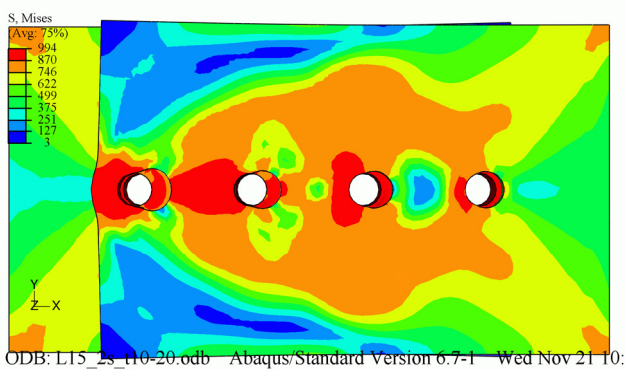
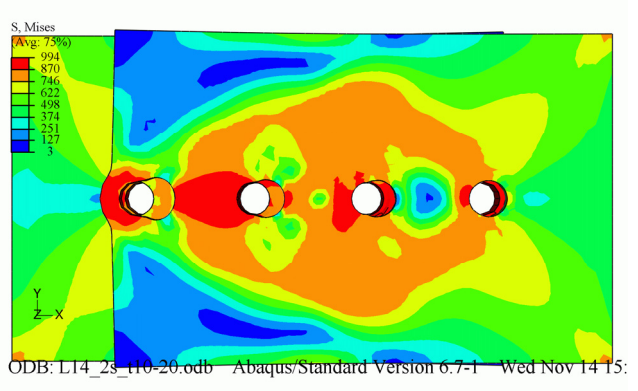
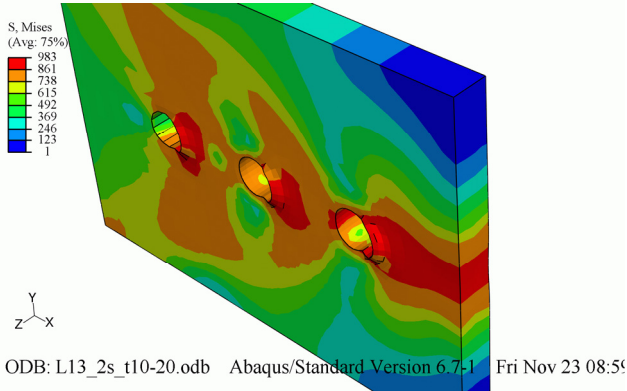
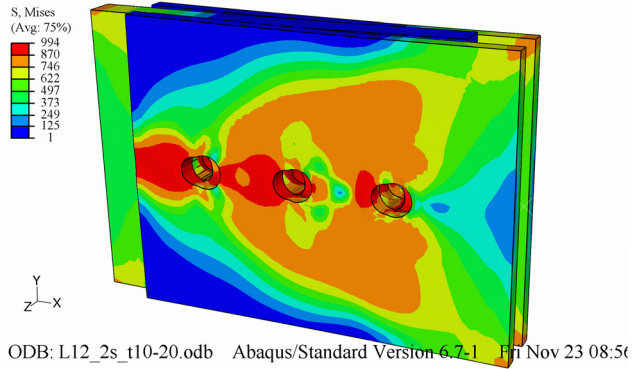
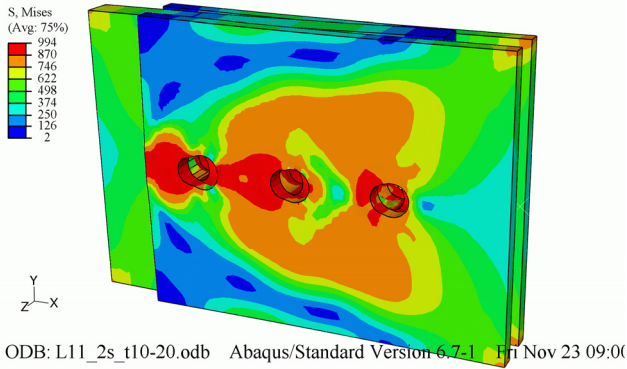
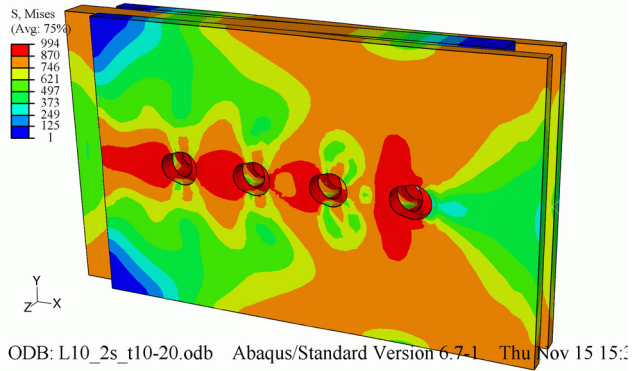
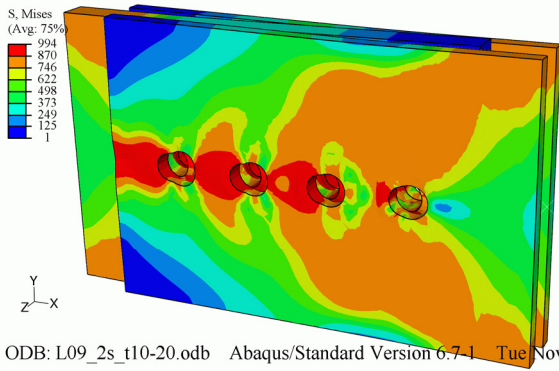


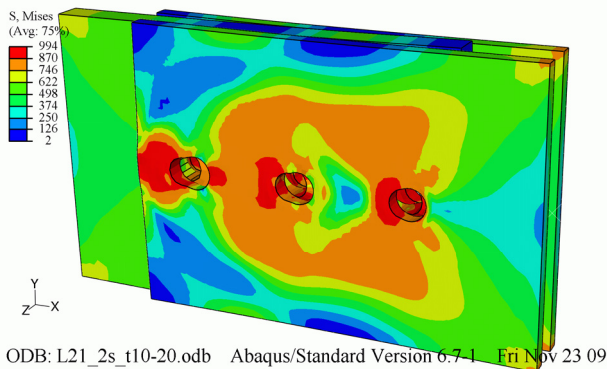
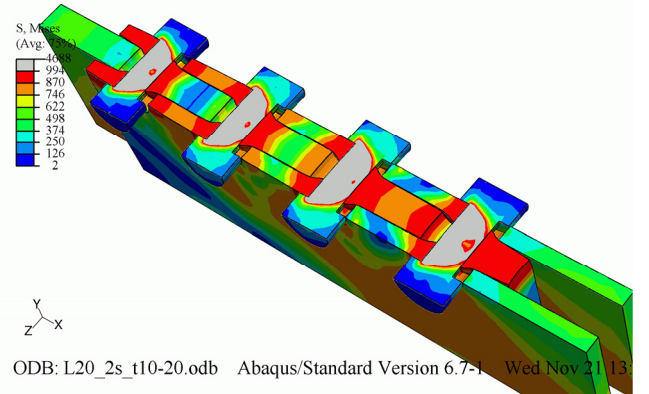
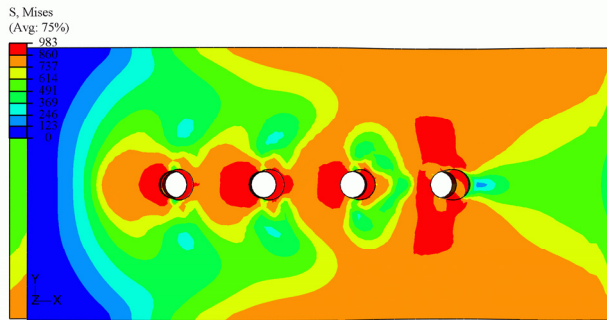
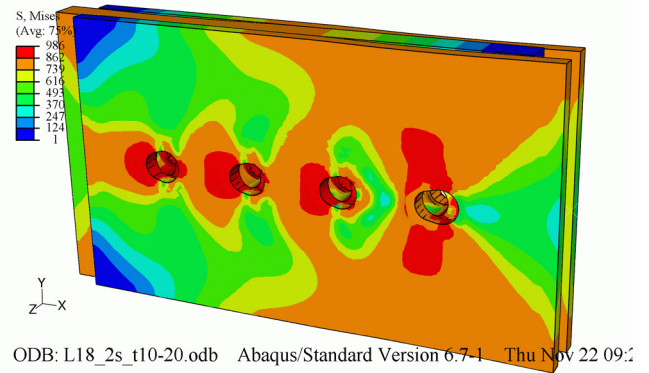
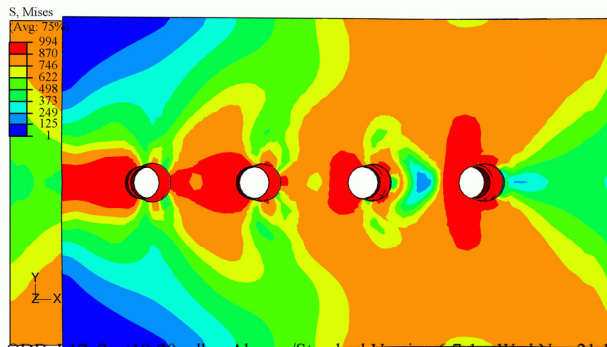




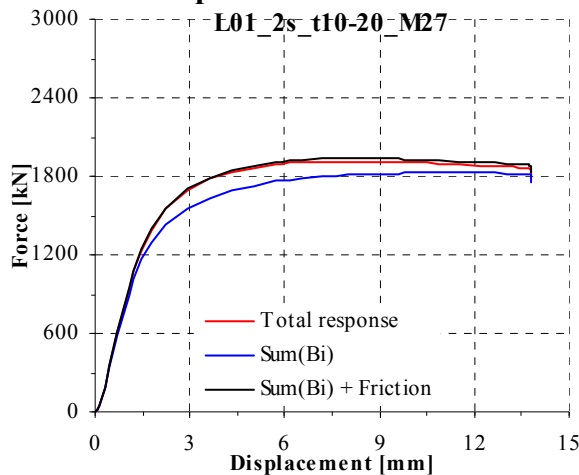
Mises stress on a deformed conbnection. The connection name is displayed on the bottom left side of the figure



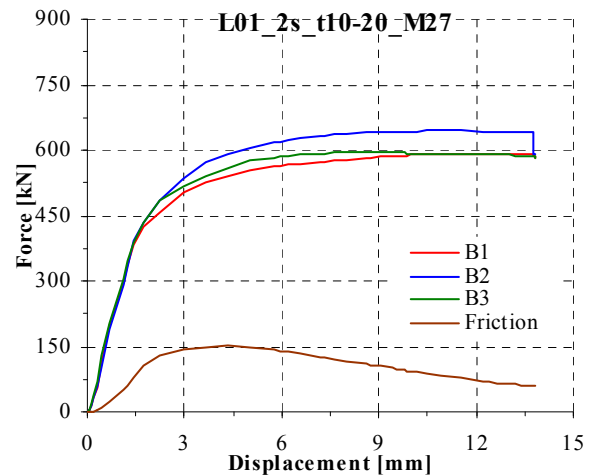


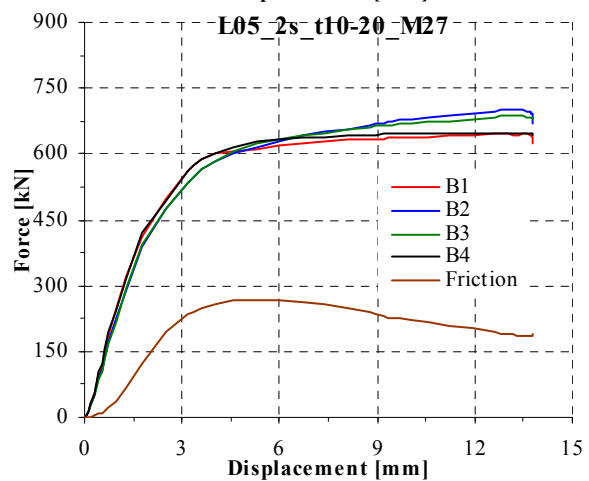
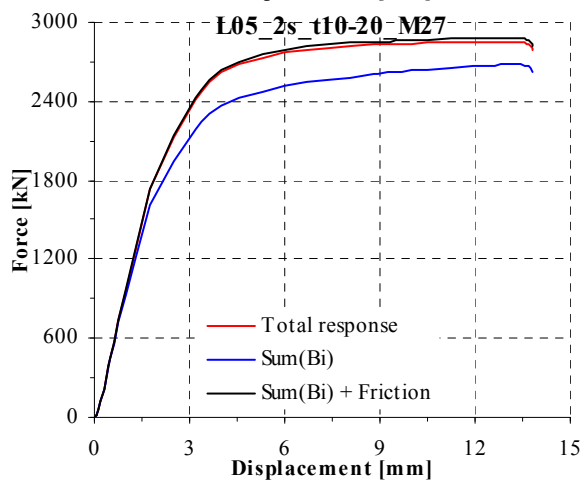
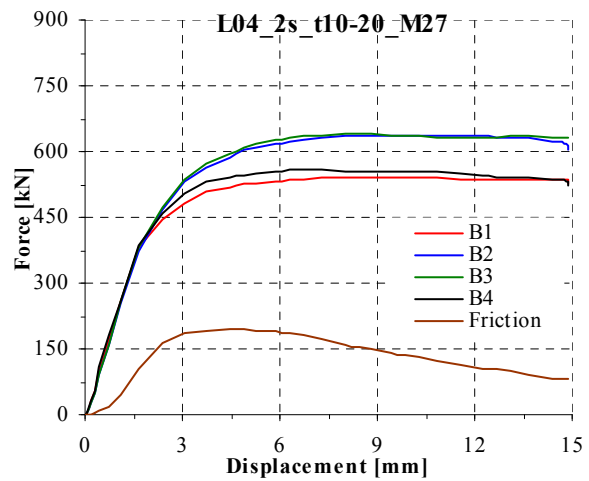
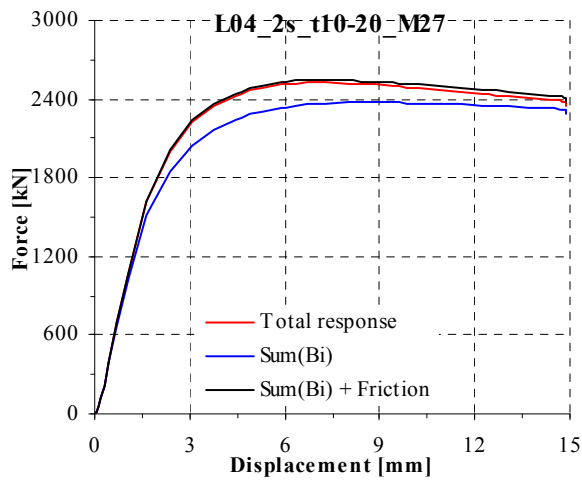
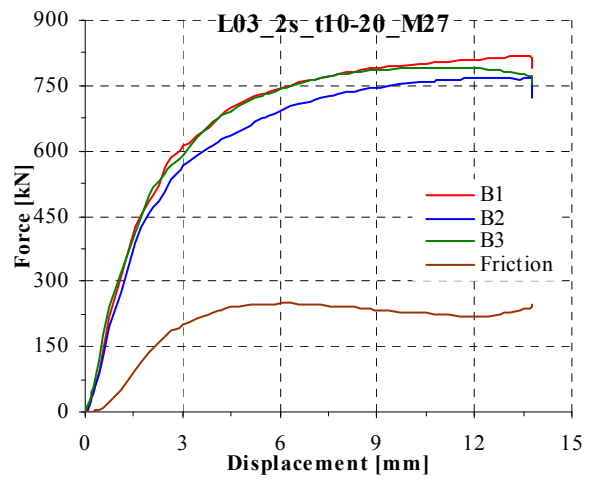
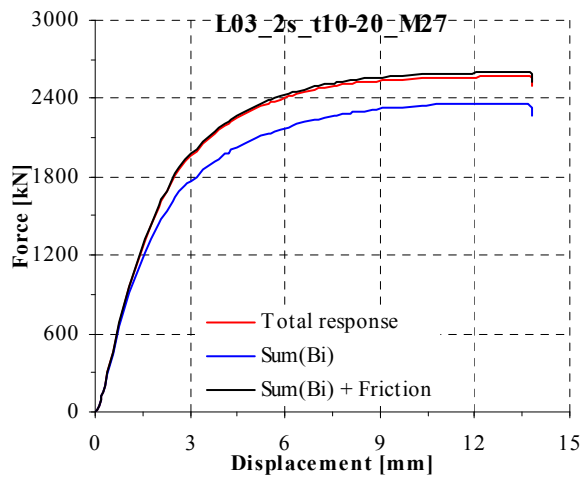
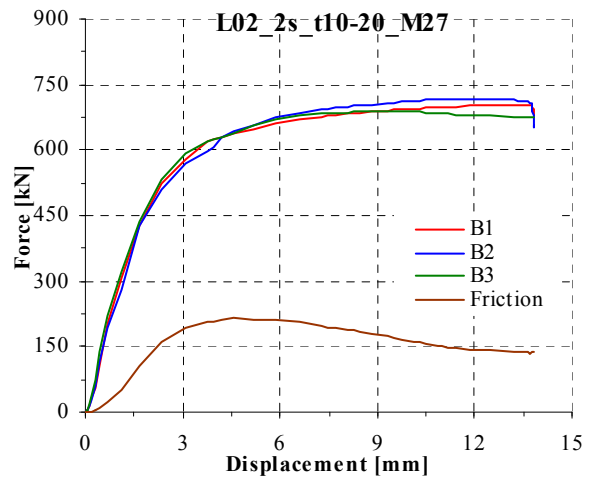
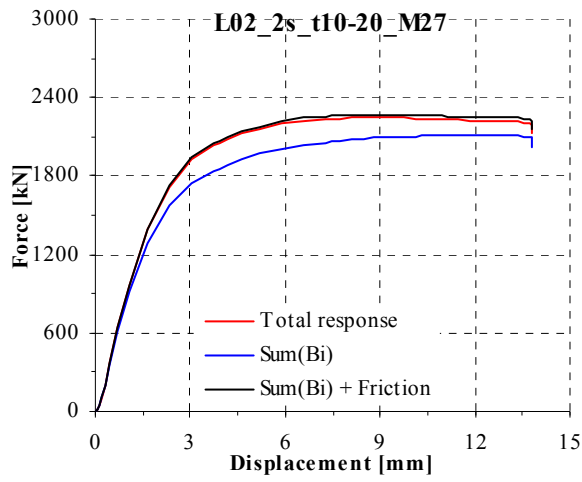


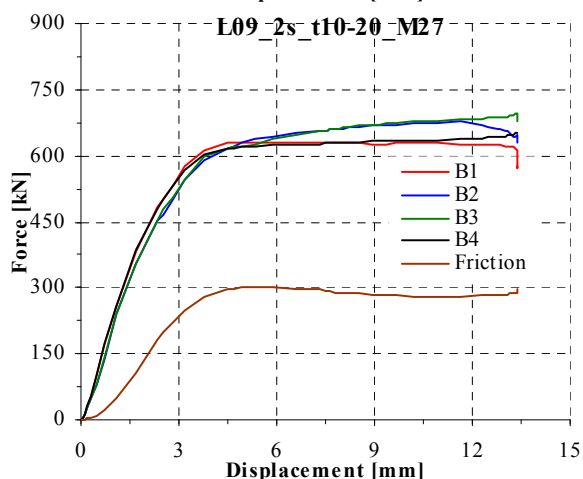
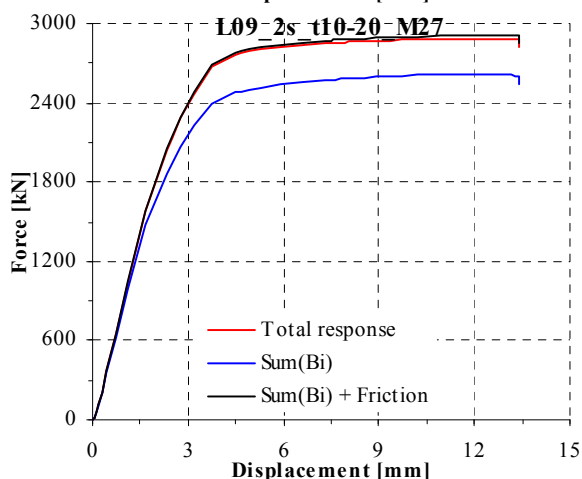
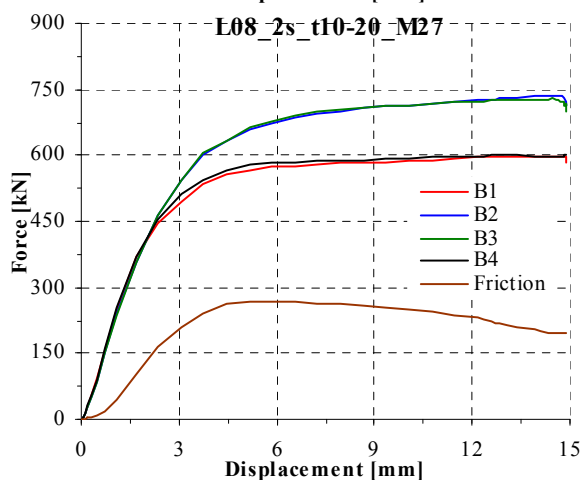
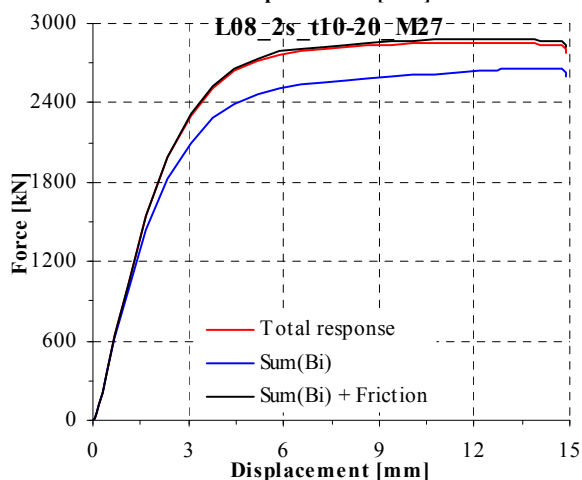
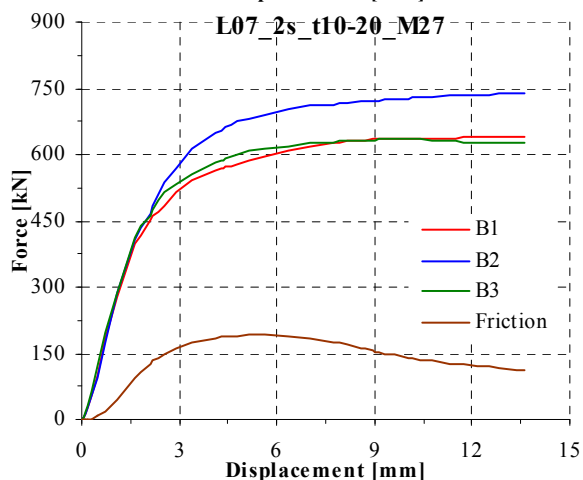
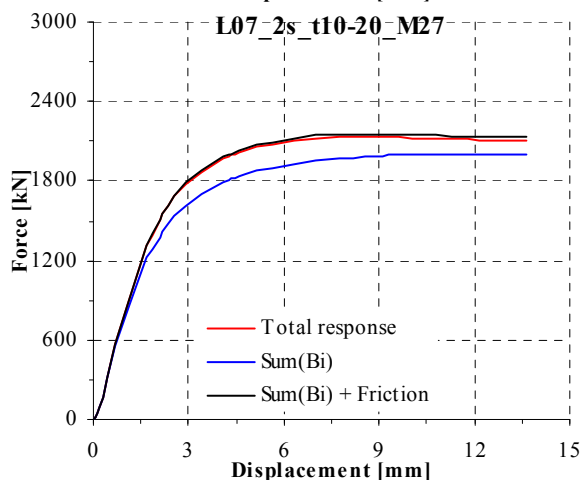
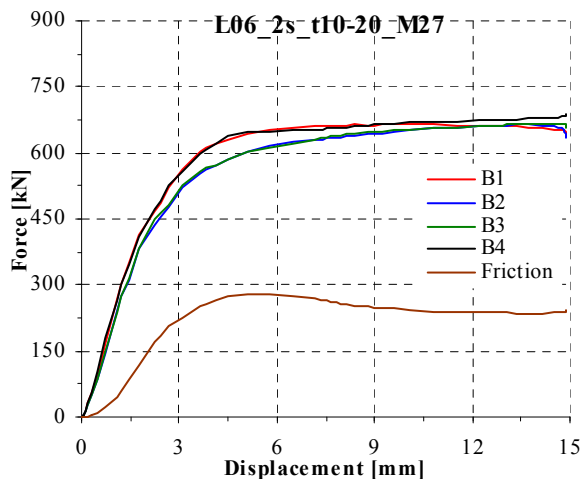
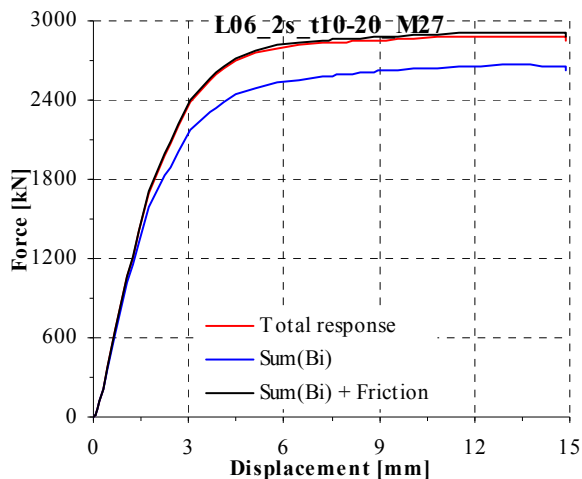
Lxx_2s_t10-20_M27; Numerical model type M3; 21 FE analyses
Experimental and numerical load-displacement curves

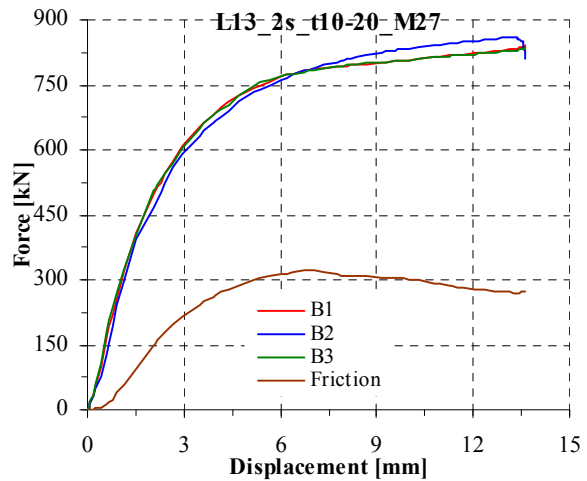
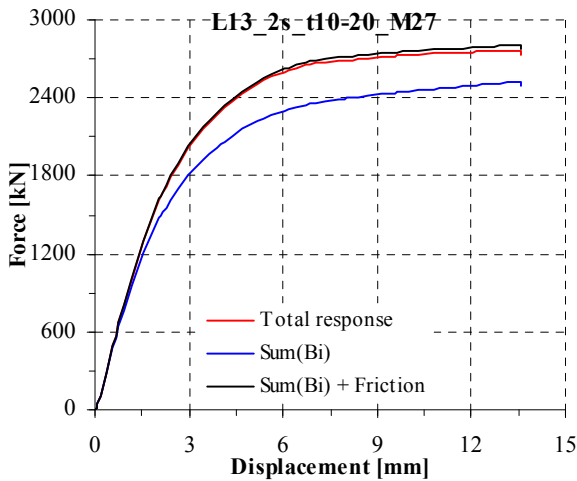
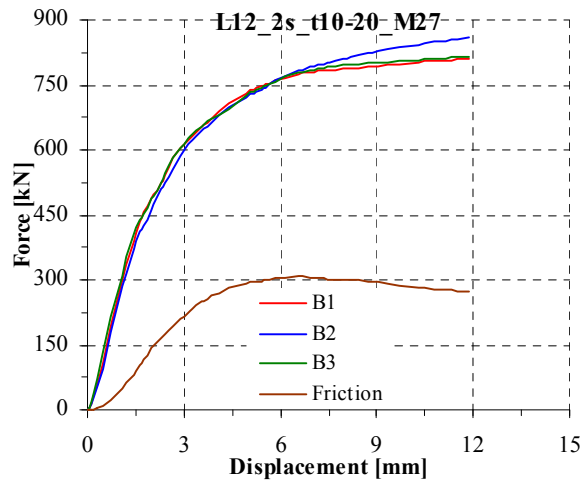
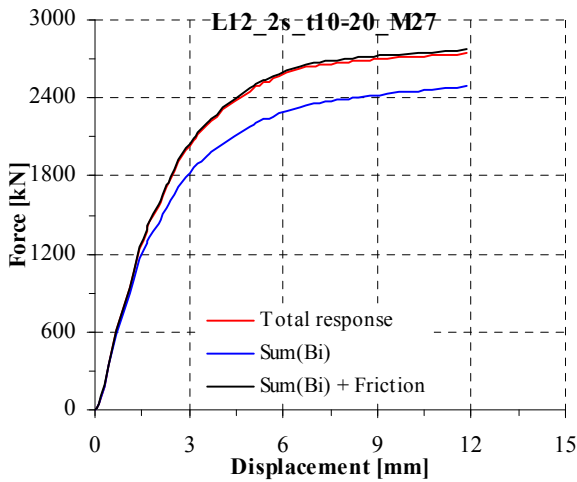
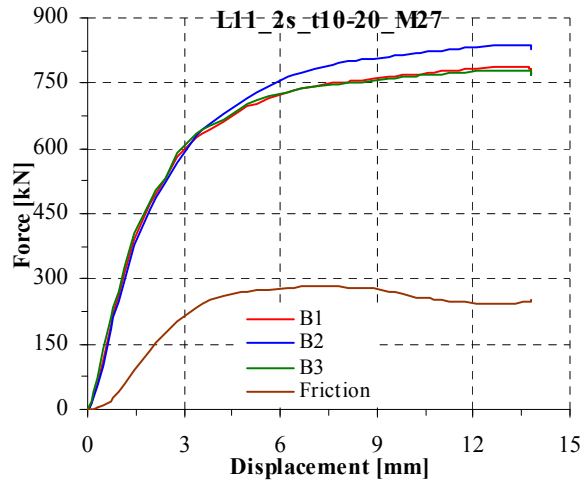
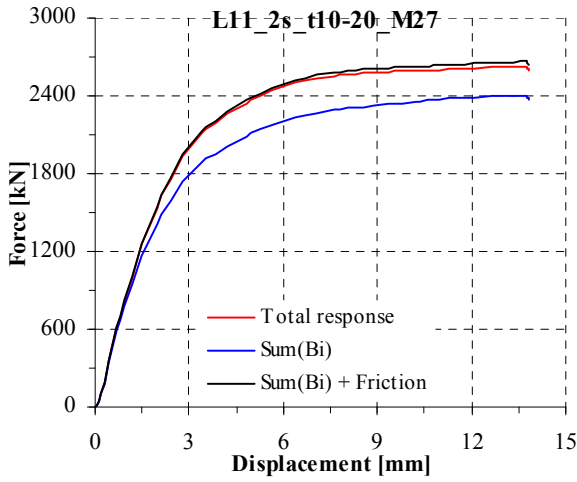
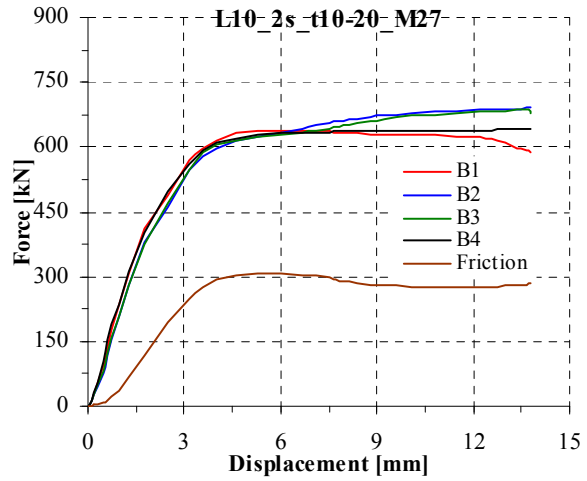
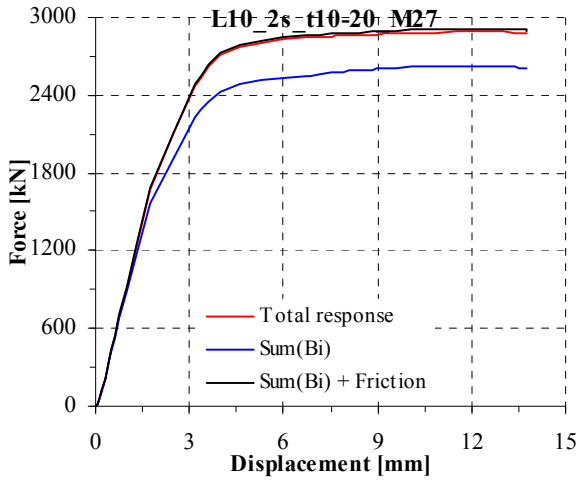


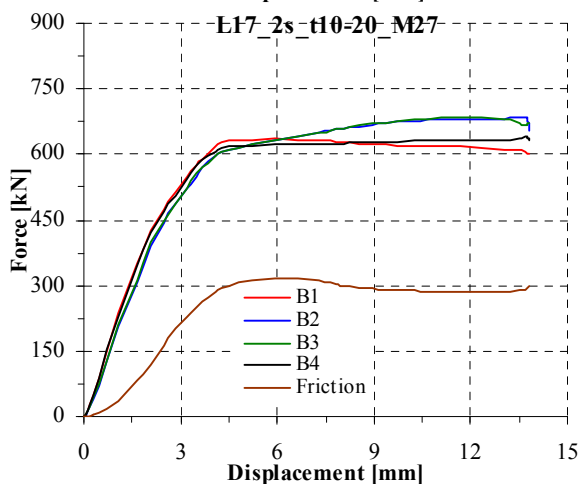
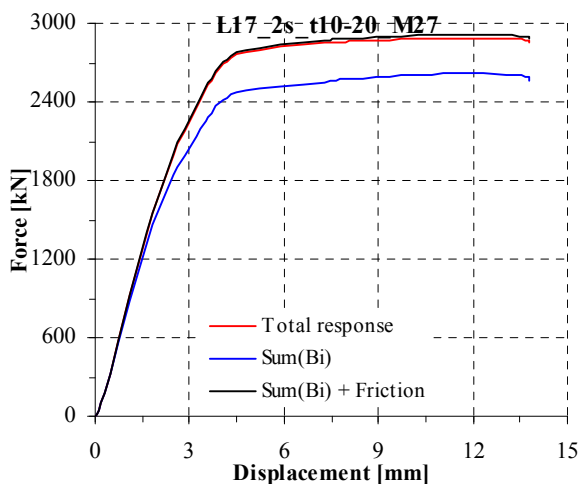
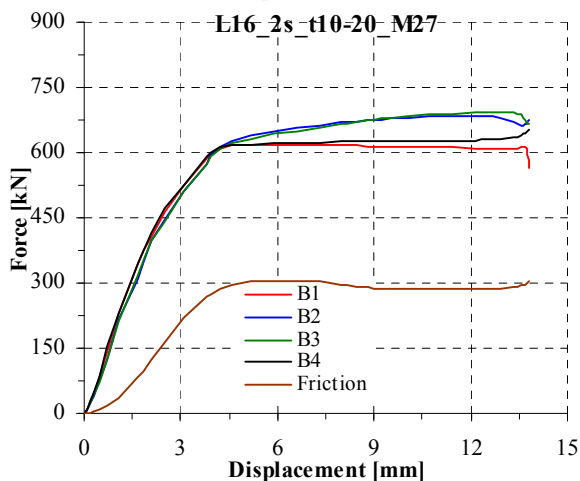
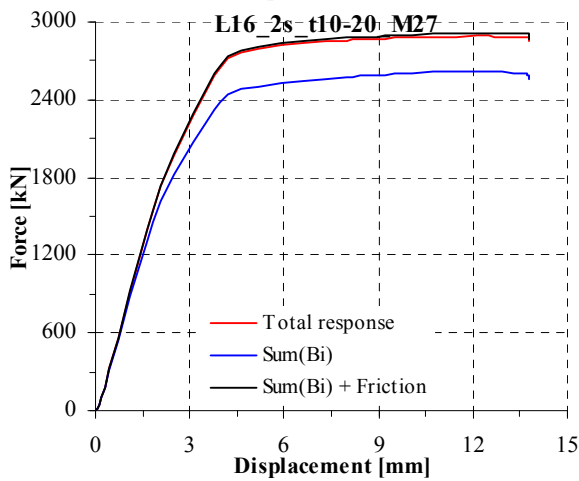
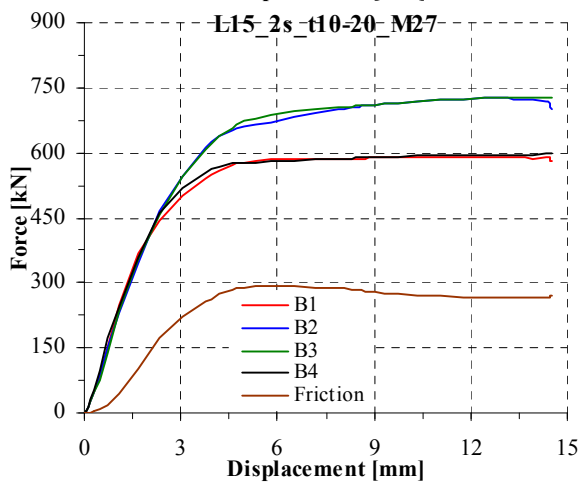
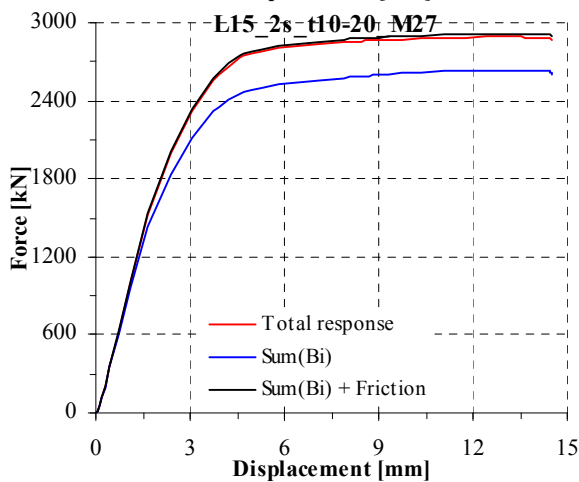
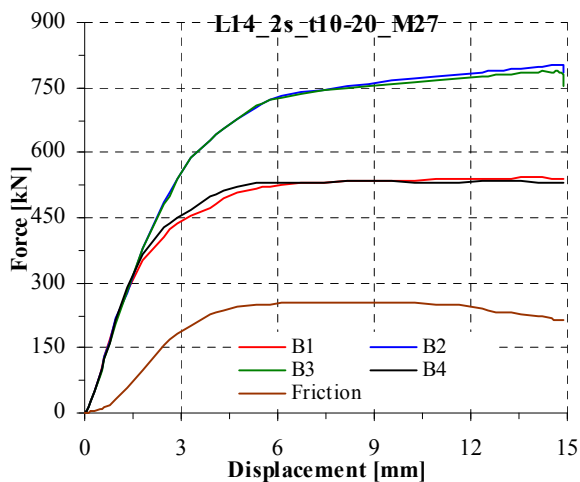
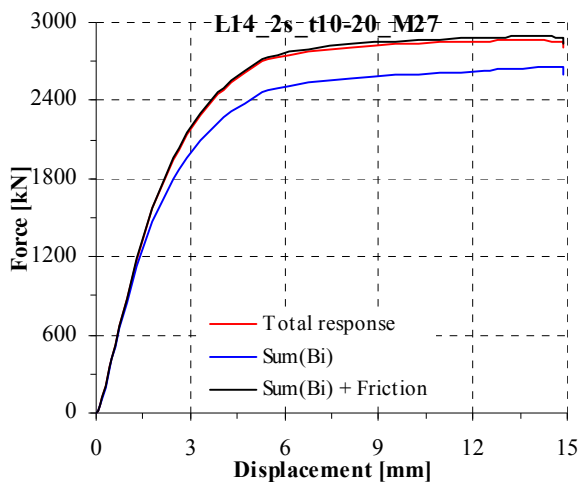
Distribution of forces between bolts and the friction force

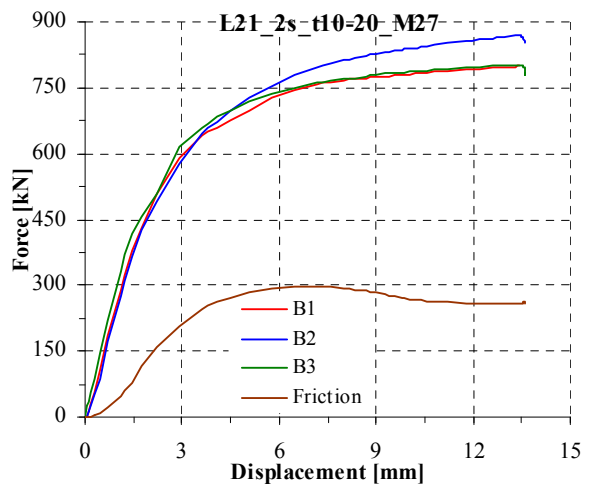
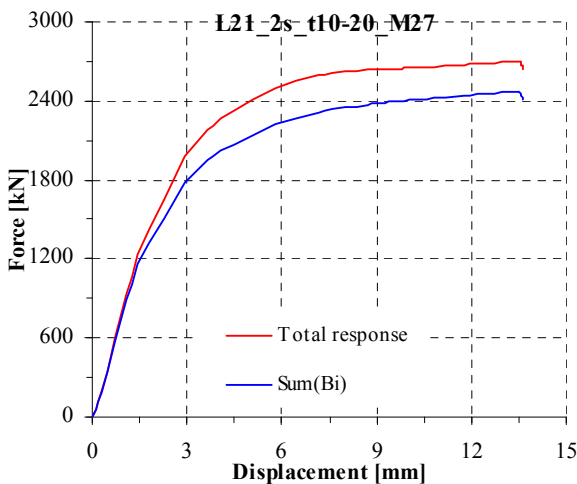
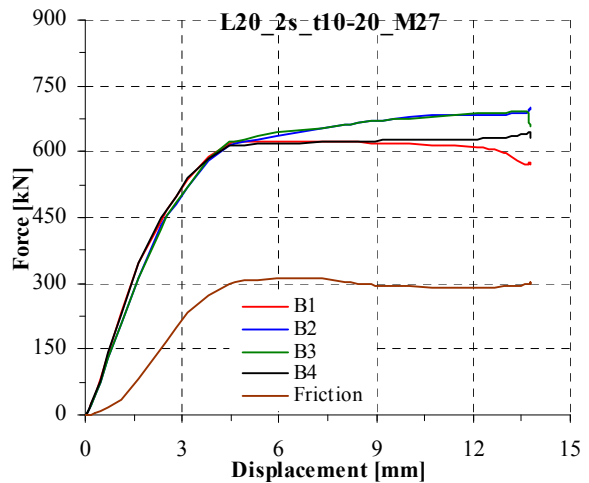
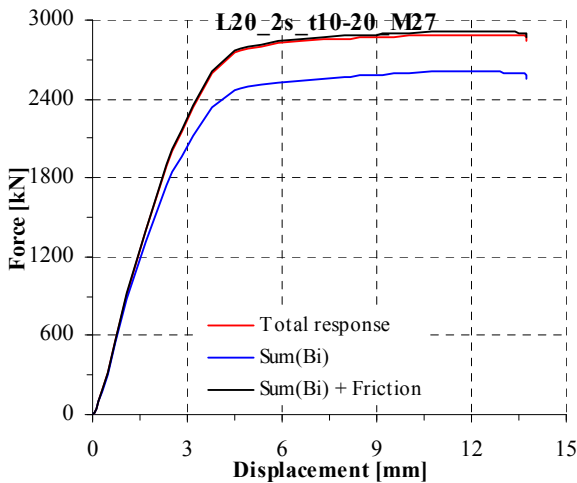
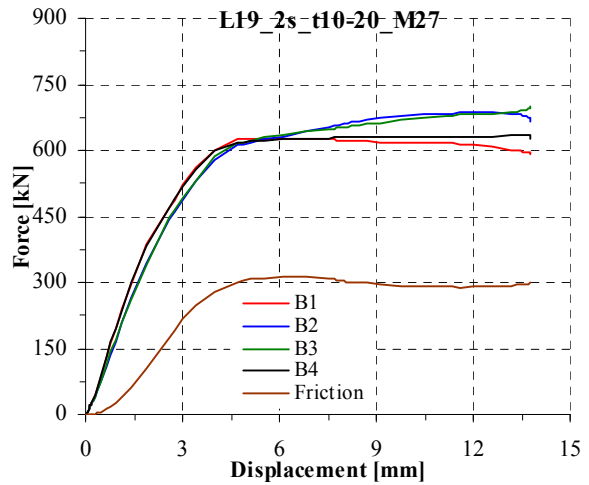
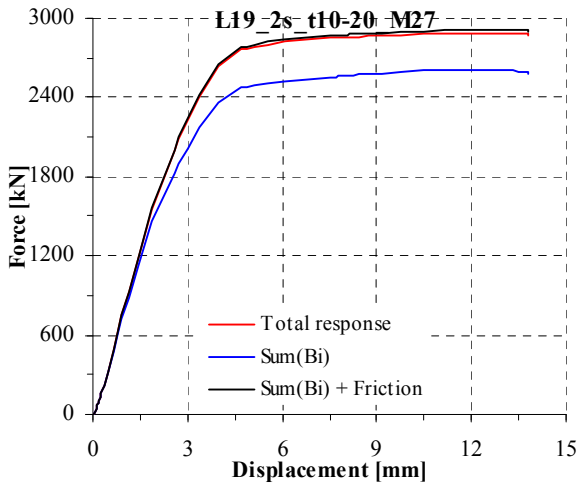
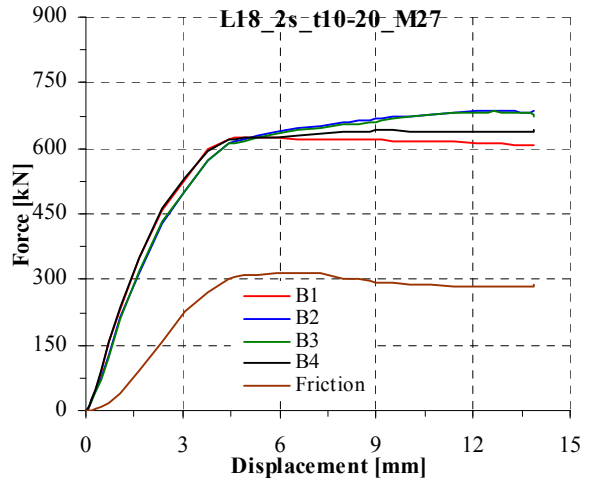
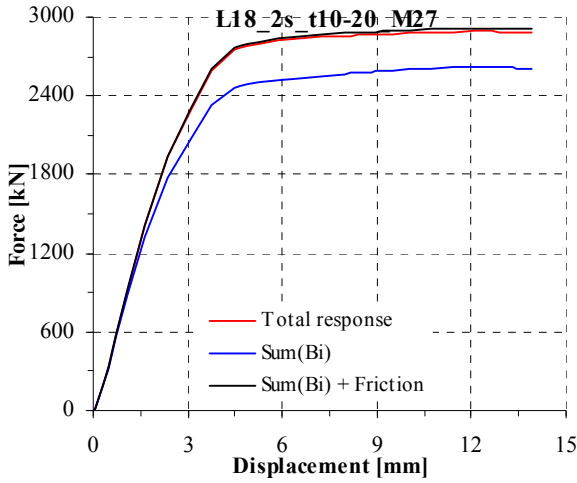




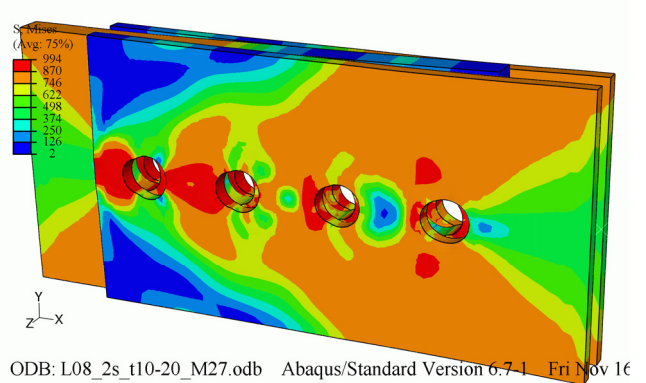
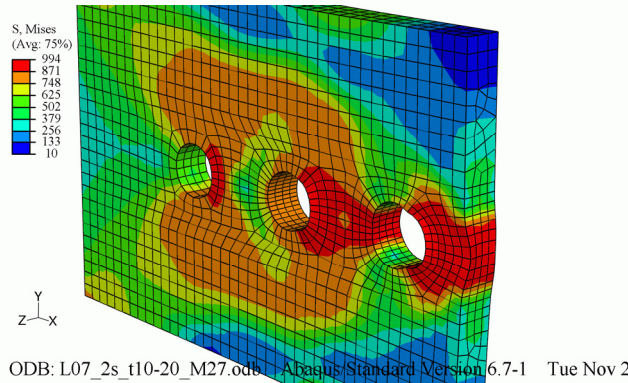
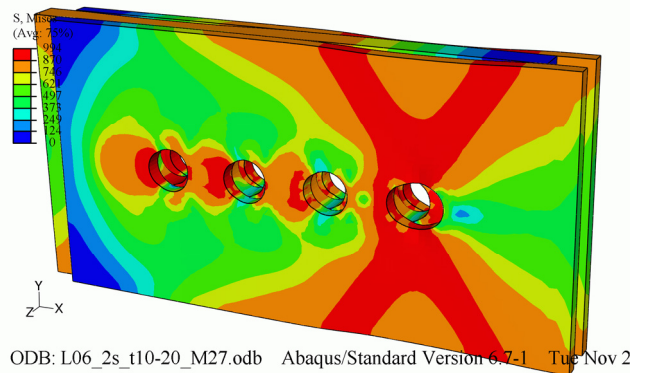
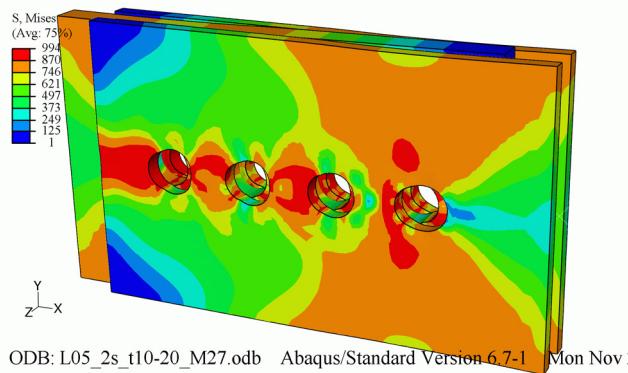
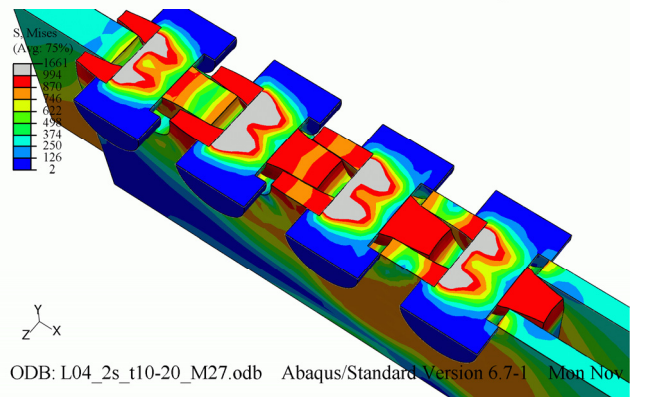
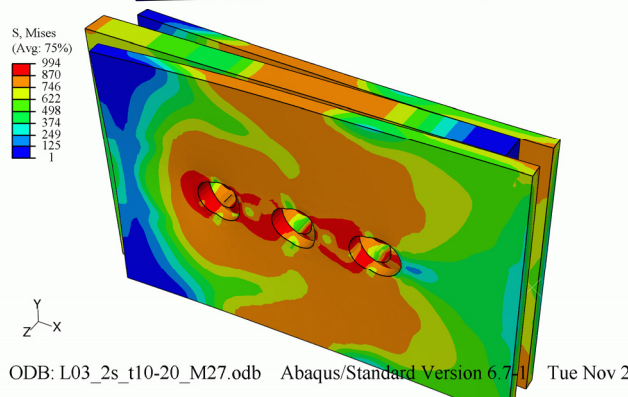
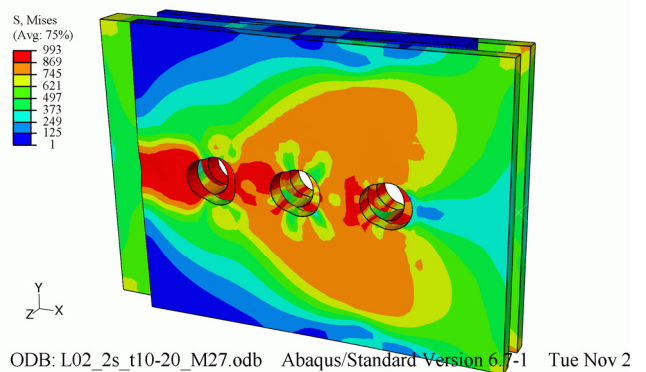
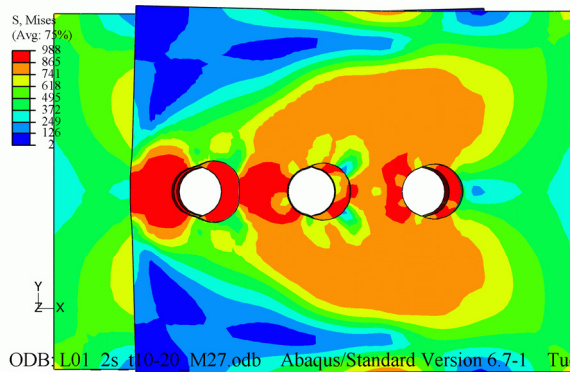


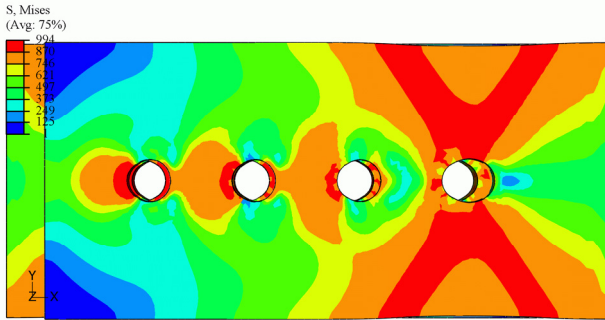




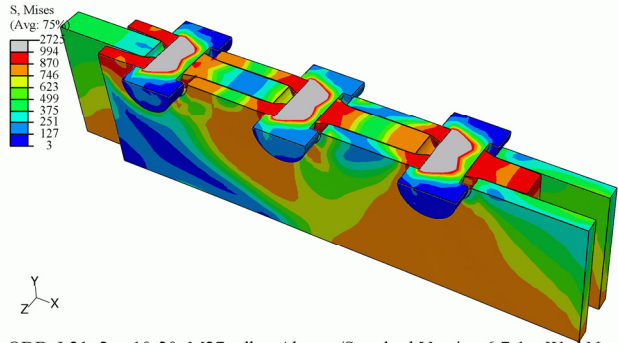


Mises stress on a deformed conbnection. The connection name is displayed on the bottom left side of the figure

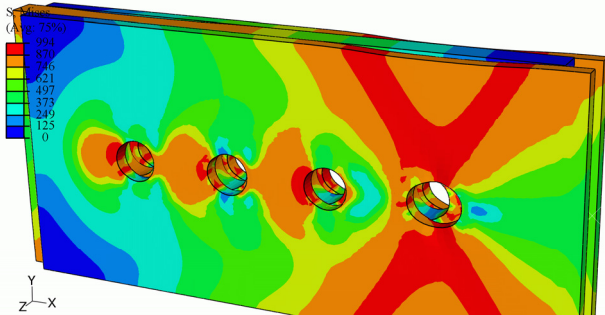




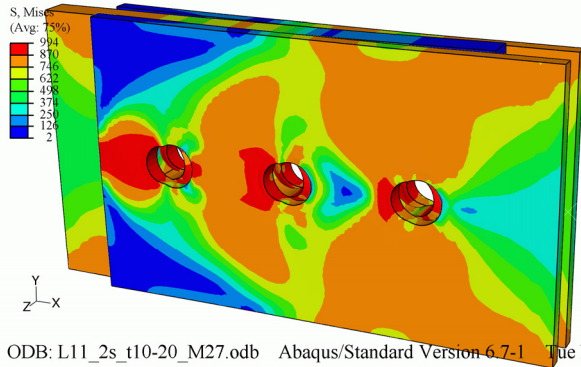
ODB: L09_2s_t10-20_M27.odb Abaqus/Standard Version 6.7-1 Thu Dec 0



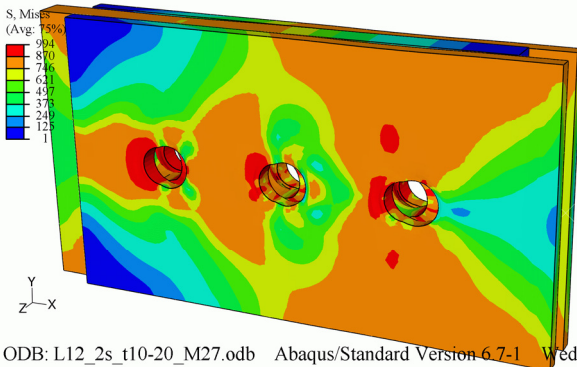
ODB: L21_2s_t10-20_M27.odb Abaqus/Standard Version 6.7-1 Wed Nov :



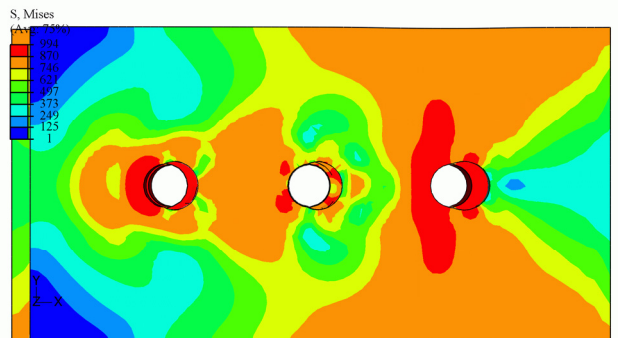
ODB: L10_2s_t10-20_M27.odb Abaqus/Standard Version 6.7-1 Mon Nov :



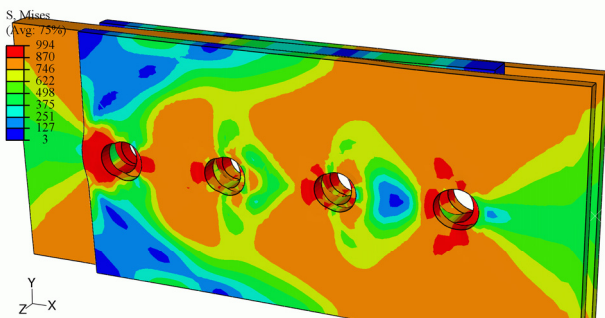
ODB: L11_2s_t10-20_M27.odb Abaqus/Standard Version 6.7-1 Tue Nov 2



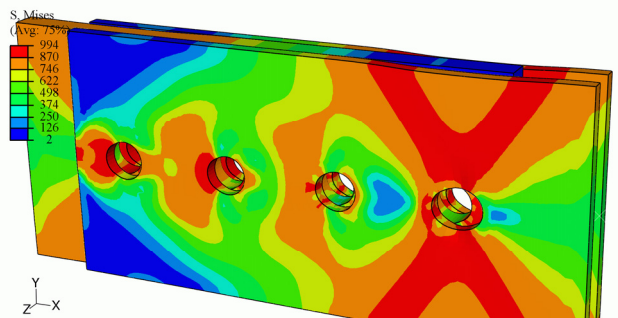
ODB: L12_2s_t10-20_M27.odb Abaqus/Standard Version 6.7-1 Wed Nov :



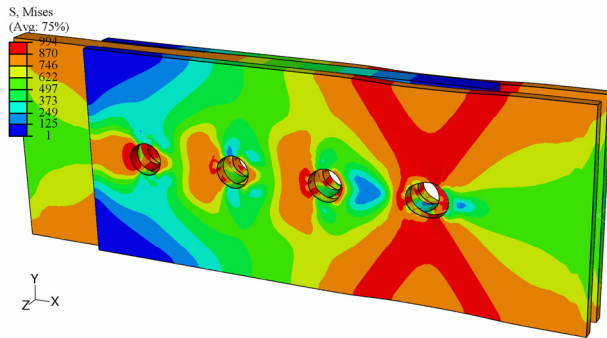
ODB: L13_2s_t10-20_M27.odb Abaqus/Standard Version 6.7-1 Wed Nov :



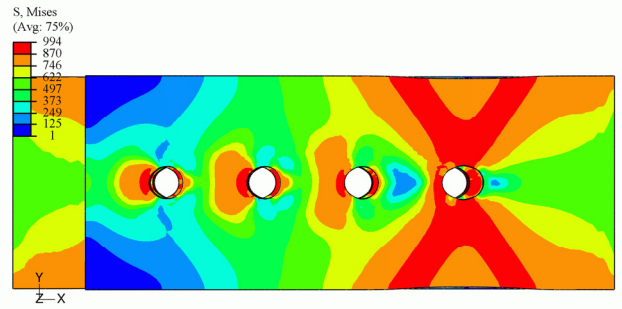
L14_22_t10-20_M27
ODB: L14_2s_t10-20_M27.odb Abaqus/Standard Version 6.7-1 Thu Nov 1



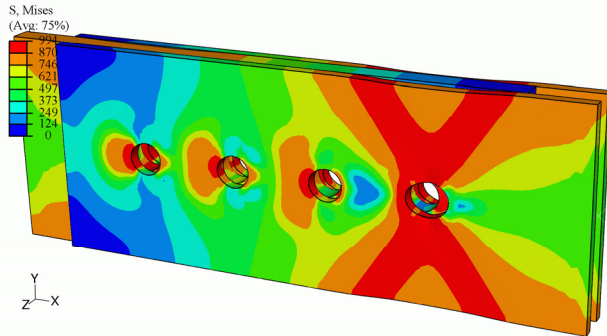
ODB: L15_2s_t10-20_M27.odb Abaqus/Standard Version 6.7-1 Tue Dec 1



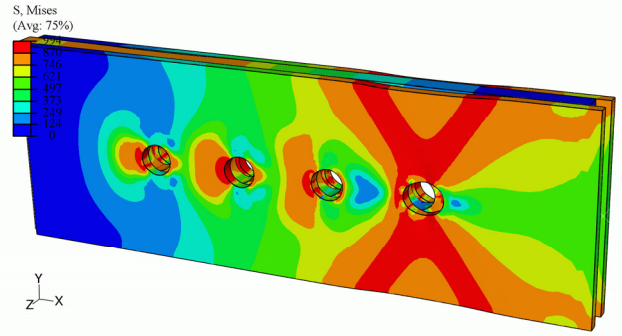
ODB: L16_2s_t10-20_M27.odb Abaqus/Standard Version 6.7-1 Mon Nov 23



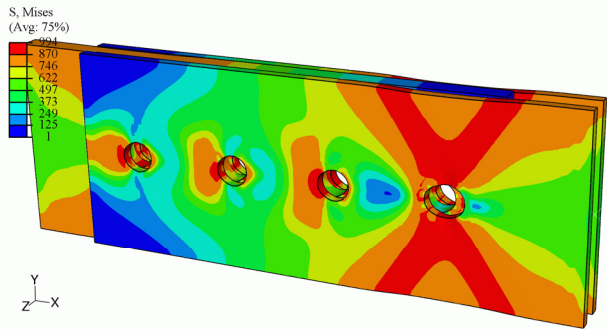
ODB: L17_2s_t10-20_M27.odb Abaqus/Standard Version 6.7-1 Mon Nov 23



ODB: L18_2s_t10-20_M27.odb Abaqus/Standard Version 6.7-1 Fri Nov 23

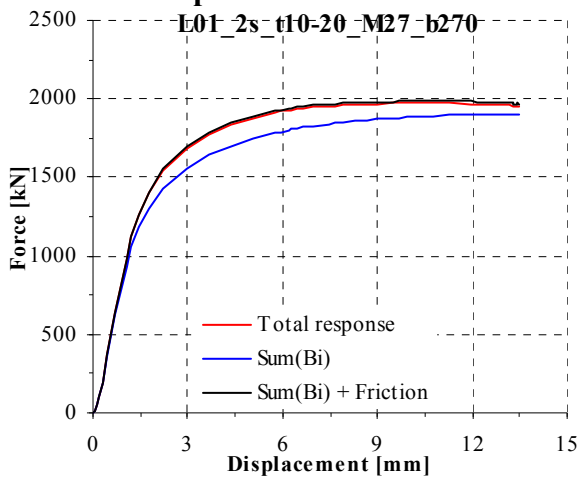


ODB: L19_2s_t10-20_M27.odb Abaqus/Standard Version 6.7-1 Mon Dec 1

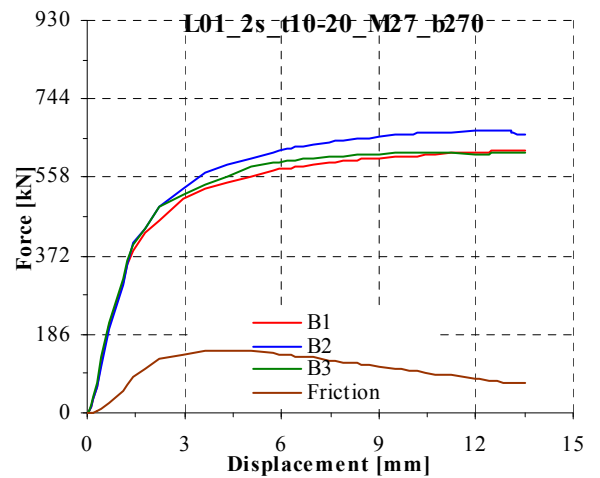


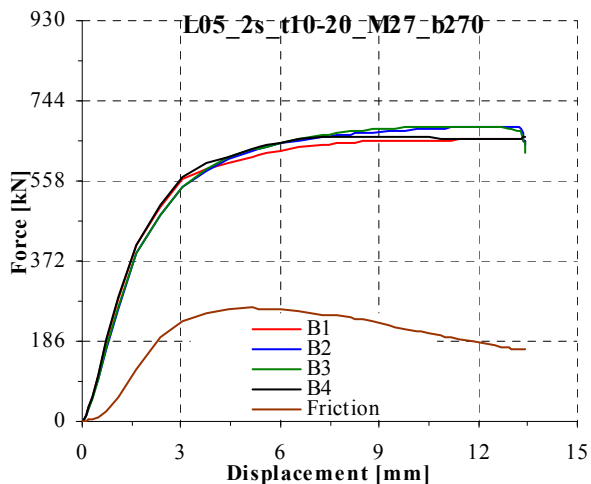
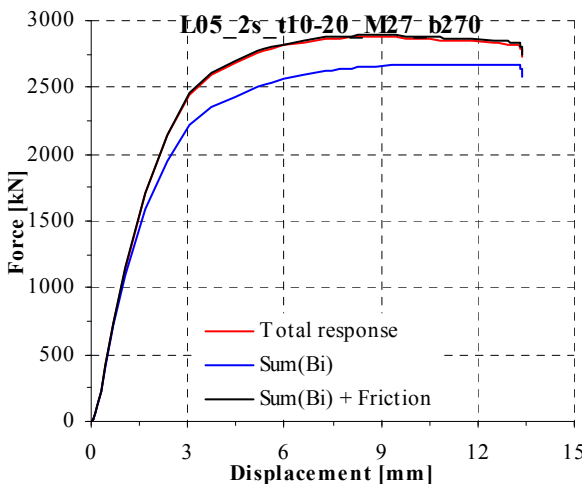
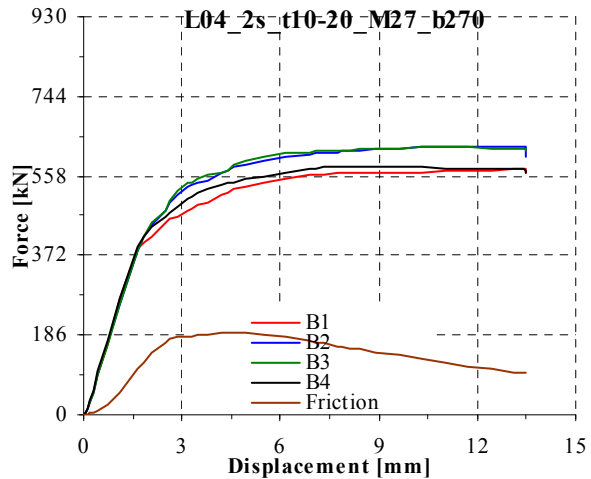
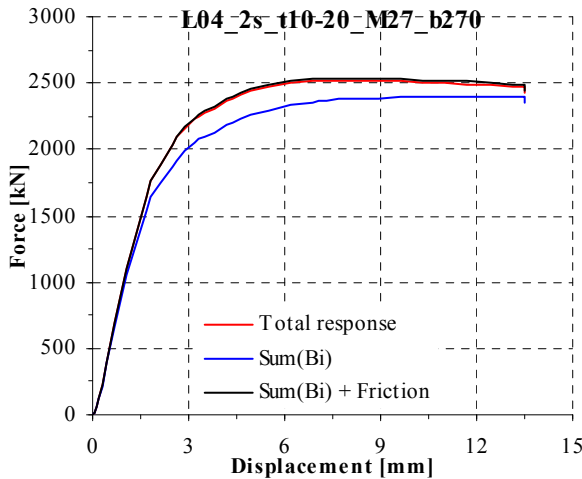
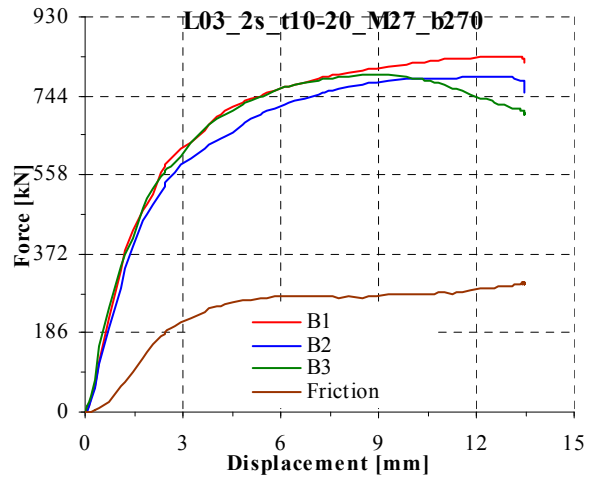
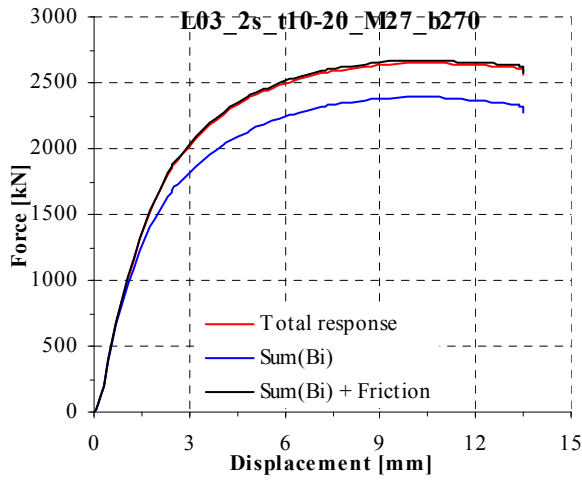
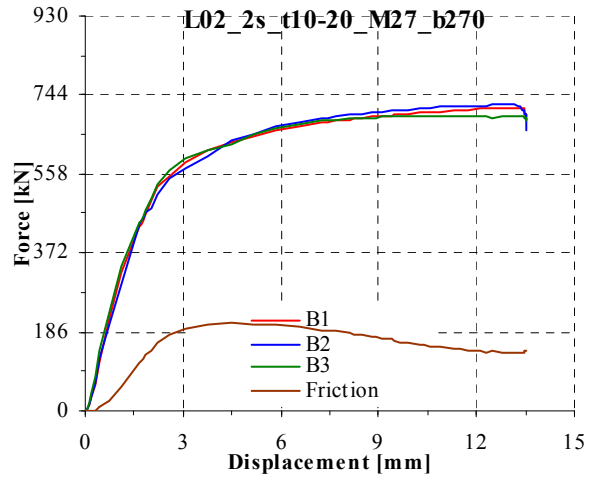
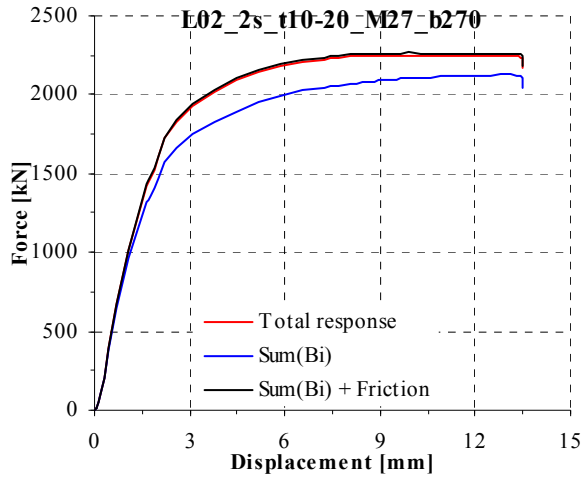
ODB: L20_2s_t10-20_M27.odb Abaqus/Standard Version 6.7-1 Tue Dec 1

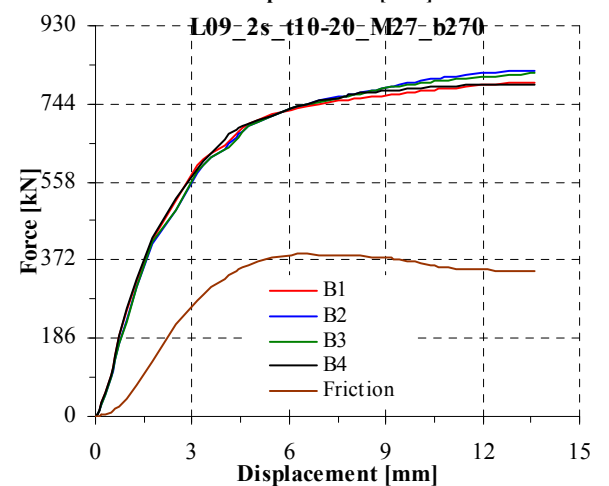
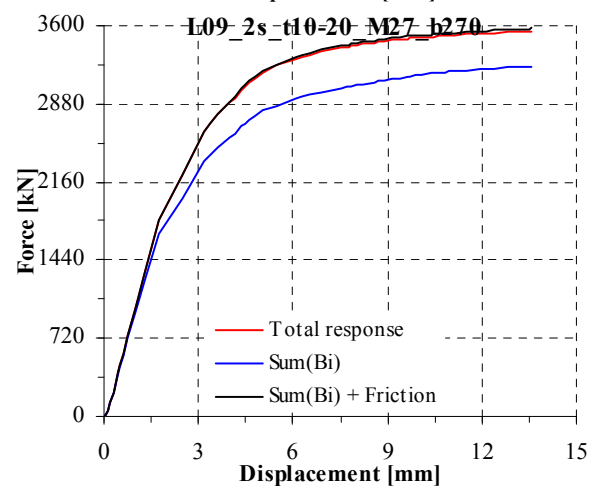
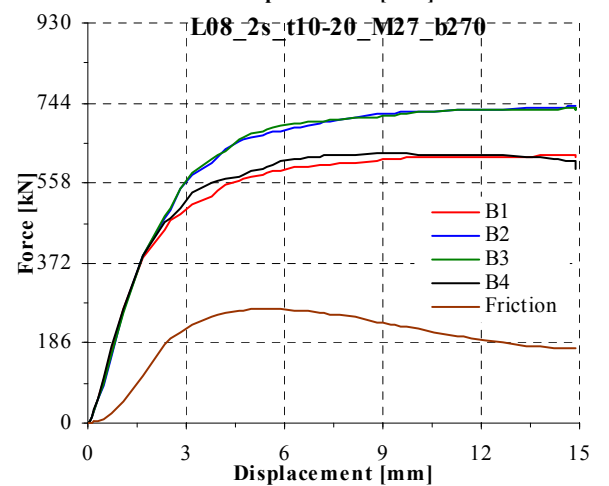
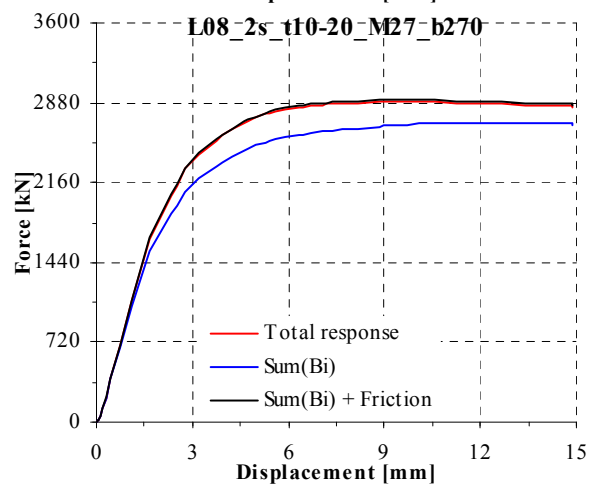
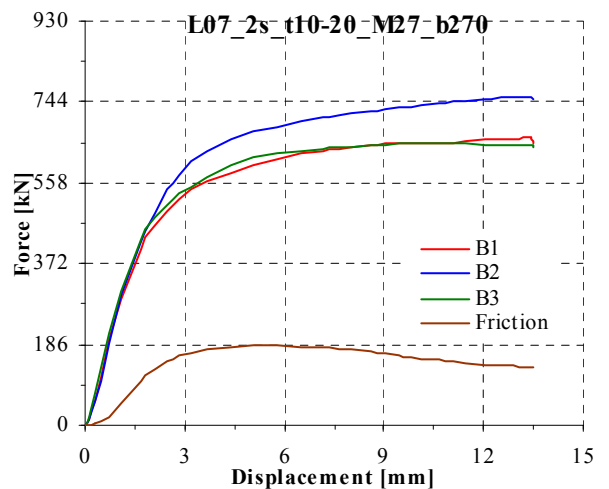
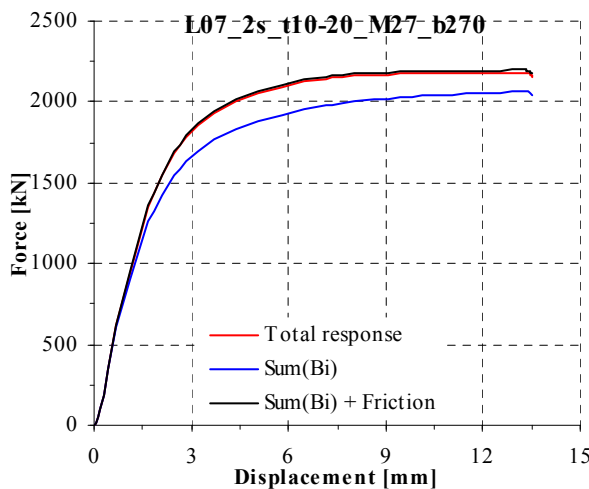
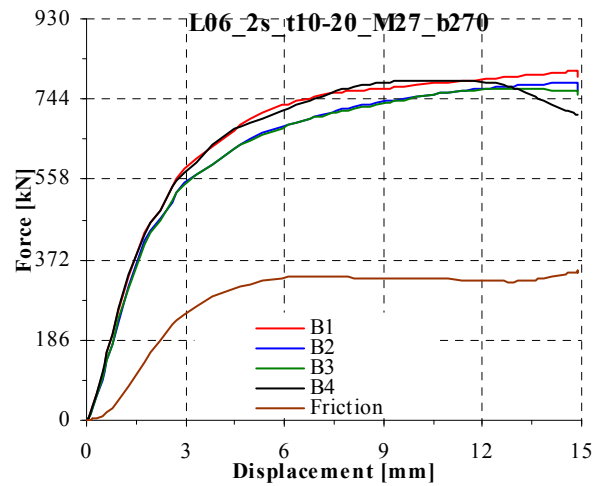
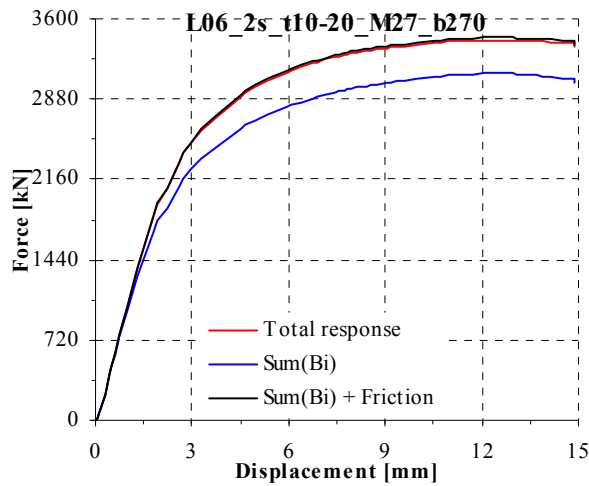
Lxx_2s_t10-20_M27_b270; Numerical model type M3; 21 FE analyses
Experimental and numerical load-displacement curves

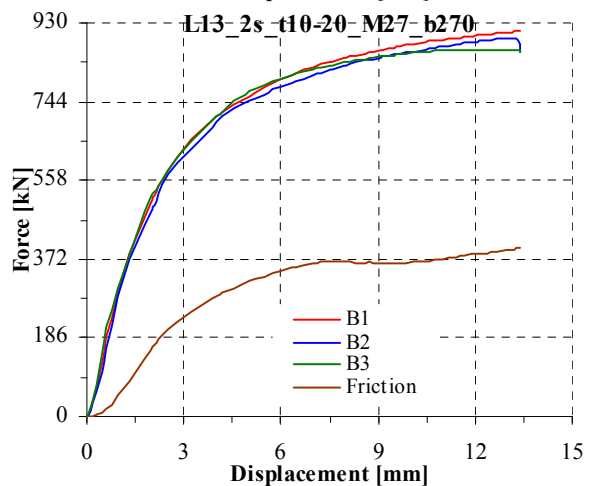
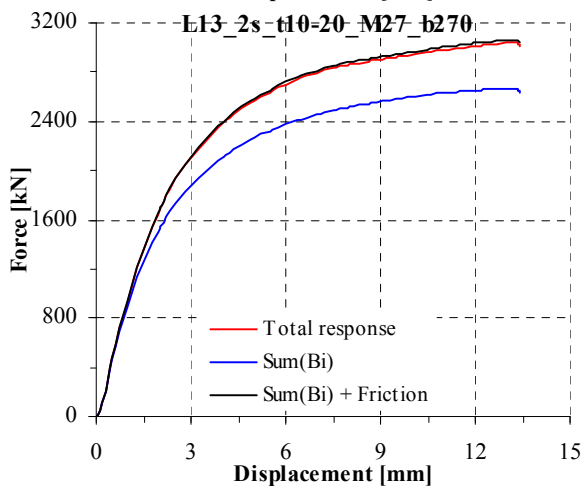
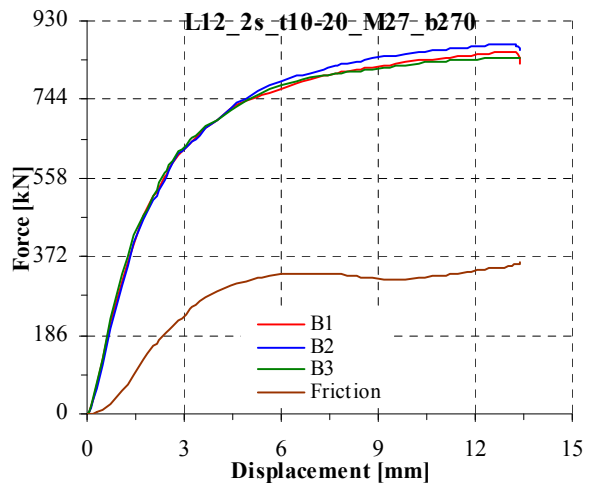
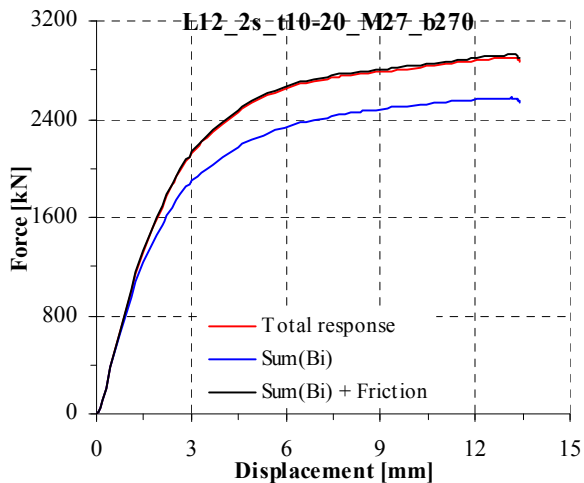
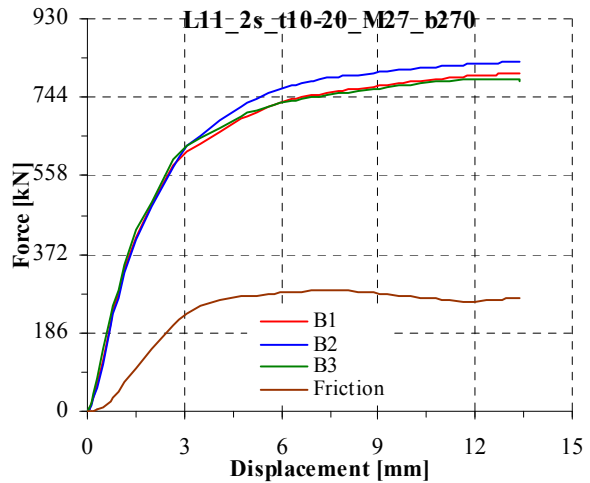
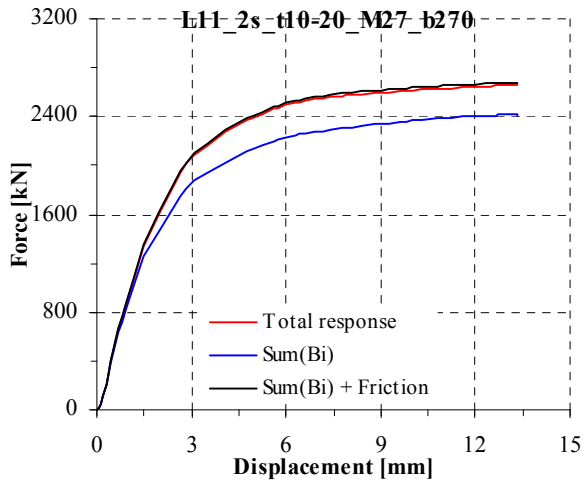
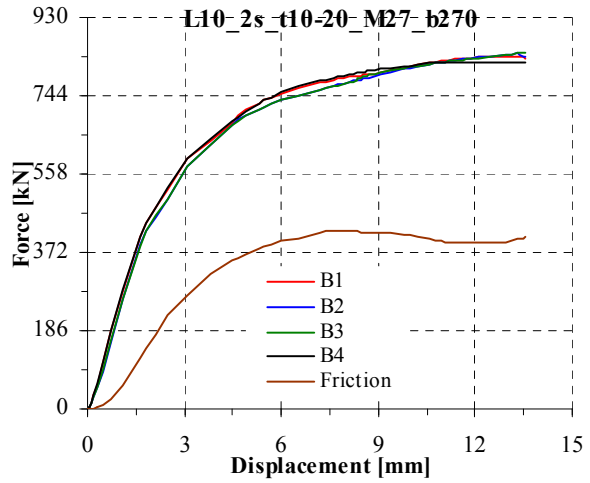
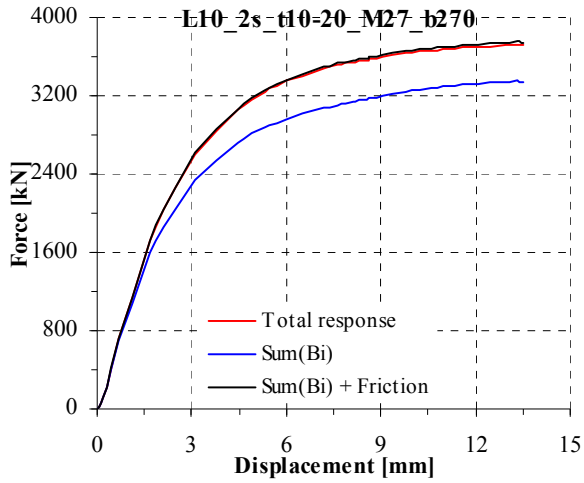


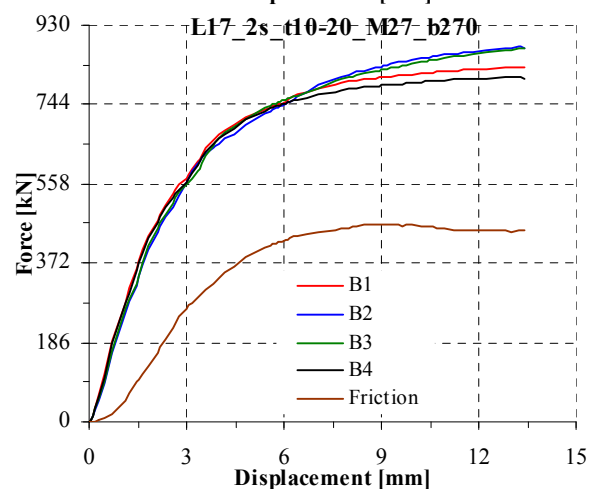
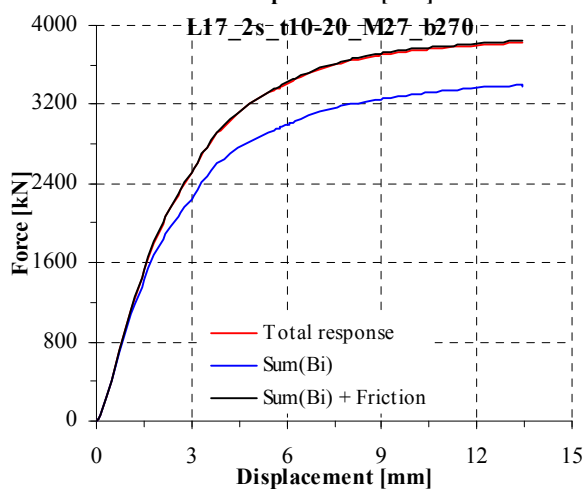
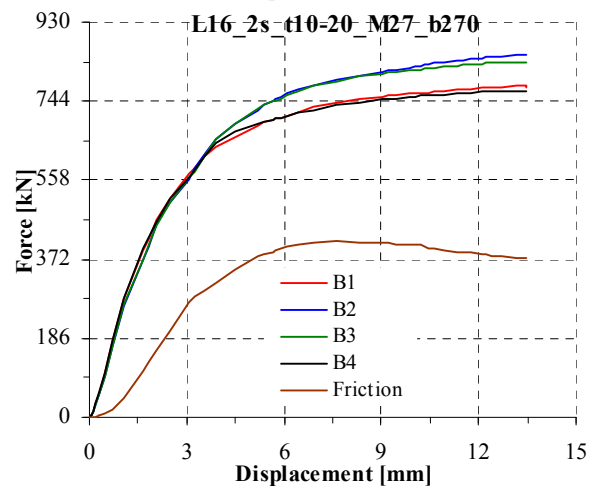
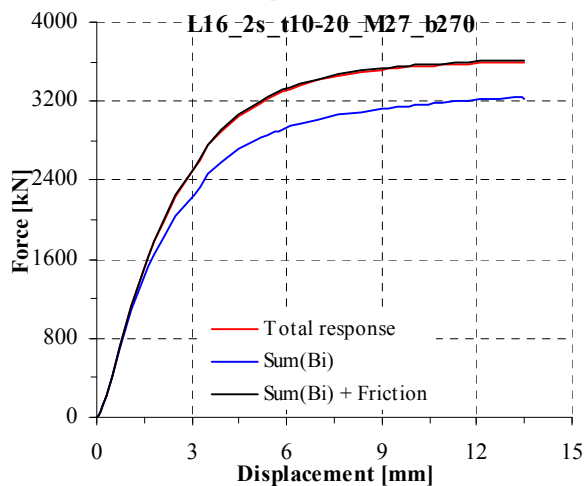
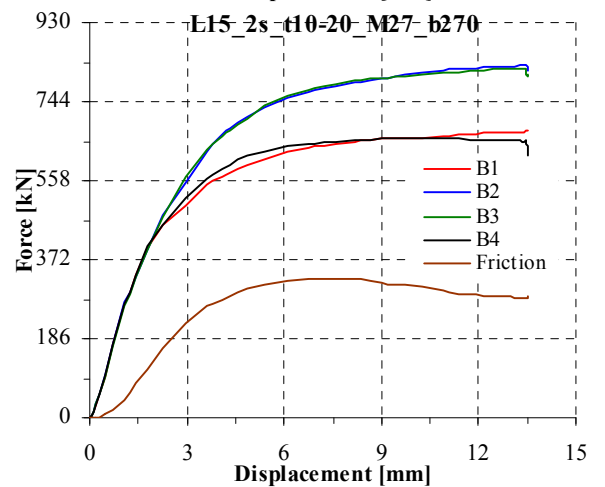
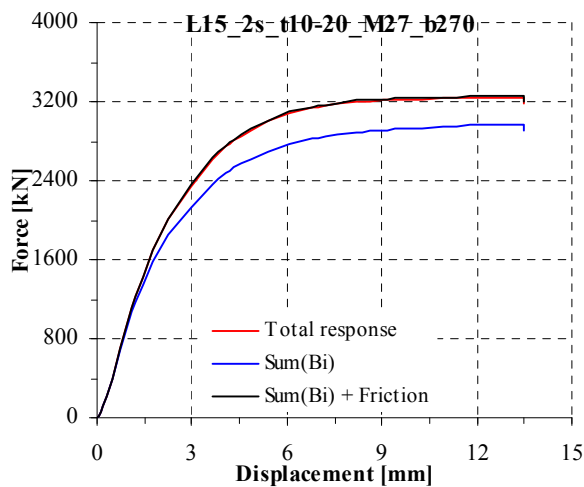
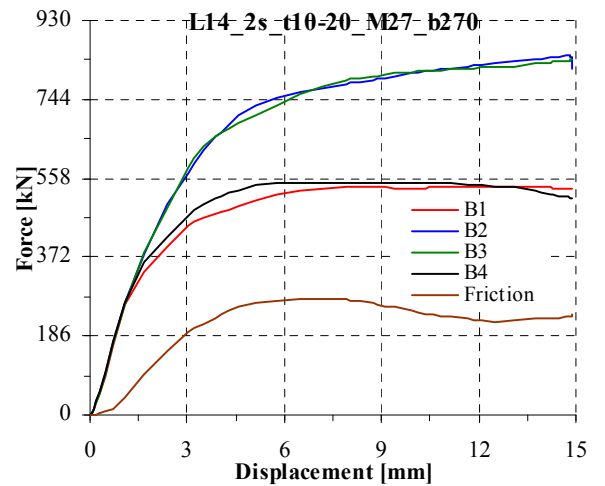
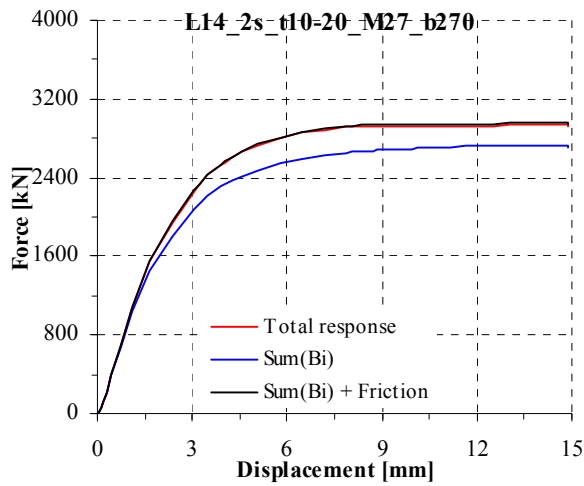
Distribution of forces between bolts and the friction force

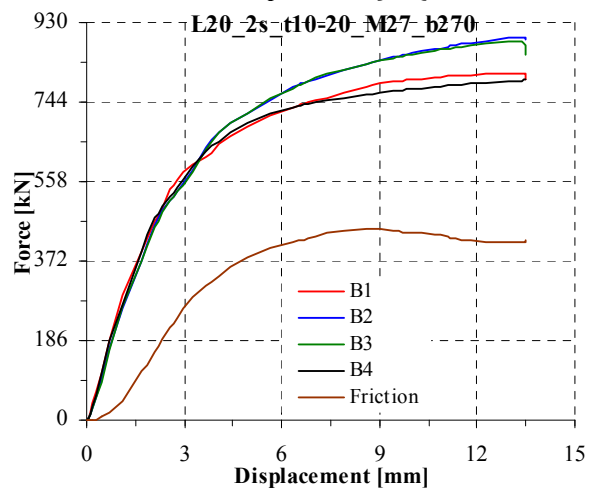
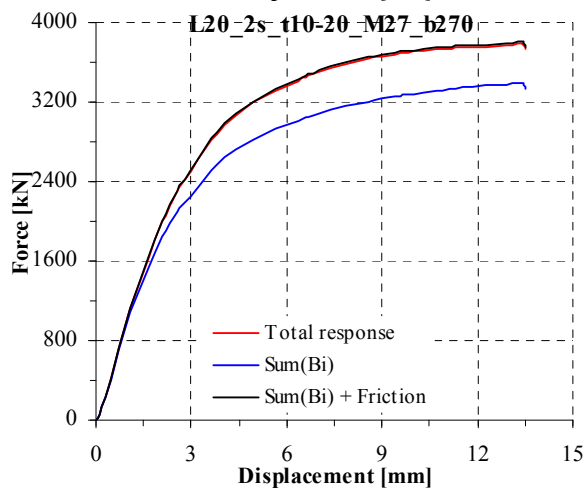
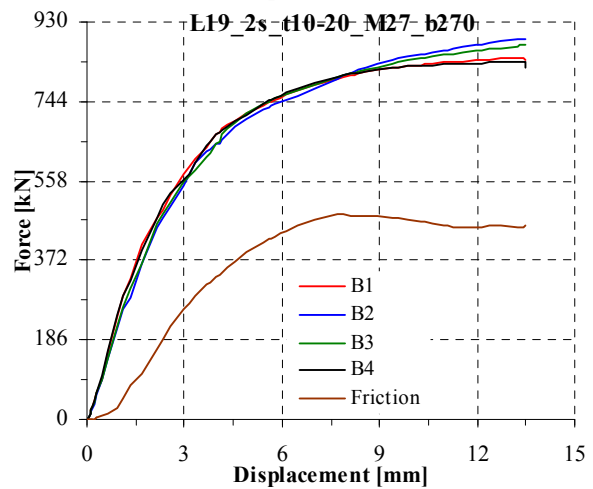
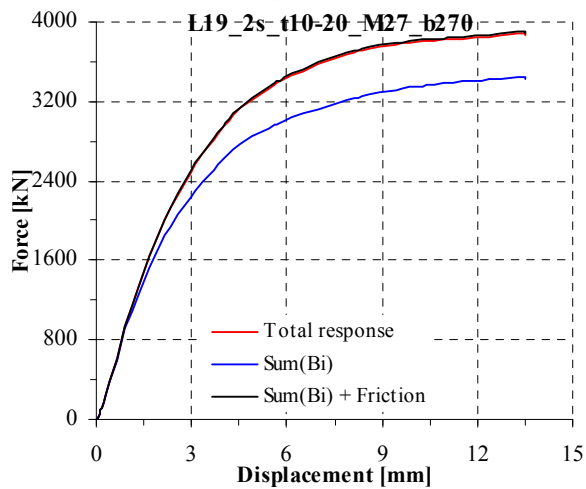
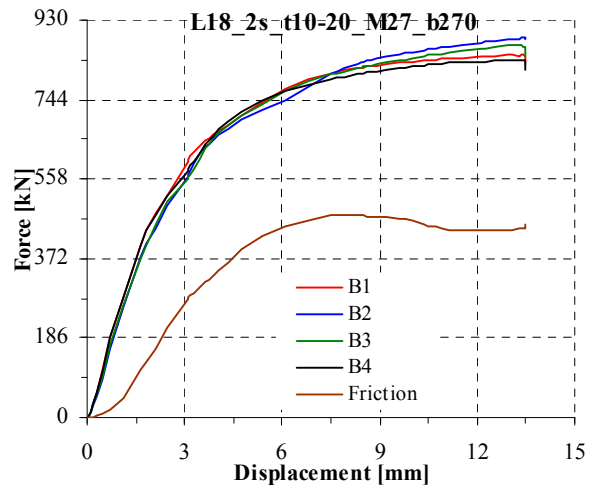
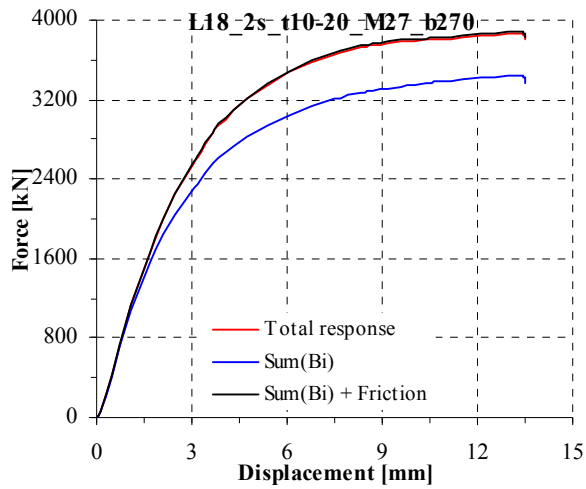


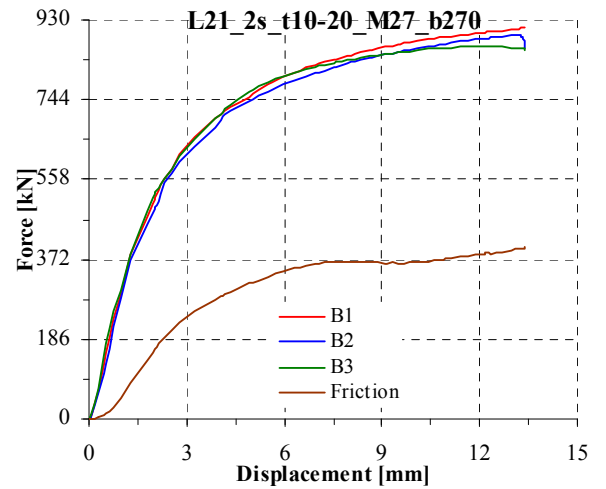
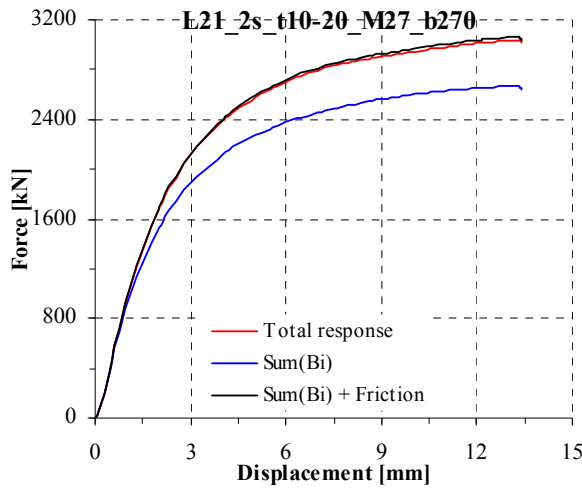




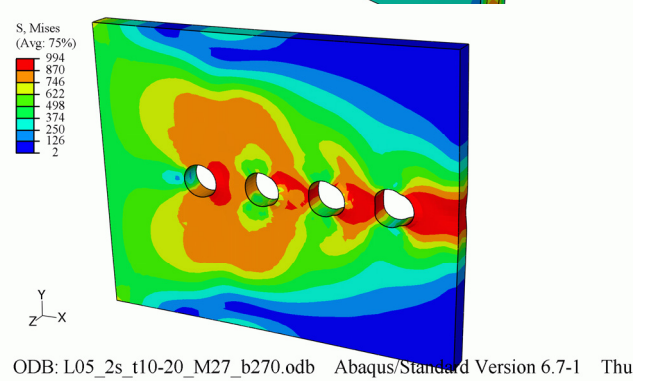
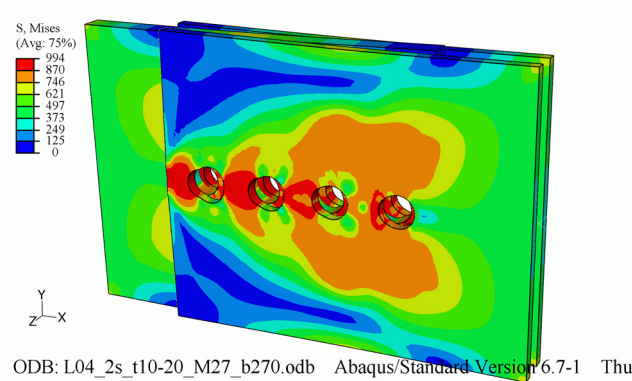
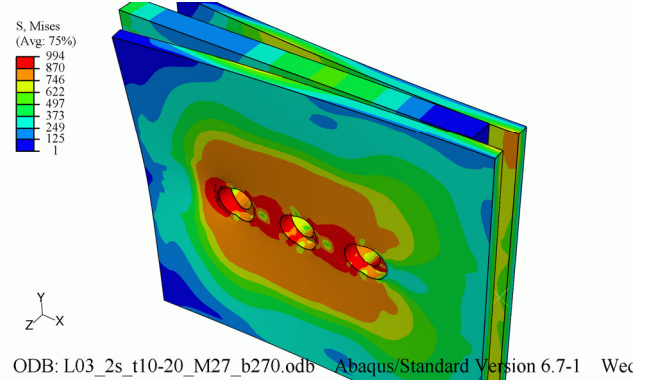
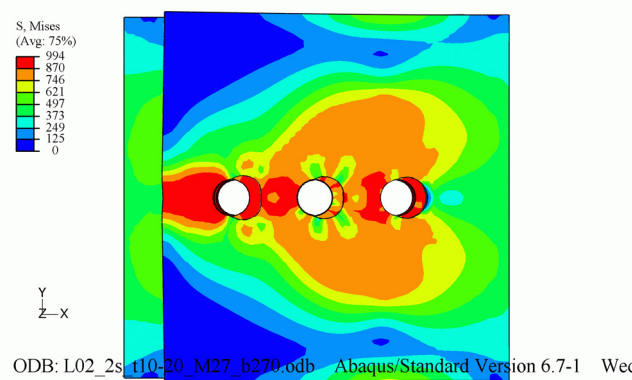
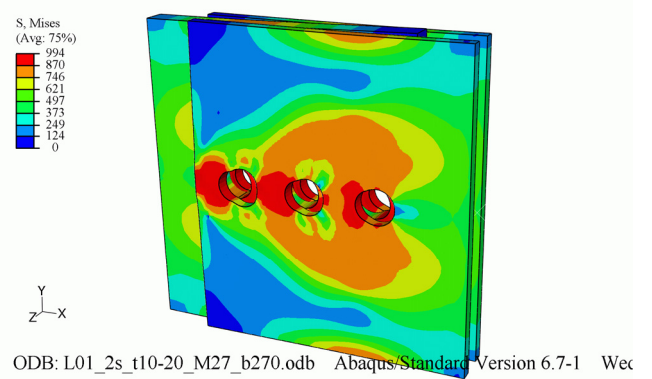
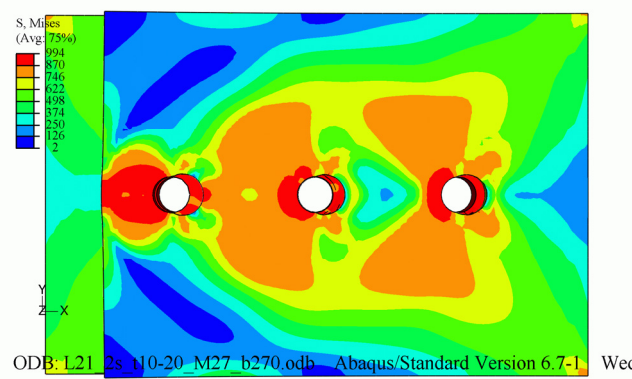


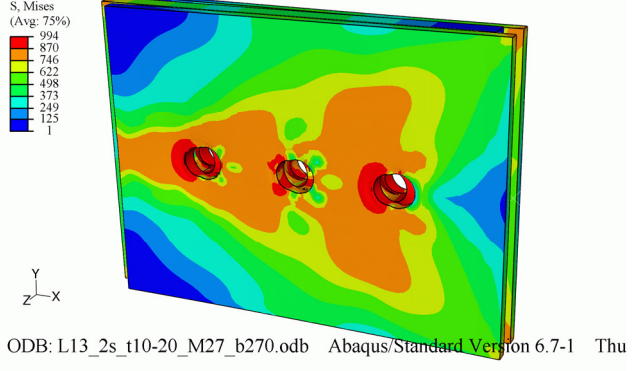
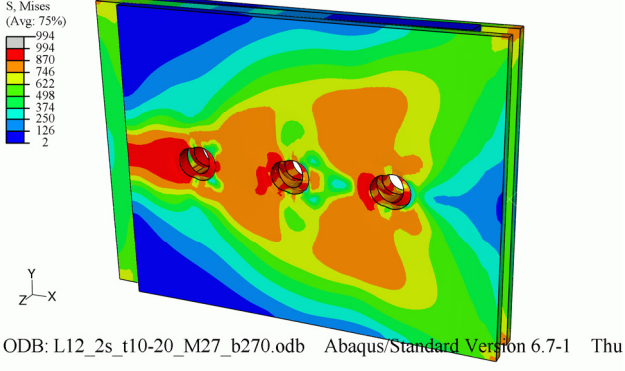
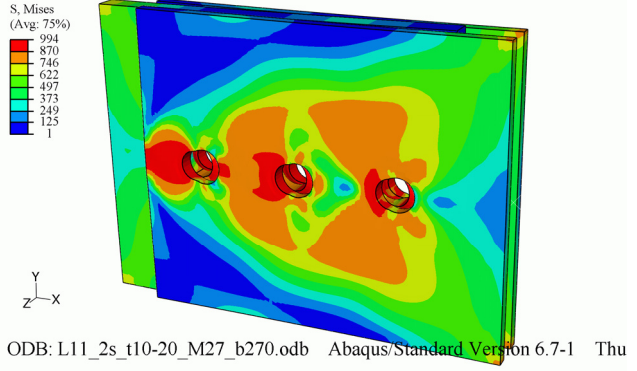
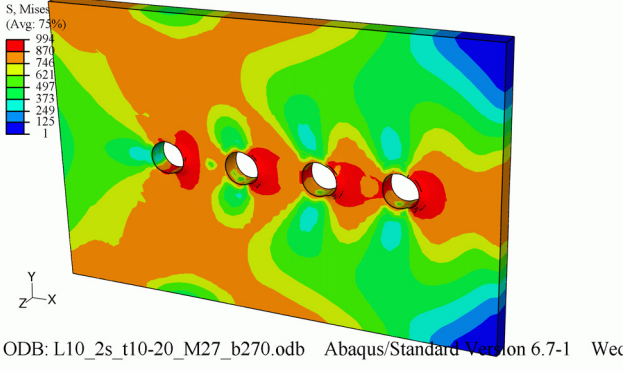
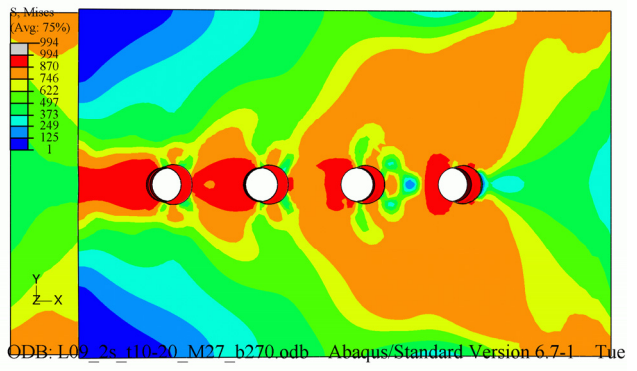
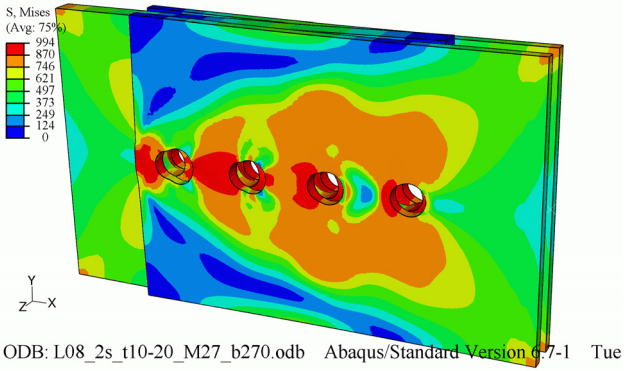
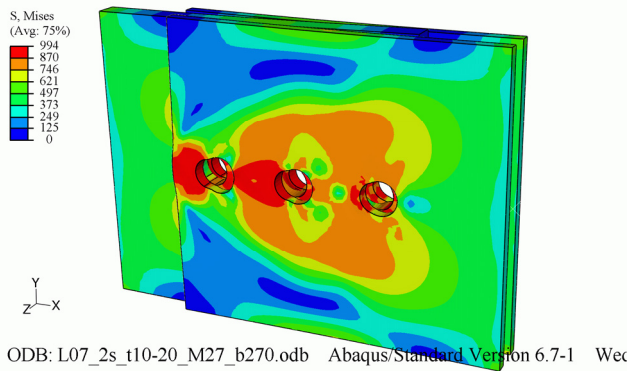
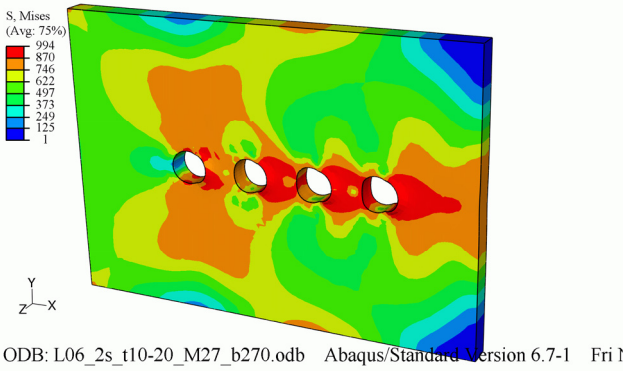


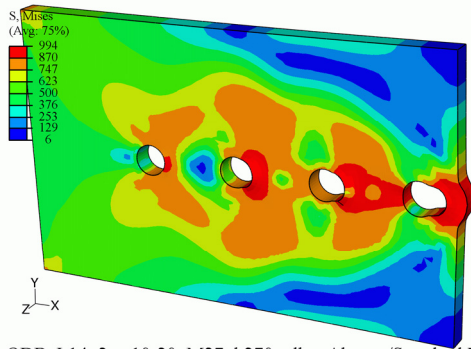




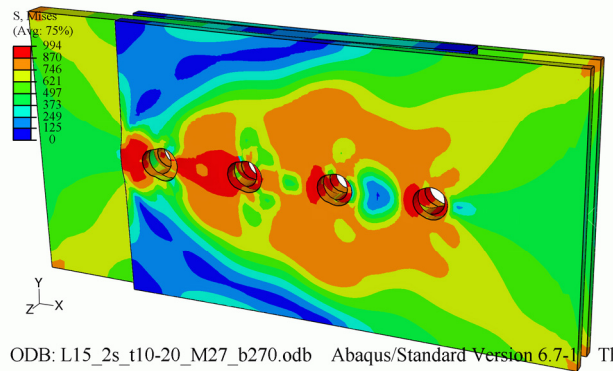
Mises stress on a deformed connection. The connection name is displayed on the bottom left side of the figure



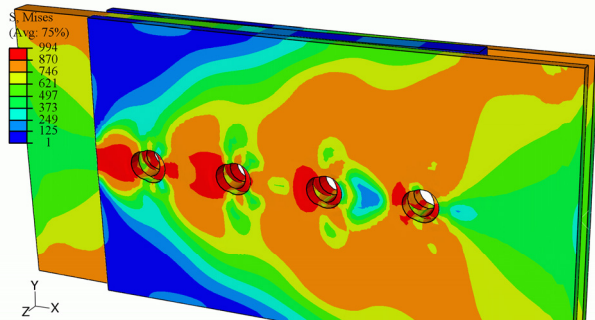




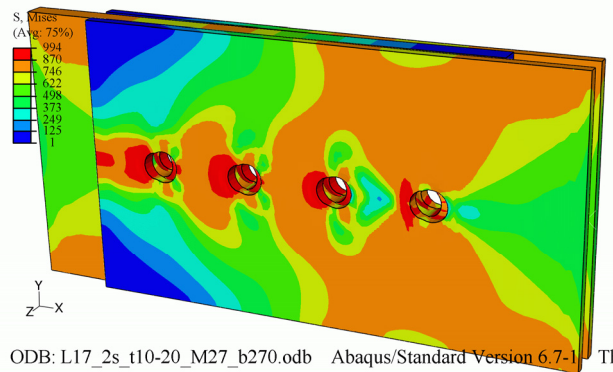
ODB: L14_2s_t10-20_M27_b270.odb Abaqus/Standard Version 6.7-1 Wec



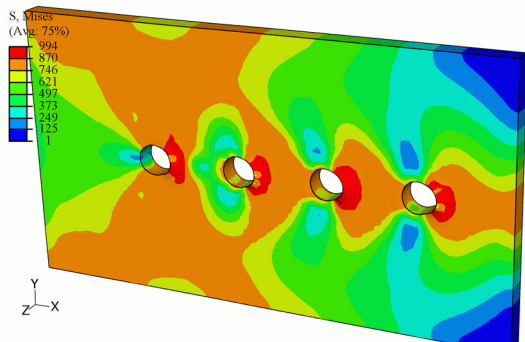
ODB: L15_2s_t10-20_M27_b270.odb Abaqus/Standard Version 6.7-1 Thu



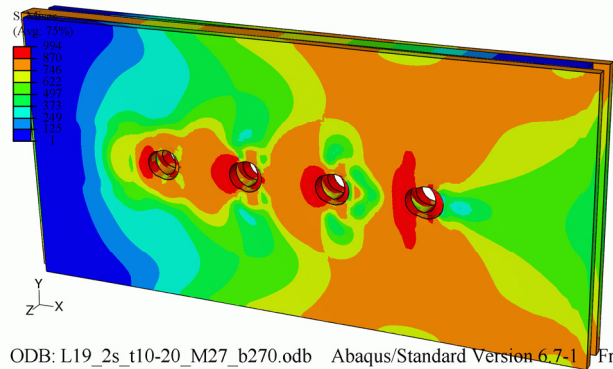
ODB: L16_2s_t10-20_M27_b270.odb Abaqus/Standard Version 6.7-1 Thu



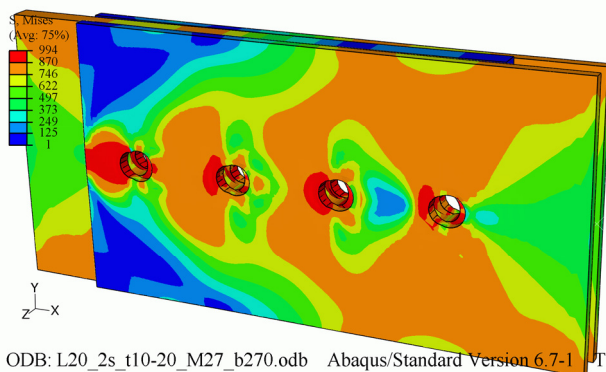
ODB: L17_2s_t10-20_M27_b270.odb Abaqus/Standard Version 6.7-1 Thu



ODB: L18_2s_t10-20_M27_b270.odb Abaqus/Standard Version 6.7-1 Mon



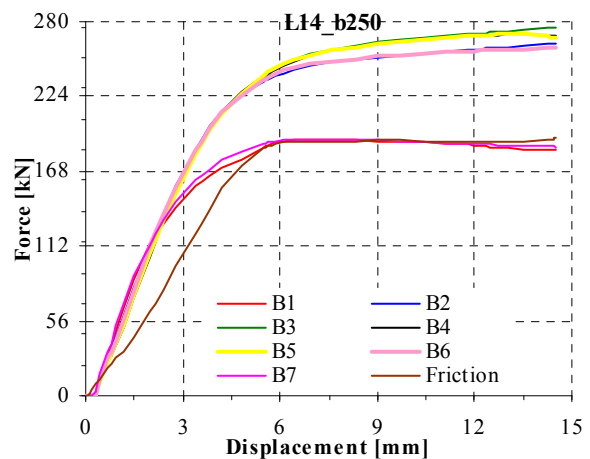
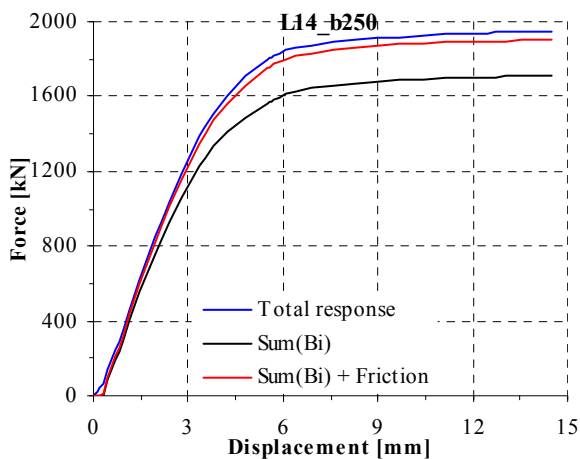
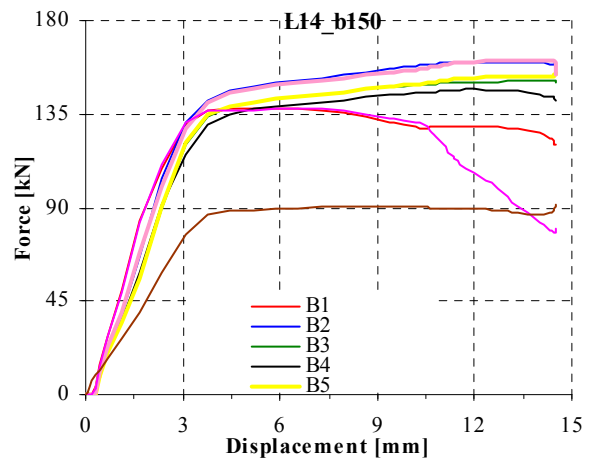
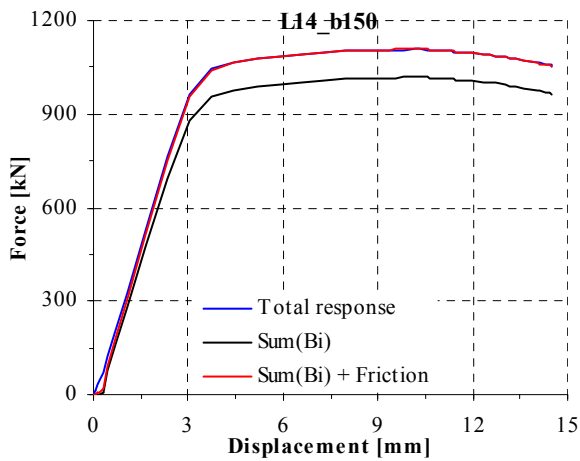
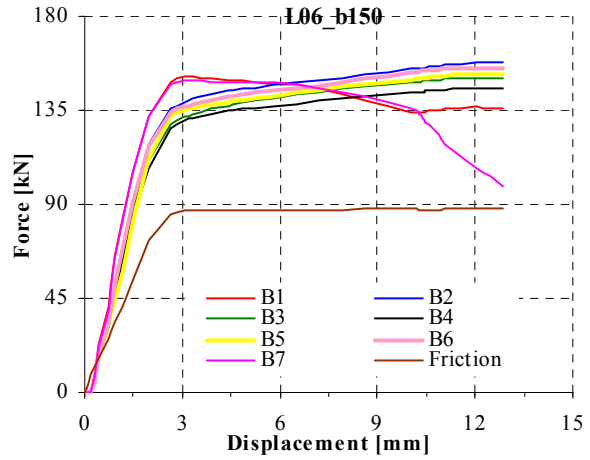
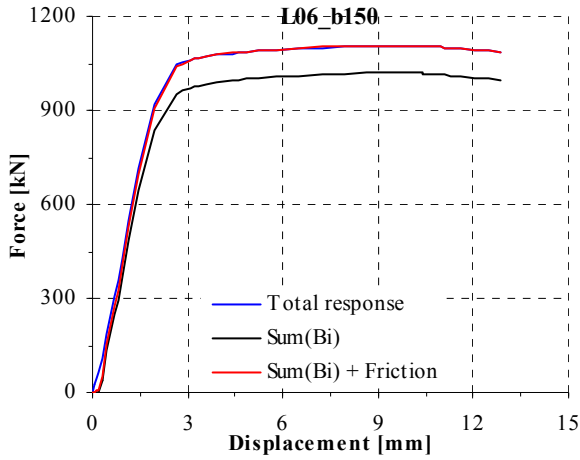
ODB: L19_2s_t10-20_M27_b270.odb Abaqus/Standard Version 6.7-1 Fri

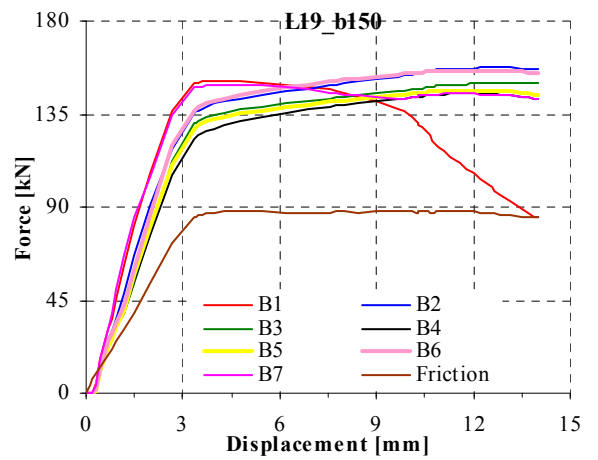
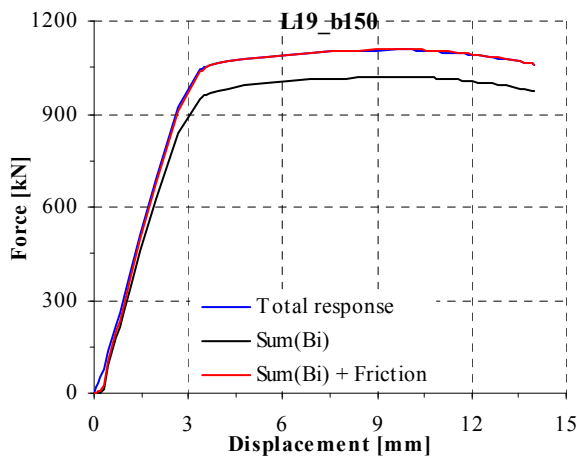
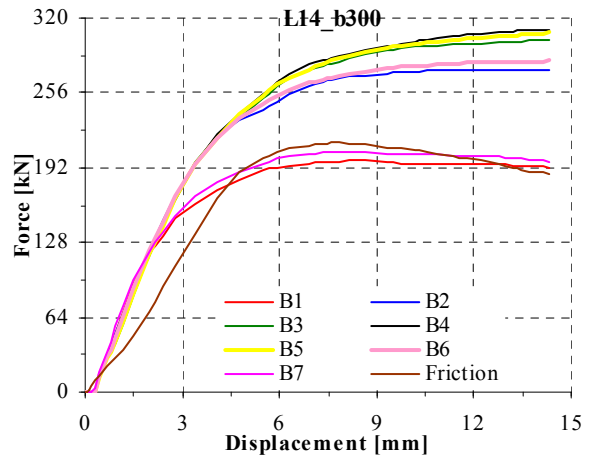
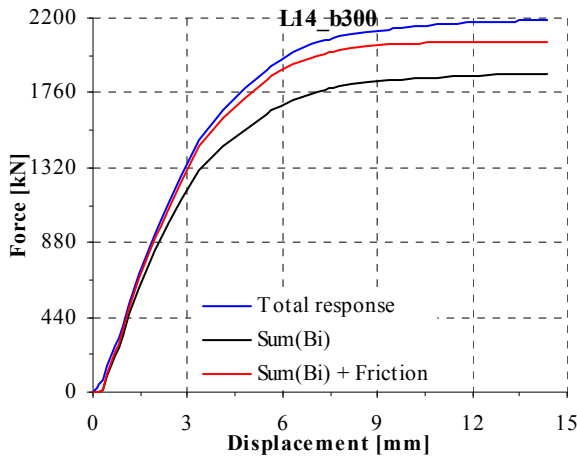


ODB: L20_2s_t10-20_M27_b270.odb Abaqus/Standard Version 6.7-1 Tue

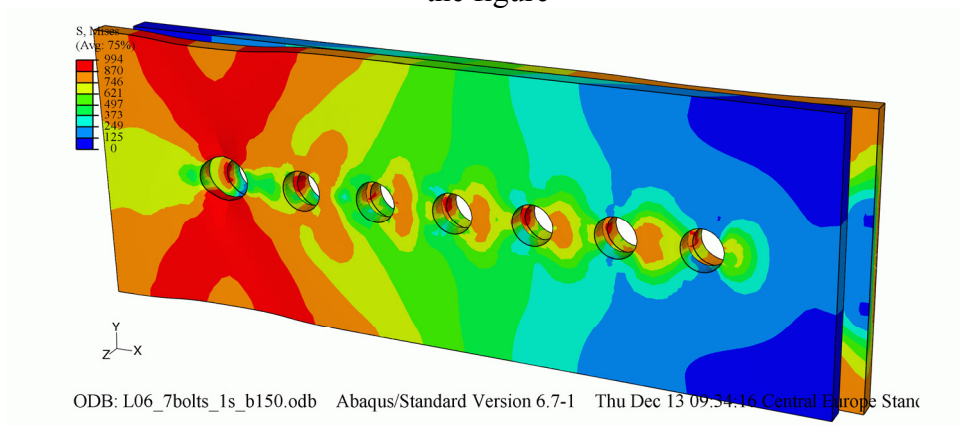
Lxx_7bolts_1s_bxxx; Numerical model type M3; 5 FE analyses
Experimental and numerical load-displacement curves

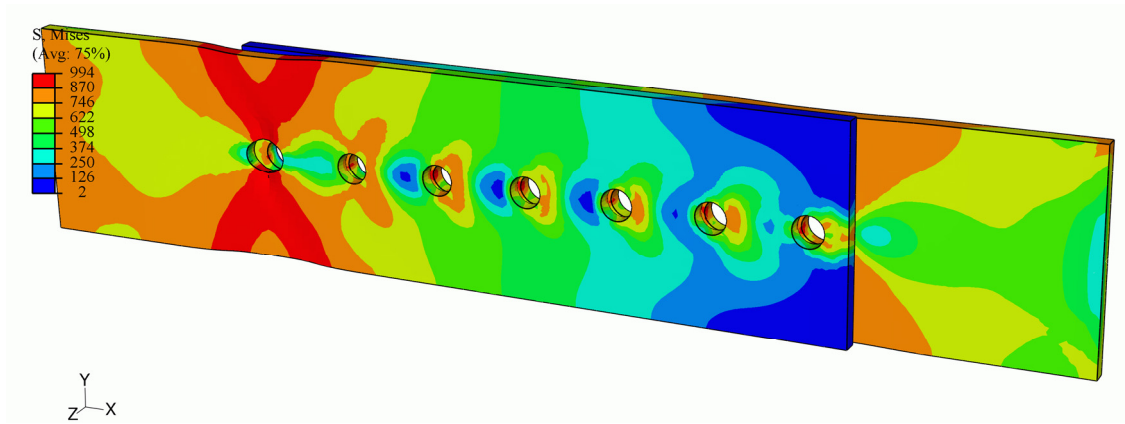
Distribution of forces between bolts and the friction force



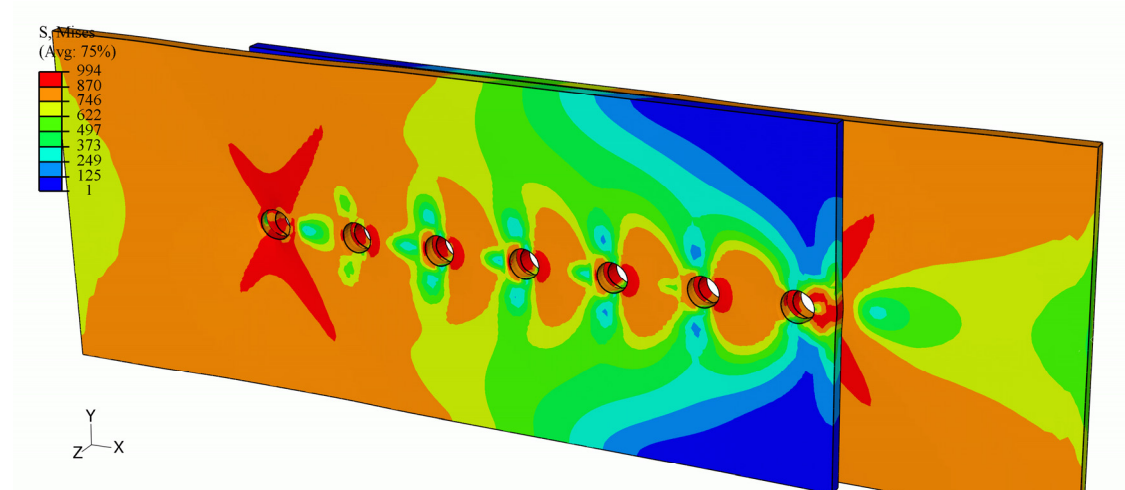


Mises stress on a deformed connection. The connection name is displayed on the bottom left side of the figure

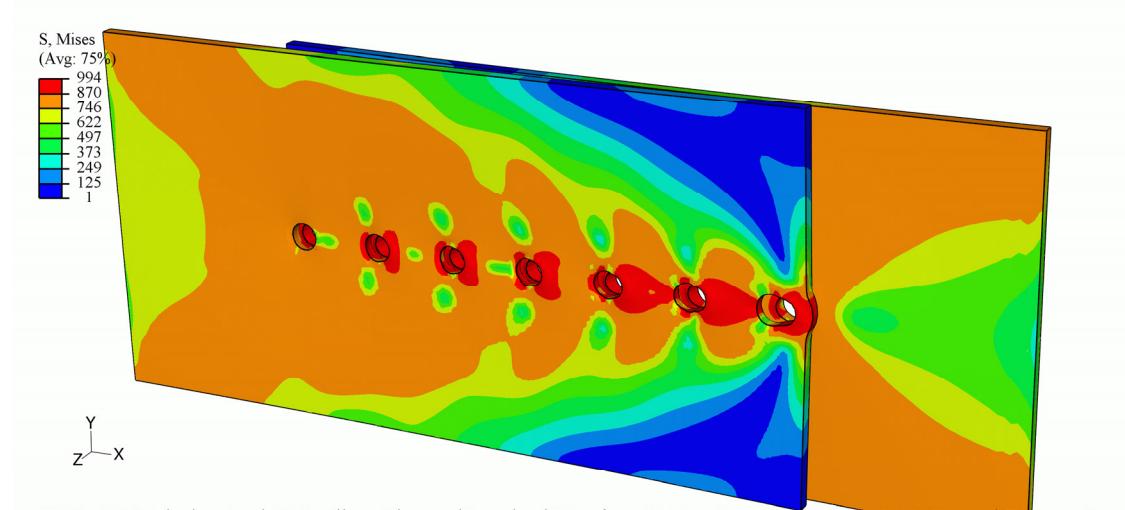




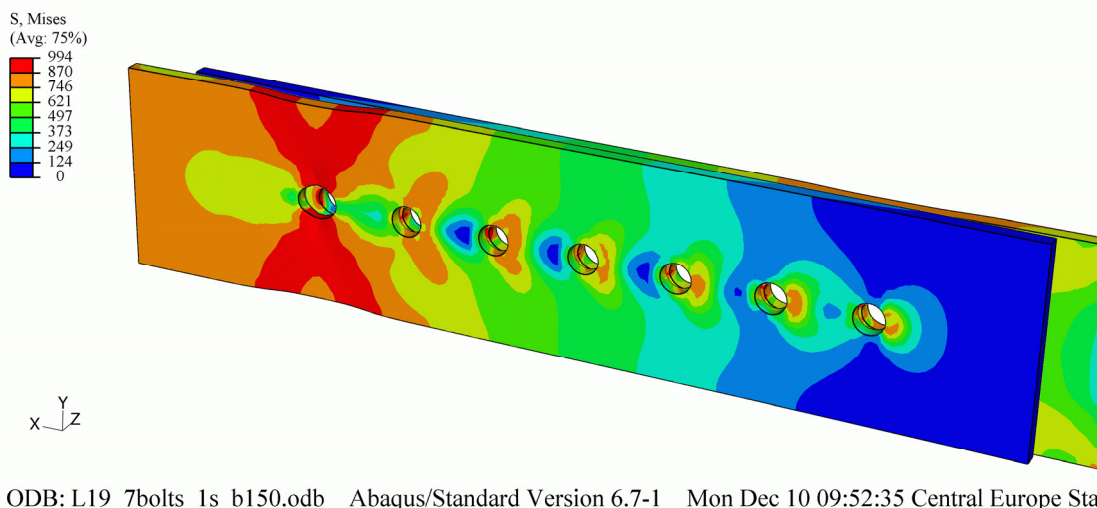
ODB: L14_7bolts_1s_b150.odb Abaqus/Standard Version 6.7-1 Mon Dec 10 09:52:06 Central Europe Star



ODB: L14_7bolts_1s_b250.odb Abaqus/Standard Version 6.7-1 Mon Dec 10 09:53:35 Central Europe Star

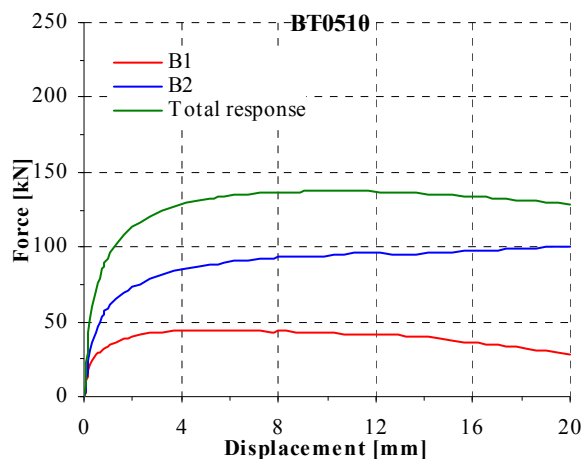


ODB: L14_7bolts_1s_b300.odb Abaqus/Standard Version 6.7-1 Tue Oct 30 16:45:13 Central Europe Star

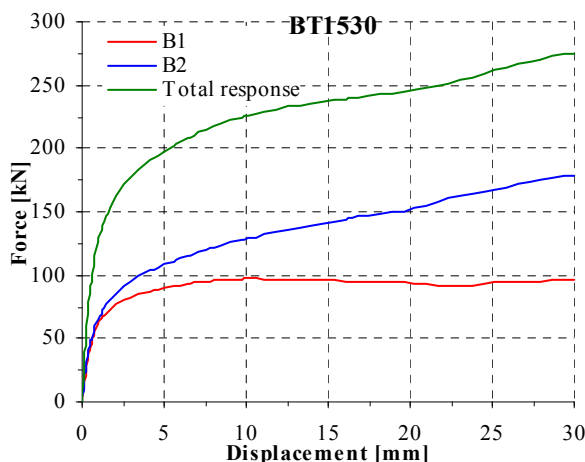
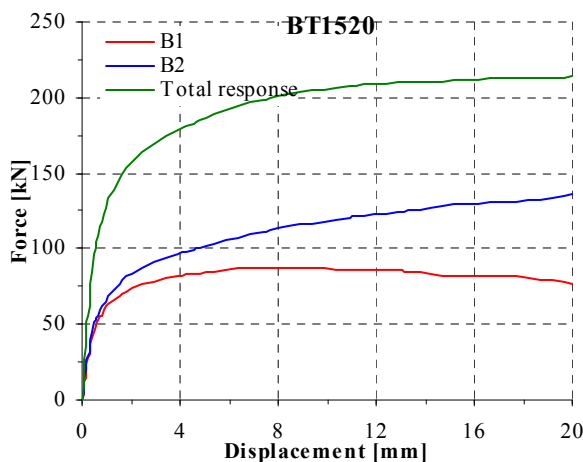
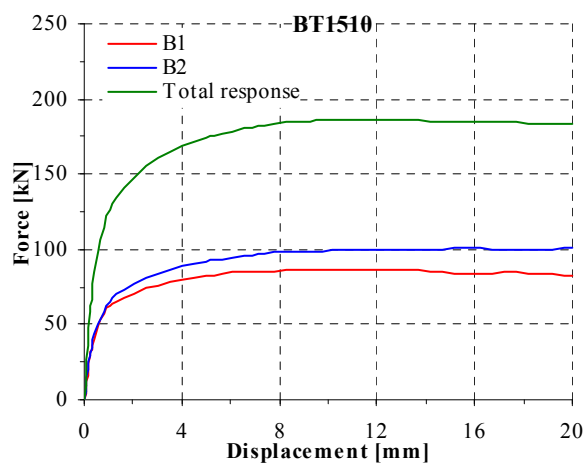
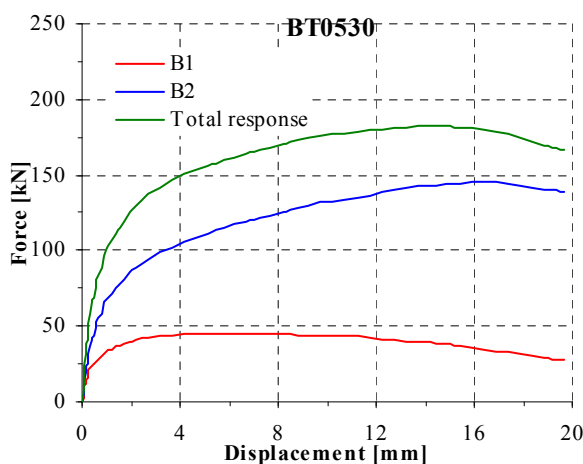
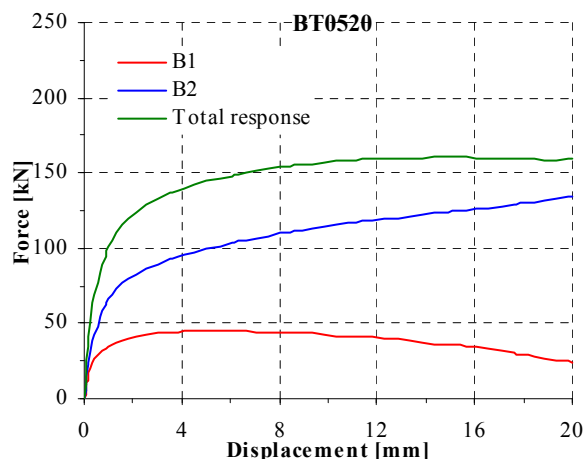


Appendix E RESULTS OF NUMERICAL FE ANALYSES, REPLICATING TESTS FROM LITERATURE

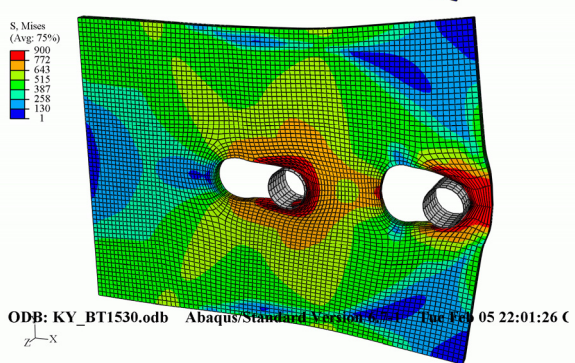
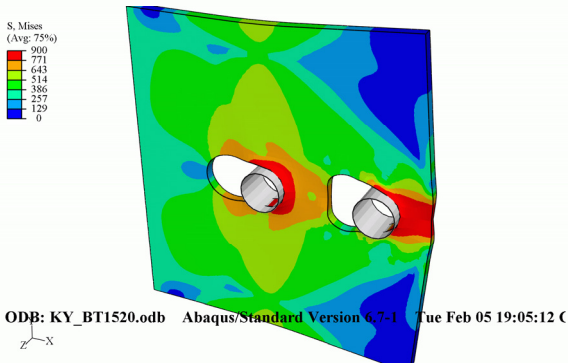
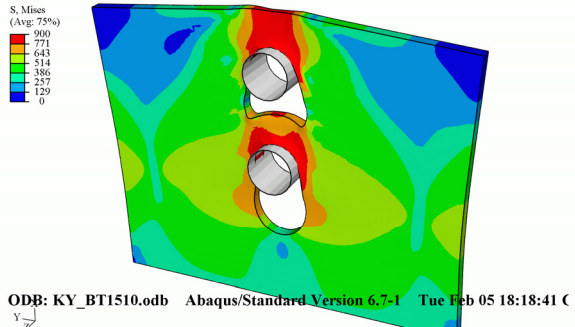
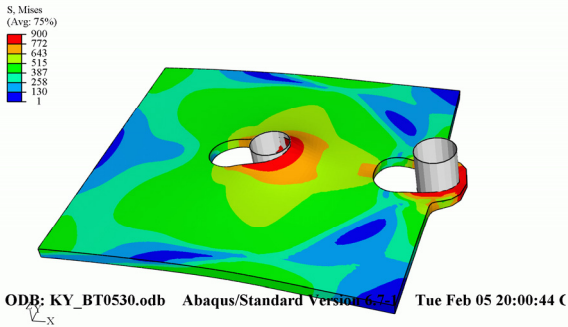
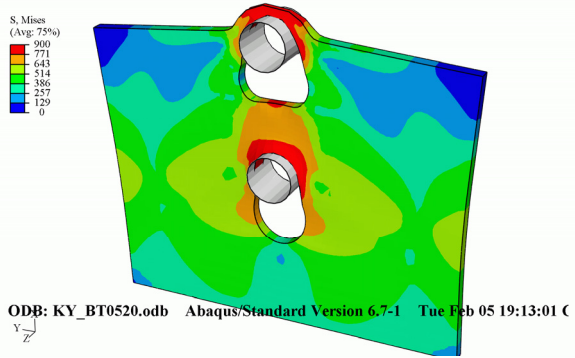
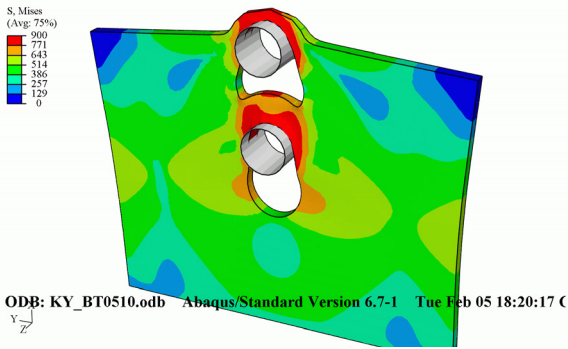
KY xxxx;(Kim, Yura, 1996) ; Numerical model type M1; 6 FE analyses
Experimental and numerical load-displacement curves



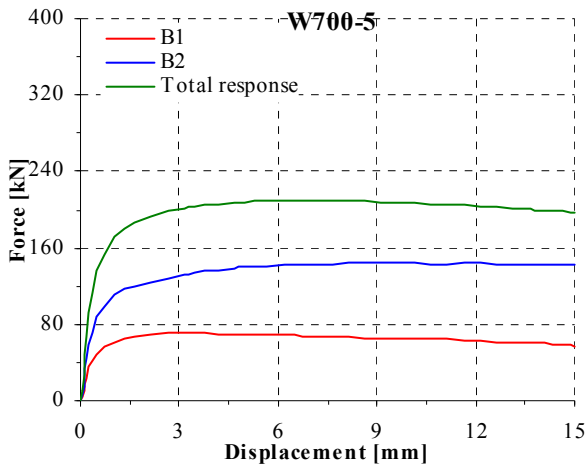
Distribution of forces between bolts and the friction force



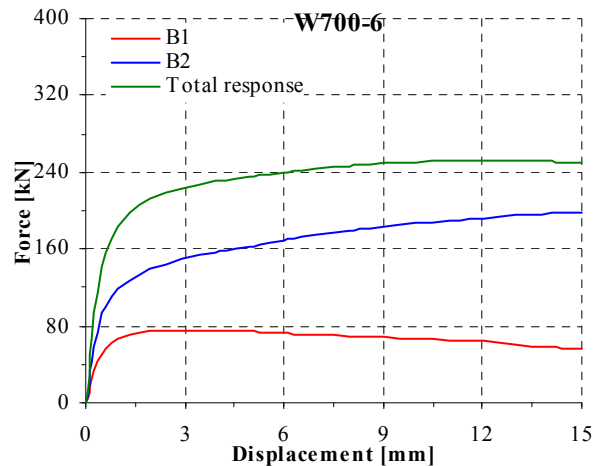
Mises stress on a deformed connection. The connection name is displayed on the bottom left side of the figure

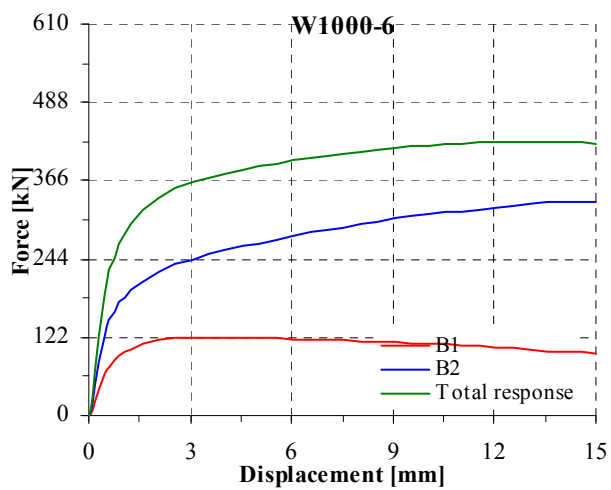
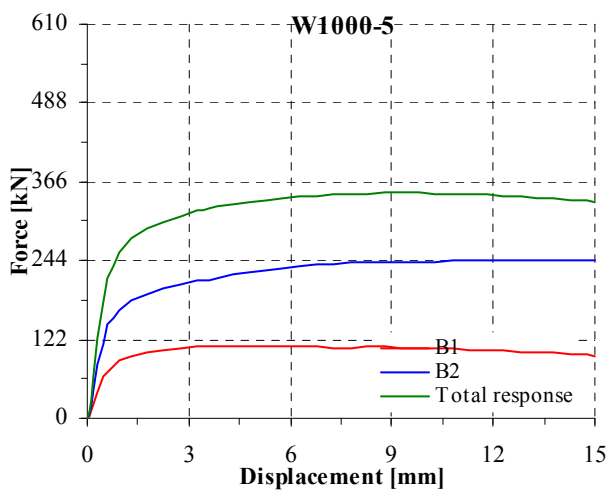
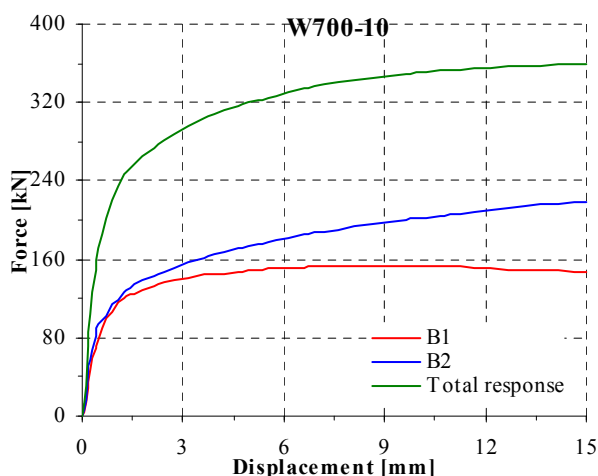
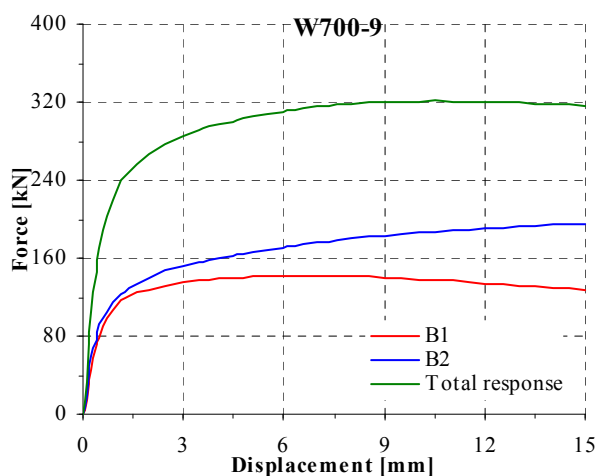
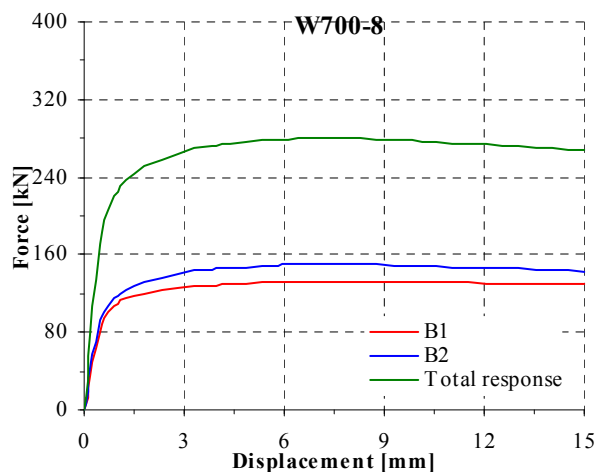
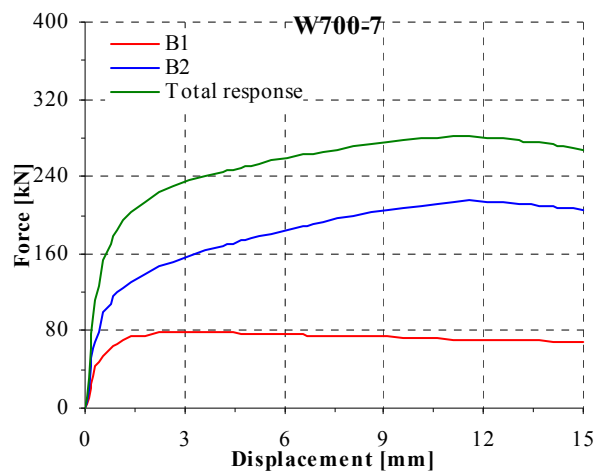


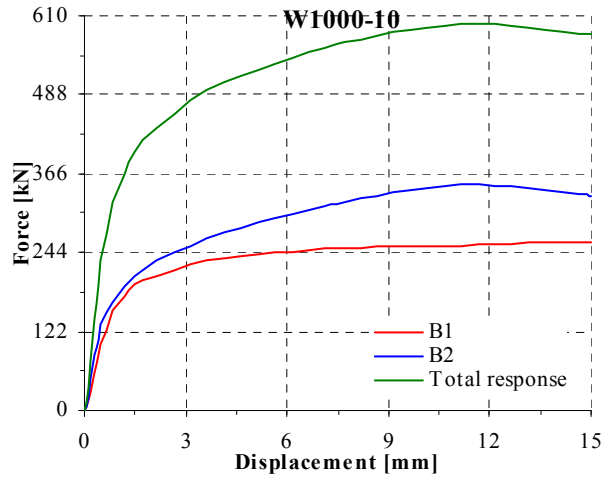
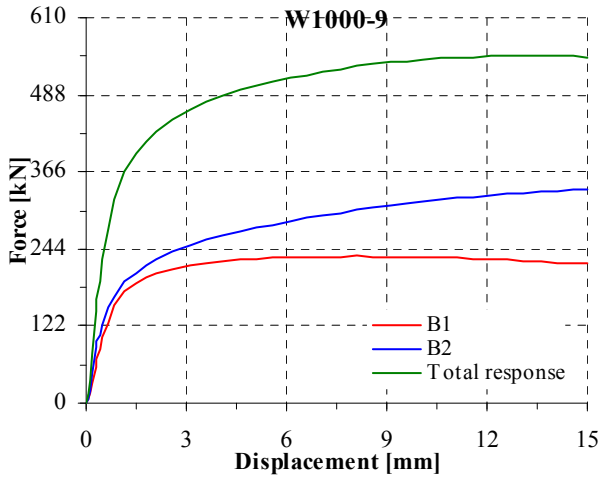
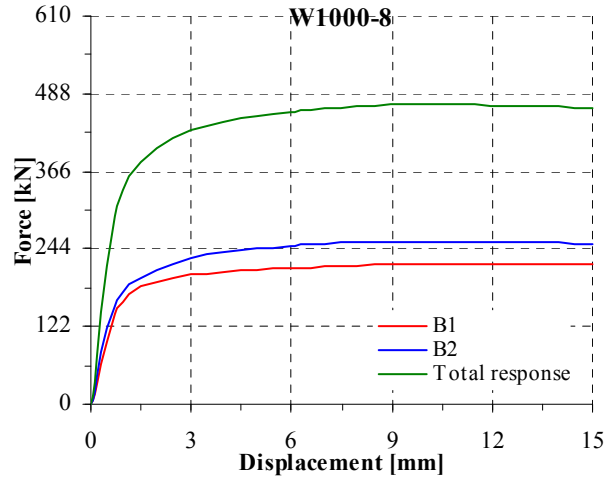
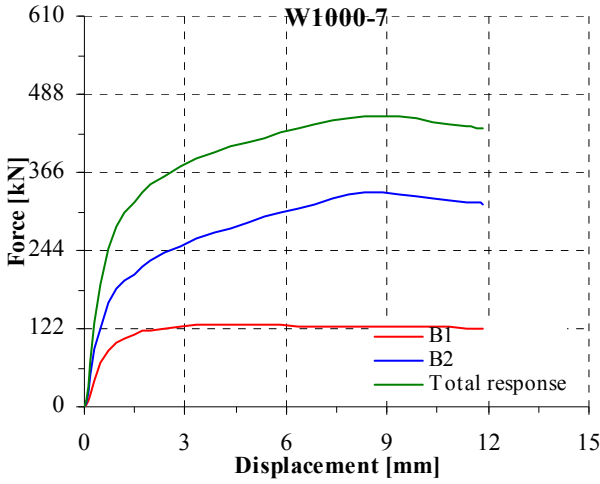
AL xxxx;(Aalberg, Larsen, 2001. 2002) Numerical model type M1; 12 FE analyses
Experimental and numerical load-displacement curves



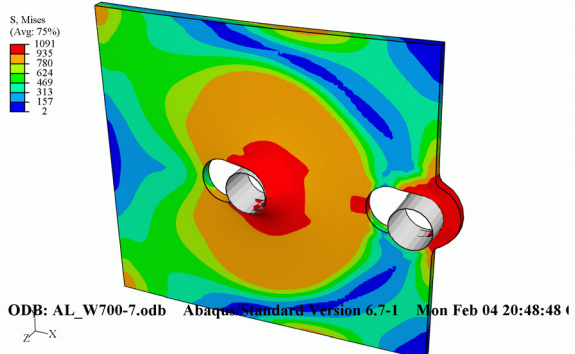
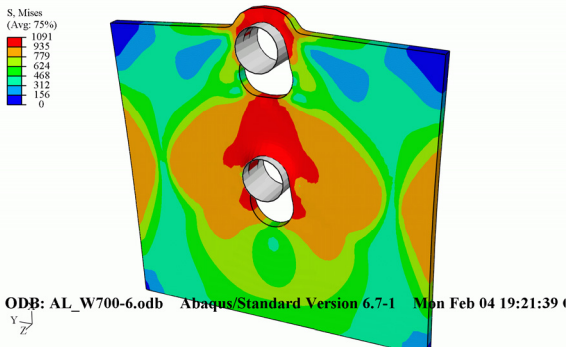
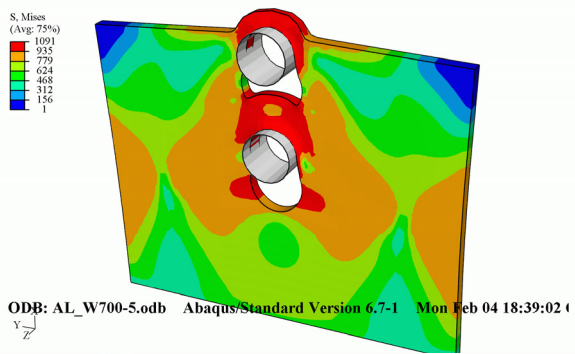
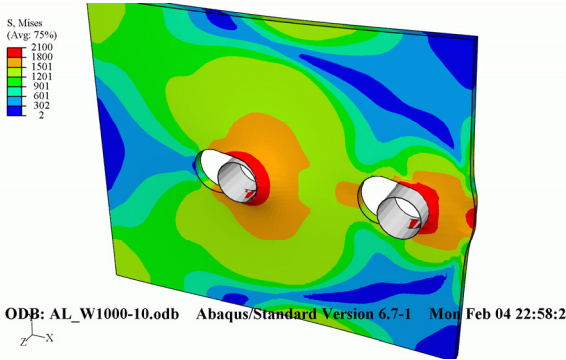
Distribution of forces between bolts and the friction force

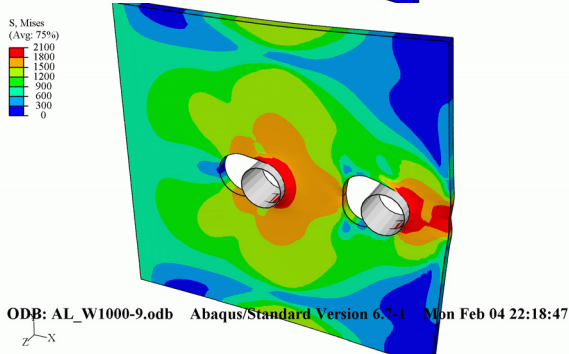
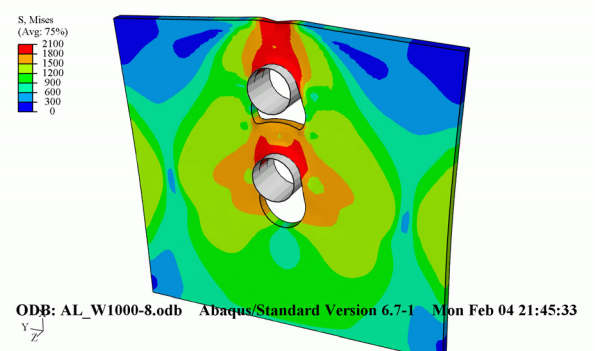
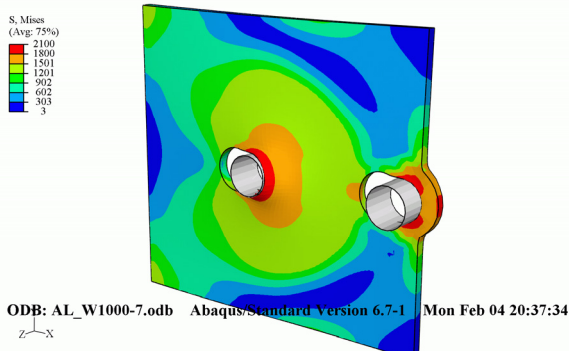
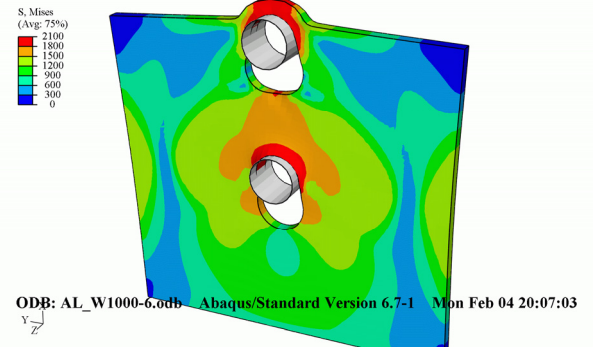
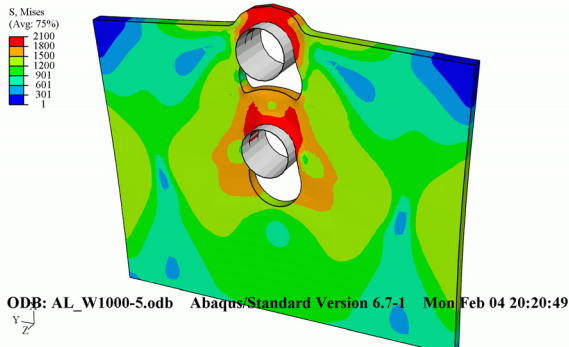
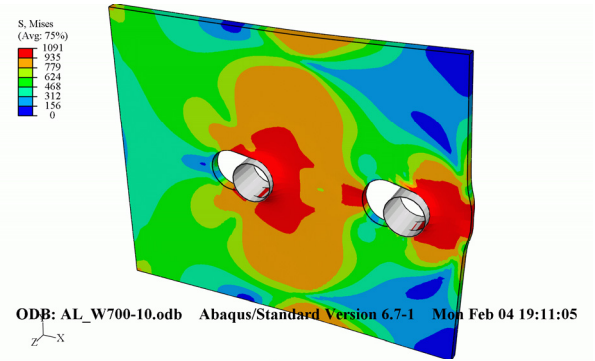
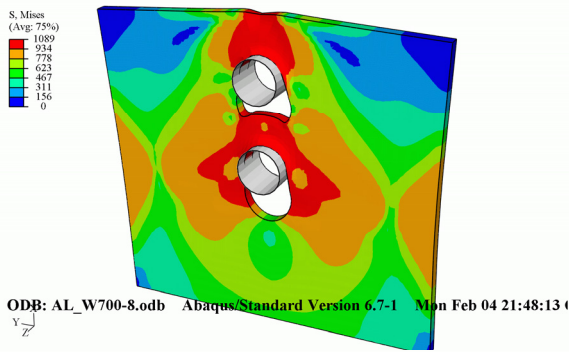




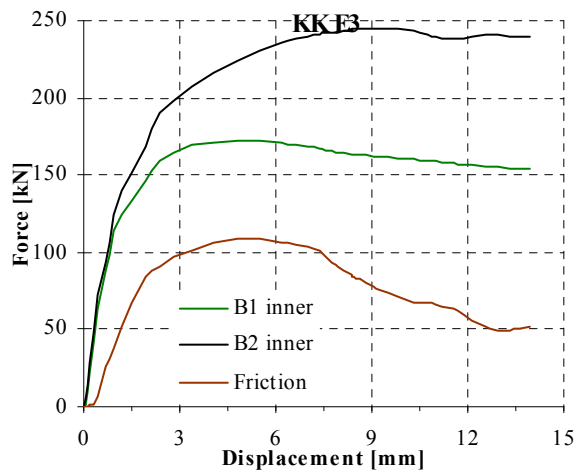
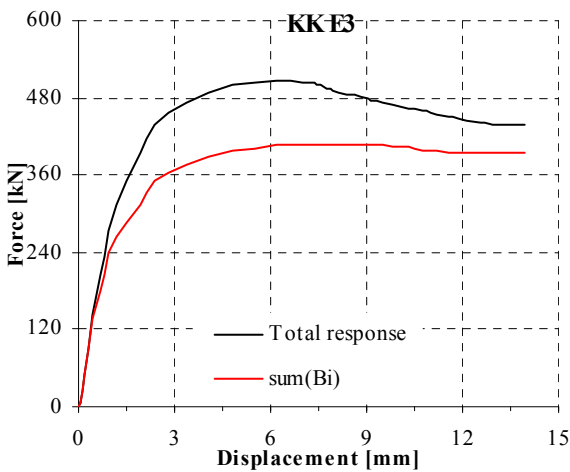
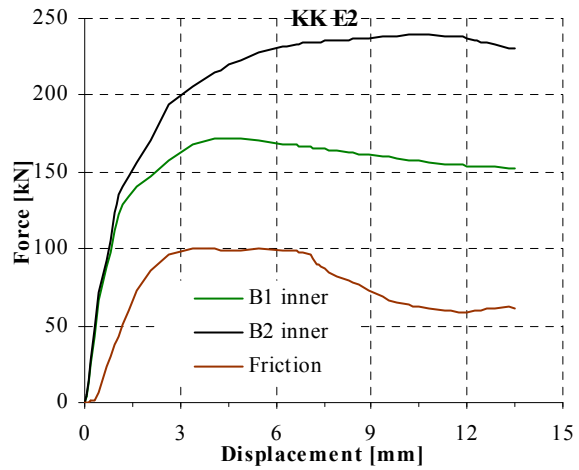
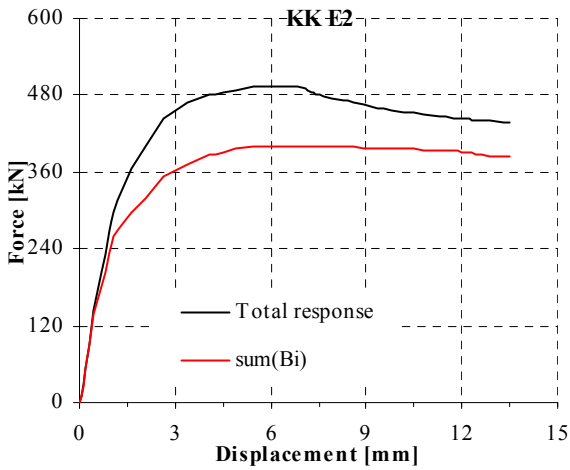
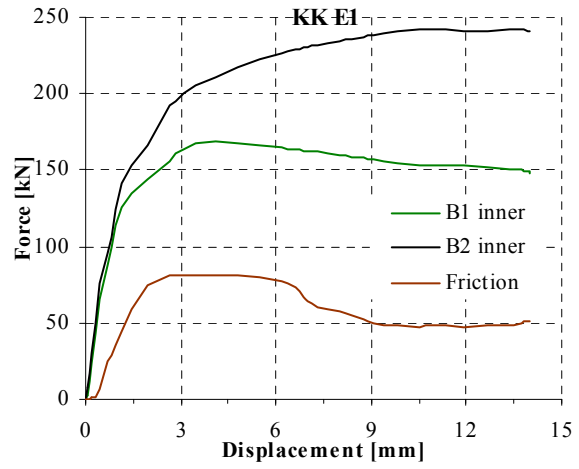
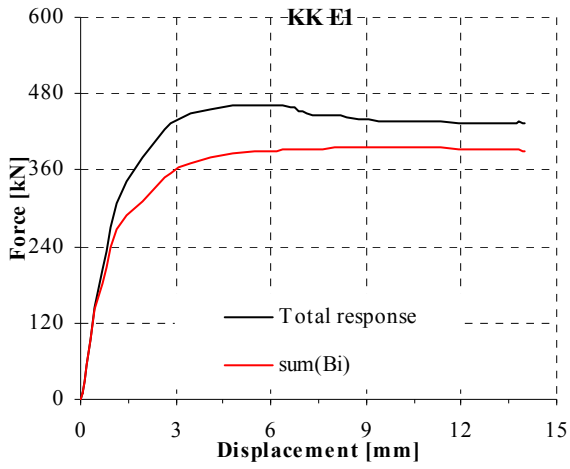


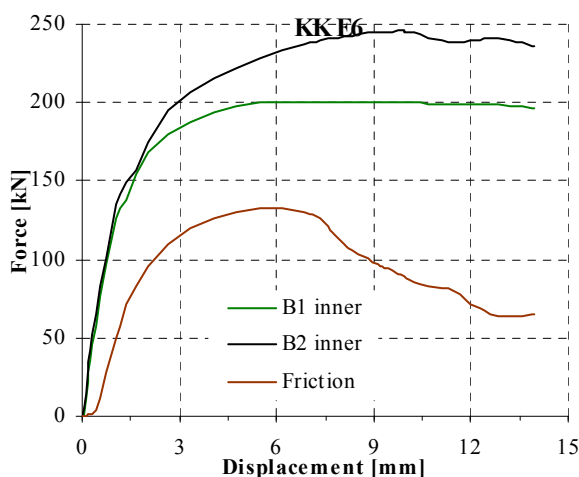
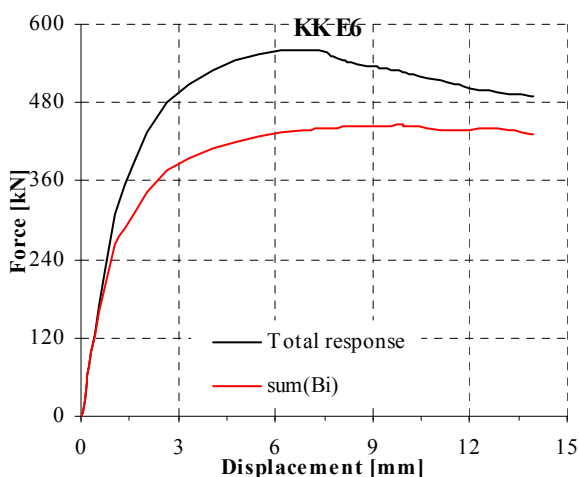
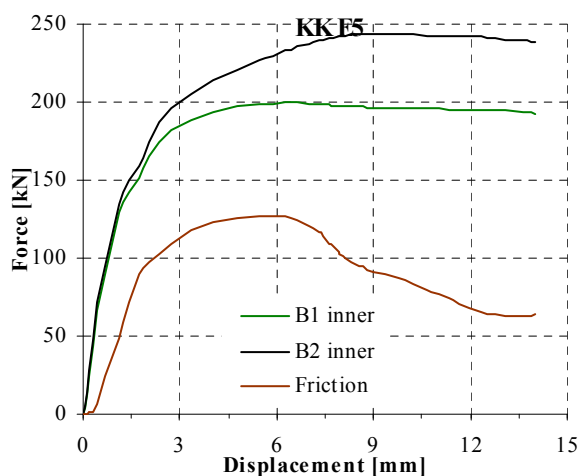
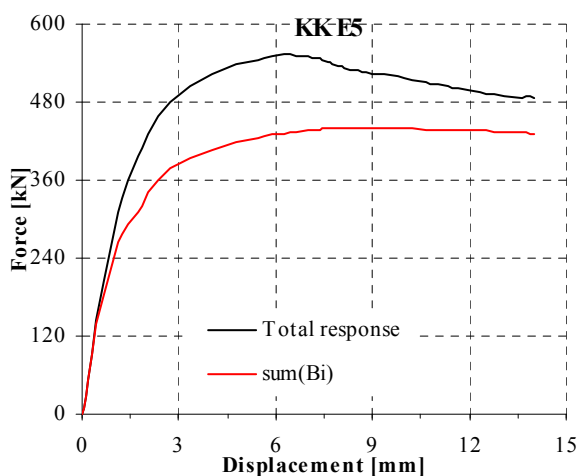
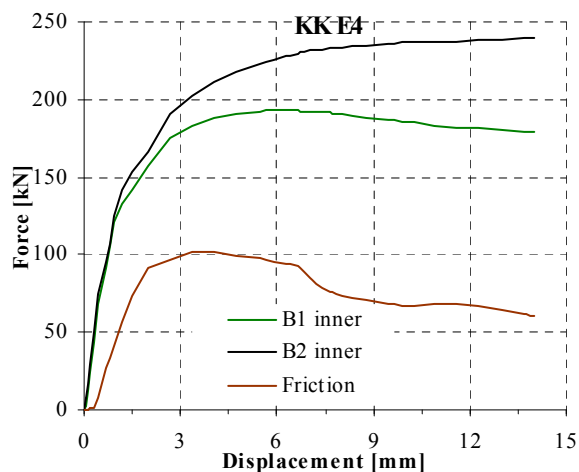
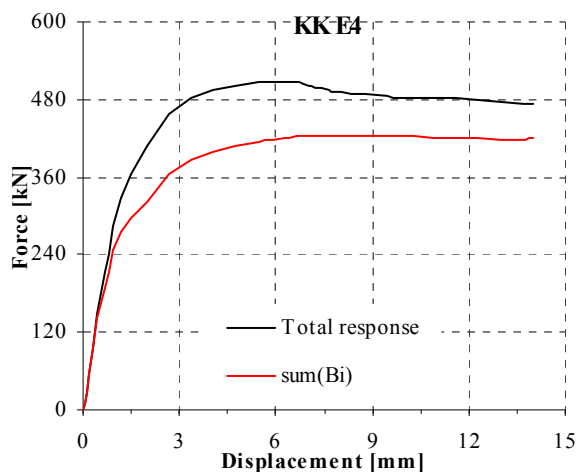
Mises stress on a deformed connection. The connection name is displayed on the bottom left side of the figure



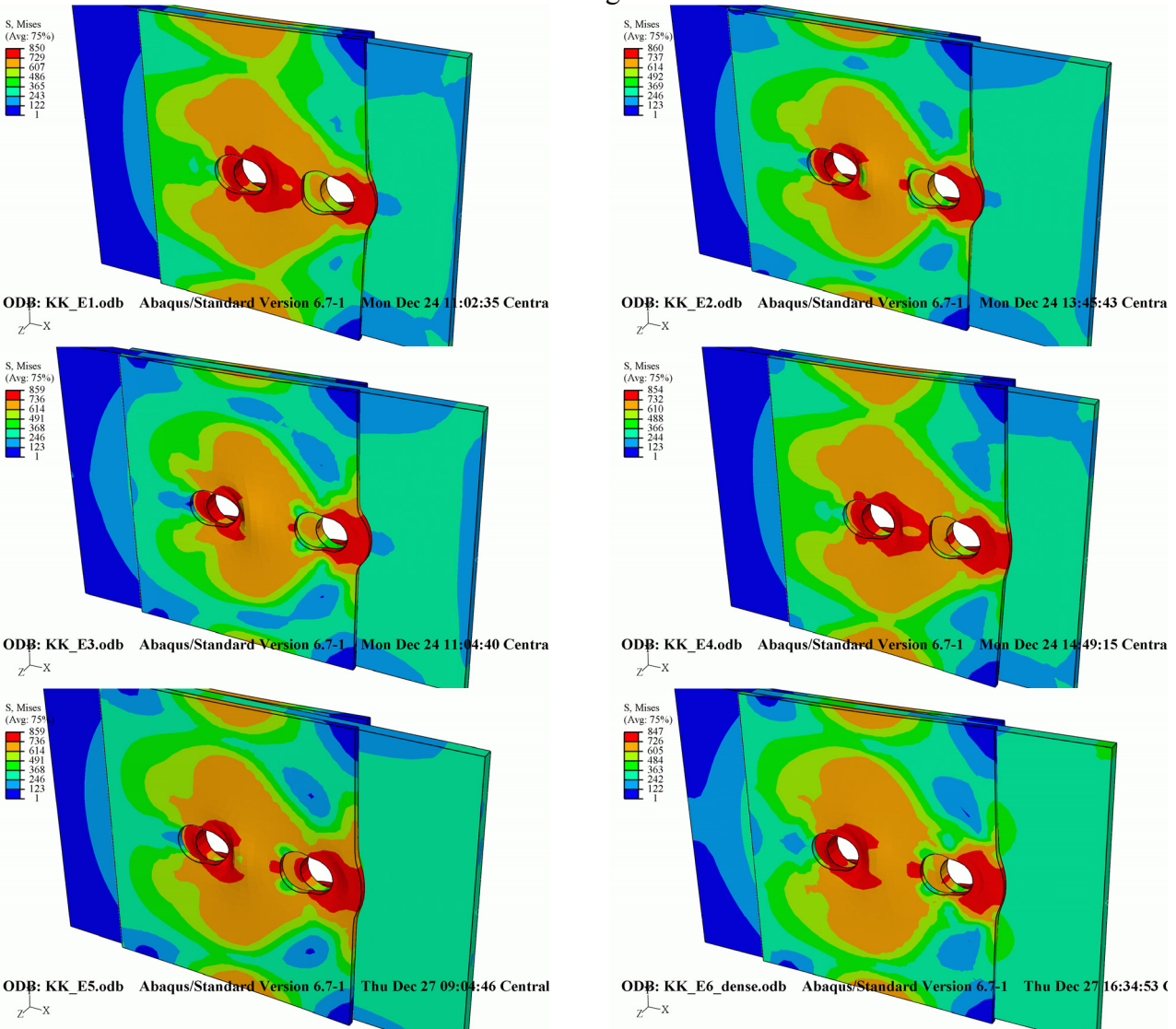


KK Ex; (Kouhi, Korteesmaa, 1990); Numerical model type M3; 6 FE analyses
Experimental and numerical load-displacement curves **Distribution of forces between bolts and the friction force**

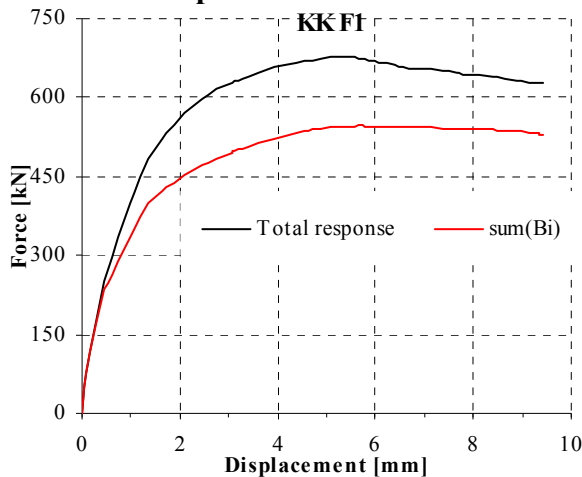




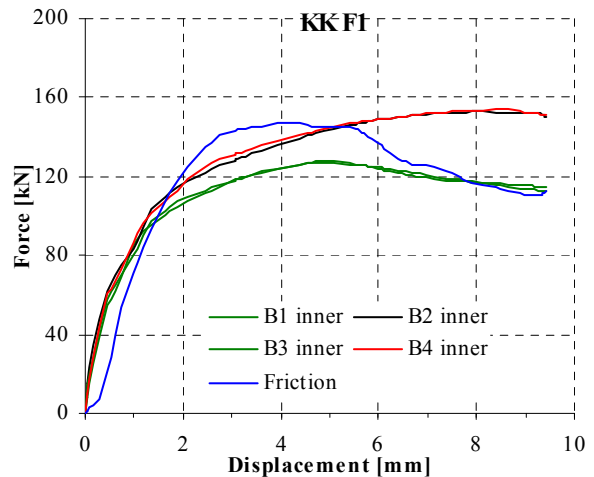
Mises stress on a deformed connection. The connection name is displayed on the bottom left side of the figure

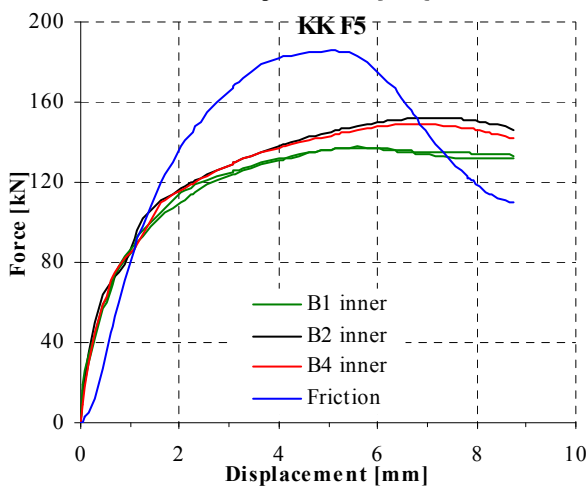
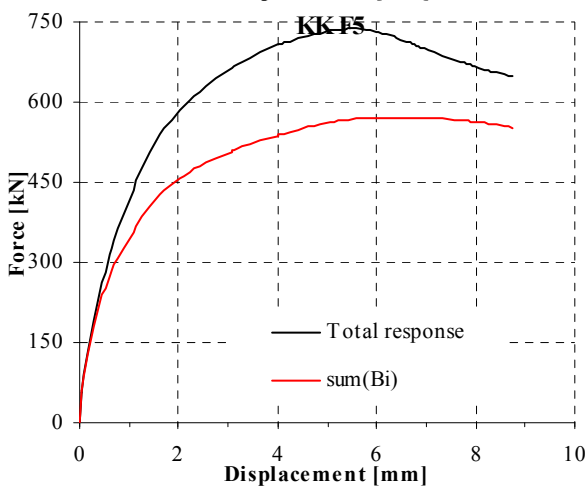
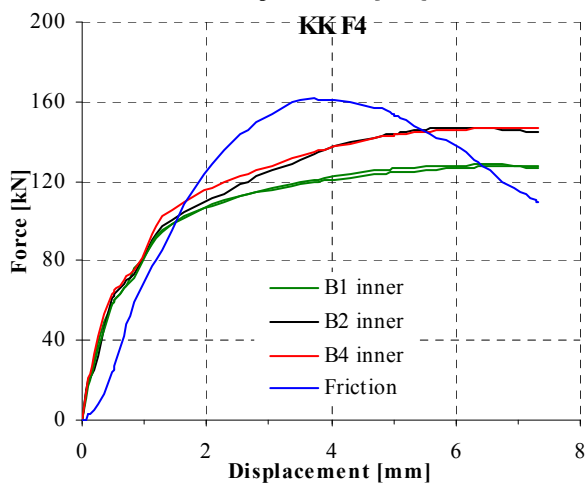
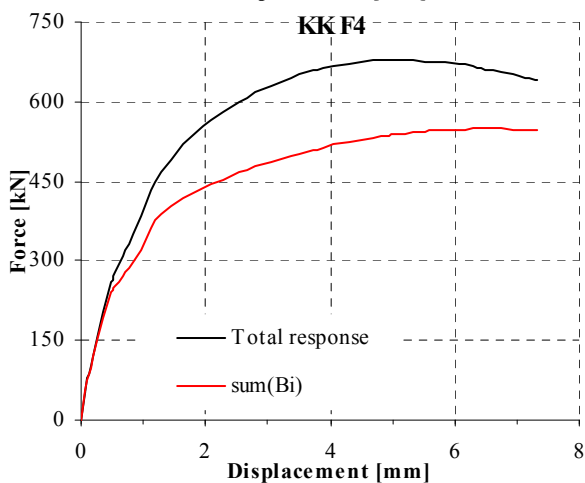
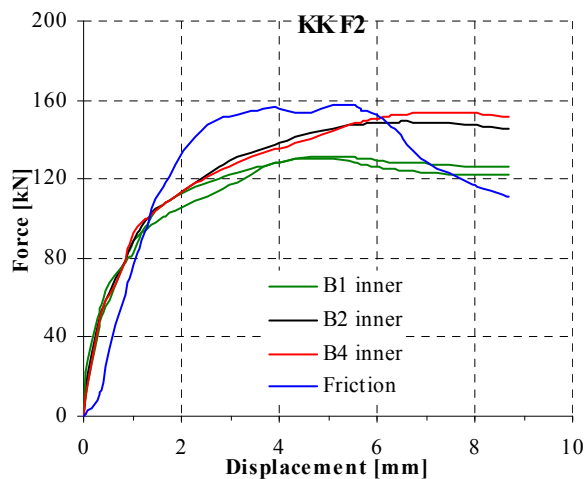
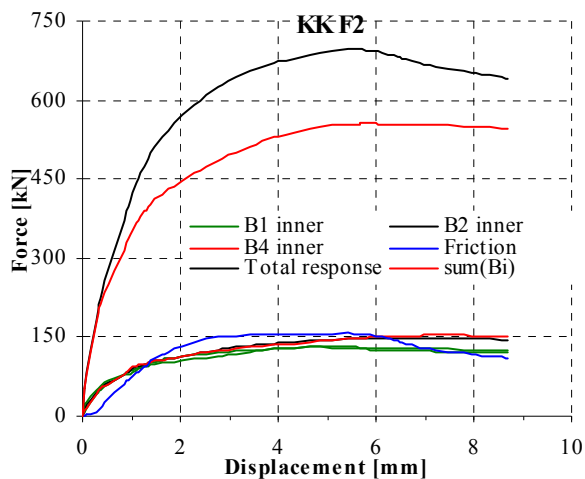


KK Fx; (Kouhi, Kortesmaa, 1990); Numerical model type M3; 4 FE analyses
Experimental and numerical load-displacement curves

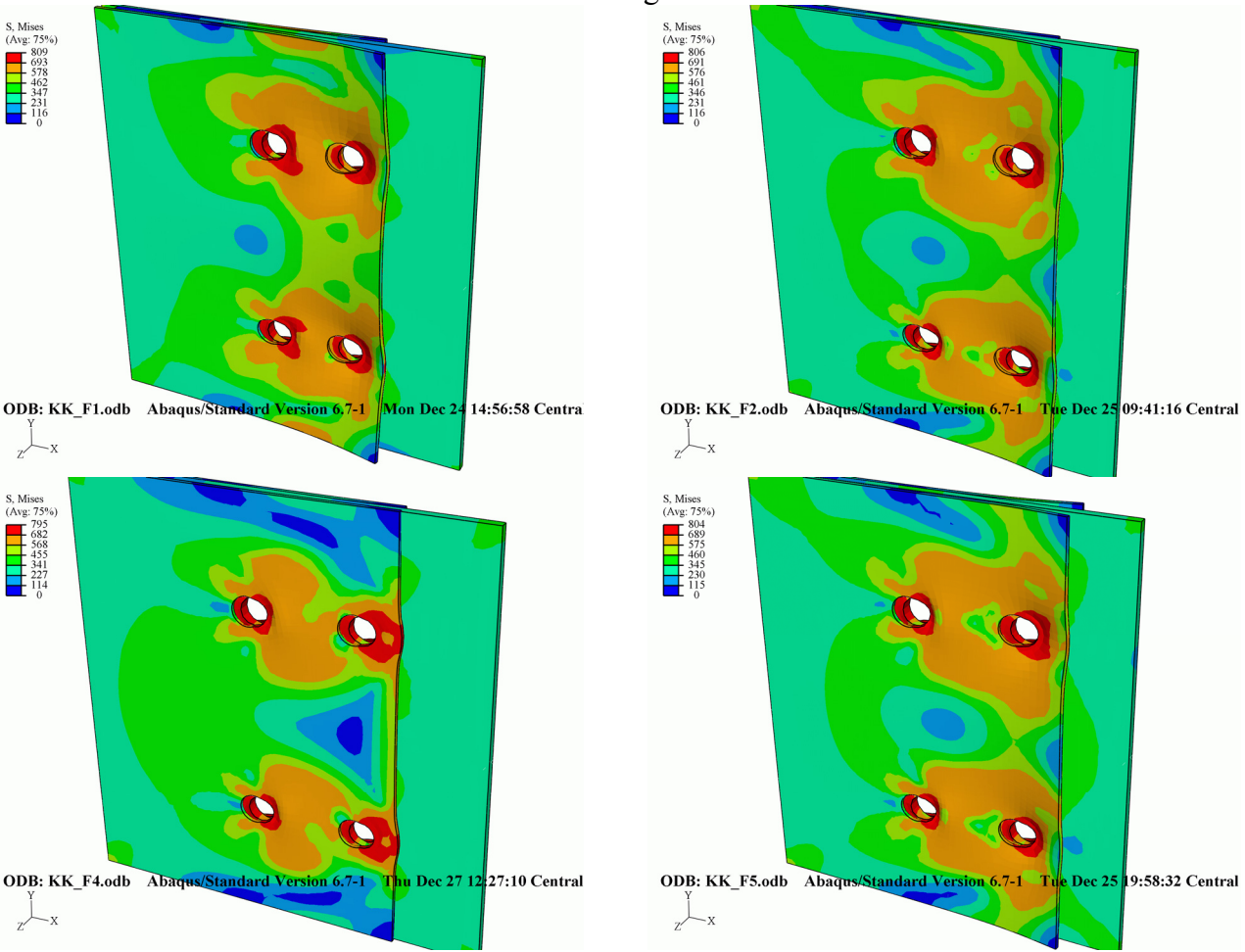


Distribution of forces between bolts and the friction force

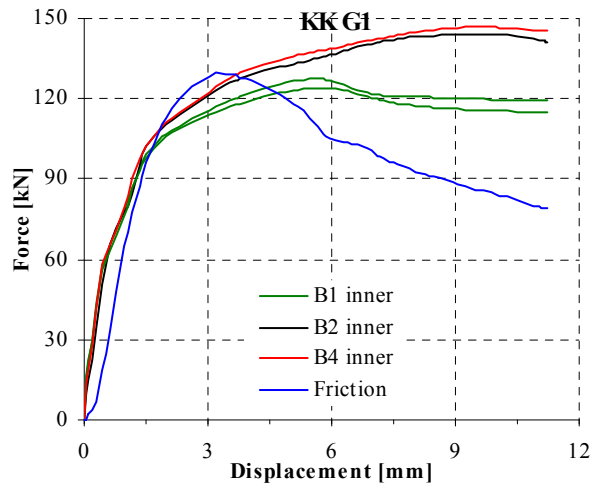
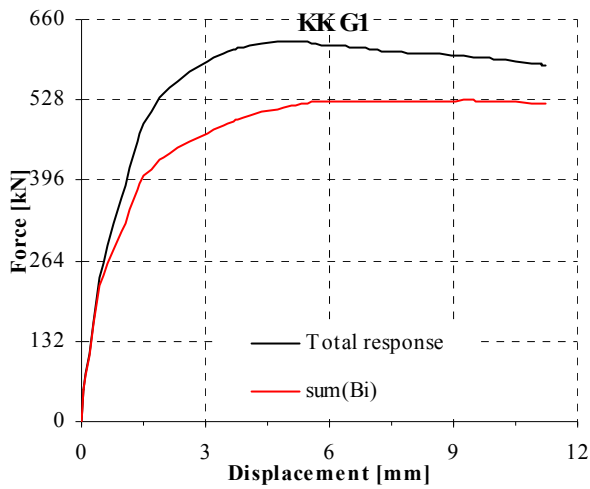


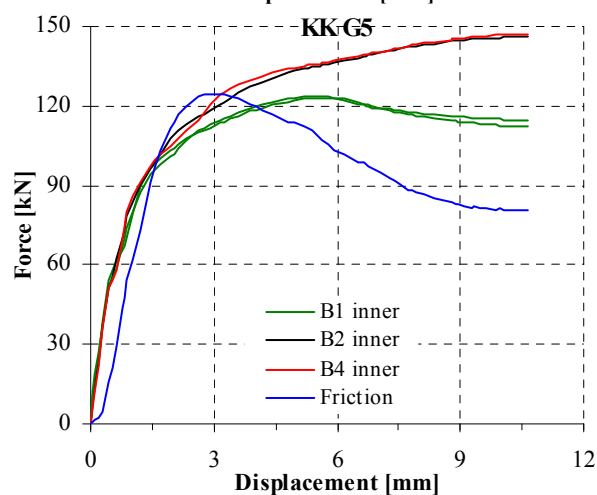
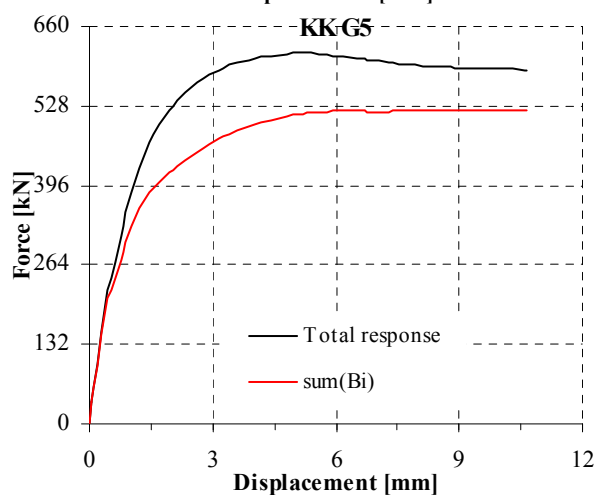
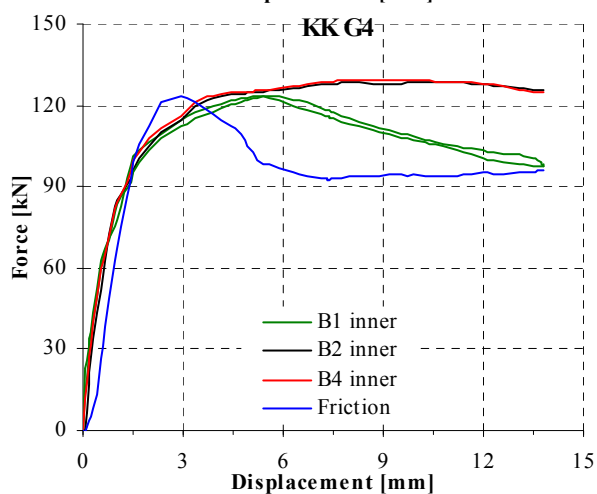
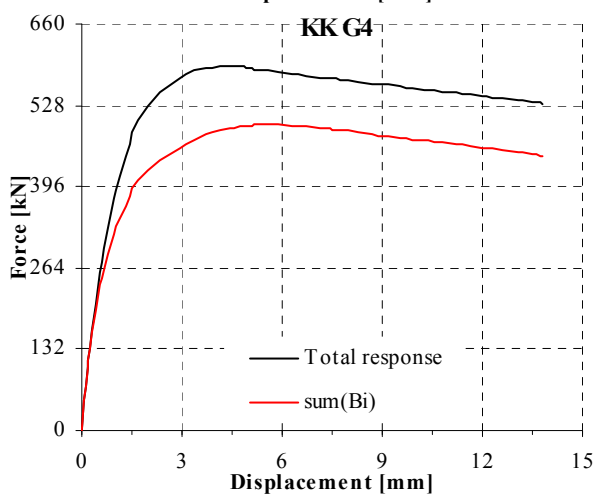
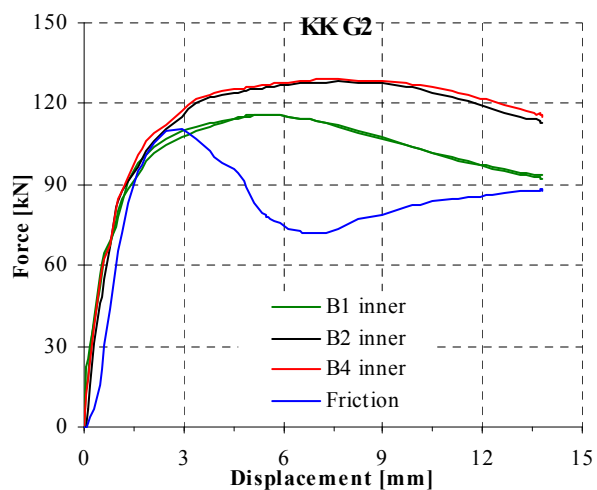
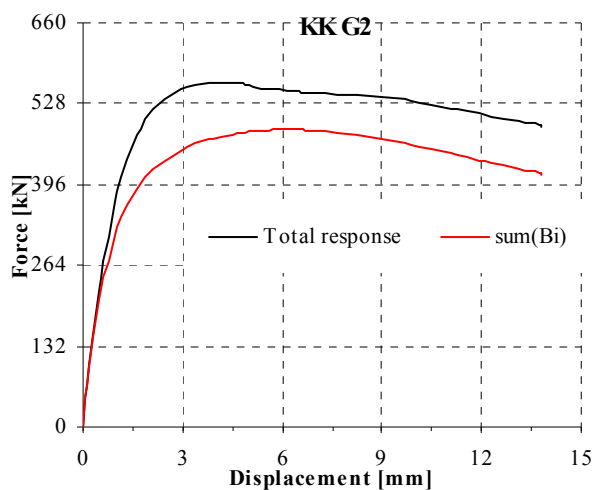


Mises stress on a deformed connection. The connection name is displayed on the bottom left side of the figure

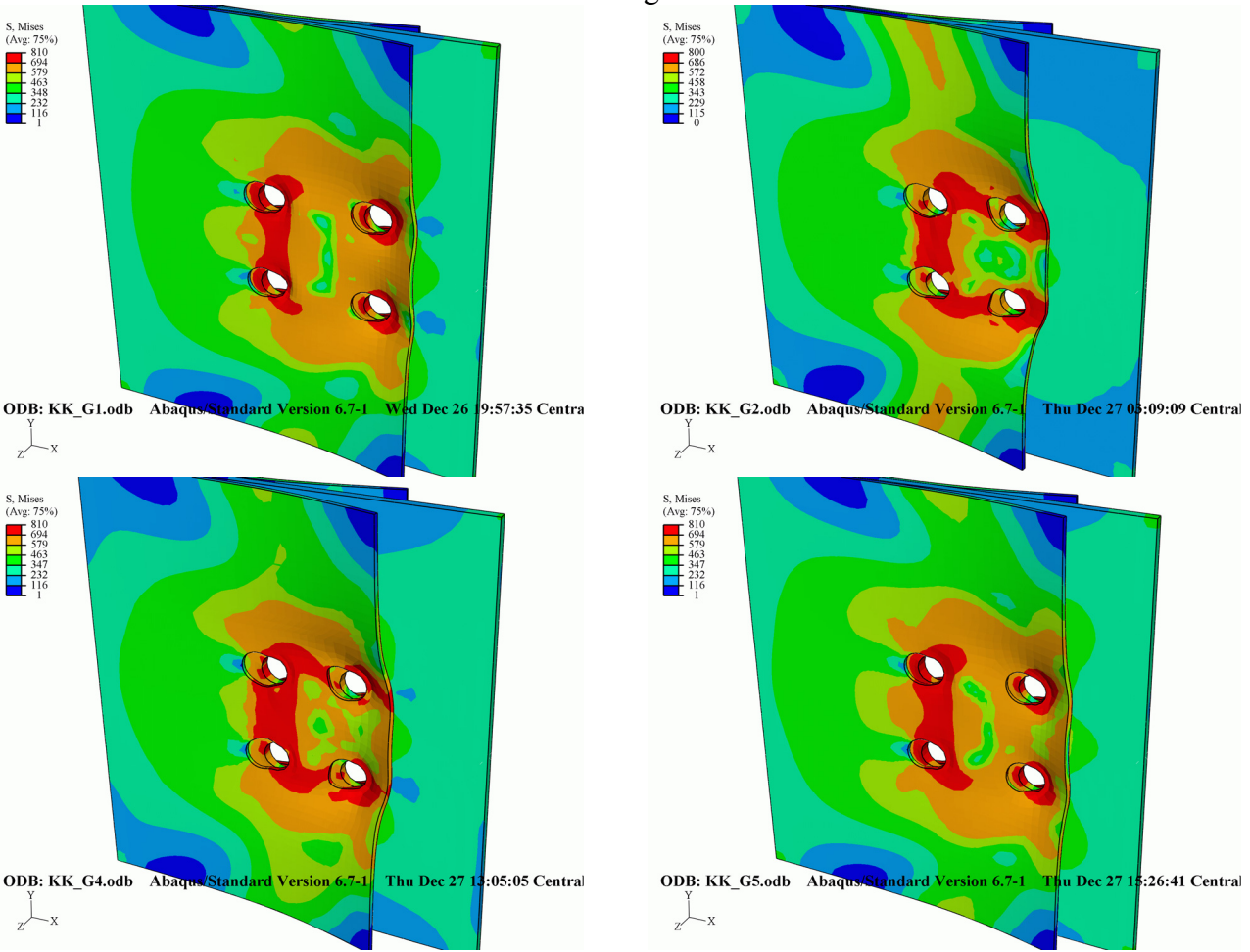


KK Gx; (Kouhi, Kortesmaa, 1990); Numerical model type M3; 4 FE analyses
Experimental and numerical load-displacement curves **Distribution of forces between bolts and the friction force**

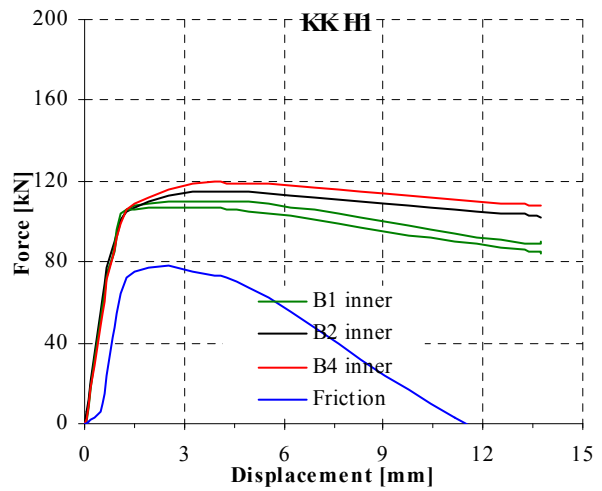
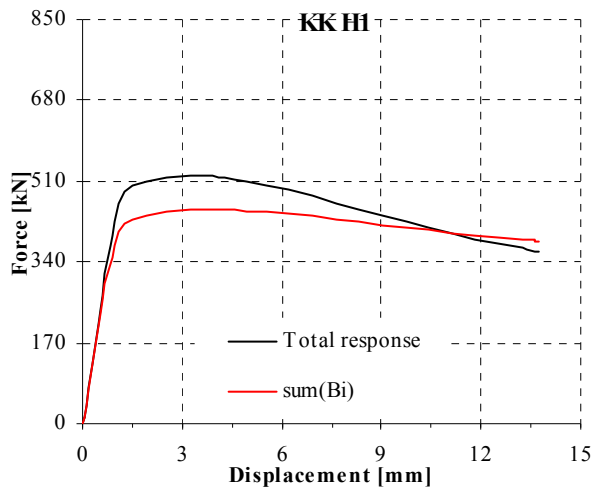


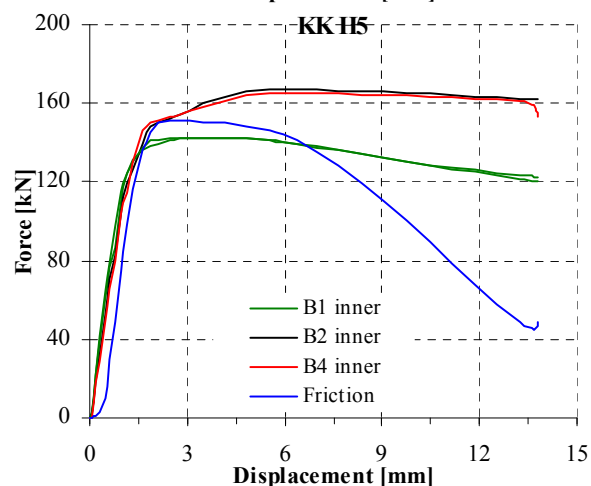
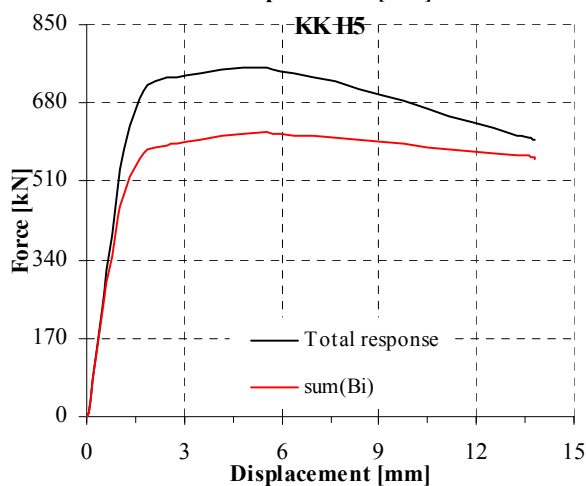
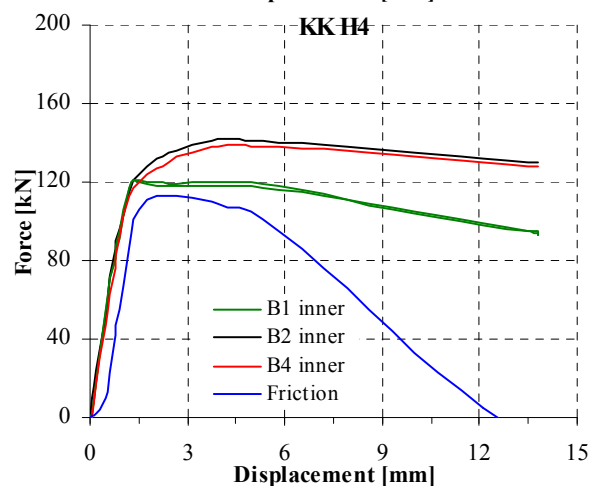
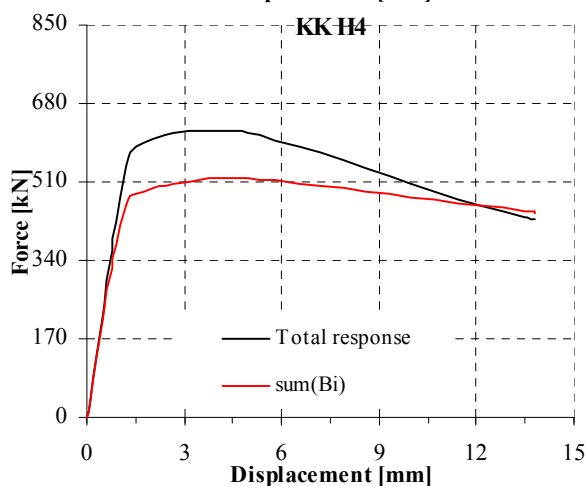
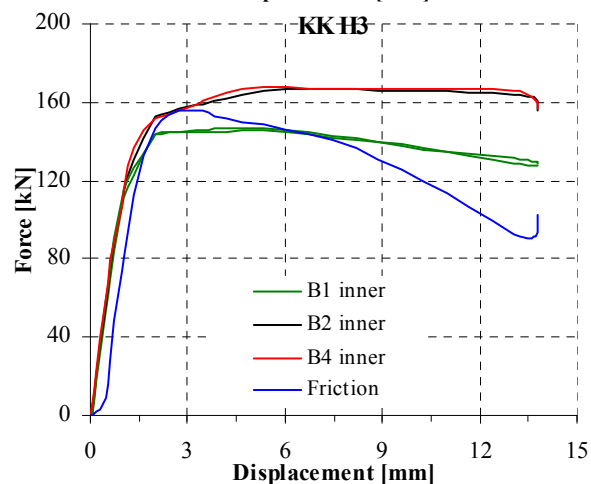
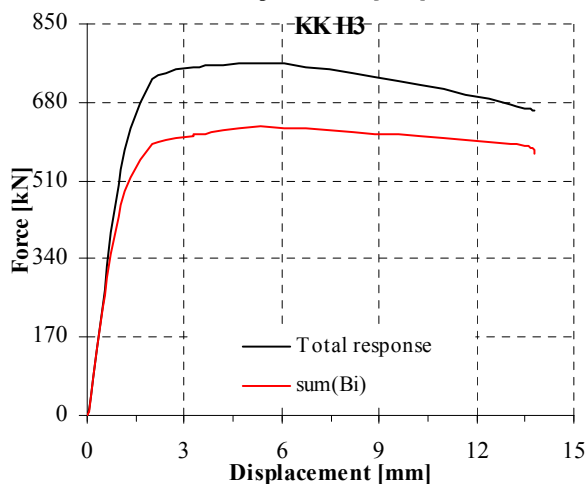
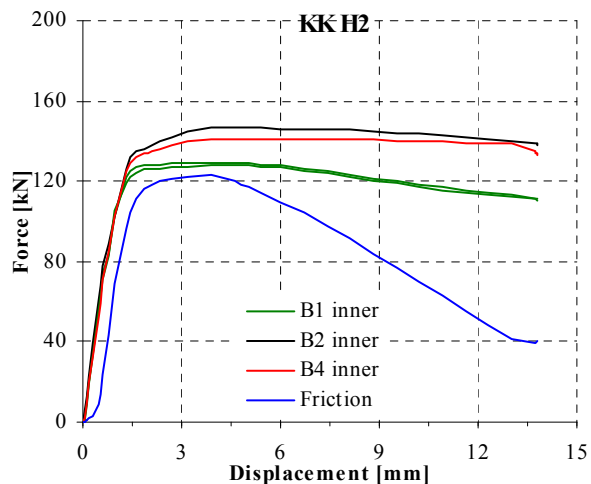
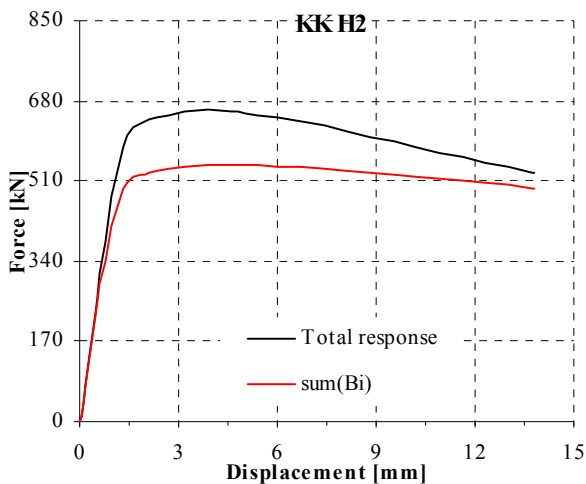


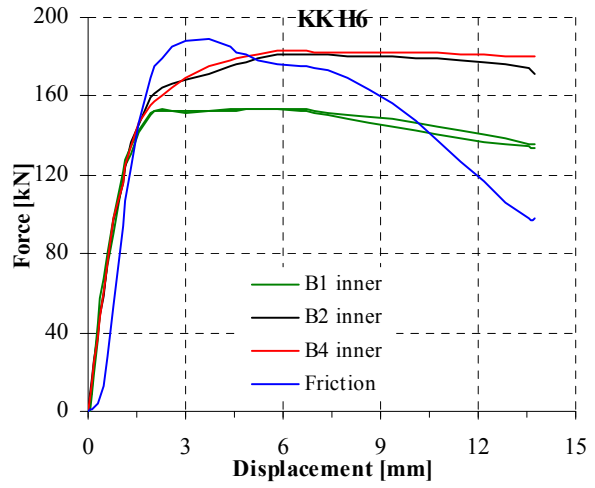
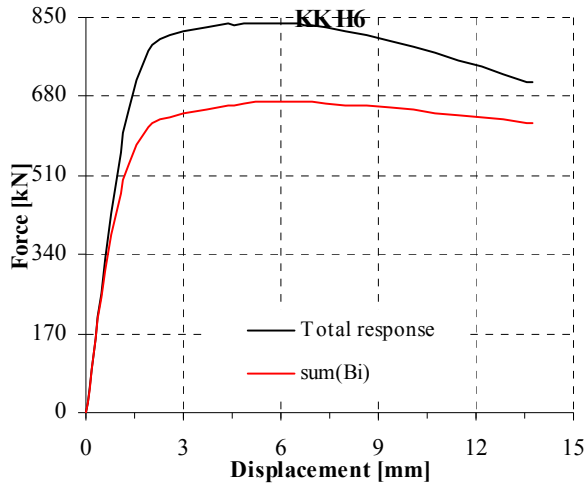
Mises stress on a deformed connection. The connection name is displayed on the bottom left side of the figure



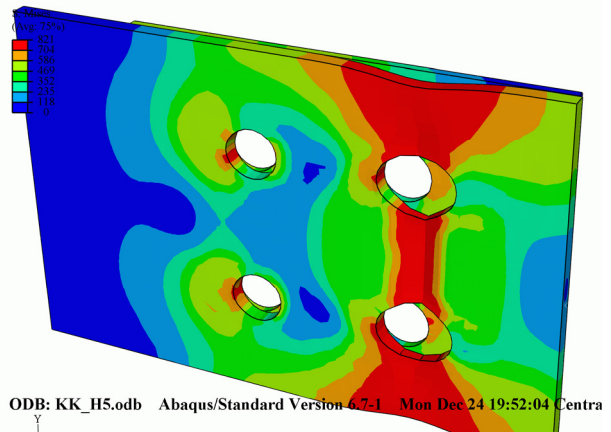
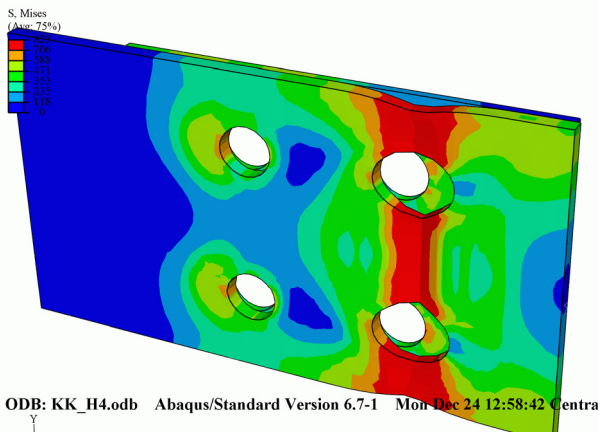
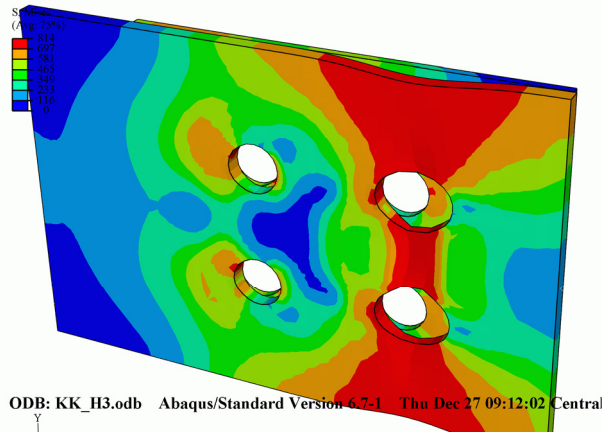
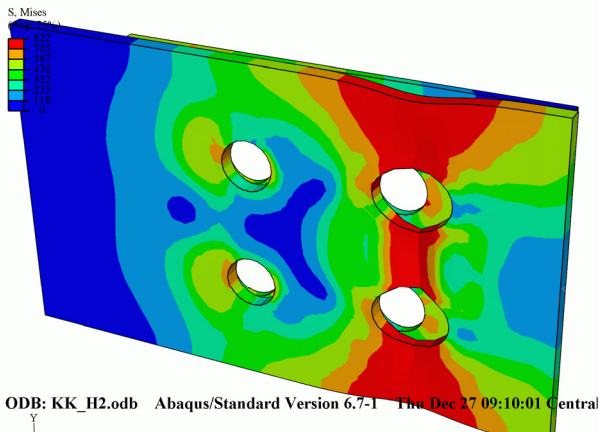
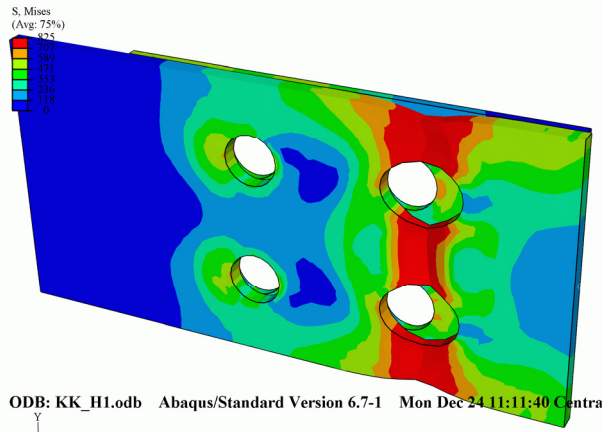
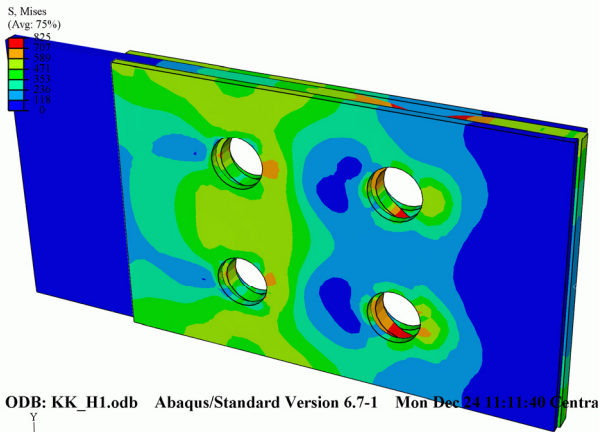
KK Hx; (Kouhi, Kortesmaa, 1990); Numerical model type M3; 6 FE analyses
Experimental and numerical load-displacement curves **Distribution of forces between bolts and the friction force**

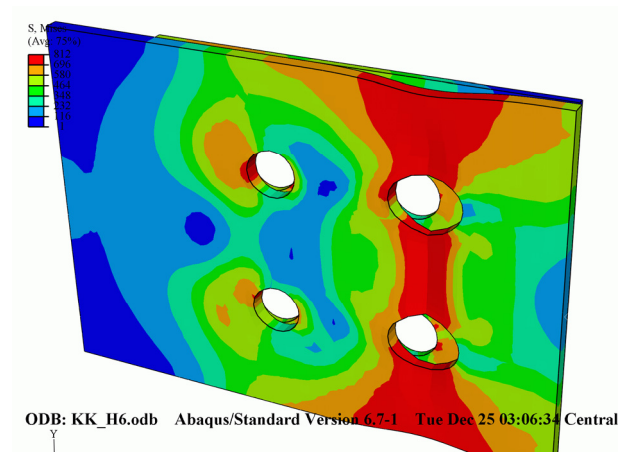






Mises stress on a deformed connection. The connection name is displayed on the bottom left side of the figure





Appendix F FACTORS USED IN BEARING RESISTANCE FORMULAS

In the following table the factors k_1 and α_b used in the Eurocode resistance formula are given. The values were calculated by nominal geometry of the connection.

Specimen name	k_{1_e2}	k_{1_p2}	α_{d_e1}	α_{d_p1}
B101	1,10	0,00	1,00	0,00
B102	1,66	0,00	0,40	0,00
B103	1,66	0,00	0,50	0,00
B104	1,66	0,00	0,67	0,00
B105	1,66	0,00	1,00	0,00
B106	2,08	0,00	0,83	0,00
B107	2,08	0,00	1,00	0,00
B108*	1,61	0,00	1,00	0,00
B109	2,50	0,00	0,33	0,00
B110	2,50	0,00	0,40	0,00
B111	2,50	0,00	0,50	0,00
B112	2,50	0,00	0,67	0,00
B113	2,50	0,00	0,83	0,00
B114	2,50	0,00	1,00	0,00
B115*	2,03	0,00	1,00	0,00
B116	2,50	0,00	0,50	0,00
B117	2,50	0,00	0,50	0,00
B118	2,50	0,00	0,50	0,00
B119	2,50	0,00	0,67	0,00
B120	2,50	0,00	0,83	0,00
B121	2,50	0,00	1,00	0,00
B122	2,50	0,00	1,00	0,00
B123	2,50	0,00	1,00	0,00
B124*	2,27	0,00	1,00	0,00
B125*	1,57	0,00	1,00	0,00
B201	1,10	1,10	1,00	0,00
B202	1,66	1,66	0,40	0,00
B203	1,66	1,66	0,67	0,00
B204	1,66	1,66	1,00	0,00
B205	1,66	2,08	1,00	0,00
B206	2,50	1,66	0,50	0,00
B207	2,50	2,08	1,00	0,00
B208	2,50	2,50	0,33	0,00
B209	2,50	2,50	0,40	0,00
B210	2,50	2,50	0,50	0,00
B211	2,50	2,50	0,67	0,00
B212	2,50	2,50	1,00	0,00
B213	2,08	1,66	0,67	0,00
PF1	1,66	1,66	0,40	0,00
PF2	2,08	1,66	0,40	0,00
PF3	2,50	1,66	0,40	0,00
PF4	1,66	2,08	0,40	0,00
PF5	2,08	2,08	0,40	0,00
PF6	2,50	2,08	0,40	0,00
PF7	1,66	2,50	0,40	0,00
PF8	2,08	2,50	0,40	0,00
PF9	2,50	2,50	0,40	0,00
PF10	0,82	0,82	0,40	0,00

Specimen name	k_{1_e2}	k_{1_p2}	α_{d_e1}	α_{d_p1}
PF11	1,24	0,82	0,40	0,00
PF12	1,66	0,82	0,40	0,00
PF13	2,08	0,82	0,40	0,00
PF14	2,50	0,82	0,40	0,00
PF15	0,82	1,24	0,40	0,00
PF16	1,24	1,24	0,40	0,00
PF17	1,66	1,24	0,40	0,00
PF18	2,08	1,24	0,40	0,00
PF19	2,50	1,24	0,40	0,00
PF20	0,82	1,66	0,40	0,00
PF21	1,24	1,66	0,40	0,00
PF22	0,82	2,08	0,40	0,00
PF23	1,24	2,08	0,40	0,00
PF24	0,82	2,50	0,40	0,00
PF25	1,24	2,50	0,40	0,00
BO050	2,50	0,00	0,32	0,00
BO0100	2,50	0,00	0,47	0,00
BO150	2,50	0,00	0,62	0,00
BO200	2,50	0,00	0,77	0,00
BT0510	2,50	0,00	0,32	0,38
BT0520	2,50	0,00	0,32	0,69
BT0530	2,50	0,00	0,32	0,99
BT1510	2,50	0,00	0,62	0,38
BT1520	2,50	0,00	0,62	0,69
BT1530	2,50	0,00	0,62	0,99
W700-1	2,50	0,00	0,32	0,00
W700-2	2,50	0,00	0,47	0,00
W700-3	2,50	0,00	0,62	0,00
W700-4	2,50	0,00	0,77	0,00
W700-5	2,50	0,00	0,32	0,38
W700-6	2,50	0,00	0,32	0,69
W700-7	2,50	0,00	0,32	0,99
W700-8	2,50	0,00	0,62	0,38
W700-9	2,50	0,00	0,62	0,69
W700-10	2,50	0,00	0,62	0,99
W1000-1	2,50	0,00	0,32	0,00
W1000-2	2,50	0,00	0,47	0,00
W1000-3	2,50	0,00	0,62	0,00
W1000-4	2,50	0,00	0,77	0,00
W1000-5	2,50	0,00	0,32	0,38
W1000-6	2,50	0,00	0,32	0,69
W1000-7	2,50	0,00	0,32	0,99
W1000-8	2,50	0,00	0,62	0,38
W1000-9	2,50	0,00	0,62	0,69
W1000-10	2,50	0,00	0,62	0,99
L01	2,50	0,00	0,50	0,42
L02	2,50	0,00	0,67	0,42
L03	2,50	0,00	1,00	0,42
L04	2,50	0,00	0,50	0,42
L04s	2,50	0,00	0,50	0,42
L05	2,50	0,00	0,67	0,42
L06	2,50	0,00	1,00	0,42
L06s	2,50	0,00	1,00	0,42
L07	2,50	0,00	0,50	0,58
L08	2,50	0,00	0,50	0,58

Specimen name	k_{1_e2}	k_{1_p2}	α_{d_e1}	α_{d_p1}
L09	2,50	0,00	0,83	0,58
L10	2,50	0,00	1,00	0,58
L11	2,50	0,00	0,67	0,75
L12	2,50	0,00	0,83	0,75
L13	2,50	0,00	1,00	0,75
L14	2,50	0,00	0,41	0,75
L15	2,50	0,00	0,50	0,75
L16	2,50	0,00	0,67	0,75
L17	2,50	0,00	0,83	0,75
L18	2,50	0,00	1,00	0,75
L18s	2,50	0,00	1,00	0,75
L19	2,50	0,00	1,00	0,75
L20	2,50	0,00	0,67	0,92
L20s	2,50	0,00	0,67	0,92
L21	2,50	0,00	0,67	0,92
L22	2,50	0,00	0,67	1,00
RE 1	2,50	0,00	0,31	0,00
RE 2	2,50	0,00	0,31	0,00
RE 3	2,50	0,00	0,47	0,00
RE 4	2,50	0,00	0,47	0,00
RE 5	2,50	0,00	0,63	0,00
RE 6	2,50	0,00	0,63	0,00
RE 7	2,50	0,00	0,79	0,00
RE 8	2,50	0,00	0,79	0,00
RE 9	2,50	0,00	0,94	0,00
RE 10	2,50	0,00	0,94	0,00
RE 11	2,50	0,00	0,31	0,00
RE 12	2,50	0,00	0,31	0,00
RE 13	2,50	0,00	0,63	0,00
RE 14	2,50	0,00	0,63	0,00
RE 17	2,50	0,00	0,63	0,00
RE 18	2,50	0,00	0,63	0,00
RE 19	2,50	0,00	0,63	0,00
RE 20	2,50	0,00	0,63	0,00
KK_E1	2,50	0,00	0,40	0,48
KK_E2	2,50	0,00	0,40	0,68
KK_E3	2,50	0,00	0,40	0,75
KK_E4	2,50	0,00	0,50	0,48
KK_E5	2,50	0,00	0,50	0,68
KK_E6	2,50	0,00	0,50	0,75
KK_F1	2,50	2,50	0,45	0,62
KK_F2	2,50	2,50	0,45	0,85
KK_F4	2,50	2,50	0,47	0,92
KK_F5	2,50	2,50	0,58	0,92
KK_G1	2,50	2,50	0,47	0,92
KK_G2	2,50	2,50	0,47	0,62
KK_G4	2,50	2,50	0,58	0,62
KK_G5	2,50	2,50	0,58	0,85
KK_H1	2,50	1,66	1,00	0,75
KK_H2	2,50	1,66	1,00	0,75
KK_H3	2,50	1,66	1,00	0,75
KK_H4	2,50	2,50	1,00	0,75
KK_H5	2,50	2,50	1,00	0,75
KK_H6	2,50	2,50	1,00	0,75
L04_b100	2,50	0,00	0,50	0,42

Specimen name	k_{1_e2}	k_{1_p2}	α_{d_e1}	α_{d_p1}
L04_b150	2,50	0,00	0,50	0,42
L04_b175	2,50	0,00	0,50	0,42
L04_b242	2,50	0,00	0,50	0,42
L06_b150	2,50	0,00	1,00	0,42
L06_b175	2,50	0,00	1,00	0,42
L06_b242	2,50	0,00	1,00	0,42
L10_b132	2,50	0,00	1,00	0,58
L10_b260	2,50	0,00	1,00	0,58
L16_b242	2,50	0,00	0,67	0,75
L16_b286	2,50	0,00	0,67	0,75
L16_b330	2,50	0,00	0,67	0,75
L14_b154	2,50	0,00	0,41	0,75
L14_b230	2,50	0,00	0,41	0,75
L14_b330	2,50	0,00	0,41	0,75
L19_b154	2,50	0,00	1,00	0,75
L19_b330	2,50	0,00	1,00	0,75
L19_b440	2,50	0,00	1,00	0,75
L16_b160	2,50	0,00	0,67	0,75
L01_1s	2,50	0,00	0,50	0,42
L02_1s	2,50	0,00	0,67	0,42
L03_1s	2,50	0,00	1,00	0,42
L04_1s	2,50	0,00	0,50	0,42
L05_1s	2,50	0,00	0,67	0,42
L06_1s	2,50	0,00	1,00	0,42
L07_1s	2,50	0,00	0,50	0,58
L08_1s	2,50	0,00	0,50	0,58
L09_1s	2,50	0,00	0,83	0,58
L10_1s	2,50	0,00	1,00	0,58
L11_1s	2,50	0,00	0,67	0,75
L12_1s	2,50	0,00	0,83	0,75
L13_1s	2,50	0,00	1,00	0,75
L14_1s	2,50	0,00	0,41	0,75
L15_1s	2,50	0,00	0,50	0,75
L16_1s	2,50	0,00	0,67	0,75
L17_1s	2,50	0,00	0,83	0,75
L18_1s	2,50	0,00	1,00	0,75
L19_1s	2,50	0,00	1,00	0,75
L20_1s	2,50	0,00	0,67	0,92
L21_1s	2,50	0,00	0,67	0,92
L22_1s	2,50	0,00	0,67	1,00
L01_2s_t10-20	2,50	0,00	0,50	0,42
L02_2s_t10-20	2,50	0,00	0,67	0,42
L03_2s_t10-20	2,50	0,00	1,00	0,42
L04_2s_t10-20	2,50	0,00	0,50	0,42
L05_2s_t10-20	2,50	0,00	0,67	0,42
L06_2s_t10-20	2,50	0,00	1,00	0,42
L07_2s_t10-20	2,50	0,00	0,50	0,58
L08_2s_t10-20	2,50	0,00	0,50	0,58
L09_2s_t10-20	2,50	0,00	0,83	0,58
L10_2s_t10-20	2,50	0,00	1,00	0,58
L11_2s_t10-20	2,50	0,00	0,67	0,75
L12_2s_t10-20	2,50	0,00	0,83	0,75
L13_2s_t10-20	2,50	0,00	1,00	0,75
L14_2s_t10-20	2,50	0,00	0,41	0,75
L15_2s_t10-20	2,50	0,00	0,50	0,75

Specimen name	k_{1_e2}	k_{1_p2}	α_{d_e1}	α_{d_p1}
L16_2s_t10-20	2,50	0,00	0,67	0,75
L17_2s_t10-20	2,50	0,00	0,83	0,75
L18_2s_t10-20	2,50	0,00	1,00	0,75
L19_2s_t10-20	2,50	0,00	1,00	0,75
L20_2s_t10-20	2,50	0,00	0,67	0,92
L21_2s_t10-20	2,50	0,00	0,67	0,92
L01_2s_t10-20_M27	2,50	0,00	0,50	0,42
L02_2s_t10-20_M27	2,50	0,00	0,67	0,42
L03_2s_t10-20_M27	2,50	0,00	1,00	0,42
L04_2s_t10-20_M27	2,50	0,00	0,50	0,42
L05_2s_t10-20_M27	2,50	0,00	0,67	0,42
L06_2s_t10-20_M27	2,50	0,00	1,00	0,42
L07_2s_t10-20_M27	2,50	0,00	0,50	0,58
L08_2s_t10-20_M27	2,50	0,00	0,50	0,58
L09_2s_t10-20_M27	2,50	0,00	0,83	0,58
L10_2s_t10-20_M27	2,50	0,00	1,00	0,58
L11_2s_t10-20_M27	2,50	0,00	0,67	0,75
L12_2s_t10-20_M27	2,50	0,00	0,83	0,75
L13_2s_t10-20_M27	2,50	0,00	1,00	0,75
L14_2s_t10-20_M27	2,50	0,00	0,40	0,75
L15_2s_t10-20_M27	2,50	0,00	0,50	0,75
L16_2s_t10-20_M27	2,50	0,00	0,67	0,75
L17_2s_t10-20_M27	2,50	0,00	0,83	0,75
L18_2s_t10-20_M27	2,50	0,00	1,00	0,75
L19_2s_t10-20_M27	2,50	0,00	1,00	0,75
L20_2s_t10-20_M27	2,50	0,00	0,67	0,92
L21_2s_t10-20_M27	2,50	0,00	0,67	0,92
L01_2s_t10-20_M27_b270	2,50	0,00	0,50	0,42
L02_2s_t10-20_M27_b270	2,50	0,00	0,67	0,42
L03_2s_t10-20_M27_b270	2,50	0,00	1,00	0,42
L04_2s_t10-20_M27_b270	2,50	0,00	0,50	0,42
L05_2s_t10-20_M27_b270	2,50	0,00	0,67	0,42
L06_2s_t10-20_M27_b270	2,50	0,00	1,00	0,42
L07_2s_t10-20_M27_b270	2,50	0,00	0,50	0,58
L08_2s_t10-20_M27_b270	2,50	0,00	0,50	0,58
L09_2s_t10-20_M27_b270	2,50	0,00	0,83	0,58
L10_2s_t10-20_M27_b270	2,50	0,00	1,00	0,58
L11_2s_t10-20_M27_b270	2,50	0,00	0,67	0,75
L12_2s_t10-20_M27_b270	2,50	0,00	0,83	0,75
L13_2s_t10-20_M27_b270	2,50	0,00	1,00	0,75
L14_2s_t10-20_M27_b270	2,50	0,00	0,40	0,75
L15_2s_t10-20_M27_b270	2,50	0,00	0,50	0,75
L16_2s_t10-20_M27_b270	2,50	0,00	0,67	0,75
L17_2s_t10-20_M27_b270	2,50	0,00	0,83	0,75
L18_2s_t10-20_M27_b270	2,50	0,00	1,00	0,75
L19_2s_t10-20_M27_b270	2,50	0,00	1,00	0,75
L20_2s_t10-20_M27_b270	2,50	0,00	0,67	0,92
L21_2s_t10-20_M27_b270	2,50	0,00	0,67	0,92
L06_7bolts_1s_b150	2,50	0,00	1,00	0,42
L14_7bolts_1s_b150	2,50	0,00	0,41	0,75
L14_7bolts_1s_b250	2,50	0,00	0,41	0,75
L14_7bolts_1s_b300	2,50	0,00	0,41	0,75
L19_7bolts_1s_b150	2,50	0,00	1,00	0,75

In the following table the factors e_1' , b_{eff} , k_1 , k_2 , k_3 , k_4 , k_5 , used in the new resistance formula are given. The values were calculated by nominal geometry of the connection.

Specimen name	e_1'	b_{eff}	k_1	k_2	k_3	k_4	k_5
B101	90	60	1,90	0,650	1,00	1,00	1,00
B102	36	72	1,30	0,830	1,00	1,00	1,00
B103	45	72	1,63	0,830	1,00	1,00	1,00
B104	60	72	1,90	0,830	1,00	1,00	1,00
B105	90	72	1,90	0,830	1,00	1,00	1,00
B106	75	81	1,90	0,965	1,00	1,00	1,00
B107	90	81	1,90	0,965	1,00	1,00	1,00
B108*	101	71	1,90	0,815	1,00	1,00	1,00
B109	30	90	0,87	1,100	1,00	1,00	1,00
B110	36	90	1,04	1,100	1,00	1,00	1,00
B111	45	90	1,30	1,100	1,00	1,00	1,00
B112	60	90	1,73	1,100	1,00	1,00	1,00
B113	75	90	1,90	1,100	1,00	1,00	1,00
B114	90	90	1,90	1,100	1,00	1,00	1,00
B115*	90	80	1,90	0,950	1,00	1,00	1,00
B116	45	90	1,30	1,100	1,00	1,00	1,00
B117	45	90	1,30	1,100	1,00	1,00	1,00
B118	45	120	0,98	1,550	1,00	1,00	1,00
B119	60	120	1,30	1,550	1,00	1,00	1,00
B120	75	120	1,63	1,550	1,00	1,00	1,00
B121	90	120	1,90	1,550	1,00	1,00	1,00
B122	105	120	1,90	1,550	1,00	1,00	1,00
B123	100	80	1,90	1,250	1,00	1,00	1,00
B124*	100	68	1,90	1,025	1,00	1,00	1,00
B125*	100	56	1,90	0,800	1,00	1,00	1,00
B201	72	72	1,90	0,425	1,00	1,00	1,00
B202	29	91	1,64	0,605	1,00	1,00	1,00
B203	48	91	1,90	0,605	1,00	1,00	1,00
B204	72	91	1,90	0,605	1,00	1,00	1,00
B205	72	98	1,90	0,673	1,00	1,00	1,00
B206	36	106	1,77	0,740	1,00	1,00	1,00
B207	72	113	1,90	0,808	1,00	1,00	1,00
B208	24	120	1,04	0,875	1,00	1,00	1,00
B209	29	120	1,25	0,875	1,00	1,00	1,00
B210	36	120	1,56	0,875	1,00	1,00	1,00
B211	48	120	1,90	0,875	1,00	1,00	1,00
B212	72	120	1,90	0,875	1,00	1,00	1,00
B213	48	98	1,90	0,673	1,00	1,00	1,00
PF1	36	114	1,64	0,605	1,00	1,00	1,00
PF2	36	123	1,52	0,673	1,00	1,00	1,00
PF3	36	132	1,42	0,740	1,00	1,00	1,00
PF4	36	123	1,52	0,673	1,00	1,00	1,00
PF5	36	132	1,42	0,740	1,00	1,00	1,00
PF6	36	141	1,33	0,808	1,00	1,00	1,00
PF7	36	132	1,42	0,740	1,00	1,00	1,00
PF8	36	141	1,33	0,808	1,00	1,00	1,00
PF9	36	150	1,25	0,875	1,00	1,00	1,00
PF10	36	78	1,90	0,335	1,00	1,00	1,00
PF11	36	87	1,90	0,403	1,00	1,00	1,00
PF12	36	96	1,90	0,470	1,00	1,00	1,00
PF13	36	105	1,78	0,538	1,00	1,00	1,00
PF14	36	114	1,64	0,605	1,00	1,00	1,00

Specimen name	e_1'	b_{eff}	k_1	k_2	k_3	k_4	k_5
PF15	36	87	1,90	0,403	1,00	1,00	1,00
PF16	36	96	1,90	0,470	1,00	1,00	1,00
PF17	36	105	1,78	0,538	1,00	1,00	1,00
PF18	36	114	1,64	0,605	1,00	1,00	1,00
PF19	36	123	1,52	0,673	1,00	1,00	1,00
PF20	36	96	1,90	0,470	1,00	1,00	1,00
PF21	36	105	1,78	0,538	1,00	1,00	1,00
PF22	36	105	1,78	0,538	1,00	1,00	1,00
PF23	36	114	1,64	0,605	1,00	1,00	1,00
PF24	36	114	1,64	0,605	1,00	1,00	1,00
PF25	36	123	1,52	0,673	1,00	1,00	1,00
BO050	20	89	0,58	1,657	1,00	1,00	1,00
BO0100	30	89	0,86	1,657	1,00	1,00	1,00
BO150	39	89	1,14	1,657	1,00	1,00	1,00
BO200	49	89	1,42	1,657	1,00	1,00	1,00
BT0510	39	150	0,68	1,482	0,68	1,00	1,00
BT0520	58	150	1,01	1,482	0,58	1,00	1,00
BT0530	77	150	1,33	1,482	0,55	1,00	1,00
BT1510	58	150	1,01	1,482	0,84	1,00	1,00
BT1520	77	150	1,33	1,482	0,66	1,00	1,00
BT1530	96	150	1,66	1,482	0,59	1,00	1,00
W700-1	20	89	0,58	1,657	1,00	1,00	1,00
W700-2	30	89	0,86	1,657	1,00	1,00	1,00
W700-3	39	89	1,14	1,657	1,00	1,00	1,00
W700-4	49	89	1,42	1,657	1,00	1,00	1,00
W700-5	39	150	0,68	1,482	0,68	1,00	1,00
W700-6	58	150	1,01	1,482	0,58	1,00	1,00
W700-7	77	150	1,33	1,482	0,55	1,00	1,00
W700-8	58	150	1,01	1,482	0,84	1,00	1,00
W700-9	77	150	1,33	1,482	0,66	1,00	1,00
W700-10	96	150	1,66	1,482	0,59	1,00	1,00
W1000-1	20	89	0,58	1,657	1,00	1,00	1,00
W1000-2	30	89	0,86	1,657	1,00	1,00	1,00
W1000-3	39	89	1,14	1,657	1,00	1,00	1,00
W1000-4	49	89	1,42	1,657	1,00	1,00	1,00
W1000-5	39	150	0,68	1,482	0,68	1,00	1,00
W1000-6	58	150	1,01	1,482	0,58	1,00	1,00
W1000-7	77	150	1,33	1,482	0,55	1,00	1,00
W1000-8	58	150	1,01	1,482	0,84	1,00	1,00
W1000-9	77	150	1,33	1,482	0,66	1,00	1,00
W1000-10	96	150	1,66	1,482	0,59	1,00	1,00
L01	77	198	1,01	1,267	0,75	1,00	1,00
L02	88	198	1,16	1,267	0,83	1,00	1,00
L03	110	198	1,44	1,267	1,00	1,00	1,00
L04	99	198	1,30	0,950	0,75	1,00	1,00
L04s	99	198	1,30	0,950	0,75	1,00	1,00
L05	110	198	1,44	0,950	0,83	1,00	1,00
L06	132	198	1,73	0,950	1,00	1,00	1,00
L06s	132	198	1,73	0,950	1,00	1,00	1,00
L07	99	198	1,30	1,267	0,66	1,00	1,00
L08	132	198	1,73	0,950	0,66	1,00	1,00
L09	154	198	1,90	0,950	0,77	1,00	1,00
L10	165	198	1,90	0,950	0,82	1,00	1,00
L11	132	198	1,73	1,267	0,65	1,00	1,00
L12	143	198	1,88	1,267	0,69	1,00	1,00
L13	154	198	1,90	1,267	0,72	1,00	1,00
L14	159	198	1,90	0,950	0,59	1,00	1,00

Specimen name	e_1'	b_{eff}	k_1	k_2	k_3	k_4	k_5
L15	165	198	1,90	0,950	0,61	1,00	1,00
L16	176	198	1,90	0,950	0,65	1,00	1,00
L17	187	198	1,90	0,950	0,69	1,00	1,00
L18	198	198	1,90	0,950	0,72	1,00	1,00
L18s	198	198	1,90	0,950	0,72	1,00	1,00
L19	242	198	1,90	0,950	0,87	1,00	1,00
L20	209	198	1,90	0,950	0,61	1,00	1,00
L20s	209	198	1,90	0,950	0,61	1,00	1,00
L21	154	198	1,90	1,267	0,61	1,00	1,00
L22	166	198	1,90	1,267	0,59	1,00	1,00
RE 1	25	114	0,57	1,650	1,00	1,00	1,00
RE 2	25	114	0,57	1,650	1,00	1,00	1,00
RE 3	38	114	0,87	1,650	1,00	1,00	1,00
RE 4	38	114	0,87	1,650	1,00	1,00	1,00
RE 5	51	114	1,16	1,650	1,00	1,00	1,00
RE 6	51	114	1,16	1,650	1,00	1,00	1,00
RE 7	64	114	1,46	1,650	1,00	1,00	1,00
RE 8	64	114	1,46	1,650	1,00	1,00	1,00
RE 9	76	114	1,73	1,650	1,00	1,00	1,00
RE 10	76	114	1,73	1,650	1,00	1,00	1,00
RE 11	25	114	0,57	1,650	1,00	1,00	1,00
RE 12	25	114	0,57	1,650	1,00	1,00	1,00
RE 13	51	114	1,16	1,650	1,00	1,00	1,00
RE 14	51	114	1,16	1,650	1,00	1,00	1,00
RE 17	51	137	0,97	2,033	1,00	1,00	1,00
RE 18	51	137	0,97	2,033	1,00	1,00	1,00
RE 19	51	89	1,49	1,233	1,00	1,00	1,00
RE 20	51	89	1,49	1,233	1,00	1,00	1,00
KK_E1	62	200	0,81	1,606	0,67	1,00	1,00
KK_E2	78	200	1,01	1,606	0,60	1,00	1,00
KK_E3	83	200	1,08	1,606	0,59	1,00	1,00
KK_E4	70	200	0,91	1,606	0,71	1,00	1,00
KK_E5	86	200	1,12	1,606	0,63	1,00	1,00
KK_E6	91	200	1,18	1,606	0,61	1,00	1,00
KK_F1	65	297	1,14	1,394	0,63	0,69	1,00
KK_F2	80	297	1,41	1,394	0,58	0,74	1,00
KK_F4	86	297	1,50	1,394	0,58	0,75	1,00
KK_F5	94	297	1,64	1,394	0,60	0,75	1,00
KK_G1	86	297	1,50	1,394	0,58	1,00	0,76
KK_G2	66	297	1,16	1,394	0,64	0,93	0,76
KK_G4	74	297	1,29	1,394	0,67	0,93	0,76
KK_G5	89	297	1,56	1,394	0,61	1,00	0,76
KK_H1	130	114	1,90	0,370	0,72	1,00	1,00
KK_H2	130	140	1,90	0,483	0,72	1,00	1,00
KK_H3	130	161	1,90	0,573	0,72	1,00	1,00
KK_H4	130	130	1,90	0,438	0,72	1,00	1,00
KK_H5	130	156	1,90	0,550	0,72	1,00	1,00
KK_H6	130	172	1,90	0,618	0,72	1,00	1,00
L04_b100	99	100	1,90	0,449	0,75	1,00	1,00
L04_b150	99	150	1,72	0,705	0,75	1,00	1,00
L04_b175	99	175	1,47	0,832	0,75	1,00	1,00
L04_b242	99	242	1,06	1,175	0,75	1,00	1,00
L06_b150	132	150	1,90	0,705	1,00	1,00	1,00
L06_b175	132	175	1,90	0,832	1,00	1,00	1,00
L06_b242	132	242	1,42	1,175	1,00	1,00	1,00
L10_b132	165	132	1,90	0,613	0,82	1,00	1,00
L10_b260	165	260	1,65	1,267	0,82	1,00	1,00

Specimen name	e_1'	b_{eff}	k_1	k_2	k_3	k_4	k_5
L16_b242	176	242	1,89	1,175	0,65	1,00	1,00
L16_b286	176	286	1,60	1,400	0,65	1,00	1,00
L16_b330	176	330	1,39	1,625	0,65	1,00	1,00
L14_b154	159	154	1,90	0,725	0,59	1,00	1,00
L14_b230	159	230	1,80	1,114	0,59	1,00	1,00
L14_b330	159	330	1,25	1,625	0,59	1,00	1,00
L19_b154	242	154	1,90	0,725	0,87	1,00	1,00
L19_b330	242	330	1,90	1,625	0,87	1,00	1,00
L19_b440	242	440	1,43	2,188	0,87	1,00	1,00
L16_b160	176	160	1,90	0,756	0,65	1,00	1,00
L01_1s	77	198	1,01	1,267	0,85	1,00	1,00
L02_1s	88	198	1,16	1,267	0,97	1,00	1,00
L03_1s	110	198	1,44	1,267	1,00	1,00	1,00
L04_1s	99	198	1,30	0,950	0,85	1,00	1,00
L05_1s	110	198	1,44	0,950	0,97	1,00	1,00
L06_1s	132	198	1,73	0,950	1,00	1,00	1,00
L07_1s	99	198	1,30	1,267	0,75	1,00	1,00
L08_1s	132	198	1,73	0,950	0,75	1,00	1,00
L09_1s	154	198	1,90	0,950	0,92	1,00	1,00
L10_1s	165	198	1,90	0,950	1,00	1,00	1,00
L11_1s	132	198	1,73	1,267	0,76	1,00	1,00
L12_1s	143	198	1,88	1,267	0,82	1,00	1,00
L13_1s	154	198	1,90	1,267	0,88	1,00	1,00
L14_1s	159	198	1,90	0,950	0,66	1,00	1,00
L15_1s	165	198	1,90	0,950	0,69	1,00	1,00
L16_1s	176	198	1,90	0,950	0,76	1,00	1,00
L17_1s	187	198	1,90	0,950	0,82	1,00	1,00
L18_1s	198	198	1,90	0,950	0,88	1,00	1,00
L19_1s	242	198	1,90	0,950	1,00	1,00	1,00
L20_1s	209	198	1,90	0,950	0,70	1,00	1,00
L21_1s	154	198	1,90	1,267	0,70	1,00	1,00
L22_1s	166	198	1,90	1,267	0,68	1,00	1,00
L01_2s_t10-20	77	198	1,01	1,267	0,85	1,00	1,00
L02_2s_t10-20	88	198	1,16	1,267	0,97	1,00	1,00
L03_2s_t10-20	110	198	1,44	1,267	1,00	1,00	1,00
L04_2s_t10-20	99	198	1,30	0,950	0,85	1,00	1,00
L05_2s_t10-20	110	198	1,44	0,950	0,97	1,00	1,00
L06_2s_t10-20	132	198	1,73	0,950	1,00	1,00	1,00
L07_2s_t10-20	99	198	1,30	1,267	0,75	1,00	1,00
L08_2s_t10-20	132	198	1,73	0,950	0,75	1,00	1,00
L09_2s_t10-20	154	198	1,90	0,950	0,92	1,00	1,00
L10_2s_t10-20	165	198	1,90	0,950	1,00	1,00	1,00
L11_2s_t10-20	132	198	1,73	1,267	0,76	1,00	1,00
L12_2s_t10-20	143	198	1,88	1,267	0,82	1,00	1,00
L13_2s_t10-20	154	198	1,90	1,267	0,88	1,00	1,00
L14_2s_t10-20	159	198	1,90	0,950	0,66	1,00	1,00
L15_2s_t10-20	165	198	1,90	0,950	0,69	1,00	1,00
L16_2s_t10-20	176	198	1,90	0,950	0,76	1,00	1,00
L17_2s_t10-20	187	198	1,90	0,950	0,82	1,00	1,00
L18_2s_t10-20	198	198	1,90	0,950	0,88	1,00	1,00
L19_2s_t10-20	242	198	1,90	0,950	1,00	1,00	1,00
L20_2s_t10-20	209	198	1,90	0,950	0,70	1,00	1,00
L21_2s_t10-20	154	198	1,90	1,267	0,70	1,00	1,00
L01_2s_t10-20_M27	105	198	1,38	0,907	0,85	1,00	1,00
L02_2s_t10-20_M27	120	198	1,58	0,907	0,97	1,00	1,00
L03_2s_t10-20_M27	150	198	1,90	0,907	1,00	1,00	1,00
L04_2s_t10-20_M27	135	198	1,77	0,680	0,85	1,00	1,00

Specimen name	e_1'	b_{eff}	k_1	k_2	k_3	k_4	k_5
L05_2s_t10-20_M27	150	198	1,90	0,680	0,97	1,00	1,00
L06_2s_t10-20_M27	180	198	1,90	0,680	1,00	1,00	1,00
L07_2s_t10-20_M27	135	198	1,77	0,907	0,75	1,00	1,00
L08_2s_t10-20_M27	180	198	1,90	0,680	0,75	1,00	1,00
L09_2s_t10-20_M27	210	198	1,90	0,680	0,92	1,00	1,00
L10_2s_t10-20_M27	225	198	1,90	0,680	1,00	1,00	1,00
L11_2s_t10-20_M27	180	198	1,90	0,907	0,76	1,00	1,00
L12_2s_t10-20_M27	195	198	1,90	0,907	0,82	1,00	1,00
L13_2s_t10-20_M27	210	198	1,90	0,907	0,88	1,00	1,00
L14_2s_t10-20_M27	216	198	1,90	0,680	0,65	1,00	1,00
L15_2s_t10-20_M27	225	198	1,90	0,680	0,69	1,00	1,00
L16_2s_t10-20_M27	240	198	1,90	0,680	0,76	1,00	1,00
L17_2s_t10-20_M27	255	198	1,90	0,680	0,82	1,00	1,00
L18_2s_t10-20_M27	270	198	1,90	0,680	0,88	1,00	1,00
L19_2s_t10-20_M27	330	198	1,90	0,680	1,00	1,00	1,00
L20_2s_t10-20_M27	285	198	1,90	0,680	0,70	1,00	1,00
L21_2s_t10-20_M27	210	198	1,90	0,907	0,70	1,00	1,00
L01_2s_t10-20_M27_b270	105	270	1,01	1,267	0,85	1,00	1,00
L02_2s_t10-20_M27_b270	120	270	1,16	1,267	0,97	1,00	1,00
L03_2s_t10-20_M27_b270	150	270	1,44	1,267	1,00	1,00	1,00
L04_2s_t10-20_M27_b270	135	270	1,30	0,950	0,85	1,00	1,00
L05_2s_t10-20_M27_b270	150	270	1,44	0,950	0,97	1,00	1,00
L06_2s_t10-20_M27_b270	180	270	1,73	0,950	1,00	1,00	1,00
L07_2s_t10-20_M27_b270	135	270	1,30	1,267	0,75	1,00	1,00
L08_2s_t10-20_M27_b270	180	270	1,73	0,950	0,75	1,00	1,00
L09_2s_t10-20_M27_b270	210	270	1,90	0,950	0,92	1,00	1,00
L10_2s_t10-20_M27_b270	225	270	1,90	0,950	1,00	1,00	1,00
L11_2s_t10-20_M27_b270	180	270	1,73	1,267	0,76	1,00	1,00
L12_2s_t10-20_M27_b270	195	270	1,88	1,267	0,82	1,00	1,00
L13_2s_t10-20_M27_b270	210	270	1,90	1,267	0,88	1,00	1,00
L14_2s_t10-20_M27_b270	216	270	1,90	0,950	0,65	1,00	1,00
L15_2s_t10-20_M27_b270	225	270	1,90	0,950	0,69	1,00	1,00
L16_2s_t10-20_M27_b270	240	270	1,90	0,950	0,76	1,00	1,00
L17_2s_t10-20_M27_b270	255	270	1,90	0,950	0,82	1,00	1,00
L18_2s_t10-20_M27_b270	270	270	1,90	0,950	0,88	1,00	1,00
L19_2s_t10-20_M27_b270	330	270	1,90	0,950	1,00	1,00	1,00
L20_2s_t10-20_M27_b270	285	270	1,90	0,950	0,70	1,00	1,00
L21_2s_t10-20_M27_b270	210	270	1,90	1,267	0,70	1,00	1,00
L06_7bolts_1s_b150	198	150	1,90	0,403	1,00	1,00	1,00
L14_7bolts_1s_b150	291	150	1,90	0,403	0,66	1,00	1,00
L14_7bolts_1s_b250	291	250	1,90	0,695	0,66	1,00	1,00
L14_7bolts_1s_b300	291	300	1,90	0,841	0,66	1,00	1,00
L19_7bolts_1s_b150	374	150	1,90	0,403	1,00	1,00	1,00